ANNUAL REVIEW

INSTITUTE FOR MOLECULAR SCIENCE

2001

Editorial Committee 2001
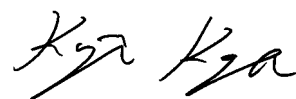
IMS 2001

This is the first annual review of the Institute for Molecular Science at the 21st century. In the last century, science and technology have made conspicuous development and have made great contribution to the establishment of materially well-off societies. In this century, molecular science has to play a central role for the establishment of the harmony between human society and natural environment by the novel concept of molecular materials.

In this annual review, recent development of researches at six departments and five research facilities are introduced in addition to the report on joints study programs of IMS last year. The reader may find out wide varieties of molecular size ranging from diatomic molecules of 0.1 nm scale to large single molecules of 100 nm scale in the individual research reports. One also feels the incoming of new areas, *i.e.*, molecular devices, biodynamics and the chemistry of the environment as important research directions.

November, 2001

KAYA, Koji
Director General, Institute for Molecular Science

CONTENT

Department of Theoretical Studies

RESEARCH ACTIVITIES II ---45

Department of Molecular Structure

RESEARCH ACTIVITIES III --59

Department of Electronic Structure

RESEARCH ACTIVITIES V --109

Department of Applied Molecular Science

RESEARCH ACTIVITIES VI --125

Department of Vacuum UV Photoscience

RESEARCH ACTIVITIES VII

Coordination Chemistry Laboratories

RESEARCH ACTIVITIES VIII --179

Laser Research Center for Molecular Science

Research Center for Molecular Materials

Equipment Development Center

Ultraviolet Synchrotron Orbital Radiation Facility

Computer Center

Abbrevations

IMS: Institute for Molecular Science
GUAS: The Graduate University for Advanced Studies

ORGANIZATION AND STAFF

Organization

The Institute for Molecular Science comprises twenty one research laboratories — each staffed by a professor, an associate professor, two research associates and several technical associates —, two research laboratories with foreign visiting professors, and five research facilities.

The laboratories are grouped into six departments and one facility for coordination chemistry:

Department of Theoretical Studies	Theoretical Studies I
	Theoretical Studies II
	Theoretical Studies III[1]
	Theoretical Studies IV
Department of Molecular Structure	Molecular Structure I
	Molecular Structure II[1]
	Molecular Dynamics
Department of Electronic Structure	Excited State Chemistry
	Excited State Dynamics
	Electronic Structure[1]
	Molecular Energy Conversion[2]
Department of Molecular Assemblies	Solid State Chemistry
	Molecular Dynamics Assemblies
	Molecular Assemblies[1]
Department of Applied Molecular Science	Applied Molecular Science I
	Applied Molecular Science II[1]
	Molecular Clusters[3]
Department of Vacuum UV Photoscience	Photochemistry
	Chemical Dynamics
	Interface Molecular Science[3]
	Synchrotron Radiation Research[2]
Coordination Chemistry Laboratories	Complex Catalysis
	Functional Coordination Chemistry
	Coordination Bond[1]

The research facilities are:

• Laser Research Center for Molecular Science	Advanced Lasers for Chemical Reaction Studies
	Advanced Lasers for Synchrotron Radiation Applications
	Advanced UV and IR Tunable Lasers
• Research Center for Molecular Materials	Organic Materials Section
	Hybrid Materials Section
	Materials Characterization Section
	Structure Control Section

• Equipment Development Center
• UVSOR (Ultraviolet Synchrotron Orbital Radiation) Facility

• Computer Center

The research facilities of ONRI (related to IMS) are:

• Center for Integrative Bioscience
• Research Center for Computational Science

1) Professors and associate professors are visiting professors from other universities.
2) Research laboratories with foreign visiting professors.
3) Professors, associate professors, and research associates, along with their positions, are transferred from other universities.

Scientific Staff

KAYA, Koji   **Professor, Director-General**

Emeritus Professors

NAGAKURA, Saburo   President, The Kanagawa Academy of Science and
                           Technology
HIROTA, Eizi   President, The Graduate University for Advanced Studies
KIMURA, Katsumi   Senior Researcher, Molecular Photonics & Photoelectron
                           Group, Communications Research Laboratory
MOROKUMA, Keiji   Professor, Emory University, U. S. A.
INOKUCHI, Hiroo   Chief Scientist of Space Utilization Research Program,
                           National Space Development Agency of Japan
MARUYAMA, Yusei   Professor, Hosei University
YOSHIHARA, Keitaro   Professor, Japan Advanced Institute of Science and
                           Technology
HANAZAKI, Ichiro
IWAMURA, Hiizu   Professor, University of the Air
SAITO, Shuji   Professor, Fukui University
IWATA, Suehiro   Professor, National Institution for Academic Degree
ITO, Mitsuo   Professor Emeritus, The Graduate University for Advanced
                           Studies, Tohoku University

Department of Theoretical Studies
  Theoretical Studies I
NAGASE, Shigeru   Professor (April '01–)
OKAMOTO, Yuko   Associate Professor
IKEGAMI, Tsutomu   Research Associate (–March '01)[1]
SUGITA, Yuji   Research Associate
TSURUSAWA, Takeshi   Technical Associate (–October '00)[2]
NAGASIMA, Takehiro   Technical Associate
YODA, Takao   IMS Fellow (–March '01), Research Associate of Research
                           for the Future Program (April '01–)
CHOE, Yoong-Kee   IMS Fellow (April '01–)
NISHIKAWA, Takeshi   Research Associate of Research for the Future Program
                           (–March '01)[3]
ITOH, Masakatsu   Research Associate of Research for the Future Program
MITSUTAKE, Ayori   Research Associate of Research for the Future Program
                           (–March '01)[4]
IMAI, Takashi   Research Associate of Research for the Future Program
                           (–June '01)[5]
YAMAGUCHI, Tsuyoshi   Research Associate of Research for the Future Program
                           (April, '01–)
RE, Suyong   JSPS Post-Doctoral Fellow (April '01–)
MAYER, Bodo   Research Fellow (from Darmstadt University of
                           Technology, Germany) (July–August '01)
KOKUBO, Hironori   Graduate Student (April '01–)
MURATA, Katsumi   Graduate Student (April '01–)
SAKAE, Yoshitake   Graduate Student (April '01–)
TAKAGI, Nozomi   Graduate Student (from Tokyo Metropolitan University)*
                           (April '01–)
FUKAMI, Kentaro   Graduate Student (from Tokyo Metropolitan University)*
                           (June '01–)

  Theoretical Studies II
NAKAMURA, Hiroki   Professor
TANIMURA, Yoshitaka   Associate Professor
ZHU, Chaoyuan   Research Associate
OKUMURA, Ko   Research Associate (–September '00)[6]
TAKAMI, Toshiya   Research Associate
SUZUKI, Yoko   Technical Associate (–April '01), Research Associate (May
                           '01–)

MISHIMA, Kenji	IMS Fellow (–March '01)[7]
KATO, Tsuyoshi	IMS Fellow
FUJISAKI, Hiroshi	IMS Fellow (April '01–)
LEE, Eok Kyun	Visiting Scientist; MONBUSHO Invited Fellow (from Korea Advanced Institute of Science & Technology, Korea) (June–August '01)
LEE, Chun-Woo	Visiting Scientist; MONBUSHO Invited Fellow (from Ajou University, Korea) (July–August '01)
OSHEROV, Vladimir I.	Visiting Scientist; JSPS Invited Fellow (from Institute of Problems of Chemical Physics, Russian Academy of Sciences, Russia) (April–May '01)
BIAN, Wensheng	Visiting Scientist; JSPS Post–Doctoral Fellow (from Shandong University, China)
MIL'NIKOV, Gennady V.	Research Fellow (from Institute of Structural Macrokinetics, Russia) (June '01–)
CHAO, Sheng-Der	Research Fellow (from University of Colorado, U.S.A.) (May '01–)
PICHL, Lukas	Graduate Student (–September '00)[8]
NAGAYA, Kuninobu	Graduate Student
KAMISAKA, Hideyuki	Graduate Student
HINO, Osamu	Graduate Student
FUKAMI, Hiroshi	Graduate Student (from Kyoto University)*

Theoretical Studies III

KIKUCHI, Takeshi	Visiting Professor (from Kurashiki University of Science and the Arts) (–March '01)
SAITO, Susumu	Visiting Professor (from Tokyo Institute of Technology) (April '01–)
KINOSHITA, Masahiro	Visiting Associate Professor (from Kyoto University) (–March '01)
SHIMOI, Yukihiro	Visiting Associate Professor (from National Institute of Advanced Industrial Science and Technology) (April '01–)
KOVALENKO, Andriy F.	Research Associate

Theoretical Studies IV

HIRATA, Fumio	Professor
YONEMITSU, Kenji	Associate Professor
SATO, Hirofumi	Research Associate
KISHINE, Jun-ichiro	Research Associate
SETHIA, Ashok	IMS Fellow (–May '01)[9]
KUWABARA, Makoto	IMS Fellow (–May '01)[10]
MORI, Michiyasu	JSPS Post-Doctoral Fellow (–January '01)[11]
SUMI, Tomonari	JSPS Post-Doctoral Fellow
IMAMURA, Chikara	Visiting Scientist (from Yamaguchi Prefectural University) (–September '00)
HARANO, Yuichi	Graduate Student (from Kobe University)* (–March '01)[12]
YAMAZAKI, Takeshi	Graduate Student
MIYASHITA, Naoyuki	Graduate Student
WATANABE, Ayumi	Graduate Student (April, '01–)

Department of Molecular Structure
Molecular Structure I

OKAMOTO, Hiromi	Professor (April '01–)
MORITA, Norio	Associate Professor
MORIWAKI, Yoshiki	Research Associate (–April '01)[13]
IMURA, Kouhei	Research Associate (July '01–)

Molecular Structure II

AKASAKA, Takeshi	Visiting Professor (from University of Tsukuba) (–March '01)[14]
AKUTSU, Hideo	Visiting Professor (from Osaka University) (April '01–)
SASADA, Hiroyuki	Visiting Associate Professor (from Keio University)

Molecular Dynamics
KITAGAWA, Teizo — Professor
KATO, Tatsuhisa — Associate Professor
MIZUTANI, Yasuhisa — Research Associate (–May '01)[15]
FURUKAWA, Ko — Research Associate (April '01–)
NAGATOMO, Shigenori — Technical Associate
HAYASHI, Naoki — Technical Associate
TOYAMA, Namiki — IMS Fellow (April '01–)
KIM, Younkyoo — Visiting Scientist; MONBUSHO Invited Fellow (from Hankuk University of Foreign Studies, Korea) (December '00–February '01)[16]
MO, Yu-jun — Visiting Scientist; MONBUSHO Invited Fellow (from Henan University, China) (–May '01)[17]
LI, Zheng-qiang — Visiting Scientist; MONBUSHO Invited Fellow (from Jilin University Changchun, China) (–May '01)[18]
HUDECEK, Jiri — Visiting Scientist; JSPS Invited Fellow (from Charles University, Czech Republic) (April '01–)
VERMA, Alan L. — Visiting Scientist; JSPS Invited Fellow (from North-Eastern Hill University, India) (–September '00)[19]
HU, Ying — Visiting Scientist; JSPS Post-Doctral Fellow (from Fudan University, China) (–January '01)[20]
UCHIDA, Takeshi — JSPS Post-Doctral Fellow
KANEMOTO, Katsuichi — JSPS Post-Doctral Fellow (–March '01)[21]
IWASE, Tadashi — Research Fellow
AKI, Michihiko — Graduate Student (–October '00)[22]
YAMAMOTO, Kohji — Graduate Student (–March '01)[23]
HARUTA, Nami — Graduate Student
OKUNO, Daichi — Graduate Student
SATO, Akira — Graduate Student
OKUBO, Shingo — Graduate Student

Department of Electronic Structure
Excited State Chemistry
NISHI, Nobuyuki — Professor
TSUKUDA, Tatsuya — Associate Professor
NAKABAYASHI, Takakazu — Research Associate
NEGISHI, Yuichi — Research Associate
AKITA, Motoko — Research Associate of Research for the Future Program
IMAI, Hiroyuki — Research Associate of Research for the Future Program
PROKOP, Petra V. — Research Associate of Research for the Future Program (October '00–)
KOSUGI, Kentaroh — Graduate Student (–March '01), Research Associate of Research for the Future Program (April '01–)
HINO, Kazuyuki — Graduate Student (from Kyushu University)*
KAMO, Satoshi — Graduate Student (from Tsukuba University)* (–March '01)

Excited State Dynamics
FUJII, Masaaki — Professor
SUZUKI, Toshinori — Associate Professor
KOHGUCHI, Hiroshi — Research Associate
SAKAI, Makoto — Research Associate
KATAYANAGI, Hideki — Technical Associate
SAEKI, Morihisa — IMS Fellow
WHITAKER, Benjamin J. — Visiting Scientist; MONBUSHO Invited Fellow (from University of Leeds, UK) (–September '00)
WATANABE, Takeshi — JSPS Post-Doctoral Fellow
MATSUMOTO, Yoshiteru — Research Fellow (April '01–)
SONG, Jae K. — Visiting Scientist (from Seoul National University, Korea) (March–June '01)
IKETAKI, Yoshimori — Visiting Scientist (from Olympus Optical Co., Ltd.) (April '01–)
ISHIUCHI, Shun-ichi — Graduate Student (–March '01), Visiting Scientist (from Keio University) (April '01–)

HOSSAIN, Delwar   Graduate Student
TSUBOUCHI, Masaaki   Graduate Student

Electronic Structure
YAMASE, Toshihiro   Visiting Professor (from Tokyo Institute of Technology)
OHSHIMA, Yasuhiro   Visiting Associate Professor (from Kyoto University)
INOKUCHI, Yoshiya   Research Associate

Molecular Energy Conversion
MO, Yu-Jun   Visiting Professor (from Honan University, China)
DE LANGE, Cornelis A.   Visiting Professor (from University of Amsterdam, the Netherlands) (May–August '01)
SWIETLIK, Roman   Visiting Professor (from Institute of Molecular Physics, Poland) (August '01–)
GRITSENKO, Victor V.   Visiting Associate Professor (from Institute for Chemical Physics Research Russian Academy of Sciences, Russia)
DU, Si-de   Visiting Associate Professor (from Fudan University, China) (June '01–)

Department of Molecular Assemblies
Solid State Chemistry
YAKUSH1, Kyuya   Professor
NAKAMURA, Toshikazu   Associate Professor
YAMAMOTO, Kaoru   Research Associate
FUJIYAMA, Shigeki   Research Associate (April '01–)
URUICHI, Mikio   Technical Associate
MAKSIMUK, Mikhail   IMS Fellow (–November '00)[24]
DROZDOVA, Olga   Visiting Scientist; MONBUSHO Invited Fellow (from Ioffe Physical Technical Institute) (–March '01)[25]
SIMONYAN, Mkhitar   Visiting Scientist (from Armenian Academy of Science) (–October '00)[26]
SWIETLIK, Roman   Visiting Professor (from Polish Academy of Sciences) (–July '01)
NAKANO, Chikako   Research Fellow
DING, Yuqin   Graduate Student
SUZUKI, Kenji   Graduate Student (–April '01)

Molecular Assemblies Dynamics
KOBAYASHI, Hayao   Professor
TADA, Hirokazu   Associate Professor
OGATA, Hironori   Research Associate
FUJIWARA, Hideki   Research Associate
OISHl, Osamu   Technical Associate
OKANO, Yoshinori   Technical Associate
TAMURA, Itaru   IMS Fellow
GRAAF, Harald   IMS Fellow
TANAKA, Hisashi   JSPS Post-Doctoral Fellow
FUJIWARA, Emiko   Research Fellow (–March '01)[27]
GRITSENKO, Victor   Research Fellow (–March '01)[28]

Molecular Assemblies
TOKUMOTO, Madoka   Visiting Professor (from Electrotechnical Laboratory) (–March '01)
KATO, Reizo   Visiting Professor (from RIKEN) (April '01–)
MORI, Takehiko   Visiting Associate Professor (from Tokyo Institute of Technology) (–March '01)
OGAWA, Takuji   Visiting Associate Professor (from Ehime University) (April '01–)
HASEGAWA, Shinji   Research Associate (–March '01)[29]

Department of Applied Molecular Science
Applied Molecular Science I
WATANABE, Yoshihito   Professor (Center for Integrative Bioscience)
KINOSITA, Kazuhiko, Jr.   Professor (Center for Integrative Bioscience) (April '01–)

INOUE, Katsuya	Associate Professor
HOSOKOSHI, Yuko	Research Associate
UENO, Takafumi	Research Associate (Center for Integrative Bioscience)
KIM, Cheal	Visiting Scientist; MONBUSHO Invited Fellow (from Seoul National Polytechnic University, Korea) (December '00–February '01)[30]
KUMAGAI, Hitoshi	JSPS Post-Doctoral Fellow
YOSHIOKA, Shiro	IMS Fellow (April '01–)
SUZUKI, Kazuharu	IMS Fellow (–March '01)[31]
NAKAI, Hidetaka	Research Fellow
YAMAHARA, Ryo	Graduate Student (from Nagoya Institute of Technology)*
MAKIHARA, Nobuyuki	Graduate Student
HARA, Isao	Graduate Student
YANG, Huijun	Graduate Student (–March '01)[32]
SUZUKI, Kentaro	Graduate Student
KATO, Shigeru	Graduate Student
OHASHI, Masataka	Graduate Student
ABURA, Tsutomu	Graduate Student
KATOH, Keiichi	Graduate Student
OKA, Yoshimi	Graduate Student (April '01–)
KOMIYA, Kazuaki	Graduate Student (from Nagoya University)* (April '01–)
YAMAZAKI, Takayuki	Graduate Student (from Nagoya University)* (April '01–)
NOGAMI, Takeo	Graduate Student (from Nagoya University)* (April '01–)
KISHIDA, Mitsumi	Graduate Student (from Nagoya Institute of Technology)* (–February '01)[33]

Applied Molecular Science II

MASUDA, Hideki	Visiting Professor (from Nagoya Institute of Technology)
IWATA, Koichi	Visiting Associate Professor (from the University of Tokyo)
OGO, Seiji	Research Associate

Molecular Clusters

KASAI, Toshio	Professor (from Osaka University)
TAKASU, Masako	Associate Professor (from Kanazawa University)
KUBO, Atsushi	Research Associate (from Kyoto University)
CHE, Dock-Chil	Research Associate (from Osaka University)
HASHIMOTO, Masahito	IMS Fellow (–March '01)[34]
SHIMIZU, Yuichiro	IMS Fellow (October '00–)
NOGUCHI, Hiroshi	JSPS Post-Doctoral Fellow
NISHIYAMA, Yusuke	Visiting Scientist (from Kyoto University)
HASHINOKUCHI, Michihiro	Graduate Student (from Osaka University)*
NOSAKA, Makoto	Graduate Student (from Kanazawa University)*
ICHIKAWA, Shinji	Graduate Student (–March '01)*[35]
FUKUYAMA, Tetsuya	Graduate Student (from Himeji Institute of Technology)* (April '01–)

Department of Vacuum UV Photoscience

Photochemistry

KOSUGI, Nobuhiro	Professor
TAHARA, Tahei	Associate Professor
TAKEUCHI, Satoshi	Research Associate
HATSUI, Takaki	Research Associate
MIZUNO, Misao	Technical Associate
OJI, Hiroshi	IMS Fellow
NAGASONO, Mitsuru	JSPS Post-Doctoral Fellow
ARZHANTSEV, Sergei Yur'evich	JSPS Post-Doctoral Fellow (–November '00), IMS Fellow (December '00–)
MANDAL, Debabrata	JSPS Post-Doctoral Fellow (November '00–)
FUJINO, Tatsuya	JSPS Post-Doctoral Fellow
FUJIYOSHI, Satoru	Graduate Student

Chemical Dynamics

| URISU, Tsuneo | Professor |
| MITSUKE, Koichiro | Associate Professor |

MIZUTANI, Masakazu — Research Associate
NONOGAKI ,Youichi — Research Associate
ONO, Masaki — IMS Fellow
IWASAKI, Kota — JSPS Post-Doctoral Fellow (–May '01)[36]
MORÉ, Sam D. — IMS Fellow (October '00–)
AZUMA ,Yasushi — Research Fellow (–March '01)[37]
YOSHIMURA, Daisuke — Research Fellow (–March '01)[38]
NODA, Hideyuki — Graduate Student (–March '01)[39]
WANG, Zhihong — Graduate Student
YAMAMURA, Shusaku — Graduate Student (April '01–)
TAKIZAWA, Morio — Graduate Student (April '01–)
FUJIKI, Satoshi — Graduate Student (April '01–)
KANBARA, Takayoshi — Graduate Student (from Okayama University)* (April '01–)
TAKABAYASHI, Yasuhiro — Graduate Student (from Okayama University)* (April '01–)
YOKOYAMA, Takahiro — Graduate Student (from Nagoya University)* (April '01–)

Interface Molecular Sicence
KUROSAWA, Kou — Professor (–March '01)[40]
KOMIYAMA, Masaharu — Professor (April '01–)
FUKUI, Kazutoshi — Associate Professor (–March '01)[41]
NAGAOKA, Shin-ichi — Associate Professor (–March '01)[42]
OKUDAIRA, Koji — Associate Professor (April '01–)
TAKASHIMA, Yoshifumi — Research Associate
KUBOZONO, Yoshihiro — Research Associate (April '01–)
TAKEZOE, Noritaka — IMS Fellow (–May '01)[43]
MATSUMOTO, Taki — IMS Fellow (April '01–)
YOSHIMURA, Daisuke — Research Fellow (April '01)
LI, Yan Jun — Research Fellow (April '01–)
YANAGITA, Hideaki — Graduate Student (–March '01)[44]
KAWASAKI, Yasuhiro — Graduate Student (–March '01)[45]
TANAKA, Takashi — Graduate Student (–March '01)[46]
SAKAKIBARA, Tsutomu — Graduate Student (–March '01)[47]
KIHARA, Takayoshi — Graduate Student (–March '01)[48]
DOI, Youichirou — Graduate Student (–March '01)[49]
YAMANE, Hiroyuki — Graduate Student (from Chiba Univ.)* (April '01–)

Synchrotron Radiation Research
LUPEI, Voicu — Visiting Profrssor (–March, '01)[50]
SKODJE, Rex Thomas — Visiting Professor (April '01–)[51]
MIL'NIKOV, Guennady — Visiting Associate Profrssor (–March, '01)[52]
WANG, Changshun — Visiting Associate Professor (June '01–)[53]
AHN, Kwang Hyun — Visiting Associate Profrssor (July '01)[54]

Coordination Chemistry Laboratories
TANAKA, Koji — Director

Complex Catalysis
UOZUMI, Yasuhiro — Professor
TANIGUCHI, Isao — Visiting Professor (from Kumamoto University)
TANAKA, Yasutaka — Visiting Associate Professor (from Shizuoka University)
YAMANOI, Yoshinori — Research Associate (April '01–)
NAKAO, Ryu — Research Fellow
SHIBATOMI, Kazutaka — Research Fellow (April '01–)
HOCKE, Heiko — Visiting Scientist; JSPS Post-Doctoral Fellow
NAKAI, Yasushi — Graduate Student (April '01–)
NAKAZONO, Maki — Graduate Student (from Nagoya City University)*
TANAKA, Hirotaka — Graduate Student (from Nagoya City University)*

Functional Coordination Chemistry
TANAKA, Koji — Professor
KAWAGUCHI, Hiroyuki — Associate Professor
MATSUO, Tsukasa — Research Associate (April '01–)
WADA, Tohru — Research Associate (April '01–)
MIZUKAWA, Tetsunori — Technical Associate

OHTSU, Hideki	Research Fellow (April '01–)
KOIZUMI, Takeaki	Research Fellow (April '01–)
SHIREN, Kazushi	Research Fellow (April '01–)
FUJIHARA, Tetsuaki	Research Fellow (April '01–)
TSUTSUI, Kanako	Research Fellow (April '01–)
TOMON, Takashi	Graduate Student
KOBAYASHI, Katsuaki	Graduate Student
KOMURO, Takashi	Graduate Student (From Nagoya University)* (April '01–)

Coordination Bond

AIDA, Takuzo	Visiting Professor (from the University of Tokyo) (–March '01)
TOKITOH, Norihiro	Visiting Professor (from Kyoto University) (April '01–)
HAMACHI, Itaru	Visiting Associate Professor (from Kyusyu University) (–March '01)
ONITSUKA, Kiyotaka	Visiting Associate Professor (from Osaka University) (April '01–)

Research Facilities
Laser Research Center for Molecular Science

FUJII, Masaaki	Director

Advanced Lasers for Chemical Reaction Studies

Advanced Lasers for Synchrotron Radiation Applications

SARUKURA, Nobuhiko	Associate Professor
OHTAKE, Hideyuki	Research Associate
MURAKAMI, Hidetoshi	IMS Fellow
KOZEKI, Toshimasa	Graduate Student
ONO, Shingo	Graduate Student
SUZUKI, Yuji	Graduate Student

Advanced UV and IR Tunable Lasers

TAIRA, Takunori	Associate Professor
KURIMURA, Sunao	Research Associate (–August '01)
LUPEI, Voicu	Visiting Professor; MONBUSHO Invited Fellow (–March '01)
JANG, Won Kweon	Visiting Associate Professor; MONBUSHO Invited Fellow
SHOJI, Ichiro	IMS Fellow
PAVEL, Nicolaie	Visiting Scientist; JSPS Post-Doctorical Fellow (–March '01)
SAIKAWA, Jiro	Graduate Student
SATO, Yoichi	Graduate Student

Research Center for Molecular Materials

WATANABE, Yoshihito	Director (–March '01)
UOZUMI, Yasuhiro	Director (April '00–)
KUWAHARA, Daisuke	Research Associate

Organic Materials Section

TANAKA, Shoji	Research Associate
TOMURA, Masaaki	Technical Associate
ZAMAN, Mohammed Badruz	IMS Fellow (–October '00)[55]
AKHTARUZZAMAN, Mohammed	Graduate Student (–January '01)[56]

Hybrid Materials Section

FUJII, Hiroshi	Associate Professor
FUNAHASHI, Yasuhiro	Research Associate (–February '01)[57]
IKEUE, Takahisa	JSPS Post-Doctoral Fellow (–March '01)[58]

Materials Characterization Section

NAGATA, Toshi	Associate Professor
ITO, Hajime	Research Associate
KIKUZAWA, Yoshihiro	Graduate Student

ITO, Kaname   Graduate Student
HINO, Takami   Graduate Student (from Kyoto University)*

Structure Control Section
SUZUKI, Toshiyasu   Associate Professor
SAKAMOTO, Youichi   Research Associate
SHIRASAWA, Nobuhiko   IMS Fellow (April '01–)
KOMATSU, Shingo   Graduate Student (from Kyushu University)*

Equipment Development Center
YAKUSHI, Kyuya   Director
WATANABE, Michio   Associate Professor

Ultraviolet Synchrotron Orbital Radiation Facility
KOSUGI, Nobuhiro   Director
KAMADA, Masao   Associate Professor
KATOH, Masahiro   Associate Professor
SHIGEMASA, Eiji   Associate Professor
KIMURA, Shin-ichi   Visiting Associate Professor (from Kobe University) (–March '01)
HORI, Yo-ichiro   Visiting Associate Professor (from Institute of Materials Structure Science) (April '01–)
HOSAKA, Masahito   Research Associate
GEJO, Tatsuo   Research Associate
KODA, Shigeru   Research Associate (–July '01)[59]
TAKAHASHI, Kazutoshi   Research Associate
MOCHIHASHI, Akira   Research Associate (August '01–)
MORÉ, Sam Dylan   Visiting Scientist; JSPS Post-Doctral Fellow (–September '00)
AZUMA, Junpei   JSPS Post-Doctral Fellow (April '01–)
TANAKA, Senku   Graduate Student
HAYAKAWA, Kousuke   Graduate Student (from Shinshu University)* (April '01–)

Computer Center
HIRATA, Fumio   Director
AOYAGI, Mutsumi   Associate Professor
NANBU, Shinkoh   Research Associate
OONO, Hitoshi   Research Associate
MINAMINO, Satoshi   Technical Associate
MAKI, Jun   IMS Fellow (April '01–)
OKADA, Kazutoshi   Research Fellow
KINOSHITA, Tomoko   Graduate Student

Research Facility of Okazaki National Research Institutes
Center for Integrative Bioscience
KITAGAWA, Teizo   Professor
WATANABE, Yoshihito   Professor (February '01–)
KINOSITA, Kazuhiko, Jr.   Professor (April '01–)
FUJII, Hiroshi   Associate Professor (February '01–)
UENO, Takafumi   Research Associate
OHTA, Takehiro   IMS Fellow (April '01–)
YOSHIOKA, Shiro   IMS Fellow (April '01–)
GOSSE, Charlie   JSPS Post-Doctoral Fellow (April '01–)
ALI, Md. Yusuf   JSPS Post-Doctoral Fellow (April '01–)
MAKI, Yasushi   Research Fellow (April '01–)
SHIMO, Rieko   Research Fellow (April '01–)
ADACHI, Kengo   Research Fellow (December '00–)
NAKAI, Hidetaka   Research Fellow
YOGO, Katsunori   Graduate Student (from Waseda University)* (April '01–)
KAWASHIMA, Keisuke   Graduate Student (from Keio University)* (April '01–)
SAKAKI, Naoyoshi   Graduate Student (from Keio University)* (April '01–)

* Carries out graduate research of IMS on Cooperative Education Program of IMS with other graduate schools.

Technical Staff

SAKAI, Kusuo	Technical Division Head
MATSUDO, Osamu	Technical Section Chief
KATO, Kiyonori	Technical Section Chief
NISHIMOTO, Fumio	Technical Section Chief
YAMANAKA, Takaya	Technical Section Chief
UEDA, Tadashi	Laser Research Center for Molecular Science
NAGATA, Masaaki	Research Center for Molecular Materials (Unit Chief)
YOSHIDA, Hisashi	Research Center for Molecular Materials (Unit Chief)
TAKAYAMA, Takashi	Research Center for Molecular Materials (Unit Chief)
SAKAI, Masahiro	Research Center for Molecular Materials
MAKITA, Seiji	Research Center for Molecular Materials
MIZUTANI, Nobuo	Equipment Development Center (Unit Chief)
SUZUI, Mitsukazu	Equipment Development Center (Unit Chief)
UCHIYAMA, Kouichi	Equipment Development Center
TOYODA, Tomonori	Equipment Development Center
KONDOU, Takuhiko	Equipment Development Center
KOBAYASHI, Kazuhiro	Equipment Development Center
HAYASHI, Kenji	Equipment Development Center
KINOSHITA, Toshio	UVSOR Facility (Unit Chief)
HASUMOTO, Masami	UVSOR Facility (Unit Chief)
YAMAZAKI, Jun-ichiro	UVSOR Facility (Unit Chief)
NAKAMURA, Eiken	UVSOR Facility
KONDO, Naonori	UVSOR Facility
MIZUTANI, Fumiyasu	Computer Center (Unit Chief)
TESHIMA, Fumitsuna	Computer Center
NAITO, Shigeki	Computer Center

List of Present Addresses

1) Department of Chemistry, University of Puerto Rico, P. O. Box 23346, San Juan, Puerto Rico 00931-3346, USA
2) Science Technology Systems Center, Government & Public Corporation Information Systems Division, Hitachi, Ltd., Shinsuna Plaza 6-27, Shinsuna 1-Chome, Koto-ku, Tokyo 136-8632
3) Office of Information Technology Research and Development, Tsukuba Advanced Computing Center, National Institute of Advanced Industrial Science and Technology, Tsukuba Central 1,Tsukuba, 305-8561
4) Department of Physics, Faculty of Science and Technology, Keio University, 3-14-1 Hiyoshi, Kouhoku-ku, Yokohama 223-8522
5) Section of Applied Chemistry, Faculty of Science and Engineering, Ritsumeikan University, 1-1-1 Nojihigashi, Kusatsu, 525-8577
6) Department of Physics, Faculty of Science, 2-1-1 Otsuka, Bunkyo-ku, Tokyo 112-8610
7) Institute of Atomic and Molecular Sciences, Academia Sinica, P. O. Box 23-166, Taipei, Taiwan
8) RIKEN, 2-1 Hirosawa, Wako 351-0198
9) Department of Chemistry, University of Houston, 4800 Calhoun Street, Houston, Texas 77204-5641, USA
10) Molecular Photoscience Research Center, Kobe University, 1-1 Rokkodai-cho, Nada-ku, Kobe 657-8501
11) Theory of Solid State Physics, Institute for Materials Research, Tohoku University, 2-1-1 Katahira, Aoba-ku, Sendai 980-8577
12) Dept. of Chemistry, Rutgers, The State University of New Jersey, 610 Taylor Road, Piscataway, New Jersey 08854, USA
13) Department of Physics, Faculty of Science, Toyama University, 3190 Gofuku, Toyama-city, Toyama 930-8555
14) Center for Tsukuba Advanced Research Alliance, University of Tsukuba, 1-1-1 Tennoudai, Tsukuba-shi, Ibaraki 305-8577
15) Molecular Photoscience Research Center, Kobe University, 1-1 Rokkodai-cho, Nada-ku, Kobe 657-8501
16) Department of Chemistry, Hankuk University of Foreign Studies, Yongin, Kyungki Do, 449-791, Korea.
17) Henan University, 95 Wenhua Rd., Zhengzhou 450002 Henau P.R.China
18) Jilin University, 123 Jie Fang Rd., Changchun, Jilin Province 130023, PR China
19) North-Eastern Hill University, Shillong, Meghalaya, India
20) Fudan University, 220 Handan Rd., Shanghai 200433, PR China
21) Department of Physics, Graduate School of Science, Osaka City University, 3-3-138 sugimoto, sumiiyoshi-ku, Osaka 558-8585
22) Graduate School of Arts and Sciences, University of Tokyo, 3-8-1 Komaba, Meguro-ku, Tokyo 153-8902

23) Molecular Photoscience Research Center, Kobe University, 1-1 Rokkodai-cho, Nada-ku, Kobe 657-8501
24) Department of Physics, Nagoya University, Furo-cho, Chikusa-ku, Nagoya 4648601, Japan
25) Department of Physics, University of Florida, PO Box 118440, Gainesville, FL 32611-8440, USA
26) Institute for Physical Research, Armenia National Academy of Sciences, IPR, Ashtarak-2,378410,Armenia
27) Research Centre for Spectrochemistry, Graduate School of Science, The University of Tokyo, Hongo, Bunkyo-ku, Tokyo 113-0033, Japan
28) Institute of Problems of Chemical Physics, RAS, 142432 Chernogolovka, Russia
29) Advanced Research Lab. Corporate Research Center, Fuji Xerox Co., Ltd. 1600, Takematsu, Minamiashigara-shi, Kanagawa, 250-0111
30) Department of Fine Chemistry, Seoul National Polytechnic University, Seoul 139-743, Korea
31) Institute of Research and Innovation, 1201 Takada, Kashiwa, Chiba 277-0861
32) Department of Genomics and Proteomics, Beijing Institute of Radiation Medicine Academy of Military Medical Sciences, Chinese National Human Genome Center at Beijing, 27 Taiping Road, Beijing 100850, P.R. China
33) Department of Applied Chemistry, Faculty of Engineering, Nagoya Institute of Technology, Gokiso-cho, Showa-ku, Nagoya 466-8555
34) Hitachi Co.Ltd., 810 Imaizumi, Ebina, Kanagawa 243-0435
35) Toyama science museum, 1-8-31, Nihinakano-cho, Toyama 939-8084
36) Shimazu Co., 380-1 Horiyamashita, Hatano, Kanagawa 259-1304
37) National Institute of Advanced Industrial Science and Technology, Higashi, Tsukuba, Ibaragi 305-8561
38) Interface Molecular Science, IMS
39) Central Research Laboratory, Hitachi, Ltd., Kokubunnji, Tokyo 185-8601
40) Department of Electrical and Electronic Engineering, University of Miyazaki, Miyazaki 889-2192
41) Research Center for Development of Far-Infrared Region, Fukui University, 3-9-1 Bunkyo, Fukui, 910-8507
42) Chemistry Group, Department of Fundamental Material Science, Faculty of Science, Ehime University, Matsuyama 790-8577
43) USHIO INC., Himeji, 671-0224 Hyogo
44) PhD student of University of Miyazaki, Miyazaki, 889-2191
45) Matsushita Electric Co., Kadoma, Osaka
46) CKD Co. Ltd., Nagoya
47) PhD student of University of Miyazaki, Miyazaki, 889-2191
48) Canon Inc.
49) Aisin Seiki Co., Ltd.
50) Institute of Atomic Physics National Institute of Laser, Plasma and Radiation Physics Solid-State's Quantum Electronics Laboratory P.O. Box MG-36, Bucharest R-76900
51) Department of Chemistry and Biochemistry Campus Box 215, University of Colorado Boulder, CO 80309 USA
52) Institute of Structural Macrokinetics, Chernogolovka Russian Academy of Science 142432 Chernogolovka Moscow Region Russia
53) Department of physics, Henan University 85, Ming Lun Street, Kaifeng, Henan, 475001, P.R. China
54) Department of Chemistry Kyung Hee University Yongin-Kun, Kyung-Ki Do, 449-701 Korea
55) Steacie Institute for Molecular Science, National Research Council of Canada, 100 Sussex Drive, Ottawa, Ontario, K1A0R6, Canada
56) Department of Electronic Chemistry, Interdisciplinary Graduate School of Science and Engineering, Tokyo Institute of Technology, 4259 Nagatsuta-cho, Midori-ku, Yokohama 226-8502
57) Applied Chemistry, Nagaya Institute of Technology, Gokiso-cho, Showa-ku, Nagoya, 466-8555
58) Department of Chemistry, Toho University School of medicine, Omorishi, Ota-ku, Tokyo 143
59) Synchrotron Light Application Center, Saga University, 1 Honjyo-cho, Saga 840-8502

COUNCIL

KAYA, Koji   **Director-General**

Councillors

Chairperson	HOSOYA, Haruo	Professor, Ochanomizu University
Vice-Chairperson	HIROTA, Noboru	Professor Emeritus, Kyoto University
	ARIKAWA, Yoshiko	Professor, Japan Women's University
	IIYOSHI, Atsuo	President, Chubu University
	ISHITANI, Akira	Executive Director, Kanagawa Academy of Science and Technology
	OHTSUKA, Eiko	Fellow, National Institute of Advanced Industrial Science & Technology
	OGINO, Hiroshi	Director, Miyagi Study Center of the University of the Air
	KAIFU, Norio	Director General, National Astronomical Observatory of Japan
	KIMURA, Yoshitaka	Director, Institute of Materials Structure Science, High Energy Accelator Research Organization
	KYOGOKU, Yoshimasa	Director, Biological Information Research Center, National Institute of Advanced Industrial Science and Technology
	GOTO, Keishi	President, Toyohashi University of Technology
	KONDOW, Tamotsu	Professor, Toyota Technological Institute, Cluster Research Laboratory
	SAHARA, Makoto	Director-General, National Museum of Japanese History
	TAKAHASHI, Riichi	President and Chief Operating Officer, Toyota Central Research & Development Laboratories,Inc.
	TSUCHIYA, Soji	Visiting Professor, Advanced Research Institute for Science and Engineering, Waseda University
	FUKUYAMA, Hidetoshi	Director, The Institute for Solid State Physics, University of Tokyo
	YAMAZAKI, Toshimitsu	Contract Resercher, RI Beam Science Laboratory, RIKEN
	YAMAMURA, Shosuke	Professor Emeritus, Keio University
	BRADSHAW, Alexander M.	Scientific Director, Max-Planck Institute for Plasma Physics
	LINEBERGER, William C.	Professor, University of Colorado

The Council is the advisory board for the Director-General.
* Two of the councillors are selected among distinguished foreign scientists.

Distinguished Research Consultants

NAGAKURA, Saburo	President, The Kanagawa Academy of Science and Technology
INOKUCHI, Hiroo	Chief Scientist of Space Utilization Research Program, National Space Development Agency of Japan
TSUCHIYA, Soji	Professor, Japan Women's University
ITO, Mitsuo	Professor Emeritus, Insitute for Molecular Science, The Graduate University for Advanced Studies, Tohoku University
HIROTA, Noboru	Professor Emeritus, Kyoto University
KONDOW, Tamotsu	Invited Professor, Toyota Technological Institute

Administration Bureau

TERAO, Shigemi	Director-General, Administration Bureau (–March '01)
KAMADA, Tohru	Director-General, Administration Bureau (April '01–)
SUNADA, Hitoshi	Director, General Affairs Department
KAWANO, Masatoshi	Director, Finance and Facilities Department (–March '01)
YUUKI, Yoshihisa	Director, Finance and Facilities Department (April '01–)
OYAMA, Takuya	Head, General Affairs Division
INDEN, Toshio	Head, Personnel Division (–March '01)
UCHIDA, Yoshio	Head, Personnel Division (April '01–)
HAYASHI, Masanori	Head, Research Cooperation Division
ONO, Yukitsugu	Head, International Affairs Division (–March '01)
KITAGAWA, Hiroshi	Head, International Affairs Division (April '01–)
IWAKAMI, Nobuyoshi	Head, Budget Division (–March '01)
HIRAI, Tokio	Head, Budget Division (April '01–)
YUUKI, Masanori	Head, Accounts Division
FUNATO, Hideaki	Head, Construction Division (–March '01)
KATOH, Masayoshi	Head, Construction Division (April '01–)
SATO, Hisashi	Head, Equipment Division

BUILDINGS AND CAMPUS

The IMS campus covering 62,343 m^2 is located on a low hill in the middle of Okazaki city. The inequality in the surface of the hill and growing trees are preserved as much as possible, and low-storied buildings are adopted for conservation of the environment. The buildings of IMS are separated according to their functions as shown in the map. The Research Office Building and all Research Facilities except for the Computer Center are linked organically to the Main Laboratory Buildings by corridors. Computer Center, Library and Administration Buildings are situated between IMS and neighboring National Institute for Basic Biology and National Institute for Physiological Sciences, because the latter two facilities are common to these three institutes.

The lodging facility of IMS called Yamate Lodge, located within ten minutes' walk, has sleeping accommodations for 15 guests and two families. Mishima Lodge, located within four minutes' walk east of IMS can accommodate 74 guests and 20 families. Scientists who visit IMS as well as the two other institutes can make use of these facilities. Foreign visiting scientists can also live at these lodgings with their families during their stays. The Okazaki Conference Center was built in April, 1997 in Mishima area, which has four conference rooms capable of between 50 and 250 attendance.

to Meitetsu Higashi-Okazaki Station

Main Gate

to National Institute for Basic Biology and National Institute for Physiological Sciences

East Gate

1. Research Office Building
2. Main Laboratory Building
3. Equipment Development Center
4. Laser Research Center for Molecular Science
5. Research Center for Molecular Materials
6. Low-Temperature Facilities Building
7. Computer Center
8. Library
9. Central Administration
10. UVSOR Facility
11. Power Station
12. Waste-Water Disposition Facilities
13. Faculty Club
14. South Laboratory Building
15. Okazaki Conference Center

Okazaki (population 330,000) is 260 km west of Tokyo, and can be reached by train in about 3 hours from Tokyo via Shinkansen and Meitetsu Line.

The nearest large city is Nagoya, about 40 km northwest of Okazaki.

RESEARCH ACTIVITIES I
Department of Theoretical Studies

I-A Prediction of Protein Tertiary Structures from the First Principles

Prediction of the three-dimensional structures of protein molecules by computer simulations is a very challenging problem in theoretical molecular science. The difficulty of the problem lies in two facts: (1) the inclusion of accurate solvent effects is non-trivial and time-consuming (2) there exist huge number of local minima in the energy function, forcing conventional simulations to get trapped in states of energy local minima. We have been exploring the strategies that allow us to overcome these difficulties.

I-A-1 Multicanonical Monte Carlo Simulation of a Small Peptide in Aqueous Solution Based on the RISM Theory

MITSUTAKE, Ayori[1]; KINOSHITA, Masahiro[2]; OKAMOTO, Yuko; HIRATA, Fumio
(*[1]Keio Univ.; [2]Kyoto Univ.*)

We report the results of multicanonical Monte Carlo simulation of a penta peptide, Met-enkephalin, in aqueous solution that is based on the reference interaction site model theory. Averages of the energy functions, end-to-end distance, dihedral-angle distributions, and radial distribution functions are calculated as functions of temperature from a single simulation run. This is accomplished by the single-histogram reweighting techniques. It is shown that the peptide is almost fully extended in aqueous solution at all temperatures, while it forms β-turn structures in gas phase at low temperatures.

I-A-2 Replica-Exchange Multicanonical and Multicanonical Replica-Exchange Monte Carlo Simulations of a Small Peptide

MITSUTAKE, Ayori[1]; SUGITA, Yuji; OKAMOTO, Yuko
(*[1]Keio Univ.*)

We recently developed the replica-exchange multicanonical algorithm and the multicanonical replica-exchange method for molecular dynamics simulations. In the first method, one first estimate the multicanonical weight factor from a short replica-exchange simulation, using the multiple-histogram reweighting techniques. One then performs a long multicanonical production run. The second method is a further extension of the first in which a replica-exchange production simulation is performed with each replica in multicanonical ensemble. In this article, we develope Monte Carlo versions of the two methods and show that these algorithms are very effective for simulations of a small peptide.

I-A-3 Examination of Parallel Simulated Annealing Using Genetic Crossover

HIROYASU, Tomoyuki[1]; MIKI, Mitsunori[1]; OGURA, Maki[1]; OKAMOTO, Yuko
(*[1]Doshisha Univ.*)

This paper proposes Parallel Simulated Annealing using Genetic Crossover (PSA/GAc). In this algorithm, there are several processes of Simulated Annealing (SA) working parallel. To exchange information between the solutions, the operation of genetic crossover is performed. Through the continuous test problems, it is found that PSA/GAc can search the solution effectively. The proposed algorithm is also applied to the prediction of protein tertiary structure. Comparing PSA/GAc to the conventional algorithm, it is also found that PSA/GAc is an effective algorithm for real world problems.

I-A-4 Solvent Effects on the Free Energy Landscape of a Short Peptide

SUGITA, Yuji; OKAMOTO, Yuko

We have studied the effects of solvent on the free energy landscape of a short peptide, Met-enkephalin, by carrying out the molecular dynamics simulations both in vacuum and in aqueous solution with explicit water molecules. The replica-exchange multicanonical algorithm, which has been recently developed by us, was employed to sample a wide conformational space. The results of the simulations were analyzed by the histogram reweighting techniques and principal component analyses. By comparing the free energy landscape in water with that in vacuum, we found that the free energy landscape is significantly changed by the solvent effects. The dependence of the free energy landscape on the different force fields is also discussed.

I-A-5 Comparison of the Numerical Efficiency of Three New Generalized-Ensemble Algorithms for Conformational Sampling of a Peptide in Explicit Water

SUGITA, Yuji; OKAMOTO, Yuko

In many systems with rough energy landscape, the conventional molecular dynamics or Monte Carlo simulation tends to get trapped in local-minimum states and cannot sample wide configurational space. To

overcome this difficulty, we have recently developed two new algorithms, namely, replica-exchange multicanonical algorithm and multicanonical replica-exchange method. In this article, we compare the numerical efficiency of these methods with that of the original replica-exchange method in simulations of a peptide with a number of explicit water molecules. We employed the average tunneling time in the energy space as a measure of the sampling efficiency. It has been shown that the sampling efficiency of the new algorithms becomes much greater than that of the original replica-exchange method.

I-B Development of Simulation Algorithms for Complex Systems

Developing a powerful simulation algorithm that can alleviate the multiple-minima problem is important in many complex systems. We have been advocating the uses of the so-called generalized-ensemble algorithms such as multicanonical algorithm and replica-exchange method.

I-B-1 Generalized-Ensemble Simulations for Systems with First-Order Phase Transition

NAGASIMA, Takehiro; SUGITA, Yuji; MITSUTAKE, Ayori[1]; OKAMOTO, Yuko
(*[1]Keio Univ.*)

Replica-exchange method is a powerful generalized-ensemble algorithm that can alleviate the difficulty of getting trapped in states of energy local minima. The method, however, fails for systems with first-order phase transition. In this article we show that the recently developed algorithms, replica-exchange multicanonical algorithm and multicanonical replica-exchange method, can be successfully applied to systems with first-order phase transition. We present our results, taking the example of the two-dimensional 10-state Potts model.

I-B-2 Li$_8$ Cluster Structures Studied by *Ab Initio* Replica-Exchange Monte Carlo Method

NISHIKAWA, Takeshi[1]; SUGITA, Yuji; OKAMOTO, Yuko; ISHIKAWA, Yasuyuki[2]
(*[1]AIST; [2]Univ. Puerto Rico*)

Interest in metal, semiconductor, and molecular clusters has been growing explosively in the past two decades due to the experimental advances that have facilitated the study of clusters. Furthermore, theoretical advances have enhanced the ability to interpret experimental results. Still lacking is the ability to routinely determine the structures of clusters. In the previous work, *ab initio* replica-exchange Monte Carlo method was developed and implemented to determine the global and local minimum configurations of Li$_6$ clusters. Gaussian98 was used for the calculations of the electronic structures. In this work, we discuss results of replica-exchange Monte Carlo simulations of Li$_8$ clusters.

I-C Theoretical Studies of Chemical Reaction Dynamics

I-C-1 Quantum Reaction Dynamics of O(^3P) + HCl on a New *ab initio* Potential Energy Surface

NOBUSADA, Katsuyuki[1]; **NAKAMURA, Hiroki; LIN, Yongjing**[2]; **RAMACHANDRAN, B.**[2]
(*[1]IMS and Hokkaido Univ.; [2]Louisiana Tech. Univ.*)

[*J. Chem. Phys.* **113**, 1018 (2000)]

Quantum reaction dynamics of O(^3P) + HCl $\leftrightarrow$ OH + Cl is studied by using a new *ab initio* potential energy surface calculated by Ramachandran *et al.* [*J. Chem. Phys.* **111**, 3862 (1999)] The hyperspherical elliptic coordinate approach is applied with an emphasis on elucidating reaction dynamics for J (total angular momentum quantum number) = 0. In terms of the previously established concept that reactive transitions are nothing but vibrationally nonadiabatic transitions at important avoided crossings, clear interpretations are given for the following dynamical features: (i) reactivity depending on potential energy surface topography, (ii) final rotational state distributions for specified initial rovibrational states, and (iii) resonance structures appearing in some reactions. Thermal rate constants are approximately estimated from the present $J = 0$ results by using the J-shift approximation. The present results are compared with our previous ones based on the different potential energy surface calculated by Koizumi-Schatz-Gordon (KSG). The calculated adiabatic potential energy curves of the present new surface have deep wells in the OH + Cl channel in contrast to the KSG potential energy surface. Consequently, the new surface leads to quite different dynamics from those on the KSG surface. Comparisons with the results obtained by quasiclassical trajectory calculations are also made.

I-C-2 Quantum-Classical Correspondence in the O(^3P) + HCl and Cl(^2P) + OH Reactions for Total Angular Momentum $J = 0$

LIN, Yongjing[1]; **RAMACHANDRAN, B.**[1]; **NOBUSADA, Katsuyuki**[2]; **NAKAMURA, Hiroki**
(*[1]Louisiana Tech. Univ.; [2]IMS and Hokkaido Univ.*)

[*J. Chem. Phys.* **114**, 1549 (2001)]

A method for carrying out quasiclassical trajectory (QCT) calculations of A + BC(v,j) reactive collisions for the special case of the total angular momentum $J = 0$ is described. Since quantum reactive scattering calculations involving heavier atoms are not straightforward for the $J > 0$ case, this method is useful to establish the extent to which classical mechanics is applicable to a particular reaction. The method is tested by comparing the results of trajectory calculations for the $J = 0$ case with analogous quantum-mechanical (QM) calculations for the O(^3P) + HCl reaction and the reverse reaction Cl(^2P) + OH. The S4 potential surface, which is based on MRCI+Q/cc-pVTZ energies scaled by the scaled external correlation method [B.

Ramachandran *et al.*, *J. Chem. Phys.* **111**, 3862 (1999)], is used for these calculations. The QCT and QM cumulative reaction probabilities are found to be in good agreement, especially for the Cl + OH reaction. The agreement between the two types of state-resolved reaction probabilities is less striking but improves considerably as the initial diatomic rotational quantum number j increases. A comparison is also made between the exact and J-shifted QCT thermal rate coefficients. These are found to be in excellent agreement, which is in keeping with similar agreement observed in the case of the quantum-mechanical exact and J-shifted thermal rate coefficients.

I-C-3 Cumulative Reaction Probability and Reaction Eigenprobabilities from Time-Independent Quantum Scattering Theory

TOLSTIKHIN, Oleg I.[1]; **OSTROVSKY, Valentin N.**[2]; **NAKAMURA, Hiroki**
(*[1]IMS and Kurchatov Inst.; [2]IMS and Univ. St. Petersburg*)

[*Phys. Rev. A* **63**, 042707 (2001)]

The cumulative reaction probability (CRP) is a gross characteristic of rearrangement collision processes defining the reaction rate constant. This paper presents a complete development of the approach to the theory of CRP that we have recently proposed [*Phys. Rev. Lett.* **80**, 41 (1998)]. In the core of this approach lies an alternative expression for CRP in terms of the outgoing wave Green's function which is formally equivalent to the Miller's definition of this quantity in terms of the scattering matrix [*J. Chem. Phys.* **62**, 1899 (1975)] and to the Miller-Schwartz-Tromp formula [*J. Chem. Phys.* **79**, 4889 (1983)], but is direct, in contrast to the former, and more suitable for practical calculations than the latter. Furthermore, our approach rests on solid grounds of time-independent quantum scattering theory and provides an appealing competitive alternative to the absorbing potential formulation given by Seideman and Miller [*J. Chem. Phys.* **96**, 4412 (1992); **97**, 2499 (1992)]. Ideologically, it is close to the approach considered earlier for a one-dimensional model by Manolopoulos and Light [*Chem. Phys. Lett.* **216**, 18 (1993)], but is formulated from scratch for realistic systems with many degrees of freedom. The strongest point of our approach is that its final working formulas are expressed in terms of the Wigner-Eisenbud matrix, so they can be easily implemented on the basis of many existing quantum scattering codes. All these features are discussed and illustrated by calculations of the CRP and reaction eigenprobabilities for two prototypical light atom transfer reactions in heavy-light-heavy triatomic systems in three dimensions for zero total angular momentum.

I-C-4 Photo-Dynamics and Reaction Dynamics of Molecules (Satellite of ICPEC XXI)

MITSUKE, Koichiro; NAKAMURA, Hiroki

The above-named satellite meeting was held in Okazaki on July 31st to August 2nd, 1999. The scientific program consisted of 21 invited lectures and 32 contributed papers covering various topics of molecular photoionization, photodissociation and chemical reaction dynamics. Several invited papers at this meeting are briefly summarized.

I-C-5 New Implementation of the Trajectory Surface Hopping Method with Use of the Zhu-Nakamura Theory

ZHU, Chaoyuan; NOBUSADA, Katsuyuki[1];
NAKAMURA, Hiroki
(*[1]IMS and Hokkaido Univ.*)

A new implementation of the trajectory surface hopping (TSH) method is proposed to treat multi-dimensional nonadiabatic dynamics by incorporating the analytical Zhu-Nakamura semiclassical theory of nonadiabatic transition. The problem of classically forbidden hops in the TSH method can now be solved and dealt with just as easily as the classically allowed hops by introducing nonvertical hopping techniques. This is made possible, because the theory can treat both classically allowed and forbidden hops accurately in a unified way. The Zhu-Nakamura theory also enables us to predetermine important regions of potential energy surface (PES) before carrying out any dynamics calculations, and thus to save a lot of computational efforts. The charge transfer processes in the collinear H_3^+ system are studied numerically to test the new TSH method. Comparing the new and old versions of TSH with exact quantum calculations, the new method shows much better agreement with the exact calculations. It also works well when all transitions are classically forbidden and the old method fails completely.

I-C-6 Significant Improvement of the Trajectory Surface Hopping Method by the Zhu-Nakamura Theory

ZHU, Chaoyuan; KAMISAKA, Hideyuki[1];
NAKAMURA, Hiroki
(*[1]GUAS*)

By taking the 3D $D^+ + H_2$ reaction system, the trajectory surface hopping method based on the Zhu-Nakamura theory is demonstrated to work much better than old one and to be very promising to treat high-dimensional electronically nonadiabatic processes. The difference between the new and old survives even at high initial vibrational states and high energies.

I-C-7 Accurate Quantum Dynamics of Electronically Nonadiabatic Chemical Reactions in the DH$_2^+$ System

KAMISAKA, Hideyuki[1]; BIAN, Wensheng[2];
NOBUSADA, Katsuyuki[3]; NAKAMURA, Hiroki
(*[1]GUAS; [2]IMS and Shandong Univ.; [3]IMS and
Hokkaido Univ.*)

Three-dimensional accurate quantum dynamics calculations are carried out for the DH_2^+ system for $J = 0$ (J: total angular momentum quantum number) by the hyperspherical coordinate approach with use of the new potential energy surfaces constructed based on the recent *ab initio* quantum chemical calculations. Not only electronically nonadiabatic reactions, *i.e.* reactive charge transfer processes, but also electronically adiabatic reactions and electronically nonadiabatic non-reactive processes are investigated. Because of the deep well on the electronically adiabatic ground surface, there appear a large number of resonances and the electronically adiabatic reactions are mostly statistical. Nonadiabatic transitions along the potential crossing seam cause deviations from the statistical behaviour and some interesting dynamical features are found.

I-D Theory of Nonadiabatic Transitions

I-D-1 Nonadiabatic Dynamics: Transitions Between Asymptotically Degenerate States

OSHEROV, Vladimir I.[1]; NAKAMURA, Hiroki
(*[1]IMS and Russian Acad. Sci.*)

Nonadiabatic transitions between asymptotically degenerate potential curves are discussed. Both crossing and noncrossing two-coupled-Morse-potential systems are studied semiclassically as well as quantum mechanically. Conditions for the appearance of a nonadiabatic transition are clarified. The case of inverse power potentials at infinity is also analyzed. Expressions of nonadiabatic transition probability are obtained.

I-D-2 Nonadiabatic Transitions due to Curve Crossings: Complete Solutions of the Landau-Zener-Stueckelburg Problems and Their Applications

ZHU, Chaoyuan; TERANISHI, Yoshiaki[1];
NAKAMURA, Hiroki

(*[1]IMS and RIKEN*)

I-D-3 New Type of Nonadiabatic Dynamics: Transitions between Asymptotically Degenerate States

OSHEROV, Vladimir I.[1]; USHAKOV, Vladimir G.[1]; NAKAMURA, Hiroki
(*[1]IMS and Russian Acad. Sci.*)

The WKB-type semiclassical analysis is carried out for a two-state model potential system, in whitch two asymptotically degenerate Morse potentials are coupled by an exponential diabatic coupling. Both crossing and non-crossing cases are treated and explicit analytical expressions for the full scattering matrix are obtained. A numerical test demonstrates the accuracy of the theory.

I-E Laser Control of Molecular Processes

I-E-1 Laser Control of Molecular Photodissociation with Use of the Complete Reflection Phenomenon

NAGAYA, Kuninobu[1]; TERANISHI, Yoshiaki[2]; NAKAMURA, Hiroki
(*[1]GUAS; [2]IMS and RIKEN*)

A new idea of controlling molecular photo-dissociation branching by a stationary laser field is proposed by utilizing the unusual intriguing quantum-mechanical phenomenon of complete reflection. By introducing the Floquet (or dressed) state formalism, we can artificially create potential curve crossings, which can be used to control molecular processes. Our control scheme presented here is summarized as follows. First, we prepare an appropriate vibrationally excited state in the ground electronic state, and at the same time by applying a stationary laser field of the frequency we create two nonadiabatic tunneling (NT) type curve crossings between the ground electronic bound state shifted up by one photon energy and the excited electronic state with two dissociative channels. In the NT-type of curve crossing where the two diabatic potential curves cross with opposite signs of slopes, it is known that the complete reflection phenomenon occurs at certain discrete energies. By adjusting the laser frequency to satisfy the complete reflection condition at the NT type curve crossing in one channel, the complete dissociation into the other channel can be realized. By taking one- and two-dimensional models which mimic the HOD molecule and using a wave packet propagation method, it is numerically demonstrated that a molecule can be dissociated into any desired channel selectively. Selective dissociation can be realized even into such a channel that cannot be achieved in the ordinary photodissociation because of a potential barrier in the excited electronic state.

I-E-2 New Way of Controlling Molecular Processes by Lasers

TERANISHI, Yoshiaki[1]; NAGAYA, Kuninobu[2]; NAKAMURA, Hiroki
(*[1]IMS and RIKEN; [2]GUAS*)

Two new ways of controlling molecular processes are proposed. One is to weep laser frequency and/or intensity at avoided crossings among dressed states to control nonadiabatic transitions there. The second is to use the intriguing phenomenon of complete reflection in the nonadiabatic tunneling type transition in the time-

independent framework. The newly completed semi-classical theory of nonadiabatic transitions can give a nice analytical formulation for these.

I-E-3 Selective Excitation Among Closely Lying Multi-Levels

NAGAYA, Kuninobu[1]; TERANISHI, Yoshiaki[2]; NAKAMURA, Hiroki
(*[1]GUAS; [2]IMS and RIKEN*)

[*Laser Control and Manipulation of Molecules*, Amer. Chem. Soc., in press]

A new idea is proposed to accomplish selective and complete excitation to any specified state among closely lying multilevels. The basic idea is to control nonadiabatic transitions among dressed states by sweeping the laser frequency periodically. Both three- and four-level models are treated by the semiclassical theory of nonadiabatic transition and conditions of complete excitation are formulated. Numerical demonstrations are presented in comparison with the π-pulse and adiabatic rapid passage.

I-E-4 Control of Molecular Processes by a Train of Linearly Chirped Pulses: Selective and Complete Excitation

NAGAYA, Kuninobu[1]; TERANISHI, Yoshiaki[2]; NAKAMURA, Hiroki
(*[1]GUAS; [2]IMS and RIEKN*)

A new scheme of controlling molecular processes is proposed. The scheme is to manipulate nonadiabatic transitions among Floquet states and can be formulated analytically. Complete selective excitation among closely lying levels and complete electronic excitation of a diatomic molecule are numerically demonstrated. This is proved to be better and more robust compared to the other methods such as the phase-lock and the adiabatic rapid passage. Experimental realizability can also be expected, since linear chirping can be now relatively easily manipulated.

I-F Theory of Multi-Dimensional Tunneling

I-F-1 Practical Implementation of the Instanton Theory for the Ground State Tunneling Splitting

MIL'NIKOV, Gennady V.[1]; NAKAMURA, Hiroki
(*[1]IMS and Inst. Struct. Macrokinetics*)

[*J. Chem. Phys.* **115**, 6881 (2001)]

The instanton theory is reformulated with use of the path integral approach and the WKB approximation to the Schrödinger equation. Both approaches are shown to provide the same results. A new practically useful semiclassical formula is derived for the tunneling splitting of the ground state, which can be implemented for high-dimensional systems. The theory is applicable to systems of arbitrary Riemannian metric and is also supplemented by a practical numerical recipe to evaluate the instanton trajectory, *i.e.* periodic orbit, in multidimensional space. Numerical examples are presented for 3D and 21D systems of HO_2 and malonaldehyde, respectively.

I-G New Methods for Scattering Calculation

I-G-1 Stable and Efficient Evaluation of Green's Function in Scattering Problem

MIL'NIKOV, Gennady V.[1]; NAKAMURA, Hiroki; HORÁČEK, Jiri[2]
(*[1]IMS and Inst. Struct. Macrokinetics; [2]IMS and Charles Univ. Prague*)

[*Comput. Phys. Commun.* **135**, 278 (2001)]

A new methodology similar to the R-matrix propagation technique is invoked to propose the practical recipe for efficiently calculating the Green's function in scattering problem. High accuracy of the proposed approach is demonstrated by taking examples of very deep tunneling and complex-valued nonlocal potential which describes low-energy dissociative attachment process between electron and molecules.

I-G-2 Use of Diabatic Basis in the Adiabatic-By-Sector R-Matrix Propagation Method in Time-Independent Reactive Scattering Calculations

MIL'NIKOV, Gennady V.[1]; NAKAMURA, Hiroki
(*[1]IMS and Inst. of Struct. Macrokinetics*)

[*Comput. Phys. Commun.* **140**, 381 (2001)]

We propose a new recipe for the *R*-matrix propagation which combines the ideas of the adiabatic-by-sector (ABS) method and the sequential diagonalization/truncation technique. The *R*-matrix is determined in the adiabatic representation but the method does not require calculations of adiabatic channel functions at

radial points inside the sector of propagation. This is a modification of the previously proposed ABS approach and can significantly reduce the computational time and memory in the energy independent part of scattering calculations. The code is checked by a test calculation of the reaction $O(^3P) + HCl \rightarrow OH + Cl$ using a LEPS potential energy surface (PES). The applicability of the method is further demonstrated by accurate quantum calculations of the endoergic reaction $H(^2S) + O_2(^3\Sigma_g^-) \rightarrow OH(^2\Pi) + O(^3P)$.

I-G-3 Regularization of Scattering Calculations at R-Matrix Poles

MIL'NIKOV, Gennady V.[1]; NAKAMURA, Hiroki
(*[1]IMS and Inst. Struct. Macrokinetics*)

Physical quantities of scattering expressed in terms of R-matrix are not well defined at *R*-matrix poles. It is shown that these unphysical singularities can be removed and the regularized expressions are obtained. The method is straightforwardly applicable to various quantities of scattering theory such as reactance matrix, Green's functions, cumulative reaction probability and density of resonance states.

I-H Theoretical Study of Dissociative Attachment

I-H-1 Study of Dissociative Electron Attachment to HI Molecule by Using R-Matrix Representation for Green's Function

KOLORENČ, P.[1]; HORÁČEK, Jiri[2]; MIL'NIKOV, Gennady V.[3]; NAKAMURA, Hiroki
(*[1]Charles Univ. Prague; [2]IMS and Charles Univ. Prague; [3]IMS and Inst. Struct. Macrokinetics*)

The new method of the calculation of scattering Green's function recently proposed by the authors is applied to the process of dessociative attachment of low-energy electrons to HI molecule previously considered by Horáček, Domcke and Nakamura. The calculation is extended to vibrationally and rotationally excited target gas molecules. The temperature dependence of the dissociative attachment cross section is studied in details.

I-I Theoretical Studies of Ultrafast Nonlinear Optical Spectroscopy of Molecules in Condensed Phases

Nonlinear optical interactions of laser fields with matter provide powerful spectroscopic tools for the understanding of microscopic interactions and dynamic processes. We attempt to provide theoretical basis for a wide class of nonlinear spectroscopic techniques, focusing on the underlying physical processes in the condensed phases.

I-I-1 Two-Dimensional Spectroscopy and the Harmonically Coupled Anharmonic Oscillators

OKUMURA, Ko; JONAS, M. David[1]; TANIMURA, Yoshitaka
(*[1]Univ. Colorado*)

Experimentally it is established that the 4th-order anharmonicity plays significant roles in many molecules; based on the local (anharmonic) modes picture with couplings between them, the Darling-Dennison coupling manifests itself, which has been confirmed experimentally. It has been shown that this order of anharmonicity can be selectively studied via the 7th order off-resonant optical processes (Okumura and Tanimura, *J. Chem. Phys.* **106**, 1687 (1997)). We obtained fairly compact analytical result for the 7th-order signal and numerically present the signal from CH stretch vibrations in methylene chloride as two-dimensional contour maps. By virtue of the two-dimensionality the results demonstrate the possibility of giving further insight into such mechanism that is not available in the one-dimensional high-resolution spectroscopy.

I-I-2 Two-Dimensional Raman and Infrared Signals Measured from Different Phase-Matching Conditions

KATO, Tsuyoshi; TANIMURA, Yoshitaka

We developed a theoretical method that can explicitly treat the phase-matching condition of two-dimensional optical measurements. This method might be a rational tool for the analysis of observed signals under non-impulsive excitation. We use this method to separate the contribution of the signal from different Liouville pathways associated with the different phase-matched condition. It is expected that the effects of mode coupling, anharmonicity of the system potential and nonlinearity of the polarizability will be pronounced by the spatial discrimination of the signal, which can be achieved experimentally.

I-I-3 Nonequilibrium Initial Conditions of a Brownian Oscillator System Observed by Two-Dimensional Spectroscopy

SUZUKI, Yoko; TANIMURA, Yoshitaka

We study effects of a nonequilibrium initial condition of a Brownian oscillator system upon two-, three-, and four-time correlation functions of an oscillator coordinate as a subject of multi-dimensional spectroscopy. A nonequilibrium initial condition is set by a displacement of a Gaussian wave packet in an oscillator potential. Such situation may be found in a vibrational motion of molecules after a sudden bond breaking between a fragmental molecule and a targeting vibrational system or a movement of wave packet in an electronic excited state potential surface created by a laser pump pulse. Multi-time correlation functions of oscillator coordinate for a nonequilibrium initial condition are calculated analytically with the use of generating functional from a path integral approach. Two-, three- and four-time correlation functions of oscillator coordinates correspond to the third-, fifth-, and seventh-order Raman signals or the first-, second-, and third order infrared signals. We plotted these correlation functions as a signal in multi-dimensional spectroscopy. The profile of the signal depends on the initial position and momentum of the wave packet in the fifth- and seventh-order Raman or the second and third order infrared measurement, which makes it possible to measure the dynamics of the wave packet directly in the phase space by optical means.

I-I-4 Higher-Order Vibrational Correlation Functions of a Single Harmonic Oscillator Nonlinearly Coupled with a Thermal Bath I: Gauss-White Noise Case

KATO, Tsuyoshi; TANIMURA, Yoshitaka

Higher-order vibrational correlation functions of a single harmonic oscillator system nonlinearly coupled with harmonic oscillators bath are studied in relation to the 2D Raman or IR spectroscopy. The nonlinear system-bath coupling models the vibrational relaxation dynamics under the presence of the elastic and inelastic relaxation mechanisms. A quantum Fokker-Planck equation is derived to describe the relaxation processes for the Gaussian-white noise. Effects of the simultaneous existence of two relaxation mechanisms, the system-bath coupling strength and the temperature are investigated and compared with the Brownian oscillator model by numerically integrating the Fokker-Planck equation. We observe new optical responses induced by the coexistence of the two relaxation mechanisms, which can possibly be very pronounced in the fifth-order Raman (or second-order IR) spectroscopy rather than the seventh-order Raman (or third-order IR)

spectroscopy.

I-I-5 Higher-Order Vibrational Correlation Functions of a Single Harmonic Oscillator Nonlinearly Coupled with a Thermal Bath II: Gauss-Markov Noise Case

KATO, Tsuyoshi; TANIMURA, Yoshitaka

A single harmonic oscillator system nonlinearly coupled to harmonic oscillators bath is considered to study the effects of the finiteness of the Gaussian-Markovian bath correlation time. The previously derived quantum Fokker-Planck equation is extended in a hierarchy form to treat arbitrary bath correlation time. The equation describes the vibrational frequency fluctuations as well as the vibrational energy relaxation processes, and can treat strong system-bath couplings. The fifth- and seventh-order Raman response functions are calculated by numerically integrating the Fokker-Planck equation for various system-bath coupling strengths and bath correlation times. Echo behaviors can be observed in the seventh-order Raman response under the slow frequency fluctuation and energy relaxation, however, such the behavior is absent in the leading fifth-order response function. This finding cannot be predicted by the available stochastic Gaussian frequency fluctuation model.

I-I-6 Two-Dimensional Spectroscopy for a Two-Dimensional Rotator in a Dissipative Environment

SUZUKI, Yoko; TANIMURA, Yoshitaka

Effects of an environment on the dynamics are more clearly characterized by the multidimensional spectroscopy than one-dimensional spectroscopy measured in the microwave absorption. We investigate the two-dimensional spectroscopy of a two-dimensional quantal rotator coupled to a Gaussian-Markovian harmonic oscillator bath by calculating a four-time correlation function of a dipole whose analytical form is derived from the generating functional. Such spectra are experimentally proved by the third order absorption. The spectra in the absence of damping are discrete and reveal transitions between eigenstates of the angular momentum quantized due to the cyclic boundary condition. The calculations for a damped rotator predict an echo signal that can be understood by the Liouville space path ways. The profile of the two-dimensional spectroscopy depends on a finite correlation time of the bath fluctuation and of a coupling strength.

I-I-7 Two-Dimensional Spectroscopy for Molecular Vibration: An Analysis of Potential Surfaces in a Dissipative Environment

MARUYAMA, Yutaka; TANIMURA, Yoshitaka

A molecular vibrational mode in condensed phases is studied using a quantum Fokker-Planck equation, which can treat a molecular system with any shape of potential coupled to a white noise heat-bath. The two-, three-, and four-time correlation functions of Raman polarizability and the dipole moment are calculated as the subject of two-dimensional (2D) spectroscopy for various potential surfaces with different heat-bath coupling strength. The temporally 2D profiles of signal are very sensitive to the potential surfaces and a coordinate dependence of the polarizability or dipole even in the strong damping case. This indicates that 2D spectroscopy allows us to access information of the potential and the polarizability or dipole in the dissipative environment, where the line shape of conventional 1D Raman or infrared spectroscopy is broadened and does not provide such information.

I-J The Condensed Phase Quantum Dynamics of Molecules and Atoms

We investigate quantum dynamics of molecules or atom in condensed phases by means of various statistical physics approaches involving the path integral and Fokker-Planck equation approaches for a reduced density matrix. Effects of dissipation on a quantum rotator, proton tunneling and electron transfer processes are investigated and compared with the classical dynamics.

I-J-1 Quantum Theory of Two-Dimensional Rotator in a Dissipative Environment: Application to Infrared Spectroscopy

SUZUKI, Yoko; TANIMURA, Yoshitaka

[*J. Phys. Soc. Jpn.* **70**, 1167 (2001)]

Quantum coherence and its destruction by coupling to a dissipative environment play important roles in time-resolved optical response. We study a two-time correlation function of a two-dimensional rotator coupled to a harmonic-oscillator bath. Generating functionals of reduced density matrix elements for the rotator degrees of freedom are calculated by diagonalizing the total Hamiltonian with the use of unitary transformations and then performing path integrals. A closed-form expression of linear absorption spectrum for a dipole rotator, *i.e.*, a Fourier transformation of the dipole two-time correlation function, is derived from the

generating functionals characterized by the bath spectral density. Based on the theory, the spectra for a methyl rotation in a toluene are depicted for various damping constants and temperatures. Because of the cyclic boundary condition that is constrained to fit the rotator degree of freedom, the energy states of the rotator in the absence of damping are discrete: the spectra consist of rotational branches, which correspond to change of the angular momentum. Owing to damping, the spectra exhibit a continuous band which is broadened as temperatures increase.

I-J-2 Two Time Correlation Function of a Two-Dimensional Quantal Rotator in a Colored Noise

SUZUKI, Yoko; TANIMURA, Yoshitaka

We study an absorption spectrum of a two-dimensional rotator coupled to a harmonic Gaussian-Markoffian heat bath. Generating functional of reduced density matrix elements for the rotator degrees of freedom in the Gaussian-White case have been developed and are presented compactly in the recent letter. We extend it to the Gaussian-Markoffian case and show the detailed calculation in this paper. A linear absorption spectrum for a dipole rotator is analytically derived from the generating functional. Representative

calculations for a methyl rotator in a toluene of the spectra are presented with the use of the analytical result. Plots for various damping strength, cutoff frequency, and temperatures take into account the environmental effect to the dynamical properties of the dipole moment.

I-J-3 Coherent Control of Nonclassical Effects in Quantum Optical Three-Level Atomic System

DU, Si-de; TANIMURA, Yoshitaka

Nonclassical effects are theoretically investigated in the interaction of a single three-level atom with a single one-mode quantized cavity field. The atom under consideration has two closely spaced excited levels and one ground-state level. When the atom is coherently excited into a superposition of the two excited states, there exists quantum interference between two transition channels which are stimulated by the cavity field initially in coherent states. We have discussed influence of quantum interference on collapses and revivals, squeezing and antibunching. It is discovered that the revival patterns strongly depend on quantum interference, and quantum interference can produce strong squeezing and antibunching. Our results are useful for understanding and controlling nonclassical effects.

I-K Theoretical Studies of Correlated Electron Systems

We study biorthogonal formulation of correlated electron system represented in the second quantized form. We illustrate the transcorrelated Hamiltonian approach and discuss the self-consistent field theory using biorthogonal orbitals.

I-K-1 Biorthogonal Approach for Explicitly Correlated Calculations Using the Transcorrelated Hamiltonian

HINO, Osamu; TEN-NO, Seiichiro[1]; TANIMURA, Yoshitaka
(*[1]Nagoya Univ.*)

A biorthogonal formulation is applied to the nonhermite transcorrelated Hamiltonian, which treats a large amount of the dynamic correlation effects implicitly. We introduce biorthognal canonical orbitals diagonalizing the nonhermite Fock operator. We also formulate many-body perturbation theory for the transcorrelated Hamiltonian. The biorthogonal self-consistent fields followed by the second order perturbation theory are applied to some pilot calculations including small atoms and molecules. We illustrate the transcorrelated Hamiltonian approach and discuss the self-consistent field theory using biorthogonal orbitals. We develop MBPT for the transcorrelated Hamiltonian based on the biorthogonal formalism. We also explain the approximate calculations of three-electron integrals, which appear in

the transcorrelated method.

I-L Development of Techniques for Prediction of Conformations and Applications to Proteins and Organic Compounds

Various techniques of prediction of conformations have been developed in this decades including proteins and organic compounds. Furthermore, the analysis of genome sequences from various species including human have been performed quite rapidly. The next significant problem is to clarify 3D structures and functions of proteins coded by genome sequences. Since the experimental techniques to determine 3D structures of proteins are still time-consuming, a predictive technique is desired. However, a prediction of protein 3D strcutures is still unsolved and difficult problem in the area of molecular biophysics. Currently, we are attempting to predict location of 3D strcuture units, so-called domains, in genome sequences by means of a kind of contact map based on the statistics of average distances between amino acids in proteins. This information can be helpful to determine the 3D structure of each structural unit. On the other hand, development of a modeling technique of organic compounds in terms of the interactions with a protein is also important especially in the field of drug design. We have applied a 3D search method to find a new potent inhibitor of an enzyme for development of a new herbicide. We also made the MD simulation of some polysacchalydes, chitosan and amylose, to clarify the relationship between their dynamical properties and the coloring bahavior with iodine.

I-L-1 Contact Maps Derived from the Statistics of Average Distances between Residues in Proteins. Application to the Prediction to the Prediction of Structiures and Active-Sites of Protein and Peptides

KIKUCHI, Takeshi
(IMS and Kurashiki Univ. Sci. Arts)

Information on various 3D structural features of proteins is extractable from statistics of protein 3D stuctures, using the method we review here. The main tool for the method is a contact map, called an average diatance map (ADM), constructuted from the statistics of average distances between residues. In spite of their simplicity, theese maps proveide various predictions on 3D structures of proteins, *e.g.*, location of domains, structural similarity between proteins, proteins structural classes, active sites in bioactive peptides, and so on. The present method is useful for practical problems encountered in protein engineering and drug design. We also demonstrate a practical application of the present method to the structure-activity relationship prediction of an insect peptidic hormone; the results have ramifications for the future development of new types of insecticides. Further, ADM can be applied for identification of functional units on genome sequences in the post-genome era.

I-L-2 Prediction of Protein 3D Folding Properties in Genome Sequences Based on the Statistics of Average Distances between Residues

KIKUCHI, Takeshi
(IMS and Kurashiki Univ. Sci. Arts)

The analyses of human genome has been proceeded quite rapidly and whole human genome will be uncovered in very near future. The next significant step is to predict the 3D structure and function of domains in an Open Reading Frame (ORF) derived from a genome analysis, *i.e.* to clarify which region in an ORF corresponds to what kind of functional domain. The average distance (ADM) method is useful and adequate for the step of prediction of domain locations on ORFs. The ADM method also gives several predictions on 3D structures of proteins. In the present work, we report the recent progress of the ADM method to treat ORFs derived from genome analyzes especially focusing on the prediction of location and folding properties of domains. The results show that the ADM method predicts folding units in a protein sequence and it corresponds to a functional domain in many cases.

I-L-3 Identification of Novel Potent Inihivitors for ATP-Phosphoribosyl Transferase Using Three-Dimensional Structural Database Search Technique

GOHDA, Keigo[1]; OHTA, Daisaku[2]; KOZAKI, Akiko[3]; FUJIMORI, Ko[4]; MORI, Ichiro[5]; KIKUCHI, Takeshi[6]
([1]Novartis Pharma; [2]Osaka Prefectural Univ.; [3]Nagoya Univ.; [4]Osaka Bioci. Cent.; [5]Nippon Glaxo; [6]IMS and Kurashiki Univ. Sci. Arts)

An efficient method to search potent inhibitors of an enzyme or a receptor is required in the process of drug design. One simple but effective strategy is to search compounds fit to the cavity of a receptor from the compound 3D database. We identified new potent inhibitors for ATP-phosphoribosyl transferase, which acts at the first step of histidine biosynthesis pathway, using a 3D database search technique. The 3D search was based on the structure of the product molecule, N-1-(5'-phosphoribosyl-1-pyrophosphate), *i.e.* bi-substrate

mimicking. Four compounds with three different chemical classes were examined. Among them, amino-(chlorophenyl)-triazolopyrimidine compounds, which are the simplest and smallest ones, showed potent activity. The structural comparison with the product molecule suggests that the simultaneous occupation of two substrate-binding sites likely enhances the enzyme inhibition. The most potent compound examined in this study was a disulfide-bond containing molecule, whose mode of action seems to be different from others.

I-L-4 Complex Formation of Chitosan with Iodine and Its Structure and Spectroscopic Properties—Molecular Assembly and Thermal Hysteresis Behavior

YAJIMA, Hirofumi[1]; KIKUCHI, Takeshi[2]; ISHII, Tadahiro[1]
(*[1]Sci. Univ. Tokyo; [2]IMS and Kurashiki Univ. Sci. Arts*)

To elucidate the factors responsible for the complexation of chitosan with iodine and to gain insight into the structures and spectroscopic properties of chitosan-iodine (CI) complexes, extensive studies were performed on the effects of iodine/chitosan concentrations and temperature on the CI complexation. That is, the several physicochemical properties of the complex in acidic solutions containing excess KI were examined by means of various spectroscopic (absorption, CD, *etc.*) and structural analyses (SAXS, *etc.*) and molecular dynamics (MD) simulations. The CI complex exhibited absorption spectra with a peak at around 500 nm, regardless of the iodine/chitosan concentrations and temperature. Correspondingly, the CI complexes exhibited mutually split CD bands with opposite signs (+, –) at around 500 nm. The CI complex showed thermal hysteresis, *i.e.*, an irreversible reaction process involved in complexation and color formation. MD calculations predicted that the irreversibility and thermal hysteresis behavior of the CI complexes are due to a crystalline-like extended compact folded conformational transition.

I-M Electronic Properties of Nanostructured Materials

I-M-1 Electronic Structure of K-Doped Carbon Nanotubes

MIYAKE, Takashi[1]; SAITO, Susumu[2]
([1]Tokyo Inst. Tech.; [2]IMS and Tokyo Inst. Tech.)

[submitted]

Alkali-metal doping is expected to provide a means of controlling electronic properties of carbon nanotubes. Previous band structure calculations support the charge-transfer picture in both K and Li doping. However, more systematic analysis is desirable, since transport properties of nanotubes are sensitive to their size and chirality. We study the effect of K doping inside a few zigzag nanotubes by using density functional method. We find that the effect depends on the diameter significantly, and it is not described fully by the simple charge-transfer picture. In particular, in the (10,0) and (12,0) tube, which are possible to produce macroscopic amount, the nearly free electron (NFE) state of the nanotube is pulled down by hybridization with the K 4s state, and crosses the Fermi level. We will discuss the influence on transport properties from the spatial distribution of the NFE state.

I-M-2 Geometries, Electronic Properties, and Energetics of Isolated Single Walled Carbon Nanotubes

KANAMITSU, Kenjiro[1]; SAITO, Susumu[2]
([1]Tokyo Inst. Tech.; [2]IMS and Tokyo Inst. Tech.)

[submitted]

Using the density-functional electronic-structure calculations, we study so-called zig-zag carbon nanotubes. From the complete geometry optimization, it is found that two kinds of bond lengths are considerably different from each other. They possess strong tube-diameter dependence. In addition, changes of the electronic band structure upon the geometry relaxation from the uniform bond-length tube are found to be sizable. Also the electronic properties and energetics obtained are discussed in detail.

I-N Theoretical Analyses on Nonlinear Behavior of Complex Systems

When material A and material B form a complex system, for example, an interface (or an interface region) newly appears between the two materials. Structure and properties of the interface are often totally different from those of the bulk materials, with the result that the complex system exhibits highly nonlinear behavior that can never be understood by superposition of the behaviors of the individual materials. We deal with a complex system in which liquid solvent or aqueous solution is one of the constituents. The integral equation theories are applied to the liquid solvent and combined with theoretical methods or computer simulation techniques for the other constituents. Some of the complex systems considered are biomolecules in aqueous solution, molecular assemblies formed by self-organization of surfactant molecules in solvent, metal-liquid interface, solvent-mediated interaction between colloidal particles, surface-induced phase transition phenomena, and entropic excluded-volume effects in colloidal and biological systems.

I-N-1 Long-range Interaction between Hydrophilic Surfaces Immersed in a Hydrophobic Fluid Containing a Hydrophilic Component at Low Concentration

KINOSHITA, Masahiro
(Kyoto Univ. and IMS)

[*Chem. Phys. Lett.* **333**, 217 (2001)]

Behavior of a hydrophobic fluid containing a hydrophilic component at low concentration, which is confined between macroparticles separated by distance *L*, is analyzed using the RISM-HNC theory. When the hydrophilicity of the macroparticle surface is sufficiently high, the following is observed. A layer within which particles of the hydrophilic component are enriched is formed around each macroparticle. As *L* decreases the two enriched layers within the confined domain continue to grow, eventually leading to a phase transition. The range of the macroparticle interaction induced can be far longer than the molecular scale.

I-N-2 Statistical-Mechanical Analysis on Entropically Driven Formation of Ordered Structure

KAMIO, Kazunori[2]; KINOSHITA, Masahiro[1]
([1]Kyoto Univ. and IMS; [2]Kyoto Univ.)

[*Kagaku Kogaku Ronbunshu* (in Japanese) in press]

Phase separation in a mixture of small and large colloidal particles and the interaction induced between a macromolecule (a large particle) and a cell membrane (a surface) immersed in smaller molecules (small particles), have been analyzed using an integral equation theory. Simplified models are employed to study the entropically driven formation of ordered structure, which is ascribed to the excluded volume effects (forces of increasing the system entropy by reduction of the total excluded volume for the small particles). In the analysis on the induced interaction, attention is focused on effects due to the packing fraction of the small particles, the diameter of the large particle, the surface curvature, presence of a small amount of particles slightly larger than the small particles, and attractive interaction between the small particles. A significant result is that great specificity is provided between the diameter of the large particle and the surface curvature. Works concerning the roles of the excluded volume effects on the "lock and key" steric interactions between macromolecules and protein folding in the biological systems, which are in progress in our group, have also been discussed.

I-N-3 Depletion Effects on the Lock and Key Steric Interactions between Macromolecules

KINOSHITA, Masahiro[1]; OGUNI, Teppei[2]
([1]Kyoto Univ. and IMS; [2]Kyoto Univ.)

[*Chem. Phys. Lett.* in press]

The hypernetted-chain (HNC) equations solved on a three-dimensional cubic grid are employed to calculate the spatial distribution of the depletion potential between a big solute of *arbitrary geometry* and a big sphere immersed in small spheres forming the solvent. Effects of the step edge on the lateral depletion force along a wall surface are analyzed and shown to be in qualitatively good agreement with a recent experimental observation. Simple model calculations are performed for the *lock and key* steric interactions between macromolecules, and it is found that the depletion effects provide the interactions with remarkably high selectivity.

I-N-4 Improvement of the Reference Interaction Site Model Theory for Calculating the Partial Molar Volume of Amino Acids and Polypeptides

KINOSHITA, Masahiro[1]; IMAI, Takashi; KOVALENKO, Andriy; HIRATA, Fumio
([1]Kyoto Univ. and IMS)

[*Chem. Phys. Lett.* **348**, 337 (2001)]

We propose a simple, efficient bridge correction of the one-dimensional reference interaction site model (RISM) theory. By combining the modified RISM method with the Kirkwood-Buff theory, the partial molar volume is calculated for the 20 amino acids and

for oligopeptides of glutamic acids in extended and a-helix conformations. The bridge correction drastically improves agreement between the calculated values and the experimental data.

I-N-5 Spatial Distribution of Depletion Potential between a Big Solute of Arbitrary Geometry and a Big Sphere Immersed in Small Spheres

KINOSHITA, Masahiro
(Kyoto Univ. and IMS)

The hypernetted-chain integral equations are solved on a three-dimensional cubic grid to calculate the spatial distribution of the depletion potential between a big solute of *arbitrary geometry* and a big sphere immersed in small spheres forming the solvent. By analyzing the potential along a specific trajectory of the big sphere, effects due to the geometric feature of the big solute (step edges, trenches, corners, changing curvature, *etc.*) can be examined in detail. As an illustration, effects of the step edge on the lateral depletion potential along a wall surface are analyzed. Along the trajectory considered, the big sphere moves at constant height, starting on the center of the wall surface and moving horizontally past the edge. The potential minimum occurs not on the center but at a location much closer to the edge. The big sphere is repelled from the edge into the wall surface, and to escape to the bulk it must overcome a significantly high free-energy barrier. A positive peak of the potential occurs near the edge on the bulk side. As another illustration, simple model calculations are performed for the *lock and key* steric interaction between macromolecules. The potential at contact (*i.e.*, the stabilization free energy) for the key that exactly fits the lock is far larger than for smaller and larger keys and considerably in excess of the value predicted by the Asakura-Oosawa (AO) theory. A very high free-energy barrier features the potential for a smaller key, preventing its access to the lock. The depletion effects on the interaction are substantially large, and the selectively given is remarkably high. The physical origin of the failure of the AO theory is discussed in detail.

I-O Electronic Structures of Polymers and Organic Molecular Crystals

In order to understand the electronic, optical, and magnetic properties of polymers and organic molecular crystals, we have investigated the electronic structures of these materials using various kinds of theoretical approaches, for examples, the density matrix renormalization group method for a model Hamiltonian, a first-principles pseudopotential method, and ab initio quantum chemical calculations. In particular, we have focused our attention mainly to phase transition phenomena accompanied by drastic changes of electronic and optical functions. The actual targets of our research are as follows: 1) Semiconductor-metal transition in doped conducting conjugated polymers, 2) Thermo- and photochromic phase transitions in polydiacetylene, 3) Neutral-ionic transition in tetrathiafulvalene-p-chloranil.

I-O-1 Charge Carriers and Semiconductor-Metal Transition in Doped Conducting Conjugated Polymers

SHIMOI, Yukihiro[1,2]; KUWABARA, Makoto[2,3]; ABE, Shuji[1]
(*[1]AIST; [2]IMS; [3]Kobe Univ.*)

We have investigated how the configurations of charge carriers evolve in non-degenerated conjugated polymers when carrier concentration increases, putting emphasis on electron correlation effects and electron-lattice coupling. For this purpose, we have applied the density matrix renormalization group method to the one-dimensional extended Hubbard-Peierls model. We found out theoretically a new configuration of charge carrier, polaron-pair state, as an intermediate configuration between polaron and bipolaron. This configuration is possible under a relatively weak electron-lattice coupling. We have shown that gaps for charge and spin excitations become quite small at highly doping concentration. Comparing the non-interacting case, correlation effects suppress the gap, indicating the significant role of electron-electron interaction on semiconductor-metal transition of which mechanism is still open question.

I-O-2 First-Principles Study of Polydiacetylene

KATAGIRI, Hideki[1]; SHIMOI, Yukihiro[1,2]; ABE, Shuji[1]
(*[1]AIST; [2]IMS*)

In order to elucidate the mechanism of thermo- and photochromic phase transitions in polydiacetylene (PDA), we have performed first-principles pseudo-potential calculations for a typical theromochromic PDA, TCDU, (poly(5,7-dodecadiyne-1,12-diyl-bis-phenylurethane)). The calculated energy surface shows that the butatrinene conformation of backbone chain is not a metastable state in TCDU, in contrast to a hypotetical PDA where the side group is replaced by a hydrogen atom. This indicates that the side group has significant influence on the geometry of the backbone, consistent with experimental observations. We have investigated how the conformation of side group affects the energy surface and band gap in order to understand the interplay between the π-electronic structure at backbone and the configuration of side group more clearly.

I-O-3 Role of Intramolecular Charge Distribution on Neutral-Ionic Transition of Tetrathiafulvalene-*p*-Chloranil

KAWAMOTO, Tohru[1]; IIZUKA-SAKANO, Takako[1]; SHIMOI, Yukihiro[1,2]; ABE, Shuji[1]
(*[1]AIST; [2]IMS*)

[*Phys. Rev. B* **64**, 205107 (2001)]

We calculated the Madelung energies of both the ground state and excited states in tetrathiafulvalene-*p*-chloranil (TTF-CA) by taking into account intra-molecular charge distribution. The distribution is found to be significant in the neutral-ionic (NI) transition. In the ionic phase, the Madelung energy depends more strongly on the intermolecular distance perpendicular to the π-stacking chains than on that along the chains. This indicates that simple single-chain models neglecting interchain electrostatic coupling are not adequate. The gain of the Madelung energy due to dimerization is concluded to be small compared with the other structural changes. We also calculated the formation energy of excited state domains, which appear in the initial process of the phase transition. A one-dimensional excited domain has the smallest energy among the possible domains with the same number of molecules, and the energy per molecule is considerably reduced in increasing the domain size. It is consistent with the experimental suggestion that a large number of excitations were generated by only one photon.

I-P Electronic Structure of a Molecule in Solution

Chemical reaction is undoubtedly the most important issue in the theoretical chemistry, and the electronic structure is a key to solve the problem. As long as molecules in the gas phase are concerned, the theory for the electronic structure has been enjoying its great success. However, when it comes to molecules in solution, the stage of theory is still an infant. We have recently proposed a new method refereed to as RISM-SCF based on the integral equation theory of molecular liquids (RISM) and the ab initio electronic structure theory (SCF).[1] The integral equation approach replaces the reaction field in the continuum models by a microscopic expression in terms of the site-site radial distribution functions between solute and solvent.

$$V_\lambda = \sum_j \int 4\pi r^2 \frac{q_j}{r} g_{j\lambda}(r) dr$$

where j and λ specify solvent and solute sites, respectively, and r denotes the solvent density. The site-site radial distribution functions $g_{\lambda j}(r)$ can be calculated from the extended RISM equation. Using V_λ the solvated Fock operator is defined as,

$$F^s = F^g - \sum_\lambda V_\lambda b_\lambda$$

where b_λ is a population operator of solute atoms. The statistical solvent distribution around solute is determined by the electronic structure or the partial charges of solute, while the electronic structure of solute is influenced by the solvent distribution. Therefore, the Hartree-Fock equation and the RISM equation should be solved in a self-consistent manner. It is this self-consistent determination of the solute electronic structure and the solvent distribution around the solute that features the RISM-SCF procedure.

The same Fock operator can be derived from a variation principle.[2] Defining the Helmholtz free energy A as following;

$$A = E_{solute} + \Delta\mu$$

where E_{solute} is the energy of solute under solvent influence, and $\Delta\mu$ is the solvation free energy represented in terms of the Singer-Chandler formula. The Fock operator for a solute molecule in solvent as well as the RISM-HNC equations can be obtained as the first order variations with respect to the wave functions and the pair correlation functions under the constraint of the orthonormality to the molecular orbitals. The latest development along this line are reported below.

References
1) S. Ten-no, F. Hirata and S. Kato, *Chem. Phys. Lett.* **214**, 391 (1993); *J. Chem. Phys.* **100**, 7443 (1994).
2) H. Sato, F. Hirata and S. Kato, *J. Chem. Phys.* **105**, 1546 (1996).

I-P-1 Theoretical Study on the Structures and Energies of Acetic Acid Dimers in Aqueous Solution

NAKABAYASHI, Takakazu; SATO, Hirofumi; HIRATA, Fumio; NISHI, Nobuyuki

The effects of hydration on the dimerization energies and structures of acetic acid dimers are studied by the reference interaction site model self-consistent-field (RISM-SCF) method. Comparisons of the RISM-SCF results are also made with those obtained from the self-consistent reaction field (SCRF) methods to examine the dielectric effects of the solvent. The RISM-SCF method predicts the marked stabilization due to solvation in the dimer structures with large dipole moments. From the decomposition analysis of the excess chemical potential, the contribution from the free carbonyl oxygen is found to be much larger than the other atoms for the stabilization of these dimers in aqueous solution. Such a stabilization in the polar dimers is not obtained from the simplest SCRF method that considers only the solute dipole.

I-P-2 Realization of Three-Dimensional Solvation Structures from the Site-Site Radial Distribution Functions in Liquids

SATO, Hirofumi; HIRATA, Fumio

We propose a new procedure to realize a three-dimensional (3D) solvation structure around a solute molecule from a set of radial distribution functions (RDF), or distance information. The method consists of the minimization of a penalty function defined as the mean-square difference of the solute-solvent interatomic distances obtained from trial 3D configurations and from target RDFs. The hydration structures around several different solute molecules are visualized to demonstrate the method.

The solvation structures realized with the present method correspond to the most plausible solvation

structure (MPSS), which looks like a "snap shot" of the molecular dynamics trajectory. However, the MPSS is essentially different from the "snap shot," since it represents an average configuration, and is therefore an observable quantity. The present procedure was originally developed for analyses of the RDF results obtained from the reference interaction site model (RISM), but can be applied straightforwardly to RDFs from other sources, such as molecular simulations and scattering experiments.

I-P-3 Solvent Effect on the Nuclear Magnetic Shielding: Ab initio Study by the Combined Reference Interaction Site Model and Electronic Structure Theories

YAMAZAKI, Takeshi[1]; SATO, Hirofumi; HIRATA, Fumio
(*[1]GUAS*)

A method for calculating the nuclear magnetic shielding constant of atoms in solution is proposed based on the *ab initio* electronic structure theory combined with the extended reference interaction site model in statistical mechanics for molecular liquids. The method is applied to a water molecule solvated in water, acetone, chloroform, and carbon tetrachloride. The results for solvation effect demonstrate capability to predict the experimental results. The theory provides a tool to investigate the solvent effect on the nuclear magnetic shielding and its temperature dependence from a molecular view point. The theory takes account for effect of the electrostatic interaction on the electronic structure of solute, but disregards the electron overlap. The effect of intermolecular overlap of electron on the nuclear magnetic shieldings is examined using a molecular cluster model.

I-Q Solvation Thermodynamics of Protein and Related Molecules

Concerning biomolecules such as protein, it is a final goal for the biochemistry and biophysics to explore the relation between conformations and biological functions. The first important step toward the goal would be to explain the conformational stability of biomolecules in terms of the microscopic structure of the molecules in solvent. It is an extremely difficult problem by any means due to the overwhelmingly large degrees of freedom to be handled, including protein and solvent. As long as the small and/or short-time fluctuations of protein around the native structure is concerned, a variety of molecular simulation techniques provides a quite powerful tool to explore the microscopic structure of protein and solvent. However, the techniques are not so effective to characterize stability of the macromolecules in solution, to which the thermodynamic limit ($V \to \infty$, $N \to \infty$, with V/N = const.) is concerned. In such a case, methods based on the statistical mechanics of liquids should be natural choice for sampling configurations of solvent interacting biomolecules. The extended RISM theory is the most promising candidate of such methods, which provides not only solvation thermodynamics but also microscopic description at the level of the pair correlation functions.[1] Obvious technical difficulties which one may face in applying the theory to such a large system are not only the computation time but also the stability of the numerical solution.[2]

Here, we present our recent effort to tackle the problem using the two theoretical tools based on the statistical mechanics of liquids: the extended RISM and the scaled particle theories (SPT).[3] The studies for the solvation thermodynamics of small molecules such as ions are also included because it is regarded as elementary processes for the solvation of biomolecules, and because it is prerequisite for studying the more complicated molecules.

References
1) M. Kinoshita, Y. Okamoto and F. Hirata, *J. Am. Chem. Soc.* **120**, 1855 (1998).
2) A. Kitao, F. Hirata and N. Go, *J. Phys. Chem.* **97**, 10231 (1993).
3) M. Irisa, K. Nagayama and F. Hirata, *Chem. Phys. Lett.* **207**, 430 (1993).

I-Q-1 Hydration Structure and Stability of Met-Enkephalin Studied by a Three-Dimensional Reference Interaction Site Model with a Repulsive Bridge Correction and a Thermodynamic Perturbation Method

KOVALENKO, Andriy; HIRATA, Fumio; KINOSHITA, Masahiro[1]
(*[1]Kyoto Univ.*)

We study the hydration structure and free energy of several conformations of Met-enkephalin in ambient water by employing the one-dimensional (1D) as well as three-dimensional (3D) reference interaction site model (RISM) integral equation theories, complemented by the hypernetted chain (HNC) closure with the repulsive bridge correction (RBC). The RBC contribution to the excess chemical potential of solvation is calculated by means of the thermodynamic perturbation theory (TPT), which crucially reduces computational burden and thus is especially important for a hybrid algorithm of the RISM with molecular simulation. The 3D-

RISM/HNC+RBC-TPT approach provides improved prediction of the solvation thermodynamics and gives a detailed description of the solvation structure of a biomolecule.

The results obtained are discussed and compared to those following from the 1D-RISM/HNC theory. The latter yields physically reasonable results for the conformational stability of biomolecules in solution, which is further improved by adding the 1D-RBC. The modified, 1D-RISM/HNC-RBC-TPT integral equation theory combined with the simulated annealing or generalized-ensemble Monte-Carlo simulation methods is capable of reliable prediction of conformations of biomolecules in solution with due account for the solvent effect at the microscopic level.

I-Q-2 Theoretical Study for Partial Molar Volume of Amino Acids and Poly-Peptides by the Three-Dimensional Reference Interaction Site Model

HARANO, Yuichi[1]; IMAI, Takashi; KOVALENKO, Andriy; KINOSHITA, Masahiro[2]; HIRATA, Fumio
(*[1]Kobe Univ.; [2]Kyoto Univ.*)

We calculate the partial molar volume (PMV) of twenty amino acids in aqueous solution at infinite dilution is by using the Kirkwood-Buff equation and the three-dimensional reference interaction site model (3D-RISM) integral equation theory for molecular liquids. As compared to the conventional, one-dimensional (1D-RISM) approach, the results exhibit drastic improvement for the quantitative agreement with experiment. The deviation from the experimental data, seen for the relatively large amino acids is discussed in terms of the "ideal fluctuation volume" introduced in the previous study based on the 1D-RISM to account for flexibility of solute molecules. Robustness of the new approach is further demonstrated by applying it to the PMV of poly-glutamic acids in aquous solution. The method provides reasonable account for the PMV increase with the chain length, both in a-helical and extended structures, whereas the 1D-RISM approach gives an unnatural decrease of the PMV for the a-helix with a complete turn of the backbone.

I-Q-3 Theoretical Study for Volume Changes Associated with the Helix-Coil Transition of Polypeptides

IMAI, Takashi; HARANO, Yuichi[1]; KOVALENKO, Andriy; HIRATA, Fumio
(*[1]Kobe Univ.*)

We calculate the partial molar volumes and their changes associated with the coil(extended)-to-helix transition of two types of peptide, glycine-oligomer and glutamic acid-oligomer, in aqueous solutions by using the Kirkwood-Buff solution theory coupled with the three-dimensional reference interaction site model (3D-RISM) theory. The volume changes associated with the transition are small and positive. The volume is analyzed by decomposing it into five contributions following the procedure proposed by Chalikian and Breslauer: the ideal volume, the van der Waals volume, the void volume, the thermal volume, and the interaction volume. The ideal volumes and the van der Waals volumes do not change appreciably upon the transition. In the both cases of glycine-peptide and glutamic acid-peptide, the changes in the void volumes are positive, while those in the thermal volumes are negative, and tend to balance those in the void volumes. The change in the interaction volume of glycine-peptide does not significantly contribute, while that of glutamic acid-peptide makes negative contribution.

I-R Collective Density Fluctuations in Polar Liquids and Their Response to Ion Dynamics

As to the model for molecular diffusion in polar liquids, there are two quite different points of view. One is the conventional rot-translation model, and the other the interaction-site description which sees the diffusion of a molecule as a correlated motion of each atom (site).[1] It is clearly advantageous to use the interaction-site description compared to the rot-translation model to account for chemical characteristics of solvent as well as solute dynamics. However, the interaction-site description has its own disadvantage in interpreting physical meaning of the results, since it does not give an explicit picture for the rotational relaxation of molecules, which can be directly probed by many experimental means including the dielectric and NMR relaxation. We have solved the problem by extracting collective modes of the density fluctuation from the site-site density correlation functions. In our recent study for dynamics of molecular liquids based on the interaction-site model, we have succeeded to abstract the collective excitations in liquids, which can be identified as optical and acoustic modes, by diagonalizing the collective frequency matrix appearing in the generalized Langevin equation. The two modes arise essentially from the rotational and translational motions of molecules.[2] We applied the method to the ion dynamics in a dipolar liquid, and could have explained successfully the peculiar size dependence of friction of alkali and halide ions in terms of response of the collective excitations in solvent to the solute displacement.[3]

In the past year, we have elaborated the memory kernel in our generalized Langevin equation base on the mode

coupling theory. We have also extended our treatment to dynamics of water and hydrated ions. Those studies as well as other related topics are reviewed below.

References
1) F. Hirata, *J. Chem. Phys.* **96**, 4619 (1992).
2) S. Chong and F. Hirata, *Phys. Rev. E* **57**, 1691 (1998).
3) S. Chong and F. Hirata, *J. Chem. Phys.* **108**, 7339 (1998).

I-R-1 Site-Site Mode-Coupling Theory for the Shear Viscosity of Molecular Liquids

YAMAGUCHI, Tsuyoshi; HIRATA, Fumio

[*J. Chem. Phys.* in press]

A mode-coupling expression for the shear viscosity coefficient of dense molecular liquids based on the interaction site model is presented. It is a natural extension of the corresponding theory for simple liquids, in which the shear stress auto correlation function is described as the linear combination of the bilinear products of the site-site dynamic structure factor. The theory is applied to water at the ambient condition. The agreement between the theory and the computer experiment is fairly good for the simplicity of the theory.

I-R-2 Solute-Shape Dependence in Solvation Dynamics: Investigated by RISM Theory

NISHIYAMA, Katsura[1]; HIRATA, Fumio; OKADA, Tadashi[1]
(*[1]Osaka Univ.*)

[*J. Mol. Liq.* in press]

A combination of the reference interaction-site model (RISM) theory and the site-site Smoluchowski-Vlasov equation has been applied to estimate solute-shape dependence of the dynamic average-energy relaxation of the solute-solvent system in a polar solvent. If the solute became larger, like octapoles, the relaxation got much slower. A plausible mechanism of the relaxation will be discussed.

I-R-3 Nonlinear Response of Solvent Molecules Induced by Instantaneous Change of Solute Electronic Structure: Studied by RISM Theory

NISHIYAMA, Katsura[1]; HIRATA, Fumio; OKADA, Tadashi[1]
(*[1]Osaka Univ.*)

[*J. Mol. Struct.* **565–566**, 31(2001)]

We have applied the reference interaction-site model (RISM) theory for the estimation of the dynamic response function of the average-energy relaxation, $S_S(t)$, of the solute-solvent systems, induced by an instantaneous change of the solute electronic structure in polar solvents. We choose the solutes including square- or cubic-like structures: initially all the atoms are electrically neutral and, then we put δ^+ and δ^- charges instantaneously. For the multipoles $S_S(t)$s show apparent dependence on d, which predicts nonlinear response of the solvent, because $S_S(t)$ is a normalized quantity irrespective of δ as far as the linear response of the solvent dynamics is assumed. On the other hand we have previously performed transient hole-burning and time-resolved fluorescence spectroscopy. We have found the difference between the dynamic response functions obtained from spectral widths and that from spectral peak shifts, implying the nonlinear solvent-response, as these two kinds of the response functions should again correspond to each other within a linear response regime. Our present results from the RISM theory can be another indicative to confirm nonlinearity suggested by our experiments. At the moment we ascribe the origin of the nonlinear solvent behavior to the larger local-density fluctuation around the solute.

I-R-4 Average Energy Relaxation and Rearrangement of Solute-Solvent Radial Distribution Function in Solvation Dynamics: A Connection between Spectroscopic Results and RISM Theory

NISHIYAMA, Katsura[1]; HIRATA, Fumio; OKADA, Tadashi[1]
(*[1]Osaka Univ.*)

[*J. Mol. Liq.* **90**, 251(2001)]

We calculate the relaxation dynamics of the average energy of solute-solvent systems as well as time-dependent solute-solvent radial distribution functions by means of the reference interaction-site model (RISM) theory. Compared with the experimental results obtained in our previous work, we suggest that the rearrangement of the further solvation shell could be important for the relaxation dynamics of the inhomogeneous spectral band width observed by means of transient hole-burning and time-resolved fluorescence spectroscopy.

I-S Developing Theories of Liquids and Liquid Mixtures

In the past few years, we have been concentrating our effort on building theories for chemical processes in solution. Our main concern in such study was to develop new theories which can describe "solvation" or "solvent effect" on chemical processes of interest by means of the statistical mechanics of liquids. A key to such development is the "RISM theory," and many intriguing chemistry as well as physics have been investigated in our group using the theory at least in qualitative level. On the hand, we are also experiencing serious break down of the theory sometime as we try to explore new problems such as the gas-liquid phase transition, protein solution, and liquid-liquid mixtures.

In what follows, we describe our challenges to explore new problems related to liquids and liquid mixtures. The challenge inevitably includes methodological development in the statistical mechanics of liquids.

I-S-1 Integral Equations for Molecular Fluids Based on Interaction Site Model: Density-Functional Formulation

SUMI, Tomonari; IMAI, Takashi; HIRATA, Fumio

[*J. Chem. Phys.* **115**, 6653 (2001)]

An integral equation for rigid-body molecules with respect to site-density distribution function under arbitrary external fields is derived by density-functional theory. Using a grand canonical partition function of molecular systems, we extend original Percus' idea to molecular fluids. The extended Percus' idea provides a relation between site-site pair distribution function and site-density distribution function under an external field composed of the site-site interaction potentials of a molecule fixed at the origin. The site-density integral equation combined with the extended Percus' relation to molecular fluids gives a closure relation of reference interaction site model (RISM) equation. The site-site pair distribution functions of homonuclear diatomic Lennard-Jones fluids obtained by the integral equation agree well with those of Monte Carlo simulation.

I-S-2 A Replica Reference Interaction Site Model Theory for a Polar Molecular Liquid Sorbed in a Disordered Microporous Material with Polar Chemical Groups

KOVALENKO, Andriy; HIRATA, Fumio

[*J. Chem. Phys.* **115**, 8620 (2001)]

We develop a replica generalization of the reference interaction site model (replica RISM) integral equation theory to describe the structure and thermodynamics of quenched-annealed systems comprising polar molecular species. It provides a successful approach to realistic models of molecular liquids, and properly allows for the effect of a quenched disordered matrix on the sorbed liquid. The description can be extended to an electrolyte solution in a disordered material containing charged chemical functionalities that determine its adsorption character. The replica RISM equations are complemented with the HNC closure and its partial linearization (PLHNC), adequate to ionic and polar molecular liquids. In these approximations, the excess chemical potentials are derived in a closed analytical form. We extend the description to a quenched-annealed system with soft-core interaction potentials between all species, in which the liquid and matrix equilibrium distributions are characterized in general by two different temperatures. The replica RISM/PLHNC-HNC theory is applied to water sorbed in a quenched disordered microporous network of atoms associated into interconnected branched chains, with activating polar groups grafted to matrix chains. The results are in qualitative agreement with experiment for water confined in disordered materials.

I-S-3 First-Principles Realization of a van der Waals-Maxwell Theory for Water

KOVALENKO, Andriy; HIRATA, Fumio

[*Chem. Phys. Lett.* in press]

We generalize the van der Waals-Maxwell description of the fluid phase diagram to account for chemical specificities of polar molecular fluids, such as hydrogen bonding in water. The theory is based on the reference interaction site model (RISM) integral equation method in the partially linearized hypernetted chain (PLHNC) approximation. The predictions for the liquid-vapor coexistence of water are in qualitative agreement with molecular simulations. The theory can be extended to electrolyte as well as non-electrolyte solutions, and to ionic liquids.

I-S-4 Thermochemistry of Solvation: A Self-Consistent Three-Dimensional Reference Interaction Site Model Approach

KOVALENKO, Andriy; TRUONG, Thanh N.[1]
(*[1]Univ. Utah*)

[*J. Chem. Phys.* **113**, 7458 (2000)]

We developed a self-consistent three-dimensional reference interaction site model integral equation theory with the molecular hypernetted chain closure (SC-3D-RISM/HNC) for studying thermochemistry of solvation of ionic solutes in a polar molecular solvent. It is free from the inconsistency in the positions of the ion-solvent site distribution peaks, peculiar to the conventional RISM/HNC approach and improves the predictions for the solvation thermodynamics. The SC-3D-RISM treatment can be readily generalized to the case of finite ionic concentrations, including the

consistent dielectric corrections to provide a consistent description of the dielectric properties of ion-molecular solution. The proposed theory is tested for hydration of the Na^+ and Cl^- ions in ambient water at infinite dilution. An improved agreement of the ion hydration structure and thermodynamics with molecular simulation results is found as compared to the conventional RISM/HNC treatment.

I-T Charge-Transfer Excitations and Fluctuations in Quasi-One-Dimensional Organic Conductors

i) In quasi-one-dimensional segregated-stack organic charge-transfer complexes with a quarter-filled band, $(TMTTF)_2X$ and $(TMTSF)_2X$, variation of physical properties under physical or chemical pressure can be viewed as a dimensional crossover. We have already studied how the crossover of the normal-phase properties above the phase transition temperatures to three-dimensional ones is achieved by increasing intermolecular overlaps between the neighboring chains and/or reducing electron correlation. The umklapp process has been essential to the confinement of fermions and to the antiferromagnetic long-range order. However, it was difficult to treat excitation spectra by the previous analytic approaches. Now a numerical approach is employed to deal with the dimensional crossover experimentally observed in excitation spectra. ii) In quasi-one-dimensional mixed-stack organic charge-transfer complexes with a half-filled band, neutral-ionic phase transitions with decreasing temperature, with increasing pressure, or with irradiation of light have been extensively investigated. Recently, complexes with inter-columnar networks have been synthesized and examined. Among them, the $(BEDO-TTF)(Cl_2TCNQ)$ complex shows an unusual phase transition accompanied with a sharp drop in the magnetic susceptibility. A completely new mechanism for the transition from the ionic to neutral phases is proposed and numerically investigated. Even in the conventional, quasi-one-dimensional complex, TTF-CA, time-resolved spectroscopic data just after the irradiation of light are accumulated during the photo-induced phase transition. We also study the dynamics of neutral and ionic domains in such a non-equilibrium condition.

I-T-1 Intra- and Inter-Chain Excitations near a Quantum Phase Transition in Quasi-One-Dimensional Conductors

YONEMITSU, Kenji

[*Mol. Cryst. Liq. Cryst.* in press]

We study intra- and inter-chain excitation spectra near a quantum phase transition in a spinless fermion model on a two-leg ladder at half filling by the finite-temperature density-matrix renormalization-group method. Above a critical strength of intrachain nearest-neighbor repulsion, a gap appears, accompanied with a long-range order of density modulation in the checkerboard pattern at zero temperature. The intrachain excitation spectra do not change so much in the gapless phase below the critical strength, while the interchain excitation spectra are considerably altered by the intrachain repulsion even in the gapless phase. Relevance to the optical conductivity in quasi-one-dimensional electron systems is suggested.

I-T-2 Collective Excitations and Confinement in the Excitation Spectra of the Spinless-Fermion Model on a Ladder

YONEMITSU, Kenji

[*Phys. Rev. B* submitted]

Intra- and inter-chain, local charge-transfer excitation spectra and the single-particle density of states are calculated by the finite-temperature density-matrix renormalization-group method in the spinless-fermion model on a ladder with varying intra-chain nearest-neighbor repulsion and with small inter-chain transfer integral at and near half filling. Collective excitations govern the low-energy intra-chain spectra, while only individual local excitations are present in the inter-chain spectra. As a consequence, at half filling, the

intra-chain repulsion affects the inter-chain spectra more sensitively than the intra-chain spectra. Meanwhile, the inter-chain transfer integral affects the intra-chain spectra more sensitively through modifying the density-density correlation strength. The difference between the intra- and inter-chain spectra in the insulating phase can be interpreted from the viewpoint of confinement. It is found that the doping dependence of the local charge-transfer excitation spectra is similar to the dependence on the inter-chain transfer integral. It is because the inter-chain motion of fermions is not band-like but incoherent. Similarities between these findings and the experimentally observed, optical conductivity spectra in the quasi-one-dimensional organic conductors, $(TMTSF)_2X$, are pointed out.

I-T-3 Quantum and Thermal Charge-Transfer Fluctuations for Neutral-Ionic Phase Transitions in the One-Dimensional Extended Hubbard Model with Alternating Potentials

YONEMITSU, Kenji

[*Phys. Rev. B* submitted]

Effects of quantum and thermal fluctuations on transitions between the ionic phase and the neutral phase are studied by applying the finite-temperature density-matrix renormalization-group method to the one-dimensional extended Hubbard model with alternating potentials at half filling. Charge-transfer fluctuations lower the energy of the neutral phase more than that of the ionic phase, which is in contrast to the spin fluctuations favoring the ionic phase. As a consequence, with increasing intermolecular overlap between the neighboring donor and acceptor sites, we expect a spin-fluctuation-induced transition from the neutral phase to the ionic phase, and a charge-transfer-fluctuation-induced transition from the ionic phase to the neutral phase, near the phase boundary. Relevance to a recently observed phase transition in a new class of

mixed-stack charge-transfer complexes is discussed.

I-T-4 Photoexcitations and Domain-Wall Dynamics near Neutral-Ionic Transitions

MIYASHITA, Naoyuki[1]; KUWABARA, Makoto[2]; YONEMITSU, Kenji
(*[1]GUAS; [2]Kobe Univ.*)

Recently, time-resolved photoreflectance spectra of TTF-CA have been measured just after photoexcitations by several groups. They are useful for the understanding of dynamical processes in the photoinduced phase transition, *e.g.*, creation and propagation of domain walls between the neutral and ionic phases. Real-time dynamics of such domain walls is studied by numerically solving the time-dependent Schrödinger equation for a one-dimensional extended Peierls-Hubbard model within the unrestricted Hartree-Fock approximation. Since thermal lattice fluctuations would be regarded as random initial conditions for lattice displacements, we add static impurities to the chain as a first step. Domain walls are generated at these impurity sites by photoexcitations. It is found that motion of domain walls depend at the early stage on the strengths of impurities and the intensity of photoexcitations.

I-T-5 New Photoinduced Phenomenon in Polymers

SUN, Xin[1,2]; FU, Rouli[2]; YONEMITSU, Kenji; NASU, Keiichiro[3]
(*[1]Fudan Univ.; [2]Natl. Lab. Infrared Phys.; [3]Inst. Mater. Struct. Sci.*)

[*Phys. Rev. A* in press]

Numerical simulation has shown that a polymeric molecule can possess a new photoinduced phenomenon, photoinduced polarization reversion, in which the electric dipole of the polymeric molecule is reversed by absorbing one photon. This paper provides an analytic theory by means of a response function to prove that a polymer with a bipolaron has a negative static polarizability and explains the physical origin of this new photoinduced phenomenon in detail. This paper also presents a dynamical calculation for the photoinduced polarization reversion, from which the relaxation time for the dipole reversion can be determined.

I-U Cooperation or Competition between Electron Correlation and Lattice Effects in One-Dimensional π-*d* Electron Systems

i) Quasi-one-dimensional π-*d* hybrid electron systems, $(DCNQI)_2M$, are known to show a metal-insulator transition originating from the collaboration of the Peierls (*i.e.*, electron-lattice) and Mott (*i.e.*, electron-electron) mechanisms, which is contrary to the MMX chains. Although stability of the insulator phase with lattice modulation of period three is known in a wide pressure range, *i.e.*, in a wide range of the π-*d* level difference, its theoretical treatment was very difficult because of strong correlation and highly nonlinear lattice effects. Strong commensurability effects on the stability are investigated by extensive numerical calculations. Another phase found nearby is consistent with the tendency observed by recent experiments. ii) Various charge-ordered phases are found accompanied with different lattice modulation patterns in quasi-one-dimensional halogen-bridged binuclear metal complexes, which are often called MMX chains. The dependence of the charge ordering, the lattice distortion and the optical conductivity spectra on the ligand, the counter ion and the halogen ion has been explained by competition between electron-lattice and electron-electron interactions, that between site-diagonal and site-off-diagonal interactions, and that between short-range and long-range interactions.

I-U-1 Strong Commensurability Effect on Metal-Insulator Transition in (DCNQI)$_2$Cu

KUWABARA, Makoto[1]; YONEMITSU, Kenji
(*[1]Kobe Univ.*)

[*Mol. Cryst. Liq. Cryst.* in press]

$(DCNQI)_2Cu$ salts, which are one-dimensional π-*d* electron systems, show unique physical properties associated with hybridization between π bands of DCNQI molecules and *d* orbitals of Cu. The metal-insulator transition is regarded as a cooperative phenomenon due to the Peierls instability in the 1/3-filled π band and the Mott instability in the *d* orbitals, 5/6 of which are occupied. We study stability of three-fold lattice distortion in the insulating state of $(DCNQI)_2Cu$ by exactly diagonalizing a two-band Peierls-Hubbard model on the 6×2 lattice. Self-doping is essentially important and caused by strong commensurability pinning, which is a consequence of moderate coupling of DCNQI π electrons with lattice and strong correlation of Cu *d* electrons.

I-U-2 Optical Excitations in XMMX Monomers and MMX Chains

KUWABARA, Makoto[1]; YONEMITSU, Kenji

(*[1]Kobe Univ.*)

We study optical excitations in $K_4[Pt_2(pop)_4X_2]$ monomers (X = Cl, Br, I), using an extended Hubbard model. We show that long-range transfer integrals and long-range Coulomb interactions are substantially large to reproduce the experimental results. Due to the strong long-range Coulomb interactions, it is expected that the optical conductivity spectra of the MMX chains have two peaks in the charge polarization phase.

I-U-3 Ground State Phases and Optical Properties in Extended Peierls-Hubbard Models for Halogen-Bridged Binuclear Metal Complexes

KUWABARA, Makoto[1]; YONEMITSU, Kenji
(*[1]Kobe Univ.*)

Mechanisms of a variety of charge and lattice ordered phases observed in halogen-bridged binuclear metal complexes are theoretically studied by applying the exact diagonalization and strong-coupling expansion methods to one- and two-band extended Peierls-Hubbard models. In $R_4[Pt_2(pop)_4I]_nH_2O$ [R = Na, K, NH_4, $(CH_3(CH_2)_7)_2NH_2$, *etc.*, pop = $P_2O_5H_2^{2-}$] containing charged MMX chains, three electronic phases are suggested by experiments. We find that the variation of the electronic phases originates not only from competition between site-diagonal electron-lattice and electron-electron interactions but also from competition between short-range and long-range electron-electron interactions. On the other hand, in $Pt_2(RCS_2)_4I$ (R = CH_3, n-C_4H_9) containing neutral MMX chains, a site-off-diagonal electron-lattice interaction and the absence of counter ions are found to be crucial to produce the recently found, ordered phase. The optical conductivity spectra are also studied, which directly reflect the electronic phases. Their dependence on the electronic phase and on model parameters is clarified from the strong-coupling viewpoint.

I-V Charge Order, Lattice Distortion and Magnetism in Two-Dimensional Organic Conductors and Metal-Complexes

i) Quasi-two-dimensional metal complexes, $Et_nMe_{4-n}Z[Pd(dmit)_2]_2$, have strong dimerization and two bands consisting of the HOMO and the LUMO, which have different degrees of anisotropy. The cation controls the relative magnitudes of inter-molecular overlaps between neighboring dimers. They were known from our previous calculations to effectively control the degree of magnetic frustration and consequently whether the ground state is antiferromagnetic or paramagnetic. In the previous analysis, the interaction strengths had to be assumed. Now close comparisons between the experimental and theoretical optical conductivity spectra enable us to quantitatively estimate the magnitudes of different interaction strengths. ii) Among quasi-two-dimensional organic conductors, the θ-phase compounds are known to show metal-insulator transitions accompanied with charge ordering. Although long-range Coulomb repulsion is generally believed to be essential to the paramagnetic charge-ordered phase, the optical conductivity spectra do not show an excitonic band expected from our previous calculations. Then additional interaction terms might be important for the charge-ordering transitions. In fact, $(BEDT-TTF)_2RbZn(SCN)_4$ that has a lattice-distorted ground state has a rather high transition temperature. Both numerical and analytic calculations indeed suggest that weak electron-lattice coupling plays an important role.

I-V-1 Optical Conductivity for Possible Ground States of Dimerized Two-Band Pd(dmit)₂ Salts

MORI, Michiyasu[1]; YONEMITSU, Kenji
(*[1]Tohoku Univ.*)

We have studied the optical conductivity for possible ground states of $Pd(dmit)_2$ salts, by exactly diagonalizing a two-band Hubbard model for a dimer. The one-dimer model is useful to reproduce the overall structure of the optical spectra, since the intra-dimer transfer integrals, Ah and Al, are an order of magnitude larger than the inter-dimer transfer integrals. Our results reproduce dominant peaks of the optical spectra measured by Tajima *et al.* and confirm their argument from the strong-coupling viewpoint. The peak position and the intensity are generally affected by electron-electron interactions. The interaction strengths are estimated and used in the estimation of effective exchange interaction strengths between dimers. The cation dependence of the magnetic properties is reconsidered.

I-V-2 Charge Ordering Patterns and Their Excitation Spectra in Two-Dimensional Charge-Transfer Compounds

MORI, Michiyasu[1]; YONEMITSU, Kenji
(*[1]Tohoku Univ.*)

Charge ordering (CO) states are found in the insulating phase of θ-$(BEDT-TTF)_2MM'(SCN)_4$ (M =

Rb, Cs, M' = Zn, Co) by various experimental studies. In the CO states, the charge density is disproportionate and the spin degrees of freedom survive. We calculated the optical conductivity spectra of some CO states in the quarter-filled extended Hubbard model by use of the random phase approximation (RPA) on the basis of the Hartree-Fock (HF) states. If the intersite interactions are essential, an excitonic effect should be significant to affect the peak positions and the spectral shape. Such excitonic effect is included in the RPA. We chose the values of intersite interaction strengths as to reproduce the experimentally observed degree of charge transfer about 0.4 in the HF calculation for each CO pattern. The conclusion from the RPA calculation is consistent with the Tajima *et al.*'s result as regards the number of peaks depending on the CO patterns. The RPA calculation shows a strongly excitonic character in the spectral shapes. However, the experimental data have no excitonic peak but rather broad bands probably ascribed to the inter-band transitions. This fact indicates that the above nearest-neighbor interaction strengths are too strong to explain the spectral shapes. To resolve this contradiction, not only the intersite interactions but also other interactions, *e.g.*, electron-lattice interactions, would be needed.

I-V-3 Paramagnetic Charge-Ordered States by Cooperation of Coulomb Repulsion with Electron-Lattice Coupling

MORI, Michiyasu[1]; YONEMITSU, Kenji
(*[1]Tohoku Univ.*)

Charge ordering is clearly seen below around 190 K in the slowly cooled θ-(BEDT-TTF)$_2$RbZn(SCN)$_4$ sample, where the crystal structure slightly changes at the transition temperature. If the same sample is rapidly cooled, the charge ordering becomes obscure from the room temperature down to about 20 K. It had been theoretically suggested that the charge ordering originates from the intersite repulsion in this quarter-filled system. Then, we previously calculated the optical conductivity spectra in the random phase approximation and showed that an excitonic effect should be significant if the intersite interaction is really essential. However, the experimental data show no excitonic peak but rather broad bands, which indicate that the intersite interaction is insufficient for the charge ordering. An additional interaction would resolve the contradiction by cooperatively stabilizing the charge ordering. We exactly diagonalize the Hamiltonian with an electron-lattice interaction suggested by X-ray diffraction experiments and compare the results with the second-order perturbation theory from the strong-coupling limit. Weak electron-lattice coupling indeed enhances the effect of long-range Coulomb repulsion on the charge ordering, but keeps the paramagnetism.

I-W Vortices in the Mixed State of High-Temperature Cuprate Superconductors

To elucidate anomalous metallic properties around the high-temperature superconductivity in copper oxides has been one of the major challenges in condensed matter physics. The key issue is competing low-energy instabilities near the superconducting ground state, including antiferromagnetic, stripe, or flux instabilities. Theoretical controversy between the spin-liquid and the Fermi-liquid approaches to the issue is far from resolution. Among the spin-liquid approach, the SU(2) gauge theory recently attracts attention because the flux state predicted by it may be related with another theory or with some numerical calculations. A criterion of whether such approach is valid or not is given by whether its consequence can be experimentally detected or not. Now, atomic resolution scanning tunneling microscope (STM) techniques are well developed. Here, we propose a promising STM experiment to detect signature of the flux state around the superconducting vortex and discuss consequences of the hidden SU(2) gauge structure in underdoped cuprates.

I-W-1 Signature of the Staggered Flux State around a Superconducting Vortex in Underdoped Cuprates

KISHINE, Jun-ichiro; LEE, Patrick A.[1]; WEN, Xiao-Gang[1]
(*[1]MIT*)

Based on the SU(2) lattice gauge field formulation of the *t-J* model, we discuss possible signature of the unit cell doubling associated with the staggered flux (SF) state in the lightly doped spin liquid. Although the SF state appears only dynamically in a uniform *d*-wave superconducting state, a topological defect [SU(2) vortex] freezes the SF state inside the vortex core. Consequently, the unit cell doubling shows up in the hopping (χ_{ij}) and pairing (Δ_{ij}) order parameters of physical electrons. We find that whereas the center in the vortex core is a SF state, as one moves away from the core center, a correlated staggered modulation of χ_{ij} and Δ_{ij} becomes predominant. We predict that over the region outside the core and inside the internal gauge field penetration depth around a vortex center, the local density-of-states exhibits staggered peak-dip structure inside the V-shaped profile when measured on the bonds. The staggered peak-dip structure has its direct

origin in the unit cell doubling associated with the SF core and the robust topological texture, which has little to do with the symmetry of the *d*-wave order parameter. Therefore the structure may survive the tunneling matrix element effects and easily be detected by STM experiment.

RESEARCH ACTIVITIES II
Department of Molecular Structure

II-A Picosecond Transient Infrared Studies on Excited States of Donor-Acceptor Systems

Molecules having an electron donor and acceptor group at both ends of a conjugated π-electron system sometimes show characteristic photophysical behavior: dual fluorescence, for example. 4-(Dimethylamino)benzonitrile (DMABN) has attracted much attention as a prototype of such compounds. The photophysics of these compounds are thought to be closely related to excited state molecular structures. We have already published static/transient infrared studies on DMABN and isotopomers in the ground state and in the charge-transfer excited state [*J. Phys. Chem. A* **104**, 4182 (2000); *Chem. Phys.* **260**, 193 (2000); *J. Phys. Chem. A* **105**, 4182 (2001)]. As an extension of that, we have studied molecular structures of excited states of DMABN and analogues by means of picosecond infrared spectroscopy.

II-A-1 Picosecond Infrared Spectrum of 4-(Pyrrol-1-yl)benzonitrile: Structure of the Excited Charge-Transfer States of Donor-Acceptor Systems

OKAMOTO, Hiromi[1,2]; KINOSHITA, Mariko[2]
(*[1]IMS; [2]Univ. Tokyo*)

[*J. Phys. Chem. A* submitted]

Picosecond transient infrared spectrum of the excited charge-transfer (CT) state of 4-(pyrrol-1-yl)-benzonitrile (PBN) has been recorded in the frequency range of 1700–920 cm^{-1}. The CT state of PBN gives several quite strong infrared bands. The band at 1219 cm^{-1} shifts toward high-frequency side with increasing delay time between pump and probe pulses. This frequency shift is attributed to vibrational relaxation. Some of the transient bands (1429, ~1290, 1219, and 964 cm^{-1}) are very close in frequencies to those observed for the benzonitrile moiety of the excited CT state of 4-(dimethylamino)benzonitrile (DMABN). This finding implies that benzonitrile groups of PBN and DMABN are decoupled from the electron donating (pyrrole or dimethylamino) groups, and it can be explained by the twisted intramolecular charge transfer model. To make this point clear, however, further discussion is necessary on the band assignments and on correlation between structure and spectral pattern.
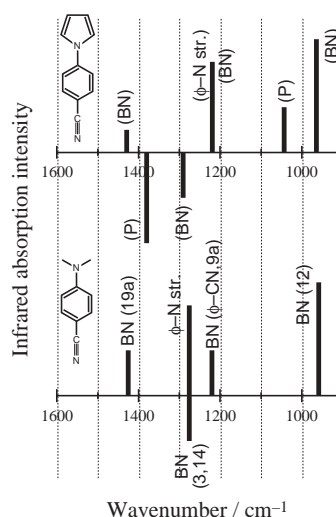
Figure 1. Transient infrared spectral patterns for the excited CT states of PBN (top) and DMABN (bottom). Tentative band assignments are given in parentheses for PBN. BN, mode of benzonitrile moiety; P, mode of pyrrole moiety.

II-A-2 Picosecond Infrared Spectra and Structure of Locally Excited and Charge Transfer Excited States of Isotope Labeled 4-(Dimethylamino)benzonitriles

**OKAMOTO, Hiromi[1,2]; KINOSHITA, Mariko[2];
KOHTANI, Shigeru[3]; NAKAGAKI, Ryoichi[3];
ZACHARIASSE, Klaas A.[4]**
(*[1]IMS; [2]Univ. Tokyo; [3]Kanazawa Univ.; [4]Max-Planck Inst.*)

[*Bull. Chem. Soc. Jpn.* submitted]

Infrared spectra of the ground, charge transfer (CT), and locally excited (LE) states of isotope-labeled 4-(dimethylamino)benzonitriles (DMABNs) in the region between 1700 and 900 cm^{-1} are reported. The isotopomers measured are normal DMABN, NC–C$_6$H$_4$–^{15}NMe$_2$ (dimethylamino nitrogen labeled DMABN), and NC–C$_6$H$_2$D$_2$–NMe$_2$ (3,5-dideuterated DMABN). Infrared spectrum of the excited CT state of DMABN-

d_2 is consistent with the previous band assignments for normal DMABN and DMABNs isotopically labeled on dimethylamino group. For the LE state of normal DMABN, three bands are observed at 1481, 1415, and 1399 cm^{-1}. This is in contrast with a previously reported transient infrared spectrum, where positions of bands due to the transient do not shift from the ground state ones. The band at *ca.* 1481 cm^{-1} is observed for normal and ^{15}N labeled DMABN, but not for DMABN-d_2. Except for this point, the band positions are almost identical for the three isotope-labeled species. The vibrational transitions observed at *ca.* 1415 and 1398 cm^{-1} are hence attributed to modes with atomic displacements localized on methyl groups and/or the part of the benzonitrile moiety adjacent to the cyano group or the cyano group itself. Quantum chemical calculations of the vibrational spectra for the CT and LE states of DMABN at present do not correctly reproduce the experimental spectra, which means that more accurate calculations are needed for a reliable analysis of these spectra.
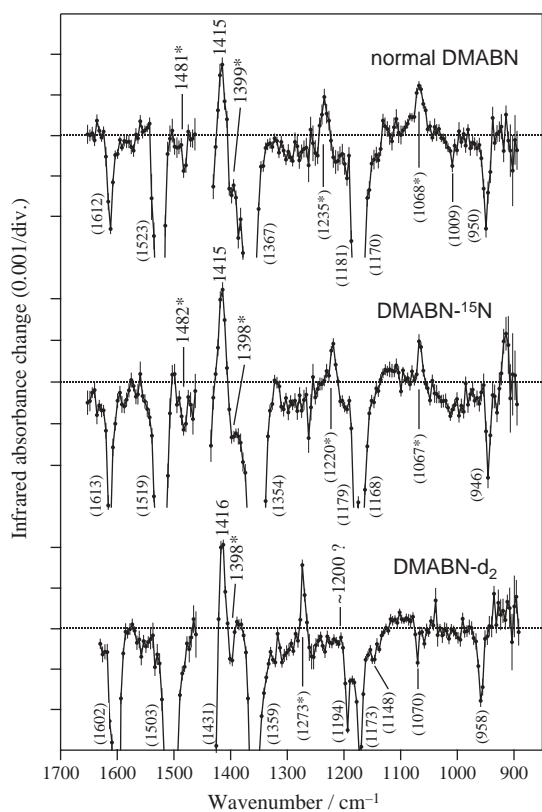
Figure 1. Transient infrared spectra of DMABN and the two isotope-labeled derivatives DMABN-d_2 and DMABN-^{15}N in cyclohexane solution at room temperature at 4 ps after excitation. Bleached bands arising from the ground state are indicated in parentheses. Negative bands due to non-totally symmetric vibrational modes (for both the ground and the excited states) are marked with asterisks.

II-B Laser Cooling and Trapping of Metastable Helium Atoms

In the past two decades, extensive developments have occurred in the laser cooling and trapping of neutral atoms, with many workers reporting the application of these techniques to such diverse atomic species as alkali atoms, alkali earth atoms, and rare gas atoms. Among these, the helium atom is unique on account of its small mass, simple energy level structure, and easy availability in two isotopic forms (^{3}He and ^{4}He) of differing quantum statistics. For this reason, we have been studying the laser cooling and trapping of helium atoms.

II-B-1 Magneto-Optical Trap of Metastable Helium Atoms with Doughnut Laser Beams: Computer Simulations

MORITA, Norio

When we intend to confine metastable helium atoms in high density in a magneto-optical trap (MOT), it is always a critical problem that the collisional ionization loss of the atoms is tremendously large under the irradiation of trapping laser light near-resonant with the cooling transition ($2s^3S_1 \rightarrow 2p^3P_2$). One of the possible methods that can let us avoid this problem may be to use laser beams with doughnut intensity profiles, because a MOT composed of such laser beams has almost negligible laser intensity around the MOT center. However, such a MOT has never been investigated so far and it is not trivial whether this type of MOT can efficiently confine the atoms. Therefore, with a computer simulation we have examined the availability of this MOT. First let us consider a one-dimensional MOT composed of doughnut laser beams: in this case, an atom lying at the center of the beam cross section and moving parallel to the beam axis receives no force from the beam, and so this atom can be neither decelerated nor trapped by the beam. This means that it is necessary to stop up the "hole" of the MOT by, for example, additional laser beams. Taking this into consideration, we can find that the simplest and most symmetric three-dimensional MOT that has no such "holes" may be a MOT with a dodecahedral beam configuration, which consists of eight doughnut beams coming from apexes of a dodecahedron to its center. Note that this configuration can easily be realized by a simple modification of a usual tetrahedral configuration. We have numerically simulated the atomic motion in this type of MOT, which is composed of eight laser beams with ($n = 0$, $l = 1$) Laguerre-Gaussian intensity profiles (the peak intensity is 20 mW/cm^2 and the radius of the peak ring is 3 mm). Consequently, we have found that any atom can be confined within a radius of 0.1 mm, in which only $< 0.5\%$ of the atoms are excited into the upper state of the cooling transition by the lasers. This means that the atomic density in the MOT can be increased by a factor of more than five in comparison with an ordinary MOT in the full saturation condition. An experiment to prove this result is now in progress.

II-C Spectroscopic Studies on Atoms and Ions in Liquid Helium

Atoms and ions in liquid helium are known to reside in bubble-like cavities due to the Pauli repulsive force between electrons. Physical properties of these exotic surroundings are determined by the potential energy of the impurity-He$_n$ system, the surface tension energy of the liquid helium, and the pressure-volume work. Spectroscopic studies of such impurity atoms and ions in liquid helium are expected not only to give information on the structure and dynamics of the bubbles but also to contribute to the study on the property of superfluid liquid helium.

II-C-1 Investigation on the Difference between Spectra of Ca Atoms in Liquid ^{3}He and ^{4}He

MORIWAKI, Yoshiki[1]; MORITA, Norio
(*[1]Toyama Univ.*)

Spectra of impurity atoms in liquid helium often explicitly reflect physical properties of the liquid. In this meaning, it may especially be interesting to investigate the difference between spectra of impurity atoms in liquid ^{3}He and ^{4}He, because even at a temperature as high as 1.4 K these liquids have much different physical properties; for example, the density is 1.62×10^{22} and 2.19×10^{22} cm^{-3} for ^{3}He and ^{4}He, respectively, and the surface tension is 0.116 and 0.336 dyn/cm for ^{3}He and ^{4}He, respectively. These differing properties are mainly caused by differences in the mass and quantum statistics between each species of He. In this work we have experimentally obtained spectra of Ca atoms in liquid ^{3}He and ^{4}He at 1.4 K and have investigated their differences. The experimental excitation spectra of the $4s^2\ {}^1S_0 \rightarrow 4s4p\ {}^1P_1$ and $4s4p\ {}^3P_{0,1,2} \rightarrow 4s5s\ {}^3S_1$ transitions are shown in Figures 1 (a) and (b), respectively. For each transition, as seen in these figures, the spectrum for liquid ^{3}He is narrow compared with the one for liquid ^{4}He, and the blue-shift of the former spectrum is smaller than the latter. This fact can qualitatively be explained with differences in the

number density and surface tension of the liquid; namely, in liquid ^{3}He, the size of a bubble formed around an impurity Ca atom is larger because of the smaller number density and surface tension of liquid ^{3}He, and this causes the Ca–He interaction the weaker. To confirm this, we have theoretically calculated these spectra, assuming a model Hamiltonian describing the Ca atom, bubble and their interactions for each liquid He. This Hamiltonian has almost the same form as assumed in our previous work on Yb$^+$ in liquid He. The spectra thus calculated are shown in Figures 1 (c) and (d), corresponding to Figures 1 (a) and (b), respectively. Comparing Figures 1 (a) and (b) with Figures 1 (c) and (d), respectively, we can see that the calculated results considerably well reproduce both widths and shifts of the experimental spectra. This fact strongly suggests that the differences observed in the experimental spectra are mainly caused by the differences in the physical properties of liquid ^{3}He and ^{4}He.
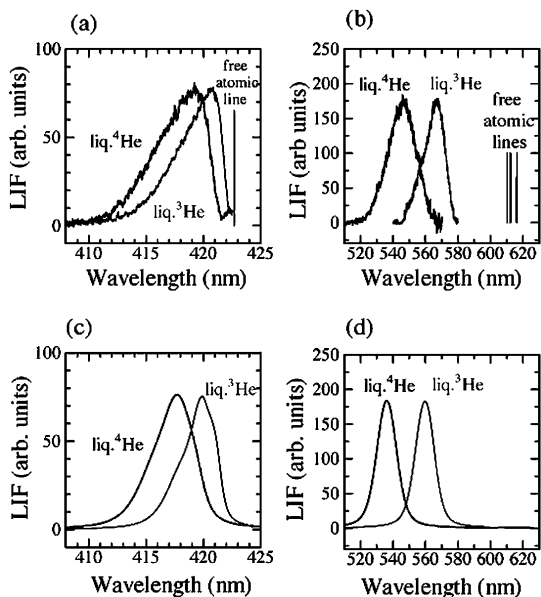
Figure 1. Excitation spectra of Ca atoms in liquid ^{3}He (gray curves) and ^{4}He (black curves): (a) and (b) show the experimental spectra of the $4s^2$ $^1S_0 \rightarrow 4s4p$ $^1P_1$ and $4s4p$ $^3P_{0,1,2} \rightarrow 4s5s$ $^3S_1$ transitions, respectively, and the theoretical spectra of those transitions are shown in (c) and (d), respectively. In (a) and (b), each transition wavelength of the free atom is also shown with a solid vertical line.

II-D Laser Spectroscopic Studies on Collisional Fine Structure Changing Transitions of Atoms and Ions

The fine structure changing transition in atoms and ions due to collisions with other particles is one of the important processes for the energy transportation in interstellar gases as well as in the atmosphere. However, unexpectedly, the number of studies so far devoted to the measurement of the cross section for this process is not so large. For this reason, we have been studying this process with laser spectroscopic methods, mainly focusing on alkali-earth ions, which have simpler energy level structures and so allow us to analyze experimental results more easily.

II-D-1 Laser Spectroscopic Measurements of Fine Structure Changing Cross Sections of Ba$^+$ Ions in Collisions with He Atoms

MORIWAKI, Yoshiki[1]; MATSUO, Yukari[2]; MORITA, Norio
(*[1]Toyama Univ.; [2]RIKEN*)

We have measured the cross section of the fine structure changing $6p$ $^2P_{3/2} \rightarrow 6p$ $^2P_{1/2}$ transition of the Ba$^+$ ion in collisions with He atoms at a room temperature. Like our similar work on Ca$^+$ and Sr$^+$, Ba$^+$ ions have been produced by laser ablation of a piece of BaTiO$_3$ placed in a vacuum chamber. The chamber is filled with He gas, and the ions produced are immediately cooled to a room temperature through collisions with the He atoms. Exciting the ions into the $6p$ $^2P_{3/2}$ level and detecting the laser-induced fluorescence from $6p$ $^2P_{3/2}$ and the sensitized fluorescence from $6p$ $^2P_{1/2}$ we have successfully obtained cross sections of the collision-induced $6p$ $^2P_{3/2} \rightarrow 6p$ $^2P_{1/2}$ transition and of the collisional quenching in the $6p$ $^2P_{1/2}$ level: $\sigma(6p$ $^2P_{3/2} \rightarrow 6p$ $^2P_{1/2}) = (2.9 \pm 0.4) \times 10^{-4}$ Å^2 and $\sigma(6p$ $^2P_{1/2} \rightarrow$ all states$) = (4.2 \pm 7.9) \times 10^{-2}$ Å^2. Figure 1 shows the cross sections for the np $^2P_{3/2} \rightarrow np$ $^2P_{1/2}$ transitions of various alkali metal atoms as well as alkali earth ions in the logarithmic scale as a function of their fine structure splittings. As seen in Figure 1, the cross sections for the alkali atoms are almost on a straight line; those for the alkali earth ions are also roughly on a straight line, but its slope is much different from the one for the alkali atoms. These exponential decreases common to both the ions and atoms can be explained by the Landau-Zener theory, as described in the previous work. On the other hand, the differing slopes of the decreases may be due to a difference between the interactions for ion-He and atom-He pairs; namely, the interaction in an ion-He pair is mainly the

monopole-induced-dipole interaction, which is stronger than for an atom-He pair. This fact may result in that, assuming the same fine structure splitting, the cross section for an alkali earth ion is much larger than for an alkali atom, as seen in Figure 1.
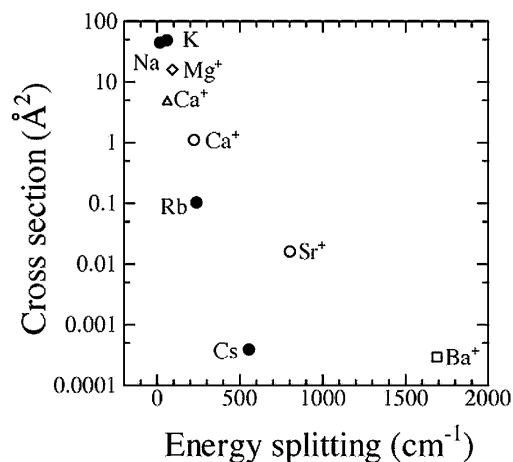
Figure 1. Fine structure changing cross sections so far measured for various alkali atoms and alkali earth ions in collisions with He atoms, as a function of their fine structure splittings; ● shows the one for the $np\ ^2P_{3/2} \to np\ ^2P_{1/2}$ transition of each alkali atom (n = 3, 4, 5 and 6, and the collision temperature T = 397, 368, 340 and 311 K for Na, K, Rb and Cs, respectively) (by Krause), ◇ Mg$^+$ $3p\ ^2P_{3/2} \to 3p$ $^2P_{1/2}$ at 1600 K (by Brust *et al.*), △ Ca$^+$ $3d\ ^2D_{5/2} \to 3d\ ^2D_{3/2}$ at 10000 K (by Knoop *et al.*), ○ Ca$^+$ $4p\ ^2P_{3/2} \to 4p\ ^2P_{1/2}$ and Sr$^+$ $5p\ ^2P_{3/2} \to 5p\ ^2P_{1/2}$ at 298 K (by Moriwaki *et al.*) and □ the present data.

II-D-2 Measurements of Fine Structure Changing Cross Sections of Ca$^+$, Sr$^+$ and Ba$^+$ Ions due to Collisions with H$_2$ and D$_2$ Molecules

**MORIWAKI, Yoshiki[1]; MATSUO, Yukari[2];
MORITA, Norio**
(*[1]Toyama Univ.; [2]RIKEN*)

Because of the vibrational and rotational degrees of freedom in molecules, fine structure changing transitions of ions due to collisions with molecules may show unique properties different from the ones in collisions with spherical atoms like He. For this reason, we have measured cross sections for such transitions of Ca$^+$, Sr$^+$ and Ba$^+$ ions in collisions with H$_2$ and D$_2$ molecules. The experimental procedure is almost the same as in the previous ion-He collision studies, except for filling the vacuum chamber with H$_2$ or D$_2$ gas instead of He. The cross sections obtained are summarized in Table 1. For the $np\ ^2P_{3/2} \to np\ ^2P_{1/2}$ transitions, as seen in Table 1, there are no drastic differences in the cross sections among each ion. This is completely different from the behavior seen in collisions with He. On the other hand, it is quite interesting that the ratio between the cross sections for the collisions with H$_2$ and D$_2$ decreases with the increase of the fine structure splitting, which is 222, 802 and 1690 cm^{-1} for Ca$^+$, Sr$^+$ and Ba$^+$, respectively. Considering this fact as well as the sizes of the splittings, we can find that not vibrational transitions but

rotational transitions of the molecules resonantly contribute to the collisional fine structure changing transitions of the ions. To confirm this, we have theoretically calculated the cross section ratios, based on a semi-classical theory (Anderson-Tsao-Curnutte theory) taking into consideration the degree of resonance between fine structure splittings of the ions and rotational transitions of the molecules. As seen in Table 1, the experimental ratios are well reproduced by our theoretical calculation.

Table 1. Fine structure changing cross sections of Ca$^+$, Sr$^+$ and Ba$^+$ due to collisions with H$_2$ and D$_2$.

Ion	Transition	Cross Sections (Å^2)		$\sigma(D_2)/\sigma(H_2)$	
		$\sigma(H_2)$	$\sigma(D_2)$	exp.	calc.
Ca$^+$	$4p\ ^2P_{3/2} \to 4p\ ^2P_{1/2}$	13.2 ± 0.6	18.7 ± 0.8	1.4	1.6
Ca$^+$	$4p\ ^2P_{1/2} \to 4p\ ^2P_{3/2}$	20.5 ± 0.9	27.1 ± 1.3	1.3	
Sr$^+$	$5p\ ^2P_{3/2} \to 5p\ ^2P_{1/2}$	22.7 ± 0.4	18.0 ± 0.4	0.82	0.7
Ba$^+$	$6p\ ^2P_{3/2} \to 6p\ ^2P_{1/2}$	11.5 ± 0.1	3.9 ± 0.2	0.33	0.3

II-E Endohedral Metallofullerenes: New Fullerene Molecules with Novel Properties

Encapsulation of one or more metal atoms inside hollow fullerene cages (endohedral metallofullerenes) has long attracted special attention because it could lead to new sperical molecules with novel properties unexpected for empty fullerenes. Great efforts have been made for the production and characterization of endohedral metallofullerenes. Up to now it has been demonstrated that group 2 and 3 metals and most lanthanide metals can be trapped inside the higher fullerenes to form soluble and relatively stable endohedral metallofullerenes. Because of the difficulty in producing pure samples in large quantities, the experimental characterization of endohedral metallofullerenes has been hindered. Recent important progress is marked by the successful isolation and purification of metallofullerenes in macroscopic quantities. This has made it possible to investigate the interesting electronic properties and chemical reactivities.

II-E-1 Structural Determination of the La@C_{82} Isomer

AKASAKA, Takeshi[1]; WAKAHARA, Takatsugu[2]; NAGASE, Shigeru[3]; KOBAYASHI, Kaoru[3]; WÄLCHLI, Markus[4]; YAMAMOTO, Kazunori[5]; KONDO, Masahiro[2]; SHIRAKURA, Shingo[2]; MAEDA, Yutaka[2]; KATO, Tatsuhisa; KAKO, Masahiro[6]; NAKADAIRA, Yasuhiro[6]; GAO, Xiang[7]; VAN CAEMELBECKE, Eric[7]; KADISH, Karl M.[7]
(*[1]IMS and Niigata Univ.; [2]Niigata Univ.; [3]Tokyo Metropolitan Univ.; [4]Bruker Japan; [5]PRN; [6]Univ. Electro-Commun.; [7]Univ. Houston*)

A stable diamagnetic monoanion of the La@C_{82} isomer was electrochemically prepared and isolated in order to disclose its cage symmetry. By measuring the ^{13}C NMR spectrum of the anion, it was determined for the first time that the isomer has C_s symmetry, as was also confirmed by density functional calculations.

II-E-2 Structure of La$_2$@C_{80} Studied by La K-Edge XAFS

KUBOZONO, Yoshihiro[1]; TAKABAYASHI, Yasuhiro[1]; KASHINO, Setsuo[1]; KONDO, Masahiro[2]; WAKAHARA, Takatsugu[2]; AKASAKA, Takeshi[3]; KOBAYASHI, Kaoru[4]; NAGASE, Shigeru[4]; EMURA, Shuichi[5]; YAMAMOTO, Kazunori[6]
(*[1]Okayama Univ.; [2]Niigata Univ.; [3]IMS and Niigata Univ.; [4]Tokyo Metropolitan Univ.; [5]Osaka Univ.; [6]PRN*)

The structure of La$_2$@C_{80} is studied by La K-edge XAFS from 40 to 295 K. The distances between the La atom and the first nearest C atoms, and between the La atom and the second nearest C atoms have been determined to be 2.42(1) Å at 40 K and 2.44(2) Å at 295 K, and 2.97(2) Å at 40 K and 2.98(3) Å at 295 K, respectively. The La–La distance has also been determined to be 3.90(1) Å at 40 K and 3.88(2) Å at 295 K. The dynamical behavior of two La atoms in the C_{80} cage is also studied based on the temperature dependence of the mean-square displacement of La–C.

II-F Electron Transfer Regulation in a Tetraheme-Cytochrome, Cytochrome c_3

Cytochrome c_3 is an electron transport protein found in several spacies of sulfate-reducing bacteria. This protein is a small (M.W. ≈ 14,000) soluble protein and posses four *c*-type hemes per molecule. Cytochrome c_3 has unique properties. It shows very low oxidation-reduction (redox) potentials (typically, –240 ~ –357 mV *vs.* NHE), and the solid film of the reduced cytochrome c_3 was shown highly electro-conductive. The macroscopic and microscopic redox potentials were determined for for a variety of sulfate-reducing bacteria. The major aims of this project is to elucidate the mechanism of the regulation of the electron transfer in cytochrome c_3 on the basis of tertiary structure. For this purpose, we have established a new and efficient expression system of *c*-type multiheme cytochromes for the first time. By the use of this expression system, structural determination of the fully reduced cytochrome c_3 from *Desulfovibrio vulgaris* Miyazaki F by NMR and analysis of oxidation-reduction properties using amino acid replacement are going on.

II-F-1 A Simple, Rapid, and Highly Efficient Gene Expression System for Multiheme-Cytochromes *c*

OZAWA, Kiyoshi[2]; YASUKAWA, Fumiko[2]; FUJIWARA, Yumiko[2]; AKUTSU, Hideo[1,2]
(*[1]IMS and Osaka Univ.; [2]Yokohama Natl. Univ.*)

It is important to establish a simple and highly efficient gene expression system of *c*-type cytochromes for the wide variety of studies such as physicochemical analyses, bioelectronics, environmental chemistry, and biotechnology. Especially, a large-scale preparation of a multiheme cytochrome *c* and its related mutants such as the amino acid replacements are very difficult. The difficulty in preparing *c*-type cytochromes is due to the complexity of the protein maturation, which needs various specific enzymes such as signal sequence peptidase and heme lyase. For this reason the heterologous expression of a *c*-type cytochrome is a special challenge. Here, we have exploited the potential of *S. oneidensis* by using the pUC-type universal vectors for *E. coli* in the transformation and have established a much more efficient gene expression system. The genes of tetraheme cytochrome c_3 and hexadecaheme high molecular weight cytochrome *c* from *Desulfovibrio vulgaris* were overexpressed in *Shewanella oneidensis* MR-1 using pUC-type vectors to yield the periplasmic holoforms. Covalent multiheme attachments were successfully performed in *S. oneidensis*. Furthermore, it was shown that *S. oneidensis* could be directly transformed by a pUC-type vector of *E. coli* through electroporation. Transcription of the heterologous gene in *S. oneidensis* could be controlled by a *lac* promotor from *E. coli*. These results indicate that *S. oneidensis* can be used as an overexpression system for *c*-type multiheme-cytochrome genes using the well established genetic techniques in *E. coli*. In conclusion, a rapid, simple, and highly efficient gene expression system of *c*-type multiheme cytochromes in a heterologous host has been established. This system would open a new horizon in various studies such as electron transfer mechanism, bioelectronics, and environmental chemistry.

II-F-2 Structure Dertemination of the Fully Reduced Cytochrome c_3 From *D. vulgaris* Miyazaki F

HARADA, Erisa[1,2,3]; FUKUOKA, Yuki[3]; OHMURA, Tomoaki[4]; FUKUNISHI, Arima[3]; KAWAI, Gota[5]; FUJIWARA, Toshimichi[2]; AKUTSU, Hideo[1,2]
(*[1]IMS; [2]Osaka Univ.; [3]Yokohama Natl. Univ.; [4]Mitsubishi Heavy Industries; [5]Chiba Inst. Tech.*)

Heteronuclear NMR spectroscopy was used for calculation of the solution structural ferrocytochrome c_3 from *Desulfovibrio vulgaris* Miyazaki F (*Dv*MF). From 3D TOCSY-HSQC and NOESY-HSQC experiments, all ^{15}N and ^1H backbone signals except N-terminus and Pro residues were assigned. To complete side chain assignment, 2D DQF-COSY, TOCSY, and NOESY experiments were performed. A total number of 633 proton signals were assigned, which correspond to 97% of the total number of expected signals. At first, NOEs from NH signals were collected using 3D NOESY-HSQC spectra. Then 2D NOESY spectra were measured. In total, 2474 NOESY constrains were obtained. Eighty four restrains of the φ torsion angle obtained from an HMQC-J experiment were used for structure calculation. After structure calculations in the early stage, the restrains of the χ_1 torsion angle were added for 16 residues. These residues showed single dominant conformers in early structural calculations, which were consistent with the values of $J_{\alpha\beta}$, $J_{\alpha\beta}$ obtained from E-COSY experiments. The final 20 structures showed no restraint violations greater than 0.3 Å. The RMSD of the top 20 conformers was 0.37 Å for backbone atoms, and 0.95 Å for heavy atoms respect to the mean structure. Although the major folding was similar to each other for the solution structure of ferrocytochrome c_3 and the crystal structure of ferricytochrome c_3, the region involving heme 1 and heme 2 was different. This is consist with the reported solution structure of *Desulfovibrio vulgaris* Hildenborough ferrocytochrome c_3, which is highly homologous with *Dv*MF cytochrome c_3. From the backbone dynamic analysis, the average value of the S^2, in the reduced state is larger than that in the oxidized state, suggesting that backbone of *Dv*MF cytochrome c_3 is slightly more rigid in the reduced state than in the

oxidized state. However, the region involving heme1 and heme2 shows more flexibility in the reduced state than in the oxidized state.

II-G Application of Optical Vortices to Spectroscopy

II-G-1 Efficient Generation of Optical Vortices and the Application to Atom Manipulation

SASADA, Hiroyuki
(IMS and Keio Univ.)

Recently optical vortices have attracted considerable attentions because of the phase singularity and the characteristic intensity distribution. In particular, the dark region is very useful to trap and guide cold atoms provided by laser cooling.[1] Several methods of generating the optical vortices have been reported so far, but their efficiencies are rather low.

We have demonstrated a simple and efficient generation of optical vortices using only glass plates and an astigmatic mode converter. A Gaussian beam successively passes N edges of thin glass plates, each of which imposes a π-phase difference to a part of the beam transmitting through the glass plate from the other part traveling in the air. The resultant beam has N nodal lines, and then is further led into a mode converter, which provides N appreciable optical vortices. The power efficiency is measured to be 72, 64, and 53% for $N = 1$, 2, and 3, respectively.

Reference
1) T. Kuga, Y. Torii, N. Shiokawa, T. Hirano, Y. Shimizu and H. Sasada, *Phys. Rev. Lett.* **78**, 4713 (1997).

II-H Molecular and Electronic Structures of Metallofullerenes

The continued interest in radical ions of fullerenes and metallofullerenes has resulted from the discovery of superconductivity in the CT complexes of alkali metals with fullerenes. Spectroscopic information concerning the electronic and spin states of the metallofullerenes has been obtained by cw- and pulsed-EPR measurements.

II-H-1 High-Field/High-Frequency ESR Study of Gd@C_{82}

FURUKAWA, Ko; OKUBO, Shingo; KATO, Tatsuhisa; KATO, Haruhito[1]; SHINOHARA, Hisanori[1]
(*[1]Nagoya Univ.*)

The X-band ESR investigations of La@C_{82}, Y@C_{82}, and Sc@C_{82} have been reported. In these metallofullerenes, the electronic structures of the metal atoms are described as $nd^1(n+1)s^2$. They have been reported that these metallofullerenes have the doublet ground states originating in the organic π radical of the C_{82} trianion via the electron transfer from metal atoms to C_{82} cage. On the other hand, the electronic structure for Gd atom is described as $4f^75d^16s^2$, and the ground high-spin state is expected. Our purpose in this work is the examination of the spin state of Gd@C_{82} and of the cage effect of the fullerene C_{82}. Highly purified Gd@C_{82} was obtained by high performance liquid chromatographic (HPLC) method. We examined Gd@C_{82} in CS_2 solutions in terms of X- and W-band ESR spectroscopy. Figure 1 shows the X-band ESR spectrum for Gd@C_{82} in CS_2 solution at 1.5 K. The spectrum pattern corresponds to that for the high-spin systems with large fine structure. The unsymmetrical spectral feature was given because of the large zero-field splitting parameter D and E, and prevented us from an easy spectral simulation. The W-band ESR measurement was performed to simplify the spectrum of Gd@C_{82}.
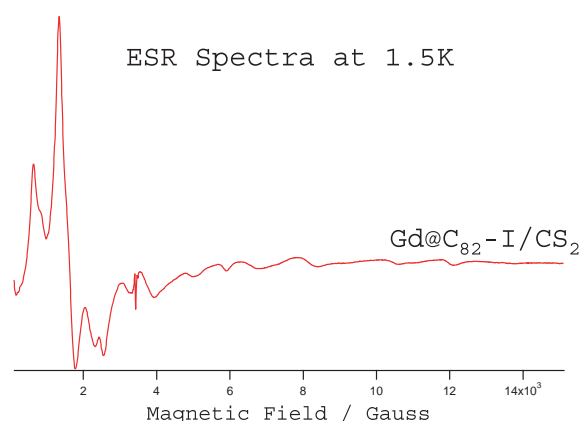
A paramagnetic metallofullerene is a nice building block for a molecular magnet. Wrapping of a metallofullerene with larger π-conjugated molecular envelopes is of great interest, which may lead to an extension of the super-molecular magnet in a 3D-fashion. Tokyo group of authors has synthesized a cyclic dimmer of metalloporphyrin,[1] as shown in the figure, and reported the big association constant of 6.7×10^5 M^{-1} for the inclusion complex of a cyclic dimmer of zinc porphyrin with C_{60} in benzene solution. The big association properties would come from the flexibility of linkers between two porphyrins. The hexamethylene linkers of the dimmer were folded to adjust the porphyrin-porphyrin distance, and the pophyrin maclocycles were slightly distorted from the planar structure so as to fit the shape of C_{60}. The electron spin state of an inclusion complex of a cyclic dimmer of metalloporphyrin with metallofullerene was investigated by means of pulsed electron spin resonance (ESR) measurement. The direct experimental evidence of the coupled spin state of $S = 3/2$ was obtained for the cyclic dimmer of copper-porphyrin with La@C_{82} by the nutation measurement of pulsed ESR. A big variety would be expected for the spin state of the inclusion complex in terms of the combination of metals on a porphyrin and a fullerene.

Reference
1) K. Tashiro, T. Aida, J.–Y. Zheng, K. Kinbara, K. Saigo, S. Sakamoto and K. Yamaguchi, *J. Am. Chem. Soc.* **121**, 9477 (1999).

ESR Spectra at 1.5K

Gd@C_{82}-I/CS_2

Magnetic Field / Gauss

Figure 1. The X-band ESR spectrum for Gd@C_{82} in CS_2 solution at 1.5 K.

II-H-2 Spin State of an Inclusion Complex of a Cyclic Dimer of Metalloporphyrin with La@C_{82}

TOYAMA, Namiki; KATO, Tatsuhisa; AKASAKA, Takeshi[1]; TASHIRO, Kentaro[2]; AIDA, Takuzo[2]
(*[1]Univ. Tsukuba; [2]Univ. Tokyo*)
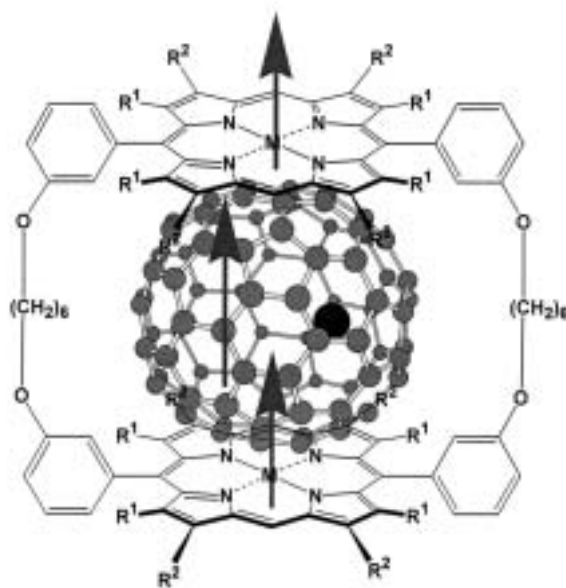
Figure 1. Molecular model of an inclusion complex of a cyclic dimmer of metalloporphyrin with metallofullerene La@C_{82}.

II-I High Field and Pulsed Electron Spin Resonance Spectroscopy

Electron spin resonance (ESR) spectroscopy has been a powerful technique for the characterization of radical species. The modern development of EPR spectroscopy enables us to investigate the heterogeneous and disordered system in detail. Especially the high frequency and pulsed EPR methods achieve the substantial resolution enhancement of spectrum. The advanced EPR spectroscopy is applied to study on the reaction mechanism in the heterogeneous system and the detection of the dication species.

II-I-1 Radical Products in Mechanochemical Dechlorination of Hazardous Organochlorine on CaO Surface

KATO, Tatsuhisa; IKOMA, Tadaaki[1]; ZHANG, Qiwu[2]; SAITO, Fumio[2]; AKIYAMA, Kimio[1]; TERO-KUBOTA, Shozo[1]
(*[1]Inst. Chem. React. Sci., Tohoku Univ; [2]Inst. Adv. Mater. Process., Tohoku Univ.*)

It is widely recognized that hazardous chlorinated organic compounds such as poly-chloro-dibenzopara-oxin (dioxin), poly-chloro-benzofuran and coplanar poly-chloro-biphenyl (PCB) are the most dangerous pollutants to our environment and health. Such great concern has led to many investigations for the complete decomposition of these toxic compounds. Recently mechanochemical method with alkaline earth metals (Mg, Ca) or their oxides have attracted attention as a practically simple and useful process to degrade chlorinated organic compounds. It is, therefore, desired to investigate the reaction mechanism of the mechanochemical dechlorination that is a solid state reaction. The advanced EPR spectroscopy is applied to study the reaction mechanism in the mechanochemical dechlorination of organochlorine using inorganic reactants. For the first time, we detected the paramagnetic products created by grinding 3-chlorobiphenyl (BP-Cl) with calcium oxide (CaO) as reactant in a ball mill, which is one of the promising ways to detoxify hazardous chlorinated organic compounds. Those products were attributed to phenoxy radicals coming from BP-Cl and trapped electrons in oxygen vacancies on the reactant surface by using high frequency and pulsed electron paramagnetic resonance spectroscopies. A radical mechanism for the destruction of organochlorine was proposed, since the good correlation between the dechlorination efficiency and the radical yield were observed. The mechanical stressing may induce the electron transfer from O^{2-} site on the surface of CaO to organic compounds and the produced organic anion radicals undergo an effective self-dissociation of the chlorine-carbon bond.

II-I-2 Facile Synthesis, Crystal Structures, and High-Spin Cationic States of All-*para*-brominated Oligo(*N*-phenyl-*m*-aniline)s

KANEMOTO, Katsuichi; KATO, Tatsuhisa; ITO, Akihiro[1]; INO, Haruhiro[1]; TANAKA, Kazuyoshi[1]
(*[1]Kyoto Univ.*)

Syntheses of both the dimer (**3**) and the trimer (**4**) of all-*para*-brominated poly(*N*-phenyl-*m*-aniline)s (**2c**) were achieved in a one-pot procedure from the parent non-brominated oligomers andbenzyltrimethyl-ammonium tribromide (BTMA·Br$_3$), see Scheme 1. An X-ray crystallographic analysis revealed that **4** has a U-shaped structure, suggesting that **2c** easily adopts helical structures. Furthermore, the redox properties were investigated by the UV-vis and EPR measurements. It was confirmed that the both **3** and **4** can be oxidized into the dications **3**$^{2+}$ and **4**$^{2+}$ with triplet spin-multiplicity. In order to identify the spin multiplicity of this species, we adopted the pulsed EPR method based on the fact that the magnetic moments with distinct spin quantum numbers (*S*) precess with their specific nutation frequency (ω_n) in the presence of a microwave irradiation field (B_1) and a static magnetic field (B_0). Figure 1 shows the relation between the EPR spectra observed at 5 K and its transient nutation spectra in a 2-D contour representation. Namely, the projection on the magnetic field axis corresponds to the usual EPR spectrum, while the projection on the frequency axis to the nutation spectrum. The intense peak observed at 3410 G (3415 G) is expected to be |1/2, +1/2> ↔ |1/2, –1/2> transition of the doublet species **3**$^+$ (**4**$^+$) and had the nutation frequency of 30.0 MHz (30.0 MHz), indicating $\omega_1 = 30$ MHz. On the other hand, two peaks at 3325 and 3510 G (3395 and 3445 G) had the same nutation frequency of 43.8 MHz (43.9 MHz), suggesting the presence of a high-spin cationic species of **3** (**4**). Here, the frequency ratio (ω_n/ω_1) of 43.8/30.0 (43.9/30.0) is in good agreement with the ratio of $\sqrt{2}$ expected for |1, 0> ↔ |1, ±1> transition of the triplet state. As a result, the high-spin species generated by excess of SbCl$_5$ can be regarded as **3**$^{2+}$ (**4**$^{2+}$).

Figure 1. Field-swept electron spin nutation spectra of (a) **3** and (b) **4** oxidized by excess $SbCl_5$ in CH_2Cl_2 at 5 K. ω_1 corresponds to 30 MHz.

Scheme 1. Molecular structures of aromatic amines.

II-J State Correlated Raman Spectroscopy

The vibrational Raman polarizability tensor responds to molecular reorientational relaxation process, and the structural environment in condensed media. The measurement of Raman scattering is a powerful technique for the study of molecular motion and of the mechanism of phase transition. We've built up the system of multichannel type detection of Raman scattering combined with the temperature controlled cell.

II-J-1 Probable Langevin-Like Director Reorientation in an Interface-Induced Disordered *SmC**-Like State of Liquid Crystals Characterized by Frustration between Ferro- and Antiferroelectricity

HAYASHI, Naoki; KATO, Tatsuhisa; AOKI, Takayuki[1]; ANDO, Tomohiro[1]; FUKUDA, Atsuo[1]; SEOMUN, San-Seong[2]
(*[1]Shinshu Univ.; [2]Univ. Dublin*)

To clarify the thresholdless, hysteresis free V-shaped switching due to frustration between ferro- and antiferroelectricity, we have studied a prototype binary mixture system. The apparent orientational order parameters, $<P_2>$ and $<P_4>$, obtained from polarized Raman scattering in thin homogeneous cells indicate that substrate interfaces induce some randomization of local in-plane directors at the tip of the V. Their correlation length, $\xi_{\parallel} \approx 3.5$ nm and $\xi_{\perp} \approx 75$ nm, have been estimated by assuming the Langevin-like reorientation. Because of the much shorter $\xi_{\parallel}$ and $\xi_{\perp}$ than the visible light wavelength, the switching process looks uniform.

II-J-2 Orientational Distributions in Smectic Liquid Crystals Showing V-Shaped Switching Investigated by Polarized Raman Scattering

HAYASHI, Naoki; KATO, Tatsuhisa; AOKI, Takayuki[1]; ANDO, Tomohiro[1]; FUKUDA, Atsuo[1]; SEOMUN, San-Seong[2]
(*[1]Shinshu Univ.; [2]Univ. Dublin*)

The polarized Raman scattering of two types of liquid crystals showing the thresholdless, hysteresis-free V-shaped electro-optic response in thin homogeneous cells was measured in the temperature range of antiferroelectric smectic phase. One sample was one component of Inui mixture [compound **a** in the Figure 1(A)] and the other was so-called Mitsui mixture [Figure 1(B)]. The apparent orientational order parameters, $<P_2>$ and $<P_4>$ were evaluated for the C–C stretching mode of phenyl ring. The obtained order parameters at the tip of the V-shaped switching were $<P_2> = 0.70$ and $<P_4> = 0.35$ for the compound **a**, $<P_2> = 0.59$ and $<P_4> = 0.20$ for the Mitsui mixture. The model calculations confirmed two extreme distribution of the local in-plane director at the tip of the V. The compound **a** exhibited a small distribution, while the Mitsui mixture did a very large distribution. The difference in the distribution of two types of liquid crystals at the tip of the V was explained by the barrier between synclinic and anticlinic ordering in adjacent layers. The small barrier gave a large distribution at the tip of the V in the dynamic switching, consequently triggered the V-shaped switching even in the first run. On the other hand, the large barrier did a small distribution and the tristable switching.

(A)

cryst. (ca. -31°C) anti* (31°C) ferri* (36°C) SmA (46°C) iso.

Inui mixture, a:b:c = 40:40:20 (by weight)

SmC$_A$* (43°C) SmX* (64°C) SmA (69°C) iso.

(B)

Mitsui mixture, d:e = 63:37 (by weight)

free-standing film; SmI* (32°C) ferri* (34°C) AF* (56°C) FI* (59°C) SmC* (79°C) SmA (100°C) iso.
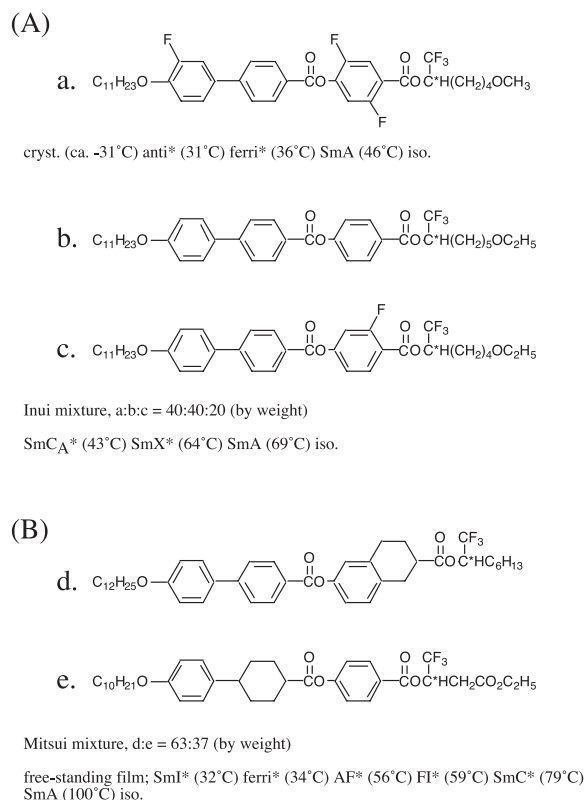
Figure 1. The Inui mixture (A) and the Mitsui mixture (B).

RESEARCH ACTIVITIES III
Department of Electronic Structure

III-A Photochemical Synthesis of Exotic Organo-Metallic Clusters with Magnetic Properties

We have succeeded to generate cluster molecular magnets of $(Co)_x(CH)_y(CH_2)_z$. Although information on the structure of the cluster molecules is not enough, *ab initio* molecular orbital calculation of $(Co)_4(CH)_4(CH_2)_4$ at B3LYP/6-31G level has suggested a deformed cubane type structure that is composed of four cobalt atoms bridged with CH carbon atoms and CH_2 groups coordinate with the cobalt atoms. Photochemical treatment of $C_5H_5Co(CO)_2$ in dichloromethane generated cobaltocene ($C_5H_5CoC_5H_5$) and $(Co)_x(CH)_y(CH_2)_z$ with keeping the chemical balance of Co atoms. The latter species became magnets at temperatures lower than 5 K in a matrix of cobaltocene and its derivatives, showing a hysteresis curve characteristic of single molecular magnets: free rotation for the inversion of external magnetic field across zero field and making their cavities wider suited for rotation. Photochemical treatment of $Co_4(CO)_{12}$ in dichloromethane produced $(CoCHCH_2)_4$. The black solid product exhibited residual cohesive magnetization with a blocking temperature of 16 K. Electronic structure of these compounds is also very interesting in relation to the origin of ferromagnetism in such cluster molecular magnets.

III-A-1 Photochemical Generation of Cluster Molecular Magnets: $(CoCHCH_2)_4$

HINO, Kazuyuki[1]; KOSUGI, Kentaroh; SEKIYA, Hiroshi[1]; HOSOKOSHI, Yuko; INOUE, Katsuya; NISHI, Nobuyuki
(*[1]Kyushu Univ.*)

Development of molecular level magnets is one of the recent topics in nanoscience and nanotechnology. In order to make magnetic molecules with high spin quantum numbers, we forcus our attention to cobalt atoms composed of 7 electrons in 3d orbitals and 2 electrons in the 4s orbital. A carbonyl compound $Co_4(CO)_{12}$ was dissolved in dichloromethane solution and high pressure mercury lamp with UV cut-off filter irradiated the solution in a closed glass vessel with a gas exhaust valve. The product solution was mixed with a large amount of anthracene for embedding product molecules in anthracene matrix. The solution was introduced into a new mass spectrometer (see AR2000, III-A-2) through a liquid chromatograph pump and the solute species were deposited as a helical belt on a titanium drum that was rotating and translating in a sample chamber under vacuum. On the opposite side of the drum, after the rotation of 180°, the solute species were photoionized and desorbed by 355 nm laser pulses. Then the ions were introduced to a reflectron mass spectrometer. The mass number of the main product was 344, and assigned to $(CoCHCH_2)_4$. The solid formed in the reaction vessel was filtrated by using a Millipore filter with a pore size of 0.2 μm. Magnetic properties of the solid photoproducts were measured with a SQUID magnetometer (Quantum Design MPMS-7S).

Figure 1-a shows $\chi_g T$ change of the photoproducts against temperatue, where χ_g is mass succeptibility. It is composed of two kinds of magnetic species. One exhibits antiferromagnetic behavior: the $\chi_g T$ value increases with increasing temperature, while the other behaves ferromagnetically at temperatures lower than 30 K. The former component is highly soluble in dichloromethane, whereas the latter is prone to precipitate in the solution. The $\chi_g T$ change of the washed precipitate shows a maximum value of 3.8×10^{-2} emu g^{-1} K at 20 K. Figure 1-b shows magnetization curves upon temperature cooling with or without magnetic field at 10 Oe. The field cooling aligns the molecular magnets along the magnetic field at temperatures lower than the blocking temperature, 16 K, where the zero-field cooling shows maximum magnetization with reducing magnetization at lower temperatures due to random orientation of the magnets. Figure 1-c shows a hysteresis curve of the magnetization. Although both the residual magnetization and the coercive force are small as compared with pure metallic magnets, the hydrogenated carbon-cobalt clusters with 4 cobalt atoms behave as magnets at temperatures lower than 16 K. In order to raise the blocking temperature, we have to increase the number of cobalt atoms up to several tens in the clusters with keeping cubane type frameworks. The origin of generating a high spin angular momentum is expected to the heavy charge transfer from cobalt atoms to carbon atoms on the basis of our molecular orbital calculation and XPS studies.
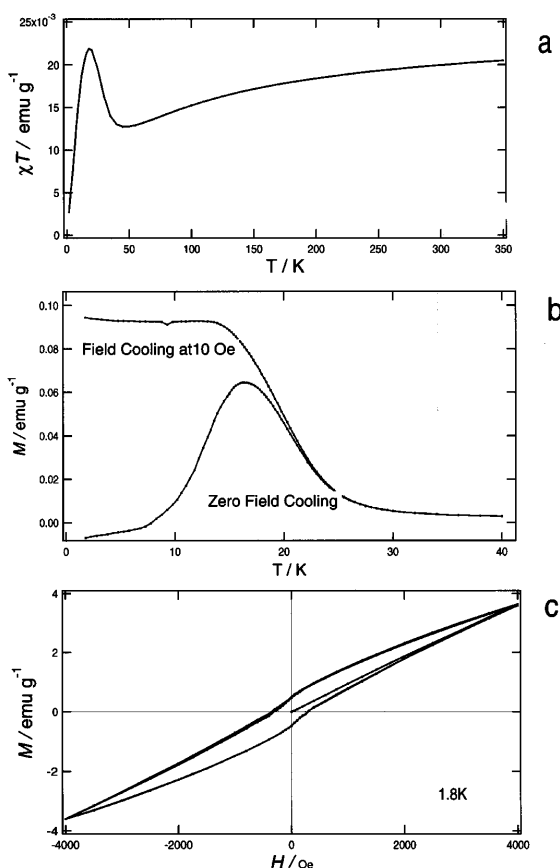
Figure 1. Magnetic properties of photoproducts from $Co_4(CO)_{12}$ and CH_2Cl_2; a: $\chi_g T$ as a function of temperature, b: Magnetization upon field cooling at 10 Oe (upper curve) and on zero field cooling (lower trace), c: hysteresis curve.

III-A-2 Magnetic Behavior of Single Molecular Magnets (Hydrated Carbon-Cobalt Clusters) Isolated in a Glassy Matrix of Cobaltocene and Its Derivatives Generated from Photochemical Reaction of $(C_5H_5)Co(CO)_2$ in Dichloromethane

HINO, Kazuyuki[1]; KOSUGI, Kentaroh; SEKIYA, Hiroshi[1]; HOSOKOSHI, Yuko; INOUE, Katsuya; NISHI, Nobuyuki
([1]Kyushu Univ.)

Photochemical reaction of $(C_5H_5)Co(CO)_2$ in dichloromethane exhibited release of CO and the following condensation reaction producing cobaltocence, $(C_5H_5)Co(C_5H_5)$, and $Co_x(CH)_y(CH_2)_z$. The latter cluster products could be generated by the photochemical reaction of solvated cobalt atoms with releasing Cl atoms from reaction intermediates. Secondary reactions also produce bicobaltocene and related compounds, $(C_5H_5)Co(C_5H_4–C_5H_4)Co(C_5H_5)$, $(C_5H_5–C_5H_4)Co(C_5H_4–C_5H_5)$, $(C_5H_5)Co(C_5H_4–C_5H_5)$, making the solid products glassy. Very fine particles were observed by a scanning electron microscope as spherical balls of the order of several hundred nm. Although the concentration of the hydrogenated carbon-cobalt clusters, $Co_x(CH)_y(CH_2)_z$, is higher in the filtrate solution, the fine particles also contains the clusters as much as approximately 5% of cobaltocene matrices as found by the laser ionization/desorption mass spectrometry of the solid products.

The $\chi_g T$ change of the fine particles behaved as a superparamagnetic material showing beautifully flat plateau at a level of 0.01 emu g^{-1} K in the temperature range from 50 K to 350 K. At the lower temperatures it increases exhibiting a maximum at 6 K as high as 0.05 emu g^{-1} K. The blocking temperature of 6 K was obtained from the ac magnetization measurement. The hysteresis curve is shown in Figure 1-a. One can see the following very intersting features characterisic of single molecular magnets in a matrix composed of bulky molecules: 1; the magnetization loop obtained after several cycles of external field modulation is located much higher than the initial magnetization rise curve, 2; at 0 (±10) Oe the magnetization decreases very quickly . These features indicate that the alighnment and the rotation of magnetic molecules following the change of the external magnetic field make the space for the magnetic molecules suited for free rotation. The orientational alignment of the spin axes of the magnets became much better when the magnets have experienced rotations forced by the change of the external magnetic field. The blocking temperature is much lower than that observed for the matrix free bulk compound as shown in III-A-1, while the residual magnetic moment at 0 Oe is much larger than the bulk material.
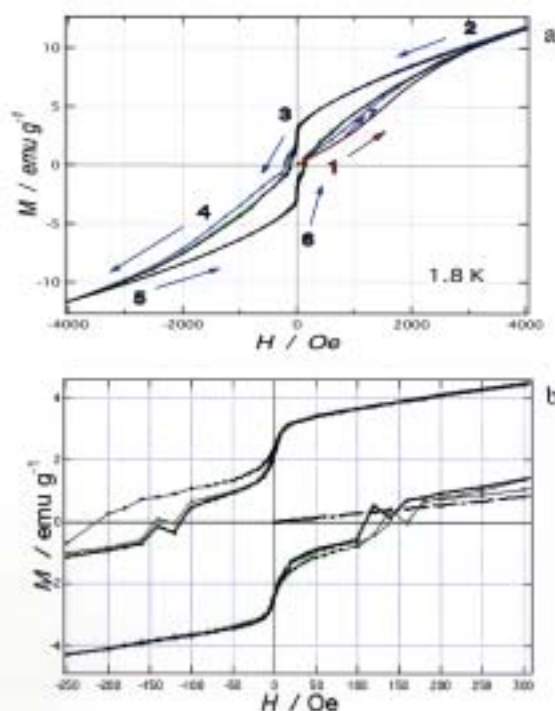
Figure 1. a: Magnetic moment hysteresis observed for $Co_x(CH)_y(CH_2)_z$ magnets in a matrix composed of $(C_5H_5)Co(C_5H_5)$ and its derivatives. Note that the initial magnetization curve is located lower than that the second magnetization loop. b: Expanded view around low magnetic field.

III-A-3 Photochemical Generation of High Spin Clusters in Solution: (Cyclopentadienyl-Vanadium)$_m$O$_n$

HINO, Kazuyuki[1]; INOKUCHI, Yoshiya; KOSUGI, Kentaroh; SEKIYA, Hiroshi[1]; HOSOKOSHI, Yuko;

INOUE, Katsuya; NISHI, Nobuyuki
(*[1]Kyushu Univ.*)

Organometallic clusters containing oxygen atoms, $(CpV)_mO_n$ ($Cp = C_5H_5$), are generated by photochemical reaction of $CpV(CO)_4$ in CH_2Cl_2 solution under control of oxygen contents. Mass spectra of single batch reactions exhibit strong signals assigned to low mass oxide clusters; $(CpV)_4O_4$, $(CpV)_5O_6$, and $(CpV)_6O_n$ ($n = 6\sim8$). Successive addition of reactant solution into the photochemical reaction vessel shows the addition of $(CpV)_{m'}$ to the low mass oxide clusters producing $(CpV)_mO_n$ ($m \gg n = 4\sim7$). The magnetic susceptibility (χ_g) of the mixture of the former low mass products shows antiferromagnetic behavior, while that of the latter high mass products is as high as 4.6×10^{-4} cm^3 g^{-1} at 10 K and the additional part due to high mass products behaves ferromagnetically at temperatures higher than 70 K.

III-B States of Neutral and Ionic Molecular Associates in Solutions

States of molecular associates particularly in aqueous solutions are of great importance in understanding the role of molecules in living organisms. We found that any ideally mixed state cannot be seen in protic-protic mixtures such as water-alcohol, water-acetic acid, and alcohol-acetic acid systems on the molecular level at solute molar fractions (χ_A) higher than 0.001. In such a system, solute-solute asociation is highly favored resulting in microscopic phase separation. Here we demonstrate that aprotic solvent such as acetonitrile can produce ideally mixed state(s) for acetic acid.

III-B-1 States of Molecular Associates in Binary Mixtures of Acetic Acid with Aprotic Polar Solvents: the Nature of Mixture States at Molecular Levels

NAKABAYASHI, Takakazu; NISHI, Nobuyuki

The structures and dynamics of liquids have received much attention over the past three decades. Our recent studies of Raman spectroscopy have shown that binary solutions of acetic acid with protic solvents do not get ideally mixed on the molecular level at acetic acid molar fractions (χ_A) higher than 0.001. In aprotic polar solvents, however, the C=O stretching band of acetic acid shows the mixing ratio dependence different from that in protic solvents. Temperature dependence of the Raman spectra of the acetic acid and acetonitrile binary solution at $\chi_A = 0.01$ is shown in Figure 1. As the temperature grows, the 1725 cm^{-1} band shifts to a lower-wavenumber, while the 1754 cm^{-1} band shifts to a higher-wavenumber. The intensity of the 1754 cm^{-1} band relative to that of the 1725 cm^{-1} band becomes larger with increasing temperature. The relative intensity between the two bands is independent of the acid concentration. These results suggest that the two bands arise from two types of acetic acid monomers in different environment. To examine the two different types of acetic acid monomers in acetonitrile, ab initio calculations are carried out with self-consistent reaction field method (B3LYP/6311++G** level). The dipole moment of a dipolar molecule becomes larger on going from the gas phase to the acetonitrile solution. Thus the C=O bond of the acetic acid monomer becomes longer and its C=O stretching mode shifts to a lower-wavenumber in acetonitrile. However, the C=O mode of the cyclic dimer in Figure 1 shows a higher-wavenumber shift in acetonitrile, because of the decrease in the C=O⋯H–C interaction. These results indicate that the C=O band of the cyclic dimer shifts to a lower-wavenumber and that of the non-complexed acetic acid monomer shifts to a higher-wavenumber as the solute-solvent electrostatic interaction decreases. The dielectric constant decreases with increasing temperature, which means that the electrostatic interaction becomes weaker as the temperature grows. Thus, the positional changes in Figure 1 can be explained when the 1725 and 1754 cm^{-1} bands are assigned to the cyclic dimer and the non-complexed acetic acid monomer, respectively. Such two bands are also observed in other aprotic polar solvents such as 1,4-dioxane, indicating that the two types of acetic acid monomers are also exist in other aprotic polar solvents. It is therefore concluded that acetic acid molecules preferentially exist as the monomeric forms in the aprotic polar solvents. This means that ideally-mixed states at molecular levels exist in the binary solutions of acetic acid and the aprotic polar solvents when the mole fraction of acet ic acid is small. From several spectroscopic studies on other binary solutions, the mixing rules at molecular levels may be proposed as follows: protic-protic binary mixtures do not easily become ideally-mixed states even when the mixing ratio is large, while ideally-mixed states at molecular levels appear in protic-aprotic polar binary mixtures at low concentrations of the protic solvent.
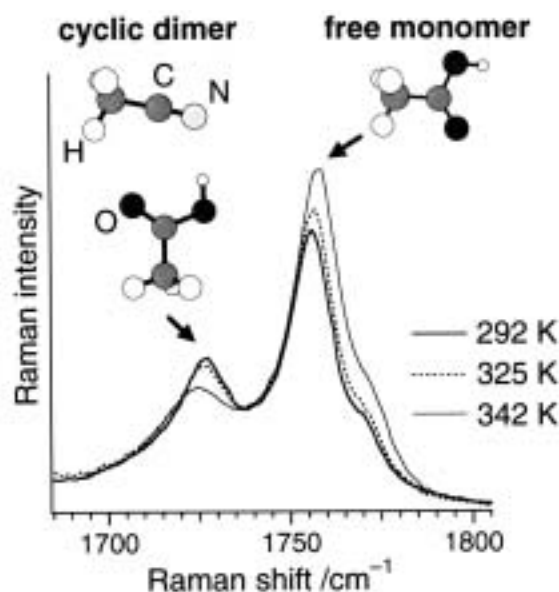
Figure 1. Temperature dependence of the C=O bands of the acetic acid and acetonitrile mixture.

III-B-2 Structure of Clusters in Methanol-Water Binary Solutions Studied by Mass Spectrometry and X-Ray Diffraction

TAKAMUKU, Toshiyuki[1]; YAMAGUCHI, Toshio[2];

ASATO, Masaki[3]; MATSUMOTO, Masaki[3]; NISHI, Nobuyuki
(Saga Univ.[1]; Fukuoka Univ.[2]; Kyushu Univ.[3])

The structure of clusters in methanol-water solutions in its dependence on the methanol mole fraction χ_M has been investigated by mass spectrometry on clusters isolated from submicron droplets by adiabatic expansion in vacuum and by X-ray diffraction on the bulk binary solutions. The mass spectra have shown that the average hydration number, (n_m), of m-mer methanol clusters decreases with increasing χ_M, accompanied by two inflection points at $\chi_M = \sim 0.3$ and ~ 0.7. The X-ray diffraction data have revealed a similar change in the number of hydrogen bonds per water and/or methanol oxygen atom at ~ 2.8 Å. On the basis of both results, most likely models of clusters formed in the binary solutions are proposed: at $0 < \chi_M < 0.3$ tetrahedral-like water clusters is the main species, at $0.3 < \chi_M < 0.7$ chain clusters of methanol molecules gradually evolve with increasing methanol content, and finery at at $\chi_M > 0.7$ the chain clusters of methanol molecules become predominant. The present results are compared with clusters previously found in ethanol-water binary solutions and discussed in relation to anomalies of the heat of mixing of methanol-water binary solutions.

III-C Ultrafast Dynamics and Structural Changes of Aromatic Cation Radicals

Release of an electron from a neutral molecule by photons induces eminent structural changes of the molecule and reorientation of solvent molecules. In particular, polar solvents stabilize the newly born cation due to Coulombic interaction causing thermal excitation of surrounding solvents and the cation. Geminate recombination of the ejected electrons and the parent cations is also expected. We have studied the ultrafast dynamics upon photoionization of aromatic molecules by time-resolved absorption and Raman spectroscopic techniques.

III-C-1 Ultrafast Relaxation Dynamics of Aromatic Cation Radicals Following Photoionization

NAKABAYASHI, Takakazu; KAMO, Satoshi[1]; SAKURAGI, Hirochika[1]; NISHI, Nobuyuki
([1]Univ. Tsukuba and IMS)

Photoionization in condensed phases has been a subject of interest for many years. Charge-pair generation, recombination, solvation and vibrational relaxation processes as well as cation structural changes can occur after photoionization of aromatic molecules in solvents. In the previous study, solvation and vibrational relaxation processes occurring on a picosecond time scale are discussed.[1] In the present study, we have measured femtosecond time-resolved absorption spectra of aromatic cation radicals (naphthalene, biphenyl, and 1,4-diphenylbutadiene) in nonpolar and polar solvents and discussed the dynamics of the photoionization in the

subpico- to picosecond time range. Figure 1 shows the time-resolved absorption spectra of the cation radical of naphthalene in cyclohexane. The broad absorption decays in several picoseconds, which can be attributable to the geminate recombination of the electrons with their parent cation radicals. The induced absorption in acetonitrile, however, shows the temporal profile different from that in cyclohexane. As shown in Figure 2, the absorption intensity first decreases in the subpicosecond range, and then increases on a 10–20 ps time scale. The absorption around 700 nm also shifts to a lower-wavelength with the delay time. The picosecond increase in the absorption intensity is observed in all the region of 600–740 nm. The temporal profile observed in ethyl acetate is similar to that in acetonitrile. The subpicosecond decay components can be ascribed to the geminate recombination of the unsolvated cation radical, which competes with the reorganization of solvent molecules. To our best knowledge, it is the first report to observe the ultrafast geminate recombination

of unsolvated aromatic cation radicals in polar solvents. The picosecond increase in the absorption intensity is observed in all the cation radicals treated, suggesting that the picosecond relaxation process increasing the cation absorption intensity occurs after the photoionization of the aromatic molecules. The time scale of the change in the absorption intensity is the same as that of the vibrational relaxation, while the intensity rise does not correlate with the dielectric relaxation time. The picosecond rise is significantly observed in highly polar solvents forming strong solvent–solute interactions. From these observations, we propose the model that the thermal excitation of the solvent shell disturbs the solvation structure of the cation radical, which causes the change in the cation absorption intensity. Contrary to the generally accepted view, this result suggests that the cation radical formed by the multi-photon ionization is solvated on a 10–20 ps time scale, because of the thermal excitation of the neighboring solvent shell.

Reference
1) T. Nakabayashi, S. Kamo, H. Sakuragi and N. Nishi, *J. Phys. Chem. A* in press.
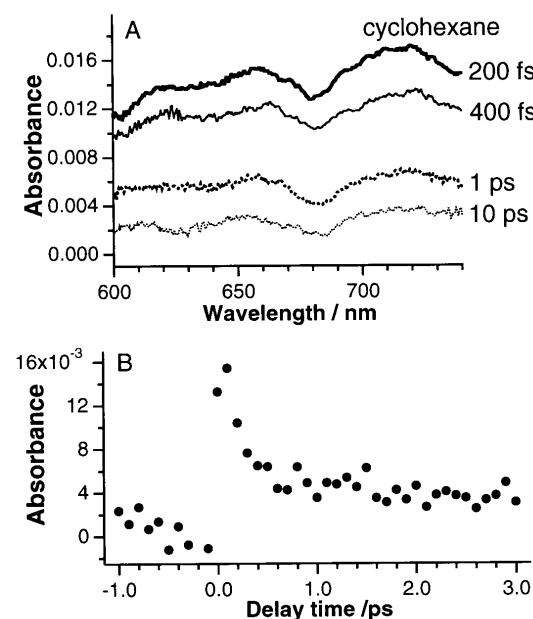
Figure 1. (A) Femtosecond time-resolved absorption spectra of naphthalene cation radical in cyclohexane. (B) Temporal profile of the absorbance due to naphthalene cation radical in cyclohexane at 685 nm.
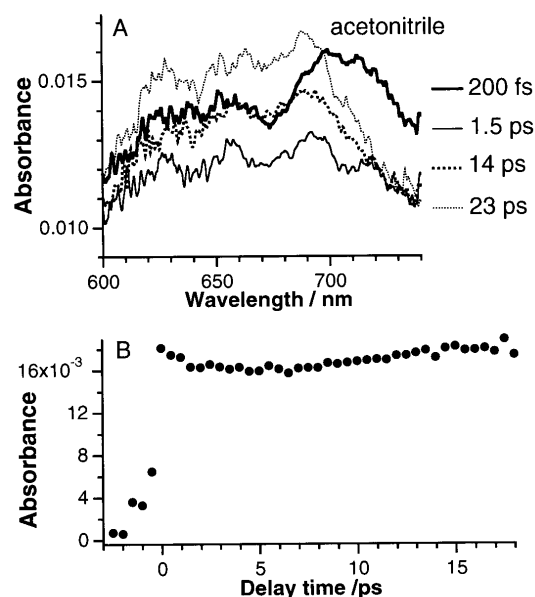
Figure 2. (A) Femtosecond time-resolved absorption spectra of naphthalene cation radical in acetonitrile. (B) Temporal profile of the absorbance due to naphthalene cation radical in acetonitrile at 685 nm.

III-D Spectroscopic and Dynamical Studies on Charge Delocalization and Charge Transfer in Molecular Cluster Ions

Electron deficiency of molecular cluster cations can attract electron rich groups or atoms exhibiting a charge transfer or a charge resonance interaction in the clusters. These interactions cause dynamical changes of structures such as proton transfer or ion-core switching in hot cluster ions.

III-D-1 Photodissociation Spectroscopy of Benzene Cluster Ions in Ultraviolet and Infrared Regions. Static and Dynamic Behavior of Positive Charge in Cluster Ions

INOKUCHI, Yoshiya; NISHI, Nobuyuki

Photodissociation spectroscopy is applied to benzene cluster ions in ultraviolet and infrared regions. In the ultraviolet photodissociation spectrum of $(C_6H_6)_3^+$, a characteristic broad band emerges at 255 nm. This band is assigned to a $\pi^* \leftarrow \pi$ transition of a solvent benzene molecule that exists in the trimer. This is in accord with a previous model of the ion cluster with a dimer ion core and a solvent benzene molecule. Infrared photodissociation spectra of $(C_6H_6)_n^+$ ($n = 3$–5) show a sharp band at 3066 cm^{-1}. The band is attributed to a C–H stretching vibration of the dimer ion core. The infrared spectra of $(C_6H_6)_n^+$ ($n = 3$–5) are fitted to model spectra produced by combining the C–H stretching bands of the dimer ion core and the solvent benzene molecule. Infrared photodissociation spectra of mixed benzene trimer ions with one or two benzene-d_6 molecules demonstrate that there is no correlation between the excited dimer ion core site in the trimer and the photofragment dimer ion species. This result implies that a dimer ion core switching occurs in photoexcited vibrational states prior to the dissociation.

III-D-2 Infrared Photodissociation Spectroscopy of Protonated Formic Acid-Water Binary Clusters, H$^+$·(HCOOH)$_n$·H$_2$O (n = 1–5). Spectroscopic Evidence of Ion Core Switch Model

INOKUCHI, Yoshiya; NISHI, Nobuyuki

Static and dynamic features of the positive charge distribution in cluster ions are very important, because they are related very much with the charge transportation in condensed phases. In this study, we apply infrared (IR) photodissociation spectroscopy to protonated formic acid-water binary clusters, H$^+$·(HCOOH)$_n$·H$_2$O (n = 1–5). We also investigate ab initio molecular orbital calculations to obtain optimized structures and theoretical IR spectra. By comparing the observed IR photodissociation spectra with the calculated ones, we discuss structures and an ion core switching process in these clusters.

The IR photodissociation spectra of H$^+$·(HCOOH)$_n$·H$_2$O (n = 1–5) are measured by using an ion guide spectrometer with two quadrupole mass filters. The MO calculations are performed by using the Gaussian 98 program package at B3LYP/6-31G(d,p) level.

Figure 1 shows the IR photodissociation spectra in 3100–3800 cm^{-1} region. For n = 1–3, there are two maxima in the IR spectra. We assign the low-frequency bands to free OH stretching vibrations of the formic acid molecules. The high-frequency bands are ascribed to asymmetric OH stretching vibrations of the water molecules. For n = 4, the high-frequency band disappears from the spectrum. For n = 5, no sharp bands exist in the spectrum. Because the free OH stretching band of water (the high-frequency band) is not observed for n = 4 and 5, the H$_2$O molecule is in the periphery of the clusters for $n \leq 3$, but it is located in an inner position of the clusters for $n > 3$. Furthermore, the theoretical calculations predict that the ion-core switch occurs from HCOOH$_2^+$ to H$_3$O$^+$ between n = 3 and 4. The most stable structures of n = 4 and 5 predicted by the theoretical calculations are also shown in Figure 1.

In the clusters of n = 4 and 5, the ion core is H$_3$O$^+$. The H$_3$O$^+$ ion core is thought to be unstable due to the lower proton affinity of water (165 kcal/mol) than that of formic acid (177.3 kcal/mol). However, the formic acid molecules surround and stabilize the H$_3$O$^+$ ion cores in the clusters. In summary, the ion core switch really occurs from HCOOH$_2^+$ to H$_3$O$^+$ between n = 3 and 4 in H$^+$·(HCOOH)$_n$·H$_2$O.
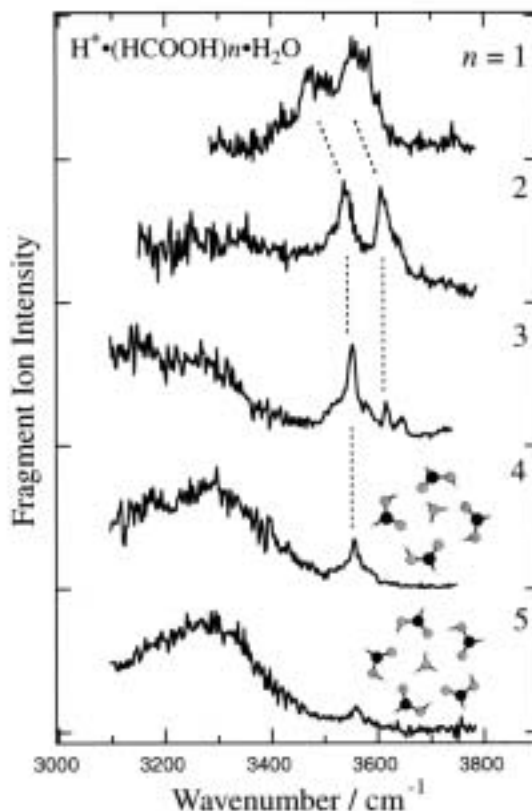
Figure 1.

III-D-3 Charge Transfer Interaction in Acetic Acid-Benzene Cation Complex

KOSUGI, Kentaroh; INOKUCHI, Yoshiya; NISHI, Nobuyuki

[*J. Chem. Phys.* **114**, 4805 (2001)]

Geometrical and electronic structures of acetic acid-benzene cation complex, (CH$_3$COOH)·(C$_6$H$_6$)$^+$, are studied experimentally and theoretically. Experimentally, a vibrational spectrum of (CH$_3$COOH)·(C$_6$H$_6$)$^+$ in the supersonic jet is measured in the 3000-3680 cm^{-1} region using an ion-trap photodissociation spectrometer. An electronic spectrum is also observed with this spectrometer in the 12000–29600 cm^{-1} region. Theoretically, ab initio molecular orbital calculations are performed for geometry optimization and evaluation of vibrational frequencies and electronic transition energies. The frequency of the strong band (3577 cm^{-1}) is close to that of the O–H stretching vibration of acetic acid and the weak one is located at 3617 cm^{-1}. On the basis of geometry optimizations and frequency calculations, the strong band is assigned to the O–H stretching vibration of the *cis*-isomer of acetic acid in

the hydrogen-bonded complex (horizontal *cis*-isomer). The weak one is assigned to the vertical *trans*-isomer where the *trans*-isomer of acetic acid interacts with the π-electron system of the benzene cation. The weakness of the high frequency band in the photodissociation spectrum is attributed to the binding energy larger than the photon energy injected. Only hot vertical *trans*-isomers can be dissociated by the IR excitation. The electronic spectrum exhibits two bands with intensity maxima at 17500 cm^{-1} and 24500 cm^{-1}. The calculations of electronic excitation energies and oscillator strengths suggest that charge transfer bands of the vertical *trans*-isomer can be observed in this region in addition to a local excitation band of the horizontal *cis*-isomer. We assign the 17500 cm^{-1} band to the charge transfer transition of the vertical *trans*-isomer and the 24500 cm^{-1} band to the π-π transition of the horizontal *cis*-isomer. The calculations also suggest that the charge transfer is induced through the intermolecular C···O=C bond formed between a carbon atom of benzene and the carbonyl oxygen atom of acetic acid.

III–E Synthesis and Characterization of Metal Clusters

Recently, metal clusters consisted of several tens or several hundreds of metal atoms have gained much attention as new nano-scaled materials because their properties are significantly different from the corresponding bulk and behave in a size-dependent manner. To exploit a synthetic method of metal clusters while controlling their size in an atomic level is a challenging task which will help us to understand the size-dependent properties of the clusters and open up many possibilities for the wide range of applications. We have addressed the issue by adopting the following approaches: 1) Chemical synthesis of the clusters in the presence of molecular capsules, which work as templates and stabilizers for the clusters and 2) characterization of the clusters by mass spectrometry. Our goal is to reveal the origin of the size-specific chemical reactions occurring on the surface of metal clusters.

III-E-1 Development of Mass Spectrometer for Metal Clusters Dispersed in Liquid Phase

NEGISHI, Yuichi; TSUKUDA, Tatsuya

Mass spectrometry is a powerful diagnostics for the metal clusters because it provides useful information complementary to that obtained from the conventional characterization by TEM; the cluster size and composition can, in principle, be characterized in an atomic resolution. We have constructed an apparatus consisting of electrospray ionization (ESI) source and time-of-flight (TOF) mass spectrometer with a reflectron as shown in Figure 1. Liquid sample containing the metal clusters is pumped through a fused silica capillary, whose end is supported in a stainless steel needle. Charged aerosol droplets are electrosprayed by

means of an electrical potential between the needle tip and a counter electrode (+3–5 kV). The cluster ions contained in the droplets are evaporated into the gas phase and further desolvated by passing through a heated capillary. A portion of the ion flow is skimmed and introduced into the acceleration region of the TOF mass spectrometer. Then, the ions are extracted in the direction perpendicular to the initial beam by applying a pulsed voltage of ~15 kV to a set of grids. The ions are stirred by several sets of ion optics and detected by either a microchannel plate (MCP) detector located at the end of the flight path of ~3.2 m (low-resolution mode) or another MCP detector with a center hole after reflected by the coaxial reflectron (high-resolution mode). Figure 2 shows a typical ESI mass spectrum of tetra-*n*-octylammonium bromide obtained in the high-resolution mode.
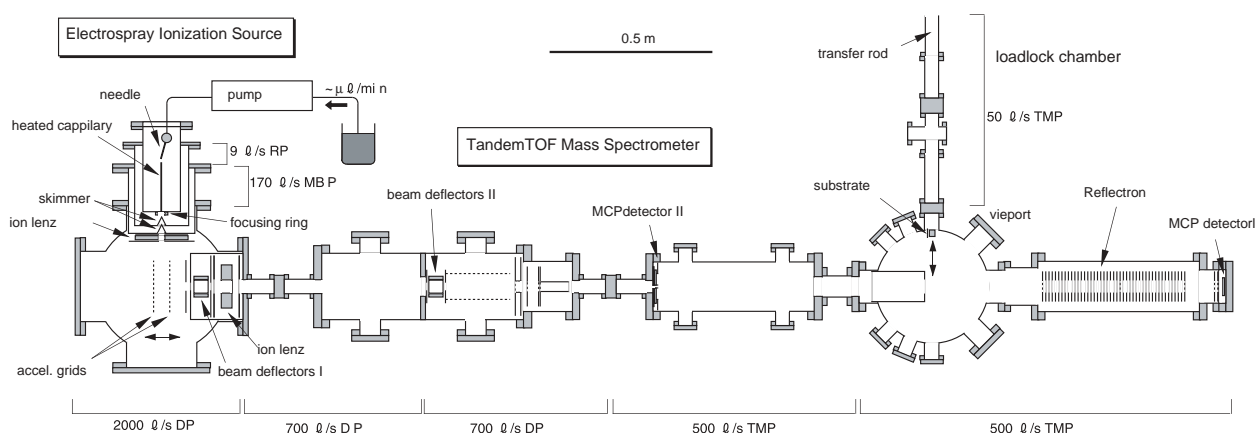
Figure 1. Schematic diagram of the experimental apparatus.
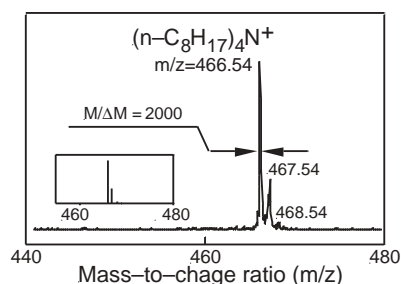
Figure 2. The positive-ion ESI mass spectrum of tetra-*n*-octylammonium bromide run in a methanol mobile phase. Inset shows the isotopic distribution of $(n\text{-}C_8H_{17})_4N^+$ calculated from the natural abundance. Mass resolution of $m/\Delta m \sim 2000$ is routinely achieved in the high-resolution mode.

III-E-2 Mass Spectroscopic Characterization of Transition Metal Clusters Encapsulated by PAMAM Dendrimers

NEGISHI, Yuichi; TSUKUDA, Tatsuya

Synthesis of metal nanoclusters using dendrimers as "nanotemplates" has been one of the most exciting topics in recent cluster chemistry.[1] The dendrimers are hyper-branched polymers, which are almost spherical in shape, sterically crowded on the exterior, and somewhat hollow on the interior. A strategy proposed for preparation of the dendrimer-encapsulated nanoparticles is rather simple:[1] Introduction of metal ions into the internal cavity of dendrimers followed by chemical reduction of the metal ions.
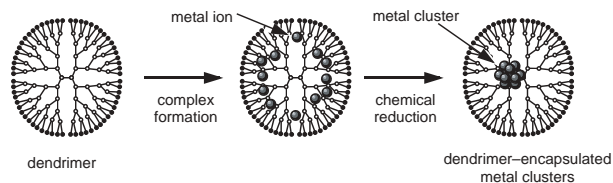
We have followed the synthetic procedures by ESI mass spectrometry. Figure 1A shows ESI mass spectra of OH-terminated poly(amido)amine dendrimers with a third generation (G3-OH). A series of prominent peaks discernible in Figure 1A are assigned to the multiply charged molecular ions of G3-OH with the ideal structure. Mass peaks interspersed between them are due to the G3-OH molecules with missing arms, which are present as contamination in the sample. Figure 1B shows mass spectrum of the complexes of G3-OH and silver ions, which are prepared by mixing 16-fold molar excess of $AgNO_3$. Clusters containing up to 10 Ag ions are recognizable whereas the larger clusters are not because of overlapping of the mass peaks due to the heterogeneity of the G3-OH sample. The chemical reduction of these complexes by $NaBH_4$ or hydrazine results in the formation of Ag clusters stabilized by G3-OH. The ESI spectrum obtained for the clusters is essentially the same with that of free G3-OH (Figure 1C). This observation suggests that the Ag clusters are passivated weakly by several G3-OH which are easily removed during the ES processes. It is conceivable that the aggregation of Ag(0) atoms proceeds outside the dendrimer because of low density of G3-OH surface and/or low partition coefficient of the Ag ions. Following studies are now underway in our group: 1) Purification of the dendrimers by gel permeation chromatography and 2) synthesis of nanoclusters by using dendrimers with higher generations having more dense surfaces.

Reference

1) R. M. Crooks *et al.*, *Topics in Current Chemistry* **212**, 81 (2001) and references therein.
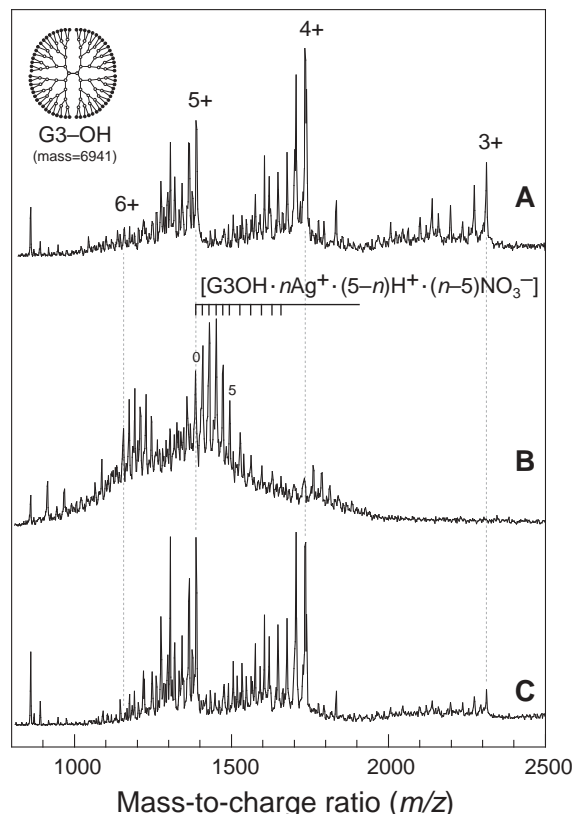
Figure 1. The ESI mass spectra of A) G3-OH PAMAM dendrimers, B) complexes between G3-OH and silver ions, C) silver clusters stabilized by G3-OH.

III-F Geometric and Electronic Structures of Negatively-Charged Molecular Clusters

The geometric and electronic structures of negatively-charged molecular clusters are among the most fundamental issues in cluster science: How do the molecular aggregates trap an excess electron and how do the structures evolve with cluster size? Among the systems studied so far, negatively-charged clusters of carbon dioxide, $(CO_2)_n^-$, have been a prototype system to address these issues. Some intriguing phenomena have been observed in the previous photoelectron spectroscopic studies of $(CO_2)_n^-$ (*Chem. Phys. Lett.* **268**, 429 (1997)): 1) Existence of distinct isomers having different anionic cores of CO_2^- and $C_2O_4^-$ ("electronic isomers"), 2) switching of the anionic core from CO_2^- to $C_2O_4^-$ and vice versa at $n = 7$ and 14, respectively ("core switching"), 3) spontaneous interconversion between $CO_2^- \cdot (CO_2)_5 \rightleftarrows C_2O_4^- \cdot (CO_2)_4$ at $n = 6$ ("electronic isomerization"). We have studied the structures of isomers for small $(CO_2)_n^-$ clusters and their isomerization processes by ab initio calculations. Structural evolution of $(CO_2)_n^-$ has been investigated by mass spectrometry.

III-F-1 *Ab initio* Study of $CO_2^- \cdot CO_2 \rightleftarrows C_2O_4^-$ Isomerization

SAEKI, Morihisa; TSUKUDA, Tatsuya; NAGATA, Takashi[1]
(*[1]Univ. Tokyo*)

[*Chem. Phys. Lett.* in press]

The potential energy surface relevant to the isomerization of $(CO_2)_2^-$ has been investigated by *ab initio* calculations including effects of electron correlation. The surface plotted against appropriate

angle parameters shows two shallow minima and a deep valley, which correspond to $CO_2^-\cdot CO_2$ (C_{2v}), $CO_2^-\cdot CO_2$ (C_s) and $C_2O_4^-$ (D_{2d}) structures, respectively. The transition states for the $C_{2v} \rightleftarrows C_s \rightleftarrows D_{2d}$ interconversion are located well below the $CO_2^- + CO_2$ dissociation limit, which allows $(CO_2)_2^-$ with sufficient internal energies to fluctuate among the isomeric forms. The calculations have also revealed quantitatively the behavior of the excess charge flow during the $CO_2^-\cdot CO_2$ $\rightleftarrows C_2O_4^-$ electronic isomerization.

Reference
1) M. Saeki, T. Tsukuda, S. Iwata and T. Nagata, *J. Chem. Phys.* **111**, 6333 (1999).
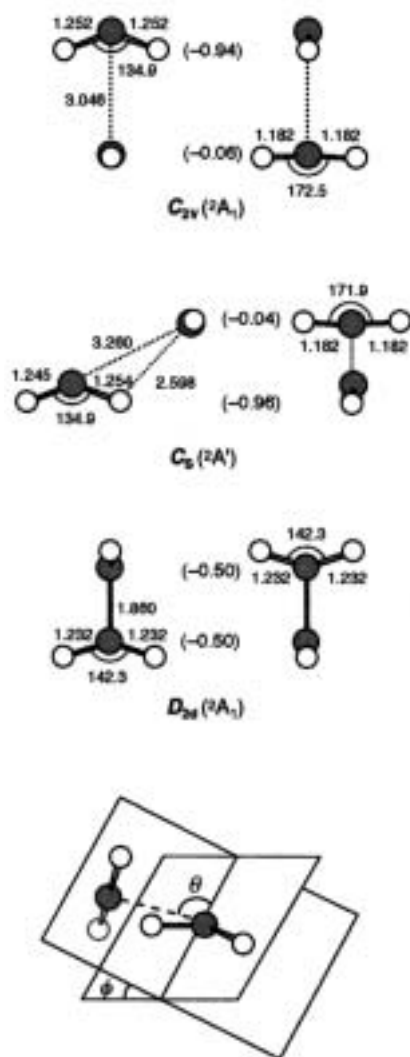
Figure 1. Top and side views of the geometries of $(CO_2)_2^-$ isomers optimized at the MP2/6-31+G* level (taken from reference 1). The digits in parentheses represent the Mulliken gross populations on the CO_2 moieties. Bond lengths and bond angles are given in Å and degrees. Also given in the figure are definitions of angle parameters θ and ϕ to describe the intermolecular motion during isomerization.
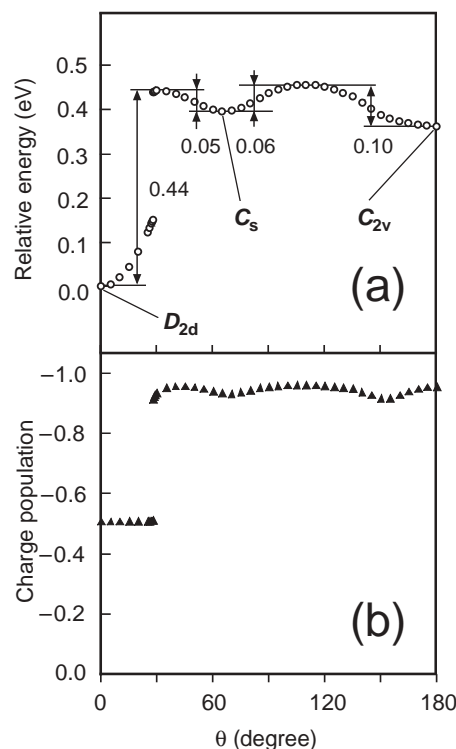
Figure 2. Potential profile along the minimum-energy path for the $(CO_2)_2^-$ isomerization (panel a) and the charge population at each transient structure (panel b) plotted against angle θ. The numbers in the panel (a) represent the barrier heights for the isomerization in electron volts. The charge population corresponds to the Mulliken gross populations on the CO_2 unit carrying a larger excess charge.

III-F-2 *Ab initio* Study of $(CO_2)_n^-$: Structures and Stabilities of Isomers

SAEKI, Morihisa; TSUKUDA, Tatsuya; NAGATA, Takashi[1]
(*[1]Univ. Tokyo*)

[*Chem. Phys. Lett.* **340**, 376 (2001)]

The geometrical structures and stabilities of $(CO_2)_n^-$ with the size range $3 \leq n \leq 6$ are investigated by *ab initio* calculations including effects of electron correlation. The calculations have shown that the structures of $(CO_2)_n^-$ can be formulated by either $CO_2^-\cdot(CO_2)_{n-1}$ or $C_2O_4^-\cdot(CO_2)_{n-2}$, and that the geometry of $(CO_2)_2^-$ dimer remains more or less in all the optimized structures. In all the sizes investigated in the present study, the most stable isomers are of the $C_2O_4^-\cdot(CO_2)_{n-2}$ form, being consistent with the results obtained in the photoelectron spectroscopic studies.[1]

Reference
1) T. Tsukuda, M. A. Johnson and T. Nagata, *Chem. Phys. Lett.* **268**, 429 (1997).

III-F-3 Structural Evolution of Large $(CO_2)_n^-$ Clusters as Studied by Mass Spectrometry

NEGISHI, Yuichi; NAGATA, Takashi[1]; TSUKUDA, Tatsuya

(*¹Univ. Tokyo*)

Negatively-charged clusters of CO_2 are generated by electron-impact ionized free jet expansion and analyzed by mass spectrometry. Figure 1 shows typical mass spectra of $(CO_2)_n^-$ covering the size range up to $n \sim 1000$ ($m/z \sim 44000$). Abrupt intensity drops in otherwise smooth distributions are observed in the size range of $n \leq 150$, whereas a series of humps are discernible in the spectra recorded in the mass range $n \geq 150$. Weak but distinct intensity anomalies are also observed in the distributions of the $(CO_2)_n^+$ cluster cations in the size range of $n \leq 150$, while oscillatory structures similar to those of $(CO_2)_n^-$ are observed in the $n \geq 150$ range. These comparisons suggest that the magic numbers associated with the small $(CO_2)_n^-$ clusters ($n \leq 150$) reflect intrinsic stabilities of ions, and that the intensity distributions of larger $(CO_2)_n^-$ cluster are mostly determined by the abundance of neutral CO_2 clusters. To find reasonable structural models for $(CO_2)_n^-$, the magic numbers are compared with the sizes predicted from the Mackay icosahedral packing sequence. For $n \leq 150$, the magic numbers observed experimentally ($n = 14, 52,$ and 146) are close to the sizes predicted for icosahedral structures having complete layers ($n = 13, 55, 147$). These similarities suggest icosahedron-like structures for small $(CO_2)_n^-$ clusters which are somewhat deformed due to the presence of anionic cores. In contrast, the distributions for larger clusters cannot be explained by icosahedral structure model, being consistent rather with the cubic structures for neutral clusters in the $n \gg 55$ range.[1]

Reference

1) J.-B. Maillet, A. Boutin and A. H. Fuchs, *J. Chem. Phys.* **111**, 2095 (1999).
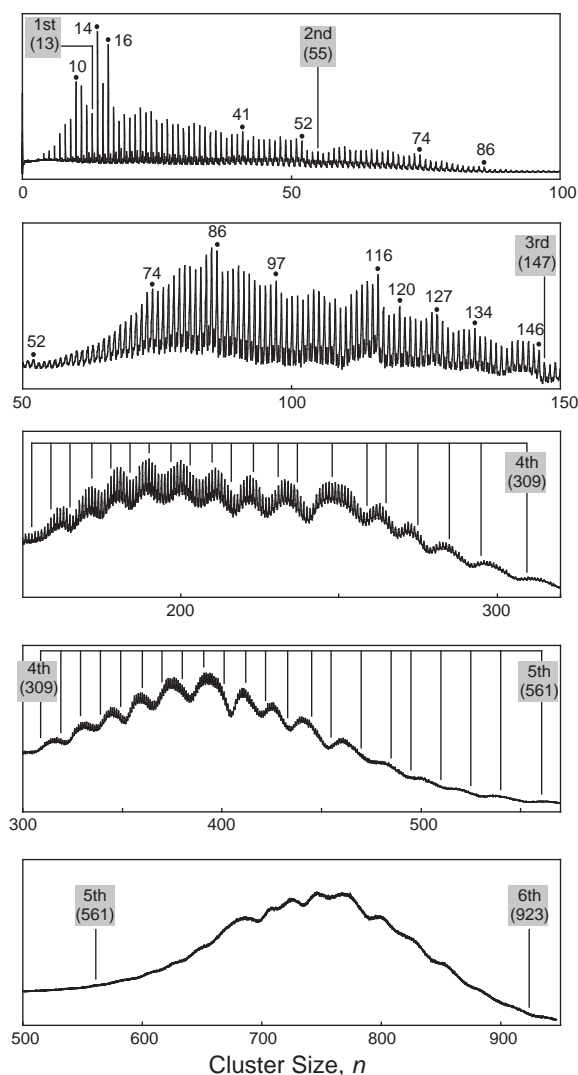
Figure 1. Typical mass spectra of $(CO_2)_n^-$. Bars in the figure represent the cluster sizes at which additional subshell structures are closed around the complete icosahedron structures. Note that these mass spectra are recorded while changing the deflection voltage so that the cluster ions of a given size range can be detected simultaneously.

III-G Spectroscopy and Dynamics of Vibrationally Excited Molecules and Clusters

This research group is studying structure and dynamics of molecules and clusters by two-color double resonance spectroscopy. New spectroscopic methods will also be developed to observe the higher vibrational state under collision-free condition.

III-G-1 Picosecond Time-Resolved Infrared Spectra of Photo-Excited Phenol-$(NH_3)_3$ Cluster

ISHIUCHI, Shun-ichi; SAKAI, Makoto; DAIGOKU, Kota[1]; UEDA, Tadashi; YAMANAKA, Takaya; HASHIMOTO, Kenro[1]; FUJII, Masaaki
([1]Tokyo Metropolitan Univ. and ACT-JST)

Picosecond time-resolved IR spectra of phenol-$(NH_3)_3$ have been measured by UV-IR-UV ion dip spectroscopy for the first time (Figure 1). It was found that the time-evolution of two vibrational bands at 3180 cm^{-1} and 3250 cm^{-1} is different from each other. The results show that two transient species are generated from the photo-excited phenol-$(NH_3)_3$ cluster. From *ab initio* calculation, the transient species are assigned to two isomers of $(NH_3)_2NH_4$ (see Special Research Activity for more detail).
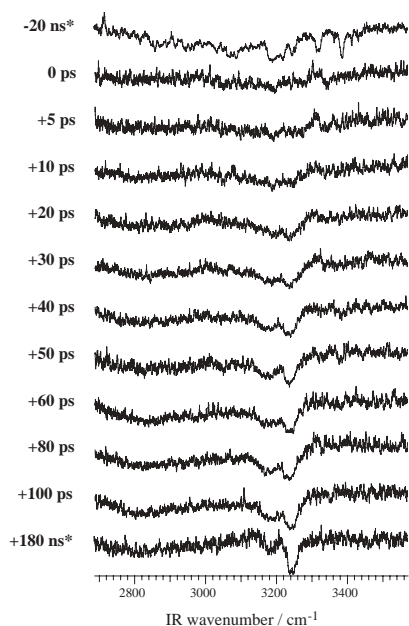
Figure 1. Picosecond time-resolved UV-IR-UV ion dip spectra of the transient species from the electronically excited PhOH-$(NH_3)_3$ which was observed by fixing the first laser ν_{UV} to the low vibronic band in the S_1 state of PhOH–$(NH_3)_3$ (281.49 nm) and monitoring $(NH_3)_2NH_4^+$ due to the ionization laser ν_{ION} (355 nm). Times indicated at the left side of each spectrum mean the delay times between ν_{UV} and the IR probe laser ν_{IR}. The spectra whose delay times are –20 ns and +180 ns (indicated by *) are obtained by nanosecond laser system, which have been reported in the previous paper (*Chem. Phys. Lett.* **322**, 27 (2000)).

III-G-2 Structure of Hydrogen-Bonded Clusters of 7-Azaindole Studied by IR Dip Spectroscopy and Ab Initio Molecular Orbital Calculation

YOKOYAMA, Hiroshi[1]; WATANABE, Hidekazu[2]; OMI, Takuichiro[1]; ISHIUCHI, Shun-ichi; FUJII, Masaaki
([1]Waseda Univ. and PRESTO; [2]AIST Shikoku, Natl. Inst. Adv. Ind. Sci. Tech.)

The IR spectrum of 7-azaindole monomer, 7-azaindole reactive and nonreactive dimers, and 7-azaindole $(H_2O)_n$ (n = 1–3) clusters in a supersonic jet from 2600 cm^{-1} to 3800 cm^{-1} have been measured using IR dip spectroscopy. The vibrational transitions in the ground state were clearly observed and were assigned to the CH and NH stretching vibrations of 7-azaindole and the OH stretching vibrations of water molecules in the clusters. The observed IR spectra of 7-azaindole monomer and 7-azaindole$(H_2O)_n$ (n = 1–3) clusters were compared to theoretical ones obtained by *ab initio* MO calculations. From a comparison, it is concluded that 7-azaindole$(H_2O)_n$ (n = 1–3) clusters have a ring structure due to a cyclic hydrogen-bond network. This conclusion is consistent with an analysis based on high-resolution spectroscopy. Similarly, the IR dip spectrum suggests that the 7-Azaindole reactive dimer has a cyclic hydrogen-bond network, forming a symmetric planer structure. It is strongly suggested from the IR spectrum and the ab initio calculations that the nonreactive dimer contains a water molecule between 7-azaindole molecules.
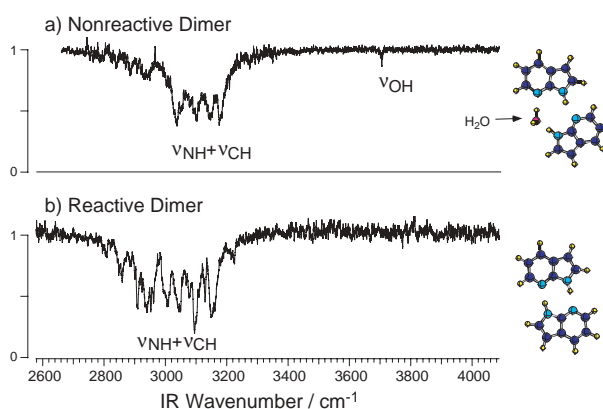
Figure 1. IR dip spectrum of (a) 7-azaindole reactive dimer and (b) nonreactive dimer. The structures concluded from the observed IR spectrum and *ab initio* calculations are also shown.

III-G-3 Structures of Carbazole-(H₂O)ₙ (n = 1–3) Clusters Studied by IR Dip Spectroscopy and a Quantum Chemical Calculation

SAKAI, Makoto; DAIGOKU, Kota[1]; ISHIUCHI, Shun-ichi; SAEKI, Morihisa; HASHIMOTO, Kenro[1]; FUJII, Masaaki
(*[1]Tokyo Metropolitan Univ. and ACT-JST*)

The IR spectra of carbazole and carbazole-$(H_2O)_n$ (n = 1–3) clusters in a supersonic jet have been measured by IR dip spectroscopy. The spectra show clear vibrational structures of both the monomer and the clusters in the 2900–3800 cm^{-1} frequency region. The observed vibrational bands are assigned to the NH stretch of carbazole and the OH stretches of H_2O molecules in the clusters. The geometries and IR spectra of carbazole-$(H_2O)_n$ clusters were calculated at the HF/6-31G and B3LYP/6-31++G(d,p) levels. From a comparison of the observed and calculated IR spectra, the structures of the cluster have been determined.

III-G-4 Structure of 1-Naphthol/Alcohol Clusters Studied by IR Dip Spectroscopy and Ab Initio Molecular Orbital Calculations

SAEKI, Morihisa; ISHIUCHI, Shun-ichi; SAKAI, Makoto; FUJII, Masaaki

The structures of 1-naphthol/alcohol clusters, 1-NpOH(ROH)$_n$ (n = 1–3; ROH = MeOH, EtOH, and t-BuOH), have been investigated by resonant two-photon ionization (R2PI) spectroscopy and ion-detected IR dip spectroscopy. Based on the calculated spectra obtained by *ab initio* MO calculations, the spectra of 1-NpOH-(MeOH)$_n$ was analyzed. The analysis elucidated that 1-NpOH(MeOH)$_{2,3}$ was a ring structure. From a similarity of the spectral pattern, the structures of 1-NpOH-(EtOH)$_n$ and 1-NpOH(t-BuOH)$_n$ were also determined to be a ring conformation. From a frequency shift of the hydrogen-bonded OH stretching vibration, the hydrogen bonding is weakened by a steric hindrance due to an alkyl group of ROH. The difference in the solvation mechanism between 1-NpOH(MeOH)$_n$ and 1-NpOH-(H$_2$O)$_n$ is discussed.

III-G-5 Structural and Dynamics of 9(10H)-Acridine and Its Hydrated Clusters. II Structual Characterization of Hydrogen-Bonding Networks

MITSUI, Masaaki[1]; OHSHIMA, Yasuhiro[1]; ISHIUCHI, Shun-ichi[2]; SAKAI, Makoto; FUJII, Masaaki
(*[1]Kyoto Univ.; [2]GUAS*)

The present paper represents fluorescence-detected infrared measurements of 9(10H)-acridone (AD) and 10 of its fluorescent hydrated clusters, AD-$(H_2O)_n$ (n = 1–5 and more), which have been performed by monitoring the fluorescence from their $^1(\pi,\pi^*)$ electronic origin transitions. In the n = 1 and 2 clusters, free N–H stretching band has been identified in addition to O–H stretching bands characteristic to water molecules acting as single proton donors. As the next solvation step, the H-bonded O–H stretches are further developed in the red-shifted region and the N–H stretch becomes involved in the hydrogen-bonds for the n = 3–5 clusters. For $n \geq 6$, more than one pair of double-donor O–H stretches appear. These spectral features are well correlated to the stepwise evolution in the hydrogen-bonding networks in AD-$(H_2O)_n$, which have been predicted by the (π,π^*) spectral-shift analysis and DFT calculations presented in paper I: water units are bound to the C=O site for n = 1 and 2, a single water chain bridges between the C=O and N–H sites above the AD aromatic rings for n = 3–5, and water bridges become branched for ng 6 and probably form three-dimensional cages at higher aggregation levels. Differences in hydrogen-bonding topologies, stabilities, and dynamical behaviors among the conformers are discussed on the basis of the experimental observations, the DFT calculations, and comparison with other hydrated aromatic clusters.

III-G-6 Internal Methyl Group Rotation in o-Cresol Studied by Pulsed Field Ionization – ZEKE Photoelectron Spectroscopy

SUZUKI, Kazunari[1]; EMURA, Yuji[2]; ISHIUCHI, Shun-ichi[3]; FUJII, Masaaki
(*[1]YAMAHA; [2]Mitsui Chemical; [3]GUAS*)

Pulsed field ionization – ZEKE photoelectron spectroscopy and (1+1) R2PI spectroscopy have been applied to cis- and trans-o-cresol. The internal rotational structure in S$_1$ has been re-assigned for the cis-isomer, and the potential curve for the internal rotation has been determined. In the PFI-ZEKE spectra recorded via different internal rotational levels in the S$_1$ state, well-resolved low-frequency bands have been observed. The low-frequency bands are assigned to internal rotational motion of the methyl group in the cation. Level energies and relative transition intensities are reproduced well by a one-dimensional rotor model with a three-fold axis potential. Potential curves for the internal rotation have been determined for both cis- and trans-o-cresol cations. The barrier height for the internal rotation is different for the two isomers in the cation, while it becomes similar in S$_1$. Contributions of steric and electronic factors to the rotational barrier are discussed.

III-G-7 Pulsed Field Ionization - ZEKE Spectroscopy of Cresoles and Their Aqueous Complex: Internal Rotation of Methyl Group and Intermolecular Vibrations

SUZUKI, Kazunari[1]; ISHIUCHI, Shun-ichi[2]; FUJII, Masaaki
(*[1]YAMAHA; [2]GUAS*)

Pulsed field ionization – ZEKE photoelectron spectroscopy and (1+1) R2PI spectroscopy have been applied to cis- and trans-m-cresol·H_2O clusters. The internal rotational structure in S_1 has been re-assigned, and the potential curve has been determined for the cluster. The PFI-ZEKE spectra of cis- and trans-isomer show low-frequency bands up to 1000 cm^{-1} above the adiabatic ionization potential IP_0. The low-frequency bands are assigned to the internal rotation of the methyl group, the intermolecular stretching and their combination bands in the m-cresol·H_2O cluster cation. Level energies and relative transition intensities are reproduced well by a one-dimensional rotor model with a three-fold axis potential. Potential curves for the internal rotation have been determined for both cis- and trans-isomers of m-cresol·H_2O cations. The effect of the cluster formation upon the internal methyl rotation, and interaction between the methyl rotation and the intermolecular vibration are discussed.

III-G-8 Butterfly Vibration of the Tetrafluorobenzene Cation Studied by Pulsed Field Ionization – ZEKE Photoelectron Spectroscopy

TAKAZAWA, Ken[1]; FUJII, Masaaki
(*[1]Natl. Res. Inst. Met.*)

The pulsed field ionization - ZEKE photoelectron spectroscopy has been applied to 1,2,4,5-tetra-fluorobenzene in a supersonic jet. The spectrum measured by selecting a specific vibronic level of butterfly vibrational mode in S_1 by the first laser shows well-resolved vibrational structure of the cation. A long progression has been assigned to the out-of-plane butterfly vibrational mode 11 with even quantum number in the cation. From the harmonisity and Franck-Condon factor, it has been concluded that the molecular structure of the tetrafluorobenzene cation is flat though that in S_1 is non-planer along the butterfly vibrational mode. The geometrical change upon ionization has been discussed in terms of the electronic structure.

III-H Ultrafast Molecular Dynamics Studied by Time-Resolved Photoelectron Imaging

Femtosecond time-resolved photoelectron imaging is a novel experimental means to probe electronic and nuclear dynamics in real time. Since photoionization can occur from any part of the potential with any multiplicity, the method provides a universal method to follow dephasing and reaction processes.

III-H-1 Photoelectron Imaging on Time-Dependent Molecular Alignment Created by a Femtosecond Laser Pulse

TSUBOUCHI, Masaaki[1]; WHITAKER, Benjamin J.[2]; WANG, Li[3]; KOHGUCHI, Hiroshi, SUZUKI, Toshinori
(*[1]GUAS; [2]Univ. Leeds; [3]Dalian Inst. Chem. Phys.*)

[*Phys. Rev. Lett.* **86**, 4500 (2001)]

Rotational wave packet revivals on an excited electronic state of pyrazine have been measured by femtosecond time-resolved photoelectron imaging for the first time. The pump pulse (324 nm) excited pyrazine to the S_1 0^0 level, and the subsequent 401 nm probe pulse ionized this level by a two-photon process. Figure 1(a) shows a typical photoelectron image measured at a time delay of 30 ps between the pump and probe pulses. The pump and probe laser polarization are both vertical in the figure. The observed image consists of three major rings with different radii corresponding to the photoelectron kinetic energies of 37, 101, and 643 meV. The sharp ring structure indicates that all of these ionization processes occur with the vibrational selection rule $\Delta v = 0$ via intermediate Rydberg states at the energy of $\omega_1 + \omega_2$. Strong anisotropy in the photoelectron image also points to atomic-like electron orbitals in the intermediate states. The Rydberg states contributing to the two outer rings were assigned to the $3s$ (^1A_g) and $3p$ ($^1B_{3u}$ or $^1B_{2u}$) Rydberg states. The time dependencies of photoelectron intensity for the three rings are shown in Figure 1(b). The two outer distributions decay as a function of time (τ = 110 ps), while the inner one grows with the same time constant, corresponding to the intersystem crossing from the S_1 to the triplet manifold.

We have analyzed these revival features based on the theory of RCS reported by Felker and Zewail.[1] For simplicity, we approximated the S_1 state of pyrazine as an oblate symmetric top. By assuming the transitions from S_1 to R_n^{3s} and to R_n^{3p} to be parallel and perpendicular, respectively, simulation of the RCS revivals agrees almost perfectly with observation, as shown in Figure 2(b). The transition from the S_1 ($^1B_{3u}$) to the $3p$ ($^1B_{3u}$ or $^1B_{2u}$) state is vibronically induced by excitation of the mode 11 (b_{3u}), making the transition a perpendicular type.

The PAD measured at each time delay was fit to the following form:

$$I(\theta) = \beta_{00}Y_{00}(\theta) + \beta_{20}Y_{20}(\theta) + \beta_{40}Y_{40}(\theta) + \beta_{60}Y_{60}(\theta),$$

where Y_{LM} are spherical harmonics. We found β_{60} to be negligible. The ratio β_{20}/β_{00} thus obtained for ionization of S_1 via the $3s$ and $3p$ Rydberg states also clearly shows the rotational revivals [Figure 1(c)]. In the present case, the pump pulse creates a time-dependent alignment $A_{20}(t)$ in the S_1 state, and the probe pulse transfers this alignment to rotational levels in the Rydberg states. Since these states are ionized instantaneously within a probe laser pulse, the PAD is modulated only by the time dependence of $A_{20}(t)$ in the S_1 state.

Reference
1) P. M. Felker, J. S. Baskin and A. H. Zewail, *J. Phys. Chem.* **90**, 724 (1986).
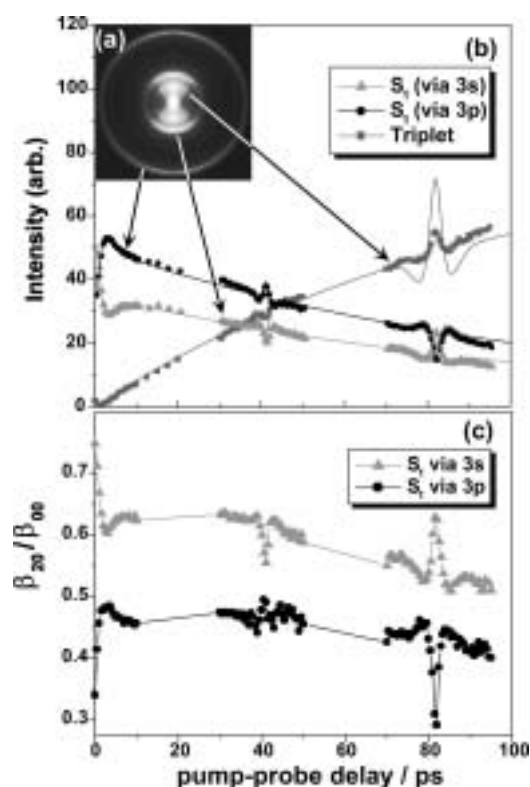
Figure 1. (a) Inverse Abel transformed photoelectron image of the [1+2'] PEI of pyrazine via the S_1 $B_{3u}(n\pi^*)$ 0^0 level observed at the time delay of 30 ps. The original image was integrated 80 000 laser shots. (b) Time evolution of three major components in the [1+2'] PEI. Circle (●), triangle (▲), and square (■) represent the angle integrated intensity for the outer (KE = 643 meV), middle (101 meV), and inner ring (37 meV), respectively. Solid lines are a simulation taking into account the rotational coherence. (c) β_{20}/β_{00} as a function of pump-probe time delay in the [1+2'] PEI.

III-H-2 Femtosecond Photoelectron Imaging on Pyrazine: Spectroscopy of 3*s* and 3*p* Rydberg States

SONG, Jae Kyu[1]; TSUBOUCHI, Masaaki[2]; SUZUKI, Toshinori
(*[1]Seoul Natl. Univ.; [2]GUAS*)

Femtosecond two-color and one-color photoelectron imaging have been applied to Rydberg states (n = 3) of jet-cooled Pyrazine. The 3s and 3p members of Rydberg series converging to the ground state (n^{-1}) of the cation and the 3s member of Rydberg series converging to an excited state of the cation (π^{-1}) were observed. Figure 1 (a) shows (2+1) REMPI spectrum of jet-cooled Pyrazine observed with our tunable femtosecond laser. There are two band systems. The first system exhibits a progression of the 6a mode, indicating the geometry change from S_0 along this mode. The second system does not indicate such a prominent geometry change. Figure 1 (b) is the He(I) photoelectron spectrum of Pyrazine adopted from the literature.[1] Here, the first system is the ground state (^2A_g) of the cation and the second system is the excited state ($^2B_{1g}$) of the cation. The spectral features in Figure 1 (a) and (b) are remarkably similar, from which the two systems in Figure 1 (a) are assigned to $3(n^{-1})$ and $3s(\pi^{-1})$ Rydberg states. The energy difference between the $3s(\pi^{-1})$ and $3s(n^{-1})$ Rydberg states is 820 meV, while the energy difference between $I_0(^2A_g)$ and $I_1(^2B_{1g})$ is 880 meV. The quantum defects calculated for the $3s(\pi^{-1})$ and $3s(n^{-1})$ Rydberg states are 0.87 and 0.86, respectively. The difference in electronic character between the $3s(\pi^{-1})$ and the $3s(n^{-1})$ Rydberg states was also evident in the photoelectron angular distributions for ionization out of these orbitals.

The spectrum shown in Figure 1(b) is strikingly different from the one reported by Turner *et al.* using a nanosecond laser[2] in that (1+2) REMPI spectrum via T_1 is completely missing in our data. This is presumably because the ionization efficiency of the rapidly-decaying Rydberg states was substantially lower with nanosecond lasers, making the $T_1 \leftarrow S_0$ spectrum more dominant.

The Franck-Condon factors in electronic transitions involving S_0, S_1, S_2, $3s(n^{-1})$, $3s(\pi^{-1})$, D_0, and D_1 were analyzed to examine conical intersections between these states, and the intersection was identified between S_1-S_2, $3s(n^{-1})$-$3s(\pi^{-1})$ and D_0-D_1. Although the electronic dephasing times for S_2-S_1 and D_1-D_0 have been estimated to be 30 fs, the photoelectron angular distribution indicated that $3s(n^{-1})$-$3s(\pi^{-1})$ dephasing is not completed within 100 fs.

References
1) H. Fridh, L. Asbrink, B. O. Jonsson and E. Linddholm, *Int. J. Mass Spectrom.* **8**, 101 (1972).
2) R. E. Turner, V. Vaida, C. A. Molini, J. O. Berg and D. H. Parker, *Chem. Phys.* **28**, 47 (1978).
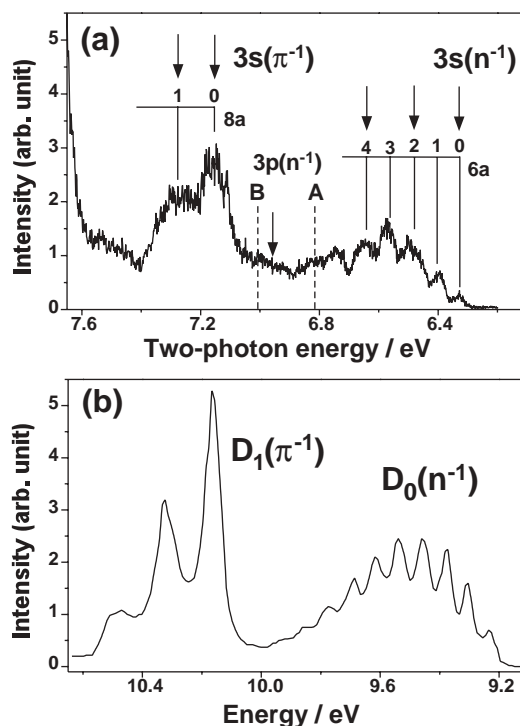
Figure 1. (a) One-color REMPI spectrum in the 325–400 wavelength region. The abscissa of the spectrum represents the two-photon energy in eV. The assignments of the vibrational progressions are indicated in the figure. The origins of 3pA and 3pB Rydberg states, although they are not visible in the spectrum, are indicated by broken lines. (b) He (I) photoelectron spectrum of Pyrazine shown on the same scale as (a). Adopted from reference 1.

III-H-3 Photoionization Dynamics of CO Studied by Photoelectron Imaging

KATAYANAGI, Hideki; MATSUMOTO, Yoshiteru; DE LANGE, Cornelis A.; SUZUKI, Toshinori

The photoelectron energy and angular distributions in (2+1) REMPI of CO via the $B^1\Sigma^+$ ($v' = 0$ and 1) states have been observed by photoelectron imaging. Jet-cooled CO molecule was ionized using UV light near 230 nm, and the photoelectrons were projected onto a position-sensitive imaging detector.

Since the $B^1\Sigma^+$ ($v' = 0$) state is the 3s member of a Rydberg series converging to the $X^2\Sigma^+$ (v^+) state of CO^+, the $\Delta v = 0$ propensity rule may be anticipated. However, off-diagonal transitions, $\Delta v = 1$–7, were observed. Figure 1 shows the observed photoelectron image. Two outer rings with strong intensity arise from $\Delta v = 0$ and 1 transitions corresponding to the photoelectron kinetic energy of 2.15 and 1.88 eV, respectively. In addition, close examination reveals that there are weak inner rings due to $\Delta v = 2$–7 transitions. The rings were separated by about 260 meV in energy. These results are in agreement with a previous work by Sha *et al.*[1] The photoelectron angular distribution exhibited high anisotropy for $v^+ = 0$ and a low value for $v^+ = 1$–7, which suggests different ionization mechanisms between the $\Delta v = 0$ and $\Delta v = 1$–7 ionization processes. The latter, off-diagonal transitions, are

ascribed to autoionization from a superexcited Rydberg state converging to the first excited ionic state ($A^2\Pi$).

In the photoelectron spectrum via $B^1\Sigma^+$ ($v' = 1$) state, the $\Delta v = 0$ transition was dominant, which is different from the spectrum via $B^1\Sigma^+$ ($v'= 0$).

References

1) G. Sha, D. Proch, Ch. Rose and K. L. Kompa, *J. Chem. Phys.* **99**, 4334 (1993).
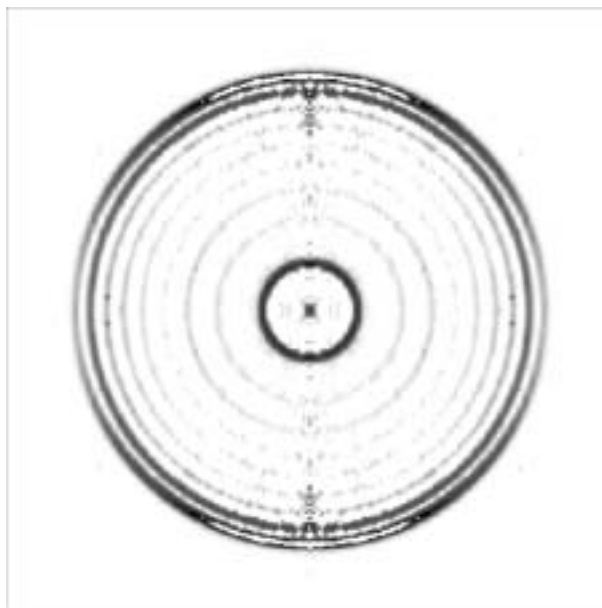
Figure 1. Inverse Abel transformed (512 × 512 pixels) photo-electron image of [2+1] REMPI of CO via the $B^1\Sigma^+$ ($v' = 0$) state. The original image was integrated for 90,000 laser shots.

III-I Bimolecular Reaction Dynamics

Chemical reactions under thermal conditions occur with various collision energies, internal quantum states, and impact parameters. The experimental data measured under such conditions are highly-averaged quantities, from which detailed feature of reactions can hardly be learned. A crossed molecular beam method allows us to observe chemical reactions of state-selected reagents at well-defined collision energy. The differential cross section (angular distribution of products) reveals impact-parameter dependence of reaction probability and reaction mechanism.

III-I-1 Differential Cross Sections for the Inelastic Scattering of NO ($X^2\Pi_\Omega$) by Ar Studied by Crossed Molecular Beam Ion-Imaging and Quantum Scattering Calculations

KOHGUCHI, Hiroshi; SUZUKI, Toshinori; ALEXANDER, H. Millard[1]
(*[1]Univ. Maryland*)

High-resolution ion-imaging combined with a crossed molecular beam method has been applied to the state-resolved differential cross sections (SR-DCSs) of inelastic scattering of NO ($j'' = 0.5$, $\Omega'' = 1/2$) + Ar → NO (j', $\Omega' = 1/2, 3/2$) + Ar at a collision energy of 516 cm^{-1}. Sensitive (j', Ω')-dependence and complex undulations of the obtained SR-DCS were investigated by comparison with rigorous theoretical calculations. The close-coupling scattering calculation without any dynamical approximation based on the two ab initio potential energy surfaces [CEPA and CCSD(T) calculations] were carried out for the theoretical SR-DCS. The above quantum features observed in the $\Delta\Omega = 0$ scattering were almost completely reproduced by the two *ab initio* surfaces consistently. Noticeable discrepancy between the two calculations, although the CCSD(T) potential energy surfaces yielded the better agreement with the experiment, was seen in the forward scattering of the middle Δj in the $\Delta\Omega = 1$ transitions. The major difference between the CCSD(T) and CEPA surfaces lying in the potential well region at the T-shaped configuration resulted in these discrepancies of the specific scattering angles in the limited (j', Ω') states.
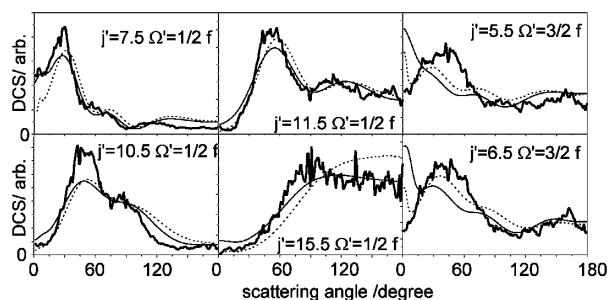
Figure 1. State-resolved differential cross sections of the NO + Ar inelastic scattering at the collision energy of 516 cm^{-1}. The initial state of the collision is $j'' = 0.5$, $\Omega'' = 1/2$ state. The thick-solid lines represent the experimental differential cross sections. The thin-solid and broken lines are the theoretical results based on the CCSD(T) and the CEPA *ab initio* PESs, respectively.

III-J Structure and Properties of Polyoxometalates with a Magnetic, Electronic, or Biological Significance

Polyoxometalates constitute model systems for the study of the electron and energy transfer in the infinite metal-oxide lattice and their simplicity allows to treat at the molecular scale the coupling of electronic and nuclear movements, which is an inherent problem for the mixed-valence systems. As is clear from such a variety of both structure and reactivity of polyoxometalates, our current works on polyoxometalates are 1) structure/reactivity relationships with particular regard to the mechanism of electron transfer reactions, 2) magnetic interaction and molecular magnetic device, 3) energy-transfer mechanism and luminescence device (including nonlinear optical device), 4) encapsulation of templates in the photo-induced self-assembly process, 5) template-exchange reaction and topology, and 6) antibacterial effects on methicillin-resistant *Staphylococcus aureus* (MRSA) and human gastric pathogen of *Helicobacter pylori*.

III-J-1 A Highly Nuclear Vanadium-Containing Tungstobismutate: Synthesis and Crystal Structure of $K_{11}H[(BiW_9O_{33})_3Bi_6(OH)_3(H_2O)_3V_4O_{10}]\cdot 28H_2O$

BOTAR, Bogdan; YAMASE, Toshihiro; ISHIKAWA, Eri
(IMS and Tokyo Inst. Tech.)

A novel and large heteropolyanion $[(BiW_9O_{33})_3Bi_6(OH)_3(H_2O)_3V_4O_{10}]^{12-}$ has been synthesized by reaction of sodium metavanadate with $Na_9[BiW_9O_{33}]\cdot 16H_2O$ in acetate buffer solutions (at pH 4.8). The present anion has a trilobal structure in which three α-B $[BiW_9O_{33}]$ units are connected to each other by an unique core $[Bi_6(OH)_3(H_2O)_3V_4O_{10}]^{15+}$. A central bismutate/vanadate-mixed core comprises three sets of two types of the BiO_6 pentagonal pyramid, the edge-sharing VO_5 square-pyramidal triad, and a VO_4 tetrahedron.

III-J-2 Photochemical Self-Assembly Reaction of β-$[Mo_8O_{26}]^{4-}$ to Mixed-Valence Cluster $[Mo_{37}O_{112}]^{26-}$ in Aqueous Media

YAMASE, Toshihiro; ISHIKAWA, Eri
(IMS and Tokyo Inst. Tech.)

Prolonged photolysis of β-$[Mo_8O_{26}]^{4-}$ in the presence of electron-donative MeOH in aqueous solutions at pH 3.3 provides stepwise self-organization to paramagnetic reddish-brown mixed-valence species $[H_{14}Mo^V_{24}Mo^{VI}_{13}O_{112}]^{12-}$. The X-ray structural analysis of the reddish brown crystals, isolated as $[NMe_4]^+$ salt, shows that $[H_{14}Mo^V_{24}Mo^{VI}_{13}O_{112}]^{12-}$ anion consists of a central T_d $[H_{10}(Mo^V_{12}O_{40})(Mo^{VI}O_2)_3]^{4-}$ core sandwiched by two $[H_2Mo^V_6Mo^{VI}_5O_{33}]^{4-}$ ligands, with overall symmetry of D_{2d}. The central $\{Mo^V_{12}O_{40}\}$ subcore (with six short Mo^V–Mo^V contacts, 2.56(1) and 2.625(7) Å) is a tetrahedral ε-Keggin structure with a cavity (in the size of ~3.3 Å) accommodating four protons, and is stabilized by capture of four $\{Mo^{VI}O_2\}$ groups with 3/4 occupancy. The $\{Mo^V_6Mo^{VI}_5O_{33}\}$ framework as the ligand consists of two sets of a dinuclear $\{Mo^V_2O_4\}$ pair with a $Mo^V\cdots Mo^V$ distance of 2.567(7) Å, two sets of the edge-shared $\{Mo^{VI}_2O_{10}\}$ octahedra, and three mononuclear groups of one $Mo^{VI}O$ and two Mo^VO_2. The Mo^V atoms in the two Mo^VO_2 groups in the ligand are separated with distance of 6.31(1) Å, being ESR-active ($<g>$ = 1.909, $g_\perp$ = 1.894, and $g_\parallel$ = 1.939 at 77 K). The structure of the $[H_{14}Mo^V_{24}Mo^{VI}_{13}O_{114}]^{12-}$ anion is slightly different from the diamagnetic species $\{[H_6Mo^{VI}_2O_{40}(Mo^VO_3)_4]-[H_3Mo^V_4Mo^{VI}_6O_{29}][H_5Mo^V_6Mo^{VI}_5O_{31}]\}^{14-}$ prepared by thermal reduction of $[Mo_7O_{24}]^{6-}$ with $N_2H_4\cdot H_2SO_4$, in both structure and mixed-valency of the ligand. The stepwise self-assembly processes from β-$[Mo_8O_{26}]^{4-}$ to $[H_{14}Mo^V_{24}Mo^{VI}_{13}O_{114}]^{12-}$ are discussed in terms of the photochemical multi (six- and four-) electron reduction of β-$[Mo_8O_{26}]^{4-}$ which results in the splitting into $\{Mo_4\}$, $\{Mo_2\}$, and $\{Mo_1\}$ fragments.

III-J-3 A Spherical Potassium-Capped Vanadium Methylphosphonate as Another ε-Keggin Fragment, $[H_6KV_{12}O_{27}(VO_4)(PO_3CH_3)_3]^{5-}$

YAMASE, Toshihiro; MAKINO, Haruyo; NARUKE, Haruo; SAN JOSÉ WÉRY, Ana Maria
(IMS and Tokyo Inst. Tech.)

An $[H_3KV_{12}O_{27}(AsO_4)_4]^{6-}$-isostructural ε-Keggin fragment anion, $[H_6KV_{12}O_{27}(VO_4)(PO_3CH_3)_3]^{5-}$, was photochemically prepared. This K^+-capped anion is formally built of nine $V^{IV}O_6$ octahedra, three PO_3C tetrahedra, and four V^VO_4 tetrahedra, one of the latter being a central VO_4^{3-} group. The capping K^+ cation lies on the C_3 axis and links two adjacent anion, to form a linear chain of the anions along c-axis.

III-J-4 Chemical Structure and Intramolecular Spin-Exchange Interaction of $[(VO)_3(SbW_9O_{33})_2]^{12-}$

YAMASE, Toshihiro; BOTAR, Bogdan; ISHIKAWA, Eri; FUKAYA, Keisuke
(IMS and Tokyo Inst. Tech.)

The crystal structure determination of tris(vanadyl)-substituted tungstoantimonate(III) $K_{11}H[(VO)_3(SbW_9$-

$O_{33})_2]\cdot27H_2O$ reveals that the $[(VO)_3(SbW_9O_{33})_2]^{12-}$ anion contains three exterior VO^{2+} groups sandwiched by two α-B $[SbW_9O_{33}]^{9-}$ ligands in $V^{IV}\cdots V^{IV}$ separation of 5.411(8)–5.464(8) Å and is stabilized by equatorial three K^+ ions triangle with virtual D_{3h} symmetry. An observable spin-exchange interaction between V^{IV} centers within the vanadyl coplanar triangle is demonstrated in terms of $S = 1/2$ and $S = 3/2$ states.

III-J-5 Synthesis and Structure of Ln(W$_5$O$_{18}$)-Capped Mixed-Ligand Polyoxotungstolanthanoate [Ln(W$_5$O$_{18}$){Ln(H$_2$O)$_2$(SbW$_9$O$_{33}$)(W$_5$O$_{18}$)}]$^{15-}$ (Ln = Sm and Er)

NARUKE, Haruo; YAMASE, Toshihiro
(IMS and Tokyo Inst. Tech.)

Polyoxotungstolanthanoate, $[Ln_2(H_2O)_2(SbW_9O_{33})\text{-}(W_5O_{18})_2]^{15-}$ (Ln = Sm and Er), possessing Ln^{3+}, trivacant α-B-Keggin $[SbW_9O_{33}]^{9-}$, and monovacant Lindqvist $[W_5O_{18}]^{6-}$ groups with a ratio of 2:1:2, was prepared and structurally characterized. In the anion the α-B-$[SbW_9O_{33}]^{9-}$ group coordinates to two $[Ln\text{-}(W_5O_{18})]^{3-}$ moieties through terminal- and bridging-O atoms at vacant and non-vacant sites, respectively. A ^{183}W-NMR spectrum for Y^{3+}-analog in aqueous solution was consistent with this anion structure.

III-J-6 Three-Dimensional Inorganic/Organic Hybrid Material, [Ni$_2$(4,4'-bipy)$_3$(H$_2$O)$_2$V$_4$O$_{12}$]·2.5H$_2$O

YANG, Lan; HU, Changwen; NARUKE, Haruo; YAMASE, Toshihiro
(IMS and Tokyo Inst. Tech.)

The title compound has been prepared by hydrothermal method and characterized by elemental analysis, IR spectroscopy, and single-crystal X-ray diffraction. The structure consists of {V$_2$O$_6$}, {Ni(1)-(4,4'-bipy)$_4$O$_2$} and {Ni(2)(H$_2$O)$_2$(4,4'-bipy)$_2$O$_2$} polyhedra, and water molecules of crystallization. The Ni atoms and one bipyridyl group lie on centers of symmetry.

III-J-7 Molecular Aspect of Energy Transfer from Tb^{3+} to Eu^{3+} in Polyoxometalate Lattices: An Approach for Molecular Design of Rare-Earth Metal-Oxide Phosphors

YAMASE, Toshihiro
(IMS and Tokyo Inst. Tech.)

The exploitation of mixed heteronuclear rare-earth-element-containing polyoxometalates to probe the multipolar nature of heteronuclear rare-earth interactions is imaginative. It appears that polyoxometallolanthanoates are ideal for this type of investigation. Three structural types of Tb^{3+}/Eu^{3+} heterolanthanide-multinuclear polyoxometalates, $K_{15}H_3[Tb_{1.4}Eu_{1.6}\text{-}(H_2O)_3(SbW_9O_{33})(W_5O_{18})_3]\cdot25.5H_2O$, $Na_7H_{19}[Tb_{4.3}\text{-}Eu_{1.7}O_2(OH)_6(H_2O)_6Al_2(Nb_6O_{19})_5]\cdot47H_2O$, and $[NH_4]_{12}H_2[Tb_{3.1}Eu_{0.9}(MoO_4)(H_2O)_{16}(Mo_7O_{24})_4]\cdot13H_2O$ are studied by crystal structures, emission and excitation spectra, and emission decay dynamics. The excitation of the Tb^{3+} $^7F_6 \rightarrow {^5D_4}$ transitions produces not only the emission lines of Tb^{3+}, but also those of Eu^{3+}, accompanied by nonexponential rise and decay curves of the emission from Tb^{3+} and Eu^{3+}. There is no significant exchange interaction between the lanthanide ions, as a result of the coordination of aqua and/or hydroxo ligands to the lanthanide ions. The mechanism of the $Tb^{3+} \rightarrow Eu^{3+}$ energy transfer is identified as a Förster-Dexter-type energy transfer from Tb^{3+} (donor) to Eu^{3+} (acceptor). The nearest-neighbor energy-transfer rates by electric dipole-dipole interactions between a Tb-Eu pair at 4.2 K are estimated to be 4.5×10^4, 4.7×10^5, and 4.9×10^3 s^{-1} and the critical radii at 4.2 K are 10.3, 10.0, and 6.17 Å for $K_{15}H_3[Tb_{1.4}Eu_{1.6}(H_2O)_3(SbW_9O_{33})(W_5O_{18})_3]\cdot25.5H_2O$ (with Tb-Eu separation of 5.05 Å), $Na_7H_{19}[Tb_{4.3}Eu_{1.7}O_2(OH)_6(H_2O)_6Al_2(Nb_6O_{19})_5]\cdot47H_2O$ (with 3.76 Å separation), and $[NH_4]_{12}H_2\text{-}[Tb_{3.1}Eu_{0.9}(MoO_4)(H_2O)_{16}(Mo_7O_{24})_4]\cdot13H_2O$ (with 6.17 Å separation), respectively. The low symmetry (C_s or C_1) of the LnO_8 (Ln = Tb and Eu) coordination polyhedra allows the nonvanishing electric-dipole transition probability for the $^7F_J \leftrightarrow {^5D_0}$ ($J = 0, 1$) transitions which leads to a faster transfer rate at high temperatures. The photoexcitation of the host lattices (tungstate, niobate, and molybdate) induced the energy transfer from the oxygen-to-metal charge-transfer {O → M (= Nb, Mo, W) lmct} triplet states to Tb^{3+} ($^7F_6 \rightarrow {^5D_4}$) and Eu^{3+} ($^7F_{0,1,2} \rightarrow {^5D_{0,1}}$). In the case of $[NH_4]_{12}H_2[Tb_{3.1}Eu_{0.9}(MoO_4)(H_2O)_{16}(Mo_7O_{24})_4]\cdot13H_2O$ this transfer is not complete and the O → Mo lmct triplet emission of molybdates is observed to provide the rate constant for the energy transfer to Tb^{3+}/Eu^{3+} sites with 4.4×10^6 s^{-1}.

III-K Structure and Exited-State Dynamics of Aromatic Clusters

Clusters containing aromatic molecules are model systems for elucidating intermolecular interactions that control macroscopic properties of the molecules in condensed phases, such as liquids and crystals. We focus on detailed correlation of dynamical behavior of photo-excited aromatic chromophore to geometry and bonding topology of the clusters. Especially, it is critically important to definitely characterize the cluster structure, and we implement various laser-based methods, such as IR–UV double resonance and rotational coherence spectroscopy (RCS), in conjunction with molecular-orbital calculations. The following subjects have been studied; 1) hydrogen-bonding networks and nonradiative dynamics of a bi-functional aromatic solvated by water molecules, 2) experimental determination of solvation structure of aromatic clusters by RCS, and 3) reexamination of electronic spectra of (benzene)$_n$ clusters.

III-K-1 Electronic Spectroscopy of 9(10H)-Acridone and Its Hydrated Clusters

MITSUI, Masaaki[1]; OHSHIMA, Yasuhiro[1,2]
(*[1]Kyoto Univ.; [2]IMS*)

The lowest $^1(\pi,\pi^*)$ electronic transition of 9(10H)-acridone (AD) and its hydrated clusters has been studied by fluorescence-based laser spectroscopy and mass-selective two-color resonance-enhanced two-photon ionization (2C-R2PI). Thirteen fluorescent hydrates as well as the monomer have been identified in fluorescence-excitation and UV–UV hole-burning measurements, and size assignments for relatively smaller clusters, AD–(H$_2$O)$_n$ ($n = 1$–6), have been conducted by 2C-R2PI. The origin bands for larger-size clusters show larger red shifts converging at *ca.* 2200 cm^{-1}, but the changes are non-monotonic with a substantial increase from $n = 2$ to 3. DFT calculations at the B3LYP/6–31G(d,p) level have predicted that the energy difference between the C=O and N–H bonded isomers is quite small (only ≈ 1 kcal/mol) for $n = 1$ and 2. The observed spectral shifts of fluorescent hydrates with $n = 1$ and 2 are well reproduced by the HOMO–LUMO gap in the calculated orbital energies of either of the N–H or C=O bonded isomers, leaving the definitive structural assignments to fluorescence-detected infrared spectroscopy described in the next section. For the larger clusters ($n = 3$–5), several minimum-energy structures have been identified within 2 kcal/mol in binding energy, among which the conformers with water molecules bridging between the C=O and N–H sites over the AD's aromatic rings are identified as the observed species, based on good agreement between the calculated and observed spectral shifts.

III-K-2 Characterization of Hydrogen-Bonding Networks in 9(10H)-Acridone and Its Hydrated Clusters

MITSUI, Masaaki[1]; OHSHIMA, Yasuhiro[1,2]; ISHIUCHI, Shun-ichi[3]; SAKAI, Makoto; FUJII, Masaaki
(*[1]Kyoto Univ.; [2]IMS; [3]GUAS*)

Fluorescence-detected infrared measurements have been performed for 9(10H)-acridone (AD) and ten of its fluorescent hydrated clusters, AD–(H$_2$O)$_n$ ($n = 1$–5 and more). In the $n = 1$ and 2 clusters, free N–H stretching band has been identified in addition to O–H stretching bands characteristic to water molecules acting as single proton donors. As the next solvation step, the H-bonded O–H stretches are further developed in the red-shifted region and the N–H stretch becomes involved in the hydrogen-bonds for the n = 3–5 clusters. For $n \geq 6$, more than one pair of double-donor O–H stretches come to appear. These spectral features are well correlated to the stepwise evolution in the hydrogen-bonding networks in AD–(H$_2$O)$_n$, which have been predicted by the (π,π^*) spectral-shift analysis and DFT calculations presented in the above section: waters units are bound to the C=O site for $n = 1$ and 2, a single water chain bridges between the C=O and N–H sites above the AD's aromatic rings for $n = 3$–5, and water bridges become branched for $n \geq 6$ and probably form three dimensional cages at higher aggregation level.

III-K-3 Microscopic Solvation Effects on Nonradiative Dynamics in 9(10H)-Acridone and Its Hydrated Clusters

MITSUI, Masaaki[1]; OHSHIMA, Yasuhiro[1,2]; KAJIMOTO, Okitsugu[1]
(*[1]Kyoto Univ.; [2]IMS*)

Nonradiative dynamics and energy-level structure of relevant electronic excited states in 9(10H)-acridone (AD) and its hydrated clusters have been studied. The fluorescence decay is very fast (≈ 10 ps) for bare AD but drastically lengthened ($> $ ns) in the clusters. Bare AD has been observed by delayed ionization and sensitized phosphorescence, which indicates the efficient formation of molecules in triplet manifold after the $^1(\pi,\pi^*)$ excitation. Several weak peaks attributable to $^3(n,\pi^*)$ transitions are identified in bare AD, but such satellites completely disappear in the fluorescent cluster spectra with $n \geq 1$. The dominant nonradiative pathway in bare AD is the $S_1(\pi,\pi^*) \rightarrow T_2(n,\pi^*)$ intersystem crossing (ISC) followed by the $T_2(n,\pi^*) \rightarrow T_1(\pi,\pi^*)$ internal conversion. This direct ISC process becomes prohibited by the energy-level inversion between S_1 and

T_2 induced by the H-bonding to the C=O site. The relaxation pathway is switched to the second-order ISC $[S_1(\pi,\pi^*) \rightarrow T_1(\pi,\pi^*)]$ in the fluorescent hydrated clusters, where the carbonyl site is H-bonded. Owing to the increasing S_1-T_2 separation, the fluorescence quantum yield becomes larger for the higher clusters, which is approaching to the bulk solution value. A small fall-off in the decay constants from $n = 2$ to 3 is correlated to the crossover in H-bonding topologies (the C=O bonded $\rightarrow$ the bridged form), which has been established in the above sections. The delayed ionization has identified new spectral features that are absent in the fluorescence excitation spectrum. They are assigned to the N–H bonded isomer(s) with $n \leq 3$, in which the ISC should be as fast as in bare AD because of the lack of the S_1-T_2 level inversion. These experimental findings demonstrate the site-specific solvation effects on the nonradiative dynamics in the hydrated clusters of AD.

III-K-4 Structural Characterization of 9-Cyanoanthracene–(Ar)$_n$ (n = 0–3)

EGASHIRA, Kazuhiro[1]; OHSHIMA, Yasuhiro[1,2]; KAJIMOTO, Okitsugu[1]
(*[1]Kyoto Univ.; [2]IMS*)

Rotational coherence spectroscopy implemented with time-resolved fluorescence depletion has been applied in a structural study of 9-cyanoanthracene (CNA) and its clusters with Ar up to three atoms. For bare CNA, C-type transients for the S_1 and S_0 states have been observed separately, yielding independent sets of rotational constants for the two states. For the Ar clusters, rotational constants as averages for S_1 and S_0 have been derived to fix the cluster geometry. The Ar atom in CNA–Ar is located 3.46 ± 0.03 Å above the central aromatic ring of CNA and displaced slightly from the ring center toward the cyano group. The plane–Ar distance is quite close to those in clusters with other polycyclic aromatic molecules. Two values (≈ 0.2 or 0.6 Å) for the displacement to the cyano group are consistent with the experimental data, and results on related aromatics–Ar show that the former is preferable. The dominant conformer of CNA–(Ar)$_2$ has been determined as a two-sided $(1 + 1)$ type: structures for each sides of the CNA plane are the same as that of CNA–Ar within the experimental uncertainties. CNA–(Ar)$_3$ has a $(2 + 1)$-type structure: one side of the substrate is the same as CNA–Ar and an Ar dimer lies 3.48 ± 0.04 Å above the other side. The determined conformations of CNA–(Ar)$_{1,3}$ are the same as the corresponding anthracene clusters, but that of CNA–(Ar)$_2$ is in contrast to anthracene–(Ar)$_2$, which has been identified as a $(2 + 0)$ type. Model potential calculations have been employed to explain the difference in structural motifs of the two closely related clusters.

III-K-5 Structural Characterization of 9-Cyanoanthracene–Water

EGASHIRA, Kazuhiro[1]; OHSHIMA, Yasuhiro[1,2];

KAJIMOTO, Okitsugu[1]
(*[1]Kyoto Univ.; [2]IMS*)

Rotational coherence spectroscopy has been applied to determine rotational constants of the two isotopic species of the 9-cyanoanthracene–water complex, CNA–H$_2$O and CNA–D$_2$O. To support the experimental observation DFT calculations [B3LYP/6-31G(d,p)] have been also performed to identify several stable conformations. The structure of the complex is found to be such that water is hydrogen-bonded to the π-electrons of the cyano group of CNA. Geometrical parameters consistent with the experimental results are evaluated.

III-K-6 Structural Characterization of 1:1 van der Waals Complexes of 9-Cyanoanthracene with Aprotic Solvents

EGASHIRA, Kazuhiro[1]; OHSHIMA, Yasuhiro[1,2]; KAJIMOTO, Okitsugu[1]
(*[1]Kyoto Univ.; [2]IMS*)

Structures of 9-cyanoanthracene (CNA) clusters microsolvated with single molecule of aprotic solvents (carbon dioxide, two isotopomers of acetonitrile, and fluoroform) have been studied by rotational coherence spectroscopy. All the observed traces exhibit pronounced C-type transients, which suggests that these species are quite close to planar asymmetric tops with their electronic transition moments pointing to in-plane directions. Weak J-type transients have been also identified for CNA–CO$_2$ and –CF$_3$H, latter of which shows A-type transients in addition. By comparing the experimental observations with B3LYP/6-31G(d,p) calculations, it is concluded that the solvent molecule is located by the side of the CN group of CNA with its molecular axis lying in the CNA molecular plane. All the cluster geometries are of C_s symmetry, in which a positively charged atom of the solvents (C, H, or H for CO$_2$, CH$_3$CN, and CF$_3$H, respectively) is close to the cyano nitrogen of CNA, while an electonegative part (O, N, or F) contacts with the 1-position hydrogen of CNA. Some geometrical parameters including the centers of mass separation are obtained from the derived rotational constants.

III-K-7 Size Reassignments of the S_1–S_0 Vibronic Spectra of Benzene Clusters

IIMORI, Toshifumi[1]; OHSHIMA, Yasuhiro[1,2]
(*[1]Kyoto Univ.; [2]IMS*)

The vibronic band systems of (benzene)$_n$ clusters in the S_1–S_0 vibronic region are revisited by mass-selective resonant two-photon ionization and ultraviolet–ultraviolet hole-burning spectroscopies. A detailed examination of the spectra of isotopomers with isotopic

mixture of C_6H_6 and C_6D_6 reveals that there is substantial fragmentation for $n \geq 3$ following photo-ionization. This observation concludes that it is necessary to correct the size assignments. Transitions which have been formerly identified to the trimer are most probably due to the tetramer. Instead, reassigned to the trimer is the band system which has been believed to be of an isomeric form of the dimer.

RESEARCH ACTIVITIES IV
Department of Molecular Assemblies

IV-A Spectroscopic Study of Organic Conductors

The reflectivity of an organic conductor provides us with a wealth of information on the electronic structure. For instance, the anisotropy of a band structure, bandwidth, effect of electron-electron correlation, and electron-molecular vibration (EMV) coupling parameters can be extracted from the analysis of the reflectivity or optical conductivity curve. We are investigating the polarized reflection spectra of various organic conductors in the spectral region of 50–33000 cm^{-1} and in the temperature range of 6–300 K. Raman spectroscopy is a complementary method to reflection spectroscopy for understanding molecular vibrations (local phonons). We are investigating the charge ordering (CO) or charge disproportionation phenomena in organic conductors using the technique of vibrational spectroscopy. The charge ordering was found in inorganic narrow-band systems such as copper, manganese, and vanadium oxides. Recently, a charge-ordered ground state has been found in several organic conductors. The Raman and infrared spectra change dramatically at CO phase-transition temperature. Our goal is the complete understanding of the CO phase transition through the interpretation of the vibrational spectra, and the drawing of a P-T phase diagram using Raman spectra.

IV-A-1 Charge Ordering in θ-(BEDT-TTF)$_2$RbZn-(SCN)$_4$ Studied by Vibrational Spectroscopy

**YAMAMOTO, Kaoru; YAKUSHI, Kyuya;
MIYAGAWA, Kazuya[1]; KANODA, Kazushi[1];
KAWAMOTO, Atsushi[2]**
(*[1]Univ. Tokyo; [2]Hokkaido Univ.*)

Spatial charge distribution in an insulating phase of θ-(BEDT-TTF)$_2$RbZn(SCN)$_4$ was investigated using polarized Raman and infrared (IR) spectroscopy. Figure 1 shows polarized Raman and IR spectra of the natural (non-substituted) and ^{13}C-substituted samples in the insulating phase. Both the Raman and IR spectra showed a complicated multiple-peak pattern stemming from two modes based on ring (ν_2) and central C=C stretchings (ν_3). From the isotope-shifts, we attributed peaks **a$_1$** and **a$_2$** to ν_2 and peaks **b$_1$**, **b$_2$**, **c$_1$**, and **c$_2$** to ν_3. While it is known that ν_2 and ν_3 commonly show a large frequency shift in proportion to a variation in the molecular charge, ν_3 provides a larger vibronic coupling effect than ν_2. Because of the strong vibronic-coupling, ν_3-related peaks showed a large Davydov splitting, allowing us to perform factor group analysis to specify the spatial pattern of the charge distribution. Meanwhile, the strong vibronic coupling causes an irregular frequency shift, hindering us to calculate the charge-disproportionation (CD) ratio from the frequency. To avoid the complicated shift due to the vibronic coupling, we used the weakly coupled mode ν_2 for the estimation of the CD ratio. The calculated ratio agrees with the value estimated by an NMR study. The agreement of the conclusions drawn by the two different approaches substantiates the explanation for the charge distribution and the reliability of this estimation method.
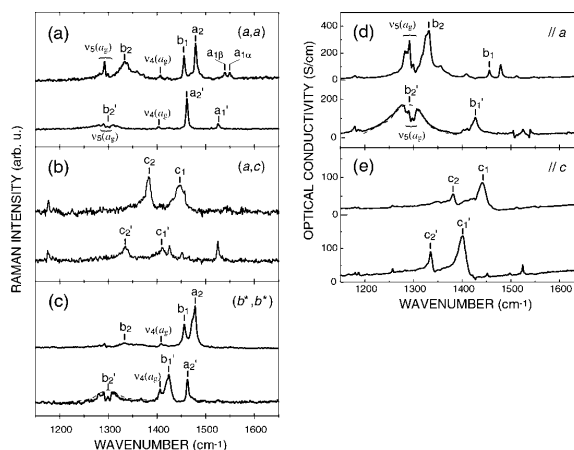
Figure 1. Polarized Raman and optical conductivity spectra of the natural (upper curve) and ^{13}C-substituted (lower curve) θ-(BEDT-TTF)$_2$RbZn(SCN)$_4$. (a), (b), and (c) show the (*a,a*), (*a,c*), and (*b*,b**)-polarized Raman spectra, and (d) and (e) show the *a*- and *c*-polarized optical conductivity spectra, respectively. (*T* = 50 K)

IV-A-2 Charge Disproportionation Ratio of (BEDT-TTF)$_3$CuBr$_4$ Studied by a Molecular Vibration Frequency

**YAMAMOTO, Kaoru; YAKUSHI, Kyuya;
YAMAURA, Jun-ichi[1]; ENOKI, Toshiaki[2]**
(*[1]Inst. Solid State Phys.; [2]Tokyo Inst. Tech.*)

Vibrational spectroscopy is a powerful tool to investigate charge distribution in charge transfer salts. Based on Raman and IR measurements for θ-(ET)$_2$Rb-Zn(SCN)$_4$, (ET: BEDT-TTF) we have proposed that a molecular charge can be estimated from the frequency of the ring C=C stretching mode (ν_2). In order to verify the reliability of the argument, we applied this analysis to other ET salts with a different molecular arrangement and band filling from the θ-type salt. The title compound (ET)$_3$CuBr$_4$ has a 3:1 stoichiometry. According to the x-ray diffraction study, the semi-

conductive salt shows charge ordering from room temperature. Raman spectra of this salt showed multiple peaks in the C=C stretching region. Based on the polarization dependence, we found two ν_2-related peaks among the multiple peaks. Figure 1 shows the reported ν_2 frequencies plotted with respect to the molecular charge. According to this plot, the observed two peaks are positioned approximately at $+0.9e$ and $+0.2e$. Supposing that there are two differently charged ET molecules ($+0.9e$ and $+0.2e$) in the ratio of 2:1, the average molecular charge is consistent with the stoichiometry. This suggests the certainty of the interpretation. This result supports the conclusion of the x-ray study proposing the presence of charge ordering, and demonstrates that the molecular-charge-estimation based on the ν_2 frequency can be applied for various systems.
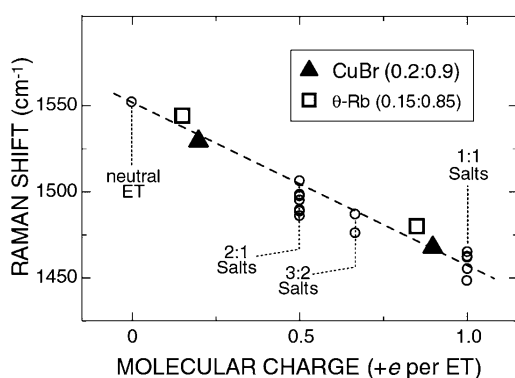
Figure 1. Raman frequencies of the ring C=C stretching (ν_2) modes *vs.* molecular charge.

IV-A-3 Charge and Molecular Arrangement in (DI-DCNQI)$_2$Ag Studied by Vibrational Spectroscopy

YAMAMOTO, Kaoru; YAKUSHI, Kyuya;
HIRAKI, Koichi[1]; TAKAHASHI, Toshihiro[1];
KANODA, Kazushi[2]; MENEGHETTI, Moreno[3]
(*[1]Gakushuin Univ.; [2]Univ. Tokyo; [3]Univ. Padova, Italy*)

(DI-DCNQI)$_2$Ag (see the inset of Figure 1) has a one-dimensional (1D) structure with a quarter-filled band. An x-ray diffraction and NMR studies revealed that there was a $4k_F$ charge-density wave (CDW) below 220 K. Both studies claim the $4k_F$ site CDW (see Figure 1c) for the insulating state of this compound. To examine the possible $4k_F$ bond CDW (see Figure 1d), we studied the molecular vibrations, since the vibronic modes are extremely sensitive to the lattice modulation such as bond CDW. As shown in Figure 1a, the optical conductivity spectrum of (DI-DCNQI)$_2$Ag shows clear vibronic bands below 3000 cm^{-1}, in contrast to (DMe-DCNQI)$_2$Cu, which is metallic with a uniform stacking structure. Because the CT dipole moments induced by EMV coupling are cancelled out in a uniform stack (1b) and $4k_F$ site CDW (1c) as shown in Figure 1, the appearance of the vibronic bands strongly suggests the $4k_F$ bond CDW (1d). Low-temperature Raman and IR measurements are in progress to examine whether the
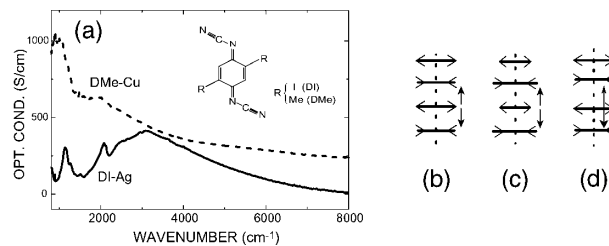
bond CDW and site CDW coexist or not.

Figure 1. (a) Optical conductivity spectra of (DI-DCNQI)$_2$Ag (solid line) and (DMe-DCNQI)$_2$Cu (dashed line) measured at room temperature. Schematic models of vibronically induced charge-transfer moment in (a) uniformly stacked, (b) $4k_F$ site CDW, and (c) $4k_F$ bond CDW. Horizontal bars and arrows represent a charge density and phase of a molecular vibration, respectively. Perpendicular arrows indicate the CT dipole moments induced by the molecular vibration.

IV-A-4 The C=C Stretching Vibrations of κ-(BEDT-TTF)$_2$Cu[N(CN)$_2$]Br and Its Isotope Analogues

MAKSIMUK, Mikhail[1]; YAKUSHI, Kyuya;
TANIGUCHI, Hiromi[2]; KANODA, Kazushi[2];
KAWAMOTO, Atsushi[3]
(*[1]IMS and Inst. Problem Chem. Phys.; [2]Tokyo Univ.; [3]Hokkaido Univ.*)

The C=C stretching modes in resonance Raman spectra and infrared reflectivity were measured at temperatures between 15 K and 300 K using various polarizations in κ-(BEDT-TTF)$_2$Cu[N(CN)$_2$]Br, its fully and partially deuterated analogues. The infrared- and Raman-active bands were re-assigned based on the factor group analysis. As shown in Figure 1, we found a Raman-active EMV-coupled ν_3 mode near 1420 cm^{-1}, which has B$_{2g}$ symmetry and shows a large downshift and broadening through the inter-dimer EMV interaction. The ν_2 and ν_3 modes are respectively the ring and bridge C=C stretching vibration, which mix with each other depending upon the positive charge on BEDT-TTF. We found that the mixing of the bridge and ring C=C stretching vibrations depended upon the symmetry of the crystal mode. The ν_{27} mode is an asymmetric ring C=C vibration, which vibrates out-of-phase within a dimer in the ν_{27} (A$_g$) crystal mode. In contrast to deuterated crystals, the non-deuterated crystals show a splitting in the ν_2, ν_3, and ν_{27}. The origin of this unusual finding is not clear at present.
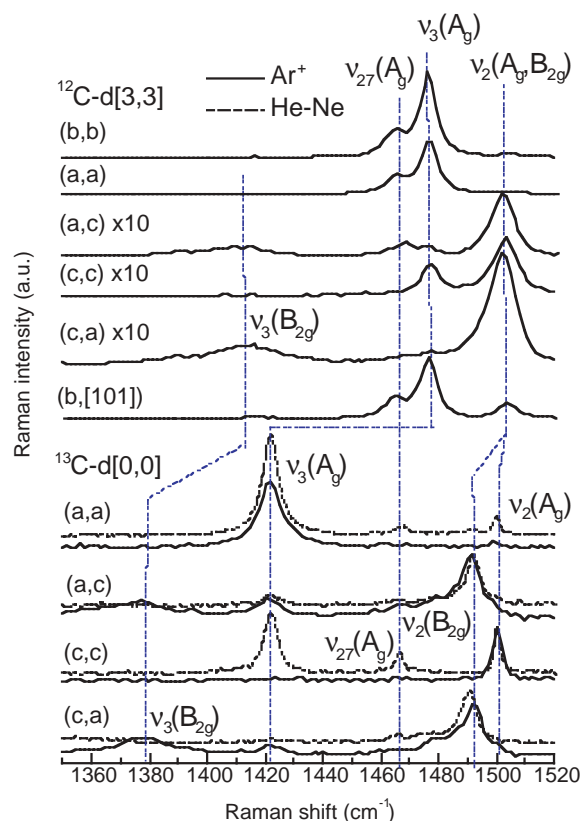
Figure 1. Raman spectra of ^{12}C-d[3,3] and ^{13}C-d[0,0] at 20 K. The intensity among the different polarizations is approximately scaled to each other in ^{12}C-d[3,3], but not scaled in ^{13}C-d[0,0]. In ^{12}C-d[3,3], three hydrogen atoms in each ethylene group are replaced by deuterium, and in ^{13}C-d[0,0], the two central ^{12}C atoms bridging the 1,3-dithiol rings are replaced by the carbon isotope ^{13}C.

IV-A-5 Plasma Frequency and Optical Effective Mass of κ-(ET-d$_8$)$_2$Cu(CN)[N(CN)$_2$]

DROZDOVA, Olga[1]; YAKUSHI, Kyuya; YAMOCHI, Hideki[2]; SAITO, Gunzi[2]
(*[1]IMS and Yoffe Inst. Phys., [2]Kyoto Univ.*)

κ-(ET)$_2$Cu(CN)[N(CN)$_2$] is a strongly correlated organic metal with superconducting transition at T_C = 11.2 K (ET-h$_8$) and T_C = 12.3 K (ET-d$_8$) at ambient pressure. Optical study was undertaken on single crystals of deuterated compound in a wide frequency region from far-IR to UV, along two main directions in the conducting (100) plane, at temperatures down to 6 K.

The tight-binding band calculation at 300 K predicts the intraband transition of the free charge carriers for two upper band branches, with the total calculated plasma frequency ~7000 cm^{-1} and the effective mass m^*/m_e = 2. However, in the experimental reflectivity spectra, the intraband transition appears at much lower frequency (ω < 300 cm^{-1} at T = 300 K). Almost no Drude peak can be found in the optical conductivity, and most of the spectral weight is contained in the broad mid-infrared peak.

Two distinctive temperature regions can be found. From 300 K down to 150 K, intensity of the mid-

infrared peak increases together with the intensity of the coupled EMV features. Below 150 K, the far-infrared reflectivity starts to grow rapidly. In the optical conductivity, it is accompanied by the shift of the spectral weight from the mid-infrared peak and EMV coupled features to the Drude peak.

The parameters of the electronic structure (ω_p, Γ_e) were obtained from the Drude-Lorentz dispersion analysis. At lower temperatures, the plasma frequency is rapidly growing (ω_p ~ 5500 cm^{-1} at 6 K). Ordinary sources of the low-temperature increase of the plasma frequency in a metal (Fermi-Dirac function, increase of the transfer integrals due to the crystal shrinking) cannot justify the observed three-to-four-fold growth. However, the growth of the plasma frequency can be explained by a temperature-dependent density of states in the strongly correlated metal accompanying a crossover from an incoherent transport at high temperatures to a coherent regime at lower T.

IV-A-6 Charge Order in θ-(BDT-TTP)$_2$Cu(NCS)$_2$

YAKUSHI, Kyuya; OUYANG, Jianyong[1]; SIMONYAN, Mkhitar[2]; MISAKI, Yohji[3]; TANAKA, Kazuyoshi[3]
(*[1]GUAS; [2]IMS and Inst. Phys. Res. ARAS; [3]Kyoto Univ.*)

[*Mol. Cryst. Liq. Cryst.* in press]

θ-(BDT-TTP)$_2$Cu(NCS)$_2$ is a highly correlated organic conductor with a quasi-two-dimensional electronic structure. We have found a charge disproportionation in θ-(BDT-TTP)$_2$Cu(NCS)$_2$ accompanying the phase transition at 250 K.[1] The magnetic properties of this compound was examined to know the pattern of the ordered charge. The paramagnetic susceptibility conforms to Curie-Weiss law down to about 30 K, makes a peak at 5–10 K, and drops to nearly zero at 1.8 K. This behavior suggests that the exchange interaction between localized charge is much weaker than that of θ-(BEDT-TTF)$_2$RbZn(SCN)$_4$ which shows a similar charge ordering phase transition. This result and the comparison of the optical conductivity with a theoretical calculation strongly suggest that the localized charge forms a vertical stripe in contrast to the horizontal stripe in θ-(BEDT-TTF)$_2$RbZn(SCN)$_4$. The horizontal stripe is more stable than the vertical stripe according to the calculation of Madelung energy in both compounds. The degree of charge disproportionation δ = 0.1–0.2, in (BDT-TTP)$^{\delta+}$(BDT-TTP)$^{(1-\delta)+}$ is also almost the same as that of θ-(BEDT-TTF)$_2$RbZn(SCN)$_4$ (δ = 0.1$_5$). The investigation of the reasoning of the different nature between θ-(BDT-TTP)$_2$Cu(NCS)$_2$ and θ-(BEDT-TTF)$_2$-RbZn(SCN)$_2$ is now in progress.

Reference
1) J. Ouyang, K. Yakushi, Y. Misaki and K. Tanaka, *Phys. Rev. B* **63**, 54301 (2001).

IV-A-7 Assignment of the In-Plane Molecular Vibrations of the Electron-Donor Molecule BDT-TTP Based on Polarized Raman and Infrared Spectra

**OUYANG, Jianyong[1]; YAKUSHI, Kyuya;
KINOSHITA, Tomoko[1]; NANBU, Shinkoh;
AOYAGI, Mutsumi; MISAKI, Yohji[2]; TANAKA,
Kazuyoshi[2]**
(*[1]GUAS; [2]Kyoto Univ.*)

To interpret the change of the vibrational spectrum accompanying the charge ordering and/or asymmetric charge distribution within the BDT-TTP molecule, we conducted the normal mode analysis of BDT-TTP. We first analyzed TTP-DO which have a TTP skeleton in order to obtain the force constants in the TTP skeleton, and then analyzed BDT-TTP based on the empirical force constants. The vibrational modes of TTP-DO are assigned with the aid of the depolarization ration of solution Raman spectra, polarized reflection and Raman spectra of single crystals. A D_{2h} symmetry is assumed for the BDT-TTP molecule and its in-plane fundamental vibrations are assigned with the aid of the polarization ratio and the correlation with TTP-DO, TTF, TMTTF, and BEDT-TTF. Normal coordinate calculation with a modified internal valence force field was carried out for the in-plane fundamental vibrations of TTP-DO and BDT-TTP. *Ab initio* calculations of the normal modes of BDT-TTP^0 and BDT-TTP$^+$ were compared with the empirical analysis. The agreement with the result of the empirical analysis was very good.

IV-A-8 Spectroscopic Study of the [0110] Charge Ordering in (EDO-TTF)$_2$PF$_6$

**DROZDOVA, Olga[1]; YAKUSHI, Kyuya; OTA,
Akira[2]; YAMOCHI, Hideki[2]; SAITO, Gunzi[2]**
(*[1]IMS and Yoffe Inst. Phys.; [2]Kyoto Univ.*)

(EDO-TTF)$_2$PF$_6$ is a novel organic metal, which undergoes a complex phase transition at 280 K. The feature of the phase transition includes a sharp metal-insulator transition with 1st order canceling of the magnetic moment, order-disorder transformation of PF$_6$, drastic change in the donor packing and shape, and a charge ordering.

IR spectra at 295 K show the Drude-like reflectivity along the stack (E||*b*), and a low background with a number of phonons for the perpendicular (E||*a**) direction. The optical conductivity for E||*b* displays a peak of 1500 Ω^{-1}cm^{-1} centered at 1200 cm^{-1}, which extrapolates smoothly to the measured conductivity σ_{dc} = 50 Ω^{-1}cm^{-1}. The peak has a distorted shape, with a dip due to the EMV coupling at 1400 cm^{-1}, and an extended high-frequency tail presumably due to the electron correlation effect. The electronic spectrum for E||*b* changes drastically below the phase transition: the peak at 1200 cm^{-1} completely disappears, and instead two charge-transfer bands emerge. The first is of D^{0}D$^+$ → D$^+$D^0 type, centered at 4500 cm^{-1}. It is the lowest electronic excitation of the low-temperature phase, and it compares well with the energy gap E_g = 0.64 eV measured on the compressed powder pellet. The second band is at 11150 cm^{-1}, corresponding to D$^+$D$^+$ → D^{2+}D^0 charge transfer.

Profound change appears in the vibrational spectra

in the region of charge-sensitive C=C stretching modes, as well. Neutral EDO-TTF has three C=C modes: ν_1 (EDO-ring, 1648 cm^{-1}), ν_2 (TTF-ring, 1538 cm^{-1}), and ν_3 (central, 1498 cm^{-1}). In the high-temperature phase, three IR and three Raman active C=C modes are allowed and can be observed in the specific polarizations. Their frequencies correspond to EDO-TTF$^{0.5+}$. Below 280 K, these are split into a total of 12 modes (6 IR + 6 R), half due to the charge-poor EDO-TTF and half due to the charge-rich ones. ν_3 and ν_1 of the charge-rich EDO-TTF were found to be strongly interacting with the 11150 cm^{-1} charge-transfer band, as evidenced by both the IR spectrum along the stacking axis, and by the selective resonance Raman effect of these modes with the 785 nm excitation wavelength in the same direction. From the ionization shifts, it was estimated that the charge on the charge-poor and charge-rich molecules is ≤ +0.1e and ≥ +0.9e, respectively, *i.e.* the charge is completely separated.
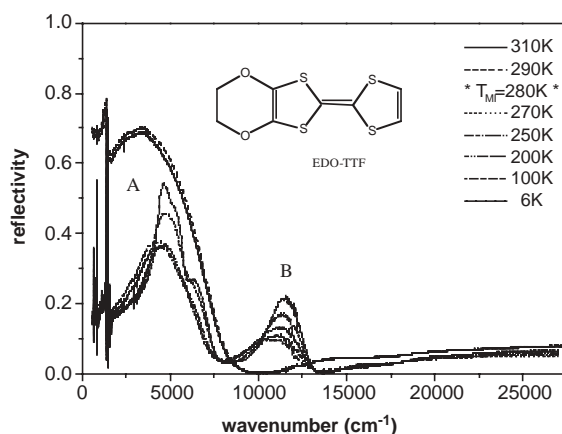
Figure 1. Temperature dependence of the reflection spectrum of EDO-TTF. The spectrum drastically changes from a metallic to insulating reflectivity at the phase transition temperature. The bands A and B correspond to the charge-transfer transitions of D$^+$D^0 → D^{0}D$^+$ and D$^+$D$^+$ → D^{0}D^{2+}, which clearly indicate the charge ordering such as D^{0}D$^+$D$^+$D^0.

IV-A-9 Structural and Spectroscopic Study of Quasi-One-Dimensional Organic Conductor, (BDTFP)$_2$X(C$_6$H$_5$Cl)$_{0.5}$ (X = AsF$_6$, PF$_6$)

**URUICHI, Mikio; YAKUSHI, Kyuya;
SHIRAHATA, Takashi[1]; TAKAHASHI, Kazuko[1];
MORI, Takehiko[2]; NAKAMURA, Toshikazu**
(*[1]Tohoku Univ.; [2]Tokyo Inst. Tech.*)

In (BDTFP)$_2$X(PhCl)$_{0.5}$ (X = PF$_6$, AsF$_6$), the BDTFP molecules are stacked along the *c*-axis with a dimerized structure. The crystal structure and polarized reflection spectra suggest a quasi-1D electronic structure along the *c*-axis. In spite of the isomorphous structure at room temperature, the PF$_6$ and AsF$_6$ salts show different kinds of phase transition. (BDTFP)$_2$PF$_6$(PhCl)$_{0.5}$ shows a magnetic phase transition at 175 K accompanying a resistivity jump, and undergoes a non-magnetic ground state. On the other hand, (BDTFP)$_2$AsF$_6$(PhCl)$_{0.5}$ shows a first-order phase transition at 250 K, and undergoes first a paramagnetic state and then an anti-ferromagnetic ground state. We determined the low-temperature

crystal structures below the phase transition temperature. In the former, the *c*-axis was doubled and thus the dimerized structure changed into a tetramerized structure. At the same time, a new charge-transfer transition appeared at 7000~8000 cm^{-1}. These two findings are consistent with the non-magnetic state. In the latter, on the other hand, dimerized structure was maintained below the phase transition temperature, and instead AsF$_6$ ion rotated with *ca.* 10° rotation of BDTFP. This structural change seems to be the origin of the first-order phase transition to a paramagnetic state.

BDTFP
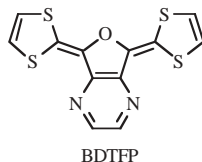
References

1) T. Ise, T. Mori and K. Takahashi, *J. Mater. Chem.* **11**, 264 (2001).
2) T. Nakamura, K. Takahashi, T. Ise, T. Shirahata, M. Uruichi, K. Yakushi and T. Mori, *Mol. Cryst. Liq. Cryst.* in press.

IV-A-10 Crystal Chemistry and Physical Properties of Superconducting and Semiconducting Charge Transfer Salts of the Type (BEDT-TTF)$_4$[A^{I}M^{III}(C$_2$O$_4$)$_3$] PhCN (A^I = H$_3$O, NH$_4$, K; M^{III} = Cr, Fe, Co, Al; BEDT-TTF = Bis(ethylenedithio) tetrathiafulvalene)

MARTIN, Lee[1]; TURNER, Scott T.[1]; DAY, Peter[1]; GUIONNEAU, Philippe[2]; HOWARD, Judith A. K.[3]; HIBBS, Dai E.[4]; LIGHT, Mark E.[4]; HURSTHOUSE, Michel B.[4]; URUICHI, Mikio; YAKUSHI, Kyuya
(*[1]Royal Inst. GB; [2]Inst. Chim. Matiere Condensee de Bordeaux; [3]Univ. Durham; [4]Univ. Southampton*)

Synthesis, structure determination by single-crystal X-ray diffraction, and physical properties are reported and compared for superconducing and semiconducting molecular charge-transfer salts with stoichiometry (BEDT-TTF)$_4$[A^{I}M^{III}(C$_2$O$_4$)$_3$] PhCN, where A^I = H$_3$O, NH$_4$, K; M^{III} = Cr, Fe, Co, Al. Attempts to substitute M^{III} with Ti, Ru, Rh, or Gd are also described. New compounds with M = Co and Al are prepared and detailed structural comparisons are made across the whole series. Compounds with A = H$_3$O$^+$ and M = Cr, Fe are monoclinic (space group *C2/c*), at 150, 120 K *a* = 10.240(1) Å, 10.232(2) Å; *b* = 19.965(1) Å, 20.04(3) Å; *c* = 34.905(1) Å, 34.97(2) Å; β = 93.69(1)°, 93.25(1)°, respectively, both with *Z* = 4. These salts are metallic at room temperature, becoming superconducting at 5.5(5) or 8.5(5) K, respectively. A polymorpoh with A = H$_3$O$^+$ and M = Cr is orthorhombic (*Pbcn*) with *a* = 10.371(1) Å, *b* = 19.518(3) Å, *c* = 35.646(3) Å, and *Z* = 4 at 150 K. When A = NH$_4^+$, M = Fe, Co, Al, the compounds are also orthorhombic (*Pbcn*), with *a* = 10.370(5) Å, 10.340(1) Å, 10.318(7) Å; *b* = 19.588(12) Å, 19.502(1) Å, 19.460(4) Å, *c* = 35.646(3) Å, 36.768(1) Å, 35.808(8) Å at 150 K, respectively, with *Z* = 4. All of the *Pbcn* phases are semiconducting with activation energies between 0.15 and 0.22 eV. For those compounds which are though to contain H$_3$O$^+$, Raman spectroscopy or C=C and C–S bond lengths of the BEDT-TTF molecules confirm the presence of H$_3$O$^+$ rather than H$_2$O. In the monoclinic compounds the BEDT-TTF molecules adopt a β" packing motif while in the orthorhombic phases (BEDT-TTF)$_2$ dimers are surrounded by monomers. Raman spectra and bond length analysis for the latter confirm that each molecule of the dimer has a charge of +1 while the remaining donors are neutral. All of the compounds contain approximately hexagonal honeycomb layers of [AM-(C$_2$O$_4$)$_3$] and PhCN, with the solvent occupying a cavity bounded by [M(C$_2$O$_4$)$_3$]$^{3-}$ and A. In the monoclinic series each layer contains one enatiomeric conformation of the chiral [M(C$_2$O$_4$)$_3$]$^{3-}$ anions with alternate layers having opposite chirality, whereas in the orthorhombic series the enantiomers form chains whicin each layer. Analysis of the supramolecular organization at the interface between the cation and anion layers shows that this difference is responsible for the two different BEDT-TTF packing motifs, as a consequence of weak H-bonding interactions between the terminal ethylene groups in the donor and the [M(C$_2$O$_4$)$_3$]$^{3-}$ oxygen atoms.

IV-B Solid State Properties of Organic Conductors with π-d Interaction

Some phthalocyanine molecules contain unpaired d-electrons in the conjugated π-electron system. Due to this nature, the itinerant π-electrons coexist with localized unpaired d-electrons in solid phthalocyanine salts, in which a one-dimensional double-chain system (metal and ligand chain) is formed. Furthermore these chains make up wide (π-band) and narrow (d-band) one-dimensional bands. The energy of the narrow band is close to the Fermi energy of the wide band. The phthalocyanine conductor is thus a two-chain and two-band system. The electronic structure of phthalocyanine conductors is analogous to that of the f-electron system, in which a narrow f-band coexists with a wide s-band and they are hybridized near the Fermi level. To understand the electronic structure of this two-band system, we are investigating the charge-transfer salts of NiPc and CoPc and their mixed crystals.

IV-B-1 Preparation and Characterization of Phthalocyanine-Based Organic Alloy $Co_xNi_{1-x}Pc(AsF_6)_{0.5}$ ($0 \leq x \leq 1$)

DING, Yuqin[1]; SIMONYAN, Mkhitar[2]; YONEHARA, Yukako[1]; URUICHI, Mikio; YAKUSHI, Kyuya
(*[1]GUAS; [2]IMS and Inst. Phys. Res. ARAS*)

The organic alloy $Co_xNi_{1-x}Pc(AsF_6)_{0.5}$ ($0 \leq x \leq 1$) was prepared and characterized by elementary analysis (EPMA), X-ray diffraction, ESR, magnetic susceptibility, Raman spectroscopy and reflection spectroscopy. These experiments show that mixed crystals are formed for a wide range of x although $CoPc(AsF_6)_{0.5}$ is not exactly isomorphous to $NiPc(AsF_6)_{0.5}$. The mixing on a molecular level is proved by the x dependence of the ESR and Raman spectra over the whole range of x. The localized spin on Co^{2+} occupies the $3d_{z^2}$ orbital, which is extended to the stacking axis. The reflection spectrum shows that this d orbital forms a one-dimensional band along the stacking axis and closely located near the Fermi level of 3/4-filled π band. We found a very weak $3d_{z^2}$-to-$3d_{x^2-y^2}$ inter-molecular charge transfer transition through the resonance effect of Raman spectrum in the alloy system. Based on the above results, we proposed a model for the energy band near the Fermi level including the 3d bands. This band model explained the differences in the magnetic and optical properties between $CoPc(AsF_6)_{0.5}$ and $NiPc(AsF_6)_{0.5}$.
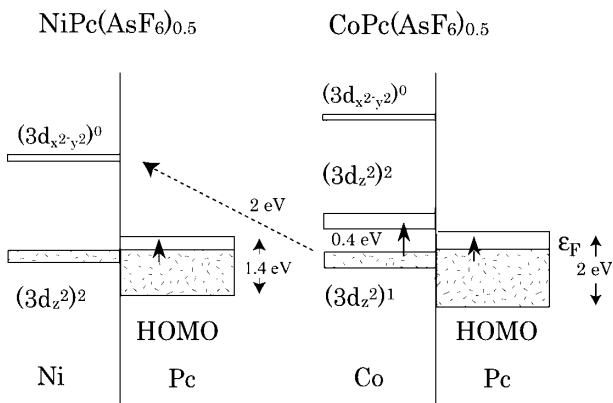
Figure 1. Schematic band structure including 3d bands. The arrows denote the optical transition along the conducting axis detected in the reflection spectra and through resonance effect of Raman spectrum.

IV-B-2 Electronic States and Infrared Spectroscopy of Nickel and Cobalt Phthalocyanines: *Ab initio* Calculations for the Neutral and Cation States

TOMAN, Petr[1]; NESPUREK, Stanislav[1]; YAKUSHI, Kyuya
(*[1]Inst. Macromolecular Chem. ASCR*)

Organic conductors such as TMTSF, BEDT-TTF,

and DCNQI have charge sensitive vibrational bands, which show red shift upon oxidation or reduction. This phenomenon comes from the reorganization of the molecular geometry. By contrast, metallophthalo-cyanine (MPc) has no such vibrational bands, because the molecular geometry is rigid against the oxidation. However, MPc has characteristic vibrational bands, the intensity of which changes upon oxidation. The reason for this change is associated with the change of the charge distribution between neutral and oxidized MPc. We calculated the frequency and intensity of the normal mode of NiPc and CoPc by the B3LYP method. This *ab initio* calculation clearly showed the ligand oxidation both in NiPc and CoPc, which agreed with the experimental observation. Besides, the calculation reproduced the frequency of the infrared-active modes, and the intensity changes of the characteristic bands: the 1291, 1356, 1471, and 1533 cm^{-1} bands of NiPc and 1290, 1468, and 1525 cm^{-1} bands of CoPc.

Using the molecular orbitals, the overlap integrals are calculated between a_{1u} HOMO a MPc and the a_{1g} $3d_{z^2}$ orbital of the adjacent molecule in $MPc(AsF_6)_{0.5}$. The extremely small overlap integral indicates no hybridization between the HOMO band and $3d_{z^2}$ band, in other words, these two bands are almost independent.

IV-B-3 Metal to Insulator Transition of One-Dimensional Bis(1,2-benzoquinonedioximato)-platinum(II), $Pt(bqd)_2$, at Low Temperatures and High Pressures

TAKEDA, Keiki[1]; SHIROTANI, Ichimin[1]; SEKINE, Chihiro[1]; YAKUSHI, Kyuya
(*[1]Muroran Inst. Tech.*)

The electrical resistivity of the high quality single crystals of one-dimensional bis(1,2-benzoquinone-dioximato)platinum(II), $Pt(bqd)_2$, has been studied at low temperatures and high pressures under hydrostatic conditions. The resistivity along the c-axis abruptly decreases with increasing pressure up to 0.9 GPa at room temperature. $Pt(bqd)_2$ with an energy gap of about 0.3 eV at ambient pressure indicates the insulator-to-metal (IM) transition at around 0.8 GPa. The x-ray diffraction and the electronic spectrum of $Pt(bqd)_2$ have been studied at room temperature and high pressures. The mechanism of the IM transition of $Pt(bqd)_2$ is discussed. Below 235 K the resistivity of $Pt(bd)_2$ increases with decreasing temperature at around 0.8 GPa. The metal-to-insulator (MI) transition for $Pt(bqd)_2$ is found at around 235 K under 0.8 GPa. This is the first example that the one-dimensional metal formed from single molecules shows the MI transition at low temperatures.

IV-C Microscopic Investigation of Molecular-Based Conductors

The aim of this research is to clarify the electronic states (charge and spin states) of molecular based compounds with curious electronic phases by microscopic point of view. Although the fundamental properties of molecular based conductors have been very well clarified, it is true that there still remain several unsolved questions in the molecular based conductors.

Microscopic investigations are advantageous for understanding the microscopic charge and spin states. To clarify the low temperature electronic states, we performed the ^{1}H, ^{13}C NMR, and ESR measurements for molecular based conductors.

IV-C-1 Possible Successive SDW Transition in (EDT-TTF)$_2$AuBr$_2$

NAKAMURA, Toshikazu

[*J. Phys. Soc. Jpn.* **69**, 4026 (2000)]

The low temperature magnetic properties in the quasi-one-dimensional system, (EDT-TTF)$_2$AuBr$_2$, were investigated by using ^{1}H-NMR and ESR techniques. (EDT-TTF)$_2$AuBr$_2$ undergoes an SDW transition at 16 K. At 6 K, an anomalous second-peak of ^{1}H-NMR spin-lattice relaxation rate, ^{1}H-T_1^{-1}, in the SDW phase has been observed. An additional increase of ^{1}H-NMR absorption line and gradual decrease of spin-spin relaxation rate, ^{1}H-T_2^{-1}, were observed below 6 K. The magnetic properties of the SDW phase observed in the present salt are discussed from microscopic points of view.
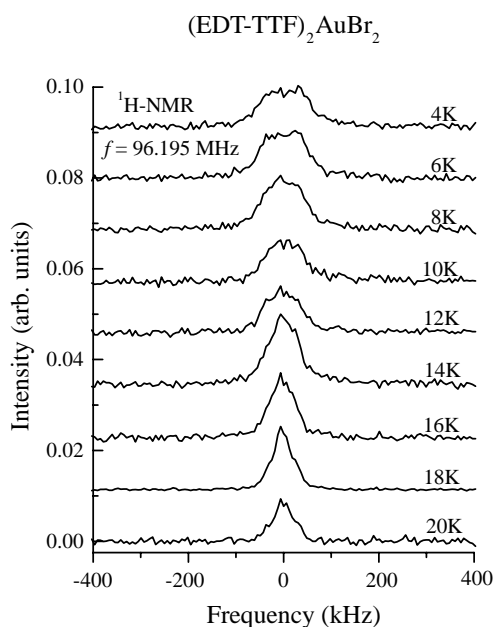
Figure 1. Temperature dependence of the ^{1}H-NMR absorption lines of powdered (EDT-TTF)$_2$AuBr$_2$ crystals.
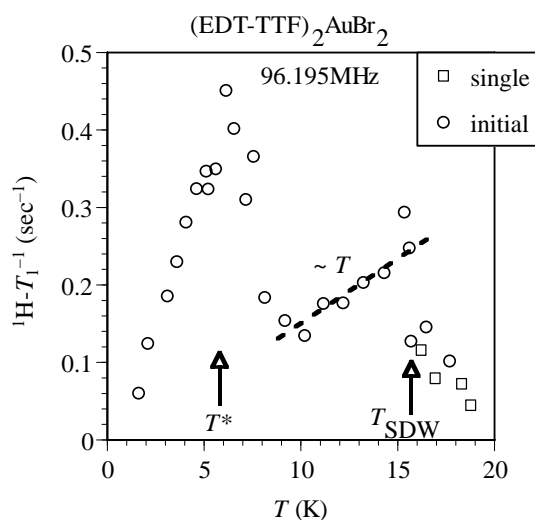
Figure 2. Temperature dependence of the ^{1}H-NMR spin-lattice relaxation rate, T_1^{-1}, in the SDW phase.

IV-C-2 Magnetic Investigation of Organic Conductors Based on TTP Derivatives

TSUKADA, Hiroshi; NAKAMURA, Toshikazu; MISAKI, Yohji[1]; TANAKA, Kazuyoshi[1]
(*[1]Kyoto Univ.*)

[*Synth. Met.* **120**, 869 (2001)]

Magnetic investigation of organic conductors based on TTP derivatives, (BDT-TTP)$_2$SbF$_6$ and (EO-TTP)$_2$-AsF$_6$, was carried out by ^{1}H-NMR measurements. The NMR spin-lattice relaxation rates, ^{1}H-T_1^{-1}, of the present salts deviate from the Korringa-like behavior at low temperatures. The low-temperature electronic states of the TTP family will be discussed from microscopic points of view.
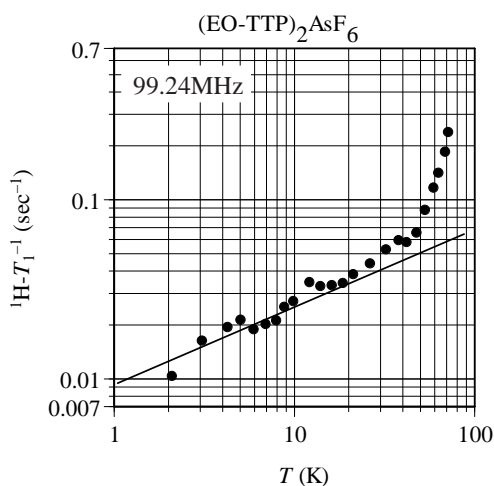
Figure 1. Temperature dependence of the ^{1}H-T_1^{-1} of (EO-TTP)$_2$AsF$_6$.

IV-C-3 Magnetic Properties of Organic Spin-Ladder Systems, (BDTFP)$_2$X(PhCl)$_{0.5}$

NAKAMURA, Toshikazu; TAKAHASHI, Kazuko[1]; ISE, Toshihiro[1]; SHIRAHATA, Takashi[1]; URUICHI, Mikio; YAKUSHI, Kyuya; MORI, Takehiko[2]
(*[1]Tohoku Univ.; [2]Tokyo Inst. Tech.*)

(BDTFP)$_2$X(PhCl)$_{0.5}$ (X = AsF$_6$, PF$_6$) are quasi-one-dimensional organic conductors with so-called two leg ladder structures; the inter-ladder interaction is one-order smaller than that in intra-ladder. Since there is a considerable dimerization within the column, the upper band is a half-filled.

Figure 1 shows the temperature dependence of the spin susceptibility of the PF$_6$ salt. Between 170 and 300 K, the spin susceptibility is almost temperature independent, but gradually increases as temperature decreases. The EPR signal intensity suddenly decreases below 170 K where the resistivity shows an abrupt jump. The EPR linewidth also shows anomaly; it abruptly decreases around 170 K, suggesting an abrupt change of the relaxation mechanism of the electron spins. It is proved that the low temperature phase of the PF$_6$ salt is spin-singlet.

Figure 2 shows the temperature dependence of the spin susceptibility of the AsF$_6$ salt. In the case of the cooling process, the spin susceptibility abruptly increases around 230 K, suggesting the existence of a phase transition. Below 200 K, the spin susceptibility of the AsF$_6$ salt shows a Curie-like enhancement. This hysteresis phenomenon indicates that the transition is of first order. The low temperature phases are undoubtedly different between the AsF$_6$ and PF$_6$ salts. Below 50 K, the spin susceptibility of the AsF$_6$ salt turns to decrease, indicating spin-gap behavior. It fits with Troyer's prediction for the undoped two-leg ladder. However an abrupt broadening of the EPR line indicates existence of a magnetic order at 14 K.

Although the electronic states of the PF$_6$ and AsF$_6$ salts at R. T. are very similar, those at low temperatures are quite different. Detailed investigations are now going on.
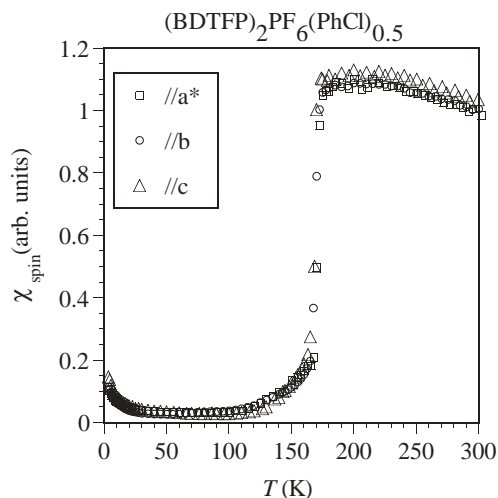
Figure 1. Temperature dependence of the spin susceptibility of (BDTFP)$_2$PF$_6$(PhCl)$_{0.5}$ determined by the EPR signal intensity of a single crystal.
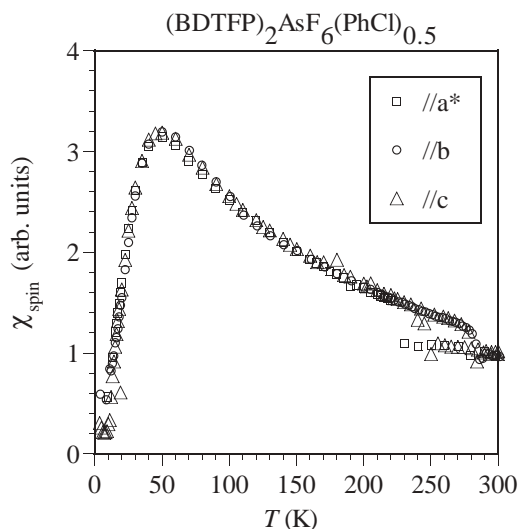
Figure 2. Temperature dependence of the spin susceptibility of (BDTFP)$_2$AsF$_6$(PhCl)$_{0.5}$ determined by the EPR signal intensity of a single crystal.

IV-C-4 EPR Investigation of the Electronic States in β'-type [Pd(dmit)$_2$]$_2$ Compounds (Where dmit is the 1,3-dithia-2-thione-4,5-dithiolato)

NAKAMURA, Toshikazu; TAKAHASHI, Toshihiro[1]; AONUMA, Shuji[2]; KATO, Reizo[2,3]
(*[1]Gakushuin Univ.; [2]Univ. Tokyo; [3]Inst. Phys. Chem. Res.*)

Magnetic investigations of organic conductors, β'-type [Pd(dmit)$_2$]$_2$, have been performed by Electron Paramagnetic Resonance (EPR) measurements. We found that most of them except one compound underwent antiferromagnetic transitions. Although they are isostructural with little differences in lattice

parameters, their spin-spin correlations and antiferromagnetic transition temperatures show strong counter ion dependence. The EPR *g*-values of Pd(dmit)$_2$ cannot be explained within the framework of isolated radical description, which is a good approximation for conventional organic conductors. The electronic structures of a series of molecular conductors based on Pd(dmit)$_2$ at ambient pressure are discussed from microscopic points of view.
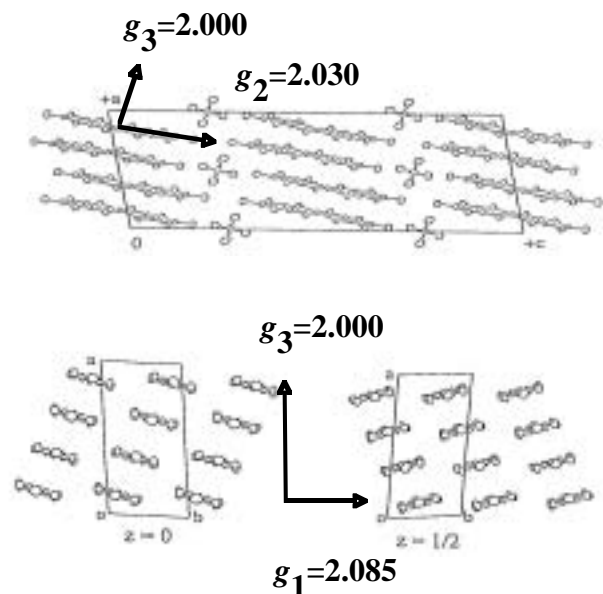
Figure 1. Determined principal axes and values β'-Et$_2$Me$_2$P-[Pd(dmit)$_2$]$_2$ on the actual crystal structure.

IV-C-5 Microscopic Investigation of Itinerant and Local Spins System, (CHTM-TTP)$_2$TCNQ

NAKAMURA, Toshikazu; TANIGUCHI, Masateru[1]; MISAKI, Yohji[1]; TANAKA, Kazuyoshi[1]; NOGAMI, Yoshio[2]
(*[1]Kyoto Univ.; [2]Okayama Univ.*)

(CHTM-TTP)$_2$TCNQ is a new organic conductor developed by Kyoto university group. This compound is composed of segregated donor (CHTM-TTP) and acceptor (TCNQ) layers. The CHTM-TTP molecules stack to form one-dimensional columns. On the other hand, there is little interaction between the TCNQ molecules. This salt shows metallic behavior down to 30 K with abrupt jump around 240 K. In order to clarify the low temperature electronic phases of this salt, we performed magnetic investigation.

Figure 1 shows the temperature dependence of the spin susceptibility determined by the EPR signal intensity. Between 240 K and 300 K, the spin susceptibility shows a gradual increase as the temperature decreases. At 240 K and 170 K, the spin susceptibility decreases abruptly. The principal values of the *g*-tensor change their absolute values both at the transition temperatures. It cannot be explained within the framework of one spin picture . These observations lead us to a conclusion that effective local moments on TCNQ decrease at 240 K, and that disappear perfectly below 170 K.
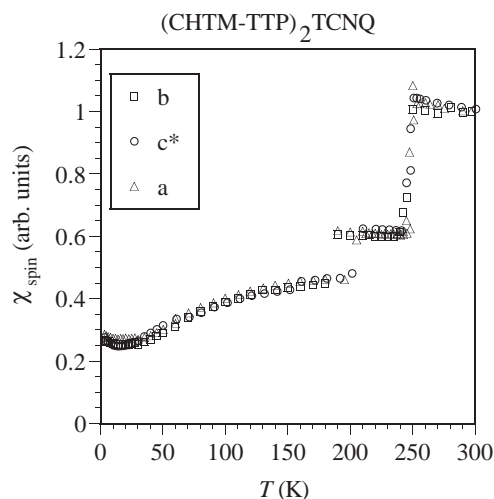
Figure 1. Temperature dependence of the spin susceptibility of (CHTM-TTP)$_2$TCNQ determined by the EPR signal intensity of a single crystal.

IV-D Development of Magnetic Organic Superconductors and Related Systems

Although the first organic superconductor $(TMTSF)_2PF_6$ called Bechgaard salt possesses one-dimensional electronic band structure, its crystal structure gave a large hint to design two-dimensional metals without one-dimensional metal instabilities. In fact, with the aid of the guiding principle on the design of molecular conductors based on simple extended Hückel tight binding band picture, we could find the first κ-type organic superconductor with typical two-dimensional cylindrical Fermi surface in 1987 ($κ$-ET_2I_3). Since a number of κ-type organic superconductors including the system with the highest-T_c record ($κ$-$ET_2Cu[N(CN)_2]Cl$; T_c = 12.8 K at 0.3 kbar) have been discovered and the κ-type molecular conductors are nowadays regarded as the most typical two-dimensional metals. However the recent development of the simple typical organic superconducting systems becomes somewhat stagnant in the last decade. On the other hand, an increasing interest is going to be attracted to the magnetic organic conducting systems where the magnetic order and superconductivity are expected to coexist.

We have recently found the systems exhibiting unprecedented superconductor-to insulator transition and the first antiferromagnetic organic superconductor constructed of BETS (= bis(ethylenedithio)tetraselenafulvalene) molecules and magnetic anions containing Fe^{3+}. Furthermore, we have recently discovered a field-induced superconducting transition in another type of two-dimensional conductor, $λ$-$BETS_2FeCl_4$.

IV-D-1 Magnetic-Field Induced Super-conductivity in a Two-Dimensional Organic Conductor

UJI, Shinya[1]; SHINAGAWA, Hideyuki[1]; TERASHIMA, Taichi[1]; YAKABE, Taro[1]; TERAI, Yoshikazu[1]; TOKUMOTO, Madoka[2]; KOBAYASHI, Akiko[3]; TANAKA, Hisashi; KOBAYASHI, Hayao
(*[1]Natl. Res. Inst. Metal; [2]Electrotechnical Lab.; [3]Univ. Tokyo*)

The application of sufficiently strong magnetic field to superconductor will, in general, destroy the superconducting state. Two mechanisms are responsible for this. The first is the Zeeman effect, which breaks apart the paired electrons if they are in a spin-singlet (but not a spin-triplet) state. The second is the so-called orbital effect, whereby the vortices penetrate into the superconductors and the energy gain due to the formation of the paired electrons is lost. In this paper we have reported resistance and magnetic torque experiments on single crystals of the quasi-two-dimensional organic conductor $λ$-$(BETS)_2FeCl_4$, where the field-induced insulator-to metal transition has been previously discovered around 10 T. We found that for magnetic fields applied exactly parallel to the conducting layers of the crystals, superconductivity is induced for fields above 17 T at a temperature of 0.1 K. The resulting phase diagram indicates that the transition temperature increases with magnetic field.
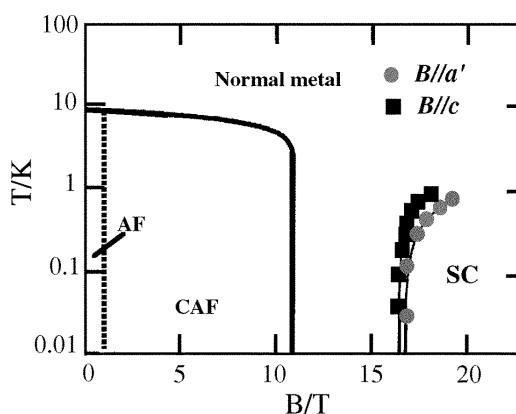
Figure 1. Temperature versus magnetic field diagram for $λ$-$(BETS)_2FeCl_4$.

IV-D-2 Superconductivity in an Organic Insulator at Very High Magnetic Fields

BALICAS, Luis[1]; BROOKS, James[1]; STORR, Kevin[1]; UJI, Shinya[2]; TOKUMOTO, Madoka[3]; TANAKA, Hisashi; KOBAYASHI, Hayao; KOBAYASHI, Akiko[4]; BARZYKIN, Victor[1]; GOR'KOV, Lev[1]
(*[1]Florida State Univ.; [2]Natl. Res. Inst. Metal; [3]Electrotechnical Lab.; [4]Univ. Tokyo*)

We investigated by electrical transport the field-induced superconducting state (FISC) in the organic conductor $λ$-$BETS_2FeCl_4$. Below 4 K, antiferromagnetic-insulator, metallic and eventually superconducting (FISC) ground state are observed with increasing in-plane magnetic field. As shown in Figure 1, the superconducting state develops progressively with decreasing temperature but is suppressed for fields sufficiently away from 33 T. The temperature-magnetic field phase diagram shows the maximum temperature of the FISC phase of about 4.2 K is realized around 33 T, which is lower than T_c of $λ$-$BETS_2GaCl_4$ ($≈ 5.5$ K). The

FISC state survives between 18 and 41 T and can be interpreted in terms of the Jaccarino-Peter effect, where the external magnetic field compensates the exchange field of aligned Fe^{3+} ions. We further argue that the Fe^{3+} moments are essential to stabilize the resulting singlet, two-dimensional superconducting state.
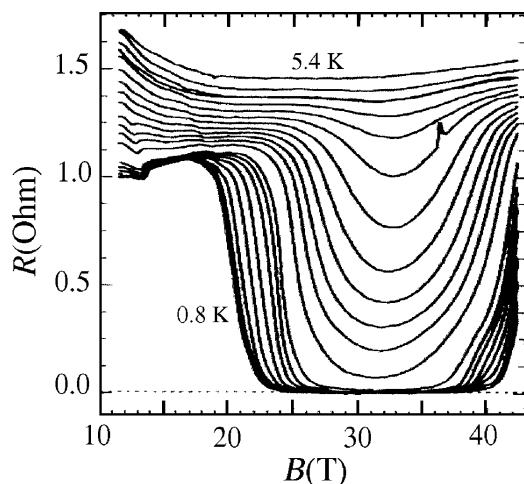
Figure 1. Resistance as a function of magnetic field B, applied along the in-plane c axis of λ-$BETS_2FeCl_4$ single crystal for temperature intervals of approximately 0.25 K, between 5.4 and 0.8 K.

IV-D-3 Novel Electronic Property in Organic Conductor: Superconductivity Stabilized by High Magnetic Field

UJI, Shinya[1]; KOBAYASHI, Hayao; BROOKS, James[2]
(*[1]Natl. Res. Inst. Metal; [2]Florida State Univ.*)

[*Adv. Mater.* in press]

Organic conductors have attracted considerable interest because of the characteristic properties relating to their low dimensionality of the electronic states. Among various organic conductors, λ-$(BETS)_2FeCl_4$ is one of the most attractive materials in the last decade because strong competition is expected between the antiferromagnetic order of the Fe moments and the superconductivity. λ-$(BETS)_2FeCl_4$ is known to have a unique phase diagram. At zero magnetic field, it shows a metal-insulator transition around 8 K, while the isostructural non-magnetic salt λ-$(BETS)_2GaCl_4$ undergoes a superconducting transition around 6 K. The metal-insulator transition in λ-$(BETS)_2FeCl_4$ is associated with the antiferromagnetic (AF) order of the Fe moments with the spins $S = 5/2$. The insulating phase is destabilized by the magnetic field above about 10 T, and a paramagnetic metallic state with ferromagnetically oriented Fe^{3+} spins is recovered. Furthermore, a field-induced superconductivity (FISC) has been recently discovered at 18–41 T. FISC has been reported for a Chevrel compounds $Eu_xSn_{1-x}Mo_6S_8$ with $T_c = 3.8$ K. As field increases, the superconductivity is destroyed at about 1 T but is restored by the field of 4 T below 0.1 K. This phenomenon is understood in terms of Jaccarino-Peter (J-P) compensation effect. Due to the

antiferromagnetic coupling between the Eu spins and the conduction electrons, the exchange polarization can be compensated by an external field leading to the reappearance of superconductivity (FISC) at high magnetic field. J-P effect is considered to be essential also for FISC of λ-$(BETS)_2FeCl_4$.
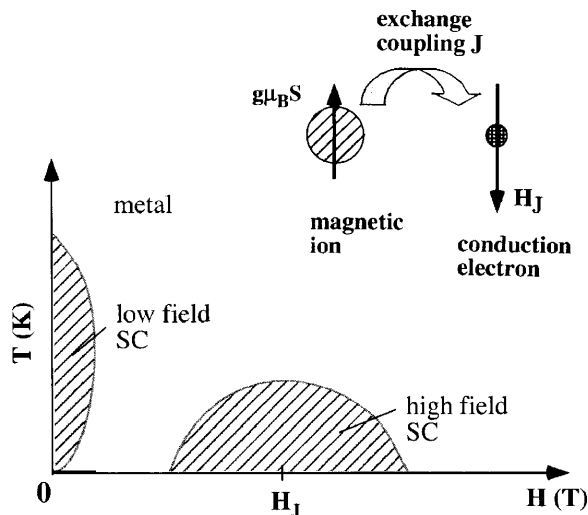
Figure 1. Schematic phase diagram of the system showing FISC and schematic picture of J-P effect.

IV-D-4 Field-Induced Superconducting Phase of λ-$(BETS)_2Fe_xGa_{1-x}Cl_4$

KOBAYASHI, Hayao; TANAKA, Hisashi; ZHANG, Bin; KOBAYASHI, Akiko[1]; TOKUMOTO, Madoka[2]; UJI, Shinya[3]; BROOKS, James[4]
(*[1]Univ. Tokyo; [2]Electrotechnical Lab; [3]Natl. Res. Inst. Metal; [4]Florida State Univ.*)

About a decades ago, we have tried to develop a series of BETS conductors with magnetic anions, with the aim of studying the π-d interaction in organic conductors. In fact, many interesting phenomena have been found in λ- and κ-$(BETS)_2FeX_4$ (X = Cl, Br). For example, λ-$(BETS)_2FeCl_4$ exhibits various phase transitions: (1) At ambient pressure, the system undergoes a coupled antiferromagnetic (AF) and insulating transition around 8.5 K. (2) At high pressure, this AF insulating state is suppressed and the superconducting phase is stabilized (> 3 kbar). (3) Furthermore, by applying magnetic field, the ground state is changed as, the AF insulating state → metallic state → superconducting state → metallic state with increasing magnetic field. In addition, with decreasing temperature, the alloy system, λ-$(BETS)_2Fe_xGa_{1-x}FeCl_4$ (0.35 < x < 0.5) exhibits the transitions as, metallic state → insulating state → superconducting state. We have recently examined the resistivities of λ-$(BETS)_2Fe_x$-$Ga_{1-x}FeCl_4$ ($x \approx 0.35$), which exhibits a subsequent metal → superconductor → insulator transition at zero magnetic field. The superconducting state can survive up to 15 T (= maximum field in this study) when magnetic field is approximately parallel to the conduction plane. Considering that the superconducting state of λ-$(BETS)_2GaCl_4$ is broken above 10 T, the phase diagram shown in Figure 1 is of special interest.
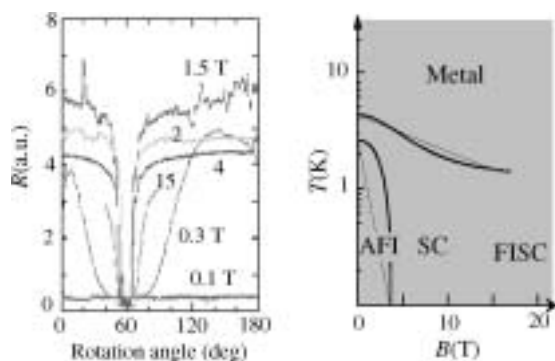
Figure 1. (a) Resistivity of λ-(BETS)$_2$Fe$_x$Ga$_{1-x}$FeCl$_4$ ($x \approx$ 0.35) for various orientation of the crystal ($T \approx$ 1–3 K) (b) Schematic T-B phase diagram.

IV-D-5 Antiferromagnetic Ordering of Fe^{3+} Ions in Organic Superconductor, κ-BETS$_2$FeCl$_x$Br$_{4-x}$

FUJIWARA, Emiko; FUJIWARA, Hideki; KOBAYASHI, Hayao; KOBAYASHI, Akiko[1]
(*[1]Univ. Tokyo*)

Recently we have found the first and second antiferromagnetic organic superconductors, κ-BETS$_2$FeX$_4$ (X = Br and Cl) which undergo antiferromagnetic transitions at 2.5 K (Br) and 0.6 K (Cl) and a superconducting transitions at 1.1 K (Br) and 0.1 K (Cl). In this work, the magnetic and electrical properties of κ-BETS$_2$FeCl$_x$Br$_{4-x}$ were examined by using one single crystal. The temperature dependence of the magnetic susceptibility and the field (H) dependence of the magnetization (M) at 2 K of κ-(BETS)$_2$FeCl$_x$Br$_{4-x}$ revealed that the Néel temperature (T_N) shifts to lower temperature with the increase of chlorine contents (x). Moreover, the easy spin axis was found to rotate from the direction parallel to a axis to b axis with increasing x. In other words, though the metamagnetic behavior of pure FeBr$_4$ system ($x = 0$) was observed for the magnetic field parallel to a, that of the FeClBr$_3$ system ($x = 1.0$) was observed for the field parallel to b. The magnetic field dependence of the electrical resistivities showed that both T_N where the resistivity step was observed and T_c decreased rapidly with the increase of x.
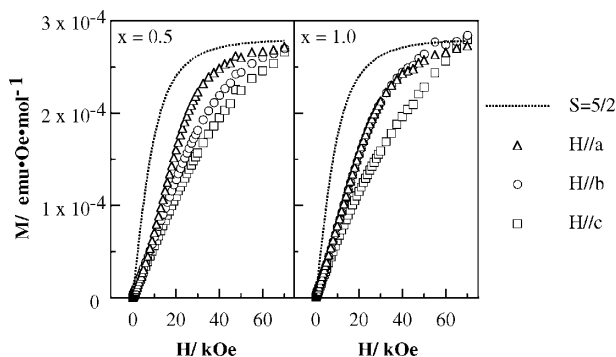
Figure 1. (a) Field (H) dependence of the magnetization (M) at 2.0 K of κ-(BETS)$_2$FeCl$_x$Br$_{4-x}$ ($x \approx$ 0.5 and 1.0). The field were applied along the three axes of crystal lattices. The Brillouin function with S = 5/2 is also shown for comparison.

IV-D-6 The *x*-Dependence of Electrical Properties and Antiferromagnetic Ordering between Fe^{3+} Ions in κ-BETS$_2$Fe$_{1-x}$Ga$_x$Br$_4$ System

FUJIWARA, Hideki; FUJIWARA, Emiko; KOBAYASHI, Hayao; KOBAYASHI, Akiko[1]
(*[1]Univ. Tokyo*)

As reported before, both κ-BETS$_2$FeBr$_4$ and κ-BETS$_2$GaBr$_4$ salts are isostructural to each other and showed superconductivity around 1 K, but the transition of GaBr$_4^-$ salt is very broad compared to the case of FeBr$_4^-$ salt. Furthermore, FeBr$_4^-$ salt exhibited the antiferromagnetic ordering of Fe^{3+} spins at 2.5 K. Therefore we have measured the magnetic and electrical properties of the alloy system κ-BETS$_2$Fe$_{1-x}$Ga$_x$Br$_4$ to investigated the gallium contents-dependence of the antiferromagnetic ordering of Fe^{3+} spins and the superconducting state. The temperature dependence of the magnetic susceptibility of κ-BETS$_2$Fe$_{1-x}$Ga$_x$Br$_4$ (Ga = 0.1 and 0.2) revealed that the Néel temperature shifts to lower temperature with the increase of the gallium contents (2.3 K for x = 0.1 and 2.1 K for x = 0.2). On the other hand, the measurement of the electrical resistivities of κ-BETS$_2$Fe$_{0.9}$Ga$_{0.1}$Br$_4$ showed that the temperature of the step-like drop of resistivities, which is in good agreement with the Néel temperature determined from the magnetic measurement, also shifts to lower temperature (2.3 K) with the increase of the gallium contents. On the other hand, the mid-point of the critical temperature of superconductivity is almost the same as that of the κ-BETS$_2$FeBr$_4$ salt (1.1 K), but the transition became broader than the case of the κ-BETS$_2$FeBr$_4$ salt.
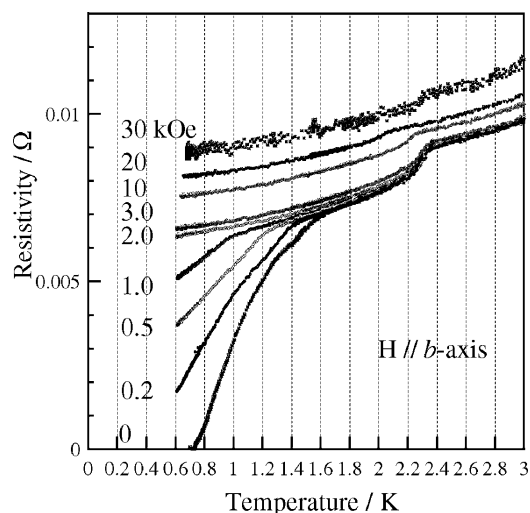
Figure 1. Magnetic field dependence of the electrical resistivities of κ-BETS$_2$Fe$_{0.9}$Ga$_{0.1}$Br$_4$.

IV-D-7 Organic Antiferromagnetic Metals Exhibiting Superconducting Transitions κ-(BETS)$_2$FeX$_4$ (X = Cl, Br): Drastic Effect of Halogen Substitution on the Successive Phase Transitions

OTSUKA, Takeo[1]; KOBAYASHI, Akiko[1];

**MIYAMOTO, Yasuhisa[1]; WADA, Nobuo[1];
FUJIWARA, Emiko; FUJIWARA, Hideki;
KOBAYASHI, Hayao**
(*[1]Univ. Tokyo*)

The magnetic and thermal properties of an organic conductor incorporating localized magnetic moments, κ-$(BETS)_2FeCl_4$ were investigated down to 60–70 mK. Similar to the Br analogue κ-$(BETS)_2FeBr_4$, κ-$(BETS)_2FeCl_4$ exhibited a successive antiferromagnetic and superconducting transitions with lowering temperature ($T_N = 0.45$ K, $T_c = 0.1$ K). That is, κ-$(BETS)_2FeCl_4$ is the second antiferromagnetic organic metal which exhibits a superconducting transition at ambient pressure. It became clear that the halogen exchange (Br $\rightarrow$ Cl) in the anions results in the strong reduction of both magnetic and superconducting transition temperatures. Resistivities showed a small drop at 0.45 K (= T_N), which gave a direct evidence of the existence of π-d interaction between π metal electrons and localized magnetic moments of Fe. In contrast to κ-$(BETS)_2FeBr_4$ exhibiting three-dimensional nature of the magnetic transition, the specific heat of κ-$(BETS)_2FeCl_4$ indicates the low-dimensionality of the spin system.
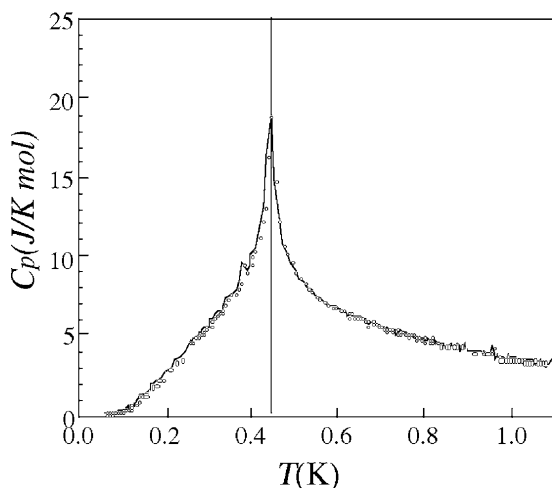
Figure 1. The specific heat of κ-$(BETS)_2FeCl_4$.

IV-D-8 A New Molecular Superconductor, κ-$(BETS)_2TlCl_4$

**GRITSENKO, Victor; TANAKA, Hisashi;
KOBAYASHI, Hayao; KOBAYASHI, Akiko[1]**
(*[1]Univ. Tokyo,*)

Since the first discovery of the κ-type organic superconductor, κ-ET_2I_3 in 1987, many organic superconductors with κ-type molecular packing were discovered. Among them, κ-$ET_2Cu[N(CN)_2]Cl$ reported in 1990 has retained the highest Tc-record of organic superconductor ($T_c = 12.8$ K) for more than 10 years. About a decade ago, we have examined seven BETS conductors with tetrahalide anions MX_4 (M = Fe, Ga, In; X = Cl, Br) from which five organic superconductors

including the first antiferromagnetic organic superconductor, κ-$(BETS)_2FeBr_4$ have been discovered so far. Recently we have examined the electrical resistivity of κ-$(BETS)_2TlCl_4$. Contrary to our previous experiments showing that the crystal was broken around 220 K, we found that the crystal could survive down to low temperatures when the cooling speed was very large. This accidental finding suggests that the resistivity measurements of this system can be made down to low temperature if the destruction of the crystal around 220 K is suppressed. Accordingly we tried to perform the resistivity measurements by using the crystal coated by epoxy resin under the expectation that "effective pressure" produced by the contraction of the epoxy resin at low temperatures will suppress the destruction of the crystal around 220 K. As was expected, we could observed the superconducting transition despite of the remaining large resistivity anomaly around 220 K.
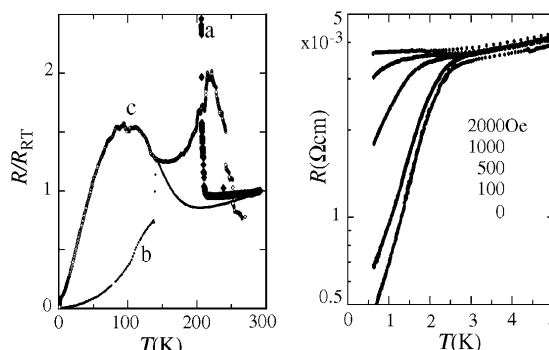
Figure 1. (a) Temperature dependence of resistivity of κ-$(BETS)_2TlCl_4$. a: slow cooling, b: fast cooling, c: slow cooling with epoxy resin. (b) Superconducting transition.

IV-D-9 Structure and Physical Properties of Divalent Magnetic Anion Salts Based on BETS Molecule

**FUJIWARA, Emiko; GRITSENKO, Victor;
FUJIWARA, Hideki; TAMURA, Itaru;
KOBAYASHI, Hayao; TOKUMOTO, Madoka[1];
KOBAYASHI, Akiko[2]**
(*[1]IMS and Electrotec. Lab.; [2]Univ. Tokyo*)

With the aim of the development of new magnetic conductors, we have investigated BETS salts involving divalent transition metal halides such as the $CoCl_4^{2-}$, $CoBr_4^{2-}$ and $MnBr_4^{2-}$ anions with magnetic moments. X-Ray crystal structure analysis of the $CoCl_4^{2-}$ salt cleared that the salt is the κ-$(BETS)_4CoCl_4(EtOH)$. κ-$(BETS)_4CoCl_4(EtOH)$ showed metallic conducting behavior down to 0.7 K and its room temperature conductivity is 1–10 S·cm^{-1}, which is consistent with the result of band structure calculation giving conventional two-dimensional Fermi surfaces. Crystal structure analysis of the $MnBr_4^{2-}$ salt indicated that the salt is θ-$(BETS)_4MnBr_4(EtOH)_2$. (Figure 1) The electrical and magnetic properties of θ-$(BETS)_4MnBr_4(EtOH)_2$ showed that the system is metallic down to *ca.* 30 K with room temperature conductivities of 10–100 S·cm^{-1} and there is only a slight antiferromagnetic interaction between the manganese 3d spins because of

anion-solvent-intermingled layer structure. With regard to the $CoBr_4^{2-}$ salt, the conducting behavior is almost the same as that of the $MnBr_4^{2-}$ salt.
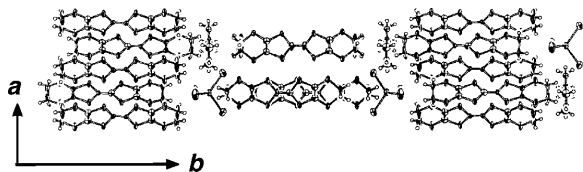
Figure 1. Crystal structure of θ-$(BETS)_4MnBr_4(EtOH)_2$ projected on to the *ac*-plane.

IV-D-10 Novel Molecular Metals Exhibiting Peculiar Magnetism Originating From Lanthanide *f* Electrons

OTSUKA, Takeo[1]; CUI, Hengbo[1]; KOBAYASHI, Akiko[1]; MISAKI, Yohji[2]; KOBAYASHI, Hayao
(*[1]Univ. Tokyo; [2]Kyoto Univ.*)

Compared with the *d*-block elements, *f*-block elements, lanthanides, will show still more unique electronic properties because of the peculiar magnetic properties of *f* orbital spins, and large magnetic moments. Since the *f* electrons are considered to be shielded by outer electrons, the spin-orbit coupling is believed to play essential role in the magnetic properties. Though the molecular metals incorporating localized *f* electrons are still very rare, the study of the '*f*-π system' will undoubtedly expand the range of functional molecular materials. We have examined the crystal structures, electronic conductivities and magnetic properties of $(BDT-TTP)_5[M(NO_3)_5]$ (BDT-TTP = 2,5-bis(1,3-dithiol-2-ylidene)-1,3,4,6-tetra-thiapentalene; M = Sm, Eu). The 4-probe resistivities measurements of $(BDT-TTP)_5[M(NO_3)_5]$ (M = Eu, Sm) showed the systems to be metallic down to 2 K, which is consistent with the two-dimensional electronic band structures. The *dc* magnetic susceptibilities were measured on SQUID (Figure 1). At first sight, weakly temperature-dependent paramagnetic susceptibility at high temperature region seems to suggest Pauli paramagnetism. The susceptibility value, however, exceeds 10^{-3} emu/mol. A contribution from Eu^{3+} ion should be taken into account. The energy levels of the lowest excited state ($J = 1$) and the ground state ($J = 0$) is very close for Eu^{3+} ion, and the excited state is easily accessed by thermal excitation. In this case, the Van Vleck paramagnetic compensation term is important. Similar but smaller Van Vleck paramagnetism was also observed in Sm system.
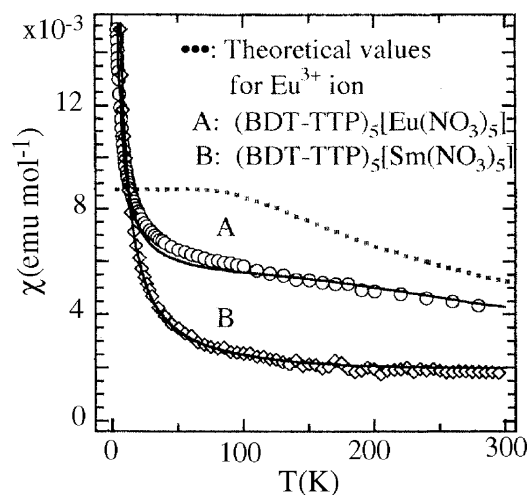
Figure 1. Paramagnetic susceptibility of $(BDT-TTP)_5$-$[M(NO_3)_5]$ (M = Eu (A), Sm (B)). The dotted curve shows the Van Vleck paramagnetism of Eu^{3+} ion.

IV-E Crystal Structure Analyses at Low Temperature and/or High Pressure

Since the molecular crystal is very soft and rich in the structural freedom, various structural phase transitions are expected by applying pressure and/or lowering temperature. Therefore the precise three-dimensional X-ray structure analyses at high pressure and/or low temperature are very important in the studies of solid state physics and chemistry of molecular crystals. The apparatus used for our present low-temperature crystal structure analyses is essentially the same to the IP (imaging plate) X-ray system equipped with liquid helium refrigerator established by us about 10 years ago. But the accuracy of the structure analysis was enhanced greatly owing to the recent slight remodeling of the apparatus. Concerning to the high-pressure X-ray structural studies, we are trying to establish the X-ray studies by combining diamond anvil cell and the IP system mentioned above. To our knowledge, accurate X-ray crystal structure determination of the soft organic crystal by diamond anvil high-pressure cell is still very rare. Very recently we have performed precise single crystal X-ray structure analysis of the crystal of organic conductor up to 2 GPa. There seems to be no difficulty to elevate the pressure up to about 5 GPa. As for the high-pressure resistivity measurements, we have recently reported the improved method of four-probe resistivity measurements for soft organic single crystals.

IV-E-1 Doubling of Lattice Constants of New Organic Superconductor κ-$(BETS)_2TlCl_4$

TAMURA, Itaru; TANAKA, Hisashi; KOBAYASHI, Hayao; KOBAYASHI, Akiko[1]
(*[1]Univ. Tokyo*)

About a decade ago, we have examined the crystal structure and electronic properties of BETS conductors with tetrahalide anions such as FeX_4^- and GaX_4^- (X = Cl, Br). Among them, three superconductors with κ-type molecular arrangements have been discovered, suggesting the ground state of κ-type BETS conductor with MX_4^- anion to be superconducting. However, from the early days of the studies of κ-$BETS_2MX_4$, it was noticed that the accurate resistivity measurements of κ-type BETS salts with relatively large anions such as $FeBr_4^-$ and $GaBr_4^-$ are difficult because the crystals frequently show small resistivity jumps. Very recently we have discovered the superconductivity of the crystal of κ-$BETS_2TlCl_4$ coated with epoxy resin (fourth κ-type BETS superconductor). But the crystal without epoxy resin was always broken around 200 K, which had prevented further studies of this system. The crystal of κ-$BETS_2TlCl_4$ has orthorhombic unit cell with the space group of Pnma. In order to examine the crystal structure of this new organic superconductor, we have tried to examine X-ray diffraction patterns at low temperature by using the crystal coated by epoxy resin and found the doubling of the lattice constant c at low temperature (see Figure 1). The lattice constants were determined as: at room temperature, $a = 11.626(2)$ Å, $b = 36.618(8)$, $c = 8.560(6)$; at 20 K, $a = 11.434(1)$ Å, $b = 36.379(5)$, $c = 16.897(5)$.
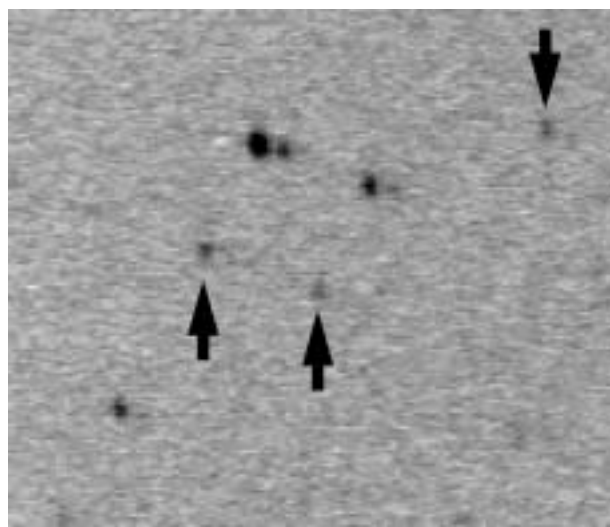
Figure 1. X-ray diffraction pattern of κ-$BETS_2TlCl_4$ at 20 K. The arrows indicate new diffraction spots developed at low temperature.

IV-E-2 High-Pressure Structure of α-(BEDT-TTF)$_2$I$_3$

TAMURA, Itaru; KOBAYASHI, Hayao

α-ET_2I_3 is one of the representative organic conductors, which undergoes a metal-insulator transition at about 135 K at ambient pressure. This metal-insulator transition is suppressed at high pressure and disappears at about 1.5 GPa. Recently, the peculiar transport property of this system observed at high pressure attracts many interests. We performed X-ray structure analyses of α-ET_2I_3 single crystal under several pressures using Diamond-anvil cell. The sample was put in a hole of gasket mounted on the Diamond anvil with 1.0 mm culet-diameter. Single crystals of α-ET_2I_3, with typical dimension of $0.28 \times 0.23 \times 0.15$ mm^3 were used. Pressures were determined by ruby fluorescence method. X-Ray intensity data were collected by using the IP system. The oscillation photographs were taken by using a rotating anode X-ray generator with a Mo target. The lattice parameters were decreased isotropically with increasing pressure. Isotropic thermal parameters were used for all the atoms except three I atoms. The reliability factor was reduced to about 8%. Usually the bond lengths within molecules are believed to be unchanged at low pressure region. However, the I–I bond length was fairly shortened with increasing pressure (Figure 1). The data collections under higher pressures are now underway.
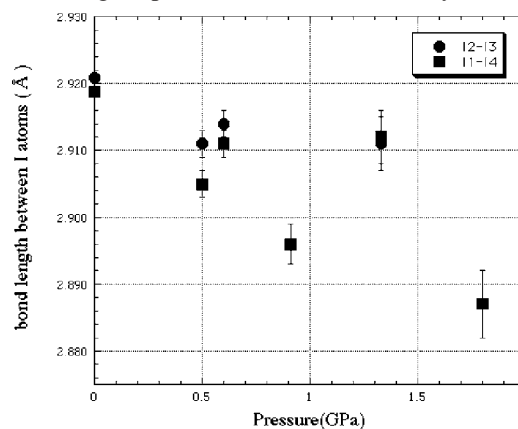
Figure 1. The pressure dependence of I–I bond length.

IV-F Development of New Molecular Conductors

The design and development of new functional molecules are most important for the progress in the field of molecular assemblies. Since the discovery of the first organic superconductors by Bechgaard and Jerome in 1980, an extremely large progress has been made in the field of molecular conductors. It is well known that all the molecular metals ever developed are the systems consisted of more than two components because the charge transfer between the molecules consisting conduction band and other molecules (or ions) has been considered to be indispensable for the carrier generation in organic systems. This means that the molecular crystal consisted of single-component molecules must be non-metallic because of the lack of the charge carriers. However, we have recently developed the first molecular metal composed of single-component molecules. This finding will indicate the possibility of the

development of various unprecedented molecular conductors such as (1) superconductors composed of single-component molecules, (2) ferromagnetic metal composed of single-component magnetic molecules and (3) molecular metals soluble in organic solvents. These systems will be future targets. In addition, we are now trying to develop pure organic ferromagnetic metal based on π donor molecules containing stable radical parts.

IV-F-1 Molecular Design and Development of Single-Component Molecular Metals

KOBAYASHI, Akiko[1]; TANAKA, Hisashi; KOBAYASHI, Hayao
(*[1]Univ. Tokyo*)

We have examined the requirements for designing single component molecular metals, based on the results of crystal structure analyses, electrical resistivity measurements and extended Hückel tight-binding band calculations of molecular conductors composed of single-component molecules of $[Ni(ptdt)_2]$ with extended TTF-ligands, ptdt. The design of π molecules with a small HOMO-LUMO gap and a TTF-like skeleton is a key step to developing single-component molecular metals. A new approach is proposed to reduce HOMO-LUMO gaps. A single-component three-dimensional molecular metal based on an analogous neutral transition metal complex molecule, $[Ni(tmdt)_2]$ were prepared and characterized. Black crystals of this compound were obtained by the electrochemical method. In the crystal, which has a triclinic unit cell containing only one molecule, the planar $[Ni(tmdt)_2]$ molecules are closely packed to form the lattice plane (021-). There are intermolecular short S···S contacts which indicate that the system is a three-dimensional conductor. The resistivity measurements shows that the system is metallic down to 0.6 K. The extended Hückel tight-binding band calculation gave three-dimensional semi-metallic Fermi surfaces. A metallic crystal was also prepared with an analogous molecule $[Ni(dmdt)_2]$. The formation of a single component molecular metal opens the possibilities of developing various types of unprecedented functional molecular systems such as single component molecular superconductors, ferromagnetic single-component molecular metals, molecular metals (or superconductors) soluble in organic solvent, *etc.*
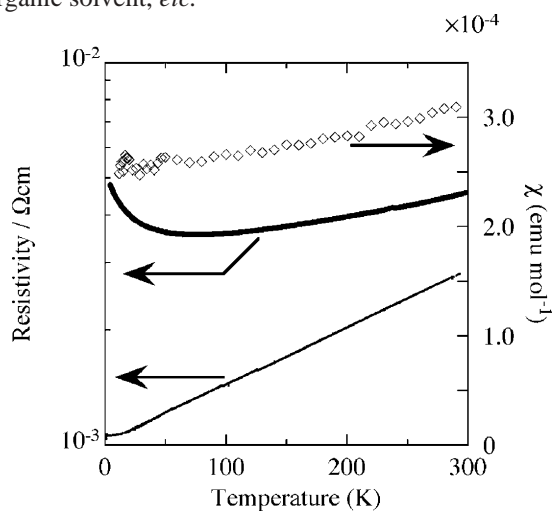
Figure 1. The susceptibility (upper) and resistivities of compacted pellet (middle) and single crystal (lower) of $[Ni(tmdt)_2]$.

IV-F-2 Single Component Conductors Containing Magnetic Transition Metals

TANAKA, Hisashi; KOBAYASHI, Hayao; KOBAYASHI, Akiko[1]
(*[1]Univ. Tokyo*)

We have recently succeeded to develop the first three-dimensional molecular metal composed of single component molecules, $[Ni(tmdt)_2]$, where tmdt (= trimethylenetetrathiafulvalenedithiolate) is a extended-TTF ligand. Since the single component molecular metal has been realized, one of the next targets will be the development of single component magnetic molecular metals. We have prepared metal complexes with magnetic ions (Cu^{2+}, Co^{2+}, *etc.*) coordinated by tmdt and dmdt (dmdt = dimethyltetrathiafulvalenedithiolate). These complexes were easily oxidized by electrochemical methods. Black crystals of neutral metal complexes were obtained for $[Cu(dmdt)_2]$ and the resistivity measurement was made on a compaction pellet sample. The room temperature conductivity was considerably high as for the compaction sample (3.0 Scm^{-1}) and the activation energy was very small ($E_a = 60$ meV). The susceptibility was consistent with the existence of localized magnetic moment of Cu^{2+}. Small antiferromagnetic interaction was observed between Cu^{2+} ions ($C = 0.327(3)$ emu K mol^{-1}, $\Theta = -4.18(6)$ K). X-Ray crystal structure analysis showed that $[Cu(dmdt)_2]$ is a non-planar molecule though the dmdt ligand moiety is ideally planar. Four sulfur atoms of two bidentate ligands coordinate the central copper atom with a distorted tetrahedral geometry.

R, R = -Me, -Me (dmdt)
-(CH₂)₃- (tmdt)
M = Cu(II), Co(II), Fe(III), Cr(III), ...
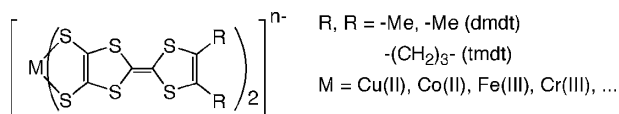
Scheme 1.
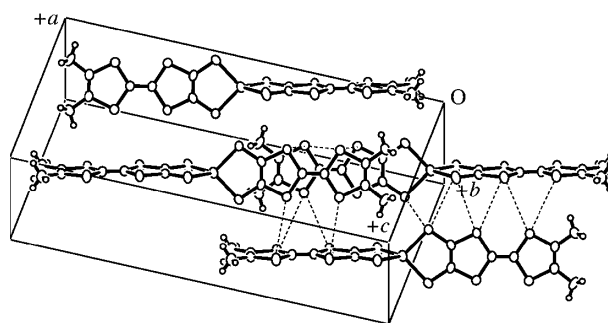
Figure 1. Crystal structure of $[Cu(dmdt)_2]$.

IV-F-3 Synthesis, Structures and Properties of New Organic Donors Connecting to a TEMPO Radical Through a Pyrrolidine Ring

FUJIWARA, Hideki; FUJIWARA, Emiko; KOBAYASHI, Hayao

The molecular conductors and superconductors containing magnetic transition metal anions have been studied for the investigation of the interplay between the conductivity and magnetism. On the other hand, several attempts have been also performed using donors containing a stable TEMPO or NN radical to investigate the interaction between conduction electrons and localized spins of the organic stable radical parts for the development of novel multifunctional materials and ferromagnetic metals. Herein we report the synthesis, structures and physical properties of new TEMPO-containing electron donors in which a TEMPO radical part connects to the EDT-TTF (**1**) or EDO-TTF (**2**) skeletons through a pyrrolidine ring. The ESR spectra of them indicated three absorption lines characteristic of the TEMPO radical. The donors are paramagnetic and showed a slight antiferromagnetic interaction at low temperature region (θ = –2.4 and –3.2 K, respectively). The CV measurement showed two pairs of reversible redox waves originated from the TTF part and one oxidation wave from the TEMPO radical part and indicated the possibility of the coexistence of both the cation-radical and localized spins.
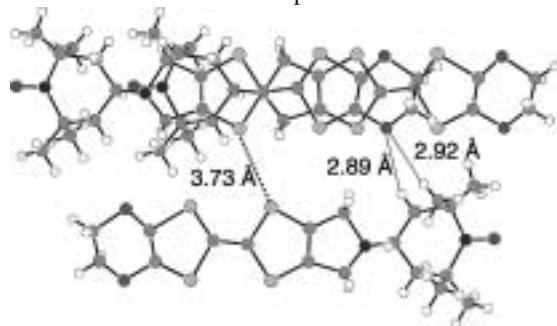
Figure 1. Crystal structure of **2**.

IV-F-4 Synthesis, Structures and Properties of New TTF and TTP Donors Containing a PROXYL Radical

FUJIWARA, Hideki; FUJIWARA, Emiko; KOBAYASHI, Hayao

To investigate the interaction between conduction electrons of the TTF-type donors and localized spins of the organic stable radical parts we have synthesized and studied the molecular conductors containing a stable TEMPO radical so far. Herein we report the synthesis, structures and physical properties of novel TTF (**1a, b**) and TTP (**2**) donors containing a PROXYL radical. X-Ray structure analysis of **1** showed that the PROXYL part has a racemic structure and connects to the TTF part in the chair-formed conformation. The ESR spectra of them indicated three absorption lines characteristic of the PROXYL radical. The donors **1a, b** are paramagnetic and showed a slight antiferromagnetic

interaction at low temperature region (θ = –2.1 and –8.7 K, respectively) and **1b** showed a rapid decrease of magnetic susceptibilities around 5 K, which seems to be originated from an antiferromagnetic transition. The CV measurement of **1a, b** showed two pairs of reversible redox waves originated from the TTF part and one oxidation wave from the PROXYL radical part and indicated the possibility of the coexistence of both the cation-radical and localized spins.

Figure 1. Crystal structure of **1a**.

IV-F-5 Syntheses, Structures and Physical Properties of New π-extended TTF Derivatives Containing a Organic Radical

FUJIWARA, Emiko; FUJIWARA, Hideki; KOBAYASHI, Hayao

We have succeeded in the syntheses of several donors **1**–**3** containing TTF moiety and 2,2,5,5-tetramethylpyrrolin-1-yloxyl (radical part) within single-molecules. Crystal structure analysis on a red crystal of the donor **3** revealed that the TTF moiety is almost planar. Electrochemical properties of the donor **1**–**3** were investigated by cyclic voltammetry. All the donors showed four pairs of reversible redox waves (E = 0.58, 0.86, 0.95, 1.67 V for **1**, E = 0.60, 0.85, 0.96, 1.63 V for **2**, E = 0.59, 0.88, 0.96, 1.69 V *vs.* Ag/AgCl in PhCN for **3**). On the other hand the aldehyde of 2,2,5,5-tetramethylpyrrolin-1-yloxyl showed one reversible redox wave (0.98 V) under the identical conditions, suggesting that the third redox process at 0.95–0.96 V occurs at radical part. The ESR spectra of benzene solutions of the donors **1**–**3** were measured to confirm the existence of the NO radical part. All of them showed three absorption lines (g = 2.0059 and a_N = 14.3–14.4 G) characteristic of the NO radical. The static magnetic susceptibilities of the donor **2**–**3** were measured by SQUID magnetometer. Both of them showed Curie-Weiss temperature dependence with slight antiferromagnetic interaction and magnetization corresponding to one S = 1/2 spin per molecule (C = 0.398 K·emu·mol^{-1}, θ = –2.3 K for 2 and C = 0.355 K·emu·mol^{-1}, θ = –0.73 K for 3). Preparation of cation radical salts of the donor **3**, where TTF moiety and radical part are expected to bear conducting and magnetic properties respectively, was carried out, and they showed semiconducting behavior.

1 : R = -SCH$_3$
2 : 2R = -SCH$_2$S-
3 : 2R = -SCH$_2$CH$_2$S-
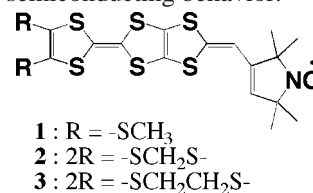
Figure 1. Structure of **1**–**3**.

IV-G Field Effect Transistors with Organic Semiconductors

The mechanism of carrier transport in organic semiconductors and carrier injection from metal electrodes becomes the most important subject to be elucidated for the construction of high performance organic thin film devices. We have studied electrical properties of organic films using field effect transistors.

IV-G-1 Electrical Properties of Phathalocyanine films Prepared by Electrophoretic Deposition

TAKADA, Masaki[1]; YOSHIOKA, Hirokazu[2];
TADA, Hirokazu; MATSUSHIGE, Kazumi[2]
(*[1]GUAS; [2]Kyoto Univ*)

Optical and electrical properties of phthalocyanine (Pc) films have long been studied because of their potential applications to gas sensors, organic light emitting devices and electronic devices including field effect transistors (FETs). Since most Pcs are insoluble in aqueous and organic solvent, Pc films studied so far were prepared by vacuum evaporation technique. We prepared Pc films onto interdigital electrodes by electrophoretic deposition of protonated Pc molecules in the mixture solution of trifluoroacetic acid and dichrolomethane. Contaminations in the films were removed by annealing treatment, and the films exhibited FET behaviors of p-type semiconductors (Figure 1). Carrier mobility, conductivity and carrier density of the films were 1.4×10^{-5} cm^2/Vs, 7.7×10^{-7} S/cm and 6.6×10^{16} cm^{-3}, respectively. These values are almost the same as those of vacuum evaporated films examined so far. It is found that electrophoretic deposition is useful for selective growth of active layers in organic devices.

IV-G-2 Field Effect Transistors with BTQBT Films

TAKADA, Masaki[1]; GRAAF, Harald;
YAMASHITA, Yoshiro[2]; TADA, Hirokazu
(*[1]GUAS, [2]Tokyo Inst. Tech.*)

The carrier mobility of organic single crystals are in the range of 1 cm^2/Vs which is comparable to that of amorphous silicon. However, most organic films in devices exhibited the mobility less than 10^{-3} cm^2/Vs due to the existence of grain boundaries. It is thus important to control molecular packing in the films of well-designed molecules. We have chosen BTQBT as the candidate for active layers of field effect transistors (FETs), since the single crystal showed large mobility and highly oriented films were prepared on various substrates. It was found that BTQBT showed p-type semiconducting behavior in air with the mobility of 0.01–0.5 cm^2/Vs, depending on growth conditions.
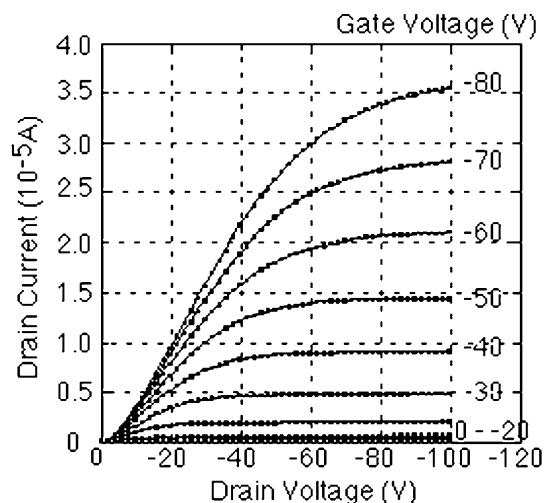
Figure 1.

IV-H Preparation and Characterization of Highly Ordered Molecular Films on Silicon Bound Through Si–C Covalent Bond

Self-assembled monolayers (SAMs) have received considerable attention because of their potential applications to molecular scale electronic devices. Covalently bond alkane SAMs formed by reaction between alkene and hydrogen terminated silicon are of increasing interest as nano-interface for molecular electronics devices fabricated on silicon microstructures. We have studied the growth manner and electronic structure of Si–C junction using scanning probe microscope such as STM (scanning tunneling microscope), AFM (atomic force microscope) and KFM (Kelvin force microscope).

IV-H-1 AFM Studies of Organic Monolayers on Silicon (111) Surfaces

ARA, Masato[1]; GRAAF, Harald; TADA, Hirokazu
(*[1]GUAS*)

Surface morphorogy of SAMs formed by the reaction between 1-dodecene, octadecene and methyl 10-undecenoate and hydrogen terminated silicon (111) surfaces were studied with contact mode AFM. Both p and n type Si(111) surfaces with atomically flat terraces were obtained by chemical etching with NH4F solution. Atomically flat surfaces were also observed in AFM images of SAMs on silicon, indicating that the molecules formed highly-oriented films. We found differences in adhesion force and contact angle depending on the molecules and density of molecules. Electronic structure at the interface will be revealed with KFM studies as well as ultraviolet photoelectron spectroscopy.

IV-I Nanolithography of Organic and Inorganic Materials for Molecular Scale Electronics

Great progress is being made in integration and miniaturization of electronic devices by various techniques of micro- and nano-lithography. Modification of chemical structure of organic compounds with scanning probe microscopes is one of the most promising ways for nano-fabrication. We have studied nano-modification of self-assembled monolayers (SAMs) grown on silicon.

IV-I-1 Microscopic Patterning on the Polysilane Films by the Laser Induced Grating Technique

OKAMOTO, Koichi[1]; TOJO, Tomoaki[1]; TADA, Hirokazu; TERAZIMA, Masahide[1]; MATSUSHIGE, Kazumi[1]
(*[1]Kyoto Univ.*)

[*Mol. Cryst. Liq. Cryst.* in press]

Microscopic patterning on polysilane thin films was observed after photoexcitation with an optical interference pattern using a nanosecond pulsed laser. The patterning processes were monitored by the diffraction of the probe beam. The observed diffraction signals consist of the transient grating component due to the temperature change and the permanent grating component due to a chemical reaction. It was found that the microscopic pattern was destroyed with prolonged laser radiation. The created microscopic pattern was observed by the optical microscope.

IV-I-2 AFM Lithography of Organic Monolayers Bound Covalently on Silicon

ARA, Masato[1]; GRAAF, Harald; TADA, Hirokazu
(*[1]GUAS*)

The alkane monolayer on silicon was degraded by applying a positive bias voltage at the substrate, which resulted in the oxidization of silicon surfaces (Figure 1). The height of the silicon oxide depends on the applied voltage, the width on the curvature radius and the humidity of the atmosphere of the AFM tip. The patterned area is available for different kinds of advanced techniques: 1) covering the oxide with other self-assembled monolayer by trichloro- or trimethoxy siliyl compounds; 2) removing of the silicon oxide by NH_4F-solution and using the established hydrogen terminated silicon for light or heat induced reaction with other alkenes or using the electrical conductive for metal plating; 3) etching of ditches by NH_4F/H_2O_2 solution and fill this ditches with metal by plating.
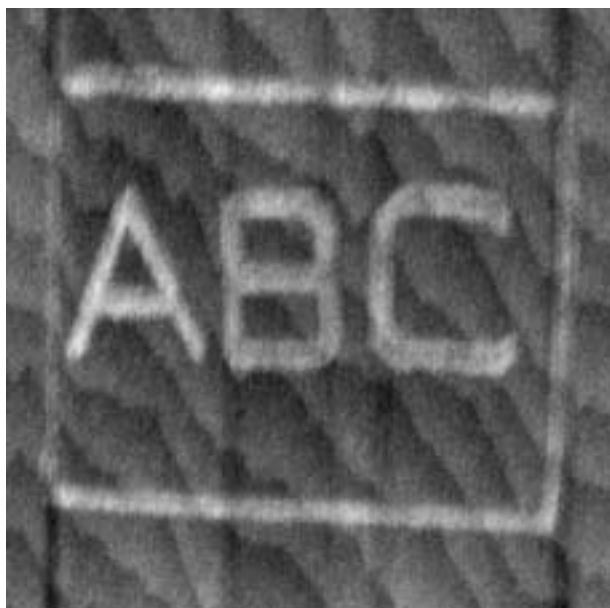
Figure 1.

IV-J Development of New Molecular Conductors

Molecular conductors at the first stage were single component systems where only one degree of freedom governs transport properties. For example, the conduction band in KCP is a one-dimensional d_{z^2} band. TTF-TCNQ has a HOMO band of TTF and a LUMO band of TCNQ, but both of them are one-dimensional pure π bands. Recently, however, increasing number of interesting systems which have "two" bands with different characters near the Fermi level, or where itinerant pπ electrons interact with localized d spins, have been reported: for example, the DCNQI-Cu salt with π and itinerant d, Pd(dmit)$_2$ salts with a two-dimensional HOMO band and a one-dimensional LUMO band, the organic superconductor (TMET-STF)$_2$BF$_4$ with a two-dimensional HOMO band and a one-dimensional HOMO band. On the other hand, in the BETS salt with FeCl$_4$, localized d spins on the Fe^{3+} ions interact with itinerant π electrons. Such multi component systems exhibit interesting physical properties derived from the interplay of many degrees of freedom. The aim of this project is to forward further development of molecular-based conductors with many degrees of freedom.

Main subjects are;

(1) Supramolecular organic conductors: Design of the *inter*-molecular interaction is indispensable in the rational development of molecular materials to still higher forms. From this point of view, we are trying to introduce supramolecular chemistry into the molecular conductor. We have a great interest in an iodine-based *halogen bond* as a supramolecular synthon. Carbon-bound iodine atoms are known to act as Lewis-acids and form short contacts with various species which can act as a Lewis-base (for example, –CN, –Cl, –Br, and =S). This non-covalent interaction (halogen bond) can be strong and directional, which would lead to 1) the reliable regulation of the molecular arrangement and orientation, 2) enhancement of an interaction between conduction electrons and functional molecules in the assembly of molecules.

(2) π-f system: 4f electrons in rare-earth ions exhibit very large anisotropic magnetic moments, as a result of the strong spin-orbit coupling and the high degeneracy due to strong correlation in a well-localized 4f orbital. This feature is never observed in 3d ions, organic π molecules nor other systems. We are trying to develop molecular conductors where 4f electrons are incorporated into a conduction π electron system. Using the heavy rare-earth complex anions [Ln(NCS)$_6$]$^{3-}$ (Ln = Ho, Er, Yb and Y) and organic donors BO and TTP, we have synthesized the first stable π-f metals that remain metallic down to very low temperature.

(3) Two-band system based on transition metal complexes: We have studied Pd(dmit)$_2$ salts with a series of pyramidal cations and found interesting supramolecular interactions through the tellurium-based secondary bond in Me$_3$Te and Et$_2$MeTe salts. These compounds demonstrate that the supramolecular interaction provides the system where two different types of Fermi surfaces coexist within the 'same' crystal. This indicates that the tellurium-based secondary bond can be used for the tuning of the molecular arrangement and thus inter-molecular interactions in the anion radical salts.

IV-J-1 Synthesis and Properties of Novel Donor-Type Metal-Dithiolene Complexes Based on 5,6-dihydro-1,4-dioxin-2,3-dithiol (edo) Ligand

WATANABE, Eiji[1]; FUJIWARA, Masahiro[1];
YAMAURA, Jun-ichi[1]; KATO, Reizo
(*[1]Univ. Tokyo*)

The donor-type metal-dithiolene complexes, where the central C=C bond in the TTF-based organic donor is replaced by the transition metal, are promising materials for the formation of molecular metals and superconductors. One drawback in the conventional donor-type metal-dithiolene complexes is their poor-solubility in usual organic solvents which gives a difficult obstacle in the preparation of the cation radical salt with high quality. We have successfully synthesized a novel donor-type metal-dithiolene complex, Ni(edo)$_2$ [edo = 5,6-dihydro-1,4-dioxin-2,3-dithiolate], and its mixed-ligand derivatives. The edo complex is an analog of the organic donor BEDO-TTF (BO) [bis(ethylenedioxo)-tetrathiafulvalene]. The BO molecule shows higher solubility in various organic solvents than other organic donors and is known to provide superconducting cation

radical salts. The obtained edo-based complexes exhibit largely improved solubility and their donor abilities have been confirmed. The cation radical salts based on these newly synthesized metal complexes have exhibited novel donor arrangements including the trimer-based κ-type one. Notably the edo ligand shows a unique repulsive inter-ligand interaction and the face-to-face overlap of the edo ligands seems difficult to occur in the crystal, which frequently leads to the twisted and spanning overlap of the metal complexes. This is in contrast to the case of BO-based cation radical salts where the organic donor BO shows a strong tendency to aggregate into a two-dimensional layered structure by the aid of both inter-molecular C–H⋯O and side-by-side heteroatom contacts. In other words, the edo unit seems to have a strong tendency to restrict the mode of overlap, as the ethylenedioxo unit within BO but in the opposite way. An origin of this unique feature of the edo ligand remains an open question. We would make the most of what the edo ligand provides (improved solubility and unique molecular arrangement) in combination with the extended π-ligands derived from TTF. In such a largely elongated π molecule, its poor solubility is a serious problem and the spanning overlap mode plays an important role in the formation of the three-dimensional electronic structure. Further studies are in progress.

Ni(edo)₂
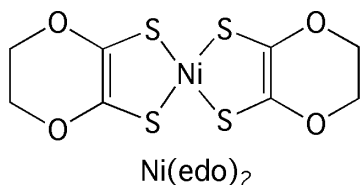
IV-J-2 Structural and Physical Properties of Conducting Cation Radical Salts Containing Supramolecular Assemblies Based on *p*BIB Derivatives (*p*BIB = *p*-Bis(iodoethynyl)benzene)

YAMAMOTO, Hiroshi[1]; MAEDA, Ryoko[2]; YAMAURA, Jun-ichi[2]; KATO, Reizo
(*[1]RIKEN; [2]Univ. Tokyo*)

A cation radical salt $(ET)_3Cl(pBIB)$ (ET = bis-(ethylenedithio)tetrathiafulvalene, *p*BIB = *p*-bis(iodo-ethynyl)benzene) salt is a unique organic metal containing supramolecular assemblies based on the *p*BIB molecule and the Cl anion, $\cdots Cl^-\cdots pBIB\cdots Cl^-\cdots$. We newly prepared chloride and bromide salts of ET with the use of di- and tetra-substituted *p*BIB derivatives: 1,4-difluoro-2,5-bis(iodoethynyl)benzene (DFBIB), 1,2,4,5-tetrafluoro-3,6-bis(iodoethynyl)-benzene (TFBIB), 1,4-bis(iodoethynyl)-2,5-dimethyl-benzene (BIDMB), and *p*-bis(iodoethynyl)benzene-d_4 (*p*BIB-d_4). The substitution effect has been studied by X-ray structure analyses, tight-binding band calculations, and resistivity measurements. The halide anion replacement $(Br^- \rightarrow Cl^-)$ as well as the deuterium and difluoro-substitutions on the *p*BIB molecule do not change the fundamental crystal structure and the metallic behavior but change the $X^-\cdots pBIB\cdots X^-$ period and the inter-chain distance. These systematic deformations of the anion framework act as *anisotropic chemical pressure* onto the donor layer and lead to a rotation of the donor molecule around the longitudinal molecular axis. The rotation of the donor molecules affects on the inter-molecular overlap integrals of HOMO and the tight-binding calculations indicate that the difluoro- and Cl⁻-substitutions increase the anisotropy of the Fermi surface. On the other hand, the tetrafluoro- and dimethyl-substitutions induce different donor arrangements that lead to semiconducting behaviors.

ET

*p*BIB
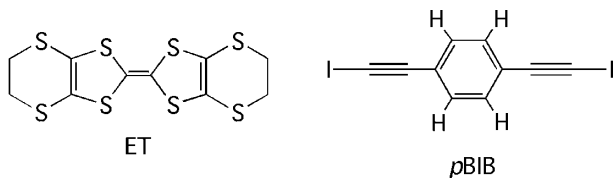
IV-K Systematic Study of Organic Conductors

Thanks to the systematic view to structure-property relationship studied particularly in BEDT-TTF-based conductors, recently our understanding of organic conductors has made a great progress. We have investigated charge ordered phases of molecular conductors, and have shown what kinds of charge ordered patterns are stable depending on the crystal structures. We have extended our molecular-orbital-calculation-based estimation of intermolecular interactions in organic conductors to πd-systems containing magnetic anions, and have discussed magnetic interactions J from the orbital overlaps. From the concept of "universal phase diagram" in the θ-phase, we can predict metal-insulator transition temperatures of a large number of organic conductors. We have applied this rule to tetrathiapentalene (TTP) compounds, verifying that this rule holds to these compounds with some shift of the metal-insulator boundary owing to the small U. We have prepared selenium containing TTP compounds, which have shown lower transition temperatures than the sulfur analogs. We also have shown that substitution of TTP donors with long alkyl chains such as ethylthio groups leads to preferable crystal structures, improving the balance of soft terminal parts and the extended core part of the long TTP molecules.

IV-K-1 Estimation of Off-Site Coulomb Integrals and Phase Diagrams of Charge Ordered States in the θ-Phase Organic Conductors

MORI, Takehiko
(Tokyo Inst. Tech. and IMS)

[*Bull. Chem. Soc. Jpn.* **73**, 2243 (2000)]

Intermolecular Coulomb repulsion, V, of the highest occupied molecular orbitals (HOMO) of BEDT-TTF (bis(ethylenedithio)tetrathiafulvalene) is calculated for various molecular geometries. The bare V is a quantity that is easily estimated under the point charge approximation. As far as the screened V in actual crystals is proportional to the calculated bare V, the usual θ-phase prefers the horizontal or diagonal stripe, whereas the vertical stripe becomes comparatively stable in the limit of the small dihedral angle (in the metallic limit) (Figure 1). The phase diagrams of the θ-phase are discussed under the combination of the static charge distribution (the atomic limit) and the Stoner model (the extended Stoner model). The model contains two order parameters: the spin polarization, S_z, and the charge order, n-1/2. This model explains why the insulating state of the Rb salt below 190 K is a paramagnetic charge-ordered state, while the Cs salt has a different insulating phase below 20 K. The lattice dimerization of the Rb salt can be explained only from V.
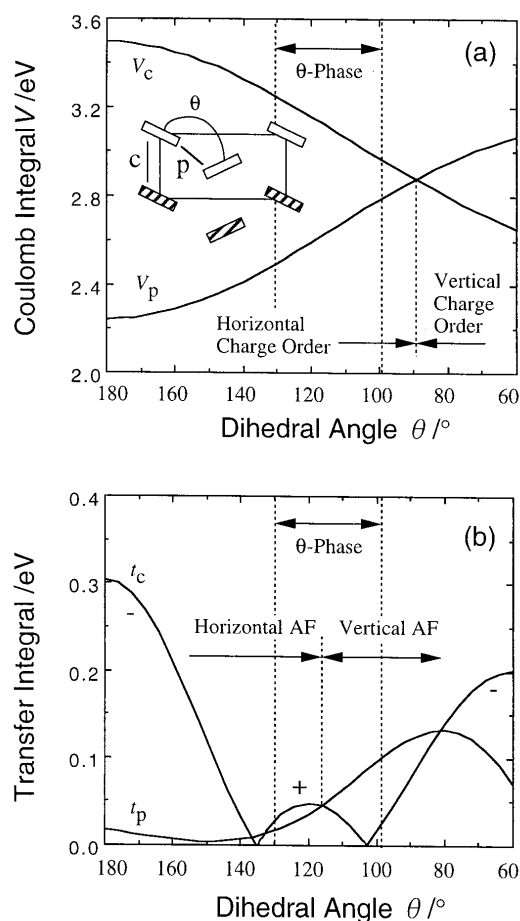
Figure 1. (a) Intermolecular Coulomb integrals, V, and (b) transfer integrals, t, between HOMO of two tilted BEDT-TTF molecules, calculated as a function of the dihedral angle, θ, in the θ-phase.

IV-K-2 Estimation of π-d Interactions in Organic Conductors Including Magnetic Anions

MORI, Takehiko[1]; KATSUHARA, Mao[2]
([1]Tokyo Inst. Tech. and IMS; [2]Tokyo Inst. Tech.)

Magnetic interactions in organic conductors including magnetic anions, such as λ-(BETS)$_2$FeCl$_4$ and κ-(BETS)$_2$FeCl$_4$ [X = Cl and Br], are estimated from the intermolecular overlap integrals: the overlaps

between anions for J_{dd}, and those between anions and donors for $J_{\pi d}$. From this, the most stable spin alignments are decided, and such quantities as the Neel and Weiss temperatures, as well as the magnitude of spin polarization on the π-molecules are evaluated on the basis of the mean-field theory of πd-systems. The calculation is extended to several other πd-conductors, which are classified depending on the magnitudes of the direct dd- and indirect πd-interactions (Figure 1).
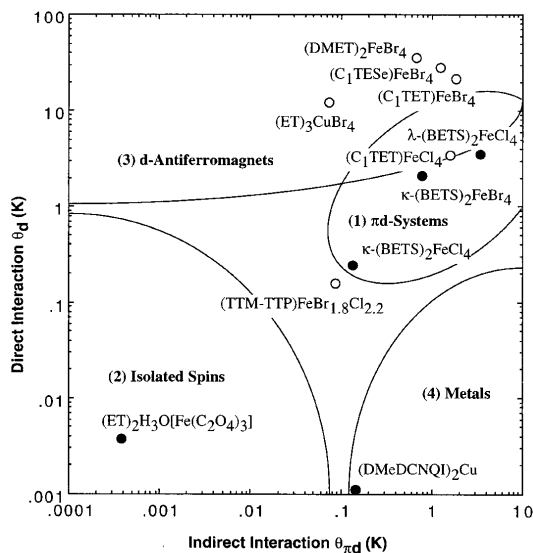
Figure 1. Calculated contributions of direct and indirect interactions to the Weiss temperatures. The closed circles designate metallic compounds at low temperatures.

IV-K-3 Tetrathiapentalene Derivatives with Long Alkyl Chains

KIMURA, Shinya[1]; KURAI, Hiroyuki[1]; MORI, Takehiko[2]; MORI, Hatsumi[3]; S. TANAKA, Shyoji[3]
(*[1]Tokyo Inst. Tech.; [2]Tokyo Inst. Tech. and IMS; [3]ISTEC*)

[*Bull. Chem. Soc. Jpn.* **74**, 59 (2001)]

Bis-fused π-electron donors having alkylthio chains, C_nTET-TTP (2-[4,5-bis(alkylthio)-1,3-dithiol-2-ylidene]-5-(4,5-ethylenedithio-1,3-dithiol-2-ylidene)-1,3,4,6-tetrathiapentalene; n = 2–4) have been synthesized. C_2TET-TTP (**1a**) forms radical-cation salts with BF_4^- and ClO_4^-, which are metallic (σ_{rt} = 900–2500 Scm^{-1}) down to helium temperatures. The I_3 salts of C_3TET-TTP (**1b**) and C_4TET-TTP (**1c**) are semiconductive from room temperature (σ_{rt} = 0.04 and 0.025 Scm^{-1}, respectively). $(C_2$TET-TTP$)_2$ClO$_4$ has uniform stacks of the donors, and has an elliptical Fermi surface characteristic of two-dimensional metals. $(C_4$TET-TTP)I_3 is dimeric, and can be regarded as a band insulator. These crystal structures demonstrate the tendency that the long alkyl chains increase the anion content, and stabilize the usual stacking structure as well as the dimerization.

C_nTET-TTP   **1a** n = 2
             1b n = 3
             1c n = 4
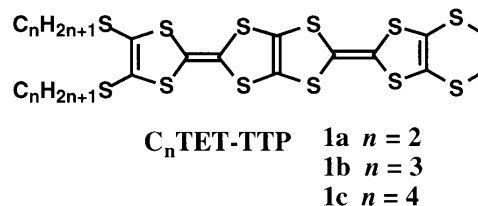
IV-K-4 TCNQ Complex with θ-Type Donor Arrangement: (TMET-TS-TTP)$_2$(TCNQ)

ARAGAKI, Masanobu[1]; HOSHINO, Hirotada[1]; MORI, Takehiko[2]; MISAKI, Yohji[3]; TANAKA, Kazuyoshi[3]; MORI, Hatsumi[4]; S. TANAKA, Shyoji[4]
(*[1]Tokyo Inst. Tech.; [2]Tokyo Inst. Tech. and IMS; [3]Kyoto Univ.; [4]ISTEC*)

[*Adv. Mater.* **12**, 983 (2000)]

A new tetrathiapentalene donor with selenium atoms, TMET-TS-TTP is prepared. (TMET-TS-TTP)$_2$-(TCNQ) has θ-type donor arrangement with a comparatively small dihedral angle (118°), and TCNQ acts as an isolated anion. This complex undergoes a metal insulator transition at 120 K accompanied by the broadening of the ESR intensity, suggesting an antiferromagnetic order.

TMET-TS-TTP
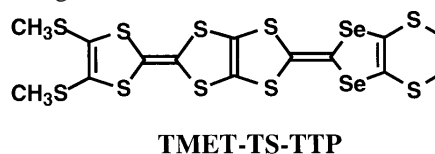
IV-K-5 Universal Phase Diagram of θ-Type TMET-TTP Salts

ARAGAKI, Masanobu[1]; HOSHINO, Hirotada[1]; MORI, Takehiko[2]
(*[1]Tokyo Inst. Tech.; [2]Tokyo Inst. Tech. and IMS*)

[*J. Phys. Soc. Jpn.* **70**, 1642 (2001)]

A new θ-type TMET-TTP salt (TMET-TTP)$_2$HSO$_4$, which has smaller dihedral angle (116°), and has 2:1 composition, is prepared. This salt undergoes a metal insulator transition at around 100 K. The ESR measurement indicates that the low-temperature insulating state is paramagnetic. Thanks to this exceptional salt, a universal phase diagram of θ-type TTP salts can be discussed similarly to θ-type ET salts. In the θ-type ET salts, the universal phase diagram holds in the uniform quarter-filled band. However, our works in the θ-type TMET-TTP salts prove that the universal phase diagram is not largely influenced by the band-filling and the position of the Fermi energy.

IV-K-6 Selenium Analogs of Tetrathiapentalene Derivatives with Long Alkyl Chains

ARAGAKI, Masanobu[1]; KIMURA, Shinya[1]; KATSUHARA, Mao[1]; KURAI, Hiroyuki[1]; MORI, Takehiko[2]
(*[1]Tokyo Inst. Tech.; [2]Tokyo Inst. Tech. and IMS*)

A novel selenium-containing bis-fused tetrathiafulvalene donor, C_2TET-TS-TTP (2-[4,5-bis(ethylthio)-1,3-dithiol-2-ylidene]-5-(4,5-ethylenedithio-1,3-dithiol-2-ylidene)-1,3,4,6-tetrathiapentalene) has been synthesized. The ClO_4^-, BF_4^-, and PF_6^- salts of C_2TET-TS-TTP are isostructural, having β-type structures. These salts are essentially metallic down to low temperatures.
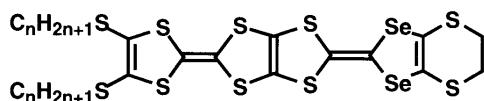
C_2TET-TS-TTP

IV-K-7 1:1 Composition Organic Metal Including a Magnetic Counteranion, (TTM-TTP)FeBr$_{1.8}$Cl$_{2.2}$

KATSUHARA, Mao[1]; ARAGAKI, Masanobu[1]; MORI, Takehiko[2]; MISAKI, Yohji[3]; TANAKA, Kazuyoshi[3]
(*[1]Tokyo Inst. Tech.; [2]Tokyo Inst. Tech. and IMS; [3]Kyoto Univ.*)

An organic donor, TTM-TTP forms 1:1 donor/anion salts with $FeCl_4^-$ and $FeBr_4$, (TTM-TTP)FeX$_4$(PhCl)$_{0.5}$ (X = Cl and Br), which have one-dimensional dimerized columns and are insulators even at room temperature. In contrast, the salt with an alloyed anion, (TTM-TTP)FeBr$_{1.8}$Cl$_{2.2}$, shows high electrical conductivity of about 1000 Scm^{-1} at room temperature and remains metallic down to 160 K. This salt has uniform, one-dimensional, donor columns. This is the first 1:1 donor/anion composition organic metal with a magnetic counteranion. These compounds exhibit weak magnetic interactions; the Weiss temperatures are around 1–3 K.
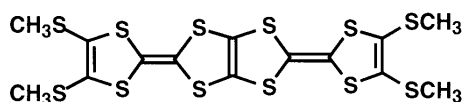
TTM-TTP

IV-K-8 Marginal Paramagnetic State of a One-Dimensional Half-Filled Alternating Chain in (TTM-TTP)AuI$_2$

KAWAMOTO, Tadashi[1]; MORI, Takehiko[2]; YAMAMOTO, Takashi[3]; TAJIMA, Hiroyuki[3]; MISAKI, Yohji[4]; TANAKA, Kazuyoshi[4]
(*[1]Tokyo Inst. Tech.; [2]Tokyo Inst. Tech. and IMS; [3]ISSP, Univ. Tokyo; [4]Kyoto Univ.*)

(TTM-TTP)AuI$_2$ has a dimerized structure along the donor stacking direction, and shows semiconducting behavior below room temperature. ESR, static magnetic susceptibility, and optical reflectance of this salt have been measured to investigate the spin state and the electronic correlation. The ESR signal has been observed from room temperature to 3 K, and the spin susceptibility shows paramagnetic behavior with a rapid decrease below 10 K. The static magnetic susceptibility is paramagnetic and has an anomaly around 10 K in agreement with the ESR result. The chain axis optical reflectance spectra show clear optical gap in the mid-infrared region. An attempt is undertaken to analyze the optical spectrum by means of the one-dimensional dimerized Hubbard model, which suggests that the on-site Coulomb repulsion, U, is small and the spin polarization is located at the marginal paramagnetic boundary. These results indicate that this compound is not a band-insulator but the Mott insulator with a small spin gap.

IV-L Organic Synthesis for Molecular Electronic Devices

The mechanism of electronic conduction through a single molecule is quite different from that of the bulk organic conductive materials. In the latter the charges are carried by soliton, however in the former theories predict that the conduction generally involves tunneling or a resonant tunneling mechanism. A few experiments support the prediction, however there is neither systematic experimental studies nor established theory for single molecular conduction. We use (1) scanning probe microscopic (SPM) technique in ultra high vacuum, and (2) planner nano-gap electrodes for the measurements. Design of the target organic molecules and the measurement system is important for reliable results. We have been preparing (1) self standing organic molecules for measurement by SPM, (2) photo-responsible molecular wires, (3) long molecular wires with low Eg which can be observed optically on nano-gap electrodes. Conduction of gold nano-particles / organic dithiols composite system is also studied.

IV-L-1 "N-Fused Porphyrin": A New Tetrapyrrolic Porphyrinoid with A Fused Tri-Pentacyclic Ring

FURUTA, Hiroyuki[1,3]; ISHIZUKA, Tomoya[1]; OSUKA, Atsuhiro[1]; OGAWA, Takuji[2,3,4]
(*[1]Kyoto Univ.; [2]Ehime Univ.; [3]JST; [4]IMS*)

The syntheses and X-ray structures of novel porphyrinoids, "N-fused porphyrins (NFPs)," and their reactivity were described. NFP was spontaneously produced from the bromo-substituted N-confused tetraarylporphyrin in a pyridine solution at room temperature. X-ray diffraction analyses revealed that the porphyrinoid core containing a fused tri-pentacyclic ring is almost planar. The deviation from the mean plane of 4e¢, for example, was within 0.30 Å. The peripheral aryl substituents were tilted 50.4, 53.5, 64.4, and 12.4° relative to the porphyrin mean plane, respectively. The occurrence of a three-centered hydrogen bonding in the NFP core was inferred by the downfield shift of the inner NH signal (*e.g.*, 8.48 ppm for 4e¢) in 1 H NMR and the short distances (within 2.4–2.9 Å) among the inner core nitrogens, N2,N3, and N4. The optical absorption spectra of NFPs exhibit Soret-like transitions around 360, 500, and 550 nm and weak Q-like bands around 650, 700, 850, and 940 nm in CH_2Cl_2. The electrode process of 4e¢ showed the first oxidation at 0.08 V and reduction at –1.37 V (*vs.* Fc/Fc+), which suggested the small energy gap attributed to the unusual long-wavelength absorption was mainly due to the rising of the HOMO energy level. The first-order rate constants (kf) for the transformation from NCPs to NFPs were largely affected by the substituents at the meso position, showing a good correlation with Hammet ó + parameters. Moreover, the reverse reaction from NFPs to NCPs was observed in the CH_2Cl_2 solution by treating with a base. Dynamic ring inversion in the tetrapyrrolic porphyrin core is discussed.

IV-L-2 Chemical Approach Toward Molecular Electronic Device

OGAWA, Takuji[1,2,3]; KOBAYASHI, Keijiro[2]; MASUDA, Go[2]; TAKASE, Takuya[2]; SHIMIZU, Yuusuke[2]; MAEDA, Seisuke[2]
(*[1]JST; [2]Ehime Univ.; [3]IMS*)

An attempt to actualize high-speed information processing system with molecular electronic devices is a fascinating approach within several other possible ideas for practical use of organic molecules for electronic devices. In order to fabricate the high-speed molecular electronic device, we need molecules of sub-micrometer size with rigid structure and high functionality. We have prepared several "molecular wires" based on porphyrin and related compounds, and studied their electronic properties by using gold nano particles and gold nano-gap electrodes.

IV-L-3 Prospects and Problems of Single Molecule Information Devices

WADA, Yasuo[1]; TSUKADA, Masaru[2]; FUJIHIRA, Masamichi[3]; MATSUSHIGE, Kazumi[4]; OGAWA, Takuji[5,7]; HAGA, Masa-aki[6]; TANAKA, Shoji[7]
(*[1]Hitachi Co.; [2]Univ. Tokyo; [3]Tokyo Inst. Tech.; [4]Kyoto Univ.; [5]Ehime Univ.; [6]Chuo Univ.; [7]IMS*)

Current information technologies use semiconductor devices and magnetic/optical discs, however, it is foreseen that they will all face fundamental limitation within a decade. This paper reviews the prospects and problems of single molecule devices, including switching devices, wires, nanotubes, optical devices, storage devices and sensing devices for future information technologies and other advanced application in the next paradigm. The operation principles of these devices are based on the phenomena occurring within a single molecule, such as single electron transfer, direct electron-hole recombination, magnetic/charge storage and legand-receptor reaction. Four possible milestones for realizing the Peta(10^{15})-floating operations per second (P-FLOPS) personal molecular supercomputer are described, and the necessary technologies are listed. These include, (1) two terminal conductance measurements on single molecule, (2) demonstration of two terminal molecular device characteristics, (3) verification of three terminal molecular device characteristics and (4) integration of the functions of "molecular super chip." Thus, 1000 times higher performance information technologies would be realized with molecular device.

IV-L-4 Synthesis and Characterization of N-Confused Porphyrinatoantimony(V): Toward Low Energy Gap Molecular Wire

OGAWA, Takuji[1,2,3]; FURUTA, Hiroyuki[4];
MORINO, Ayako[2]; TAKAHASHI, Minako[2]; UNO,
Hidemitsu[2]
(*[1]JST; [2]Ehime Univ.; [3]IMS; [4]Kyoto Univ.*)

[*J. Organomet. Chem.* 551 (2000)]

N-Confused tetraarylporphyrinatoantimony(V) dimethoxides were synthesized, and their X-ray crystallographic structure, absorption spectra and voltammetric spectra were studied. X-ray crystallographic structure revealed neutral molecules with no counter anion. From the absorption spectra and voltammetric studies we estimated their energy gaps to be about 0.2 eV less than the corresponding porphyrinatoantimony(V). The axial ligands could easily be exchanged in solvent alcohol by acid promotion. These characteristics of N-confused porphyrinatoantimony(V) indicate that they are good candidates for the molecular wire component.

IV-L-5 N-Confused Double-Decker Porphyrins

FURUTA, Hiroyuki[1,3]; KUBO, Naoko[1]; MAEDA,
Hiromitsu[1]; ISHIZUKA, Tomoya[1]; OSUKA,
Atsuhiro[1]; NANAMI, Hideki[2]; OGAWA, Takuji[2,3,4]
(*[1]Kyoto Univ.; [2]Ehime Univ.; [3]JST; [4]IMS*)

[*Inorg. Chem.* **39**, 5424 (2000)]

IV-L-6 Electronic Conductive Characteristics of Devices Fabricated With 1,10-Decanedithiol And Gold Nano Particles Between 1000 nm Electrode Gaps

OGAWA, Takuji[1,2,3]; KOBAYASHI, Keijiro[2];
MASUDA, Go[2]; TAKASE, Takuya[2]; MAEDA,
Seisuke[2]
(*[1]JST; [2]Ehime Univ.; [3]IMS*)

[*Thin Solid Films* **393**, 374 (2001)]

Electronic conductive characteristics of composite made from 1,10-decanedithiol and gold nano particles were studied with the pressed pellet and with the devices made from organic dithiols, gold nano particles and *ca.* 1 μm gap gold electrode. The I-V curve of the former pellet was ohmic and the temperature dependence $(\log(\sigma)$-1/T) of the conductance was not linear. In contrast with it, the micro-gap device exhibited sigmoidal I-V curve. The activation energy for the latter was 6×10^{-3} eV that was one order smaller than the former pellet of 4×10^{-2} eV.

IV-L-7 Synthesis and Characterization of Photo-responsive Molecular Wires Based on Ruthenium Complex Moiety and Thiol Groups

OGAWA, Takuji[1,2,3]; KOBAYASHI, Keijiro[2];
MASUDA, Go[2]; SHIMIZU, Yuusuke[2]
(*[1]JST; [2]Ehime Univ.; [3]IMS*)

[Submitted]

Molecular wires with a ruthenium complex moiety and thiol group precursors for connecting to gold electrodes were synthesized, and their optical and electrochemical properties were investigated. An electronic device was fabricated with one of the ruthenium complexes bearing two thiol groups using 2 nm gold nano-particles as connecting bond on 1-_m-gapped gold electrodes to show that the device had a sharp photo-response.

IV-M Photoelectron Spectroscopy of Organic Solids in Vacuum Ultraviolet Region

IV-M-1 Calculation of Photoelectron Angular Distributions from ω-(n-pyrrolyl)alkanethiol Self-Assembled Monolayers for Different Molecular Orbitals of Pyrrole Group

HASEGAWA, Shinji; YAKUSHI, Kyuya; INOKUCHI, Hiroo; OKUDAIRA K., Koji[1]; UENO, Nobuo[1]; SEKI, Kazuhiko[2]; MORIKAWA, Eizi[3]
([1]Chiba Univ.; [2]RCMS, Nagoya Univ.; [3]Louisiana State Univ. CAMD)

We calculated photoelectron angular distributions from ω-(n-pyrrolyl)alkanethiol self-assembled monolayers (pyrrolyl-SAMs) for different π molecular orbitals, π_N and π_C, originating from the pyrrole group. The calculations were carried out within a single-scattering approximation of photoemission process. In the approximation, the photoelectron intensity is caused by not only the self-scattering waves from a pyrrole group but also the single-scattering waves scattered in the vicinity of the pyrrole group. Therefore, the angular patterns involve information on the surface arrangement of the pyrrole groups as well as the character of the molecular orbitals.

IV-M-2 Calculated Photoelectron Angular Distributions of ω-(n-pyrrolyl)alkanethiol Self-Assembled Monolayers for Distinction between Different Arrangements of Pyrrole Groups

HASEGAWA, Shinji; YAKUSHI, Kyuya; INOKUCHI, Hiroo; OKUDAIRA K., Koji[1]; UENO, Nobuo[1]; SEKI, Kazuhiko[2]; MORIKAWA, Eizi[3]; SAILE, Volker[3]
([1]Chiba Univ.; [2]RCMS, Nagoya Univ.; [3]Louisiana State Univ. CAMD)

Photoelectron angular distributions from ω-(n-pyrrolyl)alkanethiol self-assembled monolayers (SAMs) were calculated within a single-scattering approximation of photoemission process. The calculations were carried out on two different surface structures with face-stacked and herringbone arrangements of the pyrrole groups which were deduced from molecular dynamics calculations. The characteristic angular patterns calculated for the molecular orbital originating from the pyrrole group involve information on the orientations of the pyrrole groups, which allows the distinction between these arrangements. The photoelectron angular distributions from the substituted SAMs can be used as a clue for studying the surface structures of the substituent groups.

RESEARCH ACTIVITIES V
Department of Applied Molecular Science

V-A Magnetic Structure of Oligo-Nitroxide-Transition Metal Complexes

Since one or two decades, considerable attention has been devoted to stable nitroxide radicals and their metal complexes which are now widely used as building blocks for the design of molecular-based magnetic materials. In this field, we have introduced a new strategy of employing π-conjugated polyaminoxyls as ligands in which the 2p-spins of the NO groups interact ferromagnetically ($J_1 > 0$). The dimensionality of the complex and the sign and magnitude of the exchange coupling between the neighboring spins may be readily tuned by this strategy. Depending on the nature of the additional interchain or interlayer interaction, the polymers are expected to become an antiferromagnet or ferri/ferromagnet. By modifying and extending this design strategy to bis- and tris(aminoxyl) radicals having triplet and quartet ground states, respectively, we have been able to construct with the aid of magnetic metal ions one-dimensional (1D) chain, two-dimensional (2D) network and three-dimensional (3D) parallel-crosses structures in which both the organic 2p and metallic 3d spins have been ordered in macroscopic scales. Since such a rational approach by self-assembly to the tailored extended systems having relevant physical properties is of great importance in materials synthesis. For these materials, the magnetic structures of the crystals are also interesting.

V-A-1 Magnetic Properties of Layered Complexes [M(hfac)$_2$]$_3\cdot$(R)$_2$, M = Mn(II) and Cu(II), with Trisnitroxide Radicals Having Various Metal-Radical Exchange Interactions

TANAKA, Motoko; HOSOKOSHI, Yuko; MARKOSYAN, Ashot S.[1]; IWAMURA, Hiizu[2]; INOUE, Katsuya
(*[1]IMS and M.V. Lomonosov Moscow State Univ.; [2]Kyushu Univ.*)

A series of new layered 2D-network complexes [M(hfac)$_2$]$_3$(R$_\Delta$)$_2$ of M = Mn(II) and Cu(II) with tris-nitroxide radicals R$_\Delta$ has been prepared and the magnetic properties were studied. Each triradical R$_\Delta$ has a quartet ground state and contributes not only to the formation of extended structures but essentially to the overall magnetism. Several exchange interactions, between M and nitroxide, intraradical nitroxide–nitroxide interactions, are responsible for the development of the characteristic magnetic properties in these heterospin systems. Depending on the nature of the interlayer interactions, they show either ferro/ferrimagnetic or antiferromagnetic long range order. The hierarchy of the different exchange interactions is established and the Mn–nitroxide and Cu–nitroxide exchange integrals are evaluated from the analysis of the temperature dependence of the paramagnetic susceptibility. With increasing intraradical exchange interaction, the complexes exhibit more pronounced 2D behavior.
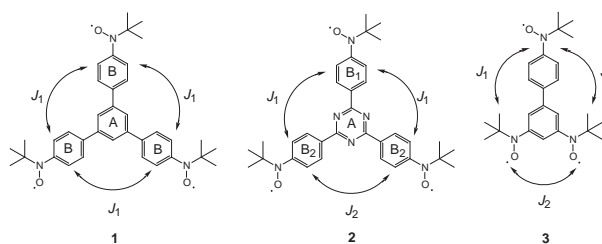
Figure 1. Triangular triradicals **1** ($J_1/k_B = 6.8$ K), **2** ($J_1/k_B = 15.3$ K, $J_2/k_B = 11.8$ K) and **3** ($J_1/k_B \approx 67$ K, $J_2/k_B > 200$ K) with three ligating sites, where A and B indicate the aromatic rings in different positions. J_1/k_B and J_2/k_B were found for the crystals of **1** and **2** or for isolated molecules of **3**. Only the radical **1** has threefold symmetry.
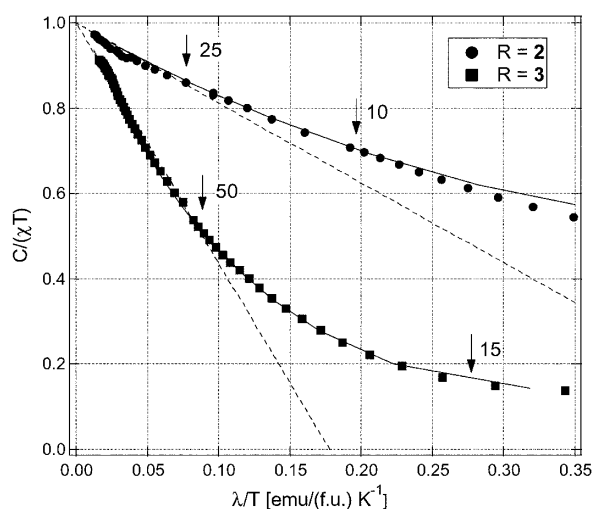
Figure 2. $C/(\chi T)$ *vs.* λ/T plots for [Mn(hfac)$_2$]$_3$(**2**)$_2\cdot$(C$_6$H$_6$)$_3$ and [Mn(hfac)$_2$]$_3$(**3**)$_2$. The solid and dot lines show the behavior for the 2D and 3D models, respectively. Some temperatures are indicated by arrows for clarity.

V-B Synthesis of Chiral Molecule-Based Magnets

The design of molecular materials with interesting magnetic and optical or electrical properties is one of the major challenges in the last few years. The synthesis and study of chiral molecular-based magnetic materials which are transparent for light are of great interest. Novel magneto-optical phenomena have been theoretically predicted and observed in chiral paramagnetic materials in 1997. Although novel properties are expected for such compounds, few examples of chiral molecular-based magnetic materials are still known. To get more insight in their properties it is therefore important to construct such chiral molecule-based magnets in a systematic way. We designed and synthesized a chiral organic radical which can be employed to construct chiral molecular-based magnets.

V-B-1 Synthesis and Structure of Chiral Molecule-Based Three-Dimensional Ferrimagnet

INOUE, Katsuya; IMAI, Hiroyuki; GHALSASI, Prasanna S.[1]; KIKUCHI, Koichi[2]; OHBA, Masaaki[3]; OKAWA, Hisashi[3]; YAKHMI, J. V.[4]
(*[1]IMS and Univ. Mumbai; [2]Tokyo Metropolitan Univ.; [3]Kyusyu Univ.; [4]Bhabha Atomic Res. Cent.*)

New chiral, transparent, high T_C = 53 K molecule-based three-dimensional ferrimagnet, $K_{0.4}[Cr(CN)_6]$-$[Mn(S)$-pn$](S)$-pnH$_{0.6}$; $((S)$-pn = (S)-1,2-diamino-propane) are synthesized. The complex was obtained as pale yellow needle crystal by the reaction of $K_3[Cr(CN)_6]$, $Mn(ClO_4)_2$, and (S)-1,2-diaminopropane dihydrochloride $((S)$-pn·2HCl). X-ray structural analysis revealed a crystallized chiral space group of hexagonal $P6_1$; moreover, the complex demonstrated a three-dimensional magnetic network. (Figure 1) The magnetic measurements of the complex show Mn^{II} and Cr^{III} ions interact ferrimagnetically and magnetic transition occurs at 53 K.

Figure 1. Crystal structure of $K_{0.4}[Cr(CN)_6][Mn(S)$-pn$](S)$-pnH$_{0.6}$. View along the *c* axis and showing the connection of helical dimetallic loops.

V-C Synthesis and Characterization of Quantum-Spin Systems

There has been considerable current interest in the study of a low-dimensional quantum-spin system with an energy gap. For such study, organic radicals will provide good examples of ideal Heisenberg spin systems, since they consist only of light elements. By the appropriate design of molecules, we can obtain a variety of spin systems. In these years, we focus on the spin-ladder system, which is interesting in terms of Haldane state and the high T_C superconductivity. For the S = 1/2 Heisenberg spin ladder with antiferromagnetic legs and rungs, the ground state of the resonating valence bond (RVB) state or the dimerized state is theoretically expected. Experimentally, the singlet ground state was observed in some ladder systems formed by Cu-based compounds. The study of spin ladder systems has been mainly devoted to that of S = 1/2, but that of S = 1 is also interesting. For the ground state of the S = 1 ladder with antiferromagnetic legs ($J_\parallel$) and rungs ($J_\perp$), the Haldane state is expected in the extreme limit of $J_\perp \to$ 0, and the dimer state in $J_\parallel \to$ 0. In its ground state phase diagram on the $J_\parallel/J_\perp$ versus the energy gap (Δ), the phase transition from the dimer state to the Haldane state through a gapless point can be expected. A similar behavior of an existence of a gapless point between two different phases with their own finite excitation gaps is known for the S = 1 Heisenberg alternating antiferromagnetic chain system.

V-C-1 Magnetic Properties of Organic Spin Ladder Systems

**HOSOKOSHI, Yuko; KATOH, Keiichi[1];
MARKOSYAN, Ashot S.[2]; INOUE, Katsuya**
(*[1]GUAS; [2]IMS and M.V. Lomonosov Moscow State Univ.*)

Novel organic polyradicals, BIP-BNO and BIP-TENO, are synthesized and crystallized to form ladder systems, where BIP-BNO and BIP-TENO denote 3,5'-bis(*N-tert*-butylaminoxyl)-3',5-dibromobiphenyl and 3,3',5,5'-tetrakis(*N-tert*-butylaminoxyl)biphenyl, respectively. The BIP-BNO crystals form a two-leg ladder of $S = 1/2$ with antiferromagnetic legs and rungs. The BIP-TENO crystals can be regarded as a two-leg ladder of $S = 1$ species. The magnetic measurements revealed that both compound have singlet ground states.
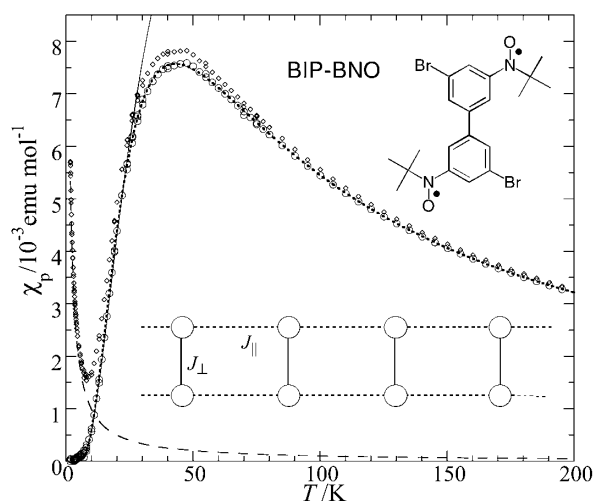
Figure 1. Temperature dependence of the paramagnetic susceptibility (χ_p) of BIP-BNO. Observed data are represented by diamonds ($\diamond$).Open circles represent data after the subtraction of the Curie impurity (broken curve). The dotted curve is the calculation for the ladder system (12 spins) with $2J_\perp/k_B = -66.4$ K and $2J_\parallel/k_B = -26$ K. The solid curve is the fit of $\chi \propto \exp(\Delta/T)/\cdot T$ with $\Delta = 47$ K.

V-C-2 Observation of Magnetization Plateau of 1/4 in a Novel Double Spin Chain of Ferromagnetic Dimmers formed by an Organic Tetraradical

**GOTO, Tsuneaki[1]; BARTASHEVICH, M. I.[1];
HOSOKOSHI, Yuko; KATOH, Keiichi[2]; INOUE,
Katsuya**
(*[1]ISSP, Univ. of Tokyo; [2]GUAS*)

We have measured the susceptibility and low temperature magnetization curve of the novel organic tetraradical crystal BIP-TENO. The susceptibility data indicate that double spin chains of ferromagnetic dimmers are formed in the crystal and the spin system is regarded as an $S = 1$ antiferromagnetic two-leg ladder. The magnetization is nearly zero up to 10 T and the spin gap is closed at 11.6 T. Above 12 T, the magnetization increases and a plateau corresponding to a quarter of the saturation magnetization appears at 44.8 T.
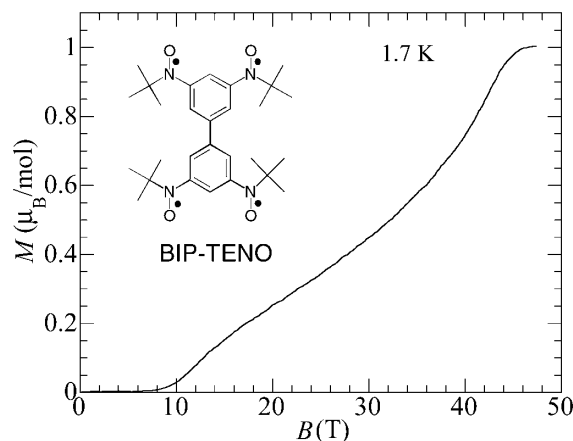
Figure 1. Magnetization curve of BIP-TENO at 1.7 K in pulsed high magnetic fields up to about 50 T.

V-D Organic Ferrimagnetism

In the last decades, the magnetism of molecule-based material has drawn much interest. After the discovery of the organic ferromagnet in 1991, search for an organic ferrimagnet attracts great interest and is considered as one of today's challenging targets in material science. Although a number of ferrimagnets are realized in inorganic-organic hybrid systems, a genuine organic ferrimagnet has not yet been realized. In 1980's, ferrimagnetism is proposed as an effective strategy to give organic materials spontaneous magnetizations by the alternant arrangement of two kinds of organic radicals having different spin-multiplicities. All the reported ferrimagnets include at least two magnetic components: bimetallic compounds or metal complexes with organic radicals. In order to achieve this challenging subject of an organic ferrimagnet from a different viewpoint, we propose here a single-component strategy: utilizing a triradical including an $S = 1$ and an $S = 1/2$ units within a molecule and connecting the $S = 1$ and $S = 1/2$ units by intra- and intermolecular antiferromagnetic interactions. Our new strategy to use a single component has the advantages of the easiness of controlling the crystal structure and the good crystallinity for quality and size.

V-D-1 Approach to a Single-Component Ferrimagnetism by Organic Radical Crystals

**HOSOKOSHI, Yuko; KATOH, Keiichi[1];
NAKAZAWA, Yasuhiro[2]; NAKANO, Hiroki[3];
INOUE, Katsuya**
(*[1]GUAS; [2]Osaka Univ.; [3]Univ. Tokyo*)

A novel organic triradical of 2-[3',5'-bis(*N-tert*-butylaminoxyl)phenyl]-4,4,5,5-tetramethyl-4,5-dihydro-1*H*-imidazol-1-oxyl 3-oxide, abbreviated as PNNBNO, were synthesized. The PNNBNO molecule includes three $S = 1/2$ spins and is regarded as the antiferromagnetic pair of an $S = 1/2$ and $S = 1$. In the crystals, the planar PNNBNO molecules stack along the b axis forming the alternant array of the $S = 1/2$ and the $S = 1$. This can be regarded as a ferrimagnetic ladder, with rungs of intramolecular antiferromagnetic interactions and legs of intermolecular antiferromagnetic interactions between the $S = 1/2$ and $S = 1$. In the static magnetic susceptibility measurements, clear ferrimagnetic behavior is observed. Moreover, we must mention that the crystals include the 3D ferrimagnetic network. Each ladder is surrounded by four neighboring ladders with the alternant alignment of the $S = 1/2$ and $S = 1$. The heat capacity measurements revealed that the effective $S = 1/2$ species (ferrimagnetic spins) undergo a magnetic phase transition at 0.28 K. This is the first example of a genuine organic ferrimagnetic material having well-defined chemical and crystal structure.
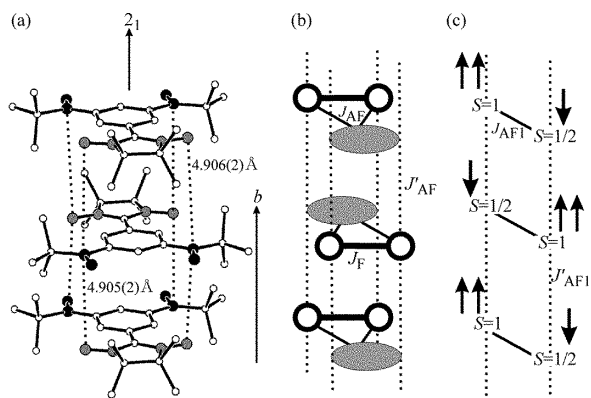
Figure 1. (a) Uniform chain structure in PNNBNO crystals. (b) Schematic illustration of the chain structure. (c) Ferrimagnetic ladder structure in the extreme limit when $J_F \rightarrow \infty$.

V-E Pressure Effects on Molecular Magnetism

'Pressure' is a powerful tool to control the molecular packings and physical properties. The molecule-based materials with small densities are 'soft' and can be expected to show large pressure effects. For the magnetic measurements with high-accuracy, we have developed a small high-pressure clamp cell made of non-magnetic Cu-Ti alloy which can be equipped to a Quantum Design SQUID magnetometer for the dc and ac magnetic measurements. The inner pressure of the clamp cell has been calibrated by the superconducting transition temperature of Pb. We have already discovered that some kind of structural change can be suppressed by pressurization. We are now studying the pressure effects on the molecule-based magnetic materials in wider range. In molecular materials, the spin density are delocalized and distributed in a molecule and the spin-density-distribution plays an important role in the exchange interactions. It is attractive to control the sign of the exchange coupling by pressurization. The pressure effects on the related compounds with similar crystal structures are studied.

V-E-1 Pressure Effect on Mn Complexes of Bisaminoxyl Radicals

HOSOKOSHI, Yuko; SUZUKI, Kentaro[1]; INOUE, Katsuya
(*[1]GUAS*)

The pressure effects on the magnetic properties of one-dimensional Mn(hfac)$_2$ complexes with 1,3-bis(*N-tert*-butylaminoxyl)benzene (**1**$_H$) and 5-halo-1,3-bis(*N-tert*-butylaminoxyl)benzene (**1**$_F$, **1**$_{Cl}$, **1**$_{Br}$) have been studied. These complexes have similar chain structures and undergo three-dimensional magnetic phase transitions at low temperature, due to weak interchain interactions. At ambient pressure, **1**$_H$ and **1**$_F$ are metamagnets with weak interchain antiferromagnetic interactrions, whereas **1**$_{Cl}$ and **1**$_{Br}$ are ferrimagnets with weak interchain ferromagnetic interactrions. The opposite sign of the interchain interactions in these materials is attributed to the different way of packing between the chains. The pressurization of the both metamagnets, results in the monotonous increase of the interchain antiferromagnetic interactions. The enhancement of T_N and H_C with applying pressure was observed. On the other hand, the both ferrimagnets show curious pressure dependences. The change of the interchain interaction is very sensitive to pressure. In some pressure region, temperature dependence of the ac susceptibility shows two peaks. One of the peaks is readily broadened in the existence of the small external DC field of 5–25 Oe. The mechanism of the interchain interaction is discussed.
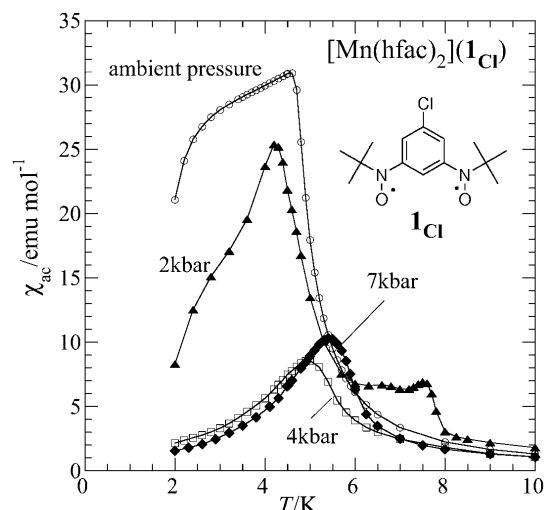
Figure 1. Temperature dependence of the ac susceptibility of [Mn(hfac)₂]·1_{Cl} under several pressures.

V-E-2 Suppression of the Structural Change under Pressure of Cu(hfac)₂ Complex with 5-Bromo-1,3-phenylenebis(*N-tert*-butyl-aminoxyl)

HOSOKOSHI, Yuko; SUZUKI, Kentaro[1]; IWAHORI, Fumiyasu[1]; INOUE, Katsuya
(*[1]GUAS*)

The pressure effect on the magnetic properties of 3:2 complex of $Cu(hfac)_2$ with 5-Bromo-1,3-phenylenebis-(*N-ter*t-butyl-aminoxyl) (1_{Br}) has been studied. At ambient pressure, sudden decrease of magnetic susceptibility at 48 K was reported, which suggests the structural change at this temperature. Our magnetic measurements under pressure revealed that the structural change is sufficiently suppressed at 6 kbar. We also found that the weak stress when the sample is dipped in oil, affects the structural change. The behavior suggests that, at 6 kbar, the high-temperature phase is preserved down to low temperature as metastable state. The enhancement of the energy barrier of the structural transition under pressure is suggested.
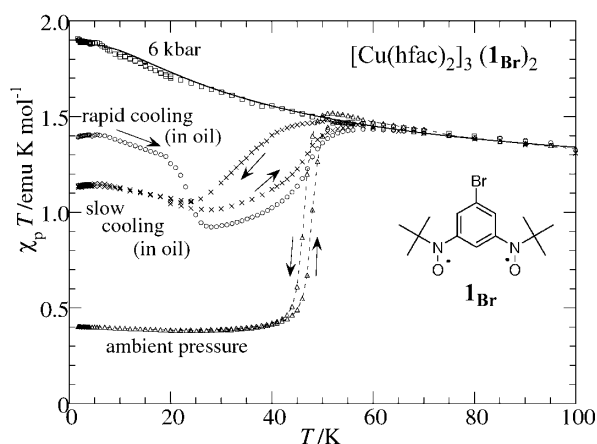
Figure 1. Temperature dependence of $\chi_p T$ of $[Cu(hfac)_2]_3 \cdot (1_{Br})_2$ at ambient pressure ($\triangle$), at 6 kbar ($\square$), and in oil ($\bigcirc$, $\times$).

V-F Bioinorganic Studies on Structures and Functions of Non-heme Metalloenzymes Using Model Complexes

Metal-containing enzymes have been widely distributed in both plants and animals and have been related to metabolic processes such as hydroxylation, oxygen transport, oxidative catalysis, electron transfer, and so on. In this project the structures and functions for the metal complexes are studied as a model of several metallo-enzymes by using some physico-chemical methods.

V-F-1 Electron Transfer Reaction Induced by Self-Assembly of Biguanidato and Violurato Complexes through Triple Hydrogen-Bond

KITAMURA, Hideki[1]; OZAWA, Tomohiro[1]; JITSUKAWA, Koichiro[1]; MASUDA, Hideki[2]; EINAGA, Hisahiko[1]
(*[1]Nagoya Inst. Tech.; [2]IMS and Nagoya Inst. Tech.*)

Hydrogen bond, which is one of the non-covalent interactions, plays an important role for controlling supramolecular synthesis through metal-induced self-assembly of organic compounds as well as covalent- and coordinate-bonds. The 1:1 mixture of $[Co(bg)_3]$ and $[Co(va)_3]$ complexes containing biguanidado (bg) and violuric acid (va) ligands, which enable formation of ADA–DAD style hydrogen bonding, respectively, gave a three-dimensional network structure constructed with triple hydrogen bonding interaction accompanying interligand proton transfer equilibrium. Internal void in this structure formed by the aggregation of the polar functions of bg and va may capture water molecule through the bonding. Moreover, an interesting electron transfer reaction, $Cu(II) + Mn(III) \rightarrow Cu(I) + Mn(IV)$, was observed in the 1:1 mixture system consisting of square planar $[Cu(va)_2]$ and octahedral $[Mn(enbg)(OH)(H_2O)]$ complexes, when the linear tape structure was generated through the interligand hydrogen bonding between va ligand and ethylenebisbiguanidato (enbg). Oxidation of Mn(III) to Mn(IV) by Cu(II) supported by the reduction potential of the complexes might be occurred through the bonding of Mn–O–Cu, which was accurately generated by the two-dimensional assembly of this linear tape.

V-F-2 A Novel Diiron Complex as a Functional Model for Hemerythrin

ARII, Hidekazu[1]; NAGATOMO, Shigenori; KITAGAWA, Teizo; MIWA, Tomohiro[1]; JITSUKAWA, Koichiro[1]; EINAGA, Hisahiko[1]; MASUDA, Hideki[2]
(*[1]Nagoya Inst. Tech.; [2]IMS and Nagoya Inst. Tech.*)

Diiron(II) complexes with a novel dinucleating polypyridine ligand, *N,N,N',N'*-tetrakis(6-pivalamido-2-pyridylmethyl)-1,3-diaminopropan-2-ol (HTPPDO), were synthesized as functional models of hemerythrin. Structural characterization of the complexes, $[Fe^{II}_2$-(Htppdo)(PhCOO)](ClO_4)_3$ (**1**), $[Fe^{II}_2(Htppdo)(p$-Cl-PhCOO)](ClO_4)_3$ (**2**), $[Fe^{II}_2(Htppdo)(p$-Cl-PhCOO)]-(BF_4)_3$ (**2'**) and $[Fe^{II}_2(tppdo)(p$-Cl-PhCOO)](ClO_4)_2$ (**3**), were accomplished by electronic absorption, and IR spectroscopic, electrochemical, and X-ray diffraction methods. The crystal structures of **1** and **2'** revealed that the two iron atoms are asymmetrically coordinated with HTPPDO and bridging benzoate. One of the iron centers (Fe(1)) has a seven-coordinate capped octahedral geometry comprised of an N_3O_4 donor set which includes the propanol oxygen of HTPPDO. The other iron center (Fe(2)) forms an octahedron with an N_3O_3 donor set and one vacant site. The two iron atoms are bridged by benzoate (**1**) or *p*-chlorobenzoate (**2**). On the other hand, Fe atoms of complex **3** are both symmetrically coordinated with N_3O_4 donors and two bridging ligands; benzoate and the propanolate of TPPDO. Reactions of these complexes with dioxygen were followed by electronic absorption, resonance Raman and ESR spectroscopies. Reversible dioxygen-binding was demonstrated by observation of an intense LMCT band for O_2^{2-} to Fe(III) at 610 (**1**) and 606 nm (**2**) upon exposure of dioxygen to acetone solutions of **1** and **2** prepared under an anaerobic conditions at –50 °C. The resonance Raman spectra of the dioxygen adduct of **1** exhibited two peaks assignable to the ν(O–O) stretching mode at 873 and 887 cm^{-1}, which shifted to 825 and 839 cm^{-1} upon binding of $^{18}O_2$. ESR spectra of all dioxygen adducts were silent. These findings suggest that dioxygen coordinates to the diiron atoms as a peroxo anion in a μ-1,2 mode. Complex **3** exhibited irreversible dioxygen binding. These results indicate that the reversible binding of dioxygen is governed by the hydrophobicity of the dioxygen-binding environment rather than the iron redox potentials.

V-F-3 A Substrate-specific α-Hydoxylation of Dipeptides Mediated upon a Co(III)-terpyridine Complex: A Functional Model for Peptidylglycine α-Hydroxylating Monooxygenase

JITSUKAWA, Koichiro[1]; IRISA, Tsuyoshi[1]; EINAGA, Hisahiko[1]; MASUDA, Hideki[2]
(*[1]Nagoya Inst. Tech.; [2]IMS and Nagoya Inst. Tech.*)

A substrate-specific α-hydroxylation of dipeptides has been found out as a functional model for peptidylglycine α-hydroxylating monooxygenase (PHM), in the reaction of the Co(III) ternary complexes containing terpyridine and dipeptide ligands under aerobic and slightly alkaline conditions.

V-F-4 Site-Selective Recognition of Amino Acids by Co(III) Complexes Containing a (N)(O)₃-Type Tripodal Tetradentate Ligand

KUMITA, Hideyuki[1]; MORIOKA, Taiju[1]; OZAWA, Tomohiro[1]; JITSUKAWA, Koichiro[1]; EINAGA, Hisahiko[1]; MASUDA, Hideki[2]
(*[1]Nagoya Inst. Tech.; [2]IMS and Nagoya Inst. Tech.*)

The bis-*N*,*N*-carboxymethy-(*S*)-phenylalaninato carbonato cobalt(III) complex, $[Co(bcmpa)(CO_3)]^{2-}$, has been prepared as a simple model that enables the recognition of an amino acid (Haa) whose coordination behaviours in solution have been characterized by electronic absorption (AB), circular dichroism (CD) and ^1H-NMR spectroscopies. The reaction of the $K_2[Co(bcmpa)(CO_3)]$ complex with amino acids (Haa) has predominantly afforded the [Co(bcmpa)(aa)] complex in the *trans*(*N*)-configuration mode, rather than in the *cis*(*N*)-form. By using amino acid derivatives with bulky substituents at their amino or carboxylate sites under a neutral condition, the reactions have been demonstrated to be initiated by coordination of the amino nitrogen site. Interestingly, the *cis*(*N*)-complex, which is isolated as a minor product, isomerizes to the *trans*(*N*)-form in the presence of active charcoal under pH 7 in an aqueous solution. The site-selective coordination of Haa to the $[Co(bcmpa)(CO_3)]^{2-}$ complex and the stereoselective isomerization of the $[Co(bcmpa)(aa)]^-$ complex have been explained to be regulated by weak non-covalent interactions within the ligands, whose origin has been discussed based on a detailed examination of the crystal structures of the *trans*(*N*)- and *cis*(*N*)-K[Co(bcmpa)(aa)] complexes.

V-F-5 Crystal Structure and Redox Behavior of a Novel Siderophore Model System: A Trihydroxamato-iron(III) Complex with Intra- and Interstrand Hydrogen Bonding Networks

MATSUMOTO, Kenji[1]; OZAWA, Tomohiro[1]; JITSUKAWA, Koichiro[1]; EINAGA, Hisahiko[1]; MASUDA, Hideki[2]
(*[1]Nagoya Inst. Tech.; [2]IMS and Nagoya Inst. Tech.*)

An iron(III) complex of a novel tripodal trishydroxamate with intramolecular hydrogen-bonding networks (**1**), tris[2-{(N-acetyl-N-hydroxy)glycyl-amino}ethyl]amine (TAHGA), has been synthesized as a siderophore model, whose crystal structure revealed the formation of the intra- and interstrand hydrogen bonding networks. Formation of the strong hydrogen bonding networks has also been demonstrated in a DMSO solution using the corresponding gallium(III) complex by ^1H-NMR spectroscopy. The amide proton peak of Ga(III)-TAHGA was quite independent on temperature in the range of 303–323 K, indicating that the amide hydrogens of the Ga(III)-TAHGA complex are well shielded from the outer sphere and are tightly protected from hydrolysis of the complex. The redox behavior of **1** in an aqueous solution exhibited higher potential (–230 mV *vs.* NHE) for its larger pM value (25.1) compared with those for natural siderophores reported hitherto, indicating that the hydrogen-bonds with the coordinating aminohydroxyl oxygens cause to lower the potential of metal ion. It is suggested that the inter- and intrastrand hydrogen-bonding interactions play an important role for not only tight holding of the iron(III) atom and its shielding from the outer sphere but also control of the redox potential of the central metal ion.

V-F-6 Characterization of an NH-π Interaction in Co(III) Ternary Complexes with Aromatic Amino Acids

KUMITA, Hideyuki[1]; JITSUKAWA, Koichiro[1]; EINAGA, Hisahiko[1]; MASUDA, Hideki[2]
(*[1]Nagoya Inst. Tech.; [2]IMS and Nagoya Inst. Tech.*)

The NH-π interaction has been detected in the crystal structures of Co(III) ternary complexes with N,N-bis(carboxymethyl)-(S)-phenylalanine (BCMPA) and aromatic amino acids including: (S)-phenylalanine ((S)-Phe), (R)-phenylalanine ((R)-Phe), and (S)-tryptophan ((S)-Trp)). Additionally, this interaction has been characterized in solution for Co(III) ternary complexes with BCMPA or NTA (NTA = nitrilotriacetic acid) and several amino acids (AA) by means of electronic absorption, circular dichroism (CD), and ^1H NMR spectroscopies. The CD intensities of the Co(III) complexes with aromatic amino acids measured in the d-d region (~ 20.5×10^3 cm^{-1}) are significantly decreased in ethanol solutions relative to water. Analogous complexes with aliphatic amino acids do not exhibit this solvent effect. The ^1H NMR spectra of the Co(III) complexes with aromatic amino acids in DMSO-d_6 exhibit up-field shifts of the N–H peaks compared with those with aliphatic amino acids, which suggest a shielding effect due to the aromaticity. The up-shift values coincide with those experimentally evaluated from the crystal structures. The magnitude in the upper field shifts agrees well with Hammett's rule, indicating that the increase of π-electron densities on the aromatic rings exerts a larger shielding effect for the NH protons. In ligand-substitution reactions of the carbonatocobalt(III) complexes with amino acids, the yields of those with aromatic amino acids are higher than the yields obtained for complexes with aliphatic amino acids. This observation is discussed in connection with the important contribution of the NH-π interaction as one of the promotion factors in the reaction.

V-F-7 Reverse Reactivity in Hydroxylation of Adamantane and Epoxidation of Cyclohexene Catalyzed by the Mononuclear Ruthenium-oxo Complexes with 6-Substituted Tripodal Polypyridine Ligands

JITSUKAWA, Koichiro[1]; OKA, Yoshiyuki[1]; EINAGA, Hisahiko[1]; MASUDA, Hideki[2]
(*[1]Nagoya Inst. Tech.; [2]IMS and Nagoya Inst. Tech.*)

The electronic character of the ruthenium complexes with tripodal polypyridine ligands, which is controlled by the substituted groups at pyridine 6-position, gives rise to differences in the reactivity for the ruthenium catalyzed hydroxylation of adamantane and epoxidation of cyclohexene with PhIO as an oxidant; Ru complexes containing electron-withdrawing groups (**1**, **3**, and **5**) promote the epoxidation, while those containing electron-donating groups (**2**, **4**, and **6**) promote the hydroxylation.

V-F-8 A Structural Model of the Ferrichrome Type Siderophore: Chiral Preference Induced by Intramolecular Hydrogen Bonding Networks in Ferric Trihydroxamate

MATSUMOTO, Kenji[1]; OZAWA, Tomohiro[1]; JITSUKAWA, Koichiro[1]; EINAGA, Hisahiko[1]; MASUDA, Hideki[2]
(*[1]Nagoya Inst. Tech.; [2]IMS and Nagoya Inst. Tech.*)

Tris[2-{(N-acetyl-N-hydroxy)-D-alanylamino}-ethyl]amine (*R*-TAAE) has been synthesized as a chiral trihydroxamate artificial siderophore with hydrogen bonding networks, whose crystal structure of the iron(III) complex revealed Λ configuration induced by interstrand hydrogen bonding networks and steric repulsion by optically active amino acid residues.

V-F-9 Crystal Structure and Solution Behavior of the Iron(III) Complex of the Artificial Trihydroxamate Siderophore with Tris(3-aminopropyl)amine Backbone

MATSUMOTO, Kenji[1]; SUZUKI, Naomi[1]; OZAWA, Tomohiro[1]; JITSUKAWA, Koichiro[1]; MASUDA, Hideki[2]
(*[1]Nagoya Inst. Tech.; [2]IMS and Nagoya Inst. Tech.*)

Microorganisms produce low molecular weight compounds called siderophores for an uptake of iron. The iron(III)-siderophore complexes are very stable and the ligand backbones as well as the iron(III)-binding groups are important for the stabilization of iron(III) complexes. Although many tripodal artificial siderophore analogues have been synthesized as ferrichrome and enterobactin analogues, tris(3-aminopropyl)amine (TRPN) has not been much employed as tripodal anchor and the details are little examined. Here, we report the synthesis of newly designed tris[{3-(N-acetyl-N-hydroxy)-glycylamino}-propyl]amine (TAGP) as a trihydroxamate artificial siderophore with TRPN anchor and the crystal structure and solution behaviors of its iron(III) complex. The crystal structure of iron(III)-TAGP complex is the first report on the trihydroxamate artificial siderophore with TRPN anchor which is very similar to the calculated lowest energy conformation of the iron(III) complex of the trishydroxamate with triscarboxylate anchor previously reported. However, the solution behaviors of these iron(III) complexes are quite different from. TAGP forms the 1:1 tris(hydroxamato)-iron(III) complex in pH 2–8, while, the ferrichrome analogue with triscarboxylate anchor forms polymeric and polynuclear iron(III) complexes, despite the higher conformational similarity between these iron(III) complexes. Interestingly, the former promotes the growth of the siderophore-auxotrophic bacterium, while the latter does not. These results suggest that the TRPN tripodal anchors are quite important not only for the stabilization of iron(III) complexes in strong acidic pH but also for the biological activity.

V-G Probing Time-Dependent Processes in Solution with Time-Resolved Spectroscopic Methods

Typical molecules in solutions experience several "collisions" in 1 ps. Therefore, many time-dependent processes in solution reach the stationary states in a picosecond time scale. Time-resolved spectroscopic techniques that can record rapidly changing phenomena with a picosecond (10^{-12} s) to sub-picosecond (10^{-13} s) temporal window are effective for probing the time-dependent processes. By using picosecond or femtosecond time-resolved spectroscopic methods, we study the rapidly changing events in solutions. In particular, we try to observe the relative translational motions and the process of intermolecular energy transfer. These processes are deeply involved in the mechanism of a chemical reaction and can determine the fate of the reactant molecules.

We started a new research project for studying the dynamic processes accompanying chemical reactions in solutions with experimental methods. For this purpose, we construct a new time-resolved spectrometer that can trace reaction kinetics in solution with a time resolution of a few hundreds of femtoseconds. With this apparatus, we try to detect time dependent transient absorption associated with electron- or charge-transfer processes, in the near-infrared region. A mode-locked Ti:sapphire laser system modified by Prof. Taira's Group, Laser Research Center for Molecular Science, is used for this study. We also study ultrafast bimolecular reaction kinetics in collaboration with Prof. Tahara's Group. Their femtosecond time-resolved fluorescence spectrometer is successfully applied for tracing ultrafast photochemical reaction between biphenyl and carbon tetrachloride.

V-G-1 Photochemical Bimolecular Reaction between Biphenyl and Carbon Tetrachloride: Observed Ultrafast Kinetics and Diffusion-Controlled Reaction Model

IWATA, Koichi[1]; TAKEUCHI, Satoshi; TAHARA, Tahei
(*[1]IMS and Univ. Tokyo*)

Reaction kinetics of an ultrafast bimolecular reaction is successfully interpreted by theories of diffusion-controlled reactions. When biphenyl is photoexcited to the first excited singlet (S_1) state in carbon tetrachloride solutions, it reacts with the solvent carbon tetrachloride in a few picoseconds. We observe this fluorescence quenching kinetics by using a fluorescence up-conversion technique with a cross correlation time of 320 fs. The obtained decay kinetics is well explained by a model function derived from Smoluchowski's theory of diffusion-controlled reactions when the fitting parameter R, distance between the reactants for the reaction, is 0.39 nm (Figure 1). A modified kinetic theory by Collins and Kimball also gives a satisfactory fit, when R is 0.40 nm and the bimolecular reaction rate constant k_{act} is 3.4×10^{11} dm^{3}mol^{-1}s^{-1}. It is suggested that molecular motions in solution for a time period of a few picoseconds is well described by a concept of diffusion.
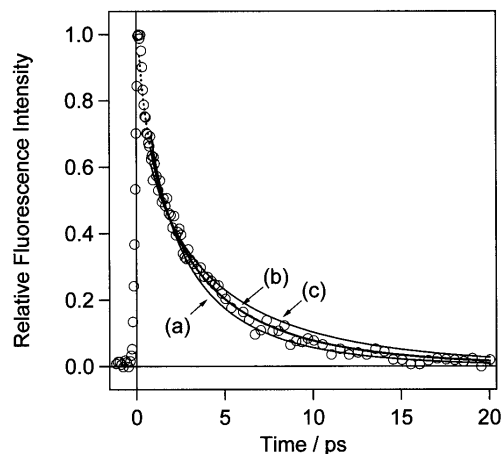
Figure 1. Fluorescence decay curves of biphenyl in carbon tetrachloride simulated by Smoluchowski's theory with the fitting parameter $R = 0.43$ nm (curve (a)), $R = 0.39$ nm (curve (b), best fit), and $R = 0.35$ nm (curve (c)). Observed fluorescence decay curve is also shown with open circles.

V-G-2 Construction of Femtosecond Time-resolved Near-infrared Absorption Apparatus for Tracing Chemical Reaction Dynamics

IWATA, Koichi[1]; KURIMURA, Sunao; TAIRA, Takunori
(*[1]IMS and Univ. Tokyo*)

It has been known that some molecular systems show strong electronic transitions associated with electron- or charge-transfer processes in the near-infrared region. Combination or overtone transitions of vibrational levels in general are also located in this spectral region. Therefore, ultrafast time-resolved near-infrared spectroscopy will be quite effective for studying kinetic processes in solution. It provides us with information, on time-dependent phenomena, that is not accessible by other spectroscopic methods. To the best of our knowledge, however, ultrafast time-resolved

near-infrared spectroscopy has been rarely used for studying chemical systems.

We are constructing a femtosecond time-resolved near-infrared absorption apparatus. The apparatus adopts a basic pump-probe scheme. Output light from a mode-locked Ti:sapphire laser (wavelength, 1030 nm; pulse width, 100 fs) is used as "probe" while its second harmonic (515 nm) is used as "pump." The probe light after the sample is detected with an electrically cooled InGaAs photodiode. Time delay between the pump and probe is controlled by an optical delay unit. We are planning to use the apparatus for tracing kinetics of electron- or charge-transfer reactions.

V-H Stereodynamics of Chemical Reactions and Photodissociation Dynamics

Ionization by metastable atoms (Penning ionization) consists of a spontaneous ionization of the intermediate collisional complex, therefore is a process of fundamental interest behind its importance in plasma and astrochemistry. It has been demonstrated that Penning ionization probes the electron density distribution of the orbital from where the electron is removed, and the collision energy dependence of the ionization cross section has been suggested to be a good measure to clarify anisotropy of intermolecular forces. The reactivity depends not only on the anisotropy of the coupling matrix of $\Gamma = <\phi_i|\Phi_{3p}>$, but also on the collision dynamics *via* stereo-anisotropic intermolecular forces, where ϕ_i is the ionized molecular orbital and Φ_{3p} is the atomic orbital of a metastable rare gas. Therefore we study how such steric effect depends on collision energy, as well as on mutual orientation of reactants.

Photo-initiated reaction of weakly hydrogen bonded halide dimer, $(HX)_2$, has a basic potentiality to produce [XHX] transient species by means of the hydrogen atom elimination from $(HX)_2$ dimer. By measuring translational energy distribution of the eliminated hydrogen atom, one can extract information about van der Waals interaction of reactants in the X + HX reaction system. We study the 243-nm photo-dissociation of the DCl clusters by using a Doppler-selected TOF (DS-TOF) technique in order to detect [ClDCl] transient species. We employed the hexapole method to select only the DCl dimer in cluster beam and to exclude any ambiguity about precursor cluster size.

V-H-1 Direct Measurement of Oscillating Behavior in Ar(^{3}P) + CH$_3$Cl → Ar + CH$_3$Cl$^+$ + e$^-$ Ionization Cross Section by Velocity and Orientational Angle Selected Collisions

OHOYAMA, Hiroshi[1]; **YAMATO, Masanori**[1]; **OKADA, Seiki**[1]; **KASAI, Toshio**[1,2]; **BRUNETTI, Brunetto G.**[3]; **VECCHIOCATTIVI, Franco**[3]
(*[1]Osaka Univ.; [2]IMS; [3]Univ. Perugia*)

Collision energy dependence of the ionization cross section for the Ar(^{3}P) + CH$_3$Cl → Ar + CH$_3$Cl$^+$ + e$^-$ reaction was determined under specific relative orientation using an oriented CH$_3$Cl beam and time-of-flight measurements. A remarkable resonance-type structure is revealed in the energy dependence of orientation angle-resolved Penning ionization cross section. This novel resonance-type structure in Penning ionization cross section could be interpreted as a new-type "nuclear-excited Feshbach resonance" in the formation of vibrational excited Rydberg states leading to a competitive dissociative exit channel.

V-H-2 2D-Measurement of Penning Ionization Cross Section upon Molecular Orientation and Collision Energy in Ar(^{3}P$_{2,0}$) + CHCl$_3$ Crossed Beam Reaction

YAMATO, Masanori[1]; **OHOYAMA, Hiroshi**[1]; **KASAI, Toshio**[1,2]
(*[1]Osaka Univ.; [2]IMS*)

The Penning ionization cross section of Ar* + CHCl$_3$ crossed beam reaction is determined as the function of both molecular orientation and relative collision energy using CHCl$_3$ oriented molecular beam. We find that, the steric opacity function at low collision energies is well correlated to the exterior electron density distribution of CHCl$_3$ molecular orbital which plays a key role in the electron exchange. At high collision energies, however, the reactivity along the molecular axis is favorable while the sideways approach is found to be unfavorable. The result of our *ab initio* calculation reveals that the collision energy dependence if specified at the sideways shows clear discrepancy with the generally accepted propensity rule based on the type of interaction potential. We propose here that this discrepancy can be ascribed to the collision energy dependent competition of product branching between Penning ionization and neutral dissociation.

V-H-3 Velocity Dependence of the Ionization Cross Section of Methyl Chloride Molecules Ionized by Metastable Argon Atoms

BRUNETTI, Brunetto G.[1]; **CANDORI, P.**[1]; **FALCINELLI, S.**[1]; **KASAI, Toshio**[2,3]; **OHOYAMA, Hiroshi**[2]; **VECCHIOCATTIVI, Franco**[1]
(*[1]Univ. Perugia; [2]Osaka Univ.; [3]IMS*)

The ionizition of methyl chloride molecules by meastble argon atom collisions is studied in a crossed beam experiment. The relative cross sections exhibit a decreading trend in the investigated collision energy range, 0.04–0.3 eV The results have been analyzed in terms of the potentioal energy interaction between the two colliding partners, using the optical potential mode. The effect of potential energy anisotropy has also been investigated by the use of a simple sudden approximation within the semiclassical framework. The experimental cross-sections appear to be rather well reproduced by the theoretical calculation with a spherically average potential and very close to the calculation performed using the poteintial for a perpendicular orientation between the C–Cl axis and the approaching direction of the excited atom.

V-H-4 Photodissociation of DCl Dimer Selected by an Electrostatic Hexapole Field Combined with Doppler-Selected TOF Technique: Observation of [ClDCl] Transient Species

CHE, Dock-Chil; HASHINOKUCHI, Mitihiro[1]; SHIMIZU, Yuichiro; KASAI, Toshio[1]
(*[1]IMS and Osaka Univ.*)

The photodissociation of DCl dimer, which is preferentially selected from the cluster beam using a hexapole electrostatic field prior to the photolysis, has been studied by a Doppler-selected time-of-flight (DS-TOF) technique at 243 nm. We observed the [ClDCl] transient species through the hydrogen atom elimination from $(DCl)_2$. By measuring the dependence of the enhancement for the photodissociated D-atom signal upon the hexapole voltage, we find that the DS-TOF spectrum exhibits two kinds of velocity components; one is fast velocity component which originates from only dimer photodissociation, and the other is slow velocity component which originates from not only dimer but also higher sizes of the DCl clusters. For the fast velocity component, the observed spectrum shows an oscillating structure, which could reflect a footprint of nascent internal states (mainly vibration) of the [ClDCl] transient species. The spacing of the observed peaks is about 1000 cm^{-1}, which is much smaller than that of the normal stretching frequency (2091 cm^{-1}) of the DCl monomer. This result suggests that the observed spectrum reflects the strong perturbation from the Cl atom in [ClDCl].

V-H-5 A New Channel of Hydrogen Elimination in the 121.6-nm Photodissociation of Formic Acid Detected by a Doppler-Selected TOF Mass Spectrometry

HASHINOKUCHI, Mitihiro[1]; KOUMURA, Ryouji; CHE, Dock-Chil; KASAI, Toshio[1]
(*[1]IMS and Osaka Univ.*)

The 121.6-nm photodissociation of formic acid was investigated by a Doppler-Selected TOF mass spectrometry (DS-TOF-MS) that enables us to map out 3D velocity distributions of photodissociated products through REMPI for the H atoms. The main channel is found to be the HCOO* formation. A new channel of H + CO + OH(X) hydrogen elimination reaction is observed. We estimate that the branching ratio to [H + HCOO*] with respect to [H + CO + OH(X)] is ~5 and those to HCOO(X), HOCO(X) and [2H + CO_2] formation channels are very small. These results show that the DS-TOF-MS method is useful to determine branching ratios and internal energy distributions of photodissociated products in both excited and ground states.

V-I Structure Determination of Neural Clusters

Over the past two decades, much attention has been paid to molecular clusters interfacing material between the gas phase and the condensed phase, from which network interactions could be analyzed at molecular level. Various spectroscopic techniques have been applied to newly synthesized clusters in order to obtain information about energetics, structures and dynamics. Bonding character and structure of clusters are usually reconstructed or modified from its constituent free molecules. Metal-ligand complexes could be treated as small sizes of clusters. Such small clusters serve as a model system for clarifying metal-ligand interaction.

we demonstrate a novel application of the electrostatic hexapole field to the supersonic beams of Al–CH_3CN and Al–NH_3 synthesized complexes for the determination of permanent dipole moments, which are relevant to the nature of dipole-induced dipole and dipole-dipole interactions between the metal atom and the ligand molecule. Second, in an attempt to clarify the weak interaction and the bonding nature between the Al atom and C_6H_6, we selected Al(C_6H_6) isomers and determined the dipole moments using the 2-meter electrostatic hexapole. We have also performed the density functional calculations (DFT) of the isomers at B3LYP/6-31G* level for obtaining geometries and electric features of the isomers.

V-I-1 Non-Destructive Selection of Geometrical Isomers of Al(C_6H_6) Cluster by a 2-Meter Electrostatic Hexapole Field

IMURA, Kohei[1]; KAWASHIMA, Takahiro[1]; OHOYAMA, Hiroshi[1]; KASAI, Toshio[1.2]; NAKASHIMA, Atsushi[3]; KAYA, Koji
(*[1]Osaka Univ.; [2]IMS; [3]Keio Univ.*)

A supersonic cluster beam which contains isomers of Al(C_6H_6) complexes is generated by a laser evaporation, and the cluster is non-destructively selected using a 2-meter-long electrostatic hexapole. The focusing curve shows clear evidence that there are two kinds of Al(C_6H_6) isomers which are slightly different from each other in geometry; namely one is an asymmetric 1,2-complex and the other one is a nearly C_{6v} symmetric 1,4-complex. The electric dipole moments of the two isomers are found to be 1.5 ± 0.1 and 1.4 ± 0.1 D, respectively. We carried out

computation using the density functional theory in order to estimate their structures. We find that the 1,2-complex is more stable than the 1,4-complex. The present work confirms that the electrostatic hexapole technique is useful for non-destructive selection of the geometrical isomers in the beam.

V-I-2 Direct Determination of the Permanent Dipole Moments and Structures of Al–CH$_3$CN and Al–NH$_3$ by Using 2-Meter Electrostatic Hexapole Field

IMURA, Kohei[1,2]; KAWASHIMA, Takahiro[1]; OHOYAMA, Hiroshi[1]; KASAI, Toshio[1,2]
(*[1]Osaka Univ.; [2]IMS*)

The supersonic beams of pure metal–ligand (1–1) complexes of Al–CH$_3$CN and Al–NH$_3$ were synthesized by a laser evaporation flow-tube-reactor method and non-destructively structure-selected by a 2-meter long electrostatic hexapole field. The permanent dipole moments of such selected complexes were determined. We find that the competing effects of "charge transfer" and "polarization" through the metal-ligand bond can be estimated by measuring the change in the magnitude of permanent dipole moments before and after the complex formation of Al–CH$_3$CN and Al–NH$_3$. The *ab initio* calculation at the MP2 level was performed in order to simulate the complex structures and to explain the experimental findings.

V-J Monte Carlo Simulation of Molecular Clusters

Monte Carlo simulation is a powerful method for studying soft matter such as polymer and gel. We performed the structure analysis of chemical gel and characterized gel with cross-linkers. For DNA in polymer solution, we simulated the linear-shaped and U-shaped motion, and studied the conditions for such motions. In both systems, we obtained qualitatively good agreement with experimental results.

V-J-1 Structure Analysis of Chemical Gel Using Monte Carlo Simulation

NOSAKA, Makoto; TAKASU, Masako

[*Trans. Mater. Res. Soc. Jpn.* **26**, 557 (2001)]

We studied the structure of gel using Monte Carlo simulation with modeled radical reactions. Simulation is performed using beads-spring model in three-dimensional continuous space. For the criterion of gel, we apply the concept of percolation to our clusters; we calculate the maximum size in all directions for each cluster, and sum up the number of percolated direction for all percolated clusters in a system. We call this the number of percolation. We obtained structure information of system from plotting the average number of percolation. We can determine whether the system has percolated clusters, and also whether the polymer network has inhomogeneous structure.

V-J-2 Characterization of Gel Using Modeled Radical Polymerization with Cross Linkers Performed by Monte Carlo Method

NOSAKA, Makoto; TAKASU, Masako; KATOH, Kouichi[1]
(*[1]Kanazawa Univ.*)

[*J. Chem. Phys.* submitted]

In this study, some physical quantities for characterization of gel are proposed. Polymer networks (gel) are investigated by Monte Carlo simulation using modeled free-radical cross-linked polymerization in continuous system. The distributions of degree of polymerization for clusters obtained in this simulation show qualitatively good agreement with the experimental results. Linkers are classified to two types according to the roles in networks, and their ratios are discussed. The normal and weighted ratios of gel are defined using percolation theory. These ratios are compared with the changes in distribution.

V-J-3 Linear-Shaped Motion of DNA in Entangled Polymer Solutions under a Steady Field

NOGUCHI, Hiroshi; TAKASU, Masako

[*J. Phys. Soc. Jpn.* **69**, 3792 (2000)]

We studied the electrophoretic behavior of DNA chains in linear-polymer solutions using Brownian dynamics with an anisotropic friction tensor. We simulated the linear-shaped motion of DNA observed in highly entangled solutions (Ueda *et al.*) using a model with a chain segment equal to 1/4 of the persistence length. A linear conformation is seen for a chain with high segment-density regions, which remain at the same positions in space, with a high anisotropy of friction, while a U-shaped conformation is seen for a chain with a low anisotropy of friction.

V-J-4 Dynamics of DNA in Entangled Polymer Solutions: An Anisotropic Friction Model

NOGUCHI, Hiroshi; TAKASU, Masako

[*J. Chem. Phys.* **114**, 7260 (2001)]

We studied the electrophoretic behavior of DNA chains in linear-polymer solutions using Brownian dynamics with an anisotropic friction model in a three-dimensional space and projected on x-axis. For the three-dimensional model with a chain segment equal to 1/8 of the Kuhn length, a chain migrates with U-shaped conformation with low anisotropy of friction. With high anisotropy of friction, a chain always migrates with linear-shaped conformation with high segment-density regions, which remain at the same positions in space. This migration mode agrees with the observation of DNA in highly entangled solutions. [Ueda *et al.*] The projection model also reproduces the linear-shaped motion. We clarified that the essential conditions for linear shaped motion are the sufficient chain length of DNA, the small mesh size, and strong confinement by entanglement with solvent polymers.

V-J-5 Eelectrophoretic Behavior of Polyelectrolytes in Gel and Polymer Solutions

NOGUCHI, Hiroshi

[*Trans. Mater. Res. Soc. Jpn.* **26**, 687 (2001)]

Electrophoresis using gel and uncrosslinked polymer solutions is widely used to separate DNA chains by chain length. We studied the electrophoretic behavior of chains using Brownian dynamics with an anisotropic friction tensor. We show the anisotropic-friction model proposed by Curtiss and Bird is an effective method to describe dynamics of polyelectrolyte chains under an electric field in gel and polymer solutions. With a low anisotropy of friction (dilute polymer solutions), a chain fluctuates between elongated and compact states with no periodicity under a steady electric field. On the other hand, with a high anisotropy of friction (gel or entangled polymer solutions), a chain oscillates periodically: Polyelectrolyte chain is trapped by gel fibers with a U-

shaped conformation, stretches out, and re-acquires a compact conformation. The above results agree well with experiments on DNA electrophoresis.

V-K Development of Broadband Solid-State NMR Spectroscopy

Ordinary NMR probes employs resonant circuits, which can be tuned only over bandwidth of a few 100 kHz. Most of the NMR probes have been well developed and are commercially available, although they are very expensive. However, solid samples often have much larger line width than the bandwidth of the resonant probe. Such examples are many of quadrupole nuclei (examples Cl, Br, I, Nb *etc.*) and metal nuclei (Pt, Rh, Hg, Pb *etc.*) having large Knight shifts. The samples containing these nuclei have been studied by rather simple methods as Hahn echo measurements or relaxation measurements by irradiating only a part of the spectral region. The whole spectra is obtained either by changing static magnetic field or by changing a carrier frequency and probe tuning. Only in a few cases, more than one carrier frequencies were employed to correlate different spectral regions.[1,2] Broadband NMR probe that does not use the resonant circuits may be necessary to conduct two-dimensional NMR experiments or automated experiments over the whole spectral range. Lowe and coworkers proposed transmission line NMR probe in 70s and it is expected to have much larger bandwidth than a normal resonant circuit.[3,4] In our study we reexamined the transmission line probe by numerical simulations and experiments.

References
1) J. Haase, M. S. Conradi, C. P. Grey and A. J. Vega, *J. Magn. Reson. A* **109**, 90 (1994).
2) J. Haase, N. J. Curro and C. P. Slichter, *J. Magn. Reson.* **135**, 273 (1998).
3) I. J. Lowe and M. Engelsberg, *Rev. Sci. Instrum.* **45**, 631 (1974).
4) I. J. Lowe and D. W. Whitson, *Rev. Sci. Instrum.* **48**, 268 (1977).

V-K-1 Numerical Simulations of the Transmission Line Probe

KUBO, Atsushi; ICHIKAWA, Shinji

The transmission line probe resembles to a circuit of a low-pass filter, which consists of π sections with a coil and two capacitors, which connect the ends of the coil to ground. To simulate the real transmission line probe, we need to include the inductive coupling between all the coils in the different π sections, which was taken into account as a parameter in the Lowe's analyses. In our analysis, we calculated the self and mutual inductance explicitly by using the Neumann's formula. The method of the simulation is based on the moment method.[1] We calculated the effective impedance, the propagation constants and the scattering matrix, which characterize the probe circuit.[2] We also calculated the strength of the rotating magnetic field as a function of carrier frequency and position. It is interesting to note that the scattering matrix is also employed in other fields as conductance of carbon nanotubes and an optical resonator.

We compared our numerical results with the analytical equations derived by Lowe. We found that their equations agree well with our numerical results, if the self-inductance of the low-pass filter was replaced by the average inductance, which is defined as the total inductance divided by the number of π sections. We considered a rectangular flat coil with a pitch p, wire length $l \gg d$ (d is the length along static magnetic field), number of turns N_i and cable impedance Z_0. We modified one of Lowe's equations and found that the rotating field at the coil center becomes an exponentially decaying function of carrier frequency ν,

$$|B_+| = (\mu_0 V_{in}/2Z_0 p)\exp(-\nu/\nu_d),$$

where $\nu_d = (2Z_0/\pi\mu_0 l)(p/d)^2$ and V_{in} is the input voltage.

To obtain large RF field, the pitch of the coil or the impedance of the probe must be small. The latter need the impedance transformation from the cable impedance of 50 Ω. The above equation also requires that ν_d must be much larger than the observed frequency, which restricts the dimensions of the coil.

We also found that the reflection of wave takes place near both ends of the coil. Since the coil near the ends have only one neighbor, their total inductance is smaller than that at the center. The reflection causes the undulation of magnitudes of currents over different π sections and also the undulation of the field strength, thus spoils the homogeneity of the magnetic field. We could also see the effect of diffraction at the carrier frequencies where the phase delay through the probe becomes close to integer multiples of π. Near these frequencies, the effective impedance showed a dispersion curve and the propagation constant became real positive, which means that the circuit absorbed the energy. Next we varied the pitch of the coil and made it smaller near both ends. This treatment suppressed the undulation of currents and thus improved the homogeneity of the RF field in the coil.

References
1) M. N. O. Sadiku, "Numerical Techniques in Electromagnetics," CRC Press; Boca (2001).
2) S. Ramo, J. R. Whinnery and T. Van Duzer, "Fields and Waves in Communication Electronics," Wiley; New York, (1994).

RESEARCH ACTIVITIES VI
Department of Vacuum UV Photoscience

VI-A Electronic Structure and Decay Mechanism of Inner-Shell Excited Molecules

This project is being carried out at the Beamline 4B of the UVSOR facility and at the surface station of the Beamline I-511 of the MAX-II facility in collaboration with the Uppsala University. Dr. Takaki Hatsui has been working as a research associate since August 2000, and Dr. Mitsuru Nagasono as a JSPS postdoctoral fellow since April 2000. We are interested in linear polarization dependence of inner-shell resonant excitations for simple molecules. We have two subprojects: (A) spin-orbit, exchange, and molecular field splittings in S 2p and P 2p excited states and (B) molecules and radicals in condensed phase and in rare gas matrix. In the subproject (A) we are happy to report here a hot result obtained by using a newly-constructed BL4B of UVSOR. In the subproject (B) we have constructed a new apparatus as shown Figure 1. For both the subprojects theoretical investigation is essential and some theoretical approaches are now under development.
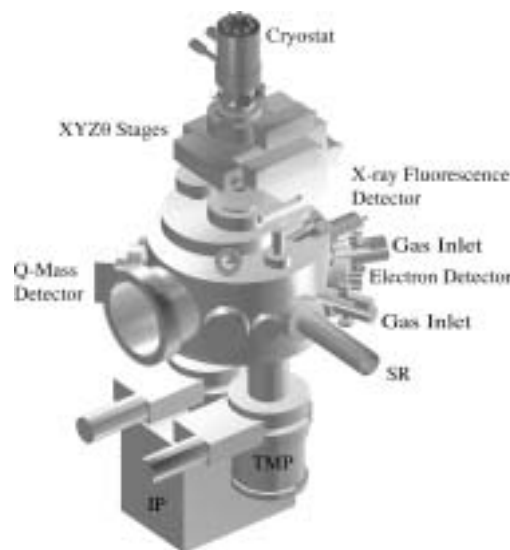
Figure 1. A new apparatus to investigate molecules and radicals in condensed phase and in rare gas matrix.

VI-A-1 Spin-Orbit and Exchange Splittings in the S 2p → π*(b₁) Excitation of SO₂

KOSUGI, Nobuhiro; HATSUI, Takaki; NAGASONO, Mitsuru; GEJO, Tatsuo; SHIGEMASA, Eiji

Figure 1 shows a part of angle-resolved photoion yield spectra (ARPIS) of SO_2, where I_0 (I_{90}) corresponds to ion yields in the direction parallel (perpendicular) to the electric vector of the linear polarized incident light. The photon energy region shown is very narrow, only 3 eV from 164 eV to 167 eV. This region includes only the S 2p excitation to the lowest unoccupied orbital of $\pi^*(b_1)$ symmetry. The S 2p orbitals have a_1, b_2 and b_1 symmetries, resulting in three S 2p-π^* (b_1) excited states of B_1, A_2, and A_1 symmetries. The ground state symmetry is A_1 and the $A_2 \leftarrow A_1$ excitation is dipole-forbidden; that is, the $a_1 \rightarrow b_1^*$ (B_1) and $b_1 \rightarrow b_1^*$ (A_1) excitations should be observed in Figure 1. Considering the spin-orbit interaction, each singlet excitation is mixed with two triplet excitations, resulting in three dipole-allowed excited states in each symmetry. The transition dipoles to the B_1 states are orthogonal to the molecular plane and these transitions give only I_{90} yields; on the other hand, the transitions to the A_1 states give both I_0 and I_{90} yields. In Figure 1, three electronic states of B_1 symmetry show vibrational fine structures, where the lowest electronic state is very weak, and the second ($^2P_{3/2}$) is stronger than the third ($^2P_{1/2}$). On the other hand, Figure 1 shows only two electronic states of A_1 symmetry, where one is located in the $^2P_{3/2}$ manifold,

and the other is in the $^2P_{1/2}$ manifold. The $^2P_{1/2}$ feature seems to be slightly stronger that the $^2P_{3/2}$ feature, though the $^2P_{3/2}$ branch is as twice large as the $^2P_{1/2}$ branch in the case of ionization. This indicates that exchange interaction is essential in the A_1 symmetry. This is reasonable, considering that the $2pb_1$ and π^*b_1 orbitals are oriented parallel. Furthermore, the singlet excited state is quite higher in energy than the triplet excited state, and the lowest state of A_1 symmetry hardly borrows intensity from the singlet component; therefore, the lowest state is invisible in the spectra as shown in Figure 1.
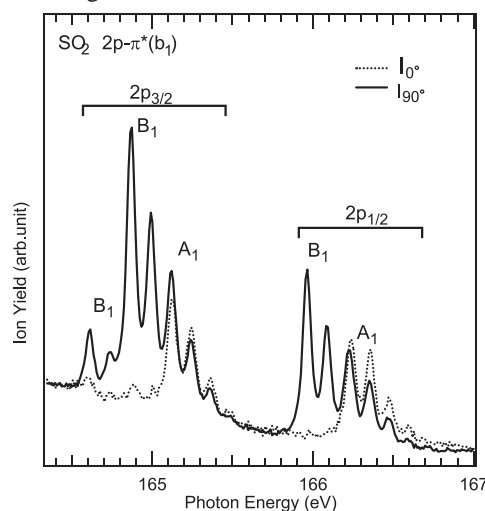
Figure 1. High resolution ARPIS of the spin-orbit split transitions to the S $2pa_1 \rightarrow \pi^*b_1$ (B_1) and S $2pb_1 \rightarrow \pi^*b_1$ (A_1) excited states of SO_2.

VI-A-2 X-Ray Photoelectron and Absorption Spectra of Fragments from NH₃/Cu(110) Induced by Soft X-Ray Irradiation

NAGASONO, Mitsuru; NORDLUND, Dennis[1,2]; NILSSON, Anders[2]; KOSUGI, Nobuhiro
(*[1]Max-lab; [2]Uppsala Univ.*)

We have studied fragments from NH_3 adsorbed on Cu(110) using N 1s x-ray photoelectron spectroscopy and x-ray absorption spectroscopy in combination with theoretical calculations. As shown in Figure 1, three N1s photoemission peaks arising under soft x-ray irradiation are assigned to NH_x ($x = 0$, 1, and 2) species on Cu(110). These peaks are enhanced in sequence of x = 2, 1, and 0; *i.e.*, at first the NH_2 species are produced from the NH_3, the NH from the NH_2, and the N from the NH. These fragments are produced by Auger stimulated dissociation (ASD) process and/or x-ray-induced electron-stimulated dissociation (XESD). In the ASD process, fragmentation of NH_3 leads to all NH_x species simultaneously. While in the XESD process, the fragmentation leads to only NH_2 species from NH_3. Therefore the XESD is a dominant process, but the ASD is a minor one. The fragments produced at the early stage correspond to NH_2 anions by considering theoretical predictions. This result suggests a charge transfer process from the Cu substrate to the adsorbed NH_2 radical prepared following the XESD process.
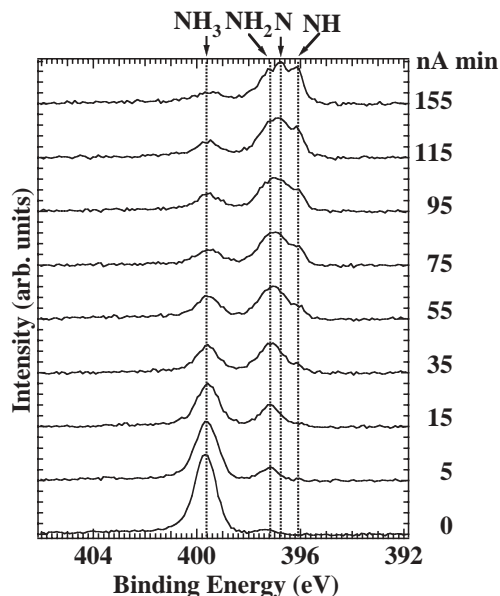
Figure 1. N 1s XP spectra of NH_3/Cu(110) as a function of exposure to x-ray.

VI-B Soft X-ray Photoelectron-Photoabsorption Spectroscopy and Electronic Structure of Transition Metal Compounds

This project is being carried out by the Kosugi group at the Beamline 1A of the UVSOR facility and at the bulk station of the Beamline I-511 of the MAX-II facility in collaboration with the Uppsala University. Dr. Hiroshi Oji has been working as a postdoctoral IMS fellow since April 2000, and Dr. Takaki Hatsui as a research associate since August 2000. We are interested in linear polarization dependence of inner-shell resonant excitations (UVSOR) for planar complex molecules/ions in the single crystal, and in resonantly-emitted photoelectron (UVSOR) and photon (MAX-II) spectroscopies for the same systems by tuning the photon energy to inner-shell resonances. In the UVSOR facility we are using crystal monochromators, which restrict the photon energy to the range higher than the Cu and Ni 2p edge (> 800 eV). Recently, we have decided to move our experimental apparatus to the BL 4B, which is a new beamline covering the lower photon energy (< 800 eV). Next year we hope we will show new results on some interesting materials containing Fe, Mn, and so on.

VI-B-1 Photoabsorption and Resonant Photoelectron Spectroscopy of a Rare-earth Borocarbide LaB₂C₂

OJI, Hiroshi; HASEGAWA, Shinji; SUZUKI, Kazuya; KOSUGI, Nobuhiro

Rare-earth borocarbides RB_2C_2 (R: rare-earth (RE) metals) are intercalation compounds in which rare-earth metal cations are intercalated in the planar BC sheets. These compounds show interesting electronic and magnetic properties, such as superconducting behavior

(T_c = 2.4 K for LuB_2C_2[1]). Therefore it is important to know their electronic structure in order to clarify the mechanism of these properties. In this study, the La 3d photoabsorption (hν ~ 830 eV) and resonant valence-band photoelectron spectra of lanthanum borocarbide (LaB_2C_2) were measured to reveal the partial density of states at the core-excited atom is enhanced in resonant photoelectron spectra. Use of the relatively high energy photons of BL1A at UVSOR facility allows us to perform the bulk-sensitive measurements. The off- (hν = 826.4 eV) and on- (834.3 eV) resonant photoelectron spectra of LaB_2C_2 in the valence region are shown in

Figure 1. Abscissa represents the binding energy relative to the Fermi level (E_F). La 3d-4f photoabsorption spectrum of LaB_2C_2 is also indicated in the inset. A La 5p band (~20 eV) and some bands near to the E_F (0–7 eV) are significantly enhanced in the on-resonant spectrum. The latter resonant enhancement suggests that some valence states near to E_F are localized on La atom. This does not support the complete donation of the three valence electrons of La to the BC sheet, but means that some valence electrons (according to the theoretical band calculation,[2] La 5d-derived electrons) of La atom are participating to the formation of the valence band of LaB_2C_2. The number of La 5d derived-valence electron localized on a La atom is roughly estimated to be 0.3.

References
1) J. van Duijn *et al.*, *Phys. Rev. B* **62**, 6410 (2000).
2) H. Harima and M. Shirai, *J. Phys. Soc.* submitted.
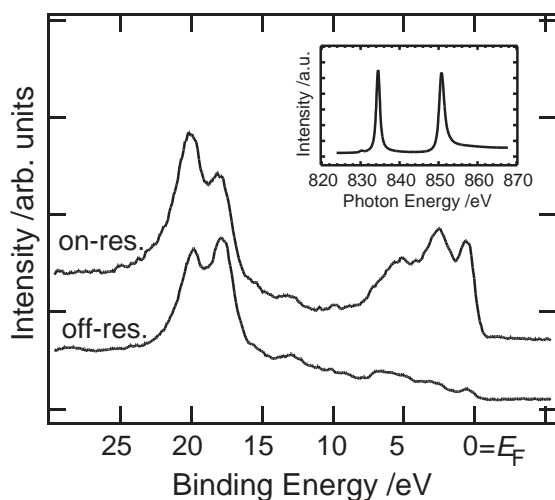
Figure 1. Off- and on-resonant valence-band photoelectron spectra of LaB_2C_2. La 3d-4f photoabsorption spectrum of LaB_2C_2 is also indicated in the inset.

VI-B-2 Cu L-Edge X-Ray Absorption Spectra of (Me$_2$-DCNQI)$_2$Li$_{1-x}$Cu

HATSUI, Takaki; TAKATA, Yasutaka[1]; KOSUGI, Nobuhiro; YAMAMOTO, Takashi[2]; TAJIMA, Hiroyuki[2]
(*[1]RIKEN; [2]Univ. Tokyo*)

Cu L-edge X-ray absorption spectra for (Me$_2$-DCNQI)$_2$Li$_{1-x}$Cu$_x$ alloys (Me$_2$-DCNQI: 2,5-dimethyl-N,N'-dicyanoquinonediimine) were measured at room temperature in order to investigate the local electronic structure around Cu atoms. Total electron yield mode was used except for the alloyed sample with $x < 0.1$, which was obtained by measuring the partial fluorescence yield. Both in the Cu L$_3$- and L$_2$-edge regions of (Me$_2$-DCNQI)$_2$Cu ($x = 1$) shows a characteristic higher-energy broad band B in addition to a lowest sharp band A associated with the transitions to the Cu 3d hole, while K$_3$Cu(CN)$_4$ with Cu 3d^{10} shows only a higher-energy band E (Figure 1). The broad band B arise from the transitions to the lowest unoccupied molecular orbital (LUMO) of Me$_2$-DCNQI molecules,

where the intensity comes from the Cu 3d components through strong hybridization with Cu. The spectral feature does not change even if the x value (the Cu content) is reduced to less than 0.1. This indicates that these alloys have nearly the same covalent bond between Cu and Me$_2$-DCNQI as (Me$_2$-DCNQI)$_2$Cu ($x = 1$).
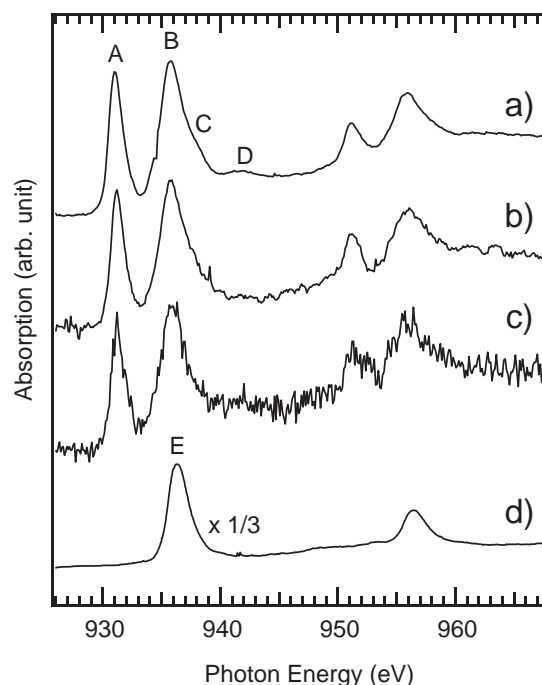
Figure 1. Cu L-edge X-ray absorption spectra of (Me$_2$-DCNQI)$_2$Li$_{1-x}$Cu$_x$ with $x = 1$ (a), $x = 0.15$ (b), and $x < 0.1$ (c). Spectrum of K$_3$Cu(CN)$_4$ is presented for comparison (d).

VI-B-3 Resonant Inelastic X-Ray Scattering of Ni Dimethylglyoxime

HATSUI, Takaki; KOSUGI, Nobuhiro; RUBENSSON, Jan-Erik[1]; KÄÄMBRE, Tanel[1]; NORDGREN, Joseph[1]
(*[1]Uppsala Univ.*)

In our previous study, we found two metal-to-ligand charge transfer (MLCT) transitions in the Ni L-edge X-ray absorption spectrum of a planar Ni complex, Ni dimethylglyoxime [Ni(Hdmg)$_2$]. The MLCT transition was proved to have close correlation with the π-backbonding. The presence of core hole in the final states of x-ray absorption, however, makes it difficult to obtain quantitative information on the bonding between metal and ligand. On the other hand, the final states of resonant x-ray inelastic scattering (RIXS) correspond to valence-excited states without core hole. In the present study, we have measured RIXS of Ni(Hdmg)$_2$ in order to clarify the bonding nature quantitatively.

Figure 1 shows RIXS spectra (a) and (b) at the higher-energy MLCT excitation. In the E_{in} // k_{out} (E_{in}: electric vector of incident x-ray, k_{out}: wavevector of emitted x-ray) geometry, the band at 860 eV is very weak in accordance with the selection rule, where the direct recombination is symmetry forbidden. The spectrum (c), obtained at the excitation far above the

ionization threshold, is similar to the resonant spectra (a) and (b). Compared with the $E_{in} \parallel k_{out}$ spectrum, peak position of the strongest peak in the $E_{in} \perp k_{out}$ spectrum (a) is shifted toward lower energy side. Based on the consideration of the selection rule and the electronic structure, the shift arises from different one-electron excitations, and the most intense peak in spectra (a) and (b) is revealed to have final states with (Ni 3d)$^{-1}$(ligand π^*)^1.
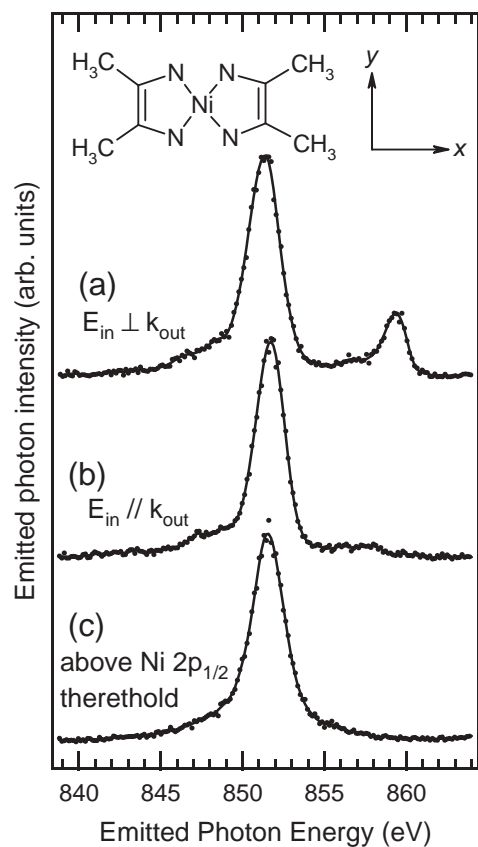
Figure 1. Resonant inelastic X-ray scattering of Ni(Hdmg)$_2$ at the excitation of MLCT band with the $E_{in} \perp k_{out}$ (a) and $E_{in} \parallel k_{out}$ (b) geometries. A non resonant spectrum is shown for comparison (c).

VI-C Observation of Vibrational Coherence (Wavepacket Motion) in Solution-Phase Molecules Using Ultrashort Pulses

With recent remarkable improvements of ultrashort-pulse lasers, we are now able to generate an optical pulse shorter than a few tens of femtoseconds. Owing to its ultrashort duration and broad frequency bandwidth, the ultrashort pulse can excite a molecule 'impulsively' to generate a coherent superposition of vibrational eigen states either in the excited state or in the ground state. This vibrationally coherent state evolves in time, which is called wavepacket motion. The observation and control of the wavepacket motion is one of the most interesting topics in modern spectroscopy. In this project, we study vibrational coherence in the condensed-phase molecules by using ultrashort optical pulses whose duration is ten ~ a few tens of femtoseconds. In this year, we attained the observation of the wavepacket motion in a photo-dissociating molecule in solution, and succeeded in measuring impulsive stimulated Raman scattering form the excited state of a polyatomic molecule for the first time.

VI-C-1 Observation of Coherent Nuclear Motion in the Photoinduced Ring-Opening Reaction of Diphenylcyclopropenone

TAKEUCHI, Satoshi; TAHARA, Tahei[1]
(*[1]IMS and RIKEN*)

When the time-resolution in time-resolved spectroscopy exceeds the period of molecular vibrations, we have a chance to observe the nuclear motions in real time. Thanks to recent progresses in short-pulse lasers, the observation of such a coherent nuclear dynamics becomes possible even during fast chemical reactions. Here, we report on our time-resolved absorption study of the coherent vibrational dynamics in the reaction of diphenylcyclopropenone (DPCP). This molecule has a highly strained three-membered ring structure. It is known that photo-excitation of DPCP causes a dissociation of the carbonyl group, giving rise to diphenylacetylene (DPA) as a product. From our sub-picosecond transient absorption measurements, we concluded that this ring-opening reaction starts form the S_2 state of DPCP, generating the product DPA in the electronically excited (S_2) state. In order to examine the nuclear dynamics during the reaction, we carried out time-resolved absorption measurements with a time resolution as good as 60–70 fs. Figure 1 depicts a temporal behavior of the absorption from the S_2 DPCP, the precursor of the reaction. The precursor absorption decays with a 0.2-ps time constant as the reaction proceeds, which is followed by a residual absorption decay (9 ps) due to the reaction product (S_2 DPA). In addition to this reaction dynamics, we found a weak but significant oscillatory modulation superposed on the decay of the precursor absorption. This modulation arises from the vibrational coherence created by the photoexcitation. The modulation period (110 fs) corresponds to a vibrational frequency of *ca.* 300 cm^{-1}. We concluded that the DPCP exhibits a coherent nuclear motion having the 300-cm^{-1} frequency during the ring-opening reaction.
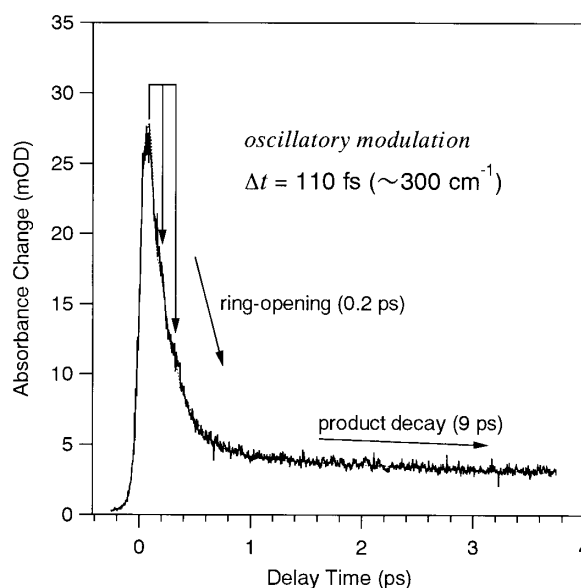
Figure 1. Time-resolved absorption of diphenylcyclopropenone in cyclohexane measured with the 295-nm excitation and 525-nm probe.

VI-C-2 Construction of Transient Resonance Impulsive Stimulated Raman Scattering Spectrometer

FUJIYOSHI, Satoru[1]; TAKEUCHI, Satoshi; TAHARA, Tahei[2]
(*[1]GUAS; [2]IMS and RIKEN*)

Time-resolved spectroscopic study of the low-frequency intra- and inter-molecular vibrations is very important to understand the structure and function of short-lived species such as reaction intermediates. However, observation of low-frequency vibrations by time-resolved frequency-domain Raman spectroscopy is extremely difficult, because a strong Rayleigh scattering often disturbs the measurements. In contrast, it is known that the Rayleigh scattering is readily separated in time-domain Raman methods such as the impulsive stimulated Raman scattering (ISRS) spectroscopy. So far, this ISRS method has been utilized to observe Raman-active low-frequency vibrations of molecular liquids in the ground state. It is highly expected that the ISRS method can also be applied to the observation of

the low-frequency vibrations of transient species. Here, we report our experimental setup constructed for the ISRS spectroscopy of transient species ("transient resonance ISRS").

Figure 1 shows the apparatus used for the transient resonance ISRS measurements. The light source is a Ti:sapphire regenerative amplifier system. The output of this amplifier (800 nm, ~0.1 ps) is divided into two parts. One portion is converted to the third harmonic at 267 nm (~0.5 ps). It is used as a pump pulse, and is focused to the sample jet to generate transient species. Another portion is converted to a visible pulse (600 nm, ~0.04 ps) in an optical parametric amplifier and subsequent frequency doubling. This visible pulse is used for the ISRS process. It is tunable in the 600–800 nm region for best resonance to the absorption of the transient species. The pulse duration of the visible pulse can be as short as 40 fs after the prism compensator. The visible pulse is divided into three, and is focused to the photoexcited portion of the sample jet with a standard BOXCARS geometry. The signal light that is diffracted in the phase matching direction is detected by a photodiode.
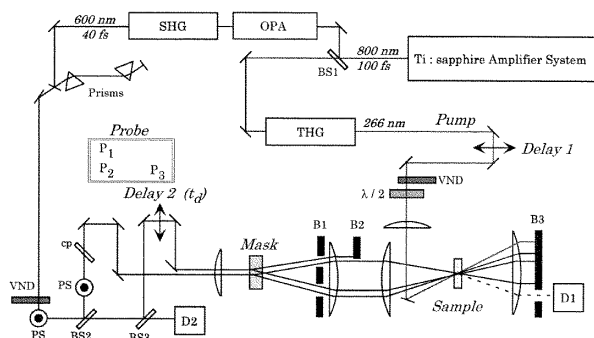
Figure 1. Apparatus of the transient-resonance-ISRS spectrometer.

VI-C-3 Observation of the Low-Frequency Vibration of S_1 *Trans*-Stilbene in Solution Using Transient Resonance Impulsive Stimulated Raman Scattering Method

FUJIYOSHI, Satoru[1]; TAKEUCHI, Satoshi; TAHARA, Tahei[2]
(*[1]GUAS; [2]IMS and RIKEN*)

Recently, we have developed a novel spectrometer for the detection of impulsive stimulated Raman scattering (ISRS) from transient species. By using this transient resonance ISRS method, we measured the low-frequency vibration of excited-state polyatomic molecules in solution, for first time. The ISRS signals obtained from *trans*-stilbene in ethanol are shown in Figure 1. Before photoexcitation (–20 ps), only a weak signal corresponding to the non-resonant electronic response of the solvent was observed (broken line). After photoexcitation (20 ps), in contrast, the intensity of the ISRS signal was strongly enhanced (solid line). The probe wavelength of the ISRS process is in resonance with the $S_n \leftarrow S_1$ transient absorption, so that the enhanced ISRS signal is attributed to S_1 trans-stilbene. The observed ISRS signal of S_1 trans-stilbene consists of a sharp peak, an oscillatory component, and a slowly decaying component. The frequency of the oscillatory component was determined to be 290 cm^{-1} by Fourier analysis, and it is equal to the frequency of an S_1 in-plane bending mode (ν_{24}) that has been observed in time-resolved frequency-domain Raman spectroscopy.[1] The present measurement successfully demonstrated a high potential of the transient resonance ISRS spectroscopy for the study of low-frequency vibrations of polyatomic molecules in the excited state.

Reference
1)T. L. Gustafson, D. M. Robert and D.A. Chernoff, *J. Chem. Phys.* **81**, 3438 (1994).
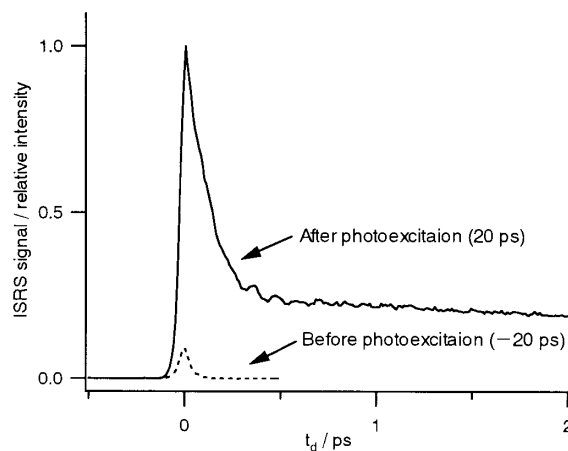
Figure 1. Transient resonance impulsive stimulated Raman scattering signals obtained from *trans*-stlibene in ethanol (pump 266 nm, probe 600 nm).

VI-D Studies of Primary Photochemical/physical Processes Using Femtosecond Electronic Spectroscopy

Ultrafast spectroscopy is playing an essential role in elucidation of photochemical reactions. Thanks to the recent advance in laser technology, we are now able to examine the dynamics of chemical reactions that take place in the femtosecond time region. In this project, we study primary photochemical/physical processes of the condensed-phase molecules using time-resolved fluorescence and absorption spectroscopy whose time-resolution is a few hundreds femtoseconds. Time-resolved fluorescence and absorption spectroscopy are complimentary to each other. The advantage of fluorescence spectroscopy lies in the fact that fluorescence originates from the transition between

the "well-known" ground state and the excited state in question. Thus time-resolved fluorescence spectroscopy can afford unique information not only about the dynamics but also other properties of the excited singlet states such as their energies and oscillator strengths. On the other hand, however, time-resolved absorption spectroscopy is considered to be more versatile because it can detect not only fluorescent excited singlet states but also other "dark" transients. In this year, we investigated the dynamics and mechanism of excited-state proton transfer of hydroxy anthraquinone derivatives, isomerization of trans-azobenzene, and photodissociation of diphenylcyclopropenone. In addition, we obtained a new crucial data about the reaction mechanism of excited-state proton transfer of 7-azaindole dimer.

VI-D-1 Femtosecond Time-Resolved Fluorescence Study of Excited-State Intramolecular Proton Transfer in Hydroxy Derivatives of Anthraquinone

ARZHANTSEV, Sergei; TAHARA, Tahei[1]
(*[1]IMS and RIKEN*)

The proton transfer is one of the most fundamental reactions and plays crucial roles in many processes in chemistry. Anthraquinone is an excellent nucleus for the study of excited state intramolecular proton transfer since the availability of many –OH and –NH_2 derivatives and the diversity of positions for substitution. In this study, we chose four α-hydroxy derivatives of anthraquinone: 1-hydroxyanthraquinone (1-HAQ), 1,4-, 1,5-, and 1,8-dihydroxyanthraquinones (DHAQ) to investigate the influence of the second hydroxyl group on photochemistry of molecules.

The steady-state fluorescence spectra of 1-HAQ, 1,5- and 1,8-DHAQs show very large Stokes shift and dual character of emission that is considered as an evidence of the proton transfer reaction in the excited state. In contrast, the fluorescence of 1,4-DHAQ is close to mirror image of absorption. There is no evidence of proton transfer reaction in the excited state.

Femtosecond time-resolved fluorescence intensities of all four molecules in hexane were measured at room temperature for a wide visible wavelength region using up-conversion method. Time-resolved fluorescence spectra were reconstructed after deconvolution taking account of the finite instrumental response. The reconstructed time-resolved fluorescence spectra are presented in Figure 1. We observed the following dynamics for molecules that show dual fluorescence. (1) Both parts of dual fluorescence exist at the time origin. (2) The intensity of short wavelength fluorescence is compatible with intensity of long wavelength fluorescence at the time origin in contrast to the steady-state spectrum. (3) All three molecules show the decrease of short wavelength fluorescence and simultaneous rise of long wavelength fluorescence in the time scale up to 10 ps. (4) In addition, 1-HAQ and 1,5-DHAQ molecules exhibit very fast decay of short wavelength fluorescence intensity in the time scale of 50 fs.

In the case of molecule that shows mirror image type fluorescence (1,4-DHAQ), we found the following dynamics. (1) The spectral changes in the time scale up to 2 ps are similar to spectral changes observed for molecules that exhibit excited state proton transfer. (2) In the time scale from 2 ps up to 50 ps the fluorescence shows the increasing intensity of short wavelength part of the spectrum.

We concluded that proton transfer in α-hydroxy derivatives of anthraquinone is barrierless type of reaction and it occurs in a time scale of several tens of femtoseconds, reflecting delocalization of the excited-state wavefunctions. We assigned the fluorescence dynamics in a few picosecond time scale to an additional proton translocation reflecting the intramolecular vibrational relaxation. It is shown that the excited-state dynamics is affected by position of the second hydroxyl group.
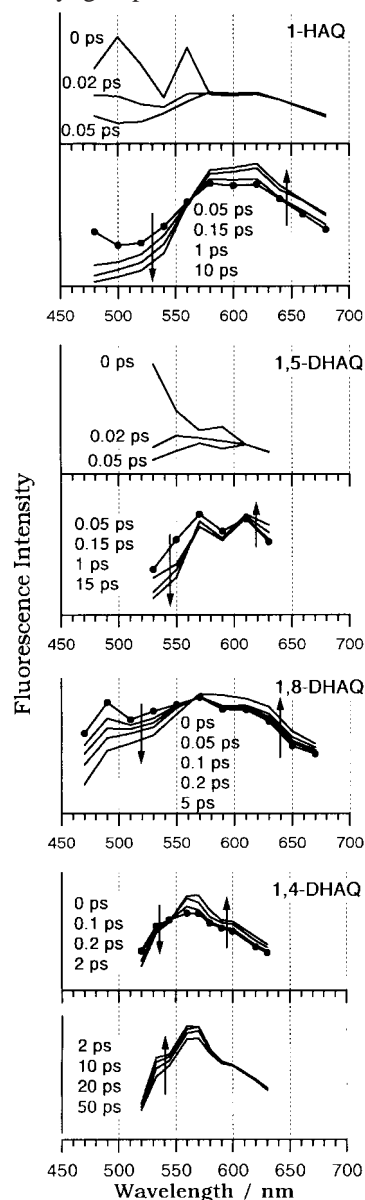
Figure 1. The reconstructed time-resolved fluorescence spectra of hydroxy derivatives of anthraquinone.

VI-D-2 Steady-State and Femtosecond Time-Resolved Fluorescence Study of *Trans*-Azobenzene with $S_2(\pi\pi^*) \leftarrow S_0$ Photoexcitation

FUJINO, Tatsuya; ARZHANTSEV, Sergei; TAHARA, Tahei[1]
(*[1]IMS and RIKEN*)

Femtosecond time-resolved fluorescence spectroscopy was performed to study the photochemistry of *trans*-azobenzene. Azobenzene in hexane was initially photoexcited to the $S_2(\pi\pi^*)$ state by 280-nm light (560 pJ, 230 fs, 82 MHz) and the time-resolved fluorescence was measured in the wavelength region from 340 to 680 nm by the up-conversion method. The observed fluorescence exhibited double exponential decay and the lifetimes were determined as ~110 and ~500 fs. The spectral analysis of the two fluorescence components showed that their intensity maxima are located at ~400 and ~650 nm. Since they showed good mirror images of the $S_2 \leftarrow S_0$, and the $S_1 \leftarrow S_0$ absorption bands, we assigned them to the fluorescence from the S_2 and S_1 states, respectively, which have planar structure around the central NN bond. The quantum yield of the $S_2 \rightarrow$ 'planar' S_1 electronic relaxation was evaluated by comparing the S_2 and S_1 fluorescence intensities, and it was found to be almost unity. It implies that almost all molecules photoexcited to the $S_2(\pi\pi^*)$ state are relaxed to the 'planar' $S_1(n\pi^*)$ state. The present time-resolved fluorescence study clarified that the isomerization pathway starting directly from the $S_2(\pi\pi^*)$ state does not exist. It was also indicated that the isomerization mechanism of azobenzene is the inversion isomerization occurring in the S_1 state, regardless of difference in photoexcitation conditions.
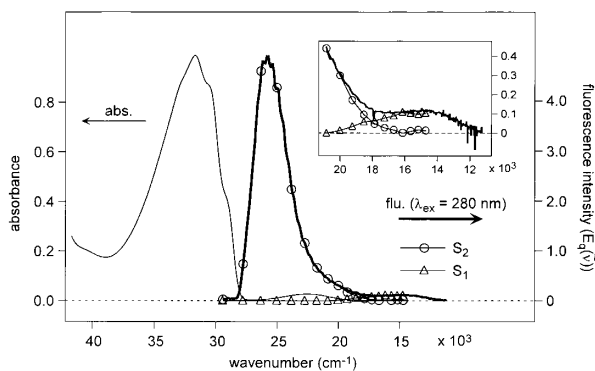
Figure 1. The absorption spectrum (left) and the steady-state fluorescence spectrum obtained with the 280-nm excitation (right). The fluorescence intensity is represented as the photon number intensity in the frequency space. In the fluorescence spectrum, open circles and open triangles represent the S_2 and S_1 fluorescence components, respectively. The wavenumber region from 22000 to 12000 cm^{-1} is expanded in the inset.

VI-D-3 A New Insight into the Relaxation Mechanisms of *trans*-Azobenzene Following the $S_2(\pi\pi^*) \leftarrow S_0$ Photoexcitation: Rotational Deactivation Process from the Vibrationally Excited $S_1(n\pi^*)$ State

FUJINO, Tatsuya; ARZHANTSEV, Sergei; TAHARA, Tahei[1]
(*[1]IMS and RIKEN*)

It is known that the quantum yield of *trans* → *cis* photoisomerization of azobenzene depends on the excitation wavelength: the S_2 excitation gives almost the half value (~0.1) of the S_1 excitation (~0.2). The photoisomerization mechanism of azobenzene has been discussed on the basis of the isomerization quantum yield, and it has been considered that the photoisomerization after the S_2 excitation proceeds differently (rotation) from that after the S_1 excitation (inversion). However, our recent spectroscopic studies clarified that S_2 azobenzene is exclusively relaxed to the 'planar' S_1 state, and hence rotational isomerization pathway from the S_2 state was ruled out. Since it is now clear that the isomerization of azobenzene occurs in the S_1 state regardless of the difference in initial photoexcitation, we need to reconsider the implication of the difference in the isomerization quantum yield between S_2 and S_1 excitation.

After the rapid decay of the S_2 state (~0.11 ps), a considerable amount of photoexcitation energy is localized in the S_1 state in the form of the vibrational excess energy, because vibrational cooling process occurs in a much longer time scale (several tens picosecond). Therefore, a significant difference between S_2 and S_1 excitation is the vibrational excess energy in the S_1 state that appears after photoexcitation. The S_1 state produced after S_2 excitation is highly vibrationally excited (hot) compared to the S_1 state generated by direct S_1 excitation. Thus, the low isomerization quantum yield of S_2 excitation is attributable to the low isomerization efficiency of the vibrationally excited S_1 state. It indicates that another relaxation channel exists especially in the vibrationally excited S_1 state.

It was reported that the isomerization quantum yields obtained with S_2 and S_1 excitation become the same (~0.2) when the rotational motion of azobenzene is prohibited by chemical modification.[1] This result suggests that the relaxation channel in the vibrationally excited S_1 state is blocked by the chemical modification. In other words, the relaxation channel, which we propose for the vibrationally excited S_1 state, is related to the rotational coordinate, although this channel does not produce the *cis* isomer but generates only *trans* S_0 azobenzene.

Reference
1)H. Rau and E. Lüddecke, *J. Am. Chem. Soc.* **104**, 1616 (1982).
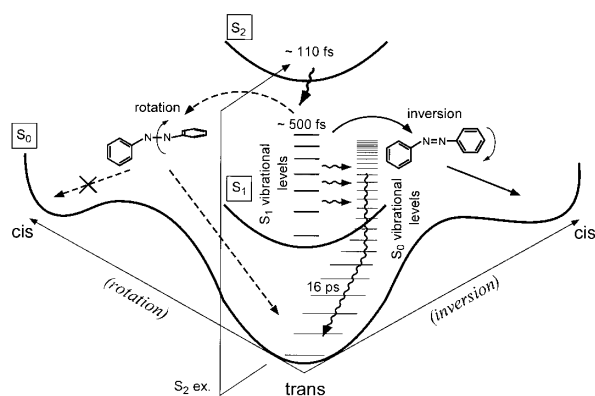
Figure 1. Schematic diagram of the relaxation and isomerization pathway of *trans*-azobenzene after the $S_2(\pi\pi^*) \leftarrow S_0$ photoexcitation.

VI-D-4 Dynamics of Photoinduced Ring-Opening Reaction of Diphenylcyclopropenone Studied by Sub-Picosecond Transient Absorption Spectroscopy

TAKEUCHI, Satoshi; TAHARA, Tahei[1]
(*[1]IMS and RIKEN*)

Since the first synthesis of cyclopropenone derivatives, the aromaticity, stability, and reactivity of their three-membered ring structure have been attracting much interest. Diphenylcyclopropenone (DPCP) is one of the molecules having such a highly strained structure. It is known that photoexcitation of DPCP causes a dissociation of the carbonyl group, giving rise to diphenylacetylene (DPA) as a product (Figure 1). This ring-opening reaction has been studied in solution by picosecond absorption spectroscopy, and it was found that the excited state of DPA is formed by the S_2 excitation of DPCP. However, the ring-opening dynamics itself was not clarified so far because of the low time resolution of the reported measurements (several tens of picoseconds). In this project, we carried out transient absorption measurements with a better (sub-picosecond) time-resolution to elucidate the ultrafast reaction dynamics.

Figure 2 shows transient absorption spectra of DPCP in cyclohexane measured with the S_2 excitation at 267 nm. For comparison, we also plot transient absorption spectra obtained by direct photoexcitation of DPA. It is readily found from this comparison that the DPCP spectra become very similar to the DPA spectra in the delay time region later than 30 ps. This spectral similarity assures that the photoexcitation of DPCP leads to the excited state of DPA. The broad peak around 430 nm recognized in the 30–60 ps time range is due to the S_1 state of DPA generated by the reaction, which then relaxes to the T_1 state ($\lambda_{max} = 410$ nm) at later delay times. In the early time region, by contrast, the DPCP spectra are significantly different from the DPA spectra. A strong band is observed around 480 nm just after photoexcitation, which is not seen in the DPA spectra. From its instantaneous rise and fast decay (0.2 ps), we assigned the 480-nm band to the initially-populated S_2 state of DPCP, the precursor of the reaction. This precursor band at 480 nm becomes

noticeable only with the good time resolution in the present study. After the fast disappearance of the 480-nm band, the DPCP spectra exhibit a broad feature extending over the entire visible region, which also looks different from the DPA spectra. We tentatively assigned this broad feature to the S_2 DPA generated right after the reaction. The spectral difference seen in the 1–10 ps time range might be due to a reaction-induced structural change of the product DPA in the S_2 state. We conclude that the ring-opening reaction starts from the S_2 DPCP with a 0.2-ps time constant, giving rise to the S_2-like DPA.
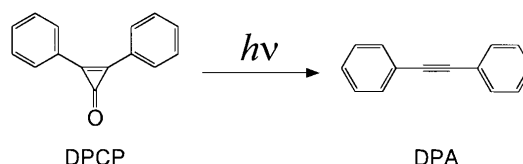
Figure 1. Photoinduced ring-opening reaction of diphenyl-cyclopropenone.
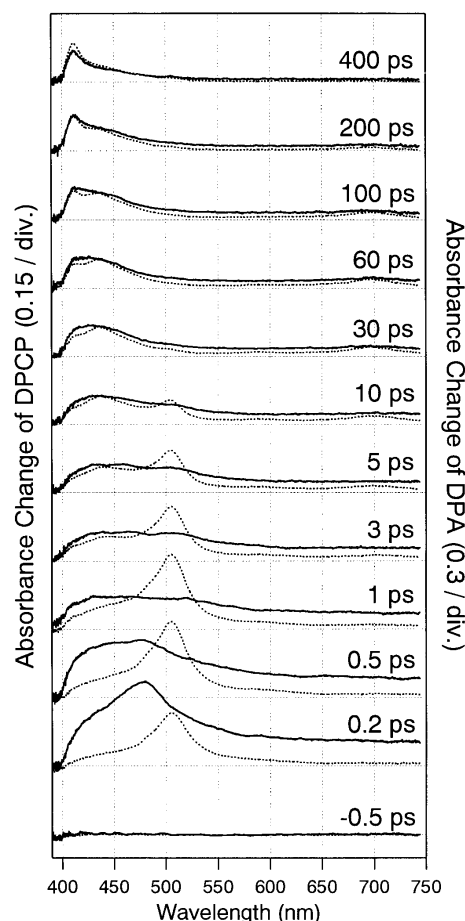
Figure 2. Transient absorption spectra of DPCP (solid) and DPA (dotted) measured in cyclohexane with the 267-nm excitation.

VI-D-5 Excitation-Wavelength Dependence of the Femtosecond Fluorescence Dynamics of 7-Azaindole Dimer: Further Evidence for the Concerted Double Proton Transfer in Solution

TAKEUCHI, Satoshi; TAHARA, Tahei[1]
(*[1]IMS and RIKEN*)

7-Azaindole dimer is a prototypical system showing the proton transfer reaction in the excited state. It is one of the ideal systems where we can examine the mechanism of the double proton transfer. An important question about the double proton transfer is whether the two protons are translocated in the concerted way or the step-wise way. These two reaction mechanisms have been the subject of intensive debates on the reaction of the 7-azaindole dimer.

Experimentally, it has been confirmed that there exist two components (0.2 ps and 1.1 ps) in the precursor dynamics of the reaction. However, as illustrated in Figure 1, these two components were assigned differently in the discussion that supports each mechanism. In the argument for the concerted mechanism, the 0.2-ps component was assigned to the $S_2 \rightarrow S_1$ electronic relaxation before the reaction and the 1.1-ps component to the actual translocation of the two protons from the S_1 state. On the other hand, in the argument supporting the step-wise mechanism, the 0.2-ps and the 1.1-ps components were assigned to the first and the second proton transfer, respectively. In other words, the two components were attributed to the formation and disappearance of the intermediate in which only one proton is transferred. Therefore, the assignment of the 0.2-ps component is the key to know which mechanism is correct.

In this project, we examined an excitation-wavelength dependence of the ultraviolet fluorescence dynamics. The experiment for the excitation-wavelength dependence is crucial to distinguish the two mechanisms. If the concerted mechanism is relevant, the change of the excitation-wavelength alters the initial population ratio of the S_2 and S_1 states, so that the relative amplitude of the 0.2-ps and 1.1-ps components should change with the excitation-wavelength. In the case of the step-wise mechanism, on the contrary, the relative amplitude of the two components is expected to be constant irrespective of the excitation wavelength, since they correspond to two successive proton-transfer steps. Figure 2 shows fluorescence decays of the dimer excited state(s) (reaction precursor) measured with six excitation wavelengths. It is clear that the precursor dynamics shows a significant excitation-wavelength dependence. In fact, the 0.2-ps component becomes smaller as the excitation wavelength gets longer. Finally, the 0.2-ps component almost vanishes when the dimer is excited at 313 nm, *i.e.*, the red-edge of the dimer absorption. These experimental data are inconsistent with the step-wise mechanism, and deny the existence of the reaction intermediate. We concluded that the proton transfer in solution starts from the S_1 state in the concerted manner with a time constant of 1.1 ps.
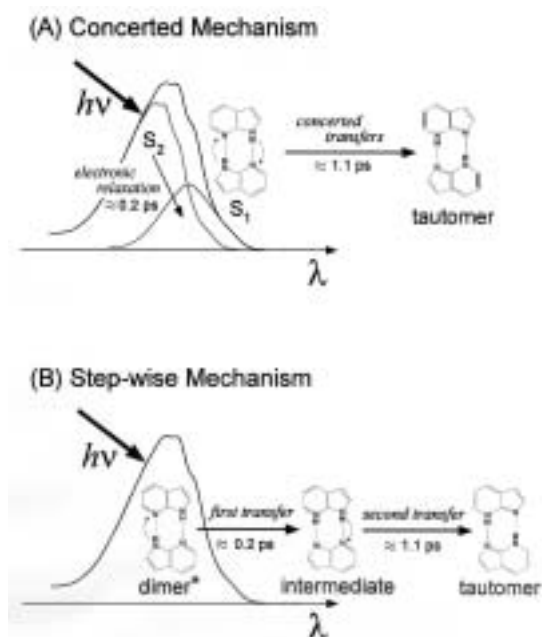
Figure 1. Two reaction mechanisms proposed for the double proton transfer of 7-azaindole dimer.
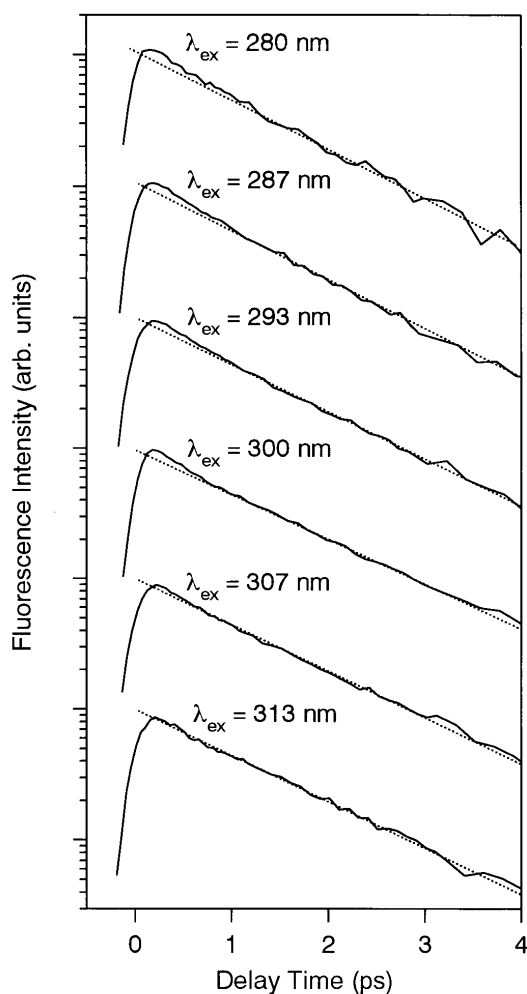
Figure 2. Logarithmic plot of the fluorescence decay of the dimer excited state(s) measured with six excitation wavelengths. The dotted straight line drawn for each data corresponds to a 1.1-ps single-exponential decay.

VI-E Studies of Photochemical Reactions Using Picosecond Time-Resolved Vibrational Spectroscopy

Time-resolved vibrational spectroscopy is a very powerful tool for the study of short-lived transient species. It often affords detailed information about the molecular structure of transients, which is not obtainable with time-resolved electronic spectroscopy. However, for molecules in the condensed phase, we need energy resolution as high as 10 cm^{-1} in order to obtain well-resolved vibrational spectra. This energy resolution is compatible only with time-resolution slower than one picosecond because of the limitation of the uncertainty principle. In this sense, picosecond measurements are the best compromise between energy resolution and time resolution for time-resolved frequency-domain vibrational spectroscopy. In this project, we study photochemical processes and/or short-lived transient species by using picosecond time-resolved Raman spectroscopy. In this year, we studied the solvated electron in water and found a novel resonance Raman enhancement due to the water molecules solvating electrons. For instrumentation, we constructed a new apparatus to perform time-resolved Raman measurements in the near-infrared region. We also demonstrated a new method for temporal fluorescence rejection in Raman spectroscopy and achieved the highest rejection efficiency at the moment.

VI-E-1 Novel Resonance Raman Enhancement of Local Structure around Solvated Electrons in Water

MIZUNO, Misao; TAHARA, Tahei[1]
(*[1]IMS and RIKEN*)

The solvated electron is the most important basic anionic species in solutions. The absorption maximum of the solvated electron in water is located around 720 nm. This absorption is assigned to the s → p electronic transition of the solvated electron. We measured picosecond time-resolved Raman spectra under the resonance condition with this electronic transition for the first time.

In the experiment, the output of picosecond Ti:sapphire regenerative amplifier was used as the light source for time-resolved Raman measurements. The third harmonic (267 nm) was used to generate solvated electrons. The fundamental pulse (800 nm) was utilized to probe Raman scattering under the condition resonant with the s → p transition of the solvated electron. Figure 1 shows picosecond time-resolved resonance Raman spectra of an indole aqueous solution. Indole is used as the electron seed molecule. A strong transient Raman band appears around 1610 cm^{-1} in accordance with the generation of the solvated electron, while only the weak OH-bend Raman band of bulk water can be observed before the pump pulse irradiation. This transient Raman band is attributable to the vibration of the solvating water molecules that strongly interact with the solvated electron in the first solvation shell. The mechanism of this resonance Raman enhancement was also discussed on the basis of the vibronic theory.
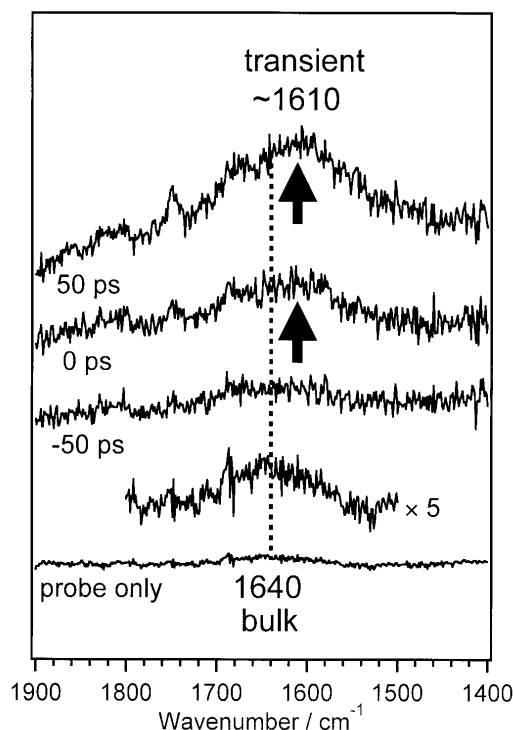
Figure 1. Picosecond time-resolved resonance Raman spectra of water in the presence of indole (1.7×10^{-3} mol dm^{-3}; pump laser 267 nm; probe laser 800 nm). The luminescence background has been subtracted from each spectrum.

VI-E-2 Construction of A Near-Infrared Time-Resolved Raman Spectrometer

MIZUNO, Misao; TAHARA, Tahei[1]
(*[1]IMS and RIKEN*)

Picosecond time-resolved resonance Raman spectroscopy is a very important tool to study the molecular structure of short-lived transient species appearing in photochemical reactions. In order to take advantage of resonance intensity enhancement, the wavelength of the probe light is required to be resonant with the absorption of the transient species. As for the time-resolved Raman measurements in the visible

region, the instrumentation has been already established for both the light source and the detector, and a large number of experiments have been performed. Some important transient species, however, show absorption in the near-infrared region, and near-infrared Raman measurements are needed to study these transients. Therefore, we constructed a new apparatus for near-infrared picosecond time-resolved resonance Raman spectroscopy. The second or third harmonics of the regeneratively amplified output of a picosecond Ti:sapphire laser are used to photoexcite the sample, and the fundamental pulse is used for the probe. Raman scattering is detected by a liquid nitrogen cooled InGaAs multi-channel detector that has sensitivity for the near-infrared light. Figure 1 shows a Raman spectrum of a water-acetonitrile mixture probed by 800 nm, which was measured using the constructed apparatus. We are now able to perform picosecond time-resolved Raman measurement for transient species that shows transient absorption in the near-infrared region.

(a)

(b)
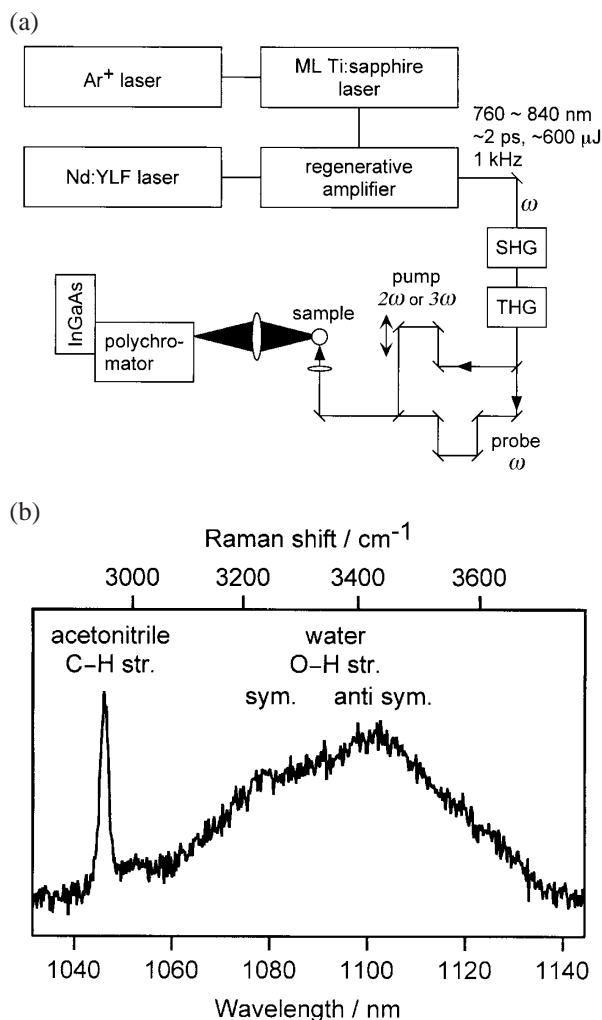
Figure 1. (a) Apparatus for the near-infrared time-resolved Raman spectroscopy. (b) Raman spectrum of a water-acetonitrile (4:1) mixture measured by an InGaAs detector. (probe wavelength 800 nm; laser energy 10 μJ; repetition rate 1 kHz)

VI-E-3 Temporal Fluorescence Rejection in Raman Spectroscopy by the Application of Femtosecond Upconversion Technique

MANDAL, Debabrata; ARZHANTSEV, Sergei; TAHARA, Tahei[1]
(*[1]IMS and RIKEN*)

Temporal fluorescence rejection is a well known and effective method for detecting weak Raman scattering from fluorescent samples. In this method, the temporal response of an ultrafast detection system acts as a "time-gate" to selectively detect the Raman signal, rejecting the longer-lived fluorescence. The efficiency of rejection is proportional to the ratio of fluorescence lifetime and the gating-time. Several techniques have been developed for this purpose, ranging from the use of ultrafast streak camera to applying nonlinear optical effects. But so far, the highest time resolution achieved has been a few picoseconds, using optical Kerr gating technique. We have developed a new method of temporal fluorescence rejection based on femtosecond upconversion. Second harmonic pulses (460 nm) from a Ti:Sapphire oscillator (Tsunami, Spectra Physics) are used to optically excite a solution of acetonitrile containing coumarin 153, a fluorophore with an intense fluorescence having a lifetime of several nanoseconds. The emission from the solution is monitored temporally by the upconversion method using the laser fundamental at 920 nm as the gate pulse. The temporal response of the apparatus is 170 fs, which was given by the fwhm of the cross correlation signal of the gate pulse and the Raman scattering from the neat solvent. Using such a short response time automatically enhances the rejection efficiency by over 1 order of magnitude compared with the previous works.

Excitation at 460 nm causes the Raman lines of acetonitrile to fall within the frequency range of coumarin 153 fluorescence, where they are undetectable in steady-state measurements. However, in the upconversion traces, the Raman response is found to strongly dominate the initial part of the signal at certain emission frequencies (Figure 1). The time resolved emission spectra (TRES) reconstructed from the decays at different emission frequencies clearly exhibit two prominent peaks at ~2250 cm^{-1} and ~2900 cm^{-1} which appear at early delay times (Figure 2a). At slightly later times the peaks vanish, leaving only the fluorescence background (Figure 2b). Comparing the TRES with the Raman spectrum of pure acetonitrile (Figure 2c) recorded with cw excitation, the peaks are assigned to the C–N and C–H stretch Raman bands of acetonitrile respectively. It is noted, however, that both the peaks in the TRES are broadened by almost 200 cm^{-1}. This band broadening results from the inevitable loss of frequency resolution inherent in femtosecond measurements. Nevertheless, our results show that femtosecond upconversion is an efficient solution to the problem of temporal fluorescence rejection in Raman spectroscopy. Additionally, by applying the shortest time-gate for this problem so far, we have achieved an upper limit in the rejection efficiency.
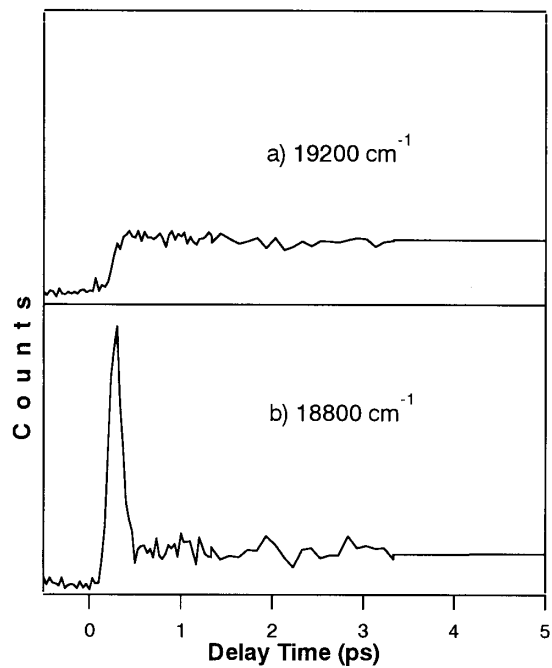
Figure 1. Time-resolved emission of coumarin 153 in acetonitrile at different emission frequencies.
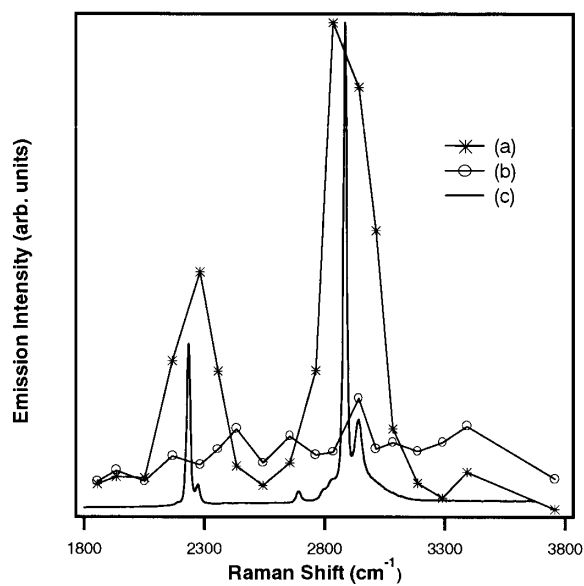
Figure 2. Reconstructed time-resolved emission spectra of coumarin153 in acetonitrile at different time-delays [time res. 160 fs] : a) 50 fs, b) 500 fs, c) Raman spectra of neat acetonitrile (measured with cw excitation).

VI-F Synchrotron Radiation Stimulated Surface Reaction and Nanoscience

Synchrotron radiation stimulated process (etching, CVD) has characteristics of low damage, low contamination, high spatial resolution, and high precision etc. In this project, nanostructures are created by using synchrotron radiation stimulated process, and the reaction mechanisms are investigated by using STM.

VI-F-1 Nanostructure Formation on Si (111) Surface Assisted by Synchrotron Radiation Illumination —Characterization by Scanning Tunneling Microscopy—

NONOGAKI, Youichi; GAO, Yongli[1]; MEKARU, Harutaka[2]; MIYAMAE, Takayuki[3]; URISU, Tsuneo
(*[1]Univ. Rochester; [2]Himeji Inst. Tech.; [3]Natl. Inst. Mater. Chem. Res.*)

[*J. Electron Spectrosc. Relat. Phenom.* **119**, 241 (2001)]

The surface structures after the synchrotron radiation (SR) stimulated removal of native oxide on Si (111) exactly oriented and 4° misoriented surfaces were investigated by scanning tunneling microscopy. The exactly oriented surface showed large regions of atomically flat Si(111)-7×7 structure, and was characterized by the formation of single bilayer steps nicely registered to the underlying crystal structure, clearly different from the disordered step edge obtained by the usual high temperature thermal cleaning. The 4° misoriented sample showed nearly uniformly spaced steps bunched and terraces terminated by 7×7 unit cells in both SR assisted and thermal cleanings, indicating that both cleanings give almost thermal equilibrium surfaces.
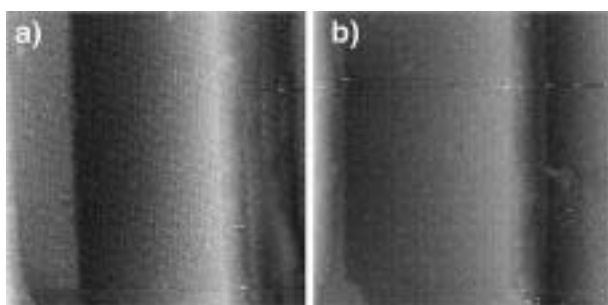
Figure 1. 50 nm × 50 nm STM images of the Si(111) 4° misoriented surfaces after 880 °C 1 min thermal (a), and the 700 °C 2 h SR stimulated cleaning (b), respectively.

VI-F-2 Construction of UHV Variable Temperature STM for *in situ* Observation of SR Stimulated Surface Reaction

NONOGAKI, Youichi; URISU, Tsuneo

We have investigated SR assisted desorption of SiO_2 on Si substrates under the various conditions and have found the significant difference between the thermal and SR-assisted desorption by STM observations. However, these STM images were not taken just after the SiO_2 desoption, since sample setting positions are different between the SR irradiation and STM observation. It is also unclear how the Si surfaces degrade during transferring the samples. To observe the time variation of the surface images more accurately, we have made a new STM system with STM and LEED as shown in Figure 1. By this system, the STM observation and SR irradiation can be conducted at the same sample position.
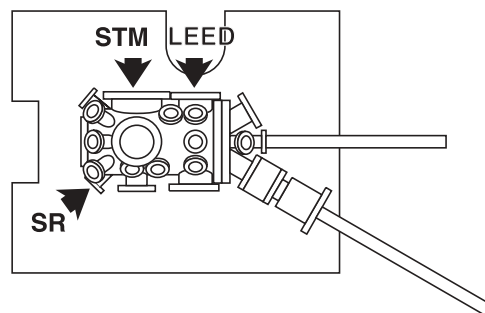
Figure 1. Schematic drawing of new STM system.

VI-F-3 Construction of Low Temperature UHV STM for Observation of Organic- or Bio-Molecules Assembled Silicon Surface

TAKIZAWA, Morio; URISU, Tsuneo

The study on organic- or bio- molecules assembled silicon surfaces is one of the important fields in nanoscience. We are now preparing low temperature STM for this purpose. The STM is equiped with VTI unit for temperature control from 2.5 K to R. T. The biomolecules which are solid, liquid and gas phase materials can be adsorbed by using a small crucible, liquid- and gas- doser, respectively. These evaporators can control a very small amount of exposure to the surfaces. Now, the chamber vacuums are reaching to less than 5.0×10^{-11} Torr (that is detection limit of our ion gauge). Although the condition is not optimized, we have got current-constant images of silicon(111) surface. In the next step, we will observe organic- or bio- molecules assembled on Si(100) surface in UHV.

VI-G Noble Semiconductor Surface Vibration Spectroscopy

As a new high sensitive and high resolution surface vibration spectroscopy technique, we are developing an infrared reflection absorption spectroscopy using buried metal layer substrate (BML-IRRAS). We are now developing a fabrication technique of BML substrate by wafer bonding. We are also investigating several surface chemical reactions on Si surfaces using this BML-IRRAS.

VI-G-1 Initial Stage of Hydrogen Etching of Si Surfaces Investigated by Infrared Reflection Absorption Spectroscopy

NODA, Hideyuki; URISU, Tsuneo; KOBAYASHI, Yoshihiro[1]; OGINO, Toshio[1]
(*[1]NTT Basic Res. Lab.*)

[*Jpn. J. Appl. Phys.* **39**, 6985 (2000)]

The initial stage of etching reactions (breaking the Si–Si back bonds) of Si(100) and Si(111) surfaces exposed to hydrogen at room temperature was investigated by buried metal layer-infrared reflection absorption spectroscopy. The peaks of SiH_2 scissors and SiH_3 deformation modes (< 1000 cm^{-1}) were successfully observed as clear indicators of the initial stage of hydrogen etching reactions. On the Si(100) surface, the hydrogen exposure dependence of these peaks indicated that the etching reaction starts in the relatively low-exposure region of ≥ 300 L (1 L = 1 $\times$ 10^{-6} Torr s). We found that the adjacent dihydride is a precursor to breaking the Si back bonds. On the Si(111) surface, it was found that the adatom's two back bonds are easily broken, and that adatom trihydride is generated at a low H-exposure of 70–500 L. Adding to this dominant reaction, the etching of the rest-atom layer was observed at H-exposures higher than 10000 L.
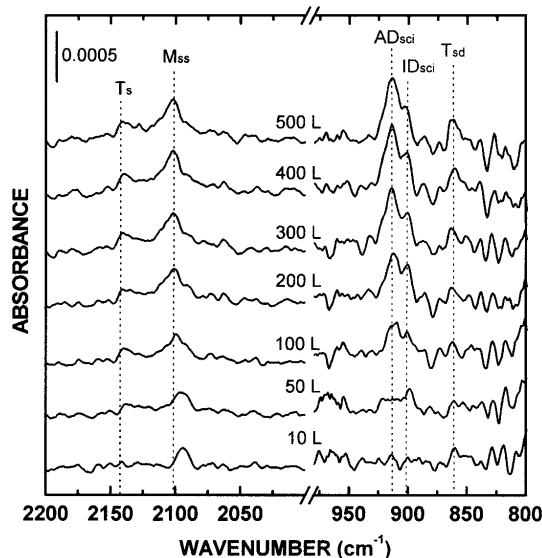
Figure 1. BML-IRRAS spectra of p-polarization for H/Si(100) formed by H-exposure at RT. The resolution is 2 cm^{-1}. H-exposure in units of Langmuir (L) is attached to each spectrum. Peak positions of SiH_n vibration modes are indicated by dotted lines. (M_{ss}: SiH symmetric stretching, T_s: SiH_3 stretching, T_{sd}: SiH_3 symmetric deformation, ID_{sci}: isolated SiH_2 scissors, AD_{sci}: adjacent SiH_2 scissors)
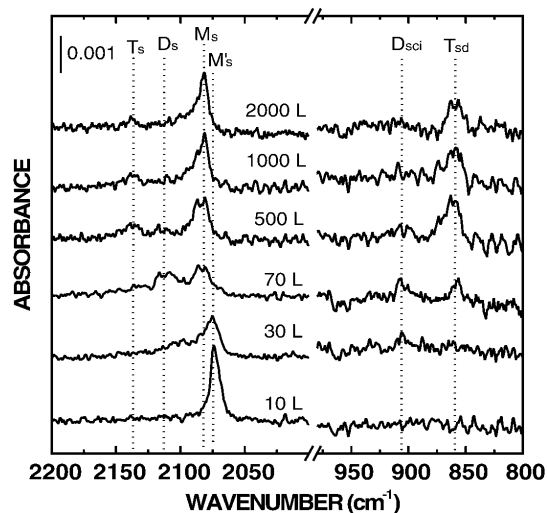
Figure 2. BML-IRRAS spectra of p-polarization for H/Si(111) formed by H-exposure at RT. The resolution is 2 cm^{-1}. H-exposure in units of L is attached to each spectrum. Peak positions of SiH_n vibration modes are indicated by dotted lines. (M_s': SiH stretching of adatom site, M_s: SiH stretching of rest-atom site, D_s: SiH_2 stretching, T_s: SiH_3 stretching, T_{sd}: SiH_3 symmetric deformation, D_{sci}: SiH_2 scissors)

VI-G-2 Nearly Ideally H-Terminated Si(100) Surfaces and IR-Line Width Broadening due to Hydrogen Diffusion into the Subsurface

WANG, Zhihong; NODA, Hideyuki; NONOGAKI, Youichi; URISU, Tsuneo

[*Surf. Sci.* submitted]

Infrared reflection absorption spectroscopy using the buried metal layer substrate (BML-IRRAS) is known to be an unique vibration spectroscopy having a high sensitivity and a high resolution in the wide energy range covering the finger print regions on the semiconductor surfaces. In the present work, dependence of the line width with the coupled monohydride symmetric stretching vibration of the H-terminated Si(100) surface on the adsorption temperature and the hydrogen exposure are investigated by BML-IRRAS method. (Figure 1) The line width significantly changes depending on the adsorption temperature and hydrogen exposure. The reason of the line width broadening is discussed, and it is strongly suggested that the hydrogen diffusion into the subsurface of Si has a significant influence on the line width broadening. The evidence of hydrogen (deuterium) diffusion into the subsurface is investigated for the first time by using IRRAS measurement.
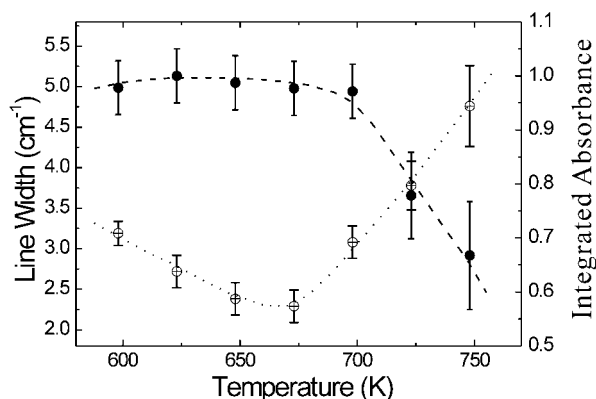
Figure 1. Dependence of line-width (○) and integrated absorbance (●) of the Si–H symmetric stretching peak on the hydrogen atom adsorption temperature.

VI-G-3 Hydrogen Diffusion and Water Reaction on the H-Terminated Si(100) Surface

WANG, Zhihong; NONOGAKI, Youichi; URISU, Tsuneo

[*Jpn. J. Appl. Phys.* submitted (2001)]

Hydrogen terminated Silicon surfaces are interesting not only from the physical studies but also from the application to semiconductor device fabrication. It is known that ideally hydrogen terminated Si(111) surface can be obtained both by wet and dry process and its passivation effects are well investigated. It is also known that the atomically flat hydrogen terminated Si(100) surface is not obtained by wet processes and the chemical reactivity of the hydrogen terminated Si(100) surfaces is also not well understood. The diffusion of hydrogen into silicon bulk is important but not well understood yet due to the difficulties of observation on bulk hydrogen. The reaction with water on H-terminated Si(100) surface is interesting from the viewpoint of understanding the first oxidation step of Si(100) surface. The authors studied these phenomena in detail by measuring the surface vibration spectra of H-terminated Si(100) surfaces using the Infrared reflection absorption spectroscopy using the buried metal layer substrate (BML-IRRAS). It has been observed that the IR line-width changes significantly depending on the hydrogen exposure and adsorption temperature. The line-width broadening was explained by diffusion of hydrogen into Si(100) bulk. The ideally H-terminated Si(100) surfaces were made and the reaction with water was also studied. It has been found that the ideally H-terminated Si(100) surface is easily attacked by water as shown in Figure 1. IR spectrum after 1000L water exposure shows that the original SiH vibration peak decrease (2100 cm^{-1}), SiH$_2$ peaks generate (~900 cm^{-1}) and the surface is oxidized (~1000 cm^{-1} band).
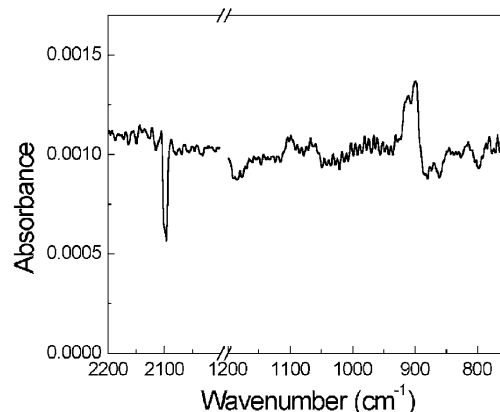
Figure 1. BML-IRRAS spectrum of water reaction with H-terminated Si (100) surface.

VI-H Integration of Bio-Functional Materials on Silicon

Integration of biofunctional materials such as lipids and proteins are expected to find an important applications in biosensors, developments of new medicines, and diagnosis of intractable diseases *etc.* In this project, we are investigating the area selective modification of Si surfaces by depositing the self assembled alkyl monolayers and the characterization by AFM and IRRAS, to integrate biomaterials such as lipids and membrane proteins on Si surfaces with controlled arrangement and orientations.

VI-H-1 Influence of Substrate Roughness on the Formation of Self-Assembled Monolayers (SAM) on Silicon(100)

MORÉ, Sam Dylan; GRAAF, Harald; BAUNE, Michael[1]; WANG, Changshun[1]; NONOGAKI, Youichi; URISU, Tsuneo
(*[1]Bremen Univ.*)

The peak shifts of the CH$_2$-vibration are an indicator of the amount of gauche-conformational disorder. We have investigated the relationship between surface roughness and morphology and the peak position.

With increasing substrate surface roughness both the symmetric CH$_2$-peak as well as the asymmetric CH$_2$-peak shift to higher wave numbers. The magnitude of the shift is about 6 cm^{-1}. The CH$_2$-peak position correlates with the trans/gauche conformational order in the aliphatic chain.

Scanning electron micrographs showed that the samples which yielded the highest signal intensity exhibited a the highest degree of roughness. This could be confirmed with laser light scattering and qualitatively with profilometer scans.

As trans/gauche oder/disorder and surface density are in close correlation, the insulating properties of

SAM-layers will depend on the microscopic order of the substrate at least for medium length C-chains. Controlling these properties would therefore mandate control of the surface roughness.
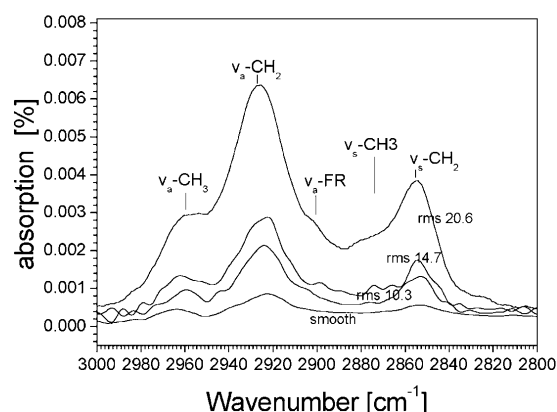
Figure 1. Symmetric (v_s) and asymmetric (v_a) CH_2 and v_a-CH_3 vibrational peaks for the smooth Si(100) and three different roughend Si (100) surfaces (a, b, c), which are covered with a aliphatic self-assembled monolayer. v_a-FR marks a Fermi-resonance and v_a-CH_3 the CH_3 asymmetric peak.
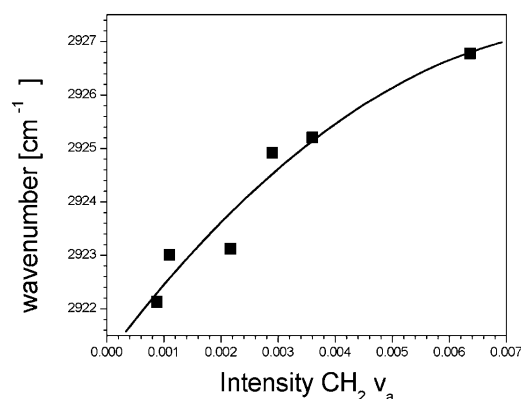
Figure 2. Peak position of the CH_2-asymmetric vibration as a function of peak intensity for an aliphatic SAM (dodecan) on roughened Si(100).

VI-H-2 Characterization of Oligo-Ethylene Glycol Ethers Bound to Self-Assembled Monolayers (SAM) on Silicon with FTIR Spectroscopy and Ellipsometry

MORÉ, Sam Dylan; WANG, Changshun[1]; URISU, Tsuneo

Amphiphilic molecules bound to self assembled monolayers (SAM) can serve as anchor molecules for supported lipid membranes. The resulting anchor entities, bound covalently to the Si-substrate, increase the non-covalently interaction of the lipid with its SAM sublayer, thus enhancing the mechanical stability of the system. Oligo-ethylene glycol molecules, which have been bound to an aliphatic chain are of special interest as the polar chain can further provide hydrophilic pockets to accommodate membrane proteins.

Two different approaches were investigated: Firstly, binding Poly-oxyethylene stearyl ethers to preexisting

functionalized self-assembled monolayers on Si(100) via an ester bond and secondly to graft undecenyl acid Brij-esters via the double bond directly to a H terminated Si(100) surface.

Only Poly-oxyethylene stearyl ethers with oxy-ethylene chainlengths of n ($O–CH_2–CH_2$) = 2 and 10. Longer chainlengths (n = 20, 23, 100) could however be attached via the direct grafting method.

Both methods lead to a significant amount of highly ordered Poly-oxyethylene stearyl domains.

VI-H-3 Deposition of Self-Assembled Alkyl Monolayers on Si and SiO$_2$

WANG, Changshun[1]; MORÉ, Sam Dylan; URISU, Tsuneo
([1]IMS and Henan Univ.)

Preparations of alkyl monolayers on Si and SiO_2 are technologically important for their potential utility. We have deposited octadecyltrichlorosilane (OTS) self-assembled-monolayers (SAM) on silicon substrates with a native oxide (nominally SiO_2) layer. Structural features of the films were characterized using Fourier transform infrared spectroscopy (FTIR) and ellipsometry. The adsorption temperature dependency of FTIR frequencies and intensities of CH_2 stretching vibration bands indicate the existence of a characteristic temperature T_c. The hydrocarbon chains observe an ordered and closely packed state when the monolayers are prepared below T_c, whilst disordered monolayers with low molecular density are formed above T_c. Moreover, dense, well-ordered alkyl SAMs are prepared on the silicon surface by the reactions of neat and dilute 1-alkenes (dodecene, octadecene, *etc.*) with the hydrogen-terminated silicon surface. The hydro-silylation reaction results in the formation of very stable silicon-carbon bonds, which yield dense monolayers as evidenced from infrared spectroscopy and ellipsometry. And the reaction is more efficient at higher temperatures than that at lower temperatures, as shown in Figure 1.
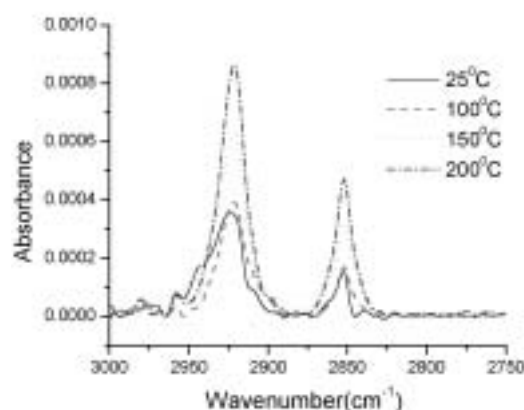
Figure 1. FTIR spectra of SAM obtained from the reaction of pure dodecene with the hydrogen-terminated Si (100) surface at different solution temperatures.

VI-I Photoionization and Photodissociation Dynamics Studied by Electron and Fluorescence Spectroscopy

Molecular photoionization is a major phenomenon in vacuum UV excitation and provides a large amount of information on fundamental electron-core interactions in molecules. Especially, neutral resonance states become of main interest, since they often dominate photoabsorption cross sections and lead to various vibronic states which are inaccessible in direct ionization. We have developed a versatile machine for photoelectron spectroscopy in order to elucidate dynamical aspects of superexcited states such as autoionization, resonance Auger decay, predissociation, vibronic couplings, and internal conversion. Two-dimensional photoelectron spectroscopy, allows us to investigate superexcited states in the valence excitation region of acetylene, nitric oxide, carbonyl sulfide, sulfur dioxide and so on. In this method, the photoelectron yield is measured as a function of both photon energy and electron kinetic energy (binding energy). The spectrum, usually represented as a contour plot, contains rich information on photoionization dynamics.

Photofragmentation into ionic and/or neutral species is also one of the most important phenomena in the vacuum UV excitation. In some cases, the fragments possess sufficient internal energy to de-excite radiatively by emitting UV or visible fluorescence. It is widely accepted that fluorescence spectroscopy is an important tool to determine the fragments and to clarify the mechanisms governing the dissociation processes of diatomic and polyatomic molecules. This year we have carried out fluorescence spectroscopy of OCS in the photon energy region of 15–30 eV.

VI-I-1 Formation and Autoionization of a Dipole-Forbidden Superexcited State of CS_2

HIKOSAKA, Yasumasa[1]; MITSUKE, Koichiro
(*[1]Inst. Mater. Struct. Sci.*)

Two-dimensional photoelectron spectroscopy has been performed in the photon energy region of 14.60–15.35 eV, in order to investigate forbidden super-excited states of CS_2. Figure 1 shows a two-dimensional photoelectron spectrum for the $CS_2^+(\tilde{B}^2\Sigma_u^+)$ band and its vicinities. The electron yield is presented as a function of both photon energy $E_{h\nu}$ and ionization energy I_E by the plots with eight tones from light to dark on a linear scale. The curve in the right panel shows a constant ionic state spectrum, which is obtained by summing electron counts along the I_E axis at each $E_{h\nu}$. Five resonances of the Rydberg states converging to $CS_2^+(\tilde{C}^2\Sigma_g^+)$ are observed at $E_{h\nu}$ = 14.69, 14.88, 14.95, 15.09, and 15.31 eV. The former two states are first assigned in this work. There exists remarkable vibrational excitation of one quantum of the anti-symmetric vibrational mode at $E_{h\nu} \sim$ 14.88 eV. A similar excitation can be seen in the two-dimensional spectrum for the $CS_2^+(\tilde{X}^2\Pi_g)$ band. This vibrational excitation is attributable to autoionization from a dipole-forbidden superexcited state which is formed through vibronic interaction with the $5p\sigma_u$ Rydberg state converging to $CS_2^+(\tilde{C}^2\Sigma_g^+)$. The forbidden superexcited state is assigned as the $v = 1$ vibrational state in the ν_3 mode of the $3d\sigma_g$ Rydberg member converging to $CS_2^+(\tilde{C}^2\Sigma_g^+)$. Preference in the autoionization of the forbidden superexcited state was discussed.
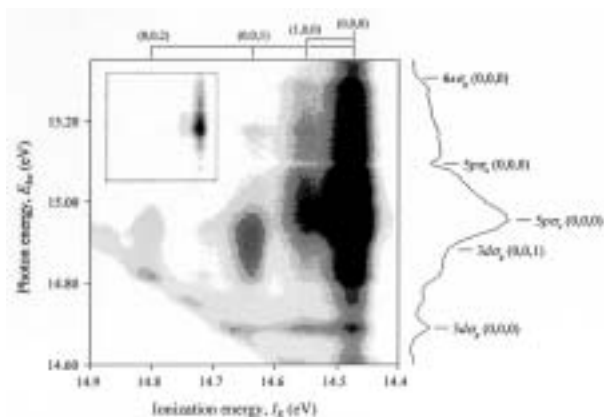
Figure 1. Two-dimensional photoelectron spectrum for the $CS_2^+(\tilde{B}^2\Sigma_u^+)$ band and its vicinities measured in the photon energy range of 14.60–15.35 eV.

VI-I-2 UV and Visible Emission Spectra from Photodissociation of OCS Using Synchrotron Radiation at 15–30 eV

MITSUKE, Koichiro

Photofragmentation of OCS in the excitation photon energy range of 15–30 eV has been studied by dispersed fluorescence spectroscopy using monochromatized undulator radiation supplied from the UVSOR facility. Figure 1 shows dispersed fluorescence spectra of OCS encompassing the wavelength region of 360–530 nm at five photon energies between 19.85 and 29.8 eV. The following emission band systems have been identified: $OCS^+ [A^2\Pi_\Omega(0,0,0) \rightarrow X^2\Pi_\Omega(0,0,v_3'')]$, $CO^+ (A^2\Pi_\Omega \rightarrow X^2\Sigma^+)$, $CS^+ (B^2\Sigma^+ \rightarrow A^2\Pi_\Omega)$, and CO $(d^3\Delta \rightarrow a^3\Pi)$. All the transitions except $OCS^+ [A^2\Pi_\Omega \rightarrow X^2\Pi_\Omega]$ are newly obtained from photodissociation of OCS in the vacuum UV region. The fluorescence excitation spectra for the $OCS^+ [A^2\Pi_\Omega(0,0,0) \rightarrow X^2\Pi_\Omega(0,0,v_3'')]$ and $CS^+ (B^2\Sigma^+ \rightarrow A^2\Pi_\Omega)$ transitions were measured in the photon energy range of 15.1–15.75 and 21.8–26 eV,

respectively. The emission spectra obtained at 20.85 and 22.9 eV exhibit atomic transitions of S [$nd^3D^o \rightarrow 4p^3P^e$ (n = 6–9)] which result from neutral dissociation of superexcited Rydberg states of OCS into S (nd^3D^o) + CO. Possible excited states of the counterpart CO were discussed on the basis of the difference in the n distribution between the two spectra.
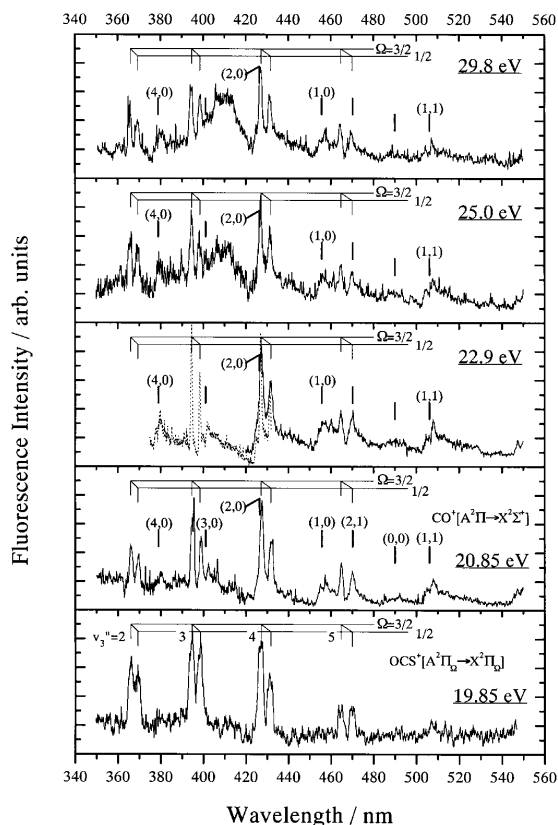
Figure 1. Dispersed fluorescence spectra of OCS encompassing the wavelength region of 360–530 nm at five photon energies between 19.85 and 29.8 eV. The thin vertical lines indicate the vibrational progression in the antisymmetric stretch v_3 mode of the OCS$^+$ [$A^2\Pi_\Omega(0,0,0) \rightarrow X^2\Pi_\Omega(0,0,v_3'')$] transition. The thick vertical lines indicate the band origins of the CO$^+$ ($A^2\Pi_\Omega$, $v' \rightarrow X^2\Sigma^+$, v'') emission-band system.

VI-J Development of a Laser-Synchrotron Radiation Combination Technique to Study Photoionization of Polarized Atoms

In conventional photoionization experiments, the most standard method has generally been taken to be measurement of energy and angular distributions of photoelectrons from randomly oriented (unpolarized) atoms or molecules. However, information obtained from these experiments is insufficient, since the initial state constituted of atoms and photons is not selected and the internal properties of final photoions and electrons are not analyzed. In this project, we have performed photoelectron spectroscopy of polarized atoms using linearly-polarized laser light, aiming at complete quantum-mechanical photoionization experiments. Initial excitation with a linearly polarized synchrotron radiation permits ensemble of atoms to be aligned along the electric vector of the light. From an angular distribution of photoelectrons from polarized atoms, we are able to gain insight into the magnitude and phase shift difference of transition dipole matrix elements of all final channels which are allowed by selection rules.

VI-J-1 Development of a Conical Energy Analyzer for Angle-Resolved Photoelectron Spectroscopy

IWASAKI, Kota[1]; MITSUKE, Koichiro
(*[1]Shimadzu Co.*)

[*Surf. Rev. Lett.* submitted]

A new angle-resolving electron energy analyzer composed of a conical electrostatic prism and position sensitive detector has been developed for gas-phase photoelectron spectroscopy. Performance tests have

been made in the energy and angular resolutions, transmission efficiency, and background level of the analyzer. Helium I photoelectron spectroscopy of Ar atoms was employed for the tests (E_{hv} = 21.22 eV). We fabricated a calibration cone electrode, on which a series of apertures of 0.5–2.0 mm in diameter are located as the test objects, and fitted this electrode in the analyzer to check the focussing efficiency by observing photoelectrons that pass through the apertures.

The 5.3 and 5.5 eV electrons produced by photo-ionization of Ar into $Ar^+(^2P_{3/2,1/2})$ were decelerated or accelerated and were made to pass through the analyzer. The photoelectron spectra were obtained by scanning the potential between the gas cell and inner cone electrode while the transmission energy is kept constant. The two peaks of the $Ar^+(^2P_{3/2,1/2})$ bands manifest symmetric Gaussian profiles, which reveals that the electric field acting upon the photoelectrons from the gas cell was not distorted. We have measured the energy resolution as a function of the transmission energy. The best energy resolution of 60 ± 1 meV (FWHM) has been achieved.

The angular resolution was evaluated from the extent of the image of the entrance apertures on the PSD detector. Figure 1 shows a typical electron image. Three spots correspond to the three entrance apertures of 1.5 and 2 mm in diameter. The angular resolution of 3° (FWHM) was estimated from the spot size for the aperture of 1.5 mm diameter. Taking into account the acceptance angle of 5.4° of the aperture from the sample

volume, we can conclude that the conical electrostatic prism has a convergence effect on the incident electrons in the azimuth direction. The diameter of the entrance aperture is the major determining factor of the angular resolution.
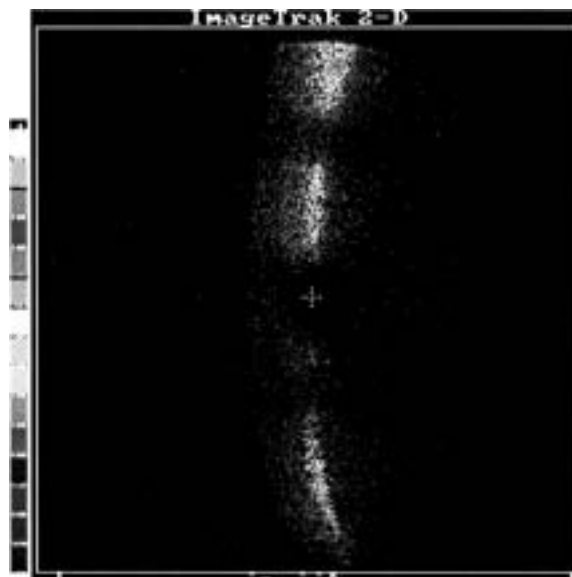
Figure 1. Photoelectron image on PSD. Three spots represent the image of three entrance holes bored on the inner cone electrode. The top spot was cut out by the edge of PSD.

VI-K Vacuum UV Spectroscopy Making Use of a Combination of Synchrotron Radiation and a Mode-Locked or Pulsed UV Laser

An ultraviolet laser system has been developed which synchronizes precisely with the synchrotron radiation (SR) from the storage ring of the UVSOR facility. A mode-locked Ti:sapphire laser is made to oscillate at the frequency of the ring in a multibunch operation mode. The delay timing between SR and laser pulses can be changed from 0 to 11 ns. The following combination studies have been performed: (1) two-photon ionization of helium atoms studied as the prototype of the time-resolved experiment, (2) laser induced fluorescence (LIF) excitation spectroscopy of $N_2^+(X\ ^2\Sigma_g^+)$ ions produced by synchrotron radiation photoionization of N_2 or N_2O, and (3) LIF excitation spectroscopy of $CN(X\ ^2\Sigma^+)$ radicals produced by synchrotron radiation photodissociation of CH_3CN.

VI-K-1 Laser Induced Fluorescence Spectroscopy of CN($X\ ^2\Sigma^+$) Radicals Produced by Vacuum UV Photoexcitation of CH₃CN with Synchrotron Radiation

MITSUKE, Koichiro; MIZUTANI, Masakazu

Synchrotron radiation-pump and laser-probe spectroscopy is employed to observe CN radicals in the vibronically ground state produced from CH_3CN. The photon energy E_{SR} of synchrotron radiation is changed from 13.6 to 18.6 eV. The laser induced fluorescence

signal is measured as a function of E_{SR} with the laser wavelength fixed at the CN($B\ ^2\Sigma^+$, $v_B = 0 \leftarrow X\ ^2\Sigma^+$, $v_X = 0$) transition. The laser and monitored wavelengths were chosen at 388 and 420.8 nm, respectively. Figure 1 shows a plot of the LIF intensity, the difference between the fluorescence signal counts with and without the laser, as a function of E_{SR}. This plot represents the yield curve for the formation of CN($X\ ^2\Sigma^+$, $v_X = 0$). The onset of 15.4 eV of the fluorescence signal indicates that the detected CN($X\ ^2\Sigma^+$) radicals result from dissociative ionization of CH_3CN

$$CH_3CN^+ \rightarrow CN(X\ ^2\Sigma^+) + CH_3^+(X\ ^1A_1'). \qquad (1)$$

The partial cross section for the formation of CN($X\ ^2\Sigma^+$)

is estimated to be 0.1–0.5 Mb and is in a reasonable agreement with that for the CH_3^+ formation.

In contrast to the photoionization efficiency curve of CH_3^+, the LIF signal intensity in Figure 1 rapidly decreases beyond the peak at 15.6 eV and settle down to the background level at > 16 eV. The absence of the LIF signal above 16 eV is ascribed to a large kinetic energy release on the way of the dissociation of CH_3CN^+. The quicker the $CN(X\,^2\Sigma^+)$ fragment escapes from the probe region, the lower its time-averaged number density becomes.
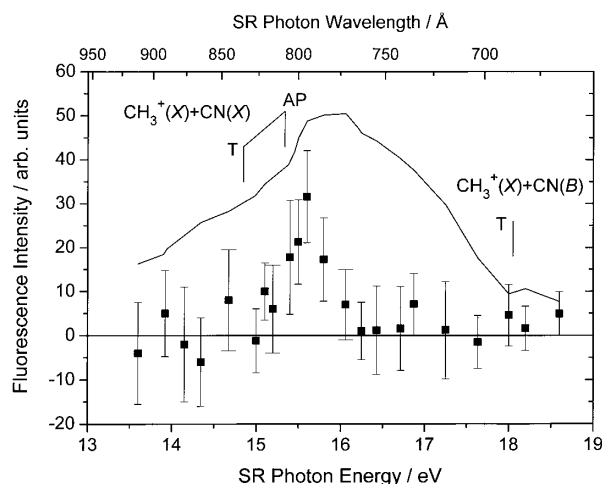
Figure 1. LIF signal intensity (■) of the $CN(X\,^2\Sigma^+, v_X = 0)$ fragment produced from CH_3CN plotted against the SR photon energy. The solid curve represents the fluorescence excitation spectrum of CH_3CN for the $CN(B\text{-}X)$ emission. In both cases, the $(X\,^2\Sigma^+, v_X = 1) \leftarrow (B\,^2\Sigma^+, v_B = 0)$ transition was monitored.

VI-L Monochromator Newly Developed on the Beam Line BL2B2 in UVSOR

A grazing incidence monochromator has been constructed which supplies photons in the energy region from 20 to 200 eV. This monochromator will bridge the energy gap between the beam lines BL3A2 and BL8B1, thus providing for an accelerating demand for the high-resolution and high-flux photon beam from the research fields of photoexcitation of inner-valence electrons, *L*-shell electrons in the third-row atom, and *4d* electron of the lanthanides.

VI-L-1 Performance of the 18 m-Spherical Grating Monochromator Newly Developed in the UVSOR Facility

ONO, Masaki; YOSHIDA, Hiroaki[1]; HATTORI, Hideo[2]; MITSUKE, Koichiro
(*[1]Hiroshima Univ.; [2]Nitto Tech. Inf. Cent. Co.*)

An 18 m-spherical grating monochromator with high resolution and high photon flux has been constructed at the bending magnet beamline BL2B2 of the UVSOR facility in the Institute for Molecular Science. The monochromator covers the energy range of 20–200 eV with three gratings. The resolving power ($E/\Delta E$) has been estimated by ion yield spectra of rare gas atoms (He, Ar and Kr) to be 2000–8000 under the conditions of a photon flux of 1×10^{10} photons s^{-1} and a ring current of 100 mA. A second-order light of 7% is contained at a photon energy of 45.6 eV.

VI-L-2 Anisotropy of Fragment Ions from SF₆ with Valence- and Sulfur *L*-Electron Excitation

ONO, Masaki; MIZUTANI, Masakazu; MITSUKE, Koichiro

Sulfurhexafluoride (SF_6) is one of the most well-known molecules that dissociate to multiple species of fragment ions after photoionization. In this research the asymmetry parameter β of the fragment ion has been measured in the energy region from the outer-valence to sulfur $2p$ electron excitation (23–200 eV).

The apparatus for the measurements of the anisotropy of fragment ions has been constructed at the end station of the beam line BL2B2 of UVSOR. The apparatus consists of two sets of an ion detector and three grids. The two ion detectors were mounted in the parallel and perpendiclar direction to the electric vector of synchrotron radiation. The difference in the sensitivity between the two ion detectors are corrected by measureing the ion yield spectra of helium and argon atoms.

Figure 1 shows the fragment ion yield from SF_6 and β parameter. The spectrum covers a wide energy range from the outer-valence electron to sulfur $2p$ electron excitation. The three peaks at > 170 eV are assigned to the resonance excitations from $2t_{1u}$ (sulfur $2p$) to unoccupied valence orbitals ($6a_{1g}$, $2t_{2g}$ and $4e_g$). Several

features around 20–60 eV are found to resemble those in the absorption spectrum. The β parameter decreases with increasing photon energy. This trend can be explained qualitatively by the assumption that SF_5^+ ions has a much more anisotropic distribution than other fragments from SF_6.
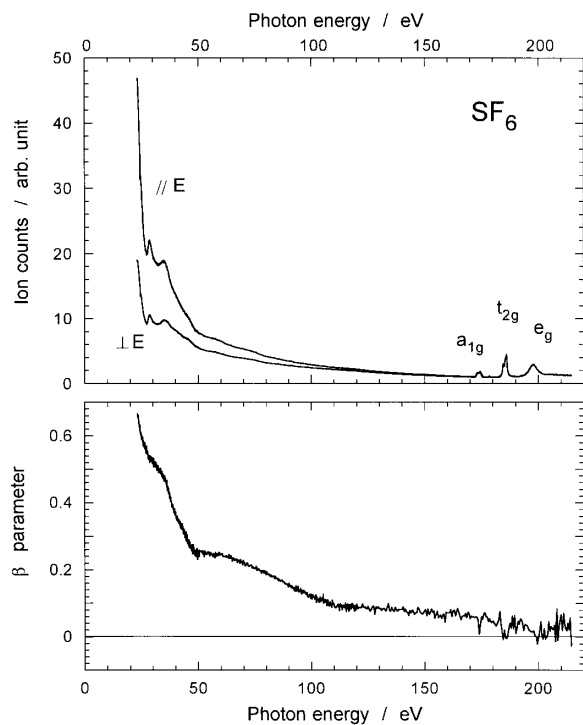
Figure 1. The fragment ion yield spectrum from SF_6 and asymmetry parameter β.

VI-M Thin Film Preparation with Chemical Vapor Deposition Using Vacuum Ultraviolet Radiation

Thin-film deposition at temperatures as low as possible is one of the key technologies for next generation of ultra-large scale integrated circuit (ULSI) fabrication. Photon-assisted chemical vapor deposition is a promising way to prepare particularly dielectric thin films. Silicon dioxide and germanium dioxide films have been prepared from tetraethoxysilane (Si–(OC$_2$H$_5$)$_4$) and tetraethoxygermanate (Ge–(OC$_2$H$_5$)$_4$) with chemical vapor deposition using vacuum ultraviolet radiation.

VI-M-1 Design and Construction of UVSOR-BL4A2 Beam Line for Nano-Structure Processing

TAKEZOE, Noritaka; YANAGIDA, Hideaki[1]; KUROSAWA, Kou; URISU, Tsuneo; NODA, Hideyuki; MEKARU, Harutaka[2]
(*[1]IMS and Univ. Miyazaki; [2]Himeji Inst. Tech.*)

Nano structures must open new windows not only for surface physics and chemistry but also for electronic and photonic devices. Synchrotron radiation stimulated surface chemical reactions have been a most promising way to fabricate nano structures, because they offer a process with the advantages of high-site selectivity by core electron excitation and also free-of damage with atomic scale. Since a new beam line with higher flux is required for the processing, we have been designing and constructing UVSOR-BL4A2 beam line for the nano structure fabrication.

VI-M-2 Characterization of SiO$_2$ Dielectric Films in Photo-Chemical Vapor Deposition Using Vacuum Ultraviolet Excimer Lamp

TOHIKAWA, Kiyohiko[1]; MIYANO, Junichi[1,2]; MOTOYAMA, Yoshikazu[1,2]; YAGI, Yusuke[1]; YANAGIDA, Hideaki[3]; KUROSAWA, Kou; YOKOTANI, Atsushi[2]; SASAKI, Wataru[2]
(*[1]Miyazaki Oki Electric Co. Ltd.; [2]Univ. Miyazaki; [3]IMS and Univ. Miyazaki*)

Photo-chemical vapor deposition using vacuum ultraviolet excimer lamp is a novel technology that deposit SiO$_2$ film at room temperature without the use of high temperature or plasma. The films contain organic impurities coming from tetraethoxysilane (TEOS) used as the precursor. The addition of O$_2$ molecules to TEOS is found to decrease C–H impurities. We show atomic concentrations in SiO$_2$ films deposited from TEOS or from TEOS with O$_2$ or N$_2$O gas.

VI-M-3 Electrical Properties of SiO$_2$ films Prepared by VUV Chemical Vapor Deposition

MOTOYAMA, Yoshikazu[1,2]; MIYANO, Junichi[1,2]; TOSHIKAWA, Kiyohiko[2]; YAGI, Yusuke[2]; KUROSAWA, Kou; YOKOTANI, Atsushi[1]; SASAKI, Wataru[1]
(*[1]Univ. Miyazaki; [2]Miyazaki Oki Electric Co. Ltd.*)

We have developed a new scheme for SiO$_2$-film preparation in which tetraethoxyorthosilicate (TEOS: Si(OC$_2$H$_5$)$_4$) is photo-dissociated by vacuum ultraviolet Xe$_2$ excimer radiation (λ = 172 nm) at room temperature. The SiO$_2$-films are included impurities of C and H atoms and/or molecules. A adding foreign gases included O atom and molecule to TEOS are effective in removal of C atom and/or molecule in SiO$_2$-film, which bring about excellent gap-filling property, but it is newly included OH impurity. We had knowledge that the electrical properties of SiO$_2$-films is correlated the amount of OH impurity by FT-IR spectra, C–V and I–V curves. Increase of OH impurity is degraded electrical properties. An only TEOS have not OH impurity, which may be using as the low-k films of next future device processes.

VI-M-4 SiO$_2$ Film Deposition on Different Substrate Materials by Photo-CVD Using Vacuum Ultraviolet Radiation

MIYANO, Junichi[1,2]; MOTOYAMA, Yoshikazu[1,2]; TOSHIKAWA, Kiyohiko[2]; YAGI, Yusuke[2]; YANAGIDA, Hideaki[3]; KUROSAWA, Kou; YOKOTANI, Atsushi[1]; SASAKI, Wataru[1]
(*[1]Univ. Miyazaki; [2]Miyazaki Oki Electric Co. Ltd.; [3]IMS and Univ. Miyazaki*)

We have prepared SiO$_2$ thin films from tetraethoxyorthosilicate (TEOS) at room temperature by photo-chemical vapor deposition using a vacuum ultraviolet (VUV) excimer lamp. We showed the affection by adding foreign gases to the raw precursor and by changing substrate materials for the growth rate and thickness uniformity and the reaction mechanism by step coverage in VUV-CVD. The SiO$_2$ film deposition behaviors by VUV-CVD depend significantly on the presence of ozone and activated oxygen by VUV photons. Then the dependence of substrate materials for the growth rate and thickness uniformity is most remarkable in case of adding O$_2$.

VI-M-5 Silica Film Preparation by Chemical Vapor Deposition Using Vacuum Ultraviolet Excimer Lamps

KUROSAWA, Kou; TAKEZOE, Noritaka; YANAGIDA, Hideaki; MIYANO, Junichi[2,3]; MOTOYAMA, Yoshikazu[2,3]; KAWASAKI, Yasuhiro[1]; YOKOTANI, Atsushi[2]
(*[1]IMS and Univ. Miyazaki; [2]Univ. Miyazaki; [3]Miyazaki Oki Electric*)

We have prepared SiO_2 thin films on silicon wafers from tetraethoxyorthosilicate (TEOS; $Si(OC_2H_5)_4$) by photo-chemical vapor deposition (photo-CVD) with the use of various excimer lamps which emit incoherent light at 308 (XeCl), 222 (KrCl), 172 (Xe_2), 146 (Kr_2) and 126 nm (Ar_2). The film deposition is observed at wavelengths shorter than 172 nm. With 10-mW/cm^2 172-nm radiation, the growth rate is 8 nm/min on the room temperature substrate. The deposition efficiency depends on the wavelength and shows the maximum value for 146-nm radiation. Addition of O_2 to TEOS induces inhibition of C and H impurity inclusion in the films.

VI-M-6 GeO$_2$ and SiO$_2$ Thin Film Preparation with CVD Using Ultraviolet Excimer Lamps

KUROSAWA, Kou; MAEZONO, Yoshinari[1]; MIYANO, Junichi[1,2]; MOTOYAMA, Yoshikazu[1,2]; YOKOTANI, Atsushi[1]
(*[1]Univ. Miyazaki; [2]Miyazaki Oki Electric*)

We have prepared SiO_2 and GeO_2 thin films from tetraethoxyorthosilicate (TEOS; $Si(OC_2H_5)_4$) and tetra-ethoxyorthogermanate (TEOG: $Ge(OC_2H_5)_4$), respectively, by chemical vapor deposition (CVD) assisted by high-energy photons. The photons are supplied from excimer lamps which emit incoherent light at 308 (XeCl), 222 (KrCl), 172 (Xe_2), 146 (Kr_2) and 126 nm (Ar_2). GeO_2 film deposition is observed for all excimer lamps used here, but SiO_2 films are obtained at wavelengths shorter than 172 nm. This is caused by a fact that the bonding energy between Si and O is much higher than that between Ge and O. The deposition rate is around 8nm/min for SiO_2 and 16nm/min for GeO_2 films. The film deposition rate increases with increasing the light intensity and with decreasing substrate temperature.

VI-M-7 Room Temperature Deposition of GeO$_2$ Thin Films Using Dielectric Barrier Discharge Driven Excimer Lamps

MAEZONO, Yoshinari[1]; YANAGIDA, Hideaki[2]; NISHI, Kota[1]; MIYANO, Junichi[1,3]; YOKOTANI, Atsushi[1]; KUROSAWA, Kou; HISHINUMA, Nobuteru[4]; MATSUNO, Hiromitsu[4]
(*[1]Univ. Miyazaki; [2]IMS and Univ. Miyazaki; [3]Miyazaki Oki Electric; [4]USHIO Inc.*)

We discuss the fabrication of GeO_2 and GeO_2/SiO_2 films at room temperature by photo-chemical vapor deposition. Excimer lamps were used for the light source, and tetraethothoxyorthosilicate (TEOS) and tetraethoxyorthogermanate (TEOG), as raw materials. We fabricated GeO_2/SiO_2 composite films from a mixed vapor of TEOS and TEOG. The refractive indices of the obtained films showed intermediate values between those of SiO_2 ($n = 1.46$) and GeO_2 ($n = 1.60$). The relationship between Ge concentratipon in the films and the refractive indices was examined. We successfully obtained a GeO_2/SiO_2 composite material of higher refractive index than that of similar composites produced by conventional methods.

VI-N Atoms and Molecules at Water-Zeolite Interfaces: Structure Determination based on AFM Observations

One of the striking capabilities of atomic force microscopy (AFM) is the direct observation of atoms and adsorbed molecules on a surface heretofore impossible, such as nonconductive materials like zeolite, under environments heretofore impossible, including underwater. The unprecedented resolution of AFM imaging enabled us to determine, for the first time, the positions of framework oxygen and extra-framework cation on a (010) surface of heulandite, a zeolite naturally occurring, and the array and the orientation structures of adsorbed molecules on its surface. Based on the *in situ* AFM observations, molecular simulations were performed to supplement the knowledge of aqueous phase adsorption processes.

VI-N-1 High-Resolution Imaging of Organic Monolayers Using Noncontact AFM

UCHIHASHI, Takayuki[1]; ISHIDA, Takao[1]; KOMIYAMA, Masaharu; ASHINO, Makoto[1]; SUGAWARA, Yasuhiro[1,2]; MIZUTANI, Wataru[1]; YOKOYAMA, Kousuke[2]; MORITA, Seizo[2]; TOKUMOTO, Hiroshi[1]; ISHIKAWA, Mitsuru[1]
(*[1]Joint Res. Cent. Atom Tech.; [2]Osaka Univ.*)

[*Appl. Surf. Sci.* **157**, 244 (2000)]

Noncontact atomic force microscopy (AFM) provides useful technique for imaging organic molecules in high resolution. Here we present our recent advances in the noncontact AFM imaging of organic materials. (I) Molecular packing structures, defects and domain boundaries were clearly observed on adenine and thymine films. The noncontact AFM images revealed detailed features of the individual nucleic acid base molecules, thus allowing us to distinguish between adenine and thymine. (II) Both ($\sqrt{3}\times\sqrt{3}$)R30° structures and c(4×2) superlattice structures were resolved on alkanethiolate self-assembled monolayer (SAM) [CH_3-$(CH_2)_8SH$] (nonanethiol) on Au(111). We found that the c(4×2) superlattice structures changed into ($\sqrt{3}\times\sqrt{3}$)R30° structures when the tip-surface distance decreased.

VI-N-2 Study of Catalyst Preparation Processes by Atomic Force Microscopy (AFM): Adsorption of a Pt Complex on a Zeolite Surface

KOMIYAMA, Masaharu; GU, Ning[1]
(*[1]Southeast Univ.*)

[*Stud. Surf. Sci. Catal.* **130**, 3173 (2000)]

Adsorption of a Pt complex commonly used for catalyst preparation onto a (010) surface of a natural zeolite heulandite was examined by *in situ* atomic force microscopy (AFM). The Pt complex appears to adsorb on the heulandite(010) surface at a three-times periodicity along the *c* axis, whereas along the *a* axis no specific periodicity was observed. Possible adsorption sites were also discussed.

VI-N-3 Recent Applications of Atomic Force Microscopy to the Study of Pyridine-Base Molecules Adsorbed on the (010) Surfaces of Heulandite and Stilbite Crystals

KOMIYAMA, Masaharu; SHIMAGUCHI, Takemi[1]
(*[1]Yamanashi Univ.*)

[“*Natural Zeolites for the Third Millennium*,” C. Colella and F. A. Mumpton, Eds., De Frede Editore; Naples p. 315 (2000)]

Liquid-phase adsorption characteristics of pyridine-base molecules, pyridine and β-picoline, on (010) surfaces of two natural zeolites, heulandite and stilbite, were examined by atomic force microscopy (AFM). These adsorption systems formed well-ordered, two-dimensional (quasi-)hexagonal adsorbed layers, with their unit-cell dimensions ranging from 0.48 nm to 0.59 nm depending on the adsorbate-substrate combinations. Although there were near registries of the adsorbed phases with respect to the substrate (010) lattices, the molecular arrays were essentially incommensurate with the substrate atomic arrangements. Orientations of the molecules within the adsorbed layers were determined from the AFM images, which were compared favorably with semiempirical molecular orbital calculations.

VI-N-4 Atomic Force Microscopy Observations of Zeolite(010) Surface Atoms and Adsorbed Molecules

KOMIYAMA, Masaharu

[*Hyomen Kagaku (J. Surf. Sci. Soc. Jpn.)* **21**, 576 (2000)]

Atomic force microscopy (AFM) is capable of directly observating surface atoms and adsorbed molecules on nonconductive materials such as zeolite, under various environments including vacuum, ambient and underwater. We have been successful in observing in situ atomic images of heulandite and stilbite (010) surfaces under aqueous environments, and molecular images of liquid-phase-adsorbed organics on these surfaces. The unprecedented resolution of the AFM imaging enabled us to determine, for the first time, the positions of framework oxygen and extra-framework cation, and the array and orientation structures of adsorbed molecules such as pyridine bases.

VI-O Soft X-Ray, Ultraviolet, Visible and Infrared Spectroscopy of Solids and Devices

Work of soft x-ray(SX), ultraviolet (UV), visible (VIS) and Infrared (IR) spectroscopy of solids have been proceeded. These are mainly performed using synchrotron radiation (beamlines BL7B, BL8B1, BL4B, BL7A and BL1A at UVSOR), owing to the wide wavelength continuity of synchrotron radiation with no structure.

VI-O-1 Reflection Spectra of $Al_{1-x}Ga_xN$

FUKUI, Kazutoshi; MIURA, Hiroshi[1]; OKADA, Akira[2]; GUO, Qixin[2]; TANAKA, Satoru[3]; HIRAYAMA, Hideki[4]; AOYAGI, Yoshinobu[4]
(*[1]Fukui Univ.; [2]Saga Univ.; [3]Hokkaido Univ.; [4]RIKEN*)

Visible, ultraviolet and vacuum ultraviolet reflection spectra of wurtzite $Al_{1-x}Ga_xN$ have been measured from 20 K to 300 K, and Kramers-Kronig analysis using of our results also presented. No drastic change in spectra between GaN and $Al_{0.14}Ga_{0.86}N$. The band gap as the function of temperature has been also presented in whole x range from 20 K to 300 K. They are well described by the Bose-Einstein expression. It suggests that the temperature shift of the band gap is mainly due to the electron-phonon interactions. The parameters of the Bose-Einstein expression are obtained by fitting.

VI-O-2 Characterization of GaN-Based Schottky Barrier Ultraviolet (UV) Detectors in the UV and Vacuum Ultraviolet (VUV) Region Using Synchrotron Radiation

MOTOGAITO, Atsushi[1]; YAMAGUCHI, Motoo[1]; HIRAMATSU, Kazumasa[1]; KOTOH, Masahiro[2]; OHUCHI, Youichiro[2]; TADATOMO, Kazuyuki[2]; HAMAMURA, Yutaka[3]; FUKUI, Kazutoshi
(*[1]Mie Univ.; [2]Mitsubishi Cable Ind. Ltd.; [3]Nikon Co. Ltd.*)

[*Jpn. J. Appl. Phys., Part 2* **40**, L368 (2001)]

Characterization of GaN-based Schottky barrier ultraviolet (UV) detectors with a comb-shaped electrode using synchrotron radiation ($h\nu = 2.2$–30 eV, $\lambda = 41$–563 nm) is described. Below $h\nu = 8.0$ eV ($\lambda > 155$ nm), the detectors are available without any photo-emission of GaN and Au electrode. Under application of reverse bias, the responsivity is increased to 0.05 A/W at ~0.4 V. The photocurrent is controlled by reverse bias. On the other hand, above $h\nu = 8.0$ eV ($\lambda < 155$ nm), the responsivity spectra are dominated by photo-emissions of Au and GaN. These results show that these Schottky type detectors with mesa structures are effective to detect vacuum ultraviolet (VUV)-UV light ($155 < \lambda < 360$ nm).

VI-O-3 Near K-Edge Absorption Spectra of the III-V Nitride

FUKUI, Kazutoshi; HIRAI, Ryousuke[1]; YAMAMOTO, Akio[1]; HIRAYAMA, Hideki[2]; AOYAGI, Yoshinobu[2]; YAMAGUCHI, Sigeo[3]; AMANO, Hiroshi[3]; AKASAKI, Isamu[3]; TANAKA, Satoru[4]

(*[1]Fukui Univ.; [2]RIKEN; [3]Meijo Univ.; [4]Hokkaido Univ.*)

[*Phys. Status Solidi B* in press]

The nitrogen and aluminum near K-edge absorption measurements of the wurtzite AlN, GaN and InN, and their ternary compounds (AlGaN, InGaN and InAlN) at various molar fractions have been performed using synchrotron radiation. Using the linear polarization of synchrotron radiation, absorption measurements with different incident light angle also performed. The spectral distribution of the nitrogen K absorption spectra clearly depends on both the incidence light angle and the molar fractions of the samples. That of the aluminum K absorption spectra also show the clear angle dependence, but it does not show the drastic molar dependence. The spectral shape comparisons among the various molar fractions, different incident angles and between two ion sites are discussed. The numerical component analysis of the K absorption spectra is also presented.

VI-P Optical Techniques for Synchrotron Radiation

The performance check of beamline BL7B at UVSOR and the development of a surface profiler for optical elements used in synchrotron radiation beamline have been proceeded

VI-P-1 Performance of IR-VUV Normal Incidence Monochromator Beamline at UVSOR

FUKUI, Kazutoshi; MIURA, Hiroshi[1]; NAKAGAWA, Hideyuki[1]; SHIMOMURA, Iwao[2]; NAKAGAWA, Kazumichi[3]; OKAMURA,

**Hidekazu[3]; NANBA, Tadao[3]; HASUMOTO,
Masami; KINOSHITA, Toyohiko[4]**
(*[1]Fukui Univ.; [2]JAERI; [3]Kobe Univ.; [4]Univ. Tokyo*)

The beamline BL7B at the UVSOR facility for solid-state spectroscopy has been opening for users after reconstruction. This beamline consists of a 3 m normal incidence monochromator and covers the spectral range from the vacuum ultraviolet to the infrared region. The optical configuration and the performance, such as photon number, purity and resolving power, are reported.

VI-P-2 Development of A Surface Profiler for Optical Elements

**KINOSHITA, Toyohiko[1]; FUKUI, Kazutoshi;
ASAKA, Shuji; YOSHIDA, Hisashi; WATANABE,
Michio; HORIGOME, Toshio[2]; MA, Peijun[3];
OHTSUKA, Ken[3]; IWANAGA, Masanao[3];
OHSHIMA, Eiichi[4]**
(*[1]Univ. Tokyo; [2]JAIST; [3]Canotec Co.,Inc.; [4]Canon Inc.*)

A surface profiler for optical elements used in synchrotron radiation beamlines has been developed. By measuring the precise positions of an incident and reflected laser beam, the surface profile of mirrors and gratings can be obtained. The profile of large mirrors up to 700 mm long and that of any other shape device such as plane and non-spherical mirrors can be also measured. The design concept and preliminary examples of profile measurements are reported.

VI-Q Dynamics and Relaxation of Atoms and Molecules Following Core-Level Excitation

Monochromatized X-ray from synchrotron radiation excites a core electron of an atom or molecule, and the core hole thereby created is usually filled by an outer-orbital electron through an Auger process. In molecules, the core electrons are localized near the atom of origin, in contrast to valence electrons, which are often delocalized over the entire molecule. Although core electrons do not participate in chemical bonding, the energy of an atomic core-level in the molecule depends on the chemical environment of the atom. Site-specific excitation and fragmentation are thus of considerable interest. To elucidate the dynamics and relaxation of atoms and molecules following core-level excitation, we have used photoelectron spectroscopy and the energy-selected-photoemission photoion coincidence method.

VI-Q-1 Site-Specific Fragmentation Following C:1s Core-Level Photoionization of 1,1,1-Trifluoroethane Condensed on a Au Surface and of a 2,2,2-Trifluoroethanol Monolayer Chemisorbed on a Si(100) Surface

NAGAOKA, Shin-ichi; TANAKA, Shin-ichiro[1]; MASE, Kazuhiko[2]
(*[1]Nagoya Univ.; [2]KEK-PF*)

We used photoelectron spectroscopy, the energy-selected-photoelectron photoion coincidence (ESPEPICO) method, the Auger-electron photoion coincidence (AEPICO) method and the ab initio method to study site-specific phenomena in the C:1s photo-ionization of 1,1,1-trifluoroethane (CF_3CH_3, TFEt) condensed on a Au surface. Site-specific excitation and occurrence of different chemical shifts at two carbon sites were evident in the total electron-yield spectrum and the photoelectron spectrum, and site-specific fragmentation was evident in the ESPEPICO spectrum. The fragmentation processes inferred from the ESPEPICO and AEPICO results were very different from those occurring in the vapor phase. We also studied the effect of the surface on the site-specific phenomena observed in a 2,2,2-trifluoroethanol (TFEtOH) monolayer chemisorbed on a Si(100) surface (CF_3CH_2OSi{substrate}). The molecular structure of TFEtOH is the same as that of TFEt except that it has a hydroxyl group substituted for one of the hydrogen atoms. Although site-specific phenomena were also observed in TFEtOH, the fragmentation process was very different from that of TFEt because of the chemisorption structure of TFEtOH on Si(100).

VI-Q-2 Si:2p Site-Specific Excitation and Fragmentation of Bridged Trihalosilyltrimethyl-silyl Molecules: Role of the Bridge and Final-State Effect

NAGAOKA, Shin-ichi; FUJIBUCHI, Tonan[1]; OHSHITA, Joji[2]; NAGASHIMA, Umpei[3]; KOYANO, Inosuke[4]
(*[1]Ehime Univ.; [2]Hiroshima Univ.; [3]AIST; [4]Himeji Inst. Tech.*)

To elucidate site-specific phenomena, we experimentally and computationally studied the spectroscopy and dynamics caused by Si:2p core-level photoexcitation of bridged trihalosilyl-trimethylsilyl molecules. We used the photoionization efficiency curve and the photoelectron photoion coincidence method to study the site-specific phenomena in the Si:2p photoexcitation of $F_3SiCH_2CH_2CH_2Si(CH_3)_3$, $F_3SiCH=CHSi(CH_3)_3$ and $Cl_3SiC{\equiv}CSi(CH_3)_3$ in the vapor phase. The site-specific excitation was revealed in the photo-ionization efficiency curves of all the molecules. The site-specific fragmentation is likely to be more evident when the distance between the two Si sites is large. For the site-specific fragmentation to occur, there should not be a triple bond between the atomic site of interest and any other near atomic-site around which bond dissociation is undesirable. Not only initial-state effect but also final-state effect is likely to contribute to the occurrence of the different chemical shifts between the two Si sites of the bridged trihalosilyl-trimethylsilyl molecules.

VI-Q-3 Site-Specific Fragmentation Caused by Core-Level Photoionization: Effect of Chemisorption

NAGAOKA, Shin-ichi; MASE, Kazuhiko[1]; NAKAMURA, Arinobu[2]; NAGAO, Masashi[3]; YOSHINOBU, Jun[3]; TANAKA, Shin-ichiro[4]
(*[1]KEK-PF; [2]Ehime Univ.; [3]ISSP; [4]Nagoya Univ.*)

We used the energy-selected-photoelectron photoion coincidence (ESPEPICO) method to clarify site-specific fragmentation caused by C:1s photoionization of 1,1,1-trifluoro-2-propanol-d_1 ($CF_3CD(OH)CH_3$, TFIP-d_1) on a Si(100) surface. The formation of the monolayer was verified by the layer-resolved shifts in the photoelectron and Auger spectra. By using high-resolution electron energy loss spectroscopy, it was shown that TFIP-d_1 is dissociatively chemisorbed like $(CF_3)(CH_3)CDO$-Si(100). Occurrence of different chemical shifts at the three carbon sites was observed by photoelectron spectroscopy. Site-specific fragmentation was clearly revealed in the ESPEPICO spectra of the monolayer at room temperature. From the results of the site-specific fragmentation, it is considered that TFIP-d_1 in the monolayer at room temperature has an O–Si bond oriented in the trans position with respect to the C–CF_3 bond. The fragmentation processes were discussed on the basis of the results of the ESPEPICO method and

the Auger-electron photoion coincidence method.

VI-Q-4 Development of Electron-Ion Coincidence Spectroscopy for Study of Vapor-Phase Dynamics

MASE, Kazuhiko[1]; NAGAOKA, Shin-ichi
(*[1]KEK-PF*)

An electron-ion coincidence spectrometer for vapor-phase dynamics study has been built. The equipment consists of an electron gun, a cylindrical mirror analyzer (CMA) and a reflectron-type time-of-flight ion mass analyzer. Sample gas is excited with the electron beam and the CMA analyzes energy of emitted or scattered electrons. Mass spectra of produced ions are measured with a multichannel scalar taking the energy-analyzed electron signal as the starting trigger.

VI-Q-5 Electron-Ion Coincidence Spectroscopy as a New Tool for Surface Analysis—an Application to the Ice Surface

TANAKA, Shin-ichiro[1]; MASE, Kazuhiko[2]; NAGASONO, Mitsuru; NAGAOKA, Shin-ichi; KAMADA, Masao; IKENAGA, Eiji[3]; SEKITANI, Tetsuji[3]; TANAKA, Ken-ichiro[3]
(*[1]Nagoya Univ.; [2]KEK-PF; [3]Hiroshima Univ.*)

Electron-ion coincidence (EICO) spectroscopy [K. Mase, M. Nagasono, S. Tanaka, M. Kamada, T. Urisu and Y. Murata, *Rev. Sci. Instrum.* **68**, 1703 (1997)] has recently been developed to investigate the process of ion desorption induced by the core level excitation. In the present study, we apply EICO spectroscopy to determine the O1s level of condensed H_2O (ice) at 100 K. The kinetic energy of O1s photoelectrons which gives the highest coincidence yield of H^+ desorption is shifted by about –0.7 eV compared to the O1s peak observed in the conventional core-level photoelectron spectroscopy. It is ascribed to a core-level shift in the O1s level from which hydrogen ions desorb. The results indicate the advantages and the possibilities of the EICO spectroscopy for surface analysis.

VI-Q-6 Photo-Stimulated Ion Desorption from TiO_2(110) Surface

TANAKA, Shin-ichiro[1]; MASE, Kazuhiko[2]; NAGAOKA, Shin-ichi; KAMADA, Masao
(*[1]Nagoya Univ.; [2]KEK-PF*)

Photo-stimulated desorption of O^+ from TiO_2(110) surface is investigated by using the electron-photoion coincidence spectroscopy. It is found that O^+ desorbs as a result of the multi-electron excitation/decay of the O1s electron, which can be explained within the expansion of the well-known Knotek-Feibelman mechanism. On the other hand, the Knotek-Feibelman mechanism does not seem to work for the O^+ desorption following the Ti-core excitation. We propose a new model in which the O^+ desorption is induced by the excitation of a Ti-

core level: the charge transfer from O2p to Ti3d induced by the Ti3p-core hole potential is responsible for the creation of O^+ ions and its desorption. A discussion on the new model is made for ion desorption from other materials.

VI-Q-7 Ion Desorption Induced by Core-Level Excitation on H_2O/Si(100) Surface

TANAKA, Shin-ichiro[1]; MASE, Kazuhiko[2]; NAGAOKA, Shin-ichi; KAMADA, Masao
(*[1]Nagoya Univ.; [2]KEK-PF*)

Ion desorption from H_2O/Si(100) induced by the O1s-excitation is investigated by the use of the photoelectron, the photon-stimulated desorption and the electron-ion coincidence spectroscopy. It is shown that ion desorption induced by the soft-X-ray is mainly caused by shake-up/off excitation accompanied with the core-excitation and with the Auger decay that results in the multi-holes final state. The core-excitation to the anti-bonding orbital or normal Auger decay that creates the two-holes final state is less important.

VI-Q-8 Resonant Auger Spectrum Following Kr:2p → 5s Photoexcitation

NAGAOKA, Shin-ichi; IBUKI, Toshio[1]; SAITO, Norio[2]; SHIMIZU, Yuichiro; SENBA, Yasunori[3]; KAMIMORI, Katsura[3]; TAMENORI, Yusuke[4]; OHASHI, Haruhiko[4]; SUZUKI, Isao H.[2]
(*[1]Kyoto Univ. Edu.; [2]Electrotechnical Lab.; [3]Hiroshima Univ.; [4]JASRI*)

Resonant Auger electron spectra following Kr:2p → 5s photoexcitation have been measured for the first time using monochromatized undulator radiation and a cylindrical-mirror electron-energy analyzer. It is found that the kinetic energy of the resonant Auger electron is higher than that of the corresponding normal Auger electron. The angular distribution of the resonant Auger electrons is nearly isotropic relative to the polarization direction of the incident light.

VI-Q-9 Molecular Deformation in the O $1s^{-1}2\pi_u$ Excited States of CO_2 Probed by the Triple-Differential Measurement of Fragment Ions

SAITO, Norio[1]; UEDA, Kiyoshi[2]; SIMON, Marc[3]; OKADA, Kazumasa[4]; SHIMIZU, Yuichiro; CHIBA, Hisashi[2]; SENBA, Yasunori[4]; OKUMURA, Hiroki[5]; OHASHI, Haruhiko[6]; TAMENORI, Yusuke[6]; NAGAOKA, Shin-ichi; HIRAYA, Atsunari[4]; YOSHIDA, Hiroaki[4]; ISHIGURO, Eiji[7]; IBUKI, Toshio[8]; SUZUKI, Isao H.[1]; KOYANO, Inosuke[5]
(*[1]Electrotechnical Lab.; [2]Tohoku Univ.; [3]LURE; [4]Hiroshima Univ.; [5]Himeji Inst. Tech.; [6]JASRI; [7]Univ. Ryukyus; [8]Kyoto Univ. Educ.*)

Measurement of mass-, energy- and angle-resolved

fragment ions revealed that the β value for C^+ with kinetic energy ≥ 3 eV is ~0.9 in the region of the O 1s → $2\pi_u$ excitation and that β value for O^+ with kinetic energy ≥ 4 eV varies from –0.23 to –0.57 across the O 1s → $2\pi_u$ resonance. These findings postulate that the CO_2 molecule excited to the lower branch of the vibronically split O $1s^{-1}2\pi_u$ excited states deforms into a bent geometry while the molecule excited to the higher branch remains in a linear geometry.

VI-Q-10 Monochromator for a Soft X-ray Photochemistry Beamline BL27SU of SPring-8

OHASHI, Haruhiko[1]; ISHIGURO, Eiji[2]; TAMENORI, Yusuke[1]; OKUMURA, Hiroki[3]; HIRAYA, Atsunari[4]; YOSHIDA, Hiroaki[4]; SENBA, Yasunori[4]; OKADA, Kazumasa[4]; SAITO, Norio[5]; SUZUKI, Isao H.[5]; UEDA, Kiyoshi[6]; IBUKI, Toshio[7]; NAGAOKA, Shin-ichi; KOYANO, Inosuke[3]; ISHIKAWA, Tetsuya[1]
(*[1]JASRI; [2]Univ. Ryukyus; [3]Himeji Inst. Tech.; [4]Hiroshima Univ.; [5]Electrotechnical Lab.; [6]Tohoku Univ.; [7]Kyoto Univ. Edu.)*

A high-resolution monochromator with varied line space plane gratings (VLSG) and spherical focusing mirrors was installed in one of three branches of BL27SU in SPring-8. The performance of the monochromator was roughly evaluated from the photo ion yield of nitrogen molecule. Furthermore, the kinetic energy of the photoelectron from Xe $5p_{3/2}$ orbital was also measured at the same photon energy with the N_2 to avoid the influence of natural width. The resolving power over 10^4 has been confirmed at the N K-edge.

VI-Q-11 Angle-Resolved Electron and Ion Spectroscopy Apparatus on the Soft X-Ray Photochemistry Beamline BL27SU at SPring-8

UEDA, Kiyoshi[1]; YOSHIDA, Hiroaki[2]; SENBA, Yasunori[2]; OKADA, Kazumasa[2]; SHIMIZU, Yuichiro; CHIBA, Hisashi[1]; OHASHI, Haruhiko[3]; TAMENORI, Yusuke[3]; OKUMURA, Hiroki[4]; SAITO, Norio[5]; NAGAOKA, Shin-ichi; HIRAYA, Atsunari[2]; ISHIGURO, Eiji[6]; IBUKI, Toshio[7]; SUZUKI, Isao H.[5]; KOYANO, Inosuke[4]
(*[1]Tohoku Univ.; [2]Hiroshima Univ.; [3]JASRI; [4]Himeji Inst. Tech.; [5]Electrotechnical Lab.; [6]Univ. Ryukyus; [7]Kyoto Univ. Edu.)*

We have designed and constructed the apparatus for the angular distribution measurements of photoejected electrons and ions from free molecules, as a part of the endstation of a *c*-branch of the beamline BL27SU, a soft X-ray photochemistry beamline at SPring-8. The experimental procedures are described in combination with the use of a capability to switch the horizontal and vertical directions of the linear polarization of the light

produced by the figure-8 undulator. As a typical example of the experimental results, we present angle-resolved energetic ion yield spectra in the O 1s excitation region of CO_2.

VI-Q-12 Resonant Auger Spectra of Kr Near the L_3 Threshold

IBUKI, Toshio[1]; OKADA, Kazumasa[2]; KAMIMORI, Katsura[2]; SASAKI, Junko[2]; YOSHIDA, Hiroaki[2]; HIRAYA, Atsunari[2]; SUZUKI, Isao H.[3]; SAITO, Norio[3]; NAGAOKA, Shin-ichi; SHIMIZU, Yuichiro; OHASHI, Haruhiko[4]; TAMENORI, Yusuke[4]
(*[1]Kyoto Univ. Edu.; [2]Hiroshima Univ.; [3]Electrotechnical Lab.; [4]JASRI)*

Auger electron spectra were studied by scanning the photon energy near the L_3 threshold of krypton. Two resonant transitions were observed in the photon energy region 1673–1678 eV for the first time. They were identified to be the resonant $3d^{-2}5s$ and $3d^{-2}4d$ states originating from the $2p_{3/2}^{-1}5s$ and $2p_{3/2}^{-1}4d$ excitations, respectively.

VI-Q-13 Auger Electron Spectra of Kr2p Holes Using Monochromatic Soft X-Rays

SUZUKI, Isao H.[1]; OKADA, Kazumasa[2]; KAMIMORI, Katsura[2]; SASAKI, Junko[2]; YOSHIDA, Hiroaki[2]; HIRAYA, Atsunari[2]; SHIMIZU, Yuichiro; NAGAOKA, Shin-ichi; TAMENORI, Yusuke[3]; OHASHI, Haruhiko[3]; IBUKI, Toshio[4]
(*[1]Electrotechnical Lab.; [2]Hiroshima Univ.; [3]JASRI; [4]Kyoto Univ. Edu.)*

Normal Auger electron spectra from Kr2p hole states, $L_{23}M_{45}M_{45}$ and $L_{23}M_{23}M_{45}$, have been measured using monochromatized synchrotron radiation and a high resolution electron spectrometer. Measured spectra were reproduced with a fitting calculation, where Voigt functions including an instrumental resolution and natural lifetime widths of related core hole states were used. At most final states estimated energies for spectral peaks agree with those by electron and ion beam techniques. Relative intensities for some peaks are appreciably different from the previous results.

VI-R Ultraviolet Photoelectron Spectroscopy of Organic Thin Film and Organic/Inorganic Interface

Electronic structures of organic film surface and organic/inorganic interface are expected to play an important role in organic-device properties. We investigated surface structures and energy alignments to clarify their electronic structures using electron spectroscopy such as photoelectron spectroscopy combined with synchrotron radiation and metastable atom electron spectroscopy.

VI-R-1 Pendant Group Orientation of Poly(2-vinylnaphthalene) Thin Film Surface Studied by Near-Edge X-Ray Absorption Fine Structure Spectroscopy (NEXAFS) and Angle-resolved Ultraviolet Photoelectron Spectroscopy (ARUPS)

MORIKAWA, Eizi[1]; SAILE, Volker[1]; OKUDAIRA K., Koji; AZUMA, Yasushi[2]; MEGURO, Kazuyuki[2]; HARADA, Yoshiya[2]; SEKI, Kazuhiko[3]; HASEGAWA, Shinji; UENO, Nobuo[2]
(*[1]Louisiana State Univ. CAMD; [2]Chiba Univ.; [3]Nagoya Univ.*)

Angle-resolved ultraviolet photoelectron spectroscopy (ARUPS) and near-edge x-ray absorption fine structure (NEXAFS) spectroscopy were applied to the investigation of the tilt angles of the naphthalene pendant groups at the surface of poly(2-vinyl-naphthalene) thin film. The NEXAFS results indicates that the mean value of tilt angle of naphthalene pendant groups with respect to the polymer surface is about 57°. In contrast to NEXAFS, which provides only an average determination of the tilt angle, ARUPS combined with a sophisticated analysis of photoelectron angular dependence offers more detailed information. Analysis by ARUPS combined with the single-scattering approximation with molecular orbital calculation indicates that the naphthalene pendant groups are tilted randomly at the polymer surface, and that the tilt angle distribution is well described as a three-dimensional isotropic random orientation, which indicates that the majority of the pendant groups is tilted at large angles with respect to the polymer surface.

VI-R-2 Origin of Indium-[perylene3,4,9,10-tetracarboxylic Dianhydride] Interface States Studied by Outermost Surface Spectroscopy Using Metastable Atoms

KERA, Satoshi[1]; SETOYAMA, Hiroyuki[1]; OKUDAIRA K., Koji; HARADA, Yoshiya[2]; UENO, Nobuo[1]
(*[1]Chiba Univ.; [2]Seitoku Univ.*)

Metastable atom electron spectra (MAES) and ultraviolet photoelectron spectra (UPS) of indium-[perylene3,4,9,10-tetracarboxylic dianhydride (PTCDA)] system prepared on a MoS_2 single crystal substrate were measured as a function of the In over-layer thickness (ΘIn). As observed by a previous UPS experiment, a new band was observed in the original PTCDA energy gap region even by the MAES which detects the outermost surface selectively (Figure 1). The ΘIn dependence of this new band intensity measured by the MAES gives a maximum at $\Theta In \sim 1$ Å, suggesting that four In atoms are reacting with one PTCDA molecule at the C=O parts. From the result of the density functional theory (DFT) methods and the enhanced intensity of the new band in the MAES, it was concluded that the new band originates from π state consisting of In 5pz AO's.
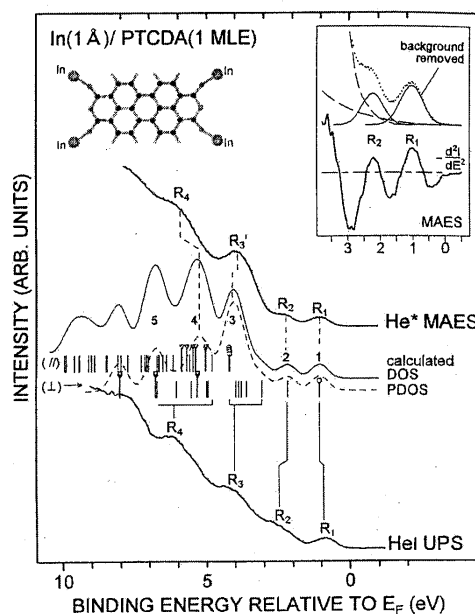
Figure 1. Comparison of the observed He*(2^3S) MAES and He I UPS of the In(1 Å)/PTCDA(1 MLE)/MoS$_2$ and the calculated results for In$_4$PTCDA. Bars show calculated MO energy levels obtained by DFT method (B3LYP/LanL2DZ). The Upper and lower bars respectively, indicate MO$_{//}$ and MO$_\perp$ states, and bars with circles show states with large contribution of In AO's (5p,5s). Bars with triangles indicate states with contribution of oxygen AO's. The calculated DOS is shown by solid curve. The PDOS, which corresponds to partial DOS for MO$_\perp$ and four contracted σ states (marked by circles in MO$_{//}$), is shown by a dashed curve. These DOS's were observed by 0.7 eV Gaussian broadening of MO's. Negative of the second derivative of the MAES ($-d^2I/dE^2$) and the MAES after background removal is shown in inset, in order to show the enhanced intensity of band R$_1$ than band R$_2$. Molecular structure of the reaction product, In$_4$PTCDA, is also shown.

VI-R-3 Surface Images of SiO₂/Si(100) Pattern using Electron Emission Microscopy with Metastable Atoms, Photons and Low-Energy Electrons

YASUFUKU, Hideyuki[1]; OKUMURA, Masao[1]; IBE, Takehiro[1]; OKUDAIRA K., Koji; HARADA, Yoshiya[2]; UENO, Nobuo[1]
(*[1]Chiba Univ.; [2]Seitoku Univ.*)

[*Jpn. J. Appl. Phys.* **40**, 2447 (2001)]

The surface images of a SiO₂ pattern on Si(100) was observed by three types of electron emission micro-scopies, *i.e.*, metastable electron emission microscopy (MEEM) with metastable he, photoelectron emission microscopy (PEEM) and low-energy electron emission microscopy (LEEM). Among these, MEEM gave the most diffused image at the pattern edges of the SiO₂ region. Furthermore, it is found that the difference in MEEM, LEEM, and PEEM images can provide new information on the spatial distribution of surface electronic state. By comparing MEEM, LEEM, and PEEM images, it is expected that we can obtain local information on surface electronic states in more detail

VI-R-4 Ultraviolet Photoelectron Spectra of Metallofullerenes, Two Ca@C₈₂ Isomers

HINO, Shojun[1]; UMISHITA, Kazunori[1]; IWASAKI, Kentaro[1]; AOKI, Masaru; KOBAYASHI, Kaoru[2]; NAGASE, Shigeru[2]; DENNIS, T. John S.[3]; NAKANE, Tomoyasu[3]; SHINOHARA, Hisanori[3]
(*[1]Chiba Univ.; [2]Tokyo Metro. Univ.; [3]Nagoya Univ.*)

[*Chem. Phys. Lett.* **337**, 65 (2001)]

Ultraviolet photoelectron spectra (UPS) of two Ca@C₈₂ isomers (III and IV) were measured with a synchrotron radiation light source. Figure 1 shows these photoelectron spectra obtained with 20 eV excitation energy. The photoelectron onset energies of isomer III and IV were 0.7 eV and 0.8 eV below the Fermi level, respectively, which indicates their semiconductive nature. When the excitation energy is tuned, spectral intensity changes as other fullerenes have shown. Their upper valence band (0–5 eV) spectra are different from those of other metallofullerenes such as La@C₈₂, Sc@C₈₂ and Gd@C₈₂ as well as those of empty C₈₂ but their lower valence band spectra (below 5 eV) are almost identical. Comparison between the UPS and *ab initio* calculation assuming transfer of two electrons from encapsulated calcium atom to the cage (*i.e.* Ca⁺²@C₈₂²⁻) suggests C_2(c) geometry for isomer III and C_s for isomer IV.
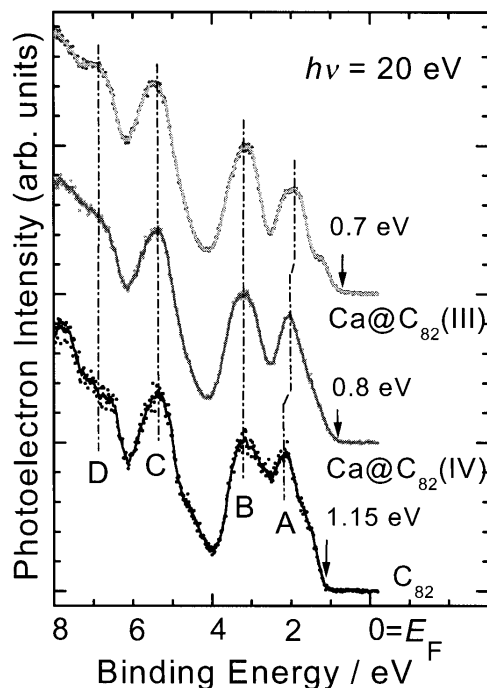
Figure 1. UPS spectra of two Ca@C₈₂ isomers and C₈₂.

VI-R-5 Chemical Reaction at the NTCDA/Metal Interfaces

MARUYAMA, Takahiro[1]; SUGAWARA, Norikazu[2]; HIRASAWA, Akira[2]; AKIMOTO, Katsuhiro[2]
(*[1]Ritsumeikan Univ.; [2]Inst. Appl. Phys., Univ. Tsukuba*)

Planar π-stacking organic molecules have been shown to be excellent model compounds for studying the growth and optoelectronic properties of organic semiconducting thin films on metal substrates.[1] In this study, we investigated the bonding of 1,4,5,8-naphthalene-tetracaboxylicacid-dianhydride (NTCDA) on Au and In by ultra-violet photoemission spectroscopy (UPS). Figures 1 and 2 show the valence band of NTCDA on Au and In, respectively, as a function of the amount of NTCDA deposition. The structures due to the highest occupied molecular orbital (HOMO) of NTCDA are seen even at low coverage on Au. However, the spectra of NTCDA deposited on Al are quite different from those on Au even at 50 Å. Taking into account the results of AES measurements, it is considered that NTCDA molecules are weakly bonded to Au substrate through the HOMO, on the other hand, a strong chemical bond between In and the anhydride group of NTCDA is formed and results in the diffusion of In atoms into NTCDA films.

Reference
1) Y. Hirose, A. Kahn, V. Aristov, P. Soukiassian, V. Bulovic and S. R. Forrest, *Phys. Rev. B* **54**, 13748 (1996).
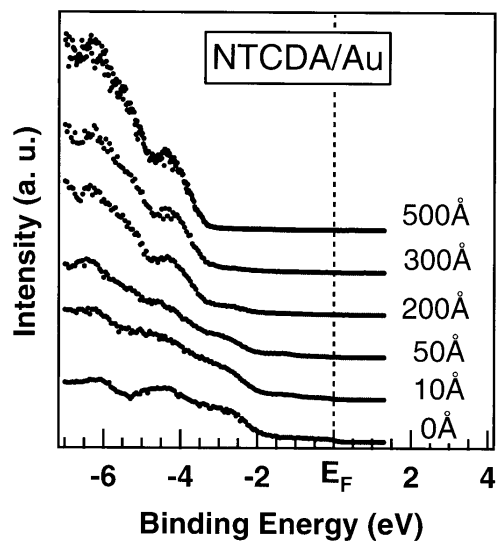
Figure 1. Valence band UPS spectra for NTCDA on Au.
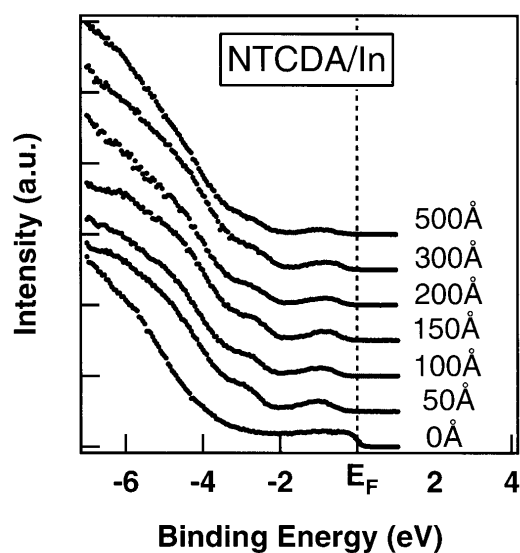
Figure 2. Valence band UPS spectra for NTCDA on In.

VI-S Study on Compact X-Ray Sources

Electron storage rings are useful and practical devices as x-ray sources because which produce a number of photons because of high electron current and various insertion devices. However, these synchrotron radiation facilities usually occupy large area and cost much. So that there have been many works to investigate compact x-ray sources such as x-ray lasers and free electron lasers. It is also useful to use laser undulator radiation or backward Compton scattering caused by the interactions of electron beams with laser photons, if we provide enough electrons to produce practical intensity of x-rays. RF-photocathode would produce dense electron beam so that it is a useful candidate of a electron source. It is necessary to search good materials as the photocathode for construction of a practical compact x-ray source. Cesium telluride has reported to have a good quantum efficiency, so that we have studied about it.

X-ray sources must be shielded for radiation safety. For constructing effective shields, we need to know how many radiations are yielded from our x-ray sources. We will use high energy electrons to produce x-rays and loss of the electrons cause radiations, it is useful to study radiations in synchrotron radiation facilities in order to estimate the yields radiations from our x-ray sources. We preliminarily measured radiations radiated from a vacuum duct of UVSOR.

VI-S-1 Preliminary Study on Photoemission from Cesium Telluride Irradiated by Polarized Photon

TAKASHIMA, Yoshifumi; KOBAYAKAWA, Hisashi[1]; TAKAGI, Masahiro[1]; KIMURA, Kenichi[1]; SUGIYAMA, Harue[1]; FURUTA, Fumio[1]; NAKANISHI, Tsutomu[1]
(*[1]Nagoya Univ.*)

Cesium telluride is a good candidate for a material to be used as a photocathode for RF-gun because of its high quantum efficiency and long life. The quantum efficiency of the photocathode for polarized photon measured with changing the incident angle of the light gives us important information about the optical constants of the materials of the photocathode.

We measured the quantum efficiency of cesium telluride by using linear polarized photon. Figure 1 shows a sketch of our experimental set up. A Xe lamp was used as a light source. The light from the Xe lamp passed through a monochrometer and a polarizer enter a vacuum chamber in which cesium telluride was evaporated on molybdenum block as a photocathode. The incident angle of the light was changed from –80° to 80°. We rotated the polarizer in order to change the direction of polarization. Figure 2 shows the quantum efficiency for the incident light of 250 nm wavelength. Closed and open circles show the quantum efficiency for the light which is polarized parallel (p-polarization) and perpendicular (s-polarization) to the incident plane, respectively. The quantum efficiency of p-polarization light has peaks at ±65°.

We assume that the quantum efficiency is proportional to (1-R) in order to calculate the optical constants of the photocathode of cesium telluride by using Fresnel formulas. R is reflectivity of the incident light from the photocathode. We obtain preliminary results of optical constants of cesium telluride. The refractive index and the extinction coefficient are 3.17 and 1.01 respectively.
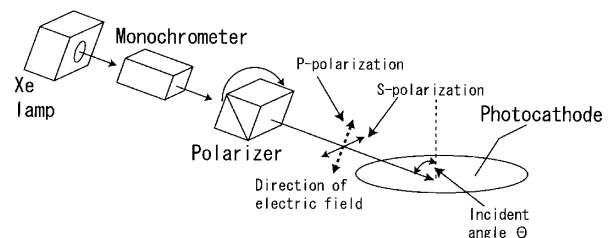
Figure 1. Sketch of experimental set up.
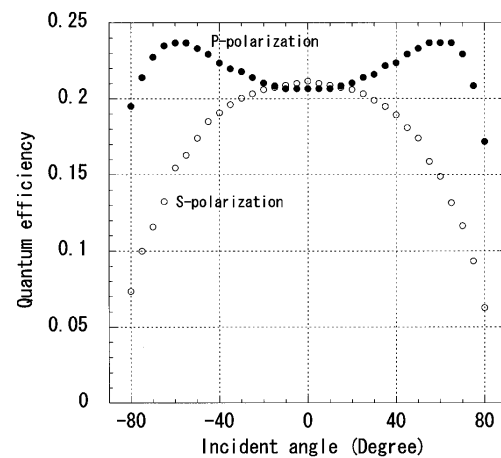
Figure 2. Quantum efficiency of cesium telluride with incident angle of light. The wavelength of the light is 250 nm. Open and closed circles show the quantum efficiency for the incident light which is polarized parallel and perpendicular to the incident plane, respectively.

VI-S-2 Study on Radiation Shielding for Synchrotron Radiation Facilities

TAKASHIMA, Yoshifumi; KOBAYAKAWA, Hisashi[1]; OKI, Sota[1]; YAMAKAGE, Masahiro[1]; TOMIHIRA, Kiyotaka[1]
(*[1]Nagoya Univ.*)

Radiation shielding for synchrotron facilities is to be effective in protecting radiations. In order to design effective shields, we need to estimate how many radiations are generated from a storage ring and

penetrate radiation shields.

Electron loss in beam ducts cause considerable stray radiations. Circulating electrons in a storage ring go out of their stable orbit if they interact with residual gases or other electrons. Electrons are also lose when they radiate high energy synchrotron radiations. These electrons are incident on the beam duct and generate electromagnetic showers around the ring.

We measured energy depositions of electromagnetic shower in NaI(Tl) scintillation counter generated by beam loss in a beam duct of UVSOR storage ring. Figure 1 shows experimental setup schematically. The diameter and thickness of the NaI(Tl) are 1 inch and 2 mm, respectively. The detection angles were 40° and 60°. Figure 2 shows pulse height distributions of energy depositions in NaI(Tl) for each detection angles. The energy deposition at 40° is larger than 60° because the incident angle of electrons in the beam duct is smaller than 40° and electromagnetic showers grow toward the incident angle.

For further study, we should measure the energy deposition in NaI(Tl) counter at smaller detection angles than 40° in order to estimate the incident angle of electrons in the beam duct. The information of the incident angle is important to calculate the spatial distribution of the dose around a storage ring. We should also investigate the absolute intensity of electromagnetic shower by comparing experimental results and theoretical calculations in order to estimate yields of radiations precisely for facilities of compact x-ray sources.
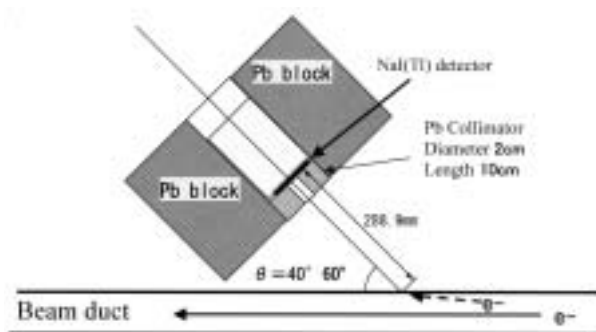
Figure 1. Experimental setup.
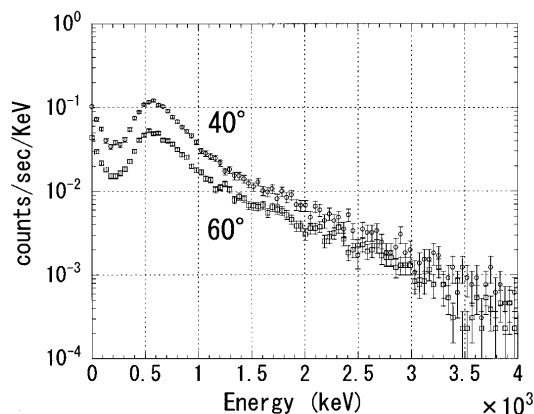
Figure 2. Pulse height distribution of energy deposition in NaI(Tl) detector. Open circles and open squares show the experimental data for detection angle of 40° and 60°, respectively.

VI-T Syntheses of Fullerene-Based New Materials with Novel Physical Properties

Fullerene-based new materials are synthesized, and the structures and physical properties are studied in wide temperature and pressure regions. The structures and transport properties of pressure-induced superconducting fulleride, Cs_3C_{60}, are studied by X-ray powder diffraction, ESR, Raman, AC susceptibility and resistivity measurements, in order to clarify the mechanism of pressure-induced superconductivity. The two-dimensional polymeric fulleride, Na_4C_{60}, is also studied in order to clarify the novel physical properties which are expected from its low-dimenionality. The structures and electronic properties of solid metallofullerenes are first clarified under high pressure, and the first evidence has been obtained for the endohedral structure and electron transfer from a metal atom to the C_{60} cage in metal endohedral C_{60}.

VI-T-1 Structure and Raman Scattering of Cs_3C_{60} under High Pressure

FUJIKI, Satoshi; KUBOZONO, Yoshihiro; EMURA, Shuichi[1]; TAKABAYASHI, Yasuhiro; KASHINO, Setsuo[2]; FUJIWARA, Akihiko[3]; ISHI, Kenji[3]; SUEMATSU, Hiroyoshi[3]; MURAKAMI, Yoichi[4]; IWASA, Yoshihiro[5]; MITANI, Tatsuoki[5]; OGATA, Hironori
(*[1]Osaka Univ.; [2]Okayama Univ.; [3]Univ. Tokyo; [4]KEK-PF; [5]JAIST*)

Raman scattering is studied for a pressure-induced superconductor Cs_3C_{60} in a pressure region from 1 bar to 62 kbar. The center frequency ω_0 for $H_g(1)$ and $H_g(2)$ Raman peaks increases by applying pressure, but the increase shows a saturation in the high-pressure region. On the other hand, the ω_0 for $A_g(1)$ and $A_g(2)$ modes increase monotonically in all pressure regions. The electron-phonon coupling constant for Cs_3C_{60} shows a rapid decrease up to 30 kbar and an increase above 30 kbar. This result may be associated with a transformation from a multiphase (body-centered orthorhombic and A15 phases) to a single phase around 20 kbar. X-ray powder diffraction pattern at 11 K under a pressure of 40 kbar shows that a superconducting phase for Cs_3C_{60} is body-centered orthorhombic.

VI-T-2 Structure and Physical Properties of Na_4C_{60} under Ambient and High Pressures

KUBOZONO, Yoshihiro; TAKABAYASHI, Yasuhiro; KAMBE, Takashi[1]; FUJIKI, Satoshi; KASHINO, Setsuo[1]; EMURA, Shuichi[2]
(*[1]Okayama Univ.; [2]Osaka Univ.*)

The structure and physical properties of two-dimensional polymeric Na_4C_{60} (body-centered monoclinic, space group $I2/m$) are studied in a wide temperature region from 12 to 300 K at 1 bar, and in a pressure region up to 53 kbar at 300 K. The temperature dependence of lattice constants suggests a structural anomaly below 100 K where the variation of spin susceptibility is observed from electron spin resonance. The thermal expansion of the unit-cell volume V is smaller than that of monomeric Rb_3C_{60} and K_3C_{60}. The compressibility of c is larger than that of a and b, which can be well explained by the repulsion between Na ions. The compressibility of the center-to-center distance in the $(10\bar{1})$ plane is ~ 1/3 times smaller than that in the (101) plane, which can be well explained by the formation of the polymer chains. Further, a possibility of a three-dimensional polymerization is discussed on the basis of the pressure dependence of $C_{60}\cdots C_{60}$ distance.

VI-T-3 Structure of $La_2@C_{80}$ Studied by La K-Edge XAFS

KUBOZONO, Yoshihiro; TAKABAYASHI, Yasuhiro; KASHINO, Setsuo[1]; KONDO, Masahiro[2]; WAKAHARA, Takatsugu[2]; AKASAKA, Takeshi[3]; KOBAYASHI, Kaoru[4]; NAGASE, Shigeru; EMURA, Shuichi[5]; YAMAMOTO, Kazunori[6]
(*[1]Okayama Univ.; [2]Niigata Univ.; [3]Univ. Tsukuba; [4]Tokyo Metropolitan Univ.; [5]Osaka Univ.; [6]Power Reactor and Nuclear Fuel Department Corporation*)

The structure of $La_2@C_{80}$ is studied by La K-edge XAFS from 40 to 295 K. The distances between the La atom and the first nearest C atoms have been determined to be 2.42(1) Å at 40 K and 2.44(2) Å at 295 K, and those between the La atom and the second nearest C atoms to be 2.97(2) Å at 40 K and 2.98(3) Å at 295 K. The La–La distance has been determined to be 3.90(1) Å at 40 K and 3.88(2) Å at 295 K. The temperature dependence of the mean-square displacement of La–C is also studied to get an insight into the dynamical behavior of two La atoms in the C_{80} cage.

VI-T-4 Structure and Electronic Properties of $Dy@C_{82}$ Studied by UV-VIS Absorption, X-Ray Powder Diffraction and XAFS

IIDA, Satoru[1]; KUBOZONO, Yoshihiro; SLOVOKHOTOV, Yuri[2]; TAKABAYASHI, Yasuhiro; KANBARA, Takayoshi; FUKUNAGA, Takeo[1]; FUJIKI, Satoshi; EMURA, Shuichi[3]; KASHINO, Setsuo[1]
(*[1]Okayama Univ.; [2]Russian Acad. Sci.; [3]Osaka Univ.*)

Two isomers of $Dy@C_{82}$ were separated by high performance liquid chromatography (HPLC), and their UV-VIS absorption spectra were measured to characterize these isomers. The crystalline powder of $Dy@C_{82}$ was obtained by removing solvent (toluene) at 250 °C under vacuum. The X-ray diffraction pattern can be indexed with fcc crystal lattice, as that in $La@C_{82}$. The lattice constant a at 298 K, 15.86(1) Å, is close to that of $La@C_{82}$, 15.78 Å. The distances between Dy and the first and second nearest C atoms are determined to be 2.52(2) and 2.86(2) Å, respectively, on the basis of Dy L_{III}-edge EXAFS. The XANES shows that the valence of the Dy atom in $Dy@C_{82}$ is +3.

VI-T-5 $Dy@C_{60}$: Evidence for Endohedral Structure and Electron Transfer

KANBARA, Takayoshi; KUBOZONO, Yoshihiro; TAKABAYASHI, Yasuhiro; FUJIKI, Satoshi; IIDA, Satoru[1]; HARUYAMA, Yusuke[1]; KASHINO, Setsuo[1]; EMURA, Shuichi[2]; AKASAKA, Takeshi[3]
(*[1]Okayama Univ.; [2]Osaka Univ.; [3]Univ. Tsukuba*)

In view of the lack of information on the structure of $M@C_{60}$ (M: alkaline earth and lanthanide metal) because of its instability and difficulties in purifying it, we have carried out and report here some structural investigations of $Dy@C_{60}$. We obtained a pure sample of $Dy@C_{60}$ by high performance liquid chromatography with aniline as an eluent, and studied it by Dy L_{III}-edge XAFS and Raman scattering. Our results show conclusively that the structure is endohedral (with the metal inside the C_{60} cage) and that electron transfer takes place between Dy and C_{60}. The Dy in $Dy@C_{60}$ is located at an off-center position, 1.25–1.30 Å, from the center of the C_{60} cage. The valence of the Dy is shown to be $+3$ on the basis of a Dy L_{III}-edge XANES study. The $A_g(2)$ Raman peak also shows that three electrons have been transferred from Dy atom to the C_{60} cage. The UV-VIS-IR spectrum suggests that the HOMO-LUMO gap is small.

RESEARCH ACTIVITIES VII
Coordination Chemistry Laboratories

Prof. Nobuhiro Tokito, Prof. Kiyotaka Onizuka took the position of Laboratory of Coordination Bond from April 2001. Prof. Takuzo Aida (Tokyo University) and Assoc. Prof. Kaku Hamachi (Kyushu University) finished their term as Adjunct Prof. of the Synthetic Coordination Chemistry in March 2001. Their effort during their term is gratefully appreciated. Prof. Isao Taniguchi (Kumamoto University) and Assoc. Prof. Yasutaka Tanaka (Shizuoka University) continue the position of the Synthetic Coordination Chemistry.

VII-A A Diversity-Based Approach to Novel Chiral Units

Catalytic asymmetric reactions have attracted significant interest for their synthetic utility. One of the most exciting and challenging subjects in research on the catalytic asymmetric synthesis is development of the novel and basic chiral units. Homochiral organic molecules bearing hetero atoms (*e.g.* nitrogen, phosphorus, *etc.*) occupy a prominent position in organic chemistry as both useful synthetic reagents and molecules of biological interest. Highly functionalized optically active bicyclic amines having a pyrrolo[1,2-*c*]imidazolone framework were identified as effective chiral agents through a diversity-based approach to new chiral amine catalysts.

VII-A-1 A Parallel Preparation of A Bicyclic *N*-Chiral Amine Library and Its Use for Chiral Catalyst Screening

UOZUMI, Yasuhiro; MIZUTANI, Kanako; NAGAI, Shin-ichi

[*Tetrahedron Lett.* **42**, 407 (2001)]

A parallel library of optically active bicyclic tertiary amines bearing *N*-chiral bridgehead nitrogen atoms was readily prepared by condensation of primary amines, cyclic amino acids, and aldehydes. The enantio-controlling ability of each of the library members was examined for the asymmetric alkylation of benzaldehyde with diethylzinc, and (3*R*,6*R*,7a*S*)-(2,3-diphenyl-6-hydroxy)hexahydro-1*H*-pyrrolo[1,2-*c*]-imidazol-1-one, which contains β-amino alcohol unit, showed high enantioselectivity.

VII-A-2 Enantioselective Desymmetrization of Meso-Cyclic Anhydrides Catalyzed by Hexahydro-1*H*-pyrrolo[1,2-*c*]imidazolones

UOZUMI, Yasuhiro; YASOSHIMA, Kayo; MIYACHI, Takamasa; NAGAI, Shin-ichi

[*Tetrahedron Lett.* **42**, 411 (2001)]

Enantioselective desymmetrization of meso compounds is a powerful synthetic means of preparing enantiomerically enriched products where plural stereogenic carbon centers are generated in one step. Enantioselective ring opening of meso cyclic anhydrides is one of the cases. Asymmetric methanolysis of meso cyclic carboxylic anhydrides including hexahydro-phthalic anhydride proceeded in toluene in the presence of (6*R*,7a*S*)-(2-aryl-6-hydroxy)hexahydro-1*H*-pyrrolo-[1,2-*c*]imidazol-1-one to give the corresponding desymmetrized mono ester acids (*e.g.* (1*S*,2*R*)-2-(methoxycarbonyl)-cyclohexane-1-carboxylic acid) with enantiomeric excesses of up to 89%.

VII-B Catalysis in Aqueous Media by Using of Amphiphilic Polymer-Supported Catalysts

Catalytic organic transformations in water using recyclable immobilized catalysts is an important goal in synthetic organic chemistry. We recently reported that several palladium-catalyzed reactions, including π-allylic substitution, carbonylation, the Heck reaction, and Suzuki-Miyaura cross-coupling, took place in water by use of palladium-phosphine complexes bound to an amphiphilic polystyrene-poly(ethylene glycol) graft copolymer (PS–PEG) resin. A chiral palladium complex and a quaternary ammonium salt immobilized on PS–PEG resin were designed and prepared, respectively. Allylic alkylation and Michael addition were investigated by using the resin-supported catalysts in water.aa

VII-B-1 Catalytic Asymmetric Allylic Alkylation in Water with a Recyclable Amphiphilic Resin-Supported *P,N*-Chelating Palladium Complex

UOZUMI, Yasuhiro; SHIBATOMI, Kazutaka

[*J. Am. Chem. Soc.* **123**, 2919 (2001)]

A novel *P,N*-chelate chiral ligand, (3*R*,9a*S*)-(2-aryl-3-(2-diphenylphosphino)phenyl)-tetrahydro-1*H*-imidazo[1,5-*a*]indole-1-one was designed, prepared, and immobilized on an amphiphilic polystyrene–poly-(ethylene glycol) graft copolymer (PS–PEG) resin. A palladium complex of the PS–PEG resin-supported *P,N*-ligand catalyzed the allylic substitution of both cyclic and acyclic allylic esters in water with high enantio-selectivity. Reactions of cyclopentenyl, cyclohexenyl, and cycloheptenyl carbonates with dialkyl malonate gave the corresponding alkylated products with enantiomeric excess ranging from 89 to 98% ee. The PS-PEG supported Pd complex was readily recovered by simple filtration and reused without loss of catalytic activity or enantioselectivity.

VII-B-2 Michael Reactions in Water Using Amphiphilic Resin-Supported Quaternary Ammonium Hydroxides

SHIBATOMI, Kazutaka; NAKAHASHI, Toshiyuki; UOZUMI, Yasuhiro

[*Synlett* 1643 (2000)]

Quaternary ammonium hydroxides were immobi-lized on a polystyrene–poly(ethylene glycol) copolymer resin. The amphiphilic polymer-supported ammonium hydroxides catalyzed Michael reaction of cyclic β-keto esters with several Michael acceptors in water to give corresponding adducts in high yields.

VII-C Electrochemical Analysis of Biological Functions of Metalloproteins and Their Mutated Molecules and Its Applications to Coordination Chemistry for Catalysis

Using surface-functionalized electrodes, biological functions and bioelectrochemical properties of metalloproteins and their mutated and redox-center modified molecules have been analyzed electrochemically to develop new bioelectrocatalytic systems and bioelectro-functional devices.

VII-C-1 Simple Methods for Preparation of a Well-Defined 4-Pyridinethiol Modified Surface on Au(111) Electrodes for Cytochrome c Electrochemistry

TANIGUCHI, Isao[1,2]; YOSHIMOTO, Soichiro[1]; YOSHIDA, Masahito[1]; KOBAYASHI, Shun-ichi[1]; MIYAWAKI, Toshifumi[1]; AONO, Yutaka[1]; SUNATSUKI, Yukinari[1]; TAIRA, Hideo[1]
(*[1]Kumamoto Univ.; [2]IMS*)

A very small amount of sulfide impurity in 4-pyridinethiol (4-PySH) modifier solution was found to interfere with the proper formation of the 4-PySH modified surface for cytochrome c electrochemistry on an Au(111) electrode. When the modification was conducted in an alkaline (*e.g.*, 0.1 M KOH) solution, in aqueous solutions under applying a potential more positive than 0.3 V *vs.* Ag/AgCl, or at a low modifier concentration (*e.g.*, 20 μM), the proper 4-PySH modified surface was obtained even using 4-PySH as received, which contained a small amount of sulfide. The selective adsorption of 4-PySH in the presence of a small amount of sulfide under these conditions was due to the rapid formation of proper 4-PySH modified surface, which prevented the sulfide from reacting with the electrode surface.

VII-C-2 Voltammetric and In Situ STM Studies on Self-Assembled Monolayers of 4- and 2-Mercaptopyridines and Thiophenol on Au(111) Electrodes

SAWAGUCHI, Takahiro[1]; YOSHIMOTO, Soichiro[2]; MIZUTANI, Fumio[1]; TANIGUCHI, Isao[2,3]
(*[1]Natl. Inst. Bioscience and Human Tech.; [2]Kumamoto Univ.; [3]IMS*)

Voltammetric and in situ STM studies were carried out for self-assembled monolayers of 4-mercapto-pyridine (4-PySH), 2-mercaptopyridine (2-PySH) and thiophenol (PhSH) on well-defined single-crystal Au(111) electrodes in aqueous solutions. A reversible voltammetric response for cytochrome c was clearly observed only at the 4-PyS/Au(111) electrode, showing that only the 4-pyridinethiolate monolayer promotes facial electron transfer reaction between the Au(111) and cytochrome c. On the basis of reductive desorption, the surface coverages of the three aromatic thiolate monolayers were found to be similar to each other; 4.6×10^{-10} mol/cm^2 for 4-PyS/Au(111), 4.7×10^{-10} mol/cm^2 for 2-PyS/Au(111), and 4.4×10^{-10} mol/cm^2 for PhS/Au(111). High-resolution STM images in perchloric acid solutions revealed p ($5 \times \sqrt{3}$R–30°) and p ($4 \times \sqrt{7}$R–40.9°) structures for the 4- and 2-pyridine-thiolate monolayers on Au(111), respectively. No structure order was observed for the PhSH monolayers. While the pyridine units of both 4- and 2-pyridine-thiolate monolayers were found to be oriented normal to the surface, 2-pyridinethiolates adsorbed through not only sulfur but also nitrogen atom of the pyridine ring. From these STM images, the orientation of the N atom of the pyridine moiety must face to the bulk solution, as in the case of 4-PyS/Au(111), in order to obtain a facile electrochemical reaction for cytochrome c.

VII-C-3 Formation of the "Nanotube" Structure of β-Cyclodextrin on Au(111) Surfaces Induced by Potential Controlled Adsorption

OHIRA, Akihiro[1]; ISHIZAKI, Takahiro[1]; SAKATA, Masayo[1]; TANIGUCHI, Isao[1,2]; HIRAYAMA, Chuichi[1]; KUNITAKE, Masashi[1]
(*[1]Kumamoto Univ.; [2]IMS*)

The self-organization of β-cyclodextrin (β-CyD) into a nanotube structure, similar to that of CyD-polyrotaxane, was found to be induced by potential controlled adsorption on Au(111) surfaces in sodium perchlorate solution without a threaded polymer. In situ scanning tunneling microscopy (STM) revealed that the cavities of β-CyD faced side ward not upward in the tube. This ordered structure can form only under conditions where the potential is controlled (–0.45 V to –0.25 V *vs.* SCE). β-CyD molecules were in a disordered state on bare Au(111) surfaces without potential control (+0 V *vs.* SCE). In addition, the desorption of β-CyD from Au surfaces was observed at a negative potential of less than –0.60 V. In the range –0.45 to –0.25 V, β-CyD molecules formed ordered array on Au(111) surfaces. Furthermore, the discontinuity of potential control led to disordered phases and the destruction of the tube structure. This indicates that by controlling the electrode potential a delicate balance of various interactions can be achieved, resulting in the self-organization of molecules on the surface.

VII-C-4 Direct Observation of Perchlorate Induced by Redox Reaction of Ferrocene Terminated Self-Assembled Monolayer Studied by in situ FT-Surface Enhanced Raman Spectroscopy

NISHIYAMA, Katsuhiko[1]; UEDA, Akihiro[1]; TANOUE, Shotaro[1]; KOGA, Tesshu[1]; TANIGUCHI, Isao[1,2]
(*[1]Kumamoto Univ.; [2]IMS*)

The incorporation of perchlorate anion into 8-ferrocenyloctanethiol (8FT) self-assembled monolayer (SAM) induced by the redox reaction at a gold wire electrode was demonstrated using in situ FT Raman spectroelectrochemistry. Upon oxidation of 8FT SAM, a band attributed to perchlorate anion was clearly observed and the band disappeared in its reduced state. On the other hand, when nitric acid was used as a supporting electrolyte, the band attributed to nitrate anion was not observed in the oxidized form of 8FT.

VII-C-5 Novel "Wet Process" Technique Based on Electrochemical Replacement for the Preparation of Fullerene Epitaxial Adlayers

UEMURA, Shinobu[1]; SAKATA, Masayo[1]; TANIGUCHI, Isao[1,2]; KUNITAKE, Masashi[1]; HIRAYAMA, Chuichi[1]
(*[1]Kumamoto Univ.; [2]IMS*)

The electrochemical replacement method to form epitaxial adlayers of fullerene on Au(111) surfaces was proposed and demonstrated by in situ electrochemical STM. The new "wet process" method consists of the transfer of Langmuir film of fullerene onto iodine-modified Au(111) surfaces at an air-water interface followed by the electrochemical removal and replacement of iodine adlayers with fullerene adlayers in solution. The fullerene adlayers prepared by this method showed excellent quality and uniformity, and they were essentially the same as epitaxial adlayers prepared by sublimation.

VII-C-6 Electrochemical and Spectroelectrochemical Studies on Cobalt Myoglobin

LI, Chen-zhong[1]; NISHIYAMA, Katsuhiko[1]; TANIGUCHI, Isao[1,2]
(*[1]Kumamoto Univ.; [2]IMS*)

The cobalt protoporphyrin-IX reconstituted myoglobin (Co-Mb) was prepared and its electrochemical and spectroelectrochemical properties were studied in comparison with native myoglobin. Unlike native myoglobin, a slow electron transfer reaction for Co(III)-Mb/Co(II)-Mb was detected by cyclic voltammogram and spectroelectrochemical methods. The chemical reduction rate of Co(III)-Mb with dithionite was also slow compared with that of native myoglobin. Direct electron transfer between Co-Mb and an In_2O_3 electrode was observed, with spectroscopic verification of different redox states of Co-Mb using an optically transparent thin layer electrode (OTTLE) cell. The reversible electrochemical redox reaction of Co(III)-Mb/Co(II)-Mb was observed using azure A, 3-amino-7-dimethylaminophenaza-thionium chloride, as an electron transfer mediator for the first time. The Nernst plot was obtained for Co-Mb with $E^{0'}$ of –100 mV *vs.* Ag|AgCl (sat. KCl) and $n = 1$ at 25 °C.

VII-C-7 Effect of Rapid Heme Rotation on Electrochemistry of Myoglobin

MIE, Yasuhiro[1]; SONODA, Kumiko[1]; KISHITA, Midori[1]; KRESTYN, Emil[1]; NEYA, Saburo[2]; FUNASAKI, Noriaki[2]; TANIGUCHI, Isao[1,3]
(*[1]Kumamoto Univ.; [2]Kyoto Pharmaceutical Univ.; [3]IMS*)

Myoglobins (Mbs) reconstituted with rotatable octamethylheme and non-rotatable etioheme were prepared and their electrochemical behavior was studied. The redox potential of octamethylheme reconstituted Mb (OMe-Mb), of which heme rotates around iron-histidine (F8-His) bond, shifted negatively by *ca.* 30 mV compared with non-rotatable etioheme reconstituted Mb (Etio-Mb). On the other hand, the redox potentials of octamethylheme and etioheme themselves were very similar to each other. Due to the similarity of the distal histidine side of the heme of these two reconstituted Mbs, the shifts of the redox potential would be attributable to the drastic change of the orientation of proximal histidine imidazole ring to the heme plane by heme rotation. The dissociation rate constant of cyanide ion from the ferrous heme iron (II) for OMe-Mb form at 5 °C and pH 7.5 was three times faster than that of Etio-Mb. The electron transfer kinetics of these Mbs showed that the heme rotation causes faster electron transfer rates in both electrode reaction and chemical reduction in solution with dithionite. The obtained heterogeneous electron transfer rates constants at an In_2O_3 electrode and first-order rate constants of the chemical reduction were 12 ($\pm$ 0.5) $\times$ 10^{-4} cm s^{-1}, 9.8 ($\pm$ 1.0) s^{-1} for OMe-Mb and 6.0 ($\pm$ 0.5) $\times$ 10^{-4} cm s^{-1}, 4.5 ($\pm$ 1.0) s^{-1} for Etio-Mb under the present experimental conditions.

VII-D Unusual Reactivities of N-Heterocycles

Among aromatic nuclei, acridines and their derivatives are still attracting considerable attention because of the many functions which they possess, including biomimetic redox reactivities, chemiluminescence, and the interaction with DNA as an intercalator. In particular the 9 position, the pare position from acridine nitrogen, in acridinium exhibits strong electrophilicity and reacts with alcohols giving rise to 9-alkoxyacridanes. 9-methyl substituted acridinium exhibited a slightly different reactivity with basic alcohol, affording the corresponding 9-alkoxyacridanes followed by an olefinic species, 9-methyleneacridane, through the 9-methyl proton abstraction by an alkoxide. Therefore, the 9 position in acridinium appears to have different electric and steric conditions as compared to the other positions, giving rise to expectations of more unique reactivity. Here we report on the unusual reactivities of the acridinium skeleton as a N-Heterocycle.

VII-D-1 An Unusually Acidic Methyl Group Directly Bound to Acridinium Cation

SUZUKI, Hiroshi[1]; TANAKA, Yasutaka[1,2]
(*[1]Shizuoka Univ.; [2]IMS*)

[*J. Org. Chem.* **66**, 2227 (2001)]

9,10-dimethylacridinium chloride (**1**: X = Cl) exhibited strong acidity of pH 3.90 (3.4×10^{-3} M, 20 °C) in an aqueous solution. H–D exchange reaction of **1** in D_2O indicated that protons in the 9-methyl group dissociated to generated H^+ ions (equation 1). This is an

$$ (1) $$

pH = 3.9 at 20 °C

1
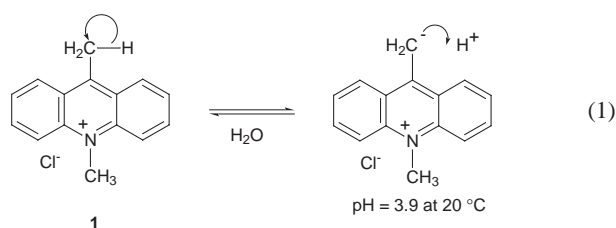
unique example of a methyl proton functioning as an acid. The conversion of **1** into **2** followed first-order kinetics with respect to the concentration of **1** over the temperature range studied (equation 2). The acidity

$$ (2) $$

k_{obs}(60 °C) = 4.25 x 10^{-5} sec^{-1}
Ea = 63.5 kJ/mol
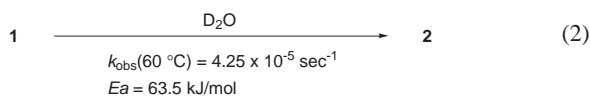
derives from the wider π face in acridinium capable of delocalizing the newly formed negative charge upon proton dissociation. PM3 calculations provided stabilization factors ($\delta\Delta H_f°$) between proton dissociated and undissociated forms of several N-heterocycles and also confirmed the acidity observed in acridinium.
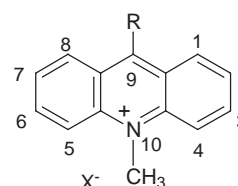
1: R=CH$_3$, X=Cl, I, CH$_3$SO$_4$
2: R=CD$_3$, X=Cl, I, CH$_3$SO$_4$

Figure 1. Chemical Structures of **1** and **2**.

a
$\delta\Delta H_f^0$ = -422.7 kJ mol^{-1}

b
$\delta\Delta H_f^0$ = -367.1 kJ mol^{-1}

c
$\delta\Delta H_f^0$ = -336.3 kJ mol^{-1}

d
$\delta\Delta H_f^0$ = -174.8 kJ mol^{-1}(1-methyl)
-289.7 kJ mol^{-1}(2-methyl)
-345.0 kJ mol^{-1}(3-methyl)
-313.8 kJ mol^{-1}(4-methyl)
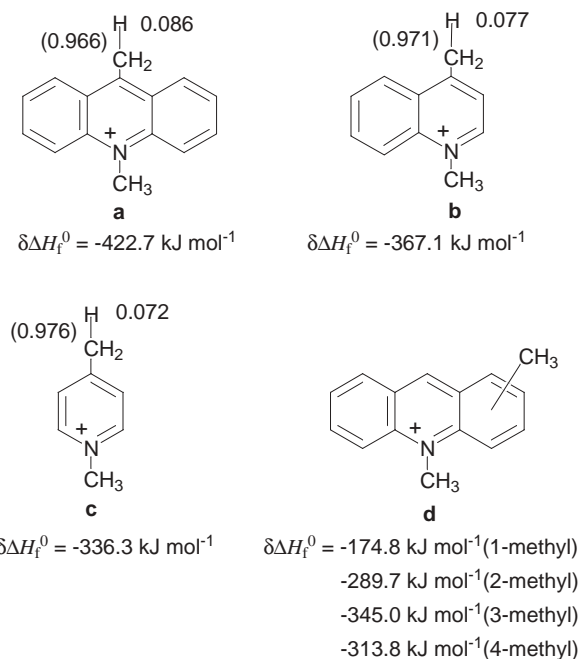
Figure 2. Model Structures for the PM3 calculation. The numbers in the structures refer to the partial charges of the dissociating proton. The numbers in parentheses refer to the bond orders between the proton and an atom bound to the proton. The difference in heat of formation ($\delta\Delta H_f°$) was calculated from $\Delta H_f°$ (undissociated form) + $\Delta H_f°$ (H_2O) – $\Delta H_f°$ (dissociated form) – $\Delta H_f°$ (H_3O^+).

VII-E Reductive Activation of Carbon Dioxide and Oxidative Activation of Water Aimed at Energy Conversion

Free energy required in the reduction of CO_2 continuously decreases with an increase of the number of electrons participated in the reduction. Accordingly, multi-electron reduction of CO_2 is much favorable compared with two-electron reduction of CO_2. An electrophilic attack of CO_2 to low valent coordinatively unsaturated metals complexes gives metal-η^1-CO_2 complexes, which can be easily converted to M-CO ones. A major problem of reduction of CO_2 in homogeneous systems is reductive cleavages of M–CO bonds (CO evolution) under the reaction condition due to accumulation of too much electrons in the central metals. A catalytic system, in which electrons required in the reduction of CO_2 are provided by ligand localized redox reactions not but metal centered ones, therefore, may open a new methodology for the reduction of CO_2. Based on the facts that naphytylidine works as not only monodentate, bidentate and bridging ligand between metals and carbonyl carbon but also electron source in the reduction of CO_2, we have been preparing a variety of meta-naphytylidine complexes to aim at multi-electron reduction of CO_2.

Much attention has been paid to high valent oxo-metal complexes from the view points of the fact that metal proteins participating in oxidation of various organic molecules contain one or multi oxo-metal conters. Among various synthetic route of metal-oxo complexes reported so far, metal aqua-complexes are reasonable precursors, since they undergo acid-base equilibrium among aqua-, hydroxo- and oxo-complexes. The distribution of those complexes can be controlled by selection of bases and pH. Polymerizaion of aqua-metal complexes upon deprotonation of aqua ligands would depress by introduction of appropriate ligands which can accept electrons generated in the hydroxy and aoxo groups. Along the line, we have prepared a series of metal-aqua complexes with dioxolene and dithiolene ligands to decrease basicity of the hydroxy and oxo ligands.

VII-E-1 Syntheses and Redox Properties of Bis(hydroxoruthenium) Complexes with Quinone and Bipyridine Ligands. Water-Oxidation Catalysis

WADA, Tohru; TSUGE, Kiyoshi; TANAKA, Koji

[*Inorg. Chem.* **40**, 329 (2001)]

A novel dimerizing ligand 1,8-bis(2,2':6',2''-terpyridyl)anthracene (btpyan) was prepared by three reactions from 1,8-diformylanthracene. Bis(ruthenium-hydroxo)complex with two 3,6-di(*tert*-butyl)-1,2-benzo-quinone ligands (3,6-tBu$_2$qui), $[Ru^{II}_2(OH)_2(3,6-tBu_2-qui)_2(btpyan)](SbF_6)_2$ ([**1**](SbF$_6$)$_2$) and with two 2,2'-bipyridine ligands (bpy), $[Ru^{II}_2(OH)_2(bpy)_2(btpyan)]$-(SbF$_6$)$_2$ ([**2**](SbF$_6$)$_2$) were synthesized by using btpyan ligand. [**1**]$^{2+}$ easily eliminated two protons by the addition of t-BuOK (2.0 equiv.) coupled with the reduction of quinone ligands in the MeOH solution, and converted to the $[Ru^{II}_2(O)_2(3,6-tBu_2sq)_2(btpyan)]^0$ (3,6-tBu$_2$sq = 3,6-di(*tert*-butyl)-1,2-semiquinone), while [**2**]-(SbF$_6$)$_2$ was not changed by the addition of large excess of t-BuOK. Electrochemical and Spectroelectrochemical measurements revealed that the $[Ru^{II}_2(O)_2(3,6-tBu_2sq)_2(btpyan)]^0$ derived from [**1**]$^{2+}$ oxidized to $[Ru^{III}_2(O)_2(3,6-t-Bu_2qui)_2(btpyan)]^{4+}$ at +1.2 V via the $[Ru^{II}_2(O)_2(3,6-tBu_2qui)_2(btpyan)]^{2+}$ in the MeOH solution. [**1**]$^{2+}$ showed higher catalytic activity for the water-oxidation in a CF$_3$CH$_2$OH/ehter solution containg water and in pH controlled-water (pH 4.0) by using modified ITO electrode, and the turnover number was 35000. The role

$$Ru(Q)(O)Ru(Q)(O)^{2+} \xrightleftharpoons[0.40V]{e^-} [Ru(Q)(O)Ru(SQ)(O)]^+ \xrightleftharpoons[0.30 V]{e^-} [Ru(SQ)(O)Ru(SQ)(O)]$$
(1)
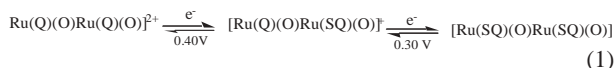
of the equilibrium of equation 1 in the O_2 evolution is evidenced by the fact that the analogous [**2**](SbF$_6$)$_2$ has no ability to catalyze the oxidation of water under the same conditions.

[**1**]$^{2+}$ [**2**]$^{2+}$
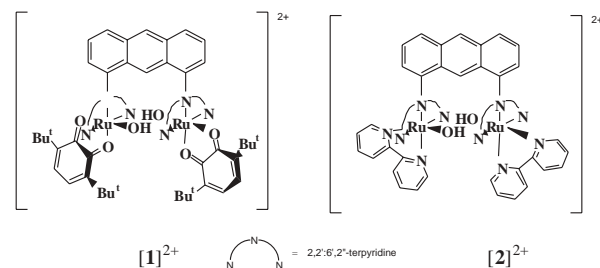
VII-E-2 A Ru–Carbene Complex with a Metallacycle Involving a 1,8-naphthylidine Framework

TOMON, Takashi; OOYAMA, Dai; WADA, Tohru; SHIREN, Kazushi; TANAKA, Koji

[*Chem. Commun.* 1100 (2001)]

The reaction of [Ru(bpy)$_2$(CO)(napy)](PF$_6$)$_2$ with HCCC(O)OH in CH$_3$OH/H$_2$O (3:2 V/V) gave [**1**](PF$_6$)$_2$. The molecular structure of **1**$^{2+}$ determined by X-ray diffraction analysis. The characteristic feature of **1**$^{2+}$ is the C–N bond formation between the CCH$_3$ group and one nitrogen of napy, and an unique five-membered metallacycle consisting of Ru–N–C–N–C(O) atoms. The metallacycle ring and the napy moiety form a co-plane despite that aromaticity of the napy ligand substantially decreased due to the attachment of CH$_3$OH to the carbon atom of 2-positon of napy. The ^{1}H-NMR spectrum of the complex **1**$^{2+}$ in CD$_3$CN/CD$_3$OD (1:1 v/v) showed the equilibrium between the carbene species and the corresponding vinylidene species. The CH$_3$O group of **1**$^{2+}$ was substituted by C$_2$H$_5$O in C$_2$H$_5$OH/CH$_3$CN. In addition, treatments of **1**$^{2+}$ with the

equivalent amount of OH⁻ at room temperature in CD_2Cl_2 gave the corresponding vinyl complex with a framework of the five membered metallacycle. The most likely path for the formation of $\mathbf{1}^{2+}$ is depicted in Scheme. The reaction of $\mathbf{1}^{2+}$ with propiolic acid would produce a vinylidene complex through π alkyne complex with monodentate napy. An intra-molecular attack of non-bonded nitrogen of napy to the α carbon of the vinylidene group must increase in acidity of the vicinal carbon of the bonded nitrogen of napy, which will induce a nucleophilic attack of CH_3OH to the C_2 carbon.
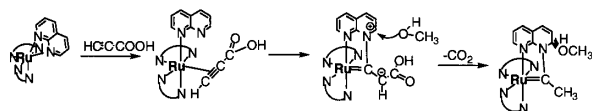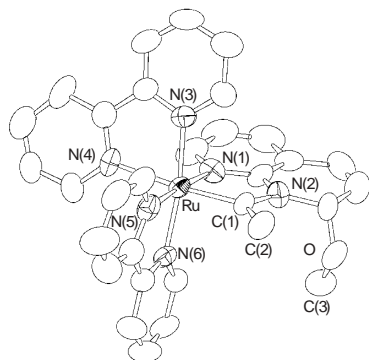
VII-E-3 Characterization of Ru(bpy)₂(CO)(COO) Prepared by CO₂ Addition to Ru(bpy)₂(CO) in Acetonitrile

FUJITA, Etsuko; CHOU, M.; TANAKA, Koji

[*Appl. Organomet. Chem.* **14**, 844 (2000)]

DMF solutions containing $[Ru(bpy)_3]^{2+}$, $[Ru(bpy)_2(CO)X]^{n+}$ (X = Cl, H, $n = 1$ or X = CO, $n = 2$), and triethanolamine (TEOA) as an electron donor have been used for photochemical CO_2 reduction. These homogeneous systems produce $HCOO^-$ and CO as the major and a minor products with a total quantum yield of approximately 15%. The CO_2 reduction system involves a photochemical cycle for $[Ru(bpy)_3]^{2+}$ and a thermal cycle for $[Ru(bpy)_2(CO)X]^{n+}$. The proposed mechanism involves reductive quenching of the $[Ru(bpy)_3]^{2+}$ excited state by TEOA to form $[Ru(bpy)_3]^+$ and reduction of $[Ru(bpy)_2(CO)X]^{n+}$ by two $[Ru(bpy)_3]^+$ molecules to produce $[Ru(bpy)_2(CO)]^0$. The latter reacts with CO_2 to form $[Ru(bpy)_2(CO)(COO)]^0$ as a common intermediate for formate and CO production. $[Ru(bpy)_2(CO)(COO)]^0$ and $[Ru(bpy)_2(CO)(COOH)]^+$ have been previously prepared by addition of two and one equivalent of OH⁻, respectively, to $[Ru(bpy)_2(CO)_2]^{2+}$. An alternative preparation of $[Ru(bpy)_2(CO)(COO)]^0$ from $[Ru(bpy)_2(CO)]^0$ is the reaction of CO_2 with a doubly reduced species generated from $[Ru(bpy)_2(CO)Cl]^+$ in acetonitrile, and the reaction is the key process of CO_2 reduction in the photochemical system.

The CV of $[Ru(bpy)_2(CO)_2]^{2+}$ in acetonitrile indicates that the two-electron reduction wave at –1.0 V *vs.* SCE is not affected by CO_2. Na-Hg reduction of $[Ru(bpy)_2(CO)_2]^{2+}$ produces a very intense blue solution of $[Ru(bpy)(CO)_2]_n$ which does not react with CO_2. The CV of $[Ru(bpy)_2(CO)Cl]^+$ indicates three reduction wave between –1.3 V and –1.9 V. The catalytic current observed under CO_2 depends on the electrolytes. The first reduction seems to be the bpy-centered reduction. Within a few minute, two tiny peaks at 395 and 510 nm disappear, indicating that intra-molecular electron transfer is taking place to form $[RuI(bpy)_2(CO)]$ with loss of a Cl ligand. The mono-reduced species does not react with CO_2.

$$[Ru(bpy)_2(CO)Cl]^{2+} \xrightarrow{\text{NaHg}} [Ru(bpy)_2(CO)]^0 \xrightarrow{CO_2} [Ru(bpy)_2(CO)(CO_2)]^0$$
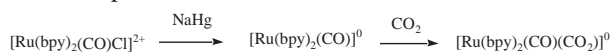
VII-E-4 Ruthenium Terpyridine Complexes with mono- and bi-Dentate Dithiolene Ligands

SUGIMOTO, Hideki; TSUGE, Kiyoshi; TANAKA, Koji

[*J. Chem. Soc., Dalton Trans.* 57 (2001)]

The reaction of $[Ru(CO)_2Cl(trpy)]PF_6$ (trpy = terpyridine) with Na_2mnt (mnt = $S_2C_2(CN)_2$) initially produced $[Ru(CO)_2(mnt-\kappa S)(trpy-\kappa^3 NN'N'')]$ (**1a**), which rearranged to $[Ru(CO)_2(mnt-\kappa^2 S)(trpy-\kappa^2 NN')]$ (**1b**) in solutions. The rearrangement from **1a** to **1b** proceeds via the penta-coordinated complex with monodentate mnt and bidentate trpy. The reaction of $[Ru(CO)_2Cl(trpy)]PF_6$ with 3,4-toluenedithiol (H_2tdt) gave $[Ru(CO)_2(tdt-\kappa^2 S)(trpy-\kappa^2 NN')]$ (**2b**) but $[Ru(CO)_2(tdt-\kappa S)(trpy-\kappa^3 NN'N'')]$ (**2a**) was not identified in the reaction. Thus, ruthenium complexes with bidentate dithiolene and bidentate terpyridine seem to be more stable than those with monodentate dithilene and tridentate terpyridine. Neither $[Ru(CO)_2(pdt-\kappa S)(trpy-\kappa^3 NN'N'')]$ (**3a**) nor $[Ru(CO)_2(pdt-\kappa^2 S)(trpy-\kappa^2 NN'N'')]$ (**3b**) (pdt = PhC(S)C(S)Ph) was obtained in the reaction of $[Ru(CO)_2Cl(trpy)]PF_6$ with Cs^+ salt of 4,5-diphenyl-dithiolate in CH_3OH under N_2. The same reaction conducted under aerobic conditions afforded $[Ru(CO)(C(O)OCH_3)(SC(Ph)C(Ph)(SC(O)OH)(trpy-\kappa^2 NN')]$ (**3**) resulting from double addition of CO_2 and CH_3OH to terminal sulfur of pdt and a carbonyl carbon of **3a**, respectively, follwed by esterification of the resultant $[Ru(CO)(C(O)OCH_3)(SC(Ph)C(Ph)(SC(O)OH)(trpy-\kappa^2 NN')]$ in CH_3OH. The addition of CO_2 to sulfur of **3a** is ascribed to the strong basicity and weak chelating ability of pdt compared with those of mnt and tdt. A series of $[RuX(dithiolene)(trpy)]^{n+}$ (X = dmso, Cl, OSO_2CF_3; $n = 0, 1$) were also prepared.
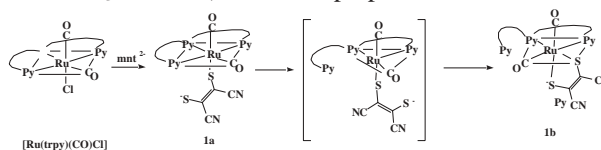
VII-E-5 Syntheses of New Ruthenium Carbonyl Terpyridine *o*-Phenylene Complexes: Strong Interaction Between Carbonyl and *o*-Phenylene Ligands

SUGIMOTO, Hideki; TANAKA, Koji

[*J. Organomet. Chem.* **622**, 280 (2001)]

Ruthenium carbonyl *o*-phenylene complexes, Ru-(CO)(3,6-Bu$_2$seq)(trpy)]PF$_6$ ([**1**]PF$_6$) and [Ru(CO)(*o*-monothiocat)(trpy)] (**2**), were prepared by the reaction of [Ru(CO)Cl$_2$(trpy)] with the corresponding *o*-phenylenes in 2-methoxyethanol. X-ray crystallographic study of [**1**]BF$_4$ indicated that the ruthenium center is coordinated by carbonyl, three nitrogens of trpy and two oxygens of 3,6-Bu$_2$seq. ESR of [**1**]PF$_6$ and **2** indicated that the electronic structures of ruthenium-*o*-phenylene unit of the complexes have Ru(II)-3,6-Bu$_2$seq and Ru(II)-*o*-monothiocat forms, respectively. Significant differences in the redox behavior and the spectroscopical properties between [**1**]PF$_6$ and **2** and [RuCl(3,5-Bu$_2$seq)(trpy)] were ascribed to the strong interaction between *o*-phenylene and carbonyl ligands through Ru(II).
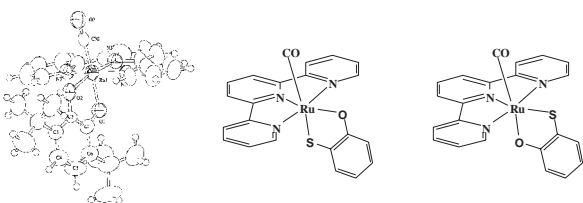
Figure 1. X-ray analysis of [Ru(CO)(*o*-monothiocat)(trpy)]$^+$.

VII-E-6 Structural and Spectroscopic Characterization of Ruthenium(II) Complexes with Methyl, Formyl and Acetyl Groups as Model Species in Multi-Step CO$_2$ Reduction

OOYAMA, Dai[1]; TOMON, Takashi; TSUGE, Kiyoshi; TANAKA, Koji
(*[1]Fukushima Univ.*)

[*J. Organomet. Chem.* **619**, 299 (2001)]

The molecular structures of Ru(II) complexes with methyl, formyl and acetyl groups [Ru(bpy)$_2$(CO)L]$^+$ (L = CH$_3$, C(O)H and C(O)CH$_3$) were examined from the view point of active species in multi-step reduction of CO$_2$ on Ru. The methyl complex was prepared by the reaction of [Ru(bpy)$_2$(OH$_2$)$_2$]$^{2+}$ with trimethylsilyl acetylene and fully characterized by infrared, Raman, ^{13}C NMR and single-crystal X-ray crystallography. Disorder of the Ru–CO and Ru–C(O)H bonds in the crystal structure of the formyl complex made it difficult to determine the bond parameters of the two groups accurately, but the molecular structure of the analogous acetyl complex, which was obtained by the reaction of [Ru(bpy)$_2$(CO$_3$)] with propiolic acid, was determined by X-ray analysis. The ruthenium–carbonyl (Ru–C–O) bond angles of the methyl and acetyl complex with 174(1) and 175.5(5)°, respectively, are in the ranges of

those of previously characterized [Ru(bpy)$_2$(CO)L]$^{n+}$ (L = CO$_2$, C(O)OH, CO and CH$_2$OH). On the other hand, the Ru–CH$_3$ and Ru–C(O)CH$_3$ bond distances showed unusual relationship against the stretching frequency in the raman spectra.
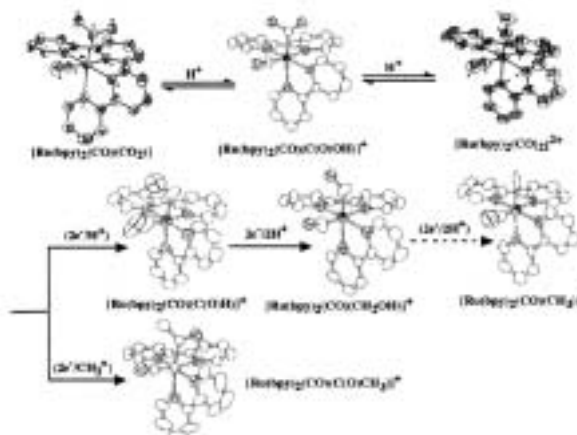
VII-F Synthesis of Transition-Metal Chalcogenido Complexes and Their Cluster-Forming Reactions

Transition-metal chalcogenido aggregates are of well-documented importance in biological systems and industrial processes such as hydrodesulfurization. A wide variety of metal chalcogenido clusters have been synthesized, in which the tetrathiometalato anions have been widely used as a building block. In this project, we are focusing on preparation of chalcogenido/chalcogenolato and silanechalcogenolato complexes as a precursor for cluster syntheses and their cluster-forming reactions.

VII-F-1 Synthesis of a Pentamethylcyclopentadienyl Complex of Tungsten with Three Different Chalcogenido (O^{2-}, S^{2-}, Se^{2-}) Ligands

KAWAGUCHI, Hiroyuki; TATSUMI, Kazuyuki[1]
(*[1]Nagoya Univ.*)

We have synthesized a pentamethylcyclopentadienyl complex of tungsten, $[PPh_4][Cp^*W(O)(S)(Se)]$ (**3**, $Cp^* = \eta^5-C_5Me_5$), in which three different chalcogenide ligands (O^{2-}, S^{2-}, Se^{2-}) are bound to the metal center. This unique mixed-chalcogenide complex is thermodynamically stable, and does not exhibit chalcogen-exchange reactions in solution. The successful route to **3** begins with the high yield synthesis of $[Cp^*W(S)_2Cl]$ (**4**) attained by the reaction between $[Cp^*WCl_4]$ and 1 equiv of $Me_3SiSCH_2CH_2SSiMe_3$. Addition of a small amount of H_2O to a THF solution of **4** under the presence of NEt_3 produced $[Cp^*WS_2O]^-$ (**5**), which was then alkylated by CH_3I or $PhCH_2Br$ to give $[Cp^*W(O)(S)(SR)]$ (R = CH_3 (**6a**), CH_2Ph (**6b**)). Finally, a terminal selenide was introduced by the reaction of **6a** or **6b** with Li_2Se_2 and PPh_4Br leading to the desired oxo/thio/seleno complex $[PPh_4][Cp^*W(O)(S)(Se)]$ (**3**).

VII-F-2 Synthesis and Reactions of Triphenylsilanethiolato Complexes of Manganese(II), Iron(II), Cobalt(II), and Nickel(II)

KOMURO, Takashi[1]; KAWAGUCHI, Hiroyuki; TATSUMI, Kazuyuki[1]
(*[1]Nagoya Univ.*)

Treatment of $Fe[N(SiMe_3)_2]_2$ with 1 and 2 equiv of Ph_3SiSH in hexane afforded $[Fe\{N(SiMe_3)_2\}(\mu–SSiPh_3)]_2$ **1** and $[Fe(SSiPh_3)(\mu–SSiPh_3)]_2$ **2**, respectively. Complex **2** reacted with Lewis bases to form the adducts $Fe(SSiPh_3)_2(L)_2$ [L = CH_3CN **3a**, 4-$^tBuC_5H_4N$ **3b**, PEt_3 **3c**, $(L)_2$ = tmeda **3d**]. The reactions of $M[N(SiMe_3)_2]_2$ (M = Mn, Co) with Ph_3SiSH in the presence of TMEDA gave rise to the corresponding silanethiolato complexes $M(SSiPh_3)_2(tmeda)$ (M = Mn **4**, Co **5**). The analogous reaction using $[Ni(NPh_2)_2]_2$ generated $Ni(SSiPh_3)_2(tmeda)$ **6**. The reaction of **3a** with $(PPh_4)_2[MoS_4]$ produced the linear trinuclear complex $(PPh_4)_2[MoS_4\{Fe(SSiPh_3)_2\}_2]$ **7**, while **3a** reacted with $(NEt_4)_2[FeCl_4]$ to afford $(NEt_4)_2[Fe_2(SSiPh_3)_2Cl_4]$ **8**. The reaction of **3a** with $[Cu(CH_3CN)_4](PF_6)$ gave the cyclic tetranuclear complex $Cu_4(SSiPh_3)_4$ **9**, in which a ligand transfer reaction occurred. Finally, when **5** was treated with $(NBu_4)F$ in THF containing PPh_3, silicon-sulfur bond cleavage took place to produce the cobalt-sulfido cluster $Co_6(\mu_3–S)_8(PPh_3)_6$ **10**.

Figure 1.

Figure 1.

i) H_2O/Et_3N / THF,   ii) PPh_4Br / CH_3CN
iii) $PhCH_2Br$ or CH_3I / THF
iv) Li_2Se_2 / THF
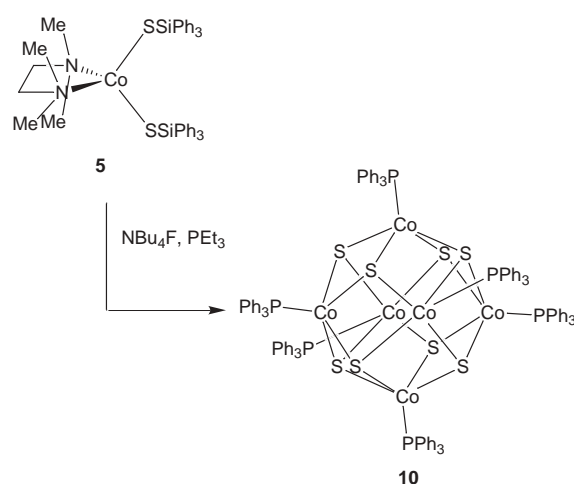
VII-G Synthesis of Compounds Having a Novel Bonding Containing Heavier Main Group Element

Low-coordinate species of main group elements of the second row such as carbenes, olefins, carbonyl compounds, aromatic compounds, and azo compounds play very important roles in organic chemistry. However, the chemistry of their heavier element homologues has been undeveloped most probably due to their high reactivity and instability under ambient conditions. Since the first isolation of stable diphosphene (P=P), silene (Si=C), and disilene (Si=Si) in 1981 by taking advantage of steric protection, various double-bond compounds containing heavier main group elements have been synthesized and characterized.

On the other hand, we have developed an extremely bulky aromatic substituent, 2,4,6-tris[bis(trimethylsilyl)-methyl]phenyl (denoted as Tbt hereafter) and 2,6-bis[bis(trimethylsilyl)methyl]-4-tris(trimethylsilyl)methylphenyl (denoted as Bbt hereafter). These substituents were found to be very effective steric protection groups for a variety of reactive species containing a heavier main group element. We have synthesized a variety of unprecedented low-coordinate compounds of heavier main group elements as stable compounds by taking advantage of kinetic stabilization using a new type of steric protection groups, Tbt and Bbt, and elucidated their properties.

VII-G-1 Separation of Orientational Disorder in the X-Ray Analysis of the Kinetically Stabilized 2-Silanaphthalene

WAKITA, Keiji[1]; TOKITOH, Norihiro[2]; OKAZAKI, Renji[1]
(*[1]Univ. Tokyo; [2]IMS and Kyoto Univ.*)

[*Bull. Chem. Soc. Jpn.* **73**, 2157 (2000)]

Cyclic electron delocalization of aromatic compounds distinctly appeared in their structure as bond length equalization. In view of the proximity in the periodic table, silicon analogues of aromatic compounds are expected to show similar structural features. However, silaaromatic compounds are highly reactive and have been observed only in low-temperature matrices or in the gas phase, except for charged systems. During the course of our study on neutral silaaromatic compounds, we have succeeded in the synthesis of the first stable 2-silanaphthalene **1** by taking advantage of an extremely bulky Tbt group. The structure of **1** was determined by X-ray crystallographic analysis, however, the severe disorder around the 2-silanaphthalene ring of **1** prevented us from discussing the detailed structure of **1** based on the X-ray analysis. Here, we report the refined crystallographic structural analysis of **1**.

The crystal structure of the stable 2-silanaphthalene **1** was refined more adequately by the separation of the disorder of overlapped two 2-silanaphthalene moieties. The bond lengths of the 2-silanaphthalene ring were in fairly good agreement with the theoretically calculated values which we previously reported.
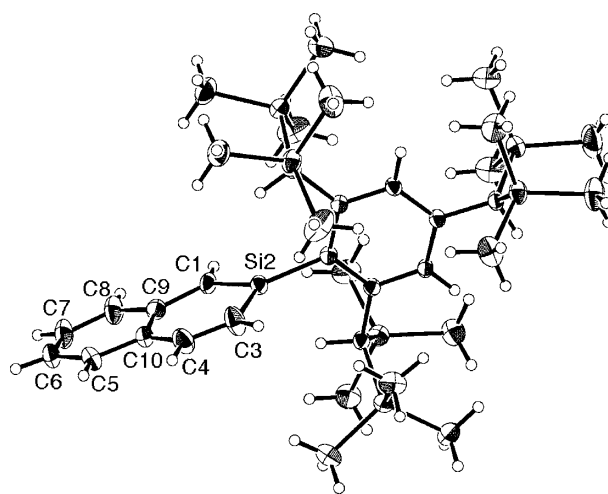
Figure 1. ORTEP drawing of 2-silanaphthalene **1** (major fragment).

VII-G-2 The First Chemical Trapping of Stibinidene, a Monovalent Antimony Compound

SASAMORI, Takahiro[1]; ARAI, Yoshimitsu[2]; TAKEDA, Nobuhiro[3]; OKAZAKI, Renji[2]; TOKITOH, Norihiro[4]
(*[1]Kyushu Univ.; [2]Univ. Tokyo; [3]Kyoto Univ.; [4]IMS and Kyoto Univ.*)

[*Chem. Lett.* 42 (2001)]

In recent decades, there has been much interest in the chemistry of monovalent species of heavier group 15 elements. Phosphinidenes (R–P̈:), phosphorus analogues of nitrenes, have long been postulated as reactive intermediates. Stibinidenes (R–S̈b:) are also interesting monovalent species of group 15 elements, but no stibinidene has been detected or trapped so far probably due to its extremely high reactivity. On the other hand, we have recently succeeded in the synthesis and characterization of the first stable distibene (TbtSb=SbTbt, **1**) and dibismuthene (TbtBi=BiTbt) by taking advantage of an efficient steric protection group, Tbt. In the final step for the synthesis of distibene **1**, that

is, deselenation reaction of (TbtSbSe)₃ (**2**) with hexamethylphosphorous triamide (HMPT), it is rational to postulate the initial formation of a stibinidene (Tbt–Sb:, **3**) as an intermediate. In this paper we wish to present the first successful trapping reaction of the intermediary stibinidene.

Deselenation of 1,3,5-trislena-2,4,6-tristibane **2** in the presence of 1,3-butadienes resulted in the formation of the corresponding [1+4]cycloadducts **4a,b** of a sterically hindered stibinidene **3**, a monovalent species of antimony. Thermal generation of **3** form **4a,b** via retro [1+4]cycloaddition reaction was suggested by the diene-exchange reaction in thermolysis of **4a,b** in the presence of another butadiene derivative.
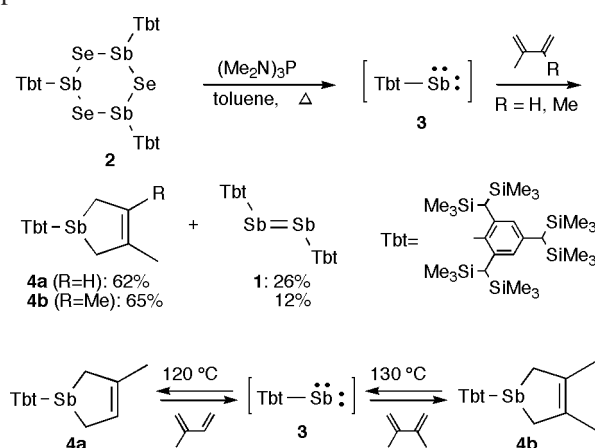
VII-G-3 Formation of Antimony-Sulfur Double-Bond Compounds and Their Trapping with Nitrile Oxides

**TOKITOH, Norihiro[1]; ARAI, Yoshimitsu[2];
SASAMORI, Takahiro[3]; TAKEDA, Nobuhiro[4];
OKAZAKI, Renji[2]**
(*[1]IMS and Kyoto Univ.; [2]Univ. Tokyo; [3]Kyushu Univ.;
[4]Kyoto Univ.*)

The chemistry of compounds featuring double-bond containing heavier group 15 elements has attracted attention in recent years. As for the low-coordinated double-bond compounds between group 15 and group 16 elements, dithioxophosphorane [RP(S)=S] and diselenoxophosphorane [RP(Se)=Se] have been synthesized as stable compounds, and thioxophosphines [RP=S] and selenoxophosphines [RP=Se] stabilized by the coordination of an amino group have been observed in solution by NMR spectroscopy. However, there are no reports about the double bond of antimony with sulfur. In this paper, we describe the formation of thioxostibine [TbtSb=S (**1**)] and dithioxostiborane [TbtSb(S)=S (**2**)] intermediates, which is confirmed by trapping reactions with nitrile oxides.

The reaction of a highly crowded dihydrostibine **3** with elemental sulfur in the presence of nitrile oxides resulted in the formation of [2+3]cycloaddition reaction products of a thioxostibine [TbtSb=S (**1**)] and a dithioxostiborane [TbtSb(S)=S (**2**)], which are among a novel class of antimony–sulfur double bond

compounds. The structures of the [2+3]cycloadducts of dithioxostiborane **2** with nitrile oxides were determined by X-ray structural analysis. Desulfurization of highly crowded antimony-containing cyclic polysulfides [TbtSbSₓ (*x* = 5 or 7)] with phosphine reagents also resulted in the formation of **1** and **2**.
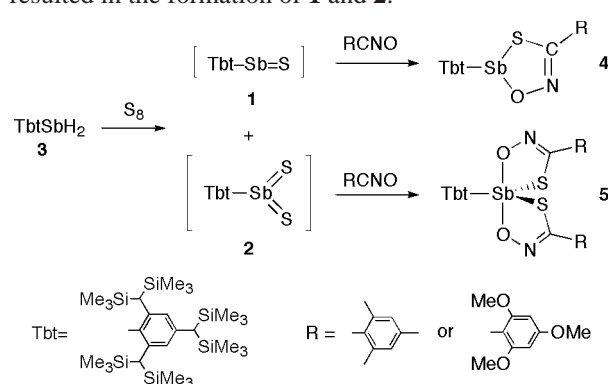
VII-G-4 Synthesis, Structures, and Reactivities of Novel Silacyclic Systems: The First Stable Silabenzene and Silacyclopropabenzene

TOKITOH, Norihiro[1]
(*[1]IMS and Kyoto Univ.*)

In the last two decades, kinetic stabilization has played an important role in the synthesis and isolation of a variety of heavier main group element compounds having an exotic structure and novel bonding. We have developed an extremely bulky and efficient steric protection group, Tbt, and applied it to the kinetic stabilization of highly reactive species of heavier main group elements. In this paper, the synthesis and isolation of the first stable silabenzene and siacyclopropabenzene are described as further application of Tbt group to the kinetic stabilization of novel conjugated ring systems containing a silicon atom.

The first stable silabenzene **2** was synthesized by the reaction of the corresponding chlorosilane **1** with (*i*-Pr)₂NLi. The crystal structure and spectroscopic properties of **2** indicated that silabenzene **2** has a completely planar, delocalized 6π-electron ring system as in the case of benzene. Interestingly, irradiation of a benzene solution of **2** with the light of 290–350 nm resulted in the formation of an unprecedented valence isomer, silabenzvalene **3**.
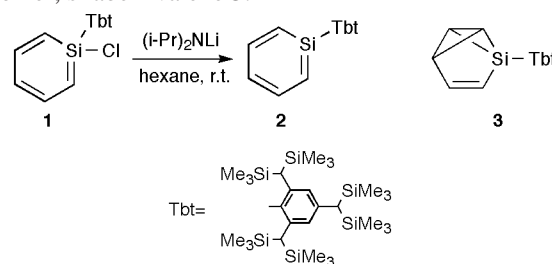
On the other hand, an overcrowded diaryldilithiosilane **4** was allowed to react with *o*-dibromobenzene to give the first stable silacyclopropabenzene **5**, which was

fully characterized by NMR spectra, FAB-MS, and X-ray structural analysis. The silacyclopropabenzene **5** thus obtained was found to be thermally very stable and have a completely planar geometry but a slightly squashed benzene ring. The crystallographic analysis revealed that no distinct bond localization is observed for the benzene moiety in contrast to its carbon analogue, *i.e.* cyclopropabenzene.
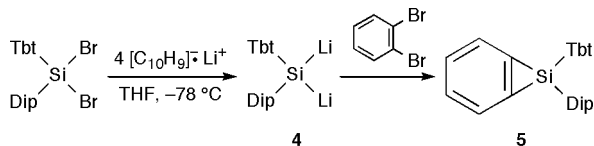
VII-G-5 Synthesis and Reactivities of the First Stable Stibabismuthene

SASAMORI, Takahiro[1]; TAKEDA, Nobuhiro[2]; TOKITOH, Norihiro[3]
(*[1]Kyushu Univ.; [2]Kyoto Univ.; [3]IMS and Kyoto Univ.*)

In recent years there has been much interest in compounds with a double bond between heavier group 15 elements. As for the case of heteronuclear double-bond compounds between heavier group 15 elements, several phosphaarsenes [RP=AsR] and phosphastibenes [RP=SbR] have been synthesized as stable compounds. However, there is no example of a heteronuclear doubly bonded system between antimony and bismuth, *i.e.* stibabismuthene. Recently, we have succeeded in the synthesis and characterization of the first stable distibene and dibismuthene [Ar–E=E–Ar (E = Sb, Bi; Ar = Tbt, Bbt)] by taking advantage of an efficient steric protection group, Tbt or Bbt group. We now report the successful application of the Bbt group to the synthesis of the first stable stibabismuthene, BbtSb=BiBbt (**1**).

The condensation reaction of an overcrowded dihydrostibine with dibromobismuthine using 1,8-diazabicyclo[5.4.0]undec-7-ene as a base afforded the first stable stibabismuthene **1**, the formation of which was evidenced by UV-vis and Raman spectra and its chemical reactivity. Thermolysis or photolysis of **1** resulted in the disproportionation reaction into the homonuclear double-bond species, distibene **2** and dibismuthene **3**.
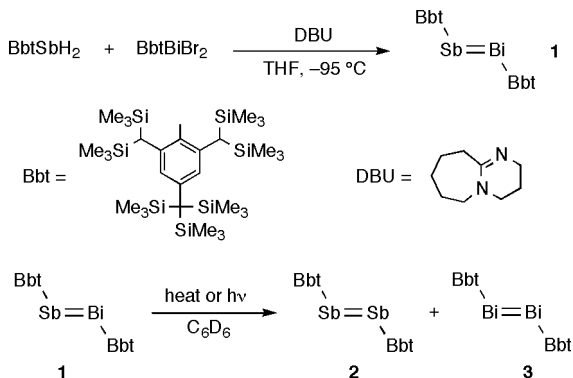
VII-G-6 Reaction of Stable Silylene–Isocyanide Complexes with BH₃·THF

TAKEDA, Nobuhiro[1]; KAJIWARA, Takashi[1]; TOKITOH, Norihiro[2]
(*[1]Kyoto Univ.; [2]IMS and Kyoto Univ.*)

In recent decades, much attention has been paid to the chemistry of silylenes (silicon analogues of carbenes). Also, silylene complexes with Lewis bases have been extensively studied and some complexes have been synthesized in low temperature matrices so far. However, their properties have not been fully disclosed yet due to their instability at ambient temperature. On the other hand, we have recently succeeded in the synthesis of the first stable silylene–Lewis base complexes **1a,b** by taking advantage of an efficient steric protection group, Tbt group. In this paper, we describe the reactivity of **1a,b** with BH₃·THF.

Stable silylene–isocyanide complexes **1a,b** reacted with BH₃·THF to give the first stable silylborane–isocyanide complexes **2a,b**. The structures of **2a,b** were determined by NMR, IR, and mass spectrometry, elemental analysis, and X-ray crystallographic analysis. Thermolysis of **2a** at 120 °C gave a 1:5 mixture of **2a** and the corresponding migration product **3a** in contrast to the previously reported intermediary silylborane–isocyanide complexes [PhMe₂SiBX₂ ← CNR], which is known to give the corresponding (boryl)(silyl)imino-methanes [(PhMe₂Si)(X₂B)C=NR] as final products. Since the isolated compound **3a** also affords the 1:5 mixture of **2a** and **3a** by heating at 120 °C, the existence of an equilibrium between **2a** and **3a** is strongly suggested.
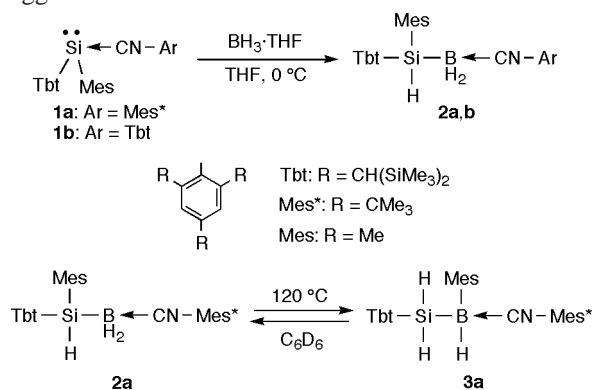
VII-G-7 Synthesis and Properties of the First Stable Germanaphthalene

NAKATA, Norio[1]; TAKEDA, Nobuhiro[1]; TOKITOH, Norihiro[2]
(*[1]Kyoto Univ.; [2]IMS and Kyoto Univ.*)

In recent years much attention has been focused on germaaromatic compounds, since they are among heavier congeners of aromatic hydrocarbons which play

very important roles in organic chemistry. Some ionic germaaromatic compounds have been successfully synthesized as stable compounds, while no isolation of a neutral germaaromatic compound has been reported probably due to its high reactivity. On the other hand, we have recently succeeded in the synthesis of kinetically stabilized silabenzene and 2-silanaphthalene, the first examples of stable neutral silaaromatic compounds, by taking advantage of an efficient steric protection group, Tbt group. Here, we report the synthesis and structure of 2-germanaphthalene **1** kinetically stabilized by the Tbt group, the first stable neutral germaaromatic compound.

The first stable 2-germanaphthalene **1** was synthesized by the dehydrobromination of bromoger-mane **2** with (i-Pr)$_2$NLi in THF at room temperature. The molecular structure of **1** was fully characterized by its ^{1}H and ^{13}C NMR spectra, which indicate the delocal-ized π–electronic structure of **1**. Moreover, the low-temperature X-ray crystallographic analysis of **1** revealed that 2-germanaphthalene ring was almost planar and the benzene ring of Tbt group was almost perpendicular to the 2-germanaphthalene ring. In addition, all the ^{1}H and ^{13}C NMR chemical shifts and the structural parameters of **1** experimentally obtained are in good agreement with the values theoretically calculated for some model compounds. UV-vis and Raman spectra of **1** also supported the aromatic character of the 2-germanaphthalene ring system.
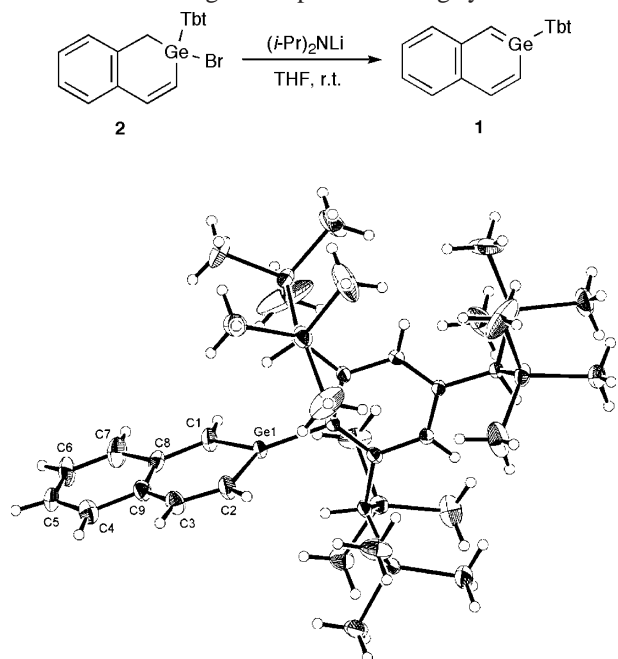
Figure 1. ORTEP drawing of 2-germanaphthalene **1**.

VII-H Development of Coordination Chemistry-based Strategies for Structural and Functional Modulation of Naturally Occurring Proteins or Enzymes

New methodologies based on coordination chemistry are actively developed which one can modulate or switch a structure and a function of naturally occurring proteins and enzymes. Using coordination chemistry on a specific site of a protein or peptide, we aim to explore a new functional molecules or chemistry-based strategy that can selectively recognize a specific surface of a protein and/or modulate its characteristic structure. Such molecules and methodologies would be expected to lead to functional change and regulation of complicated bio-macromolecules.

VII-H-1 Guest-Induced Umpolung on a Protein Surface: A Strategy for Regulation of Enzymatic Activity

HAMACHI, Itaru[1,2]; **EBOSHI, Ryoji**[1]; **WATANABE, Jun-ichi**; **SHINKAI, Seiji**[1]
(*[1]Kyushu Univ.; [2]IMS*)

This manuscript describes a new strategy to introduce an on-off switch to an engineered enzyme. We successfully demonstrated that the transition metal ion-induced charge inversion (*i.e.*, guest-induced Umpolung) occurred on a surface of semisynthetic ribonuclease S' efficiently causes sharp on-off switching of enzymatic activity. Semisynthetic ribonuclease S' (RNase S'), an RNA hydrolyzing enzyme, was employed as a suitable model. As a surface charge modulator, an unnatural amino acid bearing iminodiacetic acid group (Ida[4]) was incorporated into the S-peptide region of RNase S' by solid phase peptide synthesis. The mutant S-peptides were combined to S-protein by a self-assemble manner. The charge of the side chain of Ida[4] is a mono*anion* at neutral pH and it is inverted to a mono*cation* upon complexation with a trivalent metal cation such as Fe(III) at its iminodiacetic acid moiety. Based on the kinetic assay using single mutants, it is clear that the response to metal ions greatly depends on the charge of the original amino acid, that is, the Fe(III)-induced activity enhancement occurs at positively charged Lys or Arg site and the activity suppression occurs at negatively charged Glu or Asp site. A rationally designed double mutant displayed the sharp on-off switching (10–20 fold) of enzymatic activity which is sensitive to iron(III) concentration.

VII-H-2 Pd(en) as a Sequence-Selective Molecular Pinch for α-Helical Peptides

HAMACHI, Itaru[1,2]; **KASAGI, Noriyuki**[1]; **KIYONAKA, Shigeki**[1]; **NAGASE, Tsuyoshi**[1]; **MITO-OKA, Yasuko**[1]; **SHINKAI, Seiji**[1]
(*[1]Kyushu Univ.; [2]IMS*)

A palladium(II) ethylenediamine complex was found to selectively stabilize a-helix conformation of peptides having two histidine (His) residues at *i* and *i* + 3 or 4 positions, whereas the helix conformation of the other peptides having one or two His at different positions is destabilized. Based on CD titration, NMR spectral observation and molecular modeling calculation, we established that Pd(en) is a versatile molecular unit for binding to peptides bearing two His at a specific pattern in aqueous solution. The ethylenediamine moiety in this organometallic receptor can be chemically modified with the combination to other binding interactions, so as to facilitate the more selective binding and modulation of a protein surface. This is sharply distinguished from the simple metal ions previously reported by other researchers.

VII-H-3 Zn(II) Dipicolylamine-Based Artificial Receptor as a New Entry for Surface Recognition of α-Helical Peptides in Aqueous Solution

MITO-OKA, Yasuko[1]; **TSUKIJI, Shinya**[1]; **HIRAOKA, Takashi**[1]; **KASAGI, Noriyuki**[1]; **SHINKAI, Seiji**[1]; **HAMACHI, Itaru**[1,2]
(*[1]Kyushu Univ.; [2]IMS*)

Artificial receptors for bioactive peptides are actively developed in the field of the recent molecular recognition chemistry, because of their importance for the peptide sensing and pharmaceutical application. However, the recognition events have been exploited in organic solvents in the most cases, which are still far from the biological prospects. For the development of artificial receptors that can selectively bind a peptide/protein surface so as to inhibit or enhance the function, it is desirable to establish a design strategy for artificial receptors toward a peptide surface in aqueous solution. We describe herein that zinc(II) dipicolylamine (Zn(Dpa))-based coordination chemistry is promising for design of artificial receptors in aqueous solution toward α-helical peptides displaying two Histidine(His) on their surface ($H − i$ and $i + 4$, or $H − i$ and $i + 7$, or $H − i$ and $i + 11$). The spatial juxtaposition by a modular connector greatly influences the affinity to these peptides. To the best of our knowledge, this is the first example for the artificial receptors that can selectively bind peptides bearing two His in the distance of two or three helix pitches in perfectly aqueous solution. This motif can be readily combined with other binding motifs, so that one can design the more selective and

efficient artificial receptors toward a peptide or protein.

VII-I Synthesis and Functionality of Organometallic Dendrimers

Dendrimers are three-dimensional macromolecules with regularly hyperbranched structures, and have a wide range of potentials applicable to new functional materials. Organometallic dendrimers have attracted much attention due to their unique functions based on photochemical, redox and catalytic behaviors. This project focuses on the development of new synthetic routes toward the dendrimers that consist of organometallic species in every generation. We also examine the physical and chemical properties of these organometallic dendrimers.

VII-I-1 Living Polymerization of Aryl Isocyanides by Multifunctional Initiators Containing Pd–Pt μ-Ethynediyl Units

OHSHIRO, Nobuaki[1]; SHIMIZU, Atsushi[1]; OKUMURA, Reiko[1]; TAKEI, Fumie[1]; ONITSUKA, Kiyotaka[2]; TAKAHASHI, Shigetoshi[1]
(*[1]Osaka Univ.; [2]Osaka Univ. and IMS*)

[*Chem. Lett.* 786 (2000)]

Multinuclear acetylide complexes containing two or three Pd–Pt μ-ethynediyl units have been prepared and successfully applied to a multifunctional initiator for the living polymerization of aryl isocyanides, which gives two- or three-armed poly(isocyanide)s with a narrow polydispersity index in good yields.
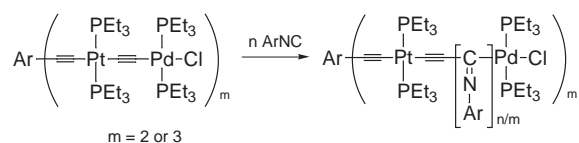
VII-I-2 Synthesis of Hyperbranched Platinum-Poly(yne) Polymers by Self Polycondensation

ONITSUKA, Kiyotaka[2]; OHSHIRO, Nobuaki[1]; FUJIMOTO, Masanori[1]; TAKEI, Fumie[1]; TAKAHASHI, Shigetoshi[1]
(*[1]Osaka Univ.; [2]Osaka Univ. and IMS*)

[*Mol. Cryst. Liq. Cryst.* **342**, 159 (2000)]

A hyperbranched polymer constructed by platinum-acetylide units has been synthesized by self poly-condensation of a dinuclear platinum complex having one terminal acetylene and two platinum-chloride groups as an AB_2 monomer in the presence of a copper catalyst in amine. The hyperbranched polymer is soluble in common organic solvents and characterized by means of spectral analyses and GPC.

VII-I-3 Synthesis of Organometallic Dendrimers by Ligand Exchange Reactions: Reversible Bonding of Dendrons to a Core in Transition Metal Acetylide Dendrimers

ONITSUKA, Kiyotaka[2]; IUCHI, Asako[1]; FUJIMOTO, Masanori[1]; TAKAHASHI, Shigetoshi[1]
(*[1]Osaka Univ.; [2]Osaka Univ. and IMS*)

[*Chem. Commun.* 741 (2001)]

Ligand exchange reactions of chloride ligands on a trinuclear palladium acetylide core with platinum acetylide dendrons having a 4-pyridyl group at a focal point result in the quantitative formation of novel organometallic dendrimers, which easily revert to the core and the dendrons by treatment with Bu_4NCl.
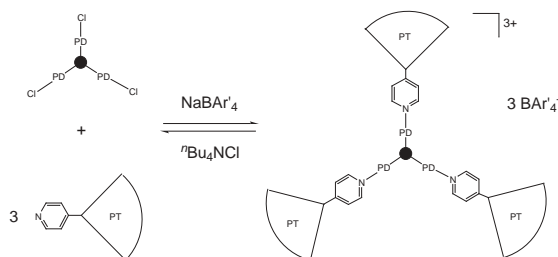
RESEARCH ACTIVITIES VIII
Laser Research Center for Molecular Science

VIII-A Developments and Researches of New Laser Materials

Although development of lasers is remarkable, there are no lasers which lase in ultraviolet and far infrared regions. However, it is expected that these kinds of lasers break out a great revolution in not only the molecular science but also in the industrial world.

In this project we research characters of new materials for ultraviolet and far infrared lasers, and develop new lasers by using these laser materials.

VIII-A-1 Supercritical-Fluid Cell with Device of Variable Optical Path Length Giving Fringe-Free Terahertz Spectra

SAITOW, Ken-ichi[1]; NISHIKAWA, Keiko[1]; OHTAKE, Hideyuki; SARUKURA, Nobuhiko; MIYAGI, Hiroshi[2]; SHIMOKAWA, Yuji[2]; MATSUO, Hitoshi[3]; TOMINAGA, Keisuke[4]
(*[1]Chiba Univ.; [2]Gakushuin Univ.; [3]Matsuo Kogyosho, Inc.; [4]Kobe Univ.*)

An optical cell suitable for supercritical fluids was constructed for measurements of far infrared absorption spectra with terahertz radiation as a light source. It was designed to withstand temperature up to 400 K and pressure up to 15 MPa. The cell has two characteristic devices; one is diamond windows set in the Brewster angle to the incident far infrared light and the other is a variable optical path length from 30 μm to 20 mm under high pressure conditions. Using the cell, fringe-free spectra of CHF_3 ranging from low-density gaseous states to high-density supercritical ones were measured in a low-energy region of 10–100 cm^{-1}.
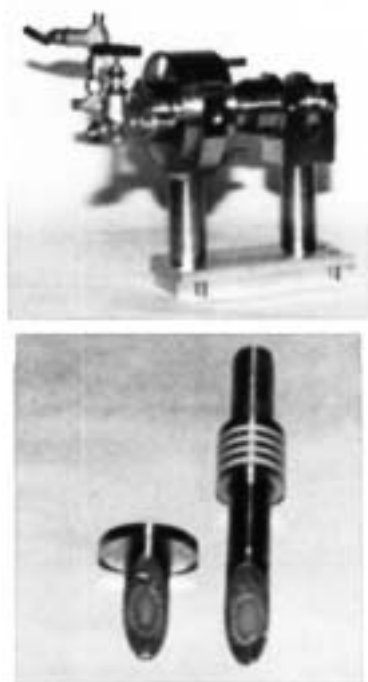
Figure 1. Photographs of an optical cell for far infrared absorption spectra measurements of supercritical fluids. The cell itself is shown in the upper part. The lower part represents flanges with diamond windows set in the Brewster angle, a cylinder, and a V packing.

VIII-A-2 Growth and Characterization of $KMgF_3$ Single Crystals by the Czochralski Technique under CF_4 Atmosphere

SHIMAMURA, Kiyoshi[1]; FUJITA, Tomoyo[1]; SATO, Hiroki[1]; BENSALAH, Amina[1]; SARUKURA, Nobuhiko; FUKUDA, Tsuguo[1]
(*[1]Tohoku Univ.*)

$KMgF_3$ (KMF) single crystals were grown by the Czochralski technique as a new candidate of vacuum-ultra-violet optical materials. The absorption edge of KMF single crystals was 115 nm. The distribution of birefringence in the radial direction was of the order of 10^{-7}. The thermal expansion coefficient of KMF single crystals along the <111> orientation was 1.98×10^{-5} K^{-1}. Together with its excellent mechanical properties, these characteristics show KMF to be superior to the current materials.
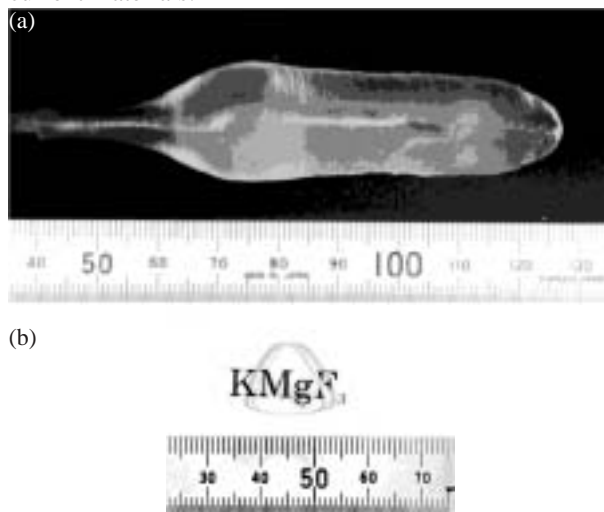
Figure 1. (a) As-grown $KMgF_3$ single crystal of 20 mm diameter pulled along the <111> orientation and (b) $KMgF_3$-wafer cut perpendicular to the growth axis with thickness of 2 mm.

VIII-A-3 Chirped-Pulse Amplification of Ultraviolet Femtosecond Pulses by Use of Ce^{3+}:LiCaAlF[6] as a Broadband, Solid-State Gain Medium

LIU, Zhenlin[1]; KOZEKI, Toshimasa; SUZUKI, Yuji; SARUKURA, Nobuhiko; SHIMAMURA, Kiyoshi[2]; FUKUDA, Tsuguo[2]; HIRANO, Masahiro[1]; HOSONO, Hideo[1,3]
(*[1]ERATO; [2]Tohoku Univ.; [3]Tokyo Inst. Tech.*)

Chirped-pulse amplification in the ultraviolet region is demonstrated by use of a broadband Ce^{3+}:LiCaAlF[6] laser medium. A modified bow-tie-style four-pass amplifier pumped by 100-mJ, 266-nm pulses from a *Q*-switched Nd:YAG laser has a gain factor of 370 and delivers 6-mJ, 290-nm pulses. After dispersion compensation, the output pulses can be compressed to 115 fs.
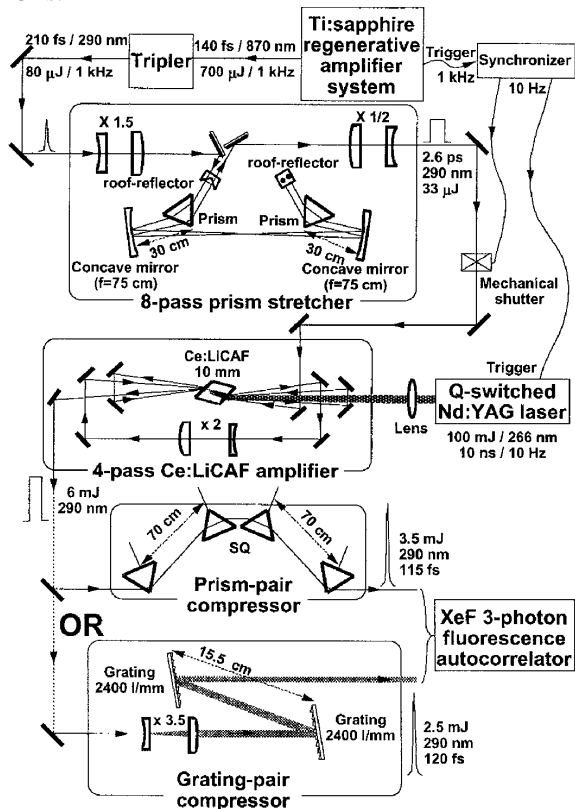
Figure 1. Experimental setup of the Ce:LiCAF CPA laser system. SQ, synthetic quartz.

VIII-A-4 Terahertz Radiation from a Shallow Incidence-Angle InAs Emitter in a Magnetic Field Irradiated with Femtosecond Laser Pulses

ONO, Shingo[1]; TSUKAMOTO, Takeyo[1]; KAWAHATA, Eiji; YANO, Takayuki; OHTAKE, Hideyuki; SARUKURA, Nobuhiko
(*[1]Sci. Univ. Tokyo*)

The optimized incidence angle and magnetic field direction geometry of an InAs terahertz radiation emitter irradiated with femtosecond laser pulses in a magnetic field is reported. The optimum geometric layout is the magnetic field direction parallel to the semiconductor surface and at an incidence angle that is slightly larger than the Brewster angle. Additionally, we also observed a center frequency shift of terahertz radiation spectrum by changing the incidence angle of the excitation laser.
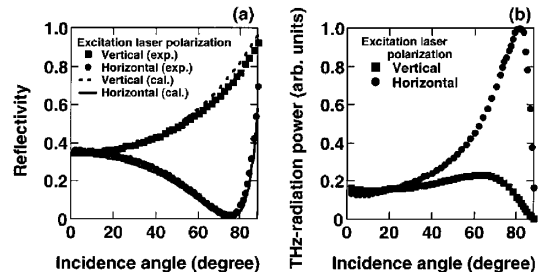
Figure 1. Angular dependence of (a) 800-nm excitation laser reflectivity and (b) THz radiation intensity from InAs. The solid and dotted curves represent the results of our theoretical calculations for $n = 3.729$ and $k = 0.448$.

VIII-A-5 Crystal Growth of Ce-Doped and Undoped LiCaAlF[6] by the Czochralski Technique under CF[4] Atmosphere

SHIMAMURA, Kiyoshi[1]; BALDOCHI, Sonia L.[1]; RANIERI, Izilda M.[1]; SATO, Hiroki[1]; FUJITA, Tomoyo[1]; MAZZOCCHI, Vera L.[2]; PARENTE, Carlos B. R.[2]; PAIVA-SANTOS, Carlos O.[3]; SANTILLI, Celso V.[3]; SARUKURA, Nobuhiko; FUKUDA, Tsuguo[1]
(*[1]Tohoku Univ.; [2]Nucleares-IPEN/CNEN-SP; [3]UNESP*)

Ce-doped and undoped LiCaAlF[6] (LiCAF) single crystals 50 mm in diameter were grown by the Czochralski technique. The formation of inclusions and cracks accompanying the crystal growth was investigated. The dependence of lattice parameters on the temperature was measured for LiCAF and LiSrAlF[6] single crystals. Linear thermal expansion coefficients for both these crystals were evaluated. Higher transmission properties for LiCAF single crystals were achieved in the UV and VUV wavelength regions.
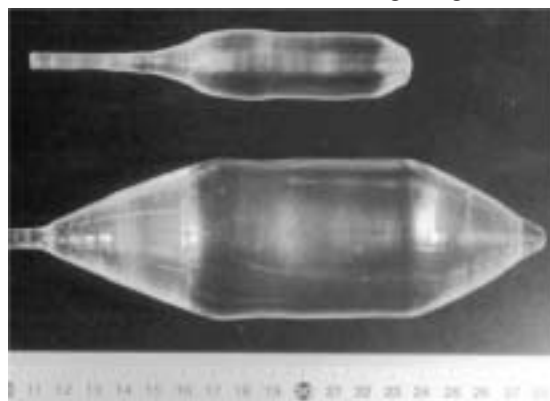
Figure 1. As-grown 2" diameter Ce-doped LiCaAlF[6] single crystal.

VIII-A-6 Ultraviolet Femtosecond Pulse Amplification with High Gain Using Solid-State, Broad-Band Gain Medium Ce³⁺:LiCaAlF₆

LIU, Zhenlin[1]; KOZEKI, Toshimasa; SUZUKI, Yuji; SARUKURA, Nobuhiko; SHIMAMURA, Kiyoshi[2]; FUKUDA, Tsuguo[2]; HIRANO, Masahiro[1]; HOSONO, Hideo[1,3]
(*[1]ERATO; [2]Tohoku Univ.; [3]Tokyo Inst. Tech.*)

Femtosecond pulse amplification with high gain in the ultraviolet region has been demonstrated using the solid-state, broad-band crystal Ce³⁺:LiCaAlF₆. With the seed pulses coming from the third harmonic generation of a cw mode-locked Ti:sapphire laser, the confocal, four-pass amplifier pumped by 15-mJ, 266-nm, 10-ns pulses from a Q-switched Nd:YAG laser demonstrates 60-dB gain and delivers 54-μJ, 289-nm, 200-fs, 10-Hz pulses. There is almost no satellite pulse even without any special single-pulse selection.
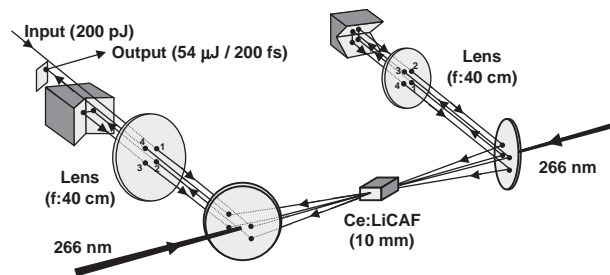
Figure 1. Experimental setup of the confocal, four-pass Ce:LiCAF amplifier. The input is the frequency-tripled output of a cw mode-locked femtosecond Ti:sapphire laser.

VIII-A-7 Terahertz Absorption Spectra of Supercritical CHF₃ to Investigate Local Structure Through Rotational and Hindered Rotational Motions

SAITOW, Ken-ichi[1]; OHTAKE, Hideyuki; SARUKURA, Nobuhiko; NISHIKAWA, Keiko[1]
(*[1]Chiba Univ.*)

Far infrared absorption spectra of neat supercritical fluoroform (CHF₃) are measured with terahertz (THz) radiation. The spectra covering from 10 to 100 cm⁻¹ are obtained at reduced temperature $T/T_c = 1.02$ on densities varied by a factor of 200. As density increases, dominant component of spectra changes from rotational to hindered-rotational motion. However, the change is nonlinear to the density. Such specificity arises from difference between bulk and local densities, and the most enhanced local density is observed near the thermodynamic state of maximum density fluctuation. In the pure fluid system, the relationship between density fluctuation and local density enhancement is experimentally presented.
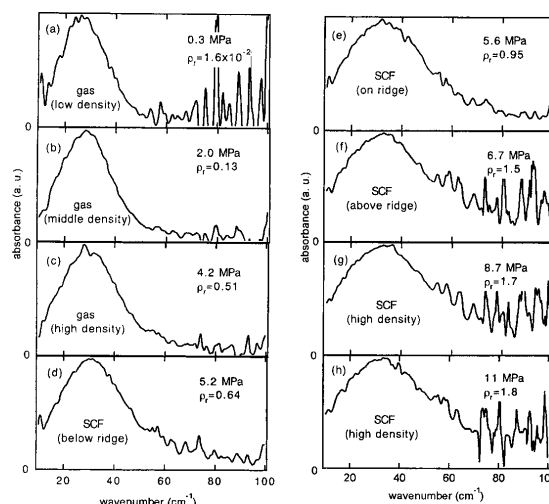
Figure 1. Far infrared absorption spectra of supercritical CHF₃ measured at reduced temperature by $T_r = T/T_c = 1.02$. The (a)–(c) are data below critical pressure (P_c) and (d)–(h) those of above P_c. The (d), (e), and (f) are ones below, on, and above the ridge, respectively. The (g) and (h) are ones at dense supercritical states above the ridge.

VIII-A-8 Observation of New Excitation Channel of Ceriumion through Highly Vacuumultraviolet Transparent LiCAF Host Crystal

KOZEKI, Toshimasa; SUZUKI, Yuji; SAKAI, Masahiro; OHTAKE, Hideyuki; SARUKURA, Nobuhiko; LIU, Zhenlin; SHIMAMURA, Kiyoshi[1]; NAKANO, Kenji; FUKUDA, Tsuguo[1]
(*[1]Tohoku Univ.*)

The transmission spectra of LiCaAlF₆ (LiCAF) and LiSrAlF₆ (LiSAF) are investigated in the ultraviolet (UV) and the vacuum ultraviolet (VUV) region. The transmission edge of LiCAF (112 nm) shows almost the same value as that of LiF. Taking into account difficulties of material processing and polishing due to the cleavage or the hydroscopic nature of LiF, LiCAF is regarded as a more suitable optical material in the UV and the VUV region. Moreover, the new excitation channel around 112 nm is discovered for Ce:LiCAF crystal. This excitation is originated not from absorption of Ceriumions but fromabsorption around the bandgap of the host crystal.
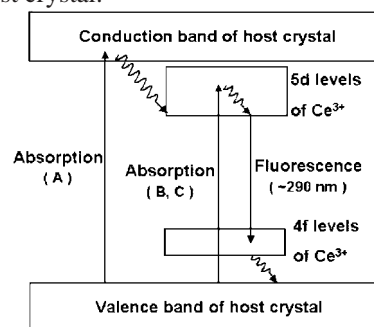
Figure 1. Schematic of energy levels and possible decay channel in Ce:LiCAF crystal.

VIII-A-9 THz-Radiation Emitter and Receiver System Based on a 2 T Permanent Magnet, 1040 nm Compact Fiber Laser and Pyroelectric Thermal Receiver

OHTAKE, Hideyuki; SUZUKI, Yuji; SARUKURA, Nobuhiko; ONO, Shingo[1]; TSUKAMOTO, Takeyo[1]; NAKANISHI, Akio[2]; NISHIZAWA, Seiji[3]; STOCK, Michelle L.[4]; YOSHIDA, Makoto[4]; ENDERT, Heirich[4]
(*[1]Sci. Univ. Tokyo; [2]Sumitomo Special Metal Co., Ltd.; [3]Shinshu Univ.; [4]Imra America, Inc.*)

Thermal receiver detectable terahertz (THz) radiation is generated from InAs irradiated with a 1040 nm, 80 fs, 180 mW, 48-MHz-repetition-rate mode-locked fiber laser in a 2 T field by a compact permanent magnet. THz radiation is monitored by means of a deuterated triglycine sulfate (DTGS) pyroelectric thermal receiver. DTGS operates at room temperature and does not require time-gating adjustment or cryogen cooling with liquid helium. The THz-radiation emitter system, including the excitation laser head, is almost the same size as a conventional notebook computer.
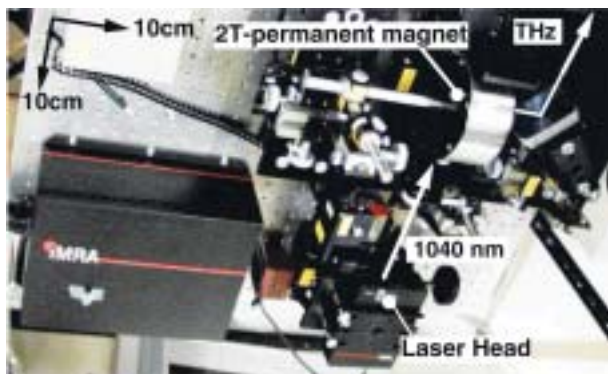
Figure 1. Photograph of THz-radiation emitter system. Laser beam is focused onto the sample with a 2 T permanent magnet.

VIII-A-10 Nanocluster Crystals of Lacunary Polyoxometalates as Structure-Design-Flexible, Inorganic Nonlinear Materials

MURAKAMI, Hidetoshi; KOZEKI, Toshimasa; SUZUKI, Yuji; ONO, Shingo[1]; OHTAKE, Hideyuki; SARUKURA, Nobuhiko; ISHIKAWA, Eri[2]; YAMASE, Toshihiro[2]
(*[1]Sci. Univ. Tokyo; [2]Tokyo Inst. Tech.*)

Lacunary polyoxometalates, large inorganic, structure-design-flexible, nanocluster crystals are found to have higher optical nonlinearity than KH_2PO_4 (KDP) by the powder second-harmonic-generation (SHG) method. Moreover, the capability of generating ultraviolet radiation down to around 300 nm is found. The basic criteria to design the high nonlinearity are also discovered by the reduction of the molecular symmetry.
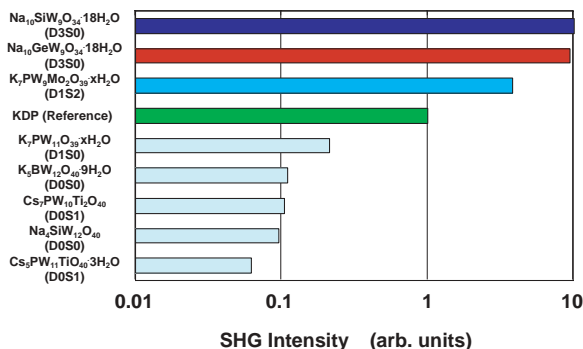
Figure 1. Powder second-harmonic-generation method results using a 1064-nm optical pulse from a Q-switched Nd:YAG laser as the fundamental radiation. Label S denotes the substitution number of metal atom.

VIII-B Development and Research of Advanced Tunable Solid State Lasers

Diode-pumped solid-state lasers can provide excellent spatial mode quality and narrow linewidths. The high spectral power brightness of these lasers has allowed high efficiency frequency extension by nonlinear frequency conversion. Moreover, the availability of new and improved nonlinear optical crystals makes these techniques more practical. Additionally, quasi phase matching (QPM) is a new technique instead of conventional birefringent phase matching for compensating phase velocity dispersion in frequency conversion. These kinds of advanced tunable solid-state light sources, so to speak "Chroma Chip Lasers", will assist the research of molecular science.

In this projects we are developing Chroma Chip Lasers based on diode-pumped-microchip-solid-sate lasers and advanced nonlinear frequency conversion technique.

VIII-B-1 Intra-Cavity Frequency Doubling of a Nd:YAG Laser Passively Q-Switched by Cr^{4+}:YAG Saturable Absorber

PAVEL, Nicolaie; SAIKAWA, Jiro; KURIMURA, Sunao; TAIRA, Takunori

[*Conf. Lasers Electro-Opt.* CTuM27 (2001)]

Frequency doubling of a diode-pumped, passively Q-switched laser could be a convenient method of generating pulsed laser sources in green region. The external-cavity frequency doubling simplifies the cavity design and the green pulses are shorter than that of the Q-switched laser. However, this method is applicable to laser sources that operate with high output powers,[1] such that acceptable conversion efficiencies can be realized. On the other hand, intra-cavity frequency doubling made uses of the high peak power that is present inside the cavity, therefore resulting in higher conversion efficiency. A disadvantage of this scheme could be the longer pulses than those produced by a comparable Q-switched laser with no intra-cavity doubling. However, if the accurate pulse width is not critical for application such pulses would reduce the possibility of various types of optical damages. In this work we report a diode-pumped Nd:YAG laser passively Q-switched by a Cr^{4+}:YAG saturable absorber (SA) and intra-cavity frequency doubled by a LBO crystal. The maximum green average power was ~1.0 W, with the laser operating at 3.8 kHz repetition frequency and 87.8-ns pulses duration (263 μJ pulse energy, ~3 kW peak power).

Figure 1 shows a schematic layout of the laser. As pump source we used a 1.55-mm diameter, 0.11 NA fiber-bundled diode (OPC-B030-mmm-FC, OptoPower Co.). We considered a Nd:YAG medium (6-mm diameter, 10-mm length, 1.3-at.%), AR coated at 808 nm on both sides. The plane mirror M1, which was coated for high reflection (HR) at 1.064 mm and high transmission (HT) at 808 nm, was used as the rear mirror of the resonator. The performances of the laser under continuous-wave (CW) operation were first investigated in a plane-plane resonator of 40-mm length. With a flat output mirror of 5% transmission at 1.064 mm we obtained a maximum output power of 8.9 W for an absorbed pump power of 21.0 W, in a laser beam with the M^2 factor of 2.2. The slope efficiency was 48.8%. The performances of the V-type cavity were next determined in CW operation. The plane mirror M^2 was HR coated at 1.064 μm and HT coated at 532 nm. The distances between mirrors M1 and M2, and M2 and M3 were 80 mm and 90 mm, respectively. With a mirror M3 of 50-cm radius and coated as 95% reflectivity at 1.064 μm, a maximum polarized infrared power of 3.8 W for 18.6 W absorbed pump power resulted. The laser beam M^2 factor was 1.14. A 3×3×10 mm^3 LBO crystal was considered for intra-cavity frequency doubling. It was designed for type I second-harmonic generation (critical phase-matching condition), therefore operating at the room temperature. Now M3 was a concave mirror of 50-cm radius and HR coated at both 1.064 mm and 532 nm wavelengths. Thus, 3.2 W green radiation for 18.6 W absorbed pump power in a beam of M^2 = 1.5 resulted.

Figure 2 summarize the output properties of the diode-pumped Nd:YAG laser, passively Q-switched by Cr^{4+}:YAG SA and intra-cavity frequency-doubled by LBO. Cr^{4+}:YAG SA crystals with unsaturated transmission T$_0$ of 90% and 80%, and that were AR coated at 1.064 mm were used. For the SA crystal of 90% initial transmission we obtained an average green power of 1.0 W for the absorbed pump-power of 14.1 W. The laser beam M^2 factor was 1.6. At this pump level the pulse width and the pulse repetition rate were 87.8 ns and 3.8 kHz and the corresponding pulse energy and peak power were 263 μJ and ~3.0 kW. A slightly higher peak power, namely 4.2 kW resulted for the SA of 80% initial transmission: the green average power was ~0.7 W and the pulse width and energy were 50 ns and 209 mJ, respectively. For comparative data on the Cr^{4+}:YAG crystal of 90% initial transmission, the LBO crystal was removed from the resonator and the mirror M3 was replaced by a 90% reflectivity mirror at 1.064 μm. Thus, an infrared maximum average power of 1.1 W resulted at 3.9 kHz and with pulses of 41.5 ns (pulse energy and the peak power were 282 mJ and ~6.8 kW, respectively). As expected, the green pulses were longer than those produced by a comparable Q-switched laser with no intra-cavity doubling. In order to explain the Q-switching results a rate-equation model that accounts for thermally induced effects in Nd:YAG rod, the ratio of the laser-beam area in medium gain to that in SA and its influence on Q-switch performances, and the SA exited state absorption (ESA) contribution was developed. The frequency doubling process was taken into account by introducing a nonlinear loss term in the flux equation rate.[2] Following the laser dynamics we have derived

analytical expressions that describes the Q-switched pulse energy, peak power, pulse width and repetition rate.[3] Using this model a good agreement between the experimental data and theory was obtained for both infrared and second-harmonic regimes.

In summary, we have reported a diode-pumped Nd:YAG laser, passively Q-switched by Cr^{4+}:YAG saturable absorber and intra-cavity frequency-doubled by LBO crystal. The laser produces high beam-quality of 263-μJ energy, 87.8-ns pulses at a pulse repetition rate of 3.8 kHz, for an average power of 1.0 W at 532 nm.

References

1) A. Agnesi, S. Dell'Acqua, E. Piccinini, G. Reali and G. Piccinno, *IEEE J. Quantum Electron.* **34**, 1480 (1998).
2) E.C. Honea, C.A. Ebbers, R. J. Beach, J. A. Speth, J. A. Skidmore, M. A. Emanuel and S.A. Payne, *Opt. Lett.* **23**, 1203 (1998).
3) N. Pavel, J. Saikawa, S. Kurimura, I. Shoji and T. Taira, *Technical Report of Japan Inst. for Electronics, Information and Commun. Engineers (IEICE)* **LQE-65**, 23 (2000).
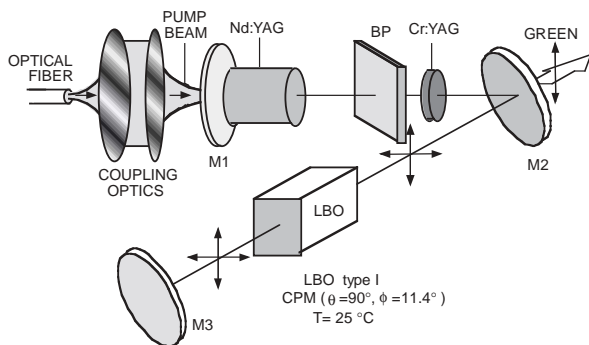
Figure 1. Schematics of the diode end-pumped Nd:YAG laser, passively Q-switched by Cr^{4+}:YAG SA and intra-cavity frequency-doubled by LBO crystal. BP: glass-plate positioned at the Brewster angle.
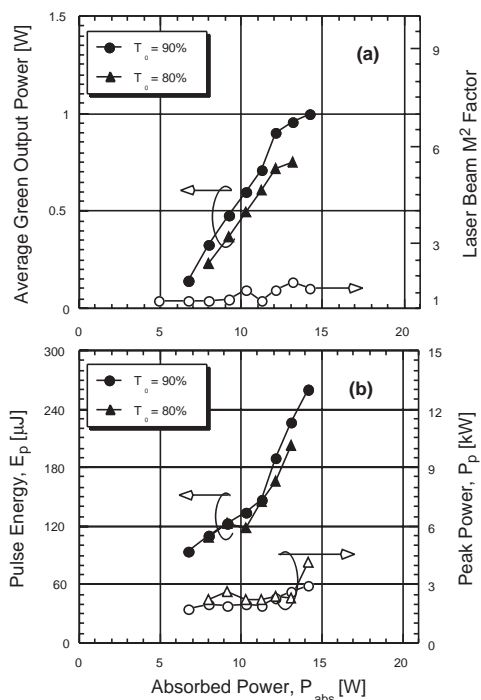
Figure 2. Output properties of diode-pumped Nd:YAG laser, passively Q-switched by Cr^{4+}:YAG and intra-cavity frequency-doubled by LBO. (a) Average power and laser-beam M^2 factor; (b) Pulse energy and pulse peak power.

VIII-B-2 Laser Emission under Resonant Pump in the Emitting Level of Highly Doped Nd Materials

LUPEI, Voicu[1]; TAIRA, Takunori; PAVEL, Nicolaie; SHOJI, Ichiro; IKESUE, Akio[2]
(*[1]IAP, Romania; [2]JFCC*)

[*Conf. Lasers Electro-Opt.* CFD4 (2001)]

Heating effects in the laser active media under pump constitute a major limitation in the construction of highly efficient or high-power solid state lasers. These effects could induce the optical distortion of the resonator or even the physical destruction of the active component. In case of neodymium-doped crystals two major sources exists: the quantum defect between the pump and laser radiation and the non-radiative processes (multiphonon relaxation, down-conversion cross-relaxation on intermediate levels, upconversion from the emitting level $^4F_{3/2}$). While the non-radiative processes constitute a physically inherent loss, the quantum defect can be controlled by the pump and emission wavelengths. In the actual diode pumped Nd laser the pump is accomplished in the $^4F_{5/2}$ level (808.7 nm) and the excitation relaxes by electron-phonon interaction to the components R_1 and R_2 of the emitting level, placed at ~945 and 860 cm^{-1} below the pump level. In absence of laser emission about 39% from the absorbed pump radiation in $^4F_{5/2}$ is transformed into heat in a 1.04 at.% Nd:YAG crystal,[1] in accord with a theoretical modeling that accounts for the non-radiative effects on the quantum efficiency.[2] In case of an efficient laser emission, when the effect of the non-radiative processes is very small and the heat generation is dominated by the quantum defect the fractional thermal load in this sample is reduced up to about 0.25. However, this figure is much larger than the value of about 0.09 in case of Yb lasers, where the pump is performed in an upper crystal field component of the emitting level.

Pumping in the emitting level or even below it could be a very efficient means for reducing the heating effects in Nd lasers. Thus, in case of Nd:YAG laser, the pump can be performed in the lower component R_1 (11425.5 cm^{-1}) of $^4F_{3/2}$ and the population of the emitting level R_2 (11509 cm^{-1}) can be accomplished by thermal population (at the room temperature about 40% of the population of $^4F_{3/2}$ level is in the R_2 level). The thermallization of the energy levels can be also used for the reduction of the lower quantum defect, between the terminal and the ground level, by pumping in a hot band of the $^4I_{9/2} \rightarrow {}^4F_{3/2}$ absorption. The spectroscopic investigation of various Nd-doped crystals shows that there are many cases when the optical transitions $X_2 \rightarrow R_1$ and $X_3 \rightarrow R_2$ are very close or nearly degenerate, leading to a two- or single-peaked broad feature: at room temperature the population of crystal field components X_2 and X_3 of $^4I_{9/2}$ could be large (in YAG

these are 0.246 and 0.178, respectively), leading to a very fairly good absorption of pump. Using these effects (thermal population—assisted pump) is equivalent with a photon cooling. However, since the quantum defect is still positive this is not evidenced as a net cooling of the same sample but only as a reduction of the thermal load. It must be noted that the attempt to observe the laser cooling in Nd:YAG[3] used the pump with 1.06 micron wavelength in order to excite the tiny fraction of thermal population from the $^4I_{11/2}$ level up to the emitting level $^4F_{3/2}$.

The room temperature absorption spectra of Nd:YAG show these two transitions collected in a two-peaked (885.7 nm and 884.4 nm) broad feature centred around 885 nm. For 1 at.% Nd the absorption coefficient for the two peaks is almost equal, ~1.75 cm^{-1}, *i.e.* much weaker than the 808.7 nm pump transition (~ 9 cm^{-1}). Laser emission has been demonstrated for 1 at.% Nd:YAG crystal[4] under 885 nm pump. However, the weak absorption of this radiation in the crystal samples precludes the construction of either microchip or high-power lasers.

Recent studies revealed that highly doped Nd:YAG laser components can be fabricated by ceramics technique.[5,6] The spectroscopic investigation shows that the intensity of the 885 nm band increases linearly with the Nd concentration, the two peaks reaching an absorption coefficient of over 14 cm^{-1} for the 9 at.% sample (Figure 1). At the same time the width of the absorption feature increases by about 25%, from 2.5 nm FWHH to 3.15 nm, by increasing the Nd concentration from 1 to 9 at.%.

In case of Nd:YAG the fractional thermal load is expected to reduce to 0.318 for 1 at.% and to 0.66 for 3.4 at.% Nd under 885 nm pump in absence of laser emission. The most important reduction will be in presence of laser emission, to 0.168 for 1.06 mm emission, *i.e.* a reduction of over 40% from the case with 808 nm pump, and to 0.058 for 940 nm emission, lower than for Yb:YAG laser and with a terminal level (852 cm^{-1}) higher than that of Yb (612 cm^{-1}).

The continuous-wave laser emission in highly doped Nd:YAG ceramics under 885 nm pump was tested with an uncoated active component of 3.4 at.% Nd and 0.87 mm thickness (Figure 2). This was placed in a 25-mm plane-concave resonator with a 50-mm radius output mirror. The 885 nm pump was provided by a Ti:sapphire laser, whose radiation was focussed to a 80 μm diameter in the active medium. For a 95% output mirror reflectivity the laser delivered 42 mW at 1.064 μm for an absorbed pump power of 194 mW; the threshold pump power and the slope efficiency were 87 mW and 37.5%, respectively. With an output mirror reflectivity of 99% the pump threshold dropped to 38 mW but the slope efficiency decreased at 16.7%, while the maximum output power was 27 mW with an optical efficiency of 14%. The improvement of laser performances is under study, by considering coated Nd:YAG ceramic components of optimized size, an improved configuration for the laser resonator as well as an increased pump power.

In conclusion this study shows that the highly doped Nd:YAG ceramics as well as many crystals with high concentrations of Nd ions could be systems of choice for low heat – high power or miniature lasers with hot band (885 nm in case of Nd:YAG) resonant pump.

References

1) T. Y. Fan, *IEEE J. Quantum Electron.* **29**, 1457 (1993).
2) V. Lupei and A. Lupei, *Phys. Rev. B* **61**, 8087 (2000).
3) T. Kushida and J. E. Geusic, *Phys. Rev. Lett.* **21**, 1172, (1968).
4) R. Lavi and S. Jackel, *Appl. Opt.* **39**, 3093 (2000).
5) I. Shoji, S. Kurimura, Y. Sato, T. Taira, A. Ikesue, and K. Yoshida, *Appl. Phys. Lett.* **77**, 939 (2000).
6) J. Lu, M. Prabhu, J. Song, C. Li, J. Xu, K. Ueda, A. A. Kaminskii, H Yagi and T. Yanagitani, *Appl. Phys. B: Lasers Opt.* **71**, 46 (2000).
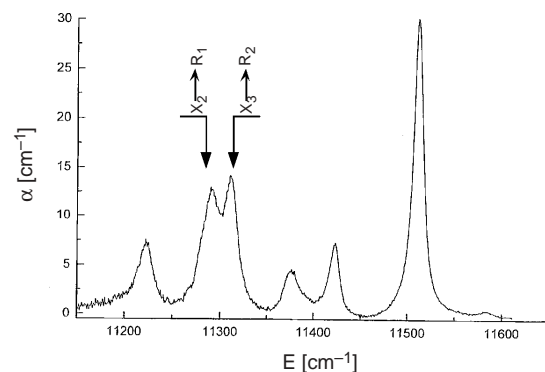
Figure 1. Room temperature $^4I_{9/2} \to {}^4F_{3/2}$ absorption spectrum of the 9 at.% Nd:YAG ceramics.
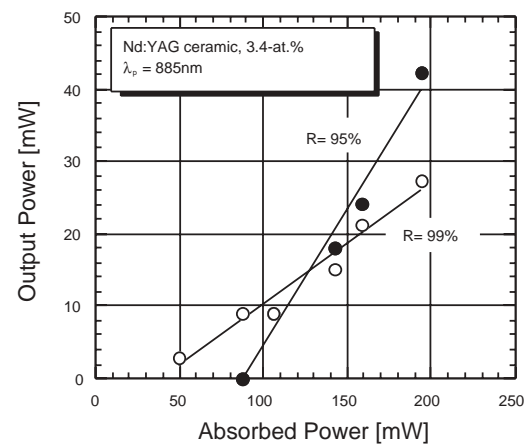
Figure 2. Output to input characteristics for the uncoated 3.4-at.% Nd:YAG ceramic pumped at 885 nm.

VIII-B-3 Thermal Birefringence in Nd:YAG Ceramics

SHOJI, Ichiro; SATO, Yoichi; KURIMURA, Sunao; LUPEI, Voicu; TAIRA, Takunori; IKESUE, Akio[1]; YOSHIDA, Kunio[2]
(*[1]JFCC; [2]Osaka Inst. Tech.*)

[*Conf. Lasers Electro-Opt.* CFD6 (2001)]

Nd:YAG ceramics are promising candidates for high-power and high-efficiency microchip laser materials because highly transparent and highly Nd^{3+}-doped samples are available without degrading thermo-mechanical properties; the thermal conductivity is as

high as that of single-crystal YAG even at high Nd^{3+} concentrations. We have succeeded in microchip laser oscillation, in which the output power from a microchip of a 3.4 at. % Nd:YAG ceramic was more than twice as high as that from a same sized microchip of a Nd:YAG single crystal at the same input power. In this work we have investigated thermal birefringence effect in the Nd:YAG ceramics, which should be useful for power scaling.

Thermal birefringence of Nd:YAG ceramics was measured with the pump-probe experiment. A Ti:sapphire laser oscillating at 808 nm was used as the pump beam. The pump beam was focused onto the sample with the radius of 80 μm. On the other hand, linearly polarized He-Ne laser beam was used as the probe beam, and only the depolarized component of the probe beam was detected by use of a polarizer. If the depolarization is defined by the ratio of the depolarized power to the total probe power, dependence of the depolarization on the absorbed pump power for the ceramic and single-crystal samples with various Nd^{3+} concentrations is shown in Figure 1. On the other hand, Figure 2 shows the depolarization as a function of Nd^{3+} concentration at the absorbed pump power of 1000 mW. We found that the depolarization is nearly the same between the ceramic and single-crystal YAG if they have equal Nd^{3+} concentrations. This result indicates that the average of the thermal birefringence induced in the Nd:YAG ceramics is nearly the same with that in the (111)-cut single crystal. Moreover, it was also found that the depolarization became larger in samples with higher Nd^{3+} concentrations even if the same pump power was absorbed. This is mainly attributed to the fact that the fractional thermal loading increases as Nd^{3+} concentration becomes higher. When lasing occurs, on the other hand, thermal birefringence is expected to be greatly reduced because the thermal loading is then independent of Nd^{3+} concentration.
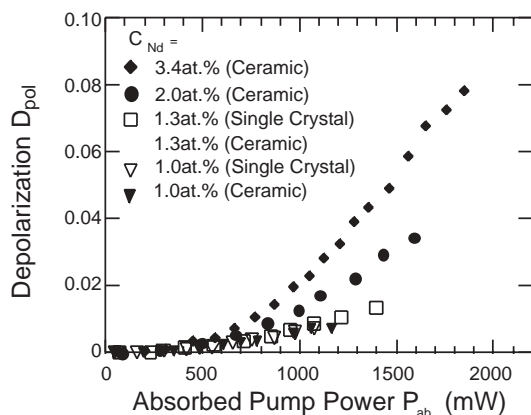
Figure 1. Dependence of the depolarization on the absorbed pump power for the ceramic and single-crystal samples with various Nd^{3+} concentrations.
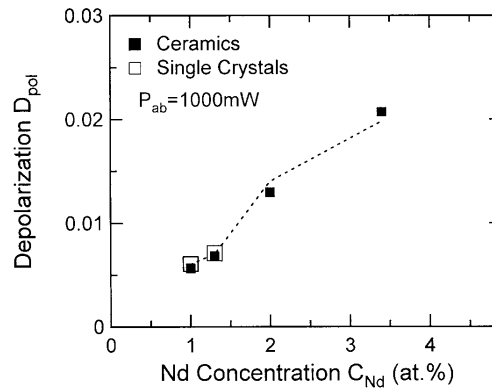
Figure 2. Depolarization as a function of the Nd^{3+} concentration for the ceramic and single-crystal samples at the absorbed pump power of 1000 mW. The dotted curve is the calculated result.

VIII-B-4 In-situ Observation of Fabrication of Nonlinear Optical Wavelength Converter

KURIMURA, Sunao; SHOJI, Ichiro; TAIRA, Takunori; RO, Jung Hoon[1]; CHA, Myoungsi[1]
(*[1]Pusan Natl. Univ.*)

MgO-doped $LiNbO_3$ (MgO:LN) has attracted much attention in quasi-phase-matched (QPM) wavelength conversion due to high resistance to photorefractive damage and low coercive field allowing a large aperture device. Since our first measurement of the coercive field, the crystal has become popular in QPM application and recent works have been verifying high performance of the material. To improve device characteristics, characterization of the domain movement is required for a device with larger aperture. Here we report in-situ monitored poling process and coercive field depending on Mg content in MgO:LN.

The experimental setup for poling is illustrated in Figure 1(a). We used transparent liquid electrode system consisting of transparent plastic blocks and o-rings. Z-cut MgO:LN wafers were sandwiched between two o-rings filled with LiCl electrodes. We observed ferroelectric 180° domains by the electro-optic imaging (EOI) technique under the crossed polarizers. Although EOI technique has a moderate spatial resolution compared with other techniques such as second-harmonic-generation microscope we previously developed, it allows in-situ observation of the poling process with a simple setup. Owing to the small velocity of domain wall in MgO:LN, real-time development was recorded by a commercial video camera. Figure 1(b) shows selected pictures describing the wall movement. Domains with reversed polarization nucleated from the right top corner in the square area directly exposed to the liquid electrode on the +C face. Walls creep very slowly and monitored current has Barkhausen pulses as we reported before. Observed bright spots work as traps of walls, making Barkhausen pulses in current.

We measured coercive fields (Ec) for forward and backward poling in 1mm-thick various crystals with different Mg concentrations of 1–7 mol%. Figure 1(c)

presents a significant reduction of coercive field with high doping of Mg. For forward poling, first polarization reversal in fresh wafers, Ec has a minimum value of 4.6 kV/mm at 5 mol%. This corresponds to the lowest defect density at this doping level in the crystal. On the other hand, for backward poling, first polarization reversal after forward poling, Ec decreases monotonically up to 7 mol%. The minimum value we observed here is 2.3 kV/mm at 7 mol%.

In conclusion, we report coercive field dependence on Mg content in LN crystals while observing polarization reversal process simultaneously with poling. Forward coercive field exhibits the minimum value of 4.6 kV/mm at 5 mol% and backward coercive field has the lowest value of 2.3 kV/mm at highest doping level of 7 mol%.

(a)

(b)

(c)
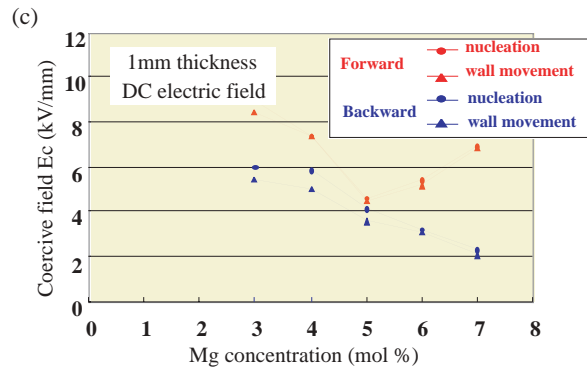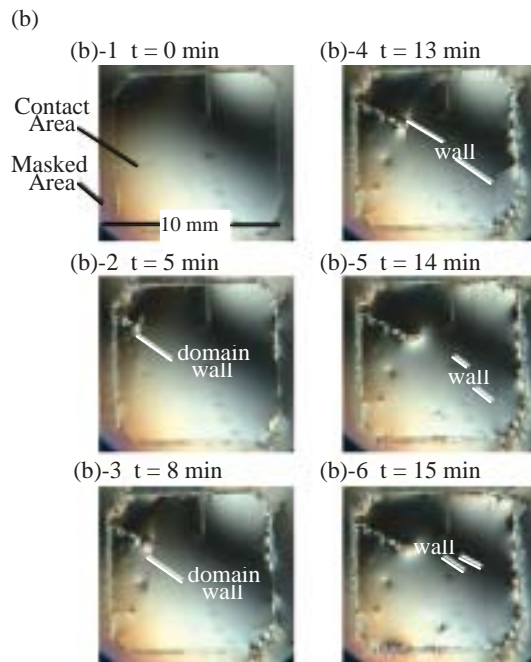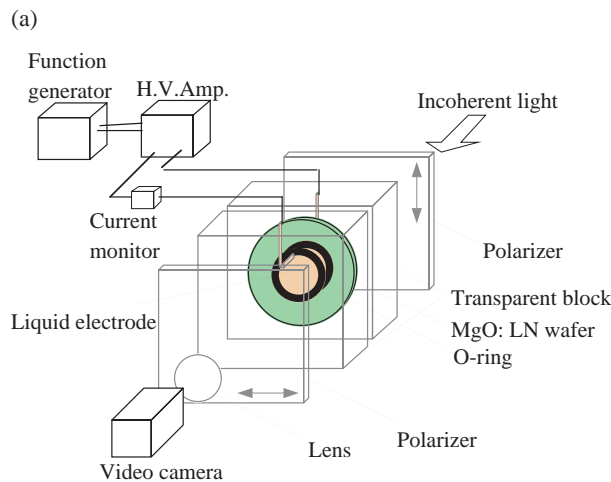
Figure 1. (a) Experimental setup of *in-situ* observation of poling process (b) time development of domains in MgO:LN during electric field poling process (c) coercive field dependence on Mg concentration in MgO:LN.

VIII-B-5 Periodical Twinning in Crystal Quartz for Ultraviolet Nonlinear Optics

KURIMURA, Sunao; FEJER, Martin[1]; SHOJI, Ichiro; TAIRA, Takunori; UESU, Yoshiaki[2]; NAKAJIMA, Hirochika[2]
(*[1]Stanford Univ., USA; [2]Waseda Univ.*)

Crystal quartz has low absorption, high chemical stability, and low thermooptic coefficients, attractive for operation in ultraviolet nonlinear optics. Growth techniques are well established because of widespread in surface-acoustic-wave and timing applications, but unfortunately, it doesn't meet the birefringent phase matching condition due to small birefringence, and electric field poling condition due to lack of ferroelectricity. We devised a new poling technique in crystal quartz using mechanical twinning and demonstrated periodical polarity reversal by using thermal stress. Figure 1 shows an observed twin structure with a period of 80 μm, obtained by thermally induced stress between patterned Cr films and a quartz. The Cr patterned substrate was heated to just below Curie temperature in order to attain reasonable film stress and reduce coercive stress. Twins tend to generate from the edge of Cr pattern and the required duty ratio of Cr to the period was more than 0.5. The depth of twins, however, were several microns, indicating not suitable for bulk nonlinear optics. New technique is under development to improve the depth profile of the twins for a practical UV generator.

(a)
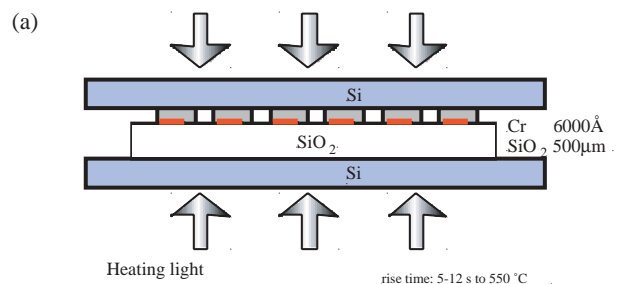
(b)
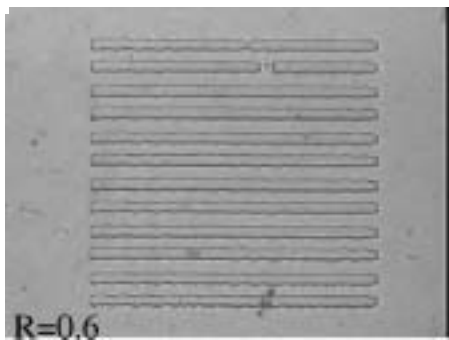
Figure 1. a) patterning method by the thermally induced in-plane stress b) observed periodical twins with a period of 80 μm period. R; duty ratio of the Cr film to the period.

Research Center for Molecular Materials

VIII-C Development of Novel Heterocyclic Compounds and Their Molecular Assemblies for Advanced Materials

Heterocycles containing sulfur and/or nitrogen atoms are useful as components of functional materials since heteroatoms in their rings are helpful to stabilize ions or ion-radical species, and extended π-conjugation decreases Coulombic repulsion. In addition intermolecular interactions caused by heteroatom contacts can be expected to form novel molecular assemblies. In this project new electron acceptors, donors, and donor-acceptor compounds based on heterocycles such as 1,2,5-thiadiazole and 1,3-dithiole were synthesized and their properties including those of the charge-transfer complexes or ion-radical salts were investigated. Unique crystal structures were constructed by using weak intermolecular interactions such as hydrogen bonding or heteroatom contacts. In addition, precisely-defined heterocyclic oligomers containing various types of functional units have been developed, which are a promising building blocks for future molecular nanotechnologies.

VIII-C-1 Linear Hydrogen-Bonded Molecular Tapes in the Co-Crystals of Squaric Acid with 4,4'-Dipyridylacetylene or 1,2-Bis(4-pyridyl)ethylene

ZAMAN, Md. Badruz; TOMURA, Masaaki; YAMASHITA, Yoshiro[1]
(*[1]IMS and Tokyo Inst. Tech.*)

The co-crystals of squaric acid with dipyridyl-type ligands, **1** and **2**, are isomorphous and form in the triclinic crystal system. The co-crystals contain linear and flat hydrogen-bonded molecular tape structures along the [120] direction (Figure 1). The squarate monoanions form a rare ten-membered dimer linked by two intermolecular O–H···O hydrogen bonds [2.511(3) Å for **1** and 2.503(2) Å for **2**]. Each component molecule forms a segregated stack along the c axis. The bond lengths of the squarate monoanion indicate the delocalization of the enolate anion.
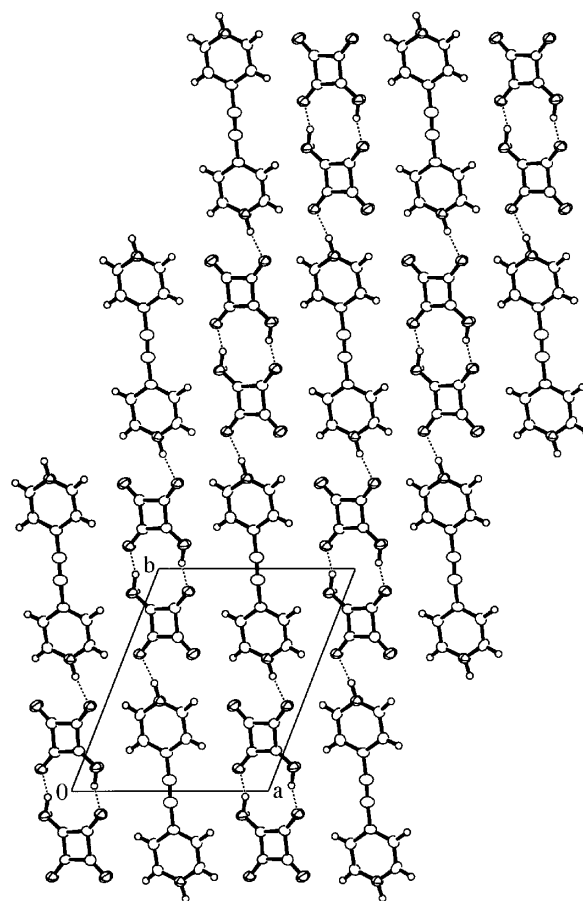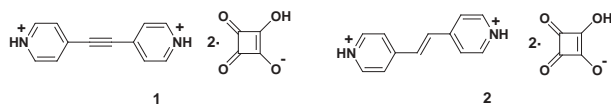
Figure 1. Packing diagram of **1** viewed along the c axis. Dotted lines show the intermolecular hydrogen bonds.

VIII-C-2 One-Dimensional Hydrogen-Bonded Molecular Tapes in 1,4-Bis[(4-pyridinium)ethynyl]-benzene Chloranilate

AKHTARZZAMAN, Md.[1]**; TOMURA, Masaaki; YAMASHITA, Yoshiro**[2]
(*[1]GUAS; [2]IMS and Tokyo Inst. Tech.*)

The crystal structure of a 1:1 co-crystal with chloranilic acid and 1,4-bis[(4-pyridyl)ethynyl]benzene contains one-dimensional hydrogen-bonded molecular tapes along the [113] direction, as shown in Figure 1. The molecular tape is nearly flat. The angles between the molecular planes of the chloranilate and the pyridinium ring, and of the pyridinium ring and the benzene ring are 7.3(2)° and 11.8(4)°, respectively. The molecular tapes are connected *via* $R_1^2(5)$ couplings with two intermolecular N–H···O hydrogen bonds [2.609(3) Å and 2.897(4) Å], where both protons of chloranilic acid have transfered to the prydine rings. The overlaps between the chloranilate-pyridinium ring-benzene ring-pyridinium ring-chloranilate are observed in the stacks of the molecular tapes. A short C–Cl···π interaction [Cl···triple bond 3.440(7) Å] exists between the stacks of the molecular tapes. It is 1.7% shorter than the sum of the van der Waals radii of Cl and C*sp*.
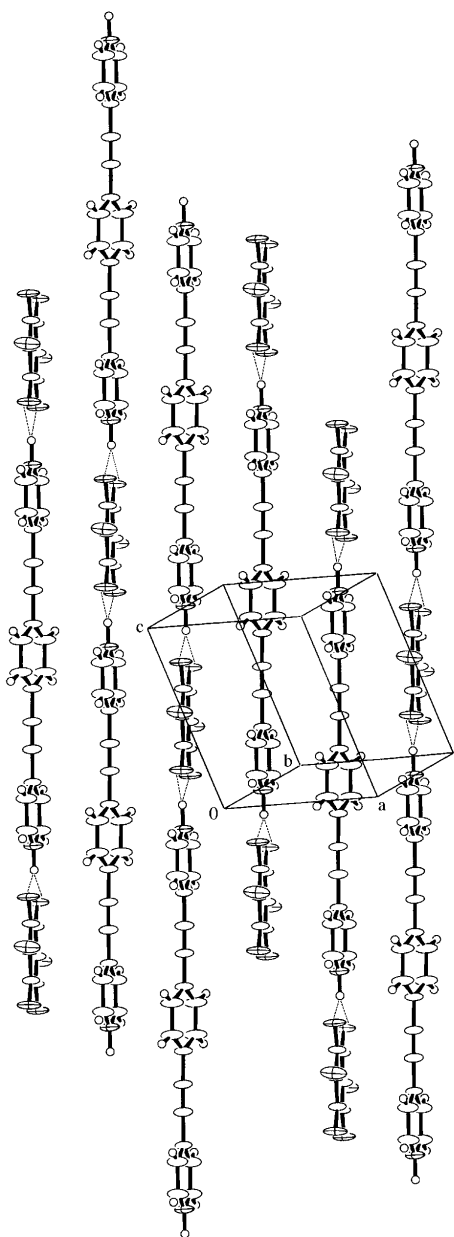
Figure 1. Packing diagram of the title compound. Dotted lines show the intermolecular N–H···O hydrogen bonds.

VIII-C-3 4,7-Bis[(4-pyridyl)ethynyl]-2,1,3-benzothiadiazole and Its Dipyridinium Diperchlorate

AKHTARZZAMAN, Md.[1]; TOMURA, Masaaki; YAMASHITA, Yoshiro[2]
(*[1]GUAS; [2]IMS and Tokyo Inst. Tech.*)

A long, rigid and conjugated bridging ligand, 4,7-bis[(4-pyridyl)ethynyl]-2,1,3-benzothiadiazole **1**, and its dipyridinium salt **2** display the bond alternation in the 2,1,3-benzothiadiazole rings, which suggests their quinonoid character. The dipyridinium dication molecules stack along the a axis and form a dimer with short S···N interheteroatom contacts [3.146(4) Å] between the two 1,2,5-thiadiazole rings. The dimer is surrounded by the perchlorate anions with a large number of intermolecular N–H···O and C–H···O hydrogen bonds, as shown in Figure 1.
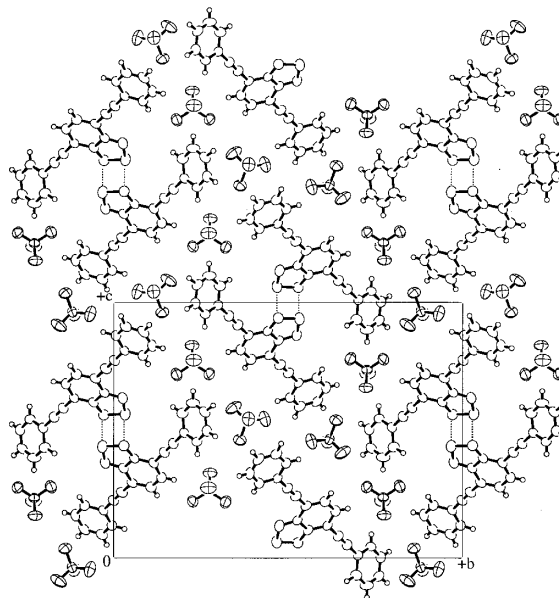
Figure 1. Packing diagram of **2** viewed along the a axis. Dotted lines show the short S···N interheteroatom contacts.

VIII-C-4 One-Dimensional Zigzag Chain Structures with Intermolecular C–H···π and C–H···O Interactions Consisted of Phthalic Acid and Pyridine Derivatives

TOMURA, Masaaki; YAMASHITA, Yoshiro[1]
(*[1]IMS and Tokyo Inst. Tech.*)

Crystal structures of co-crystals of phthalic acid with dipyridyl-type ligands, 4,4'-bipyridine or 4,4'-dipyridylacetylene, contain one-dimensional zigzag chain structures connected by intermolecular O–H···N hydrogen bonds. The edge-to-face packing (T-shaped geometry) between phthalic acid and the pyridine rings of the dipyridyl-type ligands is also observed and is

stabilized by intermolecular C–H⋯π and C–H⋯O interactions. Strong resemblance between the two crystal structures suggests robustness and reproducing ability of the supramolecular synthon formed with phthalic acid and pyridine rings. In this case, a zigzag chain structure seems to be "programmed" to form in a crystal. We have displayed that the supramolecular synthons generated by combination of simple compounds such as phthalic acid and dipyridyl-type ligands can be used in the design of one-dimensional zigzag chain structures and can realize unique preserved crystal structures.
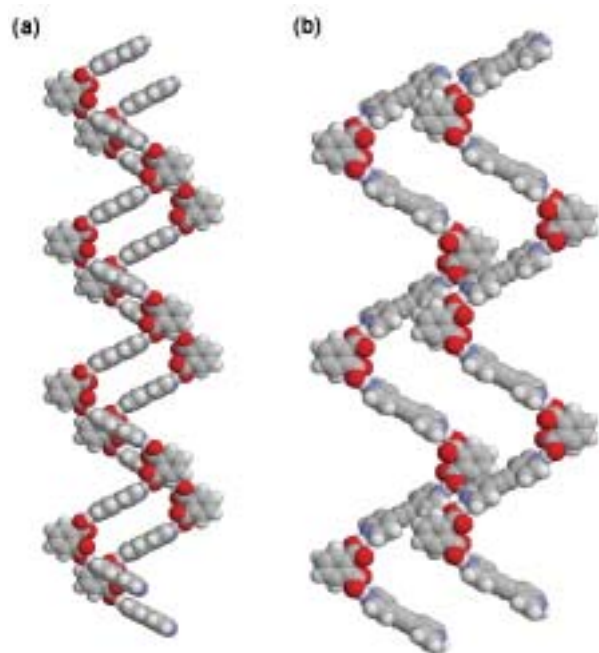
Figure 1. Two one-dimensional zigzag chain structures in the co-crystal of phthalic acid with (a) 4,4'-bipyridine and (b) 4,4'-dipyridylacetylene.

VIII-C-5 Synthesis and Crystal Structures of Decamethylferrocenium Salts of Anilate Anion Derived from Bromanilic Acid, Chloranilic Acid and Cyananilic Acid

ZAMAN, Md. Badruz; TOMURA, Masaaki; YAMASHITA, Yoshiro[1]
(*[1]IMS and Tokyo Inst. Tech.*)

Four complexes were synthesized using bis(penta-methylcyclopentadienyl)iron $Fe(C_5Me_5)_2$ as an organo-metallic donor and three anilic acids (2,5-dibromo-3,6-dihydroxy-1,4-benzoquinone; BA, 2,5-dichloro-3,6-dihydroxy-1,4-benzoquinone; CA and 2,5-dicyano-3,6-dihydroxy-1,4-benzoquinone; CNA) as an organic acceptor. The molecular-based structures with different stoichiometric ratios [1:1, 1:1:1(H$_2$O) and 2:1] of these complexes have been determined by X-ray crystallographic analysis and elemental analysis. These complexes have a one-dimensional alternated stacking arrangement as $D^+A^-D^+A^-$ type. Close contacts between the bromine atoms and oxygen atoms of the BA units

are observed in the structure $[Fe(C_5Me_5)_2](BA)$ of 1:1 composition. Interestingly, the structures $[Fe(C_5Me_5)_2]$-(CA)(H$_2$O) and $[Fe(C_5Me_5)_2](CNA)(H_2O)$ of 1:1:1 (H$_2$O) ratio contain one-dimensional molecular tape structures with the combination of the CA or the CNA units and water molecules *via* O–H⋯O hydrogen bonds. Different stoichiometric ratios and structures are found from the CNA complexes $[Fe(C_5Me_5)_2](CNA)(H_2O)$ and $[Fe(C_5Me_5)_2]_2(CNA)$.

Fe(C$_5$Me$_5$)$_2$

BA: X = Br
CA: X = Cl
CNA: X = CN
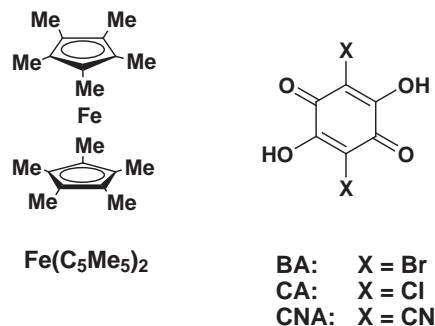
VIII-C-6 Tetrathiafulvalene with a Fused Pyrazine Ring

TOMURA, Masaaki; YAMASHITA, Yoshiro[1]
(*[1]IMS and Tokyo Inst. Tech.*)

The title compound, 2-(1,3-dithiol-2-ylidene)-2,3-dihydro-1,3-dithia-4,7-diazaindene (pyrazinotetra-thiafulvalene) forms a head-to-tail type of π-stacking centrosymmetric dimer with an interplanar distance of 3.59(1) Å. Short S⋯N interheteroatom contacts [3.10(1) Å] are observed between the two dimers, which form a two-dimensional stacking column along the [101] direction (Figure 1).
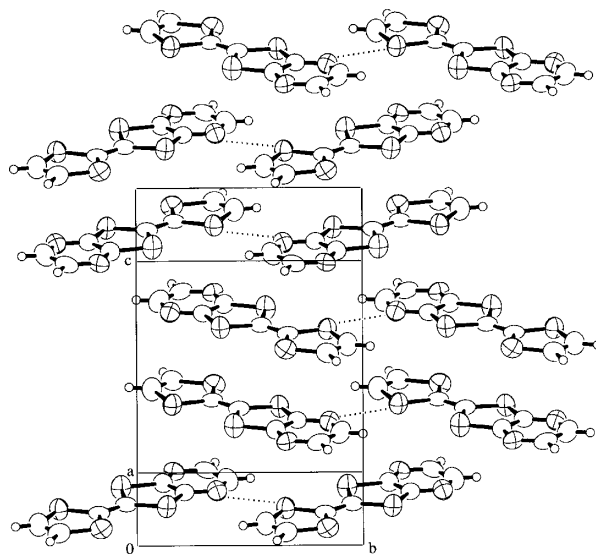
Figure 1. Packing diagram of the title compound. Short S⋯N interheteroatom contacts are indicated by dotted lines.

VIII-C-7 Hydrogen-Bonded Square Grid-Type Network in the Co-Crystal of Pyrazinotetrathiafulvalene with Chloranilic Acid

TOMURA, Masaaki; YAMASHITA, Yoshiro[1]
(*[1]IMS and Tokyo Inst. Tech.*)

For the development of functional molecular materials, we have designed the hydrogen-bonded square grid-type network using the supramolecular synthon formed with chloranilic acids and heterocyclic compounds with nitrogen. The co-crystal **1** was isolated from an acetone solution of pyrazinotetrathiafulvalene with chloranilic acid. Figure 1 shows the crystal structure of **1**. The square grid-type network with cavities and the segregated unistacks of each molecule are observed. This packing motif is essentially the same as those previously obtained from the co-crystal of chloranilic acid with quinoxaline or phenazine.[1] This fact suggests robustness and reproducing ability of the supramolecular synthon formed from chloranilic acid. Moreover, this type of segregated columnar structure is very important for organic conducting materials such as TTF-TCNQ charge transfer complex. The cavities in **1** are occupied by two water molecules. Such guest molecules in the cavities may affect physical properties of organic solids. Crystal data for **1**: $C_{14}H_6Cl_2N_2O_4S_4 \cdot (H_2O)_2$, $M = 497.35$, monoclinic, space group $P2_1/m$, $a = 3.867(3)$, $b = 22.419(9)$, $c = 11.675(4)$ Å, $\beta = 99.27(3)°$, $V = 999(1)$ Å^3, $Z = 2$, $T = 296$ K, μ(Cu-Kα) = 7.165 mm^{-1}, $R_1 = 0.0731$ and $wR_2 = 0.1841$ for 998 data with $I > 2\sigma(I)$.

Reference
1) M. Tomura and Y. Yamashita, *CrystEngComm* 16 (2000).
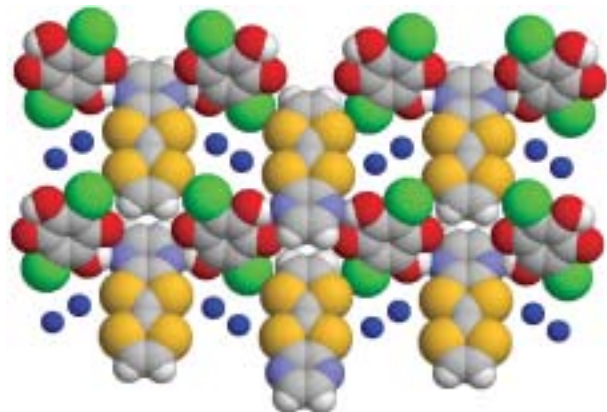
Figure 1. Crystal structure of **1** viewed along the a axis.

VIII-C-8 Hydroxyphenyl Substituted Tetrathiafulvalene Vinylogues Affording Stable Cation Radical Salts with Unusual Crystal Structures

YAMASHITA, Yoshiro[1]; TOMURA, Masaaki; IMAEDA, Ken-ichi[2]
(*[1]IMS and Tokyo Inst. Tech.; [2]IMS and Chubu Univ.*)

TTF vinylogues **1** containing hydroxy phenyl groups were newly prepared. They are stronger electron donors than BEDT-TTF and afforded their cation radical salts as single crystals upon electrochemical oxidation. The X-ray crystallographic analyses of the three cation radical salts **1a**·Au(CN)$_2$·PhCl, **1b**·PF$_6$, and **1c**·ReO$_4$·(H$_2$O)$_8$ have revealed their unusual crystal structures, where p-overlapping and hydrogen bonding play a crucial role in constructing them. The TTF vinylogue skeletons of the salts are planar and the phenyl groups are almost orthogonal to them. The two-dimensional π-overlapping[1] of the donor molecules was only found in the structure of **1a**·Au(CN)$_2$·PhCl. The structure of **1c**·ReO$_4$·(H$_2$O)$_8$ has a one-dimensional grid-like structure with a void.[2] In the structures of the three salts, hydrogen bonding between OH groups and counter anions was observed.
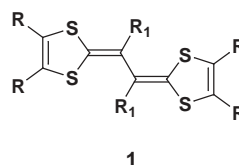
a; R, R = (CH=CH)$_2$, R$_1$ = *o*-OHC$_6$H$_4$
b; R, R = (CH=CH)$_2$, R$_1$ = *p*-OHC$_6$H$_4$
c; R, R = SCH$_2$CH$_2$S, R$_1$ = *o*-OHC$_6$H$_4$
d; R, R = SCH$_2$CH$_2$S, R$_1$ = *p*-OHC$_6$H$_4$
e; R, R = SCH$_2$CH$_2$S, R$_1$ = *o*-OBzC$_6$H$_4$
f; R, R = SCH$_2$CH$_2$S, R$_1$ = *p*-OBzC$_6$H$_4$

References
1) Y. Yamashita, M. Tomura, M. B. Zaman and K. Imaeda, *Chem. Commun.* 1657 (1998).
2) M. Tomura and Y. Yamashita, *CrystEngComm* 14 (2000).

VIII-C-9 A Molecule with a C$_1$-Homobasketane Framework

TOMURA, Masaaki; YAMASHITA, Yoshiro[1]
(*[1]IMS and Tokyo Inst. Tech.*)

We have carried out the X-ray crystallographic analysis of 6-(1,3-benzodithiol-2-ylidene)-5,7-dimethyl-1,2-diphenylpentacyclo[5.4.0.0^{2,5}.0^{3,11}.0^{4,8}]undecane **1**, which is the C$_1$-homobasketane derivative with a 1,3-dithiole moiety as the redox part. This is the first example of the crystal structure determination of a molecule with a C$_1$-homobasketane framework. Compound **1** crystallizes in the triclinic crystal system with one molecule in the asymmetric unit. The molecular structure of **1** is shown in Figure 1. The two cyclobutane rings in the cage are in puckered conformation. Due to the enhanced through-bond interaction of phenyl π systems involving a strained σ bond, the (Ph–)C–C(–Ph) bond length is significantly extended to 1.610(3) Å.
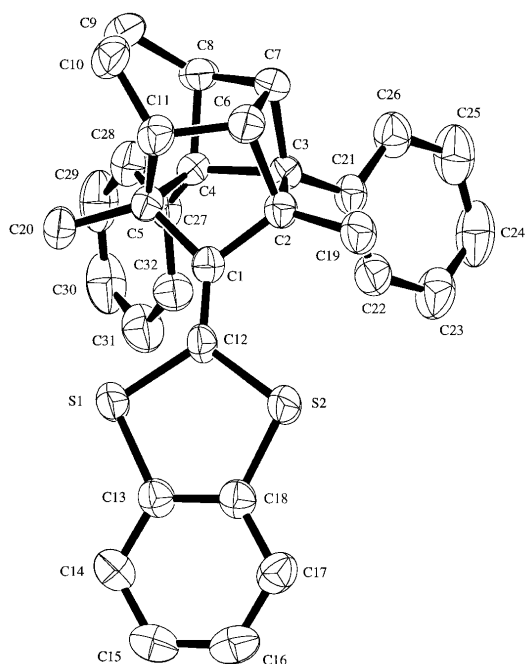
Figure 1. Molecular structure of **1**.

VIII-C-10 Real Space Observation of Individual Conformers of Oligothiophenes on Au(111) Surface

TANAKA, Shoji; YAMASHITA, Yoshiro[1]; YOKOYAMA, Takashi[2]
(*[1]Tokyo Inst. Tech.; [2]NIMS*)

The prototype of a "single molecular device" is now realized for the basic components of digital electronics (rectification, amplification and storage), however, there is still much to be learned about the molecular / supramolecular architecture on solid surface to design practical nanoscopic devices and trier large-scale integration systems. In particular, conformational identification of a π-conjugated molecule has generated a great deal of interest, because the conformational changes in the conjugated skeleton caused by the adsorption on surface will influence appreciably the electronic feature and the self-assembling ability. Here we present a real-space analysis of the molecular conformation and the self-assembling pattern of novel oligothiophenes deposited on the Au(111) surface using UHV low-temperature scanning tunneling microscopy (STM).

The samples are molecular building blocks, **BL-1** and **BL-2**, which have been designed to construct a series of multi-functional molecular wire with insulating mantle as shown in Figure 1. Figure 2a shows the twin-lobe shape of a single **BL-1** molecule, which suggests that this oligomer tends to adsorb with the main-chain parallel to the Au surface. The regular molecular ordering of **BL-1**, however, was not observed as shown in Figure 2b. In the case of the **BL-2**, the STM data shown in Figure 3a reveal that two types of well-ordered domains, *molecular stripes* and *meshes*, evolve on the Au surface. The close-up STM views of these supra-structures as shown Figure 2b-d indicate that the

molecular stripe and *meshes* consist of *s-trans* and *s-cis* conformer of **BL-2**, respectively. In solution and gas phase, the rapid exchange between the possible conformers of oligomers will occur usually. In molecular crystals, the most stable conformer would be observed predominantly. Our findings demonstrate experimentally that the control of molecular-surface interactions will be one of the key tactics to investigate individual conformers of oligomers and to construct a desired nanostructure based on them.
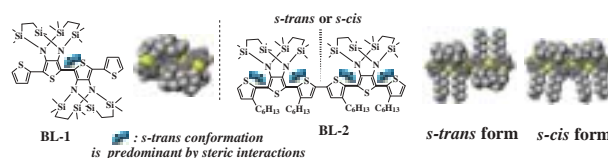
Figure 1. Molecular structure of **BL-1** and **BL-2**.

(A) 3.3 nm x 3.3 nm (Vs = -2.5 V, It = 5 pA) **(B)** 23.5 nm x 23.5 nm (Vs = -2.5 V, It = 5 pA)
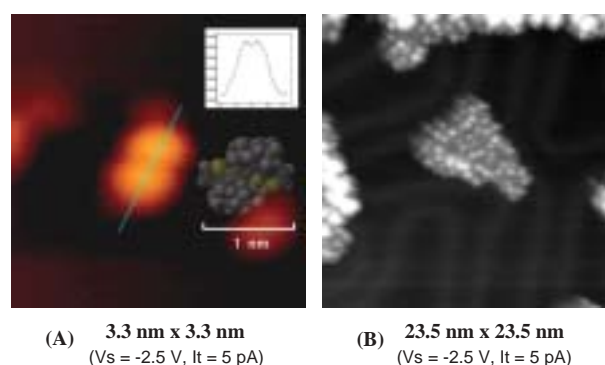
Figure 2. STM images of **BL-1** on Au(111) surface at 63 K.

(A) 98 nm x 98 nm (Vs = 2 V, It = 5 pA) **(B)** 10 nm x 10 nm (Vs = -2 V, It = 5 pA) **(C)** 5nm x5 nm (Vs = -2 V, It = 30 pA) **(D)** 10 nm x 10 nm (Vs = -2 V, It = 5 pA)
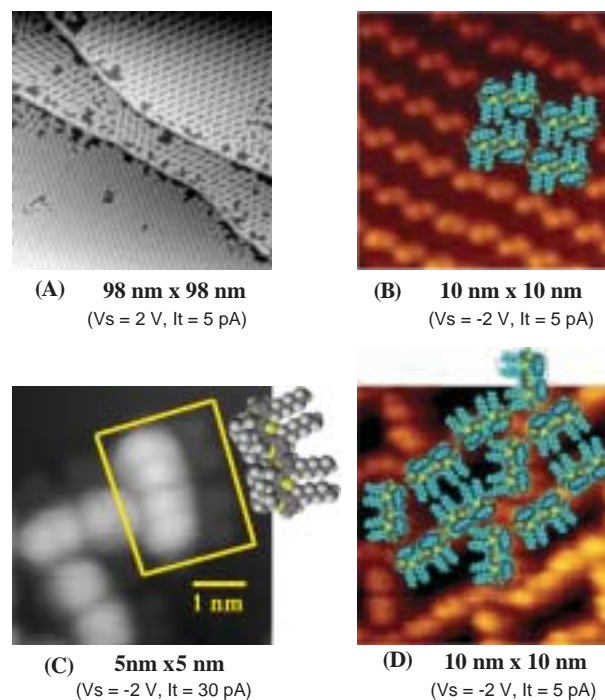
Figure 3. STM images of **BL-2** on Au(111) surface at 63 K.

VIII-C-11 Small Bandgap Polymers Involving Tricyclic Nonclassical Thiophene as a Building Block

TACHIBANA, Masamitsu[1]; TANAKA, Shoji; YAMASHITA, Yoshiro[2]; YOSHIZAWA, Kazunari[3]
([1]Kyoto Univ.; [2]Tokyo Inst. Tech.; [3]Kyushu Univ.)

The band electronic structures of one-dimensional polymers composed of thiophene, pyrrole, and tricyclic nonclassical thiophenes ([1,2,5]thiadiazolo[3,4-*b*]-thieno[3,4-*e*]pyrazine and dithieno[3,4-*b*:3',4'-*e*]-pyrazine) **1**–**2** are calculated and analyzed at the extended Hückel level of theory, with the development of highly conducting polymers in mind. The tricyclic nonclassical thiophenes that can impose quinoid-type characters to the resulting polymers are effective building blocks for the preparation of small bandgap polymers. Calculated bandgaps are discussed in view of the frontier crystal orbitals and the bond length alternation of the polymers. The homopolymer of [1,2,5]thiadiazolo[3,4-*b*]thieno[3,4-*e*]pyrazine **1a** that is predicted to have a bandgap of 0.1 eV is a good candidate for an intrinsic conducting polymer without dopants.

1a: [A]$_n$ 1b: [AT]$_n$ 1c: [AP]$_n$ 1d: [ATT]$_n$ 1e: [APP]$_n$

2a: [B]$_n$ 2b: [BT]$_n$ 2c: [BP]$_n$ 2d: [BTT]$_n$ 2e: [BPP]$_n$
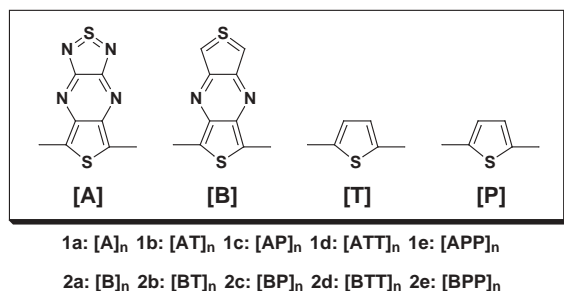
Figure 1. Polymers composed of thiophene, pyrrole, and tricyclic nonclassical thiophenes.

VIII-C-12 Prospects of Single Molecule Devices for Future High Performance Infromation Technologies

WADA, Yasuo[1]; TSUKADA, Masaru[2]; FUJIHIRA, Masamichi[3]; MATSUSIGE, Kazumi[4]; OGAWA, Takuji[5]; HAGA, Masa-aki[6]; TANAKA, Shoji
([1]Hitachi Ltd., Adv. Res. Lab.; [2]Univ. Tokyo; [3]Tokyo Inst. Tech.; [4]Kyoto Univ.; [5]Ehime Univ.; [6]Chuo. Univ.)

Current information technologies use semiconductor devices and magnetic/optical discs, however, it is foreseen that they will all face fundamental limitations within a decade. This paper reviews the prospects and problems of single molecule devices, including switching devices, wires, nanotubes, optical devices, storage devices and sensing devices for future information technologies and other advanced applications in the next paradigm. The operation principles of these devices are based on the phenomena occurring within a single molecule, such as single electron transfer, direct electron-hole recombination, magnetic/charge storage and regand-receptor reaction. Four possible milestones for realizing the Peta (10^{15})-floating operations per second (P-FLOPS) personal molecular supercomputer are described, and the necessary technologies are listed. These include, (1) two terminal conductance measurement on single molecule, (2) demonstration of two terminal molecular device characteristics, (3) verification of three terminal molecular device characteristics and (4) integration of the functions of "molecular super chip." Thus, 1000 times higher performance information technologies would be realized with molecular devices.

VIII-D Designing Artificial Photosynthesis at Molecular Dimensions

Photosynthesis is one of the finest piece of molecular machinery that Nature has ever created. Its ultrafast electron transfer and following well-organized sequence of chemical transformation have been, and will continue to be, challenging goals for molecular scientists. We are trying to mimic the function of photosynthesis by assembling molecular units that perform individual physical/chemical action. The molecular units include porphyrins, redox active organic molecules, and transition metal complexes. Our ultimate goal is to design artificial molecular systems that effect multiple chemical reactions triggered by light on the basis of molecular rationale.

Last year we focused our attention on combining "redox pool" with photoinduced electron transfer.

VIII-D-1 Synthesis and Photochemical Reactions of Multistep Redox Polymer Containing Porphyrin and Metalocenes

HINO, Takami[1]; ITO, Hajime; NAGATA, Toshi
(*[1]Kyoto Univ.*)

Photoinduced electron transfers involving porphyrins are widely studied, but utilizing the high-energy radical ion pairs for driving chemical reactions remains to be a great challenge. One of the missing features in artificial photosynthetic models based on organic molecules is the function of redox pool—that receives the oxidizing and/or reducing equivalents from the photogenerated ion pairs and retains them sufficiently long until the substrates for chemical reactions are ready. This feature is essential for photosynthetic processes to be successful, because the photogenerated high-energy states are otherwise too short-lived to cooperate with (comparatively slow) chemical reactions. In biological systems various electron-carrying substances (proteins like soluble cytochromes, or cofactors like quinones) play the role, whereas in many artificial systems solid particles with electronic band structure (metal or semiconductor nanoparticles) do that. It should be an important research topic to develop redox pools with organic and organometallic substances and utilize in molecule-based artificial photosynthetic systems.

With this goal in mind, we prepared polysiloxanes containing ferrocene and porphyrin moieties (Figure 1). The ferrocenes are present in 20-fold excess of porphyrins, so that they can serve as 'electron pool' that retains photogenerated holes on porphyrin moieties.

The desired polymer **1** was prepared by hydrosilylation of a mixture of vinylferrocene and (4-pentenyloxy)phenyl substituted porphyrin with poly(methylhydro)siloxane catalyzed by hexachloroplatinic acid (Figure 2). Purification by reprecipitation from tetrahydrofuran/methanol followed by gel permuation chromatography yielded the product with reasonably narrow size distribution ($M_w/M_n = 1.4$). The cyclic voltammogram of **1** is shown in Figure 3; a large peak of ferrocenes and two small peaks of porphyrins are observed as expected.

The photoreaction of **1** with quinones were examined. We previously reported the reductive silylation of quinones photocatalyzed by porphyrins (H. Ito, T. Hino, T. Nagata, submitted; see also Annual Review 2000). As the photoreduced product of quinones are trapped by silylating reagents, this reaction can be used to continuously pick up electrons from donor molecules. Indeed, irradiation with visible light of a mixture of the polymer **1**, 2,3,5,6-tetramethyl-1,4-benzoquinone, Me_3SiCl and pyridine in tetrahydrofuran/N,N-dimethylformamide gave the oxidized form of **1** (*i.e.* the ferrocene moieties were converted to ferrocenium) together with the reduced product, 2,3,5,6-tetramethyl-1,4-bis(trimethylsiloxy)benzene (Figure 4). The full identification, as well as the follow-up chemistry (*i.e.* reducing back to the original form) of the oxidized form of **1** is currently under way.
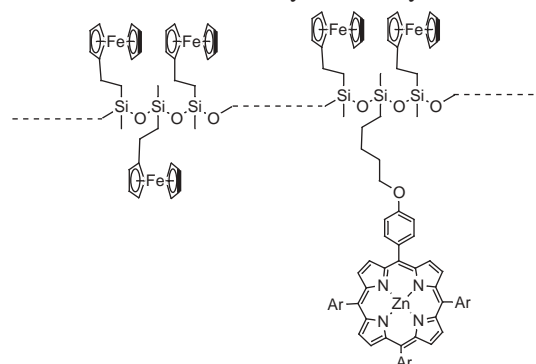
Figure 1. A redox polymer with a photoactive moiety.
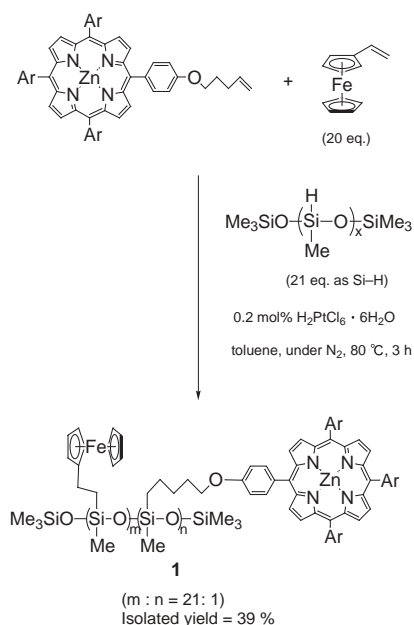
Figure 2. The synthesis of polymer **1**.

-0.10 V +0.29 V

-1.0 0 +1.0

V vs FeCp$_2$/FeCp$_2^+$
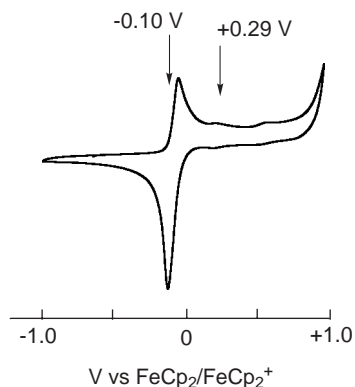
Figure 3. The cyclic voltammogram of polymer **1**. Conditions: CH$_2$Cl$_2$ with 0.1 M Bu$_4$NClO$_4$, Pt working electrode.

(4.8 eq.)
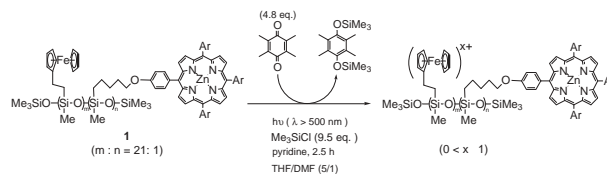
Figure 4. The photoreaction of polymer **1** with quinone and Me$_3$SiCl.

VIII-E Development of New Metal Complexes as Redox Catalysts

Redox catalysis is an important field of chemistry which translates a flow of electron into chemical transformation. It is also one of the requisites for artificial photosynthesis. This project of ours aims at developing new metal complexes that perform redox catalysis at low overpotential. Last year we focused our attention to developing terdentate ligands with strong donor character. 2,2':6',2"-Terpyridine has been the ligand of choice in this field, but our study has now revealed that 2,2':6',2"-terpyridine-1,1"-dioxide is also a good candidate for developing new catalysts.

VIII-E-1 Synthesis of Terpyridine-based Binary Ligands and Their Metal Complexes

ITO, Kaname; NAGATA, Toshi; TANAKA, Koji

In recent years, metal complexes of 2,2':6',2"-terpyridine (terpy) and their derivatives are gaining considerable attention as electrochemical catalysts. Derivatives of terpyridine are particularly suitable for electrocatalytic applications because they are chemically robust and form stable complexes with a wide variety of transition metals. On the other hand, the syntheses of terpyridine derivatives are often so troublesome that it is difficult to tune the electrochemical behavior of the metal complexes.

The *N*-oxides of pyridines are promising ligands that are easily derived from pyridine compounds by one-step peracid oxidation. Metal complexes of pyridine *N*-oxide and 2,2'-bipyridine 1,1"-dioxide are numerous, whereas the *N*-oxides of terpyridine have been much less studied. Only a few reports were published on the metal complexes of 2,2':6',2"-terpyridine 1,1',1"-trioxide (terpyO$_3$).

We prepared a series of first-row transition metal complexes of 2,2':6',2"-terpyridine 1,1"-dioxide (terpyO$_2$) are reported. Four new bis complexes [M-(terpyO$_2$)]X$_2$ (M = Mn(II), Fe(II), Co(II) and Ni(II); X = ClO$_4^-$ and BF$_4^-$) and one mono complex [Cu(terpyO$_2$)-(H$_2$O)](ClO$_4$)$_2$ were isolated and characterized, and electrochemical properties were examined. The crystal structure of the Fe(II) complex [Fe(terpyO$_2$)$_2$](ClO$_4$)$_2$ is shown in Figure 1. The ligands have non-planar conformations with an approximate C$_2$ symmetry, which makes the overall symmetry of the complex cation approximately D$_2$. The Ni(II) complex [Ni-(terpyO$_2$)$_2$](ClO$_4$)$_2$ was isostructural with the Fe(II) complex. The X-ray structure of the Cu(II) complex was also examined (Figure 2), and it was revealed that the Cu(II) ion was square-planar with the terdentate terpyO$_2$ ligand whose conformation was similar as in the Fe(II) and Ni(II) complexes.

The cyclic voltammograms of the four bis complexes revealed that the M(III)/M(II) redox potentials of the Mn(II), Fe(II) and Ni(II) complexes showed negative shifts (–0.77 to –0.24 V) compared to the terpyridine complexes, whereas the potential of the Co(II) complex showed a slightly positive shift (+0.03 V). The Fe(II) complex is particularly interesting, because the low $E_{1/2}$ value and the ease of ligand exchange (revealed by ESI-MS) make the complex promising for application as a redox catalyst. Also worth noting is the Mn(II) complex, for which another reversible wave corresponding to the Mn(IV)/Mn(III) couple was observed. The electrocatalytic properties of the terpyO$_2$ complexes is now being investigated.
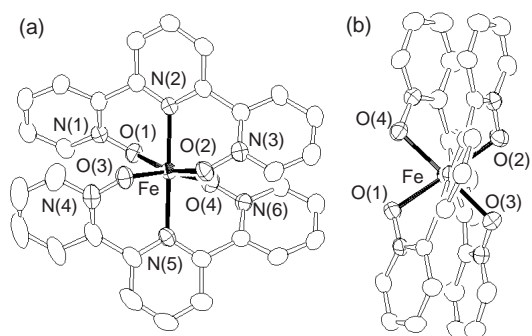
Figure 1. ORTEP view (50% probability ellipsoids) of the complex cation $[Fe(terpyO_2)_2]^{2+}$.
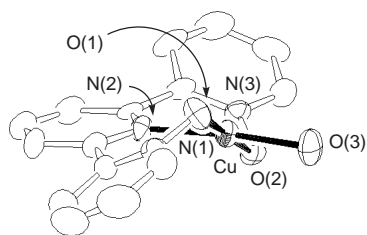
Figure 2. ORTEP view (50% probability ellipsoids) of the complex cation $[Cu(terpyO_2)(H_2O)]^{2+}$.

VIII-F Development of Organic n-Type Semiconductors for Molecular Thin-Film Devices

Organic light-emitting diodes (OLEDs) and field-effect transistors (FETs) based on π-conjugated oligomers have been extensively studied as molecular thin-film devices. Organic n-type semiconductors with low electron-injection barriers and high electron mobilities are required for highly efficient OLEDs and n-type FETs. Radical anions of an n-type semiconductor have to be generated easily at the interface with a metal electrode (electron injection), and electrons must move fast in the layer (electron mobility). Compared with organic p-type semiconductors, organic n-type semiconductors for practical use are few and rather difficult to develop. Recently, we found that perfluorinated oligomers are efficient electron-transport materials for OLEDs.

VIII-F-1 Tetradecafluorosexithiophene: The First Perfluorinated Oligothiophene

SAKAMOTO, Youichi; KOMATSU, Shingo; SUZUKI, Toshiyasu

Perfluoro-a-sexithiophene (**PF-6T**) was synthesized by the fluorination of thienyllithiums with *N*-fluoro-*N*-(phenylsulfonyl)benzenesulfonamide and the Stille and Ullmann couplings. **PF-6T** is an orange crystalline solid and slightly soluble in $CHCl_3$ and aromatic solvents such as toluene. Its structure was determined by EI-MS, elemental analysis, and X-ray crystallography. **PF-6T** exhibits bluish-green photoluminescence in solution and an orange emission in the solid state. A sharp melting endotherm was observed at 286 °C by DSC. The differential pulse voltammogram (DPV) in 1,2-dichlorobenzene showed that the redox potentials of **PF-6T** shifted positively relative to α-sexithiophene (**6T**). Single crystals of **PF-6T** were successfully grown by slow sublimation at 270 °C under a flow of 1 atm of argon. The structure of **PF-6T** is *all-trans* and planar as observed for **6T**. **PF-6T** adopts a π-stack structure with face-to-face molecules. This is quite different from the herringbone structure of **6T**, in which π-π interactions between neighboring molecules are minimized to reduce the repulsion between π-orbitals. High electron mobility is expected along the π-π stacking direction. Fabrication of n-type FETs with this new material is currently underway.

Figure 1. Perfluoro-α-sexithiophene and α-sexithiophene.

VIII-F-2 Highly Efficient Phosphorescence from Organic Light-Emitting Devices with an Exciton-Block Layer

IKAI, Masamichi[1]; TOKITO, Shizuo[1]; SAKAMOTO, Youichi; SUZUKI, Toshiyasu; TAGA, Yasunori[1]
(*[1]Toyota Central R&D Labs.*)

One of the keys to highly efficient phosphorescent emission in organic light-emitting devices is to confine triplet excitons generated within the emitting layer. We employ "starburst" perfluorinated phenylenes ($C_{60}F_{42}$) as a both hole- and exciton-block layer, and a hole-transport material 4,4',4"-tri(*N*-carbazolyl) triphenylamine as a host for the phosphorescent dopant dye in the emitting layer. A maximum external quantum efficiency reaches to 19.2%, and keeps over 15% even at high current densities of 10–20 mA/cm^2, providing several times the brightness of fluorescent tubes for lighting. The onset voltage of the electroluminescence is as low as 2.4 V and the peak power efficiency is 70–72 lm/W, promising for low-power display devices.

VIII-G The Effects of the 2D Spin-Echo NMR Experiment on a Solid-State Homonuclear Spin-1/2 Pair

The 2D spin-echo NMR experiment can reintroduce the influence of homonuclear dipolar interactions average out by magic-angle sample spinning (MAS).

VIII-G-1 Novel Structure Discovered on Two-Dimensional Spin-Echo NMR Spectra for a Homonuclear Spin-1/2 Pair in Rotating Solids

KUWAHARA, Daisuke; NAKAI, Toshihito[1]; ASHIDA, Jun[2]; MIYAJIMA, Seiichi
([1]Tokyo Univ. Agric. Tech.; [2]Kyoto Univ.)

Two-dimensional (2D) spin-echo NMR experiments have been carried out on polycrystalline $[2,3-^{13}C_2]$-*L*-alanine under magic-angle sample spinning (MAS) conditions, so that two unusual resonance lines emerged along the F_1 axis. Theoretically it was found that the line positions were determined by the sample spinning frequency and the isotropic chemical-shift difference (*Chem. Phys. Lett.* **305**, 35 (1999)). Stimulated by the result, we carried out the 2D NMR experiment using a sufficiently small t_1 increment in order to enlarge the spectral width of the F_1 domain. As a result, we found many more resonance lines on a spectrum sliced along the F_1 axis. The line distribution had a very unique and interesting structure. To elucidate the line positions theoretically, the signal for the 2D spin-echo experiment performed with any t_1 increment was calculated analytically for a homonuclear two-spin-1/2 system undergoing MAS. We showed that virtually six resonance lines (exactly twelve resonance lines) occurred on a spectrum sliced along the F_1 axis. In addition, it was demonstrated that the intensities of some resonance lines were largely dependent on the dipolar interaction. The 2D spin-echo experiment for a solid-state homonuclear two-spin system was found to have the capability of extracting information concerning the dipolar tensor under MAS conditions.

VIII-H Rotational Echo Double Resonance (REDOR) Experiments with Overtone Adiabatic Inversion Pulses

The effect of overtone adiabatic inversion pulse on solid-state ^{14}N spins was investigated.

VIII-H-1 The Observation of REDOR Phenomenon for Solid-State ^{13}C-^{14}N spin Systems with the Help of Overtone Adiabatic Inversion Pulses

KUWAHARA, Daisuke

We applied overtone adiabatic inversion pulses to ^{13}C-^{14}N spin systems in powdered *L*-alanine undergoing MAS in order to observe REDOR phenomenon. The damping of ^{13}C resonance line intensities was compared with that corresponding to the REDOR experiments with normal RF pulses having a constant frequency. We tried to establish the theoretical treatment for the REDOR experiments with adiabatic inversion pulses.

Equipment Development Center

VIII-I Development of "IMS Machines"

The technical staff of the Equipment Development Center is partly engaged in planning, researching, designing and constructing "IMS machines." This machine, crowned with the acronym of the Institute for Molecular Science, is a high-tech experimental instrument, with emphasis on new technical idea and co-operative work with members inside and outside the Institute including those in industries. We collect suggestions of new instruments once every year from all of the members of IMS.

In this fiscal year, 2000, two project themes (1 thorough 2) were adopted as IMS machines. IMS machine projects 3 (IMS machine 1999) was completed, and project 4, 5 (IMS machine 1999) are under way.

1. **A Novel Method for Intensefying Oriented Molecular Beam: Electrostatic Honeycomb Filed**
   (proposed by SHIMIZU Yuichiro, CHE Dock-Chill, HASHINOKUCHI Mitihiro, SUZUI Mitsukazu, WATANABE Michio and KASAI Toshio)
2. **The Development of a Photoion and Photoelectron CMOS Imaging Detector with High Repetition Rates**
   (proposed by GEJO Tastuo and YOSHIDA Hisashi)
3. **Vacuum-Chamber-Based High Voltage Application Apparatus to Fabricate Wide-Range Nonlinear Optical Wavelength Converters**
   (proposed by KURIMURA Sunao, TAIRA Takunori, KOBAYASHI Kazuhiro and SUZUI Mitukazu)
4. **Sorption-Pump-Type Large-Scale Dilution Refrigerator**
   (proposed by SHIBAYAMA Hideo and KONDOH Takuhiko)
5. **High-Speed Array Detector**
   (proposed by Kazuo WATANABE and Hisashi YOSHIDA)

VIII-I-1 A Novel Method for Intensefying Oriented Molecular Beam: Electrostatic Honeycomb Field

SHIMIZU, Yuichiro; CHE, Dock-Chil; HASHINOKUCHI, Mitihiro[1]; SUZUI, Mistukazu; WATANABE, Michio; KASAI, Toshio[1]
(*[1]IMS and Osaka Univ.*)

By using electrostatic hexapole field, "steric effect" in chemical reactions has been extensively studied.[1] This method enables us to control reactant molecular orientation prior to collision. Intensity of oriented molecular beam, however, inevitably becomes weaker than its un-oriented molecular beam by more than one order of magnitude due to the hexapole-selection. This is the most disadvantageous point when we wish to use oriented molecular beam. This project aims at resolving this weak point by developing a sophisticated method so-called "Electrostatic Honeycomb Field" for intensifying oriented molecular beam. Basic idea of the method is that a beam intensity is simply proportional to the number of beam lines and they can be focused on a point in space after the hexapole state-selection.

Figure 1 (top) shows photo views of the newly developed honeycomb electric field. The electric field consists of 24 pieces of electrodes which form seven sets of hexapole electric field lines. The seven beam lines are pointing at a point in downstream. Figure 1 (bottom) shows the schematic illustration of the apparatus. Seven sets of pulse valves (1 mmφ), beam skimmer (1 mmφ), and beam collimator (5 mmφ) followed by the honeycomb field (1 m long), are mounted on four pieces of supporting stainless rods (15 mmφ). All beam lines focus on to a point in the 1 m forward distance from the honeycomb filed. The honeycomb electrode is made from carbon fiber (CFPR pipe, 15 mmφ, 7.5 mmφ, 1 m long). Carbon fiber is chosen because of its light weight and high electric conduction. Polyacetal insulator is used as the electrode supporter. Beam intensity is monitored by a quadrupole mass spectrometer. As a preliminary experiment, we made comparison of the beam intensity between single-beam run and seven-beam run, and we obtained the expected beam enhancement. Additionally, we have obtained the focusing effect for acetonitrile molecule (CH_3CN, μ = 3.92 D) by use of honeycomb electric field for the first time. We are now doing to optimize the operating in order to get the most intensisve oriented molecular beam.

Reference
1)"*Steric Effects in Small Radical Formations*," in The *Chemical Dynamics and Kinetics of Small Radicals, Part II*, K. Liu and A. Wagner, Eds., Advanced Series in Physical Chemistry (World Scientific), K. Kuwata, and T. Kasai, Vol. **6**, 842-935 (1995)
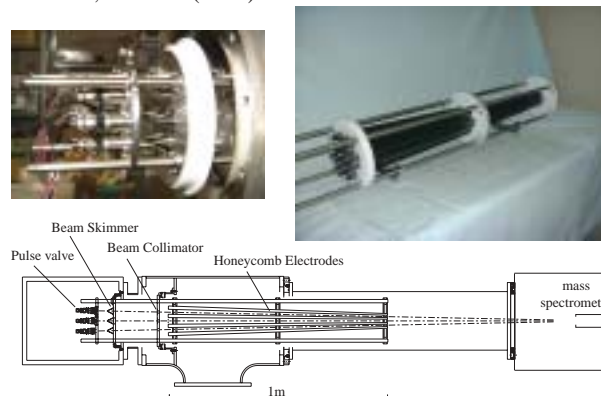
Figure 1. Honeycomb type orientational state selector. The beam source and the honeycomb electric field (top) and a schematic view of the newly designed apparatus for intense oriented molecular beam (bottom).

Ultraviolet Synchrotron Orbital Radiation Facility

VIII-J Development of the UVSOR Light Source

VIII-J-1 UVSOR Upgrade Project

KATOH, Masahiro; HAYASHI, Kenji; HONDA, Toru[1]; HORI, Yoichiro[2]; HOSAKA, Masahito; KINOSHITA, Toshio; KODA, Shigeru; TAKASHIMA, Yoshifumi; YAMAZAKI, Jun-ichiro; KITAMURA, Hideo[3]; HARA, Toru[3]; TANAKA, Takashi[3]
(*[1]KEK-PF; [2]IMS and KEK-PF; [3]RIKEN*)

Towards upgrading UVSOR, we have designed a new magnetic lattice, in which the beam emittance would be reduced and the number of the straight sections available for insertion devices would be doubled. The accelerator components necessary for the upgrade project are under development. A combined function magnet was designed, which is capable of producing both quadrupole field and sextupoles filed. A prototype was constructed and the field measurements are in progress. Some early results have shown that the required field strengths could be achieved. The beam position monitor system was replaced and successfully commissioned. The new system can measure one orbit in a second with resolution of a few microns. It will be a powerful tool in stabilizing the low emittance electron beam. An in-vacuum undulator is under construction. This will be installed in the ring, in spring, 2002, to check the performance and the effects on the electron beam. This type of device is expected to provide SR beams of higher brilliance in higher energy region above 100 eV.

VIII-J-2 Storage Ring Free Electron Laser

KATOH, Masahiro; GEJO, Tatsuo; HAMA, Hiroyuki[1]; HAYASHI, Kenji; HOSAKA, Masahito; KINOSHITA, Toshio; KODA, Shigeru[2]; SHIGEMASA, Eiji; TAKASHIMA, Yoshifumi; YAMAZAKI, Jun-ichiro
(*[1]Tohoku Univ.; [2]IMS and Saga Univ.*)

The storage ring free electron laser (FEL) at UVSOR has successfully oscillated in the wide spectral region from 590 nm to 240 nm. In these years, we have made many efforts to realize stable oscillation and high average power. As the result, the average power has exceeded 1 W, which is the world highest record as a storage ring FEL. One of the unique features of the storage ring FEL is the natural and perfect pulse-to-pulse synchronization with the synchrotron radiation pulses, which are produced in the same storage ring. By utilizing this, we have performed a pump-probe experiment, in which SR pulses from an undulator excite Xe atoms and the excited state with 1 nsec lifetime was probed by the FEL pulses.

VIII-J-3 Vacuum System Remodeling for the UVSOR Upgrading

HORI, Yoichiro; YAMAZAKI, Jun-ichiro; KATOH, Masahiro; HAYASHI, Kenji; HOSAKA, Masahito; KINOSHITA, Toshio

The beam lifetime of the UVSOR depends strongly upon both bunch size and pressure. Because a high brilliance is obtained by reducing the bunch size in the UVSOR upgrading plan designed at present, the lower operating pressure should be achieved to maintain a long beam lifetime. This project purposes to improve the present vacuum condition and to achieve the required operating pressure in the upgraded ring. We have started observation and inspection of the vacuum situation of the ring. Also the design of new beam chambers for the upgraded ring has been undertaken, where reinforcing the pumping speeds and increasing the beam position monitor are considered.

VIII-K Researches by the USE of UVSOR

VIII-K-1 Photo-Induced Phase Transition of Spin-Crossover Complex Studied by Photoelectron Spectroscopy

KAMADA, Masao; DOI, Yo-ichiro[1]; TAKAHASHI, Kazutoshi; FUKUI, Kazutoshi[1]; TAYAGAKI, Takeshi[2]; TANAKA, Koichiro[2]
(*[1]Fukui Univ.; [2]KyotoUniv.*)

The photo-induced phase transition (PIPT) of an organometal spin-crossover complex [Fe(2-pic)$_3$]Cl$_2$·EtOH has been studied by photoelectron spectroscopy. The Fe-3d and N-1s spectra showed remarkable changes due to the photo-excitation at low temperatures, indicating that the electron charge is transferred from nitrogen to Fe atoms in the PIPT. The electronic structure of the photo-induced phase is very different from that of the high-temperature phase, which is caused by thermally induced phase transition (TIPT). The valence-band spectra of the photo-induced phase is in good agreement with the cluster calculation involving the E$_g$-distortion of Fe-octahedrons, indicating that the symmetry lowering in the excited state plays an important role to cause the PIPT. It was also found that the valence-band spectra are enhanced around T_c's, indicating the dynamics of the PIPT competing with the

TIPT.

VIII-K-2 Beam-Line Systems for Pump-Probe Photoelectron Spectroscopy Using SR and Laser

KAMADA, Masao; TANAKA, Senku; TAKAHASHI, Kazutoshi; DOI, Yo-ichiro[2]; FUKUI, Kazutoshi[2]; KINOSHITA, Toyohiko[3]; HARUYAMA, Yuichi[4]; ASAKA, Shuji; FUJII, Yasuo[1]; ITOH, Minoru[5]
(*[1]Osaka City Univ.; [2]Fukui Univ.; [3]ISSP, Univ. Tokyo; [4]Himeji Inst. Tech.; [5]Shinshu Univ.*)

Since the first report by Saile, several groups have been developing new spectroscopy based on the combination of synchrotron radiation and laser light. The new spectroscopy are very attractive and interesting, since both synchrotron radiation and laser light are useful light sources with different characteristics: Synchrotron radiation provides high photon energy to investigate core-levels, while laser light is so intense to produce excited valence states with high density. Various combinations of two powerful light sources may open new scientific achievements. Combined systems for photoelectron spectroscopy using synchrotron radiation and laser light have been constructed at BL 5A and BL6A2 in the UVSOR facility, Okazaki. The systems consist of high-performance photoelectron spectrometers and mode-locked lasers. The performance of the systems is reported with a few examples.

VIII-K-3 Experiments with Combined Laser and SR at the UVSOR Facility

KAMADA, Masao

There are several ways to use SR and Laser. One is to use SR as pump and laser as probe. This is powerful to investigate many interesting phenomena concerning with core-level excitations. Second is to use laser as pump as SR as probe. This is very useful to investigate many phenomena relating with valence excitations. Third one is to use SR and laser simultaneously as 2-photon excitation. This will open the new science relating with core-level excitation too. In recent years, brilliance of SR is increased and also short- wavelength lasers are under progress. So, many persons may expect more combinations in near future such as SR-Pump + SR-Probe, Laser-Pump + Laser-Probe, Laser 2-Photon-Pump, and SR 2-Photon-Pump.

VIII-K-4 Cesiumoxide-GaAs Interface and Layer Thickness in NEA Surface Formation

MORÉ, Sam Dylan; TANAKA, Senku[1]; NISHITANI, Tomohiro[2]; NAKANISHI, Tsutomu[2]; KAMADA, Masao
(*[1]GUAS; [2]Nagoya Univ.*)

Negative electron affinity (NEA) surfaces have found applications as efficient photocathodes and the NEA surface of GaAs(100) and its superlattice is known to be a useful emitter of spin-polarized electrons with a high degree of polarization and efficiency. This can be achieved by the 'jo-jo'-technique, where Cs deposition and subsequent oxidation are repeated several times. The details of NEA surface formation, however, are not fully understood: previous reports differ considerably both in describing the method of production as well as the underlying chemical and physical mechanism. In this paper we present a systematic study of various sample treatments on GaAs(100) using photoemission spectroscopy. Analyzing the influence of the both the cesiation and oxidation on the bandbending and monitoring the photoemission yield on bulk GaAs(100), we have been able to distinguish three different regimes of activation, depending on the total thickness of the overlayer, the Cs:O ratio and the resulting chemical interaction with the substrate.

VIII-K-5 Surface Photovoltage Effects on *p*-GaAs (100) from Core-Level Photoelectron Spectroscopy Using Synchrotron Radiation and a Laser

TANAKA, Senku[1]; MORÉ, Sam Dylan; MURAKAMI, Junichi[2]; ITOH, Minoru[2]; FUJII, Yasuo[3]; KAMADA, Masao
(*[1]GUAS; [2]Shinshu Univ.; [3]Osaka City Univ.*)

The surface photo-voltage (SPV) effect on laser-excited *p*-GaAs (100) has been investigated using core-level photoelectron spectroscopy with synchrotron radiation (SR). The energy shift of the Ga-*3d* photo-electrons due to the SPV effect was remarkably dependent on the sample temperature and the laser photon-flux. The dependence in each case was well interpreted on the basis of a simple SPV formula derived from the band-bending scheme with excess photocarriers. The magnitude of the band bending was about 0.8 eV for clean *p*-GaAs (100) surfaces having no electrodes. Similar core-level shifts were observed in the Ga-3*d* and Cs-4*d* spectra of Cs/GaAs (100), indicating an unpinned behavior of the electronic states of the Cs surface layer. The time response of the SPV effect was also investigated in the nano-second range using a pump-probe method with SR and laser.

VIII-K-6 Performance Tests for the Newly Constructed Varied-Line-Spacing Plane Grating Monochromator at BL-4B

SHIGEMASA, Eiji; NAGASONO, Mitsuru; OJI, Hiroshi; HATSUI, Takaki; GEJO, Tatsuo; KOSUGI, Nobuhiro

The practical construction of the new Varied-line-spacing Plane Grating Monochromator (VLS-PGM) on BL4B at the UVSOR has begun, in order to realize

various spectroscopic studies with high resolution in the soft x-ray range (100~1000 eV). The installation has been successfully finished in October 2000. The vacuum condition was ready for obtaining the first SR light before the end of December 2000, and the first performance tests for the monochromator have been carried out.

The absolute photon flux for two gratings available so far (267 and 800 l/mm) has been measured using a Si photodiode supplied by IRD Inc. With the entrance and exit slit openings set at 25 and 10 μm, corresponding to the resolving power of 10000 at 400 eV with the 800 l/mm grating, the photocurrent from the photodiode was measured after the sample position, and converted into the absolute photon flux, taking account of the quantum efficiency of the photodiode. In this case, the resolving power in the regular spectral region for each grating is more than 3000. The throughput photon flux measured ranges from 10^8 to 10^9 photons/sec for the ring current of 100 mA, which is a little smaller than that estimated.

The inner-shell photoabsorption spectra of atoms and molecules were measured, to examine the instrumental resolution. The K-shell photoabsorption spectrum of N_2 is presented in Figure 1. The entrance and exit slits were set for achieving the resolving power of 10000. From the comparison with all available spectra of the N 1s → π* resonance of N_2, it seems to be reasonable that the resolving power obtained here is more than 5000. The photoabsorption spectra in the vicinity of the 2p ionization thresholds of S (~170 eV) for H_2S, OCS, SO_2, and CS_2 were also recorded using the 267 l/mm grating. Through the performance tests, it turned out that the resolving power more than 3000 is achieved at the entire photon energy region of interest.

Figure 1. K-shell photoabsorption spectrum of N_2.
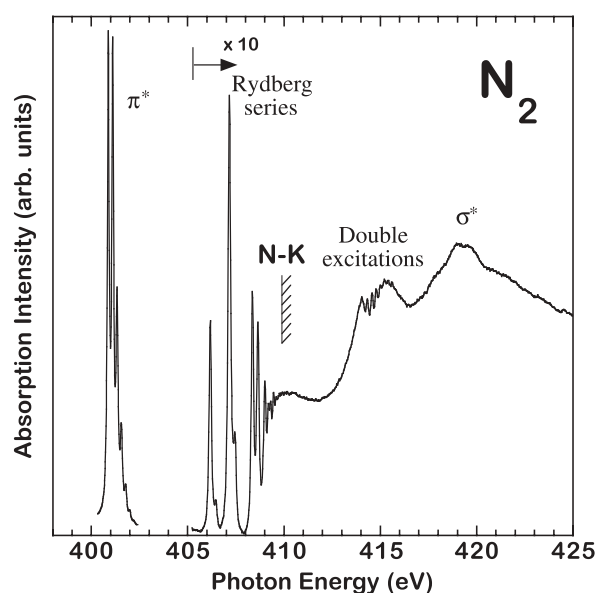
KOSUGI, Nobuhiro

High-resolution angle-resolved ion-yield spectra of N_2 have been measured using linearly polarized synchrotron radiation. The ion yield spectra (I_0 and I_{90}) measured at 0 and 90 degrees with respect to the electric vector of the light relate to the Σ ($\Delta\Lambda = 0$) and $\prod$ ($\Delta\Lambda = \pm 1$) symmetry components in the conventional photoabsorption spectrum, respectively. The Σ and $\prod$ symmetry spectra in the vicinity of the K-shell ionization threshold of N_2, except for the π* resonance are shown in Figure 1. Clear decomposition of the conventional photoabsorption spectrum into its symmetry components is observed. Concentrating on the K-shell ionization region, structures labeled from A to F, which are considered as being due to the multiple excitations, can be seen in the Σ and $\prod$ symmetry spectra. A strong and broad enhancement due to the σ* shape resonance, which is a typical single electron transition in the continuum, is found only in the Σ symmetry spectrum. A very weak structure B just above the ionization threshold, and a shoulder structure E of the shape resonance enhancement are observed in the Σ spectrum. In the $\prod$ symmetry spectrum, a structure A just above the ionization threshold, rather strong features C and D at the double excitation region, and a clear enhancement F just at the shape resonance position are detectable.

In order to elucidate the electronic structures of the spectral features observed in Figure 1, ab initio SCF-CI calculations have been performed, taking account for the transitions from $2\sigma_u$, $3\sigma_g$, and $1\pi_u$ orbitals into $1\pi_g$ (π*) orbital. As a consequence, it is found that the structure labeled F in the $\prod$ spectrum just at the shape resonance position is attributable to the triple excitations, where a simultaneous excitation of two valence electrons follows the inner-shell excitation.
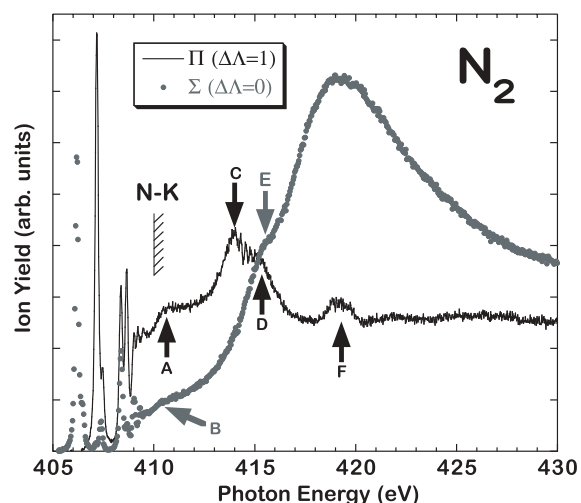
Figure 1. Symmetry-resolved K-shell photoabsorption spectrum of N_2.

VIII-K-7 High-Resolution Symmetry-Resolved K-Shell Photoabsorption Spectra of N_2

SHIGEMASA, Eiji; NAGASONO, Mitsuru; OJI, Hiroshi; HATSUI, Takaki; GEJO, Tatsuo;

VIII-K-8 Dynamical Angular Correlation in Molecular Auger Decay

GUILLEMIN, Renaud[1]; SHIGEMASA, Eiji; LE GUEN, Karine[1]; CEOLINE, Denis[1]; MIRON,

Cataline[1]; LECLERCQ, Nicola[1]; MORIN, Paul[1]; SIMON, Marc[1]
(*[1]LURE*)

The first measurements of the angular distribution of Auger electrons from fixed-in-space molecules have been performed in the C *K*-shell ionization region of CO, for both parallel and perpendicular orientation of the molecular axis with respect to the light polarization vector. The ions emitted parallel or perpendicular to the electric vector of the incident radiation determine the possible Σ or Π symmetries in the ionization channels, respectively. The angular distributions obtained for the $CO^{2+} B^1\Sigma$ Auger final state show dramatic spectral variations, which also depend on the initial ionization channels, Σ or Π. The result strongly suggests the breakdown of the two-step model in which the Auger decay is treated independently of the initial photoionization process.

VIII-K-9 Pump /Probe Experiments with FEL and SR Pulses at UVSOR

GEJO, Tatsuo; SHIGEMASA, Eiji; NAKAMURA, Eiken; HOSAKA, Masahito; KODA, Shigeru; KATOH, Masahiro; YAMAZAKI, Jun-ichiro; HAYASHI, Kenji; TAKASHIMA, Keiji; HAMA, Hiroyuki[1]
(*[1]Tohoku Univ.*)

Synchrotron radiation free electron lasers (SRFEL or FEL) has been used as a light source because of high power, high coherence and its unique temporal feature. Pump and probe experiments using FEL and synchrotron radiation (SR) pulses have been tried to perform for the last decade. This is due to the fact that the FEL pulse naturally synchronizes with the SR pulse. As the first gas-phase experiment combined FEL with SR, we have carried out the two-photon double-resonant excitation on Xe atoms, utilizing a SR pulse as a pump and an FEL pulse as a probe light.

The experiments were performed on the undulator beamline BL3A1 at UVSOR, where no monochromator is installed. An LiF filter was employed to suppress higher harmonics radiation from the undulator. The estimated photon flux is about 10^{13} photons/sec/0.1% B.W. at I = 100 mA. The FEL pulses were extracted through the backward mirror and transported to an experimental station of the BL3A1 through a series of multi-layer mirrors. The flight path of FEL, which was adjusted to synchronize timing between the FEL and the SR pulses, was about 30 m. A focusing mirror (f = 10 m) was placed in the center of the flight path to keep the beam size of FEL small throughout the transport. About 69% of the extracted power was transferred to the experimental station. The fine adjustment of the delay timing was made by using a movable optical delay system (50 cm) at the experimental station. The FEL and SR pulses introduced coaxially crossed an effusive jet of Xe atoms from a gas nozzle. The singly charged Xe ions produced in the interaction region were detected by means of a conventional channeltron.

The first experiment on the two-photon double-resonant excitation of the Xe* $5p^5nf$ autoionization states using the combination of a mode-locked laser and SR has already been successfully demonstrated by Meyer's group at LURE.[1] In the present work, the combination of FEL and the undulator radiation was chosen in place of the former. The fundamental harmonic of the undulator was adjusted to be 10.4 eV, in order to prepare the Xe* $5p^55d$ intermediate states in a first step. The Xe* $5p^54f$ autoionization resonance can be excited within the wavelength region of FEL in a second step. Because the lifetime of the intermediate states is quite short (600 ps), the synchronization between the SR and laser pulses is essential in this experiment.

The ion yield spectrum for the autoionization Xe* $5p^54f$ resonance obtained as shown in Figure 1. In this measurement the wavelength of FEL was swept by changing the gap of the helical optical klystron. During the measurement a newly developed feedback system was operated to stabilize the lasing. The asymmetric line shape described by the Fano formula has been clearly observed in Figure 1.

We are going to perform the same experiment at the beamline BL7B, where a high-resolution monochromator is installed, to improve the spectral resolution.

Reference
1) M. Gisselbrecht, A. Marquette and M. Meyer, *J. Phys. B: At., Mol. Opt. Phys.* **31** L977 (1998).
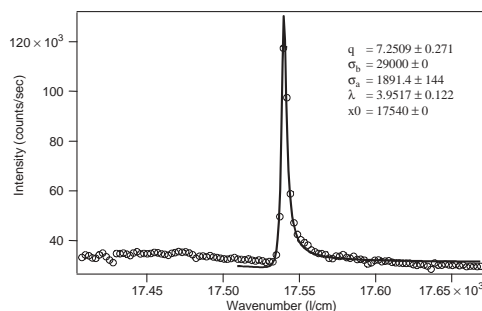
Figure 1. Two-photon ionization signal of Xe as a function of the wavelength of FEL.

Computer Center

VIII-L Theoretical Studies on Electronic Structure and Dynamics of Electronically Excited States in Polyatomic Molecules

VIII-L-1 Quantum Reactive Scattering Calculations of the O(^{1}D) + HCl Reaction Using the Global ab initio Potential Energy Surfaces of Electronic Excited States

NANBU, Shinkoh; BIAN, Wensheng; KAMISAKA, Hideyuki[1]; AOYAGI, Mutsumi; TANAKA, Kiyoshi[2]; NAKAMURA, Hiroki
(*[1]GUAS; [2]Hokkaido Univ.*)

The O (^{1}D) + HCl ($^1\Sigma^+$) reaction is quite important due to the significant role in stratospheric chemistry. The reaction is correlated with five electronic states, and there are two product channels, OH ($^2\Pi$) + Cl (^{2}P) and ClO ($^2\Pi$) + H (^{2}S) if its spin-symmetry is kept. Up to now, ab initio calculations of the ground PES and quantum wave packet calculations have been carried out along that surface, although at least three electronic potential energy surfaces are involved in this reaction.

In the present work, we have determined new global three ab initio potential energy surfaces accurately; and furthermore quantum wave packet dynamics calculations have been carried out to obtain the total reaction probabilities. The reaction probability for HCl ($v = 0, j = 0$) shows that the OH + Cl product channel via the 1^1A" state should be opened at the lower collision energy than $E_{coll} = 0.529$ eV, while the channel via 2^1A' should be closed. Although there was the discrepancy between previous theoretical works and experimental results, it was explained by our works including the electronic excited states.

VIII-L-2 Millimeter-Wave Spectroscopy of the Internal-Rotation Band of the He–HCN Cluster and Determination of the Empirical Intermolecular Potential Energy Surface

HARADA, Kensuke[1]; TANAKA, Keiichi[1]; TANAKA, Takehiko[1]; NANBU, Shinkoh; AOYAGI, Mutsumi
(*[1]Kyusyu Univ.*)

[*J. Chem. Phys.* submitted]

Millimeter-wave absorption spectroscopy was applied to the measurement of the internal-rotation band of the He–HCN cluster in the frequency region of 95–125 GHz. In total 13 rovibrational lines, split into nitrogen nuclear hyperfine structure, were observed for the fundamental internal-rotation band, $j = 1–0$.

In order to determine the empirical intermolecular potential energy surface (PES), the potential parameters were optimized by the Newton-Raphson method; the exact Schrödinger equation for the weekly bound complex was solved, and then the derivatives were evaluated. The obtained PES has a global minimum in the linear configuration (He···H–C–N) with a well depth of 27.827 cm^{-1}, and the saddle point located in the anti-linear configuration (H–C–N···He) is higher in energy than the global minimum by 8.174 cm^{-1}. The distance R_m from the He atom to the center of mass of HCN along the minimum energy path shows a large angular dependence; $R_m = 4.211$ Å and 4.104 Å in the linear and anti-linear forms, respectively, and has a minimum value of 3.513 Å in a T-shaped configuration. The rovibrational energies calculated from the empirical PES suggest that the cluster will dissociate at $l = 5$ in the first excited internal-rotation state, $j = 1$, where l denotes the quantum number for the end-over-end rotation of the cluster. This is consistent with the millimeter-wave observation of sudden disappearance of the first excited state of the intermolecular stretching vibration is located just below the dissociation limit, –0.202 cm^{-1}.

VIII-L-3 Determination of the Global Potential Energy Surfaces and Transition Wave Packet Dynamics for Polyatomic Systems

NANBU, Shinkoh; ISHIDA, Toshimasa[1]; GRAY, Stephen K.[2]; AOYAGI, Mutsumi
(*[1]Shizuoka Univ.; [2]Argonne Natl. Lab.*)

Computational algorithm for the determination of the global potential energy surfaces of polyatomic systems are developed with using the interpolant moving least squares scheme, which was proposed by Ishida and Schatz [*Chem. Phys. Lett.* **314**, 369 (1999)]. In this sheme, any derivatives in quantum-chemical calculations are not required to construct the surface and in contrast with previously developed shemes based on Shepard interpolation alone. In our new algorithm, the molecular conformations are generated with the Monte Carlo sampling, and then the ab initio calculations for all of the conformations are performed by parallel computing. Therefore, we have good advantage for computational time for the serial calculations. Application is made to the tetra-atomic systems, the 2OH $\leftrightarrow$ H$_2$O + O reaction.

Regarding to the wave packet dynamics, we are also developing the program code based on the MPI-library to make a time-evolution of the wave packet for the tetra-atomic systems.

VIII-L-4 Ab Initio Study of p-tert-Butylcalix[4]crown-6-ether Complexed with Alkyl Ammonium Cations

CHOE, Jong-In[1]; CHANG, Suk-Kyu[1]; WOOK

HAM, Seung[1]; NANBU, Shinkoh; AOYAGI, Mutsumi
(*[1]Chung-Ang Univ.*)

The conformations and energies of *p-tert*-butylcalix-[4]crown-6-ether (**1**) and its alkyl ammonium complexes have been calculated by *ab initio* (6-31G) quantum mechanics method. The cone conformation was found to be most stable for free host **1**. We have determined the binding site of these host-guest complexes focusing on the crown-6-ether or *p-tert*-butylcalix[4]arene pocket of the cone conformation of host molecule **1**. The primary binding site of host **1** for the recognition of alkyl ammonium guests was confirmed to be the central part of the crown moiety of cone conformation. The complexation energy calculations revealed that the ammonium cation without alkyl group showed the better complexation efficiency when combined with host **1**, that is in satisfactory agreement with the experimental results.

VIII-L-5 Nonadiabatic Process in Nonintegrable Quantum Systems

TAKAMI, Toshiya

We study nonadiabatic processes in classically nonintegrable systems. We have shown that extra-transitions arise from nonadiabatic couplings between eigenstates on the endpoints, and that, paradoxically, the usual adiabatic base is useless in the adiabatic limit to observe Landau-Zener transition. In order to describe the extra-transition theoretically, we introduce "boundary expansion" to obtain higher order terms of the nonadiabatic couplings. By the use of the expansion, we construct a new base which can describe non-adiabatic transition locally even in nonintegrable systems. This base is shown to be an extension of the superadiabatic base which is known as an asymptotic approximation of the exact solution. While our approach above is only for simple time-dependent nonadiabatic systems, we consider in the next applying the super-adiabatic analysis to chemical reactions. In order to analyze nonadiabatic processes on molecules in the adiabatic limit, we introduce the phase-space analysis through the method of the adiabatically renormalized Hamiltonian.

VIII-L-6 Theoretical Study of Endohedral Metalofullerene La@C_{76}

MAKI, Jun; AOYAGI, Mutsumi; KATO, Tatsuhisa; OKUBO, Shingo[1]
(*[1]GUAS*)

Endohedral metallofullerenes have attracted interests as new molecules having novel properties. We have carried out DFT calculation to get information on cage structure of La@C_{76}. Two IPR satisfying structures with T_d and D_2 symmetries are possible for C_{76} cage, while it has known from the ^{13}C NMR that empty C_{76} has D_2 symmetry. The result of geometry optimizations showed that La@C_{76} with T_d-cage is more stable. Theoretical IR spectrum of D_2-C_{76} reasonably reproduced experimental one of sublimed C_{76} films, although it was difficult to compare it with our measured IR spectra in CS_2.

VIII-L-7 Formation of HCl$^+$ (A$^2\Sigma^+$) and HBr$^+$ (A$^2\Sigma^+$) Resulting from He (2^{3}S) Penning Ionization of HCl and HBr

TOKUE, Ikuo[1]; TANAKA, Hiroyuki[1]; YAMASAKI, Katsuyoshi[1]; NANBU, Shinkoh
(*[1]Niigata Univ.*)

He (2^{3}S) Penning ionization of HCl and HBr leading to HCl$^+$ (A) and HBr$^+$ (A) has been studied optically by using a crossed-beam apparatus. The ratios of the vibrational population, $P_{v'}/P_v$ (v' = 2 and 3) of HCl$^+$ (A) and P_1/P_0 of HBr$^+$ (A), increase with the collision energy in the region of 120–200 meV. The rotational distributions of HCl$^+$ (A, v' = 0) and HBr$^+$ (A, v' = 0) can be represented by a double-Boltzmann distribution; the temperatures are 200 ± 50 and 700 ± 80 K for HCl$^+$ (A, v' = 0) and 250 ± 50 and 1200 ± 200 K HBr$^+$ (A), and are nearly independent of the collision energy. The model potential surface for He*(Li) + HCl as the entrance channel is nearly isotropic and shows a shallow dip of about 20 meV, while the surface for He + HCl$^+$ (A) as the exit channel is anisotropic and shows a deep minimum of 250 meV in the He–H–Cl collinear direction. These results suggest that at least two processes contribute to formation of these ions; one is the direct Penning ionization and the other is the formation via a temporary complex [HeHCl(A)]$^+$ by orbiting.

RESEARCH ACTIVITIES IX
Center for Integrative Bioscience

IX-A Molecular Mechanisms of Oxygen Activation by Heme Enzymes

By sharing a common prosthetic group, the heme enzymes such as cytochrome P450s, peroxidases, and catalases catalyze their own unique biological functions; monooxygenation, hydrogen peroxide dependent oxidation, and dismutation of hydrogen peroxide, respectively. Our efforts have been focused on the elucidation of the structure-biological function relationship of these heme enzymes by employing both enzymatic systems including mutants and their model systems.

IX-A-1 Molecular Engineering of Myoglobin: The Improvement of Oxidation Activity by Replacing Phe-43 with Tryptophan

OZAKI, Shin-ichi[1]; HARA, Isao; MATSUI, Toshitaka; WATANABE, Yoshihito
([1]Yamagata Univ.)

The replacement of Phe-43 in sperm whale myoglobin (Mb) by a tryptophan residue has been investigated to examine if an electron rich oxidizable amino acid residue in the heme vicinity increases oxidation activities of Mb. F43W Mb exhibits approximately 6- and 8-fold higher V_{max} values than the wild type in guaiacol and ABTS oxidations, respectively. However, the one-electron oxidation activity for F43W/H64L Mb is less that that of the F43W single mutant because the absence of histidine in the distal heme pocket suppresses the compound I formation. More than 15-fold improvement versus wild type Mb in the rates of two-electron oxidation of thioanisole and styrene are observed by the Phe-43 $\rightarrow$ Trp mutation. Our results indicate that Trp-43 in the mutants enhances both one- and two-electron oxidation activities (*i.e.* F43W Mb > Wild type Mb and F43W/H64L Mb > H64L Mb). The value of ^{18}O incorporation from $H_2^{18}O_2$ into the epoxide product for the wild type is 31%; however, the values for F43W and F43W/H64L Mb are 75 and 73%, respectively. Thus, Trp-43 in the mutants does not appear to be utilized as protein radical site in the oxidation. Furthermore, compound I of F43W/H64L Mb exhibits an absorption spectrum typical for a ferryl porphyrin radical cation, which is reduced back to the ferric state at the rate of 360 s^{-1} in the presence of thioanisole. The rate is approximately 10-fold greater than the value for H64L Mb. Our results suggest that a tryptophan in the active site of Mb mutants increases the reactivity of compound I, but the enhanced reactivity is not associated with a stable protein radical formation in the heme pocket. The oxidative protein modification of F43W/H64L Mb observed during the reaction with *m*-chlorobenzoic acid (*m*CPBA) has also been reported.

IX-A-2 Oxidative Modification of Tryptophan-43 in the Heme Vicinity of the F43W/H64L Myoglobin Mutant

HARA, Isao; UENO, Takafumi; OZAKI, Shin-ichi[1]; ITOH, Shinobu[2]; LEE, Ken-ichi[3]; UEYAMA, Norikazu[3]; WATANABE, Yoshihito
([1]Yamagata Univ.; [2]Osaka City Univ.; [3]Osaka Univ.)

The F43W/H64L Mb mutant was previously constructed to investigate the effects of electron-rich tryptophan residue in the heme vicinity on the catalysis, (Figure 1) and we found that Trp-43 in the mutant was oxidatively modified in the reaction with *m*-chloroperbenzoic acid (*m*CPBA). To identify the exact structure of the modified tryptophan in this study, the *m*CPBA-treated F43W/H64L mutant has been digested stepwise with Lys-C achromobacter and trypsin, and two oxidation products are isolated by preparative FPLC. The close examinations of the ^1H NMR spectra of peptide fragments reveal that two forms of the modified tryptophan must have 2,6-disubstituted indole substructures. The ^{13}C NMR analysis suggests that one of the modified tryptophan bears a unique hydroxyl group at the amino-terminal. The results together with Ms/Ms analysis (30 Da increase in mass of Trp-43) indicate that oxidation products of Trp-43 are 2,6-dihydro-2,6-dioxoindole and 2,6-dihydro-2-imino-6-oxoindole derivatives. (Figure 2) Our finding is the first example of the oxidation of aromatic carbons by the myoglobin mutant system.
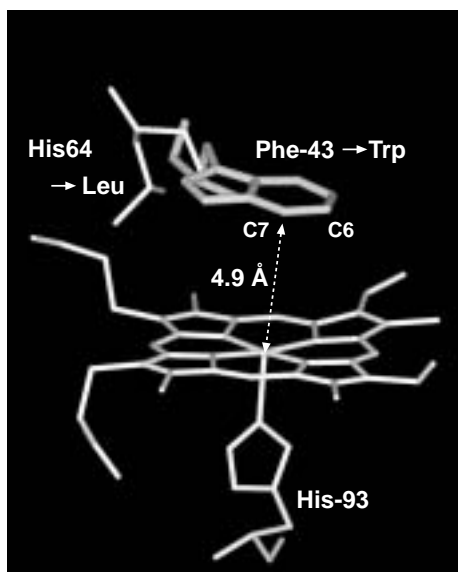
Figure 1. Calculated structure of F43W/H64L Mb using the Insight II molecular modeling program (Biosym MSI, San Diego, CA).
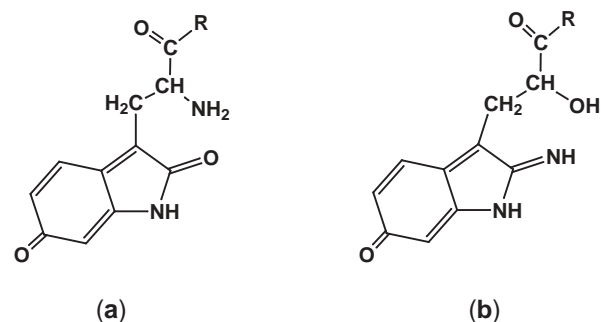
Figure 2. The oxidation products of Trp-43; (a) 2,6-dihydro-2,6-dioxoindole and (b) 2,6-dihydro-2-imino-6-oxoindole derivatives.

IX-B Model Studies of Non-Heme Proteins

Non-heme proteins play important roles in biological redox processes. Many reactions catalyzed by the non-heme enzymes are quite similar to those by hemoproteins. We are interested in the active intermediates responsible for oxidation and oxygenation by non-heme enzyme, especially the similarity and differences.

IX-B-1 (Catecholato)iron(III) Complexes: Structural and Functional Models for the Catechol-bound Iron(III) Form of Catechol Dioxygenases

YAMAHARA, Ryo[1]; OGO, Seiji; MASUDA, Hideki[1]; WATANABE, Yoshihito
(*[1]Nagoya Inst. Tech. and IMS*)

[*J. Inorg. Biochem.* in press]

The metabolic conversion of aromatic compounds to aliphatic compounds is of fundamental importance in biology. Catechol dioxygenases are mononuclear non-heme iron enzymes that catalyze the oxygenation of catechols to aliphatic acids via the cleavage of aromatic rings. These enzymes can be divided into two types: intradiol-cleaving enzymes which break the catechol C1–C2 bond, and extradiol-cleaving enzymes which break the C2–C3 or C1–C6 bond. In the last 20 years, a number of (catecholato)iron(III) complexes have been synthesized and characterized as structural and functional models for the catechol-bound iron(III) form of catechol dioxygenases. This review collects the structural and spectroscopic characteristics and oxygenation activity of (catecholato)iron(III) complexes as structural and functional models for the catechol-bound iron(III) form of catechol dioxygenases.

IX-B-2 Biomimetic Intradiol-Cleavage of Catechols with Incorporation of Both Atoms of O_2: The Role of the Vacant Coordination Site on the Iron Center

OGO, Seiji; YAMAHARA, Ryo[1]; FUNABIKI, Takuzo[2]; MASUDA, Hideki[1]; WATANABE, Yoshihito
(*[1]Nagoya Inst. Tech. and IMS; [2]Kyoto Univ.*)

[*Chem. Lett.* in press]

Since Hayaishi *et al.* have revealed that an intradiol-cleaving catechol dioxygenase, pyrocatechase, catalyzes the oxygenation of catechol to muconic acid with incorporation of two oxygen atoms of O_2 (but not of H_2O), the oxygenation mechanisms of catechol dioxygenases have been studied through investigations of model systems as well as the enzymes themselves. However, details of the O_2 insertion and aromatic ring-cleavage reactions are not yet understood. Herein, we report the first example of model system to display intradiol-cleavage of catechols with incorporation of two oxygen atoms of O_2 promoted by iron complexes (Figure 1): [Fe^{III}(^{3}L)(DBC)(DMF)] {**1**, ^{3}L = *N*-(2-hydroxyphenyl)-*N*-(2-pyridylmethyl)benzylamine, DBC = 3,5-di-*tert*-butylcatecholato, DMF = *N,N*-dimethylformamide} and [Fe^{III}(^{3}L)(DBC)Cl](PPh$_4$) (**2**).

(a)
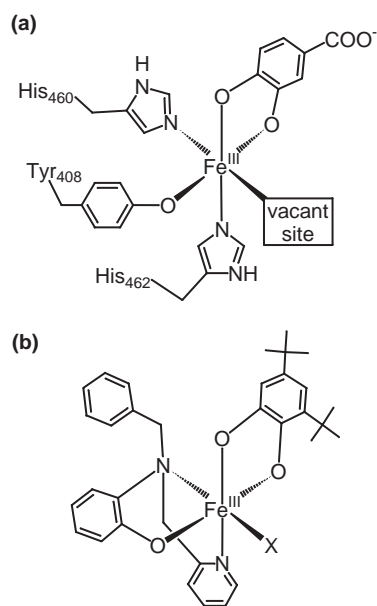
Figure 1. (a) Active site structure of a protocatechuic acid-bound form of protocatechuate 3,4-dioxygenase and (b) complexes **1** (X = Cl) and **2** (X = DMF).

(b)

IX-C Aqueous Organometallic Chemistry

Development of water-soluble organometallic catalysts is a worthy endeavor because of potential advantages such as reaction-specific pH selectivity, introduction of new biphasic processes, and alleviation of environmental problems associated with the use of organic solvents. Although the majority of these studies have been carried out with water-soluble organometallic complexes containing water-soluble phosphine ligands, few have utilized organometallic complexes containing water molecules as ligands (*i.e.* organometallic aqua complexes). These organometallic aqua complexes are promising new pH-selective catalysts since their structures drastically change as a function of pH due to deprotonation of the H_2O ligands.

IX-C-1 pH-Dependent Transfer Hydrogenation, Reductive Amination, and Dehalogenation of Water-Soluble Carbonyl Compounds and Alkyl Halides Promoted by Cp*Ir Complexes

OGO, Seiji; MAKIHARA, Nobuyuki; KANEKO, Yuichi[1]; WATANABE, Yoshihito
(*[1]Kochi Univ.*)

Recently, we reported a pH-dependent transfer hydrogenation of water-soluble carbonyl compounds with an aqua complex $[Cp*Ir^{III}(H_2O)_3]^{2+}$ (**1**, Cp* = η^5-pentamethylcyclopentadienyl) as a catalyst precursor and HCOONa as a hydrogen donor. We have extended our study with **1** to that with $[(Cp^\wedge py)Ir^{III}(H_2O)_2]^{2+}$ {**2**, $Cp^\wedge py = \eta^5$-(tetramethylcyclopentadienyl)-methyl-pyridine} and $[Cp*Ir^{III}(bpy)(H_2O)]^{2+}$ (**3**, bpy = 2,2'-bipyridine), since we expect that the ligation of pyridine and bipyridine in **1** could change its catalytic activity due to the change of the Lewis acidity of the iridium ion. Herein, we report preliminary findings of pH-dependent transfer hydrogenation, reductive amination, and dehalogenation of water-soluble carbonyl compounds and alkyl halides with **1**, **2**, and **3** as catalyst precursors and HCOONa and $HCOONH_4$ as hydrogen

donors. The pH-dependence in these reactions is discussed on the basis of (i) deprotonation processes of the catalyst precursors, (ii) pH-dependent behavior of the hydrogen donors, and (iii) pH-dependent formation of the active catalysts.
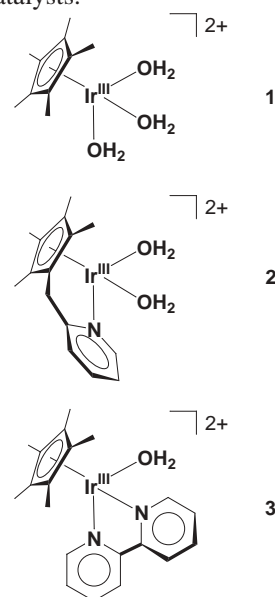
Figure 1. Complexes **1**, **2**, and **3**.

IX-D Single-Molecule Physiology

A single molecule of protein (or RNA) enzyme acts as a machine which carries out a unique function in cellular activities. To elucidate the mechanisms of various molecular machines, we need to observe closely the behavior of individual molecules, because these machines, unlike man-made machines, operate stochastically and thus cannot be synchronized with each other. By attaching a tag that is huge compared to the size of a molecular machine, or a small tag such as a single fluorophore, we have been able to image the individual behaviors in real time under an optical microscope. Stepping rotation of the central subunit in a single molecule of F_1-ATPase has been videotaped, and now we can discuss its detailed mechanism. RNA polymerase has been shown to be a helical motor that rotates DNA during transcription. Single-molecule physiology is an emerging field of science in which one closely watches individual, 'live' protein/RNA machines at work and examines their responses to external perturbations such as pulling and twisting. I personally believe that molecular machines operate by changing their conformations. Thus, detection of the conformational changes during function is our prime goal. Complementary use of huge and small tags is our major strategy towards this end.

IX-D-1 Resolution of Distinct Rotational Substeps by Submillisecond Kinetic Analysis of F_1-ATPase

YASUDA, Ryohei[1,2]; NOJI, Hiroyuki[1]; YOSHIDA, Masasuke[1,3]; KINOSITA, Kazuhiko, Jr.[1,2]; ITOH, Hiroyasu[1,4]
(*[1]CREST Team 13; [2]Keio Univ.; [3]Tokyo Inst. Tech.; [4]Hamamatsu Photonics*)

The enzyme F_1-ATPase has been shown to be a rotary motor in which the central γ-subunit rotates inside the cylinder made of $\alpha_3\beta_3$ subunits. At low ATP concentrations, the motor rotates in discrete 120° steps, consistent with sequential ATP hydrolysis on the three β-subunits. The mechanism of stepping is unknown. Here we show by high-speed imaging that the 120° step consists of roughly 90° and 30° substeps, each taking only a fraction of a millisecond. ATP binding drives the 90° substep, and the 30° substep is probably driven by release of a hydrolysis product. The two substeps are separated by two reactions of about 1 ms, which together occupy most of the ATP hydrolysis cycle. This scheme probably applies to rotation at full speed (~130 revolutions per second at saturating ATP) down to occasional stepping at nanomolar ATP concentrations, and supports the binding-change model for ATP synthesis by reverse rotation of F_1-ATPase.
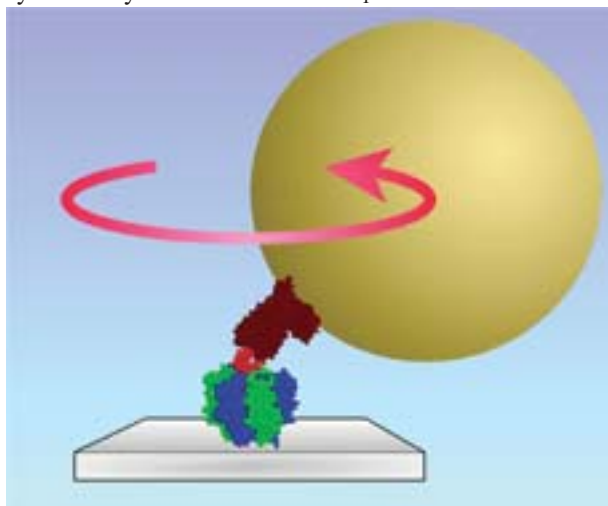
Figure 1. Imaging F_1 rotation through a gold bead. The cylinder made of three α (blue) and three β (green) subunits was fixed on a glass surface, and a 40-nm gold bead was attached to the central γ subunit (red) through streptavidin and BSA (brown) that served as glue. When the bead was attached obliquely as shown in the figure, rotation of the γ subunit resulted in a circular movement of the bead image. The rotation angle was estimated from the circular trajectory of the bead movement.

IX-D-2 Purine but Not Pyrimidine Nucleotides Support Rotation of F_1-ATPase

NOJI, Hiroyuki[1,2]; BALD, Dirk[1,3]; YASUDA, Ryohei[1]; ITOH, Hiroyasu[1,4]; YOSHIDA, Masasuke[1,3]; KINOSITA, Kazuhiko, Jr.[1,5]
(*[1]CREST Team 13; [2]PREST; [3]Tokyo Inst. Tech.; [4]Hamamatsu Photonics; [5]Keio Univ.*)

The binding change model for the F_1-ATPase predicts that its rotation is intimately correlated with the changes in the affinities of the three catalytic sites for nucleotides. If so, subtle differences in the nucleotide structure may have pronounced effects on rotation. Here we show by single-molecule imaging that purine nucleotides ATP, GTP, and ITP support rotation but pyrimidine nucleotides UTP and CTP do not, suggesting that the extra ring in purine is indispensable for proper operation of this molecular motor. Although the three purine nucleotides were bound to the enzyme at different rates, all showed similar rotational characteristics: counterclockwise rotation, 120° steps each driven by hydrolysis of one nucleotide molecule, occasional back steps, rotary torque of ~40 piconewtons (pN)·nm, and mechanical work done in a step of ~80 pN·nm. These latter characteristics are likely to be determined by the rotational mechanism built in the protein structure, which purine nucleotides can energize. With ATP and GTP, rotation was observed even when the free energy of hydrolysis was –80 pN·nm/molecule, indicating ~100% efficiency. Reconstituted F_oF_1-ATPase actively translocated protons by hydrolyzing ATP, GTP, and ITP, but CTP and UTP were not even hydrolyzed. Isolated F_1 very slowly hydrolyzed UTP (but not CTP), suggesting possible uncoupling from

rotation.

IX-D-3 Direct Observation of DNA Rotation during Transcription by *Escherichia coli* RNA Polymerase

HARADA, Yoshie[1,2]; OHARA, Osamu[3]; TAKATSUKI, Akira[1]; ITOH, Hiroyasu[2,4]; SHIMAMOTO, Nobuo[5]; KINOSITA, Kazuhiko, Jr.[1,2]
(*[1]Keio Univ.; [2]CREST Team 13; [3]Kazusa DNA Res. Inst.; [4]Hamamatsu Photonics; [5]Natl. Inst. Genetics*)

Helical filaments driven by linear molecular motors are anticipated to rotate around their axis, but rotation consistent with the helical pitch has not been observed. 14S dynein and non-claret disjunctional protein (ncd) rotated a microtubule more efficiently than expected for its helical pitch, and myosin rotated an actin filament only poorly. For DNA-based motors such as RNA polymerase, transcription-induced supercoiling of DNA supports the general picture of tracking along the DNA helix. Here we report direct and real-time optical microscopy measurements of rotation rate that are consistent with high fidelity tracking. Single RNA polymerase molecules attached to a glass surface rotated DNA for .100 revolutions around the right-handed screw axis of the double helix with a rotary torque of > 5 pN nm. This real-time observation of rotation opens the possibility of resolving individual transcription steps.
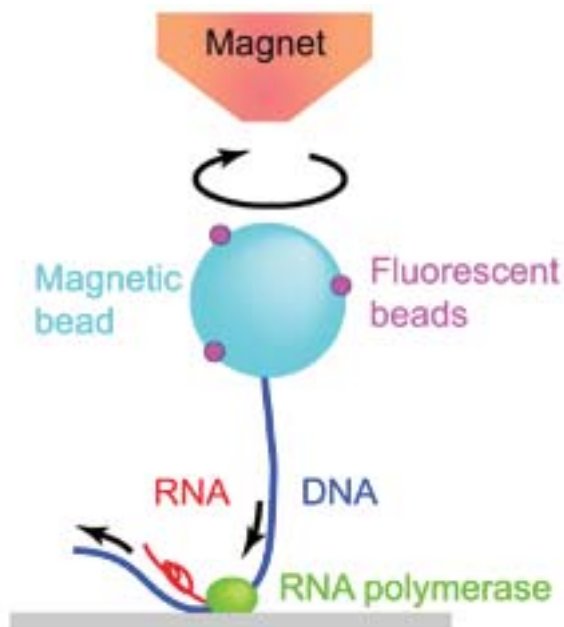
Figure 1. Observation of DNA rotation by RNA polymerase. The magnetic bead was pulled upwards by a disk-shaped neodymium magnet, to which a conical iron piece was attached to enhance the magnetic force. Magnetization was vertical and did not prevent bead rotation. Daughter fluorescent beads served as markers of rotation.

IX-E Electronic Structure and Reactivity of Active Sites of Metalloproteins

Metalloproteins are a class of biologically important macromolecules that have various functions such as oxygen transport, electron transfer, oxidation, and oxygenation. These diverse functions of metalloproteins have been thought to depend on the ligands from amino acid, coordination structures, and protein structures in immediate vicinity of metal ions. In this project, we are studying the relationship between the structures of the metal active sites and functions of metalloproteins.

IX-E-1 Structural Model of Active Site of Protocatechuate 3,4-Dioxygenase: Trigonal Bipyramidal Ferric Aqua Complex with Sterically Hindered New Salen Ligand

FUJII, Hiroshi

Protocatechurate 3,4-dioxygenase (3,4-PCD) has been found in soil bacteria and known to serve as a part of degrading aromatic molecules in nature. The enzyme is classified into an intradiol dioxygenase and contains a ferric iron as a catalytic reaction site. The enzyme cleaves catechol analogies bound to ferric iron site into aliphatic products with incorporating both atoms of molecular. It has been proposed that the enzyme activates an iron bound catecholate to react with an oxygen molecule, but not an iron bound oxygen molecule as most non-heme iron enzymes. Thus, the structure of the ferric iron site has been thought essential to understand the unique reaction of 3,4-PCD. Previous crystal structure of 3,4-PCD from *Pseudomonas putida* reveals a unique trigonal bipyramidal ferric iron site with four endogenous protein ligands (Tyr408, Tyr447, His460, and His462) and a solvent-derived water molecule. To understand the structure-function relationship of 3,4-PCD, there have been attempted over several decades to prepare inorganic model complexes that mimic the ferric iron site of 3,4-PCD, however, no ferric iron complex with the same coordination structure that in the enzyme has been characterized definitively. In this paper, we report the successful attainment to the ferric iron active site of 3,4-PCD by using sterically hindered salen ligand (Figure 1). Characterization of the present model complex reveals the roles of the iron bound water ligand in the enzyme on the unique trigonal bipyramidal structure and the catechol degradation reaction.
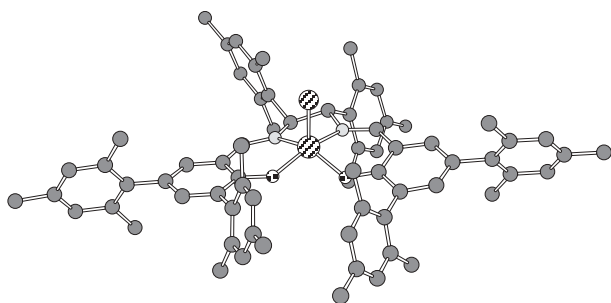
Figure 1. Structure of sterically hindered iron(III) salen complex prepared in this project.

IX-E-2 Synthesis and Characterization of High Valent Iron Porphyrin Complexes as Models for Reaction Intermediates of Cytochrome *c* Oxidase

FUJII, Hiroshi; FUMOTO, Yumiko[1]; ONO, Noboru[1]
(*[1]Ehime Univ.*)

Cytochrome c oxidase (CcO) is the terminal oxidase that reduces molecular oxygen to water, coupling with proton pumping across the mitochondrial inner membrane. Since discovery of this enzyme, many structural and functional studies have been done to understand its reaction mechanism. Recent X-ray analyses reveal that this enzyme contains a binuclear center, heme-a_3-Cu_B site, as a reaction site. The binuclear center of the resting enzyme is ferric/cupric form. The binuclear active site is reduced to a ferrous/cuprous form by two electrons from cytochrome c through the Cu_A and heme a site. The ferrous/cuprous form of active site reacts with O_2 to yield an internal dioxygen adduct, intermediate A state, which is further converted to intermediate P and F by the aid of the electrons and protons. Although the intermediates P and F have been studied by resonance Raman and flash-flow absorption spectroscopies, the electronic states of these intermediates are not still clear. To reveal the electronic states of these intermediates and to understand the reaction mechanism of CcO, we have synthesized model complexes of the heme-a_3 site of cytochrome c oxidase. The model complex contains a formyl group at pyrrole-β position to mimic the heme a_3 and mesityl groups to stabilize high valent oxo iron species (see Figure 1). We have succeeded in the preparation of a high valent oxo iron porphyrin complex as a model for the intermediate P by the oxidation of the ferric model complex with mCPBA or ozone.
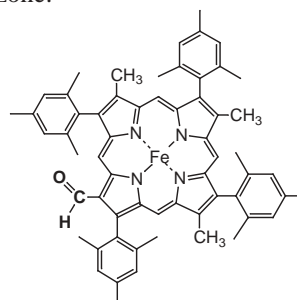
Figure 1. Structure of model complex prepared in this project as models for heme-a and heme-a_3 site of cytochrome c oxidase.

IX-F Molecular Mechanism of Heme Degradation and Oxygen Activation by Heme Oxygenase

Heme oxygenase (HO), an amphipathic microsomal proteins, catalyzes the regiospecific oxidative degradation of iron protoporphyrinIX (heme) to biliverdinIXα, carbon monoxide, and iron in the presence of NADPH-cytochrome P-450 reductase, which functions as an electron donor. Heme oxygenase reaction is the biosynthesis processes of bile pigments and CO, which is a possible physiological messenger. Recent development in the bacterial expression of a soluble form of heme oxygenase has made it possible to prepare in the large quantities for structural studies. In this project, we are studying the molecular mechanism of heme degradation and the oxygen activation by heme oxygenase using various spectroscopic methods.

IX-F-1 A Role for Highly Conserved Carboxylate, Aspartate-140, in Oxygen Activation and Heme Degradation by Heme Oxygenase-1

FUJII, Hiroshi; ZHANG, Xuhong[1]; TOMITA, Takeshi[2]; IKEDA-SAITO, Masao[2]; YOSHIDA, Tadashi[1]
(*[1]Yamagata Univ.; [2]Tohoku Univ.*)

Heme oxygenase (HO) catalyzes the oxygen-dependent degradation of heme to biliverdinIXα, CO, and free iron ion via three sequential monooxygenase reactions. Although the distinct active site structure of HO from cytochrome P450 families suggests unique distal protein machinery to activate molecular oxygen, the mechanism and the key amino acid for the oxygen activation have not been clear. To investigate the functionality of highly conserved polar amino acids in the distal helix of HO-1, we have prepared alanine mutants: T135A, R136A, D140A, and S142A, and found drastic changes in the heme degradation reactions of D140A. In this paper, we report the first evidence that D140 is involved in the oxygen activation mechanism in HO-1. The heme complexes of HO mutants examined in this study fold and bind heme normally. The pKa values of the iron bound water and autooxidation rates of the oxy-form are increased with R136A, D140A, and S142A mutations, but are not changed with T135A mutation. As the wild type, T135A, R136A, and S142A degrade heme to verdohemeIXα with H_2O_2 and to biliverdinIXα with the NADPH reductase system. On the other hand, D140A heme complex forms compound II with H_2O_2 and no heme degradation occurs. For the NADPH reductase system, the oxy form of D140A heme complex is accumulated in the reaction and only 50% of heme is degraded. The stopped flow experiments suggest that D140A can not activate iron bound dioxygen and hydroperoxide properly. To investigate the carboxylate functionality of D140, we further replaced D140 with glutamic acid (D140E), phenylalanine (D140F), and asparagine (D140N). D140E degrades heme normally but D140N shows reactivity similar to D140A. D140F loses heme degradation activity completely. All of these results indicate that the carboxylate at position 140 is essential to activate the iron bound dioxygen and hydroperoxide. On the basis of the present findings, we propose an oxygen activation mechanism involving the hydrogen-bonding network through the bridging water and D140 side chain.
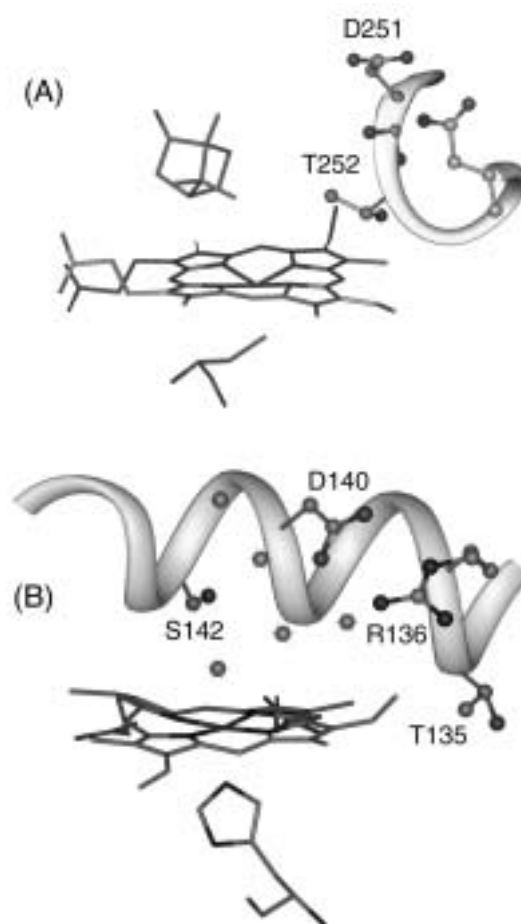
Figure 1. Active site structures of cytochrome P450 (A) and heme oxygenase (B).

IX-F-2 Catalytic Mechanism of Heme Oxygenase Through EPR and ENDOR of Cryoreduced Oxy-Heme Oxygenase and Asp 140 Mutants

DAVYDOV, Roman[1]; KOFMAN, Viktoria[1]; FUJII, Hiroshi; YOSHIDA, Tadashi[2]; IKEDA-SAITO, Masao[3]; HOFFMAN, M. Brian[1]
(*[1]Uni. Northwestern; [2]Yamagata Univ.; [3]Tohoku Univ.*)

Heme oxygenase (HO) catalyzes the O_2- and NADPH-cytochrome P450 reductase-dependent conversion of heme to biliverdin and CO through a process in which the heme participates both as prosthetic group and substrate. It was proposed that the first mono-oxygenation step of HO catalysis is the conversion of the heme to α-meso-hydroxyheme, through a process in which an electron provided by NADPH-cytochrome P450 reductase reduces the first heme to the ferrous state and molecular of dioxygen binds to form a metastable O_2-bound complex, which then is reduced by a second electron to generate hydroperoxy ferric-HO. It was further thought that the hydroperoxy-ferric HO is the reactive hydroxylating species, rather than a high-valent ferryl active intermediate as in the case of cytochrome P450cam. However, neither the putative hydroperoxo-ferric-HO intermediate nor the a-meso-hydroxyheme product had been detected during physiological HO catalysis until our recent EPR and ENDOR study of oxy-ferrous HO cryoreduced at 77 K. In the present study we have generated a detailed reaction cycles for the first mono-oxygenation step of HO catalysis. We employed EPR and ^{1}H, ^{14}N ENDOR spectroscopies to characterize the intermediates generated by 77 K radiolytic cryoreduction and subsequent annealing of wild-type oxy-HO and D140A, F mutants.
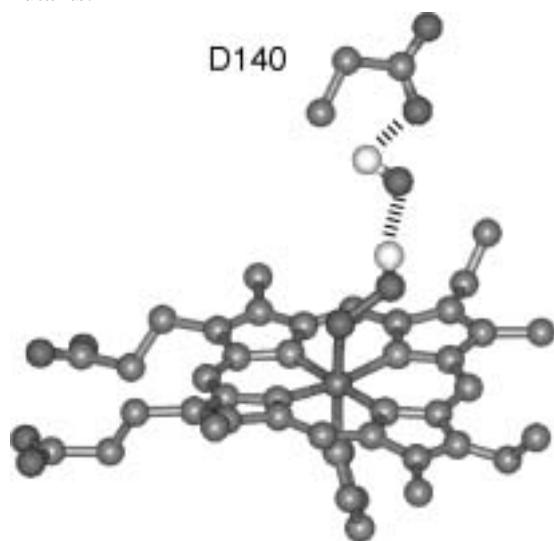
Figure 1. Structure of ferric hydroperoxide intermediate in HO.

IX-G Biomolecular Science

Elucidation of a structure-function relationship of metalloproteins is a current subject of this group. The primary technique used for this project is the stationary and time-resolved resonance Raman spectroscopy excited by visible and UV lasers. The main themes that we want to explore are (1) mechanism of oxygen activation by enzymes, (2) mechanism of active proton translocation and its coupling with electron transfer, (3) coupling mechanism of proton- and electron transfers by quinones in photosynthetic reaction center, (4) higher order protein structures and their dynamics, and (5) reactions of biological NO. In category (1), we have examined a variety of terminal oxidases, cytochrome P450s, and peroxidases, and also treated their enzymatic reaction intermediates by using the mixed flow transient Raman apparatus and the Raman/absorption simultaneous measurement device. For (2) the third generation UV resonance Raman (UVRR) spectrometer was constructed and we are going to apply it to a giant protein like cytochrme c oxidase. More recently, we succeeded in pursuing protein folding of apomyoglobin by combining UV time-resolved Raman and rapid mixing device. In (3) we succeeded in observing RR spectra of quinones A and B in bacterial photosynthetic reaction centers for the first time, but we have focused our attention on detecting tyrosine radical for the P intermediate of terminal oxidases. Some positive evidence was obtained for cytochrome bo. For (4) we developed a novel technique for UV resonance Raman measurements based on the combination of the first/second order dispersions of gratings and applied it successfully to 235-nm excited RR spectra of several proteins including mutant hemoglobins and myoglobins. Nowadays we can carry out time-resolved UVRR experiments with nanosecond resolution to discuss protein dynamics. With the newly developed third generation UV Raman spectrometer, we have succeeded in isolating the spectrum of tyrosinate in ferric Hb M Iwate, which was protonated in the ferrous state, and the deprotonated state of Tyr244 of bovine cytochrome c oxidase. As a model of Tyr244, an imidazole-bound *para*-cresol was synthesized and its UV resonance Raman was investigated. For (5) we purified soluble guanylate cyclase from bovine lung and observed its RR spectra. To further investigate it, we are developing an expression system of this protein.

IX-G-1 Presence of the Heme-oxo Intermediate in Oxygenation of Carbon Monoxide by Cytochrome c Oxidase Revealed by Resonance Raman Spectroscopy

KIM, Younkyoo[1]; SHINZAWA-ITOH, Kyoko[2];
YOSHIKAWA, Shinya[2]; KITAGAWA, Teizo
(*[1]Hankuk Univ.; [2]Himeji Inst. Tech.*)

Resonance Raman and absorption spectra were examined for the species generated upon incubation of oxidized bovine cytochrome c oxidase at pH 8.0 with carbon monoxide in the presence or absence of O_2. The anaerobic incubation yielded the CO isotope sensitive bands at 517 and 578 cm^{-1} for $^{12}C^{16}O$, at 512 and 563 cm^{-1} for $^{13}C^{16}O$, at 508 and 574 cm^{-1} for $^{12}C^{18}O$, and at 503 and 557 cm^{-1} for $^{13}C^{18}O$, indicating the formation of heme $a_3^{2+}CO$ adduct. The aerobic incubation with CO employing both $^{16}O_2$ and $^{18}O_2$ yielded the oxygen isotope-sensitive bands at 804 and 768 cm^{-1}, respectively. These bands were identified by excitation at 441.6 and 607 nm but not at 413.1, 421.3, and 590 nm, a result which is consistent with the P intermediate absorption maxima occurring near 439 and 607 nm. The frequencies of the oxygen isotope sensitive bands are in agreement with those observed for the P intermediate in the O_2 reduction by the fully reduced enzyme and in the H_2O_2 reduction by the oxidized enzyme. The other ironoxo species, the F intermediate, observed for both of the above referenced reactions was not generated in this study.

IX-G-2 Protein Conformation Change of Myoglobin upon Ligand Binding Probed by Ultraviolet Resonance Raman Spectroscopy

HARUTA, Nami[1]; AKI, Michihiko[2]; OZAKI, Shin-ichi[3]; WATANABE, Yoshihito; KITAGAWA, Teizo
(*[1]GUAS; [2]Univ. Tokyo; [3]Yamagata Univ.*)

Conformational change of myoglobin (Mb) accompanied by binding of a ligand was investigated with the 244 nm-excited ultraviolet resonance Raman spectroscopy (UVRR). The UVRR spectra of native sperm whale (sw) and horse (h) Mbs and W7F and W14F swMb mutants for the deoxy and CO-bound states enabled us to reveal the UVRR spectra of Trp7, Trp14, and Tyr151 residues, separately. The difference spectra between the deoxy and CO-bound states reflected the environmental or structural changes of Trp and Tyr residues upon CO binding. W3 band of Trp7 near the N-terminus exhibited a change upon CO binding, while Trp14 did not. Tyr151 in the C-terminus also exhibited a definite change upon CO binding, but Tyr103 and Tyr146 did not. The spectral change of Tyr residues was characterized through solvent effects of a model compound. The corresponding spectral differences between CO- and *n*-butylisocyanide-bound forms were much smaller than those between the deoxy and CO-bound forms, suggesting that the conformation change in the C- and N- terminal regions is induced by the proximal side of heme through the movement of iron. Although the swinging up of His64 upon binding of a bulky ligand is noted by X-ray crystallographic analysis, UVRR spectra of His for *n*-butylisocyanide bound form did not detect the exposure of His64 to solvent.

IX-G-3 UV Resonance Raman Characterization of Model Compounds of Tyr[244] of Bovine Cytochrome *c* Oxidase in Its Neutral-, Deprotonated Anion-, and Deprotonated Neutral Radical-Forms: Effects of Covalent Binding between Tyrosine and Histidine

AKI, Michihiko[1]; NARUTA, Yoshinori[2]; LE, T. Huu[2]; SATO, Teizi[2]; KITAGAWA, Teizo
(*[1]Univ. Tokyo; [2]Kyushu Univ.*)

A model compound of Tyr[244]-His[240] of bovine cytochrome c oxidase was synthesized and examined with UV resonance Raman (UVRR) as well as UV visible absorption spectroscopy and pH titration. Owing to the covalent linkage between imidazole and phenol, the pKa of phenolic OH and imidazolic $N_\delta H$ groups were lowered by 1.1 and 2.3, respectively. UVRR measurements of *ortho*-imidazole-bound *para*-cresol (Im♦CrOH), its deprotonated anion (Im♦CrO$^-$), and deprotonated neutral radical (Im♦CrO$^\bullet$), and their imidazole perdeuterated, cresol perdeuterated, and ^{18}O derivatives allowed assignments of Raman bands to the imidazole and phenol modes. Unexpectedly, some of imidazole vibrations were resonance enhanced upon $\pi\pi^*$ transition of phenol, although they were not observed for the corresponding equimolar mixture of imidazole and p-cresol, indicating delocalization of π electrons between the imidazole and phenol rings via the covalent linkage. Such features were appreciably changed by incorporation of a bulky group at imidazole C^2 position, causing staggered conformation. The C–O stretching RR band was observed only for a radical state at 1530 cm^{-1}. Y8a band is not shifted upon deprotonation, although it was shifted by 12 cm^{-1} for unmodified p-cresol. The UVRR difference spectra of the anion and radical with regard to the neutral states are discussed in relation with the corresponding difference spectra of the enzyme.

IX-G-4 Synthesis, Structure, and H_2O_2-Dependent Catalytic Functions of Disulfide-Bridged Dicopper(I) and Related Thioether-Copper(I) and Thioether-Copper(II) Complexes

OHTA, Takehiro; TACHIYAMA, Takashi[1]; YOSHIZAWA, Kazunari[1]; YAMABE, Tokio[1]; UCHIDA, Takeshi; KITAGAWA, Teizo
(*[1]Kyoto Univ.*)

A disulfide-bridged dicopper(I) complex, [Cu$_2$-(Py$_2$SSPy$_2$)](ClO$_4$)$_2$ (**1**) (Py$_2$SSPy$_2$ = bis{2-[*N,N*-bis(2-pyridylethyl)amino]-1,1-dimethylethyl}disulfide), a thioether-copper(I) complex, [Cu(^{i}PrSPy$_2$)](ClO$_4$) (**2**) (^{i}PrSPy$_2$ = *N*-(2-isopropylthio-2-methyl)propyl-*N,N*-bis-2-(2-pyridyl)ethylamine), and a thioether-copper(II) complex, [Cu(PheSPy$_2$)(H$_2$O)](ClO$_4$)$_2$ (**3**) (PheSPy$_2$ = *N*-(2-methyl-2-phenethylthio)propyl-*N,N*-bis-2-(2-pyridyl)ethylamine), were newly synthesized by the reactions of Cu(ClO$_4$)$_2$·6H$_2$O with a thiol ligand of Py$_2$-

SH (*N,N*-bis[2-(2-pyridyl)ethyl]-1,1-dimethyl-2-mercaptoethylamine) and thioether ligands of ^{i}PrSPy$_2$ and PheSPy$_2$, respectively. For complexes **1** and **2**, X-ray analyses were performed. Complex **1** crystallizes in the triclinic space group $P\bar{1}$, and complex **2** crystallizes in the orthorhombic space group *Pbca* with the following unit cell parameters: for **1**, a = 15.165 (3) Å, b = 22.185 (4) Å, c = 14.989 (3) Å, α = 105.76 (1)°, β = 90.82 (2)°, γ = 75.23 (1)°, and Z = 2; for **2**, a = 17.78 (2) Å, b = 17.70 (1) Å, c = 15.75 (1) Å, and Z = 8. Complex **1** is the first structurally characterized example obtained by the redox reaction Cu(II) + RSH → Cu(I) + RSSR and has two independent structures (**1a**, **1b**) which mainly differ in S–S bond distances, Cu(I)···Cu(I) separations, and C–S–S–C dihedral angles of the disulfide units. The S–S bond distances of 2.088(7) Å in **1a** and 2.070(7) Å in **1b** are indicative of significant activation of the S–S bonds by the dicopper centers. Fragment molecular orbital (FMO) analyses and molecular orbital overlap population (MOOP) analyses based on the extended Hükel method clarify the preferable formation of the disulfide S–S bond in **1** rather than the formation of a thiolate-copper(II) complex within the Py$_2$S$^-$ ligand framework. Catalytic functions of complexes **1–3** were investigated with peroxides (H$_2$O$_2$ and ^{t}BuOOH) as oxidants. Complex **1** catalyzed the selective oxidation of cyclohexane to cyclohexanol and mediated the cyclohexene epoxidation in the presence of H$_2$O$_2$. A transient dark green intermediate observed in the reaction of **1** with H$_2$O$_2$ is characterized by UV-vis, EPR, and resonance Raman spectroscopies, identifying it as a Cu(II)–OOH species, **1**(OOH). The resonance Raman features of the ν(O–O) bands at 822 and 836 cm^{-1}, which are red-shifted to 781 and 791 cm^{-1}, respectively, upon introduction of H$_2^{18}$O$_2$, are indicative of formation of two kinds of Cu–OOH species rather than the Fermi doublet and the significant weakening of the O–O bonds. These mechanistic studies demonstrate that by virtue of the electron-donating ability of the disulfide unit the Cu–OOH species can be actually activated for one-electron oxidation, which has been reported so far unfavorable for other vibrationally characterized Cu–OOH species.

IX-G-5 UV Resonance Raman Detection of a Ligand Vibration on Ferric Nitrosyl Heme Proteins

TOMITA, Takeshi[1]; HARUTA, Nami[2]; AKI, Michihiko[3]; KITAGAWA, Teizo; IKEDA-SAITO, Masao[1]
(*[1]Tohoku Univ.; [2]GUAS; [3]Univ. Tokyo*)

The Fe^{3+}–nitric oxide (NO) complexes formed from the reactions of NO with heme proteins are of significant physiological relevance. Microbial denitrification catalyzed by cytochrome P450nor, is initiated by the formation of a Fe^{3+}–NO complex. The delivery of NO by a blood-sucking insect, *Rhodnius prolixus*, to its victims is via the ferric, not ferrous, NO complex of nitrophorin. The affinity of NO for Fe^{3+} is

much lower than that for Fe^{2+}, thereby facilitating the transfer of NO. While vibrational spectroscopy has been applied extensively to explore heme-ligand systems, its application to Fe^{3+} heme-NO complexes have been scarce, primarily because of the weak vibrational signals from the NO moieties. Thus, the development of an efficient and highly sensitive method to detect the ligand vibrations in Fe^{3+} heme NO complexes is necessary. Here, we report an innovative and highly sensitive UV resonance Raman (RR) spectroscopic method for detecting the NO stretching frequency of a variety of Fe^{3+} NO heme proteins, including myoglobin (Mb), horseradish peroxidase (HRP), mammalian heme oxygenase isoform 2 (HO-2), and FixLH.

IX-G-6 Elucidation of the Differences between the 430 and 455-nm Absorbing Forms of P450-Isocyanide Adducts by Resonance Raman Spectroscopy

TOMITA, Takeshi[1]; OGO, Seiji; EGAWA, Tsuyoshi[2]; SHIMADA, Hideo[2]; OKAMOTO, Noriaki[3]; IMAI, Yoshio[3]; WATANABE, Yoshihito; ISHIMURA, Yuzuru[2]; KITAGAWA, Teizo
(*[1]Tohoku Univ.; [2]Keio Univ.; [3]Osaka Prefecture Univ.*)

Alkylisocyanide adducts of microsomal P450 exist in two interconvertible forms, each giving the Soret maximum around 430 or 455 nm. This is demonstrated with a rabbit liver P4502B4. Resonance Raman spectra of the 430 and 455 nm forms were examined with typical P450s of the two types as well as with P450 2B4, because the 430 nm form of P4502B4 is liable to change into P420. P450cam and P450nor were selected as a model of the 430 and 455 nm forms, respectively. For *n*-butyl isocyanide (CNBu) adduct, the Fe(II)–CNBu stretching band was observed for the first time at 480/467 cm^{-1} for P450cam and at 471/459 cm^{-1} for P450nor with their ^{12}CNBu/^{13}CNBu derivatives. For P450cam, another ^{13}C-isotope sensitive bands were observed at 412/402, 844/835, and 940/926 cm^{-1}, but not with P450nor. The C–N stretching mode was identified by FTIR at 2116/2080 cm^{-1} for P450cam and at 2148/2108 cm^{-1} for P450nor for the ^{12}C/^{13}C derivatives. These findings suggest that the binding geometry of isocyanide differs between the two forms, bent and linear structures for P450camCNBu and P450norCNBu, respectively. In contrast, in the ferric state, the Raman ^{13}C isotopic frequency shifts and the IR C–N stretching frequencies (2213/2170 and 2215/2172 cm^{-1}) were similar between P450cam and P450nor, suggesting similar bent structures for both.

IX-G-7 Observation of an Isotope Sensitive Low Frequency Raman Band Specific to Metmyoglobin

HIROTA, Shun[1]; MIZOGUCHI, Yasutaka[1]; YAMAUCHI, Osamu[2]; KITAGAWA, Teizo
(*[1]Nagoya Univ.; [2]Kansai Univ.*)

An iron(III)-histidine stretching (ν_{Fe-His}) Raman band is searched through isotope-sensitivity for low frequency resonance Raman bands of *metMb*, *metHb*, and its α and β subunits. A band at 218 cm^{-1} of natural abundance *metMb* exhibited a low frequency shift for ^{15}N-His-labeled *metMb* (–1.4 cm^{-1} shift), while the strong porphyrin bands at 248 and 271 cm^{-1} did not shift significantly. The frequency of the 218-cm^{-1} band of *metMb* decreased by 1.6 cm^{-1} in D$_2$O, probably due to N$_\delta$-deuteration of the proximal His, in a similar manner to that of the ν_{Fe-His} band of deoxyMb in the D$_2$O. This 218-cm^{-1} band was shifted slightly to a lower frequency in H$_2$^{18}O, whereas it did little upon ^{54}Fe isotopic substitution (< 0.3 cm^{-1}) presumably because of the six-coordinate structure. This band was absent for the hydroxy*metMb* and cyano*metMb*. For *metHb* and its α and β subunits, however, the frequencies of the band around 220 cm^{-1} were not D$_2$O-sensitive. These results suggest an assignment of the band around 220 cm^{-1} to a pyrrole tilting mode, which contains the Fe–His stretching character for *metMb* but not for *metHb* and its subunits. The differences in the isotope-sensitivity of this band in different proteins are considered to reflect the heme structure including the Fe–His geometry specific to individual proteins.

IX-G-8 A Novel Diiron Complex as a Functional Model for Hemerythrin

ARII, Hidekazu[1]; NAGATOMO, Shigenori; KITAGAWA, Teizo; MIWA, Tomohiro[1]; JITSUKAWA, Koichiro; EINAGA, Hisahiko[1]; MASUDA, Hideki[1]
(*[1]Nagoya Inst. Tech.*)

Diiron(II) complexes with a novel dinucleating polypyridine ligand, *N,N,N',N'*-tetrakis(6-pivalamido-2-pyridylmethyl)-1,3-diaminopropan-2-ol (HTPPDO), were synthesized as functional models of hemerythrin. Structural characterization of the complexes, [Fe^{II}$_2$-(Htppdo)(PhCOQ)](ClO$_4$)$_3$ (**1**), [Fe^{II}$_2$(Htppdo)((*p*-Cl)-PhCOO)](ClO$_4$)$_3$, (**2**), [Fe^{II}$_2$(Htppdo)((*p*-Cl)PhCOO)]-(BF$_4$)$_3$ (**2'**) and [Fe^{II}$_2$(tppdo)((*p*-Cl)PhCOO)](ClO$_4$)$_2$ (**3**), were accomplished by electronic absorption, and IR spectroscopic, electrochemical, and X-ray diffraction methods. The crystal structures of **1** and **2'** revealed that the two iron atoms are asymmetrically coordinated with HTPPDO and bridging benzoate. One of the iron centers (Fe(**1**)) has a seven-coordinate capped octa‐hedral geometry comprised of an N$_3$O$_4$ donor set which includes the propanol oxygen of HTPPDO. The other iron center (Fe(**2**)) forms an octahedron with an N$_3$O$_4$ donor set and one vacant site. The two iron atoms are bridged by benzoate (**1**) or *p*-chlorobenzoate (**2**). On the other hand, both Fe atoms of complex **3** are both symmetrically coordinated with N$_3$O$_4$ donors and two bridging ligands; benzoate and the propanolate of TPPDO. Reactions of these complexes with dioxygen were followed by electronic absorption, resonance Raman and ESR spectroscopies. Reversible dioxygen-binding was demonstrated by observation of an intense LMCT band for O$_2$$^{2-}$ to Fe(III) at 610 (**1**) and 606 nm

(**2**) upon exposure of dioxygen to acetone solutions of **1** and **2** prepared under an anaerobic conditions at –50 degreesC. The resonance Raman spectra of the dioxygen adduct of **1** exhibited two peaks assignable to the ν(O–O) stretching mode at 873 and 887 cm^{-1}, which shifted to 825 and 839 cm^{-1} upon binding of O$^{18}_2$. ESR spectra of all dioxygen adducts were silent. These findings suggest that dioxygen coordinates to the diiron atoms as a peroxo anion in a μ-1,2 mode. Complex **3** exhibited irreversible dioxygen binding. These results indicate that the reversible binding of dioxygen is governed by the hydrophobicity of the dioxygen-binding environment rather than the iron redox potentials.

IX-G-9 Effects of Metal Ions on the Electronic, Redox, and Catalytic Properties of Cofactor TTQ of Quinoprotein Amine Dehydrogenases

ITOH, Shinobu[1]; TANIGUCHI, Masato[2]; TAKADA, Naoki[2]; NAGATOMO, Shigenori; KITAGAWA, Teizo; FUKUZUMI, Shunichi[2]
(*[1]Osaka City Univ.; [2]Osaka Univ.*)

Model compounds of novel organic cofactor TTQ (tryptophan tryptophylquinone) of quinoprotein methylamine and aromatic amine dehydrogenases have been shown to interact with a series of metal ions in anhydrous organic media. Spectroscopic analyses including UV-vis, NMR. and resonance Raman indicate that the metal ion binds to the TTQ model compounds at their *o*-quinone moiety, the binding mode of which is similar to that proposed for the interaction between cofactor TTQ and a cationic species in the native enzymes. The binding constants K_{ML} for the metal ion complexes of TTQ model compounds have been determined from the spectral changes in UV-vis due to the complex formation. Remarkable enhancement of the oxidizing ability of the TTQ model compounds by the complexation with metal ions has been demonstrated as a large positive shift in the one-electron reduction potentials E^0_{red} of the complexes as compared to those of the TTQ model compounds in metal free form (*e.g.* ΔE^0_{red} = 1.17 V for the Mg^{2+} complex and ΔE^0_{red} = 1.16 V for the Sc^{3+} complex). The complexes can oxidize not only benzylamine but also aliphatic amines in anhydrous acetonitrile, whereas no reaction takes place in the absence of the metal ion under otherwise the same experimental conditions. Kinetic studies have revealed that the reaction proceeds via a transamination mechanism involving iminoquinone and product imine intermediates to yield the oxidized products and the reduced TTQ. The ESR spectra of the half-reduced species of TTQ model compounds; *i.e.* semiquinone radical anions, are detected successfully. The spin distribution derived from the hyperfine structures indicates that the spin is partially delocalized on the indole ring connected at the 4-position of the quinone skeleton. This indicates that the indole group plays an important role as a part of the electron transfer pathway from the reduced TTQ to a blue copper protein in biological systems.

IX-G-10 Active Site Models for Galactose Oxidase Containing Two Different Phenol Groups

TAKI, Masayasu[1]; KUMEI, Hideyuki[1]; NAGATOMO, Shigenori; KITAGAWA, Teizo; ITOH, Shinobu[2]; FUKUZUMI, Shunichi[1]
(*[1]Osaka Univ.; [2]Osaka City Univ.*)

Model complexes of the active site of galactose oxidase (GAO) have been developed using a new ligand carrying two different phenol groups, N-[(2-hydroxy-3-methylthio-5-tert-butylphenyl)methyl]-N-[(2-hydroxy-3,5-di-tert-butylphenyl)methyl]-2-(2-pyridyl)ethylamine (L1H$_2$). Deprotonated ligand L1^{2-} forms a dimeric Cu(II) complex, [Cu(II)$_2$(L1^{2-})$_2$], in the solid state, the structure of which has been determined by X-ray crystallographic analysis. The dimeric Cu(II)-diphenolate complex can be converted into the monomeric complex, [Cu(II)(L1^{2-})(X)] (X = py, AcO, and PhCH$_2$OH), in solution by adding exogenous ligands such as pyridine (py), acetate (AcO$^-$), or benzyl alcohol (PhCH$_2$OH). The structure and physicochemical properties (UV-Vis, ESR, redox potential) of [Cu(II)(L1^{2-})(X)] have been explored as a model for the resting state of the enzyme. One-electron oxidation of [Cu(II)(L1^{2-})(py)] and [Zn(II)(L1^{2-})(py)] by (NH$_4$)$_2$-[Ce^{IV}(NO$_3$)$_6$] (CAN) yielded the corresponding phenoxyl radical/phenolate complexes, Cu(II)(L1$^{\bullet-}$) and Zn(II)(L1$^{\bullet-}$), respectively, which have also been characterized by UV-Vis, resonance Raman, and ESR. The structure, physicochemical properties and reactivities of the diphenolate and phenoxyl radical/phenolate complexes of L1H$_2$ are compared to those of the corresponding monophenolate and monophenoxyl radical complexes in order to obtain further insight into the role of Tyr 495 in the native enzyme.

IX-G-11 Active Site Structure of SoxB-Type Cytochrome *bo*$_3$ Oxidase from Thermophilic Bacillus

UCHIDA, Takeshi; TSUBAKI, Motonari[1]; KUROKAWA, Tatsuki[2]; HORI, Hiroshi[3]; SAKAMOTO, Junshi[3]; KITAGAWA, Teizo; SONE, Nobuhito[2]
(*[1]Himeji Inst. Tech.; [2]Kyushu Inst. Tech.; [3]Osaka Univ.*)

Two-subunit SoxB-type cytochrome *c* oxidase in *Bacillus stearothermophilus* was over-produced, purified, and examined for its active site structures by electron paramagnetic resonance (EPR) and resonance Raman (RR) spectroscopies. This is cytochrome *bo*$_3$ oxidase containing heme B at the low-spin heme site and heme O at the high-spin heme site of the binuclear center. EPR spectra of the enzyme in the oxidized form indicated that structures of the high-spin heme O and the low-spin heme B were similar to those of SoxM-type oxidases based on the signals at g = 6.1, and g = 3.04. However, the EPR signals from the Cu$_A$ center

and the integer spin system at the binuclear center showed slight differences. RR spectra of the oxidized form showed that heme O was in a 6-coordinated high-spin (ν_3 = 1472 cm^{-1}), and heme B was in a 6-coordinated low-spin (ν_3 = 1500 cm^{-1}) state. The Fe^{2+}–His stretching mode was observed at 211 cm^{-1}, indicating that the Fe^{2+}–His bond strength is not so much different from those of SoxM-type oxidases. On the contrary, both the Fe^{2+}–CO stretching and Fe^{2+}–C–O bending modes differed distinctly from those of SoxM-type enzymes, suggesting some differences in the coordination geometry and the protein structure in the proximity of bound CO in cytochrome bo_3 from those of SoxM-type enzymes.

IX-G-12 First Synthetic NO-Heme-Thiolate Complex Relevant to Nitric Oxide Synthase and Cytochrome P450nor

SUZUKI, Noriyuki[1]; HIGUCHI, Tsunehiko[1]; URANO, Yasuteru[1]; KIKUCHI, Kazuya[1]; UCHIDA, Takeshi; MUKAI, Masahiro[2]; KITAGAWA, Teizo; NAGANO, Tetsuo[1]
(*[1]Univ. Tokyo; [2]RIKEN*)

We have already succeeded in the synthesis of a stable Fe^{III}-porphyrin-alkanethiolate complex, in which the sulfur atom is sterically protected from reactive molecules such as O$_2$ and NO by bulky groups. We report here some, spectroscopic and electrochemical properties of the first synthetic NO–heme–thiolate complex, prepared by the use of SR.

IX-G-13 Effects of a Thiolate Axial Ligand on the $\pi \rightarrow \pi^*$ Electronic States of Oxoferryl Porphyrins: A Study of the Optical and Resonance Raman Spectra of Compounds I and II of Chloroperoxidase

EGAWA, Tsuyoshi[1]; PROSHLYAKOV, A. Denis[2]; MIKI, Hideho[3]; MAKINO, Ryu[4]; OGURA, Takashi[5]; KITAGAWA, Teizo; ISHIMURA, Yuzuru[1]
(*[1]Keio Univ.; [2]Michigan State Univ.; [3]Zeon Kasei Co. Ltd.; [4]Rikkyo Univ.; [5]Univ. Tokyo*)

Optical absorption and resonance Raman spectra have been investigated for enzymatic intermediates, compounds I and II, of chloroperoxidase (CPO) which contains a thiolate-ligated iron porphyrin. Compound I of CPO (CPO-I), an oxoferryl porphyrin π cation radical, gave an apparently asymmetric single-peaked Soret band at 367 nm, for which band fitting analyses revealed the presence of two transition bands around 365 and 415 nm. Compound II of CPO (CPO-II), an oxoferryl neutral porphyrin, gave a split Soret spectrum with two bands (blue and red Soret bands) at 373 and 436 nm. Thus both CPO-I and CPO-II can be categorized as hyperporphyrins. The maximum extinction coefficients (ε_b and ε_r) and energies (E_b and E_r) of the blue and red Soret bands of CPO-II were found to fall on an $\varepsilon_b/\varepsilon_r$ versus E_b–E_r correlation line derived from data reported for six- coordinate ferrous derivatives of cytochrome P450 and CPO, Corresponding data for CPO-I did not fall on the correlation line. Resonance enhancement of the Fe^{IV}=O stretching (ν_{FeO}) Raman band was found for CPO-I when Raman scattering was excited at wavelengths within both transition bands around 365 and 415 nm, while the ν_{FeO} Raman band was not identified for CPO-II at any of the excitation wavelengths examined here. These findings suggest that the thiolate axial ligand causes Soret band splitting of CPO-II through configuration interaction between the sulfur $\rightarrow$ porphyrin e$_g$* charge transfer and porphyrin a$_{1u}$,a$_{2u}$ $\rightarrow$ e$_g$* transitions, while the FeO portion is important in determining the shape of the Soret band of CPO-I.

IX-G-14 Characterization of Imidazolate-Bridged Dinuclear and Mononuclear Hydroperoxo Complexes

OHTSU, Hideki[1]; ITOH, Shinobu[2]; NAGATOMO, Shigenori; KITAGAWA, Teizo; OGO, Seiji; WATANABE, Yoshihito; FUKUZUMI, Shunichi[1]
(*[1]Osaka Univ.; [2]Osaka City Univ.*)

Dinucleating ligands having two metal-binding sites bridged by an imidazolate moiety, Hbdpi, HMe$_2$bdpi, and Hme$_4$bdpi (Hbdpi = 4,5-bis(di(2-pyridylmethyl)-aminomethyl)imidazole, HMe$_2$bdpi = 4,5-bis((6-methyl-2-pyridylmethyl)(2-pyridylmethyl)amino-methyl)imidazole, HMe$_4$bdpi = 4,5-bis(di(6-methyl-2-pyridylmethyl)aminomethyl)imidazole), have been designed and synthesized as model ligands for copper-zinc superoxide dismutase (Cu, Zn–SOD). The corresponding mononucleating ligands, MeIm(Py)$_2$, MeIm(Me)$_1$, and MeIm(Me)$_2$ (MeIm(Py)$_2$ = (1-methyl-4-imidazolylmethyl)bis(2-pyridylmethyl)amine, MeIm(Me)$_1$ = (1-methyl-4-imidazolylmethyl)(6-methyl-2-pyridylmethyl) (2-pyridylmethyl)amine, MeIm(Me)$_2$ = (1-methyl-4-imidazolylmethyl)bis(6-methyl-2-pyridylmethyl)amine), have also been synthesized for comparison. The imidazolate-bridged Cu(II)–Cu(II) homodinuclear complexes represented as [Cu$_2$(bdpi)-(CH$_3$CN)$_2$](ClO$_4$)$_3$·CH$_3$CN·3H$_2$O (**1**), [Cu$_2$(Me$_2$bdpi)-(CH$_3$CN)$_2$](ClO$_4$)$_3$ (**2**), [Cu$_2$(Me$_4$bdpi)(H$_2$O)$_2$](ClO$_4$)$_3$· 4H$_2$O (**3**), a Cu(II)–Zn(II) heterodinuclear complex of the type of [CuZn(bdpi)(CH$_3$CN)$_2$](ClO$_4$)$_3$·2CH$_3$CN (**4**), Cu(II) mononuclear complexes of [Cu(MeIm(Py)$_2$)-(CH$_3$CN)](ClO$_4$)$_2$·CH$_3$CN (**5**), [Cu(MeIm(Me)$_1$)(CH$_3$-CN)](ClO$_4$)$_2$ (**6**), and [Cu(MeIm(Me)$_2$)(CH$_3$CN)]-(ClO$_4$)$_2$ (**7**) have been synthesized and the structures of complexes **5**–**7** determined by X-ray crystallography. The complexes **1**–**7** have a pentacoordinate structure at each metal ion with the imidazolate or 1-methyl-imidazole nitrogen, two pyridine nitrogens, the tertiary amine nitrogen, and a solvent (CH$_3$CN or H$_2$O) which can be readily replaced by a substrate. The reactions between complexes **1**–**7** and hydrogen peroxide (H$_2$O$_2$) in the presence of a base at –80 degreesC yield green solutions which exhibit intense bands at 360–380 nm,

consistent with the generation of hydroperoxo Cu-(II) species in all cases. The resonance Raman spectra of all hydroperoxo intermediates at –80 degreesC exhibit a strong resonance-enhanced Raman band at 834–851 cm^{-1}, which shifts to 788–803 cm^{-1} (Δv = 46 cm^{-1}) when ^{18}O-labeled H_2O_2 was used, which are assigned to the O–O stretching frequency of a hydroperoxo ion. The resonance Raman spectra of hydroperoxo adducts of complexes **2** and **6** show two Raman bands at 848 (802) and 834 (788), 851 (805), and 835 (789) cm^{-1} tin the case of $H_2{}^{18}O_2$, Δv = 46 cm^{-1}), respectively. The ESR spectra of all hydroperoxo complexes are quite dose to those of the parent Cu(II) complexes except **6**. The spectrum of **6** exhibits a mixture signal of trigonal-bipyramid and square-pyramid which is consistent with the results of resonance Raman spectrum.

IX-G-15 Oxygenation of Phenols to Catechols by a (μ-η²:η²-peroxo)dicopper(II) Complex. Mechanistic Insight into the Phenolase Activity of Tyrosinase

ITOH, Shinobu[1]; KUMEI, Hideyuki[2]; TAKI, Masayasu[2]; NAGATOMO, Shigenori; KITAGAWA, Teizo; FUKUZUMI, Shunichi[2]
(*[1]Osaka City Univ.; [2]Osaka Univ.*)

Mechanistic studies on the oxygenation of phenolates to the corresponding catechols by a (μ-η²:η²-peroxo)dicopper(ll) comp]ex have been carried out to provide sjgnificant insight into the mechanism of pheno]ase activity of tyrosinase. Treatment of [Cu-(L^{py2Bz})]PF$_6$ (L^{Py2BZ} = *N,N*-Bis[2-(2-pyridyl)ethyl]-α,α-dideuterio-benzylamine) with molecular oxygen in acetone at –94 °C gave a (μ-η²: η²-peroxo)dicopper(II) complex, the formation of which has been confirmed by its characteristic UV-vis [λ$_{max}$ = 364 and 530 nm (ε = 26400 and 1500 M^{-1} cm^{-1})] and resonance Raman spectra ($v_{O(16)-O(16)}$ = 737 cm^{-1}, $v_{O(18)-O(18)}$ = 697 cm^{-1}) as well as the ESR-silence and the observed stoichiometry of Cu:O_2 = 2:1. Addition of lithium salts of *p*-substituted phenols into the solution induces oxygenation at its *o*-position to give the corresponding catechols in good yields, but no C–C or C–O coupling dimer is produced. The reaction obeys pseudo-first-order kinetics in the presence of excess amount of substrate and shows a Mjchaelis-Menten type saturation phenomenon. The reactivity of the substrates increases as the electron-donating nature of the *p*-substituent increases. In addition, no catechol formation was observed when a bis(μ-oxo)dicopper(III) was employed instead of the ((μ-η²:η²-peroxo)dicopper(II) complex under the same experimental conditions. All these results suggest that the oxygenation of phenolates to catechols by the ((μ-η²:η²-peroxo)dicopper(II) comp]ex proceeds via *electrophilic attack* of the peroxo species to the phenolate in a binary complex between the peroxo species and the substrate.

IX-G-16 Differences in Changes of Subunit Interfacial Contacts upon Ligand Binding to the α or β Subunits of Ni–Fe Hybrid Hemoglobin Probed by UV Resonance Raman Spectroscopy

NAGATOMO, Shigenori; NAGAI, Masako[1]; SHIBAYAMA, Naoya[2]; KITAGAWA, Teizo
(*[1]Kanazawa Univ.; [2]Jichi Medical School*)

To see the α1-β2 subunit contacts in the half-ligated hemoglobin A (HbA), ultraviolet resonance Raman (UVRR) spectra of Ni–Fe hybrid Hb have been examined under various solution conditions. Our previous studies demonstrated that Trpβ37, Tyrα42 and Tyrα140 are mainly responsible for UVRR spectral differences between deoxyHbA and COHbA (Nagai, M., Wajcman, H., Lahary, A., Nakatsukasa, T., Nagatomo, S., and Kitagawa, T. *Biochemistry* **38**, 1243 (1999)). The half-ligated α^{Ni}β^{COFe} and α^{COFe}β^{Ni} at pH 6.7 in the presence of IHP as well as α^{Ni}β^{deoxy} and α^{deoxy}β^{Ni} stayed in the complete T structure similar to deoxyHbA. Upon ligand binding to Fe hemes, Trp residues are changed toward the R-like contact to a similar extent in α^{Ni}β^{CO} and α^{CO}β^{Ni}. The spectral changes of Tyr and Trp are not synchronous and also different between α^{Ni}β^{COFe} and α^{COFe}β^{Ni}. It is not until pH 8.7 with α^{Ni}β^{deoxy} that Tyr residues change upon ligand binding in the presence of IHP, while they changed at pH 6.7 in the absence of IHP. The structural change of Tyr residues is induced by binding of CO, but not NO, to α heme, while they were induced similarly by binding of CO and NO to β-heme. Structural changes of Trp residues are induced by the CO binding to either α- or β-heme. These observations directly indicate that the phenomenon occurring at the α1-β2 interface is different between ligand binding to α- and β-hemes and that it is greatly influenced by IHP. Thus in this study, we supplement our previous study on NOHb regarding the mechanism of the change of Tyr residues.

IX-G-17 Resonance Raman Studies of the Oxygen Sensing Signal Transducer Protein HemAT from *Bacillus Subtilis*

AONO, Shigetoshi[1]; KATO, Toshiyuki[1]; MATSUKI, Mayumi[1]; NAKAJIMA, Hiroshi[1]; OHTA, Takehiro; UCHIDA, Takeshi; KITAGAWA, Teizo
(*[1]JAIST*)

HemAT-Bs is a heme-containing signal transducer protein responsible for aerotaxis of *Bacillus subtilis*. The recombinant HemAT-Bs expressed in *E. coli* was purified as the oxy form in which O_2 was bound to the ferrous heme. Although the electronic absorption spectra of HemAT-Bs were similar to those of myoglobin, HemAT-Bs showed some unique character-istics in its resonance Raman spectra. O_2-bound HemAT-Bs showed the v(Fe–O_2) band at 560 cm^{-1}, which suggests a unique hydrogen bonding to the bound O_2 *i.e.*, the hydrogen bonding between a distal amino acid residue and the proximal oxygen atom of the bound O_2. Deoxy HemAT-Bs showed the v(Fe–His) band at 225 cm^{-1}, which indicates a relatively stronger hydrogen bonding to the proximal His and/or a less strained Fe–His bond compared with myoglobin. CO-

bound HemAT-Bs showed the ν(Fe–CO) ,and ν(C–O) bands at 494 and 1964 cm^{-1}, respectively. These results indicate that a histidine is an axial ligand of the heme in HemAT-Bs.

IX-G-18 Time-Resolved UV Resonance Raman Investigation of Protein Folding: Characterization of Kinetic and Equilibrium Intermediates of Apomyoglobin

HARUTA, Nami[1]; KITAGAWA, Teizo
(*[1]GUAS*)

The equilibrium acid-unfolding intermediate and kinetic folding intermediates of apomyoglobin were investigated by 244 nm-excited UV resonance Raman spectroscopy combined with a new rapid mixer. The dead time for mixing in the newly constructed flow-mixer was determined to be 150 μs with UV Raman spectral changes of imidazole to imidazolium upon mixing with an acid. The pH-jump experiments of apomyoglobin (apoMb) from 2.2 to 5.6 conducted with this device demonstrated the presence of three folding intermediates. Based on the analysis of W3 and W7 bands of Trp 7 and Trp14, the first intermediate, formed before 250 μs, involved inclusion of Trp14 into an α-helix from a random coil. In the second intermediate, formed around 1 ms after the start of folding, the surroundings of both Trp7 and 14 were significantly hydrophobic, suggesting the formation of hydrophobic core. In the third intermediate appearing around 3 ms, the hydrophobicity was relaxed to the same level as that of the pH 4 equilibrium intermediate, which was investigated in detail with the stationary state technique. The change from the third intermediate to the native state takes time longer than 40 ms, while the appearance of the native spectrum after the mixing of the same solutions was confirmed separately.

IX-G-19 Raman Spectroscopy of Proteins

KITAGAWA, Teizo; HIROTA, Shun[1]
(*[1]Nagoya Univ.*)

Infrared (IR) and Raman spectroscopy are the main methods to measure the vibrational spectrum of proteins. When a molecular vibration is accompanied by a change of dipole moment, the mode is IR active, and when the vibration is accompanied by a change of polarizability, the mode is Raman active. For a molecule with a center of symmetry, mutual exclusion occurs. Accordingly, the two methods are complementary. In the case of synthetic homopolypeptides with a specific geometry, IR and Raman active modes are often different from each other because of their symmetry properties. For general proteins, however, there is no symmetry, and therefore selection rules are not helpful for band assignments. In practice, some modes are stronger for Raman and others are stronger for IR.

The most important benefit of Raman in comparison with IR spectroscopy in observing the vibrational spectra of proteins is that the measurement of aqueous solutions is much easier with the former, because the Raman scattering from water is very weak. Since the technique can be applied to crystals as well as to solutions, it is also useful to compare structures of a protein in solution and crystalline phases. Another important characteristic of Raman spectroscopy is the possibility of resonance enhancement. When the excitation wavelength of Raman scattering approaches an absorption maximum of an electronic transition of a molecule, some of the molecular vibrations gain strong enhancement of Raman intensity. This is called the resonance Raman effect. Under resonance conditions, very dilute solutions can be used for Raman measurements under conditions when ordinary Raman bands are not seen. As a result, the spectrum becomes simpler. In such a case, as detailed information on the molecular structure can be derived from the spectrum of a biopolymer with a molecular weight of 10^5 as can be found for small molecules. By selecting an appropriate excitation wavelength, different chromophores of the same molecule can be monitored. Accordingly, for colored proteins, visible excitation of Raman scattering provides structural information on a chromophore and UV excitation selectively brings about the vibrational spectra of side chains of aromatic residues and the polypeptide skeleton.

IX-G-20 Identification of Tyrosine Residues Involved in Ligand Recognition by the Phosphatidylinositol 3-Kinase Src Homology 3 Domain: Circular Dichroism and UV Resonance Raman Studies

OKISHIO, Nobuyuki[1]; TANAKA, Toshiyuki[2]; NAGAI, Masako[1]; FUKUDA, Ryuji[1]; NAGATOMO, Shigenori; KITAGAWA, Teizo
(*[1]Kanazawa Univ.; [2]Univ. Tsukuba*)

Src homology 3 (SH3) domains are small non-catalytic protein modules capable of mediating protein-protein interactions . We previously demonstrated that the association of a ligand peptide RLPI (RKLPPRPSK) causes environmental and structural changes of Trp55 and some of seven Tyr residues in the phosphatidylinositol 3-kinase (PI3K) SH3 domain by circular dichroism (CD) and 235-nm excited UV resonance Raman (UVRR) spectroscopies [Okishio, N., *et al. Biopolymers* **57**, 208 (2000)]. In this work, the affected Tyr residues were identified as Tyr12, Tyr14, and Tyr73 by the, CD analysis of a series of mutants, in which every single Tyr residue was replaced by a Phe residue. Among these three residues, Tyrl4 was found to be a main contributor to the UVRR spectral change upon the RLPl binding,. Interestingly, CD and UVRR analyses revealed that RLPl associates with the Y14F and Y14H mutants in different ways. These results suggest that Tyr14 plays a crucial role in the ligand recognition, and the amino acid substitution at Tyr14 affects the mode of

PI3K SH3-ligand interaction. Our findings give an insight into how SH3 domains can produce diversity and specificity to transduce a certain signal within cells.

IX-H Fast Dynamics of Photoproducts in Solution Phases

Picosecond time-resolved resonance Raman (ps-TR³) spectroscopy is a promising technique to investigate ultrafast structural changes of molecules. However, this technique has not been used as widely as nanosecond TR³ spectroscopy, mainly due to the lack of light source which has suitable repetition rates of pulses and wavelength tunability. In order to obtain qualified TR³ spectra, first we need two independently tunable light sources for pump and probe pulses. Second, the repetition rate should be higher than kiloHertz to keep a moderate average laser power without making the photon density of probe pulse too high. We succeeded in developing light sources for ps-TR³ spectroscopy having wide tunability and kHz repetition, and applied them to study fast dynamics of photo-excited molecules. For carbonmonoxy myoglobin (MbCO), vibrational relaxation with the time constant of 1.9 ps was observed for CO-photodissociated heme. For Ni–octaethylporphyrin in benzene, differeces in rise times of population in vibrationally excited levels among various modes were observed in the anti-Stokes spectra for the first time. This technique has been applied to identify the trans ligand of CO in the CO-bound transcriptional factor, Coo A.

On the other hand, we have constructed a nanosecond temperature-jump apparatus using a water absorption in near infrared. The new apparatus based on a Nd:YAG laser was combined with a time-resolved Raman measurement system and applied successfully to explore thermal unfolding of ribonucelase A.

IX-H-1 Ultrafast Dynamics of Myoglobin Probed by Time-resolved Resonance Raman Spectroscopy

MIZUTANI, Yasuhisa; KITAGAWA, Teizo

Recent experimental work on the ultrafast dynamics of myoglobin carried out in this laboratory is summarized with a stress on structural and vibrational energy relaxation. Studies on the structural relaxation of myoglobin following CO photolysis revealed that the structural change of heme itself caused by CO photodissociation is completed within the instrumental response time of the time-resolved resonance Raman apparatus used (~2 ps). In contrast, changes in the intensity and frequency of the iron-histidine (Fe–His) stretching mode upon dissociation of the trans ligand were found to occur in the picosecond regime. The Fe–His band is absent for the CO-bound form, and its appearance upon photodissociation was not instantaneous in contrast with that observed in the vibrational modes of heme, suggesting appreciable time evolution of the Fe displacement from the heme plane. The band position of the Fe–His stretching mode changed with a time constant of about 100 ps, indicating that tertiary structural changes of the protein occurred in a 100-ps range. Temporal changes of the anti-Stokes Raman intensity of the ν_4 and ν_7 bands demonstrated immediate generation of vibrationally excited heme upon the photodissociation and decay of the excited populations, whose time constants are 1.1 ± 0.6 and 1.9 ± 0.6 ps, respectively. In addition, the development of the time-resolved resonance Raman apparatus and prospects in this research field are described.

IX-H-2 Time-Resolved Resonance Raman Study of the Exciplex Formed between Excited Cu-Porphyrin and DNA

KRUGLIK, G. Sergei[1]; MOJZES, Peter[2]; MIZUTANI, Yasuhisa; KITAGAWA, Teizo; TURPIN, Pierre-Yve[3]
(*[1]B. I. Stepanov Inst. Phys.; [2]Charles Univ.; [3]Univ. Pierre*)

The photoinduced reversible process of exciplex formation and decay between the water-soluble cationic metalloporphyrin 5,10,15,20-tetrakis[4-(*N*-methyl-pyridyl)] (Cu(T4MPyP)) and calf- thymus DNA has been studied by a picosecond time-resolved resonance Raman (ps-TR³) technique. For a detailed analysis of the exciplex properties, the following model compounds have also been investigated: double-stranded poly-nucleotides poly(dA-dT)$_2$, poly(dG-dC)$_2$, and poly(dA-dC). poly(dG-dT), single-stranded poly(dT), and the 32-mer d[(Gr)$_7$ATAT(GC)$_7$]$_2$. Additional Raman measurements have also been done in using cw and 20-ns laser sources. It is shown that this reversible exciplex is formed, with a yield depending on the nucleic base sequence, in less than 2 ps after photoexcitation, between photoexcited Cu(T4MPyP) and C=O groups of thymine residues in all thymine-containing sequences of nucleic acids. Such a rapid exciplex building process implies that it involves porphyrin molecules initially located, in the steady state of this interaction, at AT sites of the nucleic acids. This has two main consequences, which contradict previously reported assumptions (Strahan *et al.*, *J. Phys. Chem.* **96**, 6450 (1992)): (i) Although the binding mode of the porphyrin actually depends on the base sequence, there is no preferential binding of Cu(T4MPyP) to the various sites of DNA,

and (ii) there is no photoinduced ultrafast porphyrin translocation from GC to AT sites of DNA. In addition, it is shown that with surrounding water molecules an exciplex can also be formed in ~1 ps, whose spectral characteristics are not distinguishable from those formed with thymine residues. However, these two exciplex species can be distinguished from each other by their relaxation kinetics: the lifetime of the exciplex formed with water lies in the 3–12 ps range, while that of the exciplex formed with nucleic acids lies in the nanosecond time domain (1–3 ns). A set of possible routes is discussed for each of the exciplex building/decay processes.

IX-H-3 Ultrafast Structural Relaxation of Myoglobin Following Photodissociation of Carbon Monoxide Probed by Time-Resolved Resonance Raman Spectroscopy

MIZUTANI, Yasuhisa; KITAGAWA, Teizo

Studies on the structural relaxation of myoglobin following CO photolysis revealed that the structural change of heme itself caused by the cleavage of the Fe–CO bond is completed within the instrumental response time (~2 ps) of the time-resolved resonance Raman apparatus used. In contrast, changes in the intensity and frequency of the iron-histidine stretching [ν(Fe–His)] mode were found to occur in the picosecond regime. The ν(Fe–His) band is absent for the CO-bound form, and its appearance upon photodissociation was not instantaneous in contrast with the changes observed in the vibrational modes of heme, suggesting appreciable time evolution of the Fe displacement from the heme plane. Same behaviors were observed for the model compound of the heme part without protein matrix. Therefore the intensity change in ν(Fe–His) is not associated with protein relaxation following the CO photodissociation. The band position of the ν(Fe–His) mode changed with a time constant of about 100 ps, while that of the model compound without the protein matrix showed no shift. This indicates that tertiary structural changes of the protein occurred in a 100-ps range.

RESEARCH FACILITIES

The Institute for Molecular Science includes five research facilities. This section describes their latest equipment and activities. For further information please refer to older IMS Annual Review issues (1978–2000).

Laser Research Center for Molecular Science

This Center was established in 1997 by reorganization of a part of the Instrument Center. The new Center is composed of three research groups which are asked to develop new lasers suitable for pioneering researches in the new field of molecular science. The three groups are
1. Advanced Lasers for Chemical Reaction Studies,
2. Advanced Lasers for Synchrotron Radiation Applications
   and
3. Advanced UV and IR Tunable Lasers.

The Laser Research Center are equipped with excimer lasers and all-solid-state light sources in various temporaland spectral regions, including femtosecond and nanosecond Optical Parametric Oscillators (OPO). The synchronously femtosecond OPO (OPAL; SPECTRA PHYSICS) is tunable from 1.1 μm up to 1.6 μm. The nanosecond OPO has extraordinarily wide tuning range form 420 nm down to 2.2 mm. The Laser Center also has a fluorescence analyzer (FLUOROLOG2; SPEX) which is composed of a xenon lamp house, and double and single monochromators for spectroscopy. The detector is changeable by rotating a mirror (CCD and PM). Using these instruments, one can carry out various experiments not only in the ultrafast temporal region but also in the steady-state photon-counting region.

Research Center for Molecular Materials

The center was established by reorganization of Chemical Materials Center, Low-Temperature Center, and a part of Instrument Center in 1997. This center plays important roles in the preparation of novel chemical materials, management of chemicals in the institute, and support of liq. N_2 and He. Four research groups in the center cover the following four general research fields. 1) Preparation of Novel Heterocyclic Compounds and their Molecular Assemblies. 2) Electronic Structures and Reactivities of Metalloproteins. 3) Molecular Design of Artificial Photosynthesis System. 4) Organic Molecular Materials with Novel Electronic Properties. In addition to the research activities, the center supports the instruments including high filed NMR, EPR and MALDI-TOF mass spectrometers, SQUID, X-ray diffractometers. The center accepts the elemental analyses and mass spectrometric measurements.

Equipment Development Center

A number of research instruments have been designed and constructed at the mechanical, electronic and glass work sections in this Facility. Examples of our works in this fiscal year are listed below.
   Ion stack
   Ion beam bender
   Ion(Einzel) lens
   Supporter for the quadruple mass filter
   Interlock circuit of UVSOR BL4B beamline
   High precision dual delayed gate pulser
   High speed valve controller for molecular beam source
   30KV Fast rising pulse generator
   Data acqusition system for Acousto-Optical spectrometer
   Vacuum gauge for halogen gas
Development of IMS Machines
   Equipment Development Center is also engaged in developing IMS Machines. This activity is described in detail in section "RESEARCH ACTIVITIES."

Ultraviolet Synchrotron Orbital Radiation Facility

The UVSOR accelerator complex consists of a 15 MeV injector linac, a 600 MeV booster synchrotron, and a 750 MeV storage ring. The magnet lattice of the storage ring is the so-called double-bend achromat. The double RF system is routinely operated for user beam time, and the lifetime of the electron beam has been improved to about 5 hours at 200 mA. The storage ring is normally operated under multi-bunch mode with partial filling. The single bunch operation is also conducted about three weeks a year, which provides pulsed synchrotron radiation (SR) for time-resolved experiments. Typical beam currents under multi-bunch and single-bunch modes are 200 mA and 50 mA, respectively. Construction of a new beam position monitoring system and an orbit feedback system was completed by the end of March 2001.

Eight bending magnets and two insertion devices are available for utilizing SR. The bending magnet with its radius of 2.2 m provides SR, whose critical energy is 425 eV. There is a total of 20 beamlines operational at

UVSOR, which are classified into two categories. 11 of them are so-called "Open beamlines," which are open to scientists of universities and research institutes belonging to the government, public organizations, private enterprises and those of foreign countries. The rest of the 9 beamlines are so-called "In-house beamlines," which are dedicated to the use of the research groups within IMS. We have two soft X-rays (SX) stations each equipped with a double-crystal monochromator, eight EUV and SX stations with a grazing incidence monochromator, four VUV stations with a normal incidence monochromator, one (far) infrared station equipped with FT interferometers, one station with a multi-layer monochromator, and four non-monochromatized stations for irradiation of white-light.

The planar undulator is composed of 24 pairs of permanent magnets, the period of which is 84 mm. The fundamentals from the undulator provide quasi-monochromatic intense radiation in the photon energy region from 8 to 52 eV. The helical undulator was installed in 1996, which can also be used as the helical optical klystron for free electron laser (FEL) experiments. The undulator supplies the perfect circular polarization in the photon energy range of 2–45 eV, and the elliptic polarization up to 200 eV. It was finally decided in 2000 that the superconducting wiggler for BL7A, which has a fatal problem on its cryogenic system, would be removed from the storage ring. An in-vacuum type undulator will be installed at the straight section, after removing the wiggler, in March 2002. Recently, a combination of the non-monochromatized undulator radiation at BL3A1 with FEL has led us to the success of realizing two-photon experiments for Xe atoms. To our knowledge, this is the first result indicating the practical usability of FEL in the whole world.

Discussion with users, concerning the improvements and upgrades of the beamlines at UVSOR, has been continuously made as series of UVSOR workshops. As a result, about one third of beamlines have been upgraded in recent years. BL 6B, which was originally constructed for IR experiments, is under renewal for nano-scale photochemical reaction experiments. A new high-resolution beamline BL4B in the SX region has been successfully constructed lately and its performance tests have been terminated at the end of January 2001. Several novel results for simple molecules have emerged from this beamline, using photoabsorption and angle-resolved photoion yield spectroscopy under high-resolution condition. More recently, discussion for the rebuilt and rearrangement of several old beamlines has been initiated, on the basis of the review and evaluation report on the present status of UVSOR in 2000.

In spring 2001, we had one-month shutdown to perform periodic maintenance for the rings and beamlines and to check the incidental facilities in UVSOR. During the regular shutdown period for about one month in summer 2001, similar maintenance is under progress. There were lots of trouble in one year (from September 2000 to August 2001) due mainly to the superannuated laboratory equipment, as usual, but fortunately, they did not seriously affect the user's beam time. It should be noted that the incident of the leakage of toxic BF_3 gas happened at BL3A2 on the 22nd of December 2000. It was fortunate that nobody's health was damaged by this accident due to a small amount of the leakage gas. A new safety system for the handling of toxic gas has been introduced to prevent further undesirable accidents.

All uses are required to refer to the beam-line manuals and the UVSOR guidebook (latest revision in 1999), on the occasion of conducting the actual experimental procedures. Those wishing to use the open and in-house beamlines are recommended to contact with the stationmaster/supervisor and the representative, respectively. For updated information of UVSOR, http://www.uvsor.ims.ac.jp/.

Computer Center

Since April 1 of 2000, Computer Center of IMS has been reorganized as Research Center for Computational Science in Okazaki National Research Institute. The main super-computers at the Center consist of the vector parallel system of Fujitsu VPP5000 and the scalar parallel system of SGI 2800. The VPP5000 system has 30 vector CPU-nodes, and has 256 GB of main memory. SGI 2800 has 256 CPU and 256 GB of memory. The NEC SX-5 and the IBM SP2 parallel computers are also installed for the general purpose computations. These vector and parallel computers are actively utilized mainly for the large scale molecular science simulations. The computers are linked to international networks through Science Information Network(SINET). About 25% of the computer time is dedicated by the research staff at IMS. The remaining 75% is given out as research grants to scientists outside the institute in molecular science and related field, e.g. bioscience, bioinfomatics. As of March 2001, the number of project group was 162, consisting of 643 users. The library programs of the Center amount to 807. Among them, more than 150 programs can be executed immediately. Information on the library program can be found on our center's home-page (http://ccinfo.ims.ac.jp/). The Quantum Chemistry Literature Database (QCLDB) has also been developed by the QCLDB group in collaboration with the staff member of computer center, and this database can be accessible through our home page.

SPECIAL RESEARCH PROJECTS

IMS has special research projects supported by national funds. Three projects in progress are:
(a) Chemical Reaction Dynamics
(b) Molecular Photophysics and Science
(c) Novel Material Science

These three projects are being carried out with close collaboration between research divisions and facilities. Collaborations from outside also make important contributions. Research fellows join these projects.

(a) Chemical Reaction Dynamics

Folding Mechanism of Protein Molecules Studied by Generalized-Ensemble Algorithms

OKAMOTO, Yuko; SUGITA, Yuji; NAGASIMA, Takehiro; YODA, Takao; KOKUBO, Hironori[1]; MURATA, Katsumi[1]; SAKAE, Yoshitake[1]
(*[1]GUAS*)

Proteins are the most complicated molecules that exist in nature. Since protein structures are closely related to their biological functions, the understanding of their folding mechanism from the first principles is not only very challenging but also very important a problem in theoretical molecular science. To be more specific, it is widely believed that three-dimensional structure of proteins is determined by their amino-acid sequence information. However, nobody has completely succeeded in predicting it solely from the amino-acid-sequence information (prediction from the first principles.)

There are two elements for the difficulty. One element is that the inclusion of accurate solvent effects is non-trivial because the number of solvent molecules that have to be considered is very large. The other element for the difficulty is that there exist huge number of local minima in the energy function, and simulations by conventional techniques will necessarily get trapped in one of the local minima without ever finding the energy global minimum. Generalized-ensemble algorithms are new simulation algorithms that can alleviate this second difficulty (for reviews, see Refs.1-3). We have been developing new generalited-ensemble algorithms. We found that the replica-exchange method and its extension are particularly promising.[3]

The goal of the present project is to further develop and test the effectiveness of generalize-ensemble algorithms in the protein folding problem and to succeed eventuallyin the prediction of tertiary structures of proteins from the first principles.

References
1) Y. Okamoto, *Recent Res. Devel. Pure & Appl. Chem.* **2**, 1 (1998).
2) U. H. E. Hansmann and Y. Okamoto, *Ann. Rev. Comput. Phys. VI*, Ed., D. Stauffer, World Scientific, pp. 129–157 (1999).
3) A. Mitsutake, Y. Sugita and Y. Okamoto, *Biopolymers (Pept. Sci.)* **60**, 96 (2001).

Development and Applications of Basic Theories of Nonadiabatic Transitions, Chemical Reactions, and Their Control

NAKAMURA, Hiroki; ZHU, Chaoyuan; MIL'NIKOV, Gennady V.[1]; TERANISHI, Yoshiaki[2]; NAGAYA, Kuninobu[3]; KAMISAKA, Hideyuki[3]; BIAN, Wensheng[4]; FUJISAKI, Hiroshi
(*[1]IMS and Inst. Struct. Macrokinetics, Russia; [2]IMS and RIKEN; [3]GUAS; [4]IMS and Shandong Univ.*)

Based on the Zhu-Nakamura theory[1] of non-adiabatic transition due to potential curve crossing, we are developing new semiclassical methods to effectively deal with electronically nonadiabatic chemical reactions. First, we incorporate our Zhu-Nakamura theory into the trajectory surface hopping (TSH) method. Taking the DH_2^+ system as a typical example of seam crossing, we have tested the idea in comparison with the old version of TSH based on the Landau-Zener formula and the exact quantum calculations. Not only the collinear but also 3D reaction systems are studied, and the Zhu-Nakamura theory was found to improve the method significantly. This is very encouraging, since this tells us that we can apply this new method to large reaction systems. We are planning to apply this method to conical crossing case also, which is an application of the nonadiabatic tunneling case of Zhu-Nakamura theory. We further plan to develop semiclassical methods with use of Zhu-Nakamura theory even with all the phase effects included.

In order to develop the above mentioned general methods, we have to further work out to formulate basic theories of nonadiabatic transitions applicable to other cases such as Renner-Teller type transition.

Another important project we are working on is the laser control of molecular processes. Here again, the various types of nonadiabatic transitions play essential roles, since in the so called dressed state picture we can create potential curve crossing by shining molecules by laser and further more we can control nonadiabatic transitions at the newly created avoided crossings by manipulating lasers. We have proposed the following two new ideas for that;[1,2] (1) usage of the complete reflection phenomenon, and (2) control by a train of linearly chirped pulses. The first idea is based on the intriguing phenomenon occurring in the nonadiabatic tunneling type transition and can be realized by using a stationary laser field. The second is to use the inter-

ference phenomenon in nonadiabatic transitions induced by periodical chirping of laser frequencies. Since the basic analytical theories are available, we can design necessary conditions analytically. The idea can be applied to dynamic processes in an external field other than laser, namely to NMR and ESR problems.

References
1) C. Zhu, Y. Teranishi and H. Nakamura, *Adv. Chem. Phys.* **117**, 127 (2001).
2) K. Nagaya, Y. Teranishi and H. Nakamura, in "*Laser Control and Manipulations of Molecules*," American Chemical Society (in press).

Proton Tunneling in a Dissipative Environment: Raman Response and ReactionRate

TANIMURA, Yoshitaka

A double well potential system coupled to a colored Brownian oscillators bath is considered to study tunneling dynamics in a dissipative environment. The quantum Fokker-Planck equation for a colored noise bath in a low temperature is reduced in a multi-dimensional hierarchy form. A chemical reaction rate and Raman response spectrum are calculated for various coupling strength and temperature. Compared with the classical results, which are obtained by solving classical Fokker-Planck equation, we investigate the effects of tunneling processes on the reaction rate and spectrum. In the quantal case, the low frequency peak is observed in the Raman spectrum, which is due to the level splitting of vibrational levels induced by tunneling.

Constructing Molecular Theory of Chemical Process in Solution

HIRATA, Fumio; SATO, Hirofumi; KOVALENKO, Andriy; SETHIA, Ashok; IMAI, Takashi; SUMI, Tomonari; YAMAGUCHI, Tsuyoshi; HARANO, Yuichi; YAMAZAKI, Takeshi; WATANABE, Ayumi; KINOSHITA, Masahiro[1]; NISHIYAMA, Katsura[2]
(*[1]Kyoto Univ.; [2]Osaka Univ.*)

Our current research interests and activities are concentrated upon three important chemical processes in solution, in each of which solvent plays essential role: (A) the electronic structure of a molecule in solution, (B) solvation thermodynamics of protein and related molecules, (C) characterization of spatial and temporal density fluctuation in molecular liquids, and (D) molecular theory of electrode-solution interface.

The RISM theory, an integral equation theory of molecular liquids, is our main machinery to attack the problem, which is coupled with other theoretical methodologies including the ab initio molecular orbital method, molecular simulations, and the generalized Langevin equation. Problems on which we have been working along the four lines are as follows:

1. Solvent effect on nuclear magnetic shielding of a molecule in solution.
2. Partial molar volume of biomolecules and their stability upon pressure.
3. Stability of peptide and protein conformations in aqueous solution.
4. Solvation dynamics and thermodynamics of ions and molecules.
5. Non-equilibrium free energy surface related to electron transfer reactions
6. Dynamical coupling between intra- and inter molecular motions in liquids.
7. Description of collective excitation in liquids by interaction site model.
8. Path integral theory of a hydrated electron.
9. Developing DFT theories of molecular liquids.
10. Gas-liquid phase transition.
11. Theory of liquids confined in porous media.
12. Structure of alcohol-water mixture.

Imaging of Chemical Dynamics

SUZUKI, Toshinori; KOHGUCHI, Hiroshi; KATAYANAGI, Hideki; MATSUMOTO, Yoshiteru

We have constructed a crossed molecular beam apparatus and continued improving its performance over the past 6 years by introducing various new techniques of molecular beams and ion imaging. Its high performance has been proven by observing rotationally inelastic scattering of NO molecule with Ar, where state-resolved differential cross sections were observed, for the first time, for both fine-structure conserving and changing collisions. Based on this success, we set the next target of research at the $O(^1D)$ reactions with hydrides, since it is important in the stratosphere. In the year of 2001, some modifications were made on the apparatus to increase the signal level. One is a new light path of 157 nm light for photolysis of molecular oxygen: a new configuration allows a straight through propagation of F2 laser light in the source chamber for which higher flux of 157 nm light. This required reconstruction of a bulkhead and readjustment of a skimmer and a pulsed valve. Another is introduction of pulsed valves that generate much shorter pulses of molecular beams than before. With the courtesy of Professor Uzi Even, we introduced solenoid valves that allow the pulse duration of only 50 microsecond or less. Such a short pulse duration reduces scattering of an molecular beam by a skimmer that would otherwise significantly reduce the flux of high intensity beam. In addition, an oil diffusion pump (2000 L/s) in the $O(^1D)$ beam chamber was replaced with a hybrid turbo molecular pump (1600 L/s) to suppress the contamination of a focusing lens for 157 nm light by back streaming of pump oils. The backup pump was also changed from a rotary pump to an oil-free scroll pump. All of these improved the performance of our crossed beam machine, and we are currently working on reactive scattering experiments on $O(^1D) + H_2$ as a test case.

Stereodynamics and Active Control of Chemical Reactions by Using Electrostatic Hexapole State-Selector and Polarized Laser Excitation

CHE, Dock-Chil[1]; HASHINOKUCHI, Mitihiro[1,2];

SHIMIZU, Yuichiro[1]; FUKUYAMA, Tetsuya[1,3]; KASAI, Toshio[1,2]
([1]IMS; [2]Osaka Univ.; [3]Himeji Inst. Tech.)

Since mutual orientation between colliding reactants plays a key role in chemical reaction, so-called "steric effect" becomes important for understanding stereo-dynamics of elementary reactions in the gas phase, and to control them actively. Although orientation dependences of "*atom (spherical)-molecule (vector)*" reactions have been studied, the steric effect of "*molecule (vector)-molecule (vector)*" reaction has not been studied so far using oriented molecules. Typical examples of the "*molecule-molecule*" reaction are the OH + NO radical reaction and the $(Si)_n$ + OH cluster reaction, which our special research project challenges. Our experimental strategy is to select molecular orientation by use of hexapole state-selector and/or linearly polarized laser. Thus, we have built a new crossed-beam apparatus with a 1-m long hexapole electric field and we have installed a new set of tunable YAG-dye laser system. There are three on-going objectives of our special project as presented in the following.

1) We investigate the photodissociation of the DCl dimer, which is preferentially size-selected by the hexapole electric field. We succeeded in detecting [ClDCl] transient species through the hydrogen elimination from $(DCl)_2$ by a Doppler-selected TOF technique. The structure of the observed TOF spectrum represents a vibrational state distribution of [Cl–D···Cl], reflecting strong perturbation from the adjacent Cl atom in [ClDCl].

2) We are investigating the reaction of oriented-OH with aligned-NO. The OH radicals are produced by a dc-discharge of H_2O seeded in Ar. We then state-select their orientation by the hexapole. NO is aligned by the linearly polarized UV laser. The hydrogen atom in the OH + NO $\rightarrow$ NO_2 + H reaction and NH product in the OH + NO $\rightarrow$ NH + O_2 reaction are detected by REMPI and LIF, respectively. Orientation dependence of the branching ratio of the two reaction channels should provide an insight into details of stereodynamics.

3) We investigate the cluster reaction of OH with Si_n. Metal cluster source using laser vaporization is newly constructed. We temporarily obtain the result that Si monomer and dimer concentrations in the cluster beam can be control by changing the timing of the vaporization laser. Experiment is now being carried out to clarify steric effects on reactivity in van der Waals interaction within the cluster.

Monte Carlo Simulation of Chemical Gel

TAKASU, Masako; NOSAKA, Makoto; KATOH, Kouichi[1]
([1]Kanazawa Univ.)

Gel is an important material used in engineering and medicine. We studied the structure of chemical gel using Monte Carlo simulation with modeled radical reactions. Simulation is performed using beads-spring model in three-dimensional continuous space. For the criterion of gel, we apply the concept of percolation to

our clusters; we calculate the maximum size in all directions for each cluster, and sum up the number of percolated direction for all percolated clusters in a system. We call this the number of percolation. We obtained structure information of system from plotting the average number of percolation. We can determine whether the system has percolated clusters, and also whether the polymer network has inhomogeneous structure.

The distributions of degree of polymerization for clusters obtained in this simulation show qualitatively good agreement with the experimental results. Linkers are classified to two types according to the roles in networks, and their ratios are discussed. The normal and weighted ratios of gel are defined using percolation theory. These ratios are compared with the changes in distribution.

Electronic Structure and Decay Mechanism of Inner-Shell Excited Molecules

KOSUGI, Nobuhiro; HATSUI, Takaki

This project is being carried out at the Beamline 4B of the UVSOR facility and at the Beamline I-511 of the MAX-II facility in collaboration with the Uppsala University. We are investigating linear polarization dependence of inner-shell resonant excitations for simple molecules. We are also investigating resonantly-emitted photoelectron and photon (fluorescence) spectroscopies for the same systems by tuning the photon energy to inner-shell resonances. In the UVSOR facility we are using crystal monochromators, which restrict the photon energy to the range higher than the Cu and Ni 2p edge (> 800 eV). Recently, we have decided to move our experimental apparatus to the BL 4B, which is a new beamline covering the lower photon energy (< 800 eV). In these studies theoretical investigation is essential and some theoretical approaches are also under development.

Time-Resolved Spectroscopic Study of Photochemical Dynamics in Condensed Phase

TAHARA, Tahei; TAKEUCHI, Satoshi; FUJINO, Tatsuya; ARZHANTSEV, Sergei; MANDAL, Debabrata; MIZUNO, Misao; FUJIYOSHI, Satoru

Time-resolved spectroscopy is one of the most powerful tools for the studies of chemical reactions. It enables us to directly observe the temporal changes occurring in the course of chemical reactions. Thanks to drastic advance of the laser technology, we are now able to study ultrafast dynamics of the primary chemical processes with pico/femtosecond time-resolution. The aims of this project are (1) development of new techniques and methods in time-resolved spectroscopy, and (2) application of pico/femtosecond spectroscopy to the study of the dynamics of the condensed-phase molecules. Our research activities of this year are summarized as follows, in the order of time-resolution of the experiments. First, by utilizing 'extremely-short' optical pulses ($\Delta t \sim$ ten–a few tens of femtoseconds), we carried out time-resolved measurements to observe

vibrational coherence (wavepacket motion) in the excited-state molecules. We observed the wavepacket motion of a photodissociating excited-state molecule in pump-probe measurements, and measured impulsive stimulated Raman scattering of an excited-state polyatomic molecule for the first time. Secondly, with use of time-resolved fluorescence and absorption spectroscopy having a few hundreds femtoseconds time-resolution, we studied excited-state proton transfer of hydroxy anthraquinone derivatives, isomerization of trans-azobenzene, and photodissociation of diphenyl-cyclopropenone. Thirdly, we applied picosecond time-resolved Raman spectroscopy to the study of solvated electrons and found a novel resonance Raman effect of the solvating molecules. We also demonstrated high potential of the up-conversion technique for temporal fluorescence rejection in Raman spectroscopy.

Theoretical Study of Vibrational States for AlNC/AlCN

MINAMINO, Satoshi; NANBU, Shinkoh; AOYAGI, Mutsumi

The character of the low-lying electronic states of AlNC strongly depends on the bond distance of Al-NC, because the covalent states are lying closely to the ionic states. Especially, due to the electronic ground state having the ionic character, the bending vibrational motion has a quite strong anharmonicity, and the motion is characterized as a large amplitude motion (LAM). Therefore, in general, the observed spectrum has the complicated vibronic structures and it is difficult to understand the molecular conformation having the LAM. In this study, we determined the global potential energy surfaces of the electronic ground state for the isomerization of AlNC/AlCN, and we elucidated the vibrational structures of the complicated vibronic states by solving the exact Schrödinger equation for the nuclear motion. Calculated results are in good agreement with the dispersed fluorescence spectra observed by Fukushima.

Reference
1) M. Fukushima, *Chem. Phys. Lett.* **283**, 337 (1998).

Ultrafast Protein Dynamics Probed by Time-Resolved Resonance Raman Spectroscopy

KITAGAWA, Teizo

Ultrafast protein dynamics were examined with myoglobin (Mb) using picosecond time-resolved resonance Raman spectroscopy with a stress on structural and vibrational energy relaxation. Studies on the structural relaxation of Mb following CO photolysis revealed that the structural change of heme itself (core expansion), caused by CO photodissociation, is completed within the instrumental response time of the time-resolved resonance Raman apparatus used (~2 ps). In contrast, changes in the intensity and frequency of the iron–histidine (Fe–His) stretching mode upon dissociation of the trans ligand were found to occur in the picosecond regime. The Fe–His stretching band is absent for the CO-bound form, and its appearance upon photodissociation was not instantaneous, in contrast with that observed in the vibrational modes of heme, suggesting appreciable time evolution of the Fe displacement from the heme plane. The intensity reflected the out-of-plane displacement of iron, and 80% of the movement occurred in 2 ps but the remaining 20% occurred in 40 ps. The band position of the Fe–His stretching mode changed with a time constant of about 100 ps, indicating that tertiary structural changes of the protein occurred in a 100-ps range. This rate was dependent on viscosity of solvent ($k = \eta^{-0.3}$), indicating that the small change at the Fe–His bond is communicated to the protein surface through a conformation change, and conversely the change of Fe–His bond is controlled by the surface of the protein. Temporal changes of the aniti-Stokes Raman intensity of the ν_4 and ν_7 bands demonstrated immediate generation of vibrationally excited heme upon the photodissociation and successive decay of excited populations, whose time constants were 1.1 ± 0.6 and 1.9 ± 0.6 ps, respectively. This technique has been applied to identify an axial residue of a sensor protein, CooA, for which geminate recombination of photodissociated CO is very fast ($\tau = 70$ ps) and therefore the Fe–His (His77) stretching Raman band could be detected only transiently with this technique.

(b) Molecular Photophysics and Science

Development of a Near-Field Ultrafast Spectroscopy System

IMURA, Kohei; OKAMOTO, Hiromi

We are constructing an apparatus for space- and time-resolved spectroscopic measurements, by combining near field optical microscopy and ultrafast time-resolved technique. With this apparatus, we aim at nanometer spatial resolution and femtosecond temporal resolution at the same time. Various photophysical phenomena probed under such extremely high space and time resolution can be of considerable significance not only in physics and chemistry but also in biology, and thus will open a new research activity. We plan to make use of this experimental methodology to investigate basic problems on chemical processes of mesoscopic structures. This technique also has a potential to shed a new light on nano-scale material science.

Experimental arrangement is schematically depicted in Figure 1. A spatial resolution of better than 100 nm is achieved by a nanometer-sized aperture of an optical fiber tip (SNOM tip). In so-called 'illumination and collection' mode, a sample is excited by the near-field radiation on the fiber tip introduced through the optical fiber, and emitted light is collected through the same fiber tip. The collected emission is dispersed in a monochromator and detected by a CCD detector. Ultrafast measurements are possible by a pump-probe optical correlation method with 100 fs pulses from a mode-locked Ti:sapphire laser.
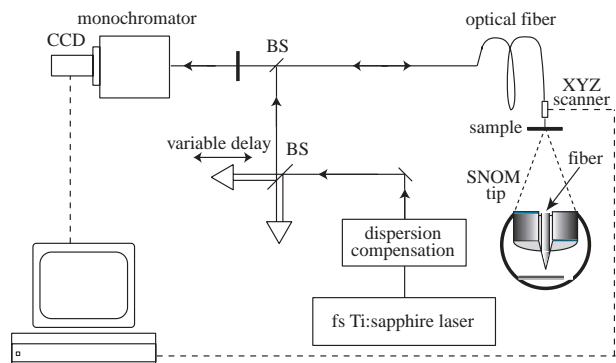
Figure 1. Schematic view of the experimental setup.

(1) Laser Cooling and Trapping of Metastable Helium Atoms
(2) Laser Spectroscopic Studies of Atoms and Ions in Liquid Helium

MORITA, Norio; MORIWAKI, Yoshiki[1]
(*[1]Toyama Univ.*)

In studies on "laser cooling and trapping of metastable helium atoms," we have been constructing a new laser trapping apparatus for realizing the Bose-Einstein condensation of metastable He atoms. We have also been making additional LNA ($La_{1-x}Nd_xMgAl_{11}$-

O_{19}) lasers necessary for the new apparatus. On the other hand, in "laser spectroscopic studies of atoms and ions in liquid helium," we have experimentally observed some interesting differences between spectra of Ca atoms in liquid ^4He and ^3He, and the cause of these differences has successfully been clarified through our theoretical calculation (see II-C-1). In addition, motivated by experimental results so far obtained in this project, we have also measured fine structure changing cross sections of Ba^+ ions in collisions with He atoms (see II-D-1) and of Ca^+, Sr^+ and Ba^+ ions in collisions with H_2 and D_2 molecules (see II-D-2).

Structure, Relaxation and Control of Reactive Cluster Studied by Two-Color Laser Spectroscopy

FUJII, Masaaki

A molecular cluster is a microscopic system of solution and/or crystal, and is thought to provide detailed information on relaxation and reaction dynamics in condensed phase. However the molecular clusters which have been studied are mainly static system which has no reaction pathway after photo-excitation, and consequently spectroscopic information which concerns the reaction mechanism has not been obtained sufficiently. In this research project started from 2000, we will apply various laser spectroscopy to the reactive clusters to reveal detailed mechanism of intracluster reaction.

For the ground state, the structure of the cluster can be determined by the combination of the IR dip spectroscopy and ab initio MO calculations.[1] The IR dip spectroscopy is a kind of IR-UV double resonance spectroscopy which provides the spectrum which corresponds to the infrared absorption spectrum of the cluster (see Figure 1). Briefly, a tunable IR laser is introduced to the clusters and is scanned its frequency over the fundamental vibrational region (typically $2400\sim4000$ cm^{-1}). Then a tunable UV laser, of which the frequency is fixed to the S_1 origin of a specific cluster, is introduced and resonant enhanced multi-photon ionization signal via S_1 is monitored. When the IR laser is resonant to a vibrational level of the cluster, the ion signal decreases much because of loss of the population in the vibrational ground state. Thus, the IR absorption spectrum of the cluster can be measured by this depletion spectroscopy. The same spectrum can be obtained when the fluorescence intensity from S_1 is monitored instead of the ion current.

The IR spectrum in the excited state S_1 can also be measured by the depletion spectroscopy, when the UV laser is introduced before the IR laser shot (the UV-IR fluorescence dip spectroscopy; see Figure 2). The molecule is excited to S_1 by the UV laser, and the fluorescence intensity is monitored as well as the IR dip spectroscopy for S_0. Then the S_1 molecules are further excited to the vibrationally excited level in S_1 by the IR laser. In general, the fluorescence quantum yield decreases in the higher vibronic level. Thus, the total

fluorescence intensity decreases when the IR laser frequency resonant to the vibrational level in S_1.

Similarly, the IR spectrum of the ionic cluster can be measured by the depletion spectroscopy (mass-selected ion dip spectroscopy; see Figure 3). The ionic cluster can be prepared by the multiphoton ionization via S_1, and the ion current due to the cation cluster of the specific size can be measured through a mass-filter. When the ionic cluster is vibrationally excited by the IR laser, the cluster is dissociated by the vibrational predissociation. Therefore, the IR transition can be measured by the decrease of the parent cluster. The same spectrum can be obtained by monitoring the enhancement of fragments (mass-selected multiphoton dissociation spectroscopy). In addition to these "dip" spectroscopies, the PFI-ZEKE photoelectron spectroscopy[2] and the nonresonant ionization detected IR spectroscopy[3] are also important method to obtain the spectral information in the cation and the overtone states. Based on these spectroscopic techniques, we have measured the IR spectra of solvated clusters,[4] such as phenol/ammonia,[5] naphthol/alcohol,[6] carbazole/water[7] and 7-azaindole dimmers,[8] and have discussed the relation between the structure and intracluster reactions.

From 2001, we have been developing the new time-resolved IR spectroscopy for the reactive clusters. The pico-second time-resolved vibrational spectroscopy is one of the ideal way to reveal the reaction mechanism directly. Here, we will demonstrate its usefulness by applying the hydrogen transfer reaction in photoexcited $PhOH–(NH_3)_n$ cluster.[9] Figure 4 shows the principle of the picosecond time-resolved UV-IR-UV ion dip spectroscopy. The reactive cluster ($PhOH–(NH_3)_n$ in present case) is excited to S_1 by a picosecond UV laser ν_{UV} and the photochemical reaction (hydrogen transfer) is triggered. The final reaction product, *i.e.* $(NH_3)_{n-1}$-NH_4, is ionized by a nanosecond UV laser ν_{ION} which is irradiated after 100 ns from ν_{UV} and the population of the reaction product is monitored as a mass peak of $(NH_3)_{n-1}NH_4^+$. A picosecond tunable IR laser ν_{IR} is irradiated after t ps from ν_{UV} and is scanned over vibrational region. If ν_{IR} is resonant to vibrational levels of the transient species, the population of the final reaction product decreases due to the vibrational predissociation of the transient species. Therefore, the vibrational transitions of the transient species at t ps can be observed as decrease of ion current of $(NH_3)_{n-1}$-NH_4^+.

Figure 5 shows a diagram of the experimental apparatus rebuilt in the Laser Research Center of the Institute for Molecular Science. The femtosecond mode lock Ti:sapphire laser was regeneratively amplified at 10 Hz and was stretched to 3 ps (TSA 10/GCR-130: Spectra Physics). The typical power of the regeneratively amplified picosecond pulse was 5.6 mJ at 800 nm. Twenty percent of this pulse was frequency-doubled and was used to pump an optical parametric generator (OPG; TOPAS-400: Light Conversion). The signal light of this OPG was frequency-doubled and was used as the excitation laser ν_{UV}. Second OPG (TOPAS-800: Light Conversion) was pumped by 40% of the fundamental pulse. The frequency-doubled idler light of the second OPG and the remainder fundamental pulse were differentially mixed in a KTA crystal and were converted to the 3 μm IR laser ν_{IR}. The power of ν_{IR} was < 100 mJ. The pulse width of ν_{UV} and ν_{IR} was 3~4 ps. Third harmonic of nanosecond Nd^{3+}:YAG laser (INDI-40: Spectra Physics) was employed as the ionization laser ν_{ION}. Two YAG lasers (INDI-40 and GCR-130 which pumps the regenerative amplifier) were synchronized electrically within 1 ns-accuracy. Two UV lasers ν_{UV} and ν_{ION} were combined coaxially by a beam combiner and focused by a 250 mm focal lens. The IR pulse ν_{IR} was introduced into a vacuum chamber from the opposite side of the two UV lasers and was focused by a CaF_2 250 mm focal lens. The configuration that ν_{UV} and ν_{IR} are counter-propagated is convenient for the optical alignment, but this configuration lowers the time resolution than the pulse duration. The effective time resolution was ~20 ps.

The phenol vapor at room temperature was seeded in NH_3/Ne (0.5%) premix gas (2 atm) and the mixture was expanded into a vacuum chamber (typically 1×10^{-5} Torr) through a pulse valve (General Valve Series 9). The nozzle diameter was 400 mm. The laser beams were focused at 15 mm below the nozzle. The produced cations were pushed into a detector chamber by a repeller at an appropriate voltage (typically 15 V·cm^{-1}), and were detected by a channel multiplier (Murata Ceratron) through a quadrupole mass filter (EXTREL). All laser systems were operated at 10 Hz, however, ν_{IR} was irradiated at 5 Hz through a chopper. Thus we could obtain a $\nu_{UV} + \nu_{IR} + \nu_{ION}$ signal and a $\nu_{UV} + \nu_{ION}$ signal alternatively. These two signals were separately integrated and stored in a digital boxcar system (4420/4422: EG&G PARC) after amplification by a pre-amplifier (5113: EG&G) . The integrated signal was recorded by a personal computer as a function of the IR laser frequency. The fluctuation of the condition of the pulse valve was suppressed by calculating the ratio between the two signals.

Time resolved UV-IR-UV ion dip spectra of phenol–$(NH_3)_3$ are shown in Figure 6. The numbers in the left hand sides of each spectrum indicate the delay time from ν_{UV} to ν_{IR}. Here the spectrum at –20 ns corresponds to the IR spectrum of $PhOH–(NH_3)_3$ in S_0, in which the sharp bands around 3400 cm^{-1}, the broad bands at ~3200 cm^{-1} and the very broad background are assigned to the degenerated antisymmetric stretch vibration ν_3 in NH_3, the totally symmetric stretch vibration ν_1 in NH_3 and the OH stretch vibration ν_{OH} in phenol, respectively.[5] The spectrum at +180 ns shows the vibrational transitions of the final reaction product via S_1, *i.e.* $(NH_3)_2NH_4$, and 1) two intense bands at 3180 cm^{-1} and 3250 cm^{-1} and 2) a broad band at 2700~3100 cm^{-1} which have been assigned to vibrational transitions concerned with NH_4.[5]

Let us discuss the time-resolved IR spectra from 0 to 100 ps, in which the excited state hydrogen transfer dynamics would be shown. One can see that the vibrational bands rise with increasing delay time. The spectral feature at +100 ps is already similar to that of the final reaction product (+180 ns). This time scale is consistent with that expected from previous studies.[5] Here, the intense band at 3250 cm^{-1} rises slower than the band at 3180 cm^{-1}. The relative intensities of the two bands become comparable at 40 ps, thereafter, the

higher band at 3250 cm^{-1} clearly grows further. Thus, the rising time constant of the band at 3250 cm^{-1} is apparently different from that of the 3180 cm^{-1}-band. This remarkable difference between the two intense bands suggests that each vibrational transition is derived from different species. The existence of two transient species are naturally interpreted by considering the isomers of $(NH_3)_2NH_4$; the most stable NH_3–NH_4–NH_3 and the meta-stable NH_4–NH_3–NH_3. The co-existence of isomers is strongly supported by ab initio calculations.

In summary, it is demonstrated that the picosecond UV-IR-UV ion dip spectroscopy is a powerful tool to explore the dynamics of the intracluster reaction. We have successfully measured the picosecond time resolved IR spectra of the transient species for the ESHT of PhOH–$(NH_3)_3$ for the first time.

References

1) R. Yoshino *et al.*, *J. Phys. Chem. A* **102**, 6227 (1998).

2) T. Omi *et al.*, *Chem. Phys. Lett.* **252**, 287 (1996); S. Ishiuchi *et al.*, *Chem. Phys. Lett.* **283**, 243 (1998).

3) K. Takazawa *et al.*, *Chem. Phys. Lett.* **189**, 592 (1992); K. Müller-Dethlefs *et al.*, *Z. Naturforsch., A: Phys. Sci.* **39**, 1089 (1984); *Chem. Phys. Lett.* **112**, 291 (1984); K. Müller-Dethlefs and M. C. R. Cockett, "*Zero Kinetic Energy (ZEKE) Photoelectron Spectroscopy*," Chapter 7, "*Nonlinear Spectroscopy for Molecular Structure Determination*," R. W. Field *et al.*, Eds., Blackwell Science; Oxford (1998) and references therein.; E. W. Schlag, "*ZEKE Spectroscopy*," Cambridge University Press; Cambridge (1998) and references therein.

4) K. Suzuki, Y. Emura, S. Ishiuchi and M. Fujii, *J. Electron Spectrosc.* **108**, 13 (2000); K. Suzuki, S. Ishiuchi and M. Fujii, *Faraday Discuss.* **115**, 229 (2000); K. Sakota, N. Yamamoto, K. Ohashi, H. Sekiya, M. Saeki, S. Ishiuchi, M. Sakai and M. Fujii, *Chem. Phys. Lett.* **341**, 70 (2001).

5) S. Ishiuchi, M. Saeki, M. Sakai and M. Fujii, *Chem. Phys. Lett.* **322**, 27 (2000).

6) M. Saeki, S. Ishiuchi, M. Sakai and M. Fujii, *J. Phys. Chem. A* in press.

7) M. Sakai, K. Daigoku, S. Ishiuchi, M. Saeki, K. Hashimoto and M. Fujii, *J. Phys. Chem. A* in press.

8) H. Yokoyama, H. Watanabe, T. Omi, S. Ishiuchi and M. Fujii, *J. Phys. Chem. A* in press.

9) S. Ishiuchi, M. Sakai, K. Daigoku, T. Ueda, T. Yamanaka, K. Hashimoto and M. Fujii, *Chem. Phys. Lett.* in press.
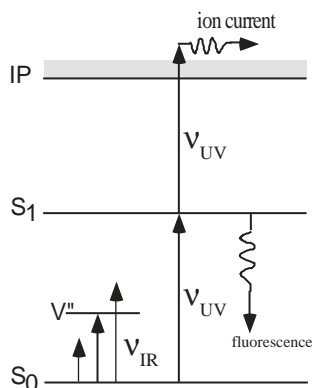
Figure 1. Principle of the IR Dip Spectroscopy. The IR transition in the ground state cluster can be measured.
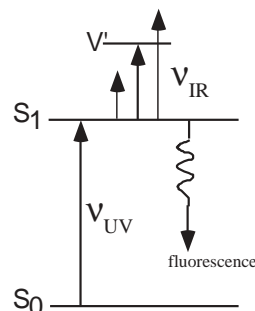
Figure 2. Principle of the UV-IR Fluorescence Dip Spectroscopy. The IR transition of the cluster in the S1 state can be obtained.
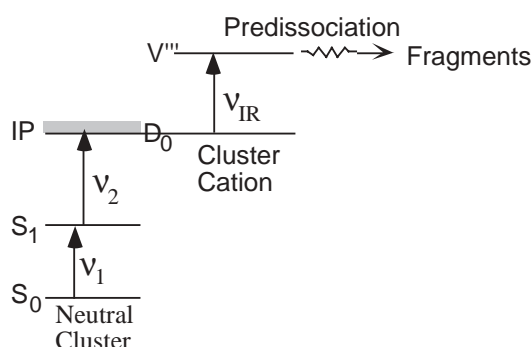
Figure 3. Principle of the mass-selected IR Ion Dip Spectroscopy. The IR transition of the cluster cation can be measured by the depletion of the parent cluster cation. The same spectrum can be measure by monitoring the enhancement of the fragments produced by the IR predissociation.
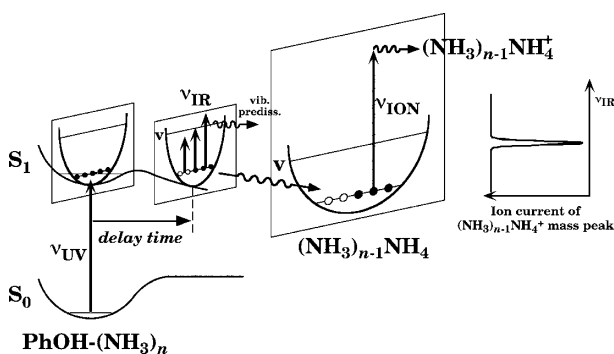
Figure 4. Principle of picosecond time-roselved UV-IR-UV ion dip spectroscopy. Potential curves of S_0 and S_1 are schematically drawn along O-H stretch coordinate. Potential curves in different sections on the S_1 O–H stretch coordinate are drawn along arbitrary N–H stretch coordinates.
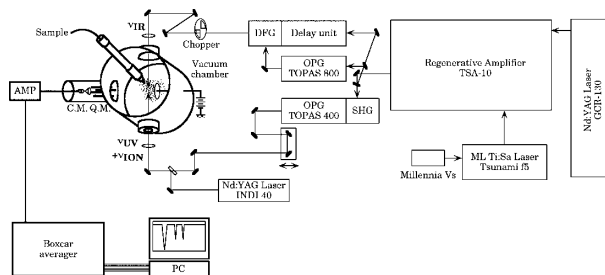
Figure 5. Schematic diagram of the experimental apparatus.
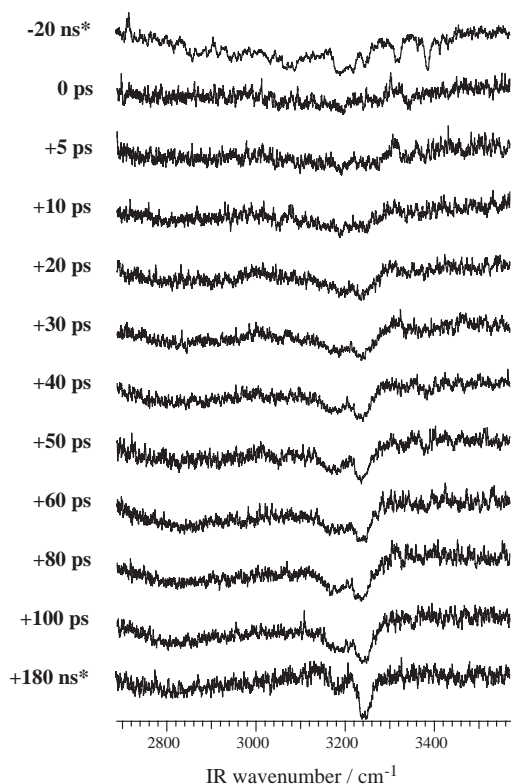
Figure 6. Picosecond time-resolved UV-IR-UV ion dip spectra of the transient species from the electronically excited PhOH–$(NH_3)_3$ which was observed by fixing ν_{UV} to the low vibronic band in the S_1 state of PhOH–$(NH_3)_3$ (281.49 nm) and monitoring $(NH_3)_2NH_4^+$ due to ν_{ION} (355 nm). Times indicated at the left side of each spectrum mean the delay times between ν_{UV} and ν_{IR}. The spectra whose delay times are -20 ns and $+180$ ns (indicated by *) are obtained by nanosecond laser system, which have been reported in the previous paper.[5)]

SR-Pump and Laser-Probe Experiments for the Photofragmentation Dynamics of Molecules

MITSUKE, Koichiro

Synchrotron radiation-laser combination techniques developed at UVSOR in Okazaki were employed for probing ionic and neutral photofragments produced in the vacuum ultraviolet. First, CN neutral fragments were dissociated from CH_3CN by excitation with synchrotron radiation in the photon energy E_{SR} range of 13.6 to 18.6 eV [*J. Electron Spectrosc. Relat. Phenom.* **119**, 155 (2001)]. Observed CN radicals were in the vibronically ground state. The laser induced fluorescence (LIF) signal was measured as a function of E_{SR} with the laser wavelength fixed at the CN ($B\ ^2\Sigma^+$, $\nu_B = 0$ $\leftarrow X\ ^2\Sigma^+$, $\nu_X = 0$) transition. The laser and monitored wavelengths were chosen at 388 and 420.8 nm, respectively. We constructed a novel optics containing spheroidal and spherical mirrors and an optical fiber in order to improve the collection efficiency of the fluorescence. The onset of 15.4 eV of the fluorescence signal indicates that the detected CN ($X\ ^2\Sigma^+$) radicals result from dissociative ionization of CH_3CN

$$CH_3CN^+ \rightarrow CN\ (X\ ^2\Sigma^+) + CH_3^+\ (X\ ^1A_1'). \tag{1}$$

The partial cross section for the formation of CN ($X\ ^2\Sigma^+$) is estimated to be 0.1–0.5 Mb and is in a reasonable agreement with that for the CH_3^+ formation previously reported.

Second, N_2^+ ($X\ ^2\Sigma_g^+$, $\nu_X = 0$ and 1) ions resulting from direct ionization or autoionization of N_2 were detected by the LIF excitation spectroscopy using the $B\ ^2\Sigma_u^+ \leftarrow X\ ^2\Sigma_g^+$ transition. The LIF signal counts were measured in the E_{SR} range of 15.6 to 16.6 eV where numerous Rydberg states converging to N_2^+ ($A\ ^2\Pi_u$) exist. The fluorescence yield curves for the $\nu_X = 0$ and 1 vibrational levels were comparable with the relative partial photoionization cross sections for the respective levels. Several Rydberg states are found to exhibit stronger peak intensities in the $\nu_X = 1$ curve, suggesting enhancement in the branching ratio of the $\nu_X = 1$ level. We performed Franck-Condon calculations to evaluate the relative partial cross sections by using an approximate expression:

$$\sigma(\nu_X) \propto n^{*-3}\ |\langle \nu_g | \nu_R \rangle|^2\ |\langle \nu_R | \nu_X \rangle|^2 \Big/ \sum_{\nu_X'} |\langle \nu_R | \nu_X' \rangle|^2 \tag{2}$$

Here, we assumed that the neutral ground state N_2 ($X\ ^1\Sigma_g^+$, $\nu_g = 0$) is primarily photoexcited to the Rydberg state having a vibrational level ν_R and an effective principal quantum number n^* and subsequently autoionized into N_2^+ ($X\ ^2\Sigma_g^+$, ν_X).

Decay and Dissociation Dynamics of Core Excited Molecules

SHIGEMASA, Eiji; GEJO, Tatsuo

The new grazing incidence monochromator (Varied-line-spacing Plane Grating Monochromator; VLS-PGM) on BL4B at UVSOR has been successfully installed by the end of December 2000. The first photons through this monochromator were observed on the 16th of January in 2001, and from that day on, the performance tests for the monochromator have been initiated. As a consequence, it turned out that the maximum resolving power achieved, is more than 3000 at the entire photon energy region of interest, and the throughput photon flux measured by a calibrated silicon photodiode ranges from 10^8 to 10^9 photons/sec/100mA when the resolving power in the regular spectral region is set to be more than 3000. The performance of the present VLS-PGM is high enough to perform various spectroscopic investigations on molecular core-levels with high-resolution. The dynamics of molecular inner-shell excitation and relaxation processes is complex even for simple molecules, and thus advantageous to use various experimental techniques together with such a high performance monochromator in the soft x-ray region.

Two types of electron-ion coincidence experiments are in planning and the construction of the related spectrometers has been started; a high luminosity double toroidal analyzer (DTA) and a threshold electron analyzer. DTA equipped with a two-dimensional detector makes it possible to measure the angular distribution and kinetic energy of electrons/ions simultaneously. The combination of the present DTA with a time-of-flight mass spectrometer can be a

powerful tool to study the state-to-state photo-dissociation dynamics following the molecular core-level excitation and ionization. Threshold electron spectroscopy has proved to be very powerful in the investigation of electron correlation phenomena not only in atoms but also in molecules. In the angle-resolved photoion spectroscopy applied to the inner-shell excitations of linear molecules, the parallel and perpendicular transitions are distinguishable. Thus, it is expected that the combination between a threshold electron spectrometer and an angle-resolved photoion spectrometer can provide a rare opportunity to obtain threshold electron spectra including the symmetry information on the excited states, which can be called as symmetry-resolved threshold electron spectra. We are hoping that the basic tunings of the apparatuses will be finished before the end of November 2001.

A new project towards utilizing the free electron laser (FEL) developed at UVSOR has been initiated in 2000. Two-photon double-resonant excitation of the autoionization Xe* $5p^54f$ resonance via the Xe* $5p^55d$ intermediate state has been chosen to demonstrate the practical usability of FEL, since the resulting spectrum has already been measured at LURE in France using the combination of a conventional mode-locked laser and synchrotron radiation (SR). Finally, the similar spectrum has been successfully derived. It is found that the spectrum obtained is characterized by a typical asymmetric Fano-type line profile. We are now planning on performing further detailed investigations on atomic photoionization processes utilizing the combination between FEL and SR.

(c) Novel Material Science

Theory for Electronic Properties of Molecular Conductors and Insulators: Dimensional Crossovers Induced by Correlation

YONEMITSU, Kenji; KISHINE, Jun-ichiro; MORI, Michiyasu[1]; KUWABARA, Makoto[2]; MIYASHITA, Naoyuki[3]
(*[1]Tohok Univ.; [2]Kobe Univ.; [3]GUAS*)

In low-dimensional molecular materials, electron correlations are essential for the understanding of novel electronic phases. i) Variation of physical properties in quasi-one-dimensional organic conductors, $(TMTTF)_2X$ and $(TMTSF)_2X$, under physical or chemical pressure can be viewed as a dimensional crossover. With increasing inter-molecular overlaps between the neighboring chains and/or reducing electron correlation, the electronic dimensionality in the normal phase above the phase transition temperatures continuously changes from one to three. The optical conductivity spectra are also known to show a similar crossover with lowering energy scale. Anisotropic excitation spectra are studied by using the finite-temperature DMRG technique for a spinless-fermion model on a two-leg ladder. *Intra*-chain electron correlation is found to sensitively affect the *inter*-chain excitation spectrum, while the *inter*-chain inter-molecular overlap to sensitively affect the *intra*-chain spectrum. These results are opposite to the intuition, but nicely explained by the collective motion and/or confinement of fermions in the chains. ii) Quasi-one-dimensional π-d hybrid electron systems, $(DCNQI)_2M$, are known to show a metal-insulator transition originating from the collaboration of the Peierls and Mott mechanisms. Strong commensurability effects on the insulator phase with lattice modulation of period three are studied by using the exact diagonalization and DMRG techniques. With strong electron correlation among the d electrons, self-consistent lattice modulation strongly block the charge transfer between the π and d orbitals in order to keep the commensurability condition even the π-d level difference is widely varied. A transition to the incommensurate phase requires a large deviation of the π-d level difference from the optimal case. iii) Among quasi-two-dimensional organic conductors, the θ-phase compounds are known to show metal-insulator transitions accompanied with charge ordering. Although long-range Coulomb repulsion is believed to be essential to the paramagnetic charge-ordered phase, the optical conductivity spectra do not show an excitonic band expected from our random-phase-approximation calculations. Then additional interaction terms might be important for the charge-ordering transitions. In fact, $(BEDT\text{-}TTF)_2Rb\text{-}Zn(SCN)_4$ shows a discontinuous transition accompanied with lattice modulation at a rather high temperature. The transition temperatures are lower when lattice modulation does not take place in similar compounds. Exact diagonalization calculations and the second-order perturbation theory from the strong-coupling limit show indeed that weak electron-lattice coupling enhances the effect of long-range Coulomb repulsion on the charge

order coexisting with paramagnetism.

Pulsed Methods of Electron Spin Resonance Spectyroscopy

KATO, Tatsuhisa; FURUKAWA, Ko

Electron spin resonance (ESR) spectroscopy has been a powerful technique for the characterization of radical species. The modern development of ESR spectroscopy enables us to investigate the transient phenomena in detail. The pulsed ESR spectroscopy gives us the prototyped demonstration of the time-dependent spectroscopy. Some time-dependent measurements were experimentally performed and compared with the theoretical model calculation. The advanced ESR method was applied to the study on the high spin state of $Gd@C_{82}$ described in section II-H-1, of an inclusion complex of a cyclic dimmer of metalloporphyrin with $La@C_{82}$ in section II-H-2, and of dications of aromatic amines in section II-I-2, and to the study on the reaction mechanism in the heterogeneous system on CaO surface in section II-I-1.

Synthesis of Palladium Clusters Stabilized by Molecular Capsules and their Catalytic Properties

SAKURAI, Hidehiro[1]; HIRAO, Toshikazu[1]; NEGISHI, Yuichi; TSUKUDA, Tatsuya
(*[1]Osaka Univ.*)

Recently, colloidal dispersions of transition metal clusters with nanometer scale have gained much attention as a new class of catalysts. They show superior catalytic properties for some organic reactions compared with the monometallic complexes due to their unique electronic and geometric structures. The important task for understanding their size–specific properties and wide range of applications is to exploit a preparative method of the clusters having a well-defined size and morphology. We have addressed these issues by utilizing various host molecules, such as cyclodextrines (CD) and calixarene compounds, as stabilizing reagents of the metal clusters. Chemical reduction of palladium ions in the presence of these molecular capsules results in the formation of stable colloidal solutions as shown in Figure 1. The size distributions of the Pd clusters fall in the range of 2–6 nm in all the cases. By considering the fact that these clusters are too large to be accommodated into an internal cavity of a single molecule, a number of molecules are involved in the stabilization of a single cluster. Namely, the Pd cluster is encapsulated as a guest into the hydrophobic space made by several CDs or calixarenes.

Their catalytic activities toward Suzuki-Miyaura coupling reactions are also studied, motivated by the fact that palladium (0) complexes, such as $Pd(PPh_3)_4$, act as good catalysts for the cross-coupling reactions between organic halides and organometallic compounds. We found the Pd clusters promotes the

coupling reactions of *m*-iodophenol and phenylboronic acid at room temperature leading to the formation of hydroxybiphenyls with excellent yields. Studies concerning the detailed mechanisms of the reactions are now underway.
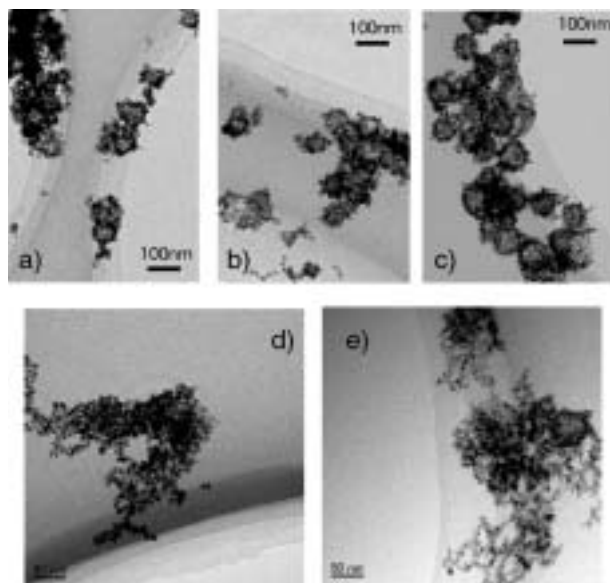

Figure 1. TEM images of Pd clusters stabilized by a) α–CD, b) β–CD, c) γ–CD, d) calix [6] arene *p*–sulfonic acid, and e) calix [8] arene *p*–sulfonic acid.

Spectroscopic and Physico-Chemical Studies of Organic Conductors

YAKUSHI, Kyuya; YAMAMOTO, Kaoru; URUICHI, Mikio; NAKANO, Chikako; DING, Yuqin; DROZDOVA, Olga; MAKSIMUK, Mikhail; SIMONYAN, Mkhitar

Photo-excitation spectrum within visible and infrared region contains much information on the local and extended electronic structure in the organic charge transfer (CT) salts. Our main research implements are the microscopic reflection and Raman spectroscopies, which enable us to perform polarized measurements on small single crystals of CT salts. Among the various information that can be extracted from these spectroscopies, we have particular interest on the molecular vibrations and possible collective excitations to investigate charge localization and superconducting phenomena.

Vibrational signals in the spectra allow us to investigate the local charge density on each molecule through the frequency shift and spectral selection rule. Based on the properties, we are now investigating the charge ordering (CO) or charge disproportionation phenomena in one-dimensional systems, $(DI-DCNQI)_2$-Ag and $(EDO-TTF)_2PF_6$, and two-dimensional systems, θ-$(BEDT-TTF)_2RbZn(SCN)_4$, θ-$(BDT-TTP)_2Cu(NCS)_2$, and $(BEDT-TTF)_2CuBr_4$ via the two spectroscopies.

On the other hand, electric transport properties are governed by the band structure and collective low-energy excitations. Particularly, it is widely recognized that the latter one is essential to be studied to understand characteristic phenomena realized in highly correlated systems. These excitations appear in the far-infrared spectrum of which observation requires exceptionally large single crystals, and thus the infrared study has remained an uncultivated field in the CT salt research. We are trying to observe good quality far-infrared spectra of organic superconductor κ-$(ET-d_8)_2Cu(CN)$-$[N(CN)_2]$. We have revealed so far that almost no Drude peak can be found in the optical conductivity down to far-infrared region and most of the spectral weight is contained in the broad mid-infrared peak in spite of the tight-binding band calculation predicting the presence of free electron excitations.

We have studied the electronic structures of certain phthalocyanine metal complexes, in which unpaired d-electrons localizing on phthalocyanine molecules coexist in the itinerant conjugated π-electron system. Such a d-π double band structure is a reminiscent of the f-electron system, in which a narrow f-band coexists with a wide s-band and they are hybridized near the Fermi level. To make sure the presence of d-π interaction, we prepared mixed crystal of NiPc and CoPc, and then investigated the ESR, magnetic susceptibility, reflectance and Raman spectra.

Broad-Line Solid State NMR Investigation of Electronic States in Molecular-Based Conductors

NAKAMURA, Toshikazu; FUJIYAMA, Shigeki

Broad-line solid state NMR is a powerful method that gives us crucial information about the fundamental electronic properties and about the detailed electronic structures of molecular based compounds. Investigation of such electronic phases in molecular based conductors is important to understand the unsolved fundamental problems in the field of solid state physics. The aim of this project is to clarify the electronic states (charges and spins) of molecular based compounds by microscopic point of view.

Quasi-one-dimensional organic conductors, $(TMTTF)_2X$, have been extensively studied so far because of their various ground states such as spin-Peierls, AF, IC-SDW and superconductivity. The temperature dependences of resistivity of TMTTF salts have broad minima around 100 K. The insulating states at low temperatures have been believed as Mott-Hubbard insulators since strong dimerization of the donor molecules might reduce the system half-filled. However a recent report of ac-conductivity suggesting strong ferroelectric response for TMTTF series provokes a new question about validity of the simple Mott-Hubbard ground state. To investigate the low temperature electronic phases, we synthesized ^{13}C substituted TMTTF molecules; the two central carbon sites, of which hyperfine coupling constants are much larger than those of hydrogen sites, have been labeled with ^{13}C. We investigated the charge configurations and spin dynamics in the low temperature phases of $(TMTTF)_2X$.

The following topics are also now going on.
[1] Magnetic investigation of itinerant and local hybrid

spins system, (CHTM-TTP)$_2$TCNQ

[2] Low temperature Electronic Phases in (EDT-TTF)$_2$-X.

[3] Magnetic properties of organic spin-ladder systems, (BDTFP)$_2$X

[4] Magnetic structures of the antiferromagnetic states in Pd(dmit)$_2$ families

In this project, we are preparing a new NMR system to study more detailed electronic structure from microscopic points of view. We also try to carry out experiments with new devices under unconventional circumstance.

Development of New Organic Conductors and Their Physical Properties

KOBAYASHI, Hayao; FUJIWARA, Hideki; FUJIWARA, Emiko; TANAKA, Hisashi; TAMURA, Itaru; KOBAYASHI, Akiko[1]
(*[1]Univ. Tokyo*)

With the aim of development of solid state physics and chemistry of molecular materials, we have tried to develop new types of molecular metals and super-conductors and to improve the methods of X-ray structure analysis at high pressure. The main results obtained in the last year are as follows. (1) development of single-component molecular metal: Although a vast number of molecular metals have been developed, the mechanism of carrier generation in the organic metals ever developed is rather simple. That is, every system utilizes the charge transfer phenomena between the molecules forming conduction band and other chemical species to generate the carriers. We have recently reported the first single-component molecular metal. As one of the next targets, we are going to start to examine the possibility of the development of ferromagnetic molecular metal composed of single-component molecules (2) discovery of field-induced super-conducting state: In contrast to the isomorphous system without magnetic moments λ-(BETS)$_2$GaCl$_4$, λ-(BETS)$_2$FeCl$_4$ undergoes a unique π-d coupled anti-ferromagnetic insulating transition around 8 K, which was suppressed by applying magnetic field higher than 11 T. Firthermore, we have recently found field-induced superconductivity at $17\ \mathrm{T} < H < 41$. In addition, we have also found that the superconductivity of the first antiferromagnetic organic superconductor κ-(BETS)$_2$-FeBr$_4$ to be a "bi-functional molecular system" whose superconducting state can be switched on or switched off by controlling the magnetic state of anions. (3) high-pressure single crystal X-ray structure analysis on organic metal: We have recently made the accurate X-ray crystal structure analysis on α-ET$_2$I$_3$ by using diamond anvile high-pressure cell up to 2 GPa. There seems no special difficulty to elevate the applied pressure (up to 10 GPa).

Preparation and Characterization of Highly Ordered Molecular Films on Silicon Bound Through Si–C Covalent Bond

ARA, Masato[1]; GRAAF, Harald; TADA, Hirokazu
(*[1]GUAS*)

Self-assembled monolayers (SAMs), have received considerable attention because of their potential applications to molecular scale electronic devices. Covalently bond alkane SAMs formed by reaction between alkene and hydrogen terminated silicon are of increasing interest as nano-interface for molecular electronics devices fabricated on silicon micro-structures. We have studied (a) growth manner and electronic structure of Si-C junction using scanning probe microscope such as STM (scanning tunneling microscope), AFM (atomic force microscope) and KFM (Kelvin force microscope), (b) surface morphology of SAMs formed by the reaction between 1-dodecene, octadecene and methyl 10-undecenoate prepared on hydrogen terminated silicon (111) surfaces, and (c) degradation process of alkane monolayer film due to the a positive bias voltage at the substrate.

As a consequence, we have achieved atomically flat terraces on both p and n type Si(111) surfaces by means of chemical etching technique. The atomically flat surface was confirmed to be maintained after the growth of SAMs, indicating that the molecules formed highly oriented films. Detail investigation on the electronic structure at the interface using KFM and ultraviolet photoelectron spectroscopy is under progress. In addition, we succeeded in a preparation of a lithographically patterned alkane monolayer on silicon surface (Figure) by controlling the degradation of the film via the bias voltage applied on the AFM tip. The patterned area is available for different kinds of advanced techniques: 1) covering the oxide with other self-assembled monolayer by trichloro- or trimethoxy siliyl compounds; 2) removing of the silicon oxide by NH$_4$F-solution and using the established hydrogen terminated silicon for light or heat induced reaction with other alkenes or using the electrical conductive for metal plating; 3) etching of ditches by NH$_4$F/H$_2$O$_2$ solution and fill this ditches with metal by plating.

Design and Synthesis of Organic Ferrimagnets

HOSOKOSHI, Yuko; KATOH, Keiichi; INOUE, Katsuya

Molecule-based magnets have attracted current interests. After the discovery of an organic ferromagnet in 1991, construction of an organic ferrimagnet is one of today's challenging targets in material science. Alternant alignment of two kinds of spins with different spin-multiplicities yields spontaneous magnetizations. Ferrimagnetism is an effective strategy to give spontaneous magnetizations to molecular materials. The use of antiferromagnetic exchange couplings, is advantageous to obtaining magnet with higher T_C. We can control the antiferromagnetic interactions easier than ferromagnetic ones. Although a number of ferri-magnets are realized in inorganic-organic hybrid systems, a genuine organic ferrimagnet has not yet been realized. All the reported ferrimagnets include at least two magnetic components: bimetallic compounds or metal complexes with organic radicals. In order to achieve this challenging subject of an organic ferri-magnet from a different viewpoint, we propose a single-component strategy: utilizing a triradical including an *S*

= 1 and an $S = 1/2$ units within a molecule and connecting the $S = 1$ and $S = 1/2$ units by intra- and intermolecular antiferromagnetic interactions. We have succeeded in synthesizing the first example of a genuine organic ferrimagnetic material having well-defined chemical and crystal structure. This material undergoes the 3D phase transition at 0.28 K. The advantage of utilizing organic molecules is demonstrated aiming to a single component ferrimagnet. (see V-D).

Formation of Nano-Reaction Field and Integration of Bio-Functional Materials on Si

URISU, Tsuneo

Integration of biofunctional materials such as lipids and proteins are expected to find important applications in biosensors, developments of new medicines, and diagnosis of intractable diseases etc. Up to now, almost of all these kinds of works have been made on the surfaces of gold. In the present work, we are considering to integrate bio-functional materials on Si surfaces, for which various structures, even nano-structures can be made easily by using conventional semiconductor processes and good matching with high density electric circuits is expected. We are going to make highly controlled nanostructures on Si surfaces by using synchrotron radiation etching, and after that, by area selective deposition of several kinds of alkyl monolayers on the surface, functionalized surfaces such as hydrophobic, hydrophilic and amphiphilic surfaces are made. By these area selectively functionalized surfaces, we expect that biofunctional materials such as lipids and membrane proteins are arranged with position and orientation controlled. In this year, we have attained the construction of the synchrotron radiation beam line for the etching experiments, clean rooms for the preparation of biomaterials, and draft for the self assembled monolayer depositions on Si. We have succeeded the good quality of self assembled alkyl monolayers on Si and SiO_2.

Development of New Materials Based on Fullerene and Carbon Nanotube in Nanometer Scale

KUBOZONO, Yoshihiro; TAKABAYASHI, Yasuhiro; FUJIKI, Satoshi; KANBARA, Takayoshi

New materials based on fullerenes and carbon nanotubes with novel physical properties are studied in various scale from bulk to nanometer size. In 2000, the superconducting transition temperature, T_c, of 52 K was reported in a field effect transistor (FET) with C_{60} crystals. The T_c was the highest among fullerene super-conductors. Very recently, the T_c increases to 117 K in FET with C_{60}-tribromomethane crystals. The T_c is comparable to that of copper oxide-based ceramics. This clearly shows a possibility for C_{60}-based super-conducting device which can be used in high-speed computing and medical imaging. Fullerene and fullerene based materials showed various novel physical properties in bulk solid. Through 1990s, solid state chemistry and physics contributed to the development

of fullerene-based new materials in solid state. The appearance of C_{60}-based FET superconductor opened a way to develop new materials by combination of chemistry, physics and electronics. In the FET, the atomic level control of interface is very important to bring out its functionality. In the present project, we propose a development of new materials in various scale from bulk to nanometer size. Now, we prepare FET with C_{60} thin films which should have higher potential in application than crystal-based FET. Further, the superconductors with higher T_c are searched in FET with C_{60} encapsulating atoms (M@C_{60}) and carbon nanotube encapsulating fullerenes (peapod). Further, the studies on heterojunction diodes with metallofullerenes and peapod are now in progress. These studies are linked to development of device in nanometer scale. The STM/STS and AFM dual probe methods will be applied to study atomic level structures and interface structures in the devices.

Asymmetric Transition Metal Catalysis in Aqueous Media

UOZUMI, Yasuhiro; SHIBATOMI, Kazutaka; HOCKE, Heiko; YASOSHIMA, Kayo; NAKAO, Ryu; TANAKA, Hirotaka; NAKAZONO, Maki; YAMANOI, Yoshinori

Catalytic asymmetric reactions have attracted significant interest for their synthetic utility. One of the most exciting and challenging subjects in research on the catalytic asymmetric synthesis is development of the novel and basic chiral units. Homochiral organic molecules bearing hetero atoms (*e.g.* nitrogen, phosphorus, *etc.*) occupy a prominent position in organic chemistry as both useful synthetic reagents and molecules of biological interest. In this specail project, highly functionalized optically active pyrrolo[1,2-*c*]-imidazolone framework was identified as a novel basic chiral unit through a diversity-based approach.

A parallel library of optically active bicyclic tertiary amines bearing N-chiral bridgehead nitrogen atoms was readily prepared by condensation of primary amines, cyclic amino acids, and aldehydes. The enantio-controlling ability of each of the library members was examined for the asymmetric alkylation of benz-aldehyde with diethylzinc, and (3*R*,6*R*,7a*S*)-(2,3-diphenyl-6-hydroxy)hexahydro-1*H*-pyrrolo[1,2-*c*]-imidazol-1-one, which contains β-amino alcohol unit, showed high enantioselectivity. Enantioselective desymmetrization of meso compounds is a powerful synthetic means of preparing enantiomerically enriched products where plural stereogenic carbon centers are generated in one step. Enantioselective ring opening of meso cyclic anhydrides is one of the cases. Asymmetric methanolysis of meso cyclic carboxylic anhydrides including hexahydrophthalic anhydride proceeded in toluene in the presence of (6*R*,7a*S*)-(2-aryl-6-hydroxy)-hexahydro-1*H*-pyrrolo[1,2-*c*]imidazol-1-one to give the corresponding desymmetrized mono ester acids (*e.g.* (1*S*,2*R*)-2-(methoxycarbonyl)cyclohexane-1-carboxylic acid) with enantiomeric excesses of up to 89%.

On the other hand, catalytic organic transformations in water using recyclable immobilized catalysts is an

important goal in synthetic organic chemistry. We recently reported that several palladium-catalyzed reactions, including π-allylic substitution, carbonylation, the Heck reaction, and Suzuki-Miyaura cross-coupling, took place in water by use of palladium-phosphine complexes bound to an amphiphilic polystyrene-poly(ethylene glycol) graft copolymer (PS-PEG) resin. A novel *P,N*-chelate chiral ligand, (3*R*,9a*S*)-(2-aryl-3-(2-diphenylphosphino)-phenyl)-tetrahydro-1*H*-imidazo[1,5-*a*]indole-1-one having pyrrolo[1,2-*c*]-imidazolone framework was designed, prepared, and immobilized on an amphiphilic polystyrene-poly-(ethylene glycol) graft copolymer (PS-PEG) resin. A palladium complex of the PS-PEG resin-supported *P,N*-ligand catalyzed the allylic substitution of both cyclic and acyclic allylic esters in water with high enantio-selectivity. Reactions of cyclopentenyl, cyclohexenyl, and cycloheptenyl carbonates with dialkyl malonate gave the corresponding alkylated products with enantiomeric excess ranging from 89 to 98% ee. The PS-PEG supported Pd complex was readily recovered by simple filtration and reused without loss of catalytic activity or enantioselectivity.

Heterolytic Cleavage of C–H bond in Alkanes

SUZUKI, Hiroshi[1]; TANAKA, Yasutaka[1,2]
(*[1]Shizuoka Univ.; [2]IMS*)

Alkanes were understood to be inert toward the heterolytic cleavage of their C–H bonds in a mild reaction condition. In particular the p*Ka* value for the methane C–H ($\equiv$C–H $\rightleftarrows$ H$^+$ + $\equiv$C$^-$) is about 49. When one of four protons was substituted with an electron withdrawing group such as nitro the p*Ka* potently decreases; *e.g.*, nitromethane has the p*Ka* value of 10.2 in water. If an aryl group was adopted as the substituent the decrease in the p*Ka* value was also observed. Thus, several aromatics undergo H-D exchange reaction of protons in a methyl side chain which is covalently bound to the aromatic ring. The mechanism of this type of reaction could also be considered as being initiated by nucleophilic attack of a base ion on a methyl hydrogen resulting in heterolytic cleavage of the C–H bond to afford a carbanion and a proton. Consequently, the presence of a strong base and/or vigorous conditions such as high temperature are inevitably required. Among aromatic nuclei, acridines and their derivatives are still attracting considerable attention because of the many functions which they possess, including biomimetic redox reactivities, chemiluminescence, and the interaction with DNA as an intercalator. In particular the 9 position, the pare position from acridine nitrogen, in acridinium exhibits strong electrophilicity and reacts with alcohols giving rise to 9-alkoxy-acridanes. 9-methyl substituted acridinium exhibited a slightly different reactivity with basic alcohol, affording the corresponding 9-alkoxyacridanes followed by an olefinic species, 9-methyleneacridane, through the 9-methyl proton abstraction by an alkoxide. Therefore, the 9 position in acridinium appears to have different electric and steric conditions as compared to the other positions, giving rise to expectations of more unique reactivity. We report on the unusual acidity of protons in methyl groups substituted onto acridinium skeleton at the 9 position. The p*Ka* of these methyl protons was estimated to be slightly higher than that of acetic acid at room temperature, showing that the methyl protons in the acridinium are functioning as an organic protic acid.

Reductive Activation of Carbon Monoxide derived from Carbon Dioxide and Oxidative Activation of Hydroxy- and Oxo-Groups Derived from Water

TANAKA, Koji: WADA, Tohru; MIZUKAWA, Tetsunori; KOBAYASHI, Katsuaki; TOMON, Takashi

An electrophilic attack of CO_2 to coordinatively unsaturated low valent metal complexes affords M-η^1-CO_2 complexes, which are easily converted to M-CO ones in both protic and aprotic media. Organic synthesis through M-CO complexes derived from CO_2 is highly desired from the viewpoint of utilization of CO_2 as C1 resources. A major problem of the reduction of CO_2 using homogeneous catalysis is reductive cleavages of M-CO bonds under reductive conditions because of accumulation of too much electrons in the central metals. Such unfavorable CO evolution in the reduction of CO_2 is expected to depress effectively by utilization of ligand localized redox reactions rather than metal centered one. A flexible ligand having an ability to change the bonding modes among monodentate, bidentate and bridging form to connect metals and carbonyl carbon of M-CO bonds would meet the requirements of smooth M-η^1-CO_2 formation and depression of reductive cleavage of M–CO bond under reductive conditions.

Neutralization energy generated by reactions between acids and bases is merely wasted as thermal energy into air. Proton gradient (Δp) between inside and outside of a cell is depicted as the sum of electric activity ($\Delta \psi$) and chemical activity (ΔpH) components. $\Delta p = \Delta \psi - Z\Delta$pH ($Z = 2.303RT/F$). Proton gradient is equivalent to the neutralization energy because the neutralization reaction takes place upon removal of separating membrane. Thus, neutralization energy results from the formation of water. Biological system effectively creates and consumes neutralization energy in various reactions. Acids and bases, therefore, have potential energy sources, which are provided by chemical bondings (chemical energy). Along this line, we tried to convert the neutral energy to electronic energy by using ruthenium-aqua complexes.

Rational Synthesis of Metal-Chalcogenido Clusters

KAWAGUCHI, Hiroyuki; MATSUO, Tsukasa; KOMURO, Takashi[1]; TATSUMI, Kazuyuki[1]
(*[1]Nagoya Univ.*)

Metal–chalcogenide clusters are of fundamental interest by virtue of their relevance to bioinoganic chemistry, catalysis, and materials science. One of challenging topics in this chemistry is to develop rational syntheses or stepwise syntheses of metal-

chalcogen clusters, whereby small metal-chalcogen fragments assemble into desirable higher molecularity sulfur complexes. For this purpose, we find it attractive to utilize silanechalcogenolato complexes as precursors to metal-chalcogenolato clusters. The use of silane-chalcogenolates has the two following advantages in exploring the synthetic method for clusters. First, silicon–chalcogen bond is labile and is readily cleaved in a mild condition. Secondly, the reactivity of silane-thiolato ligands can be regulated by steric and electronic properties of substituents on silicon. However, the coordination chemistry of silicon-chalcogen ligands has yet to be explored. In this project, we have prepared silanecalcogenolate complexes of transition metals. Studies of reactions of silicone-chalcogen bonds coordinated at a metal center are now in progress.

Developments and Researches of New Laser Materials

SARUKURA, Nobuhiko; OHTAKE, Hideyuki; LIU, Zhenlin; KOZEKI, Toshimasa; ONO, Shingo[1]
(*[1]Sci. Univ. Tokyo*)

Although development of lasers is remarkable, there are no lasers which lase in ultraviolet and far infrared regions. However, it is expected that these kinds of lasers break out a great revolution in not only the molecular science but also in the industrial world.

In this project we research characters of new materials for ultraviolet and far infrared lasers, and develop new lasers by using these laser materials.

Development and Research of Advanced Tunable Solid State Lasers

TAIRA, Takunori; KURIMURA, Sunao; SHOJI, Ichiro; PAVEL, Nicolaie; SATO, Yoichi; SAIKAWA, Jiro

The use of diode lasers to pump solid-state lasers opens new horizon in laser science. Diode-pumped solid-state lasers are compact, reliable, and efficient sources of coherent radiation. They can provide excellent spatial mode quality and narrow linewidths. The high spectral power brightness of these lasers has allowed high efficiency frequency extension by nonlinear frequency conversion. Moreover, the availability of new and improved nonlinear optical crystals makes these techniques more practical. Recently attention has been directed to the trivalent ytterbium ion doped YAG. The advantages of Yb:YAG lasers for a high power, high stability and wide tunability laser operation are well recognized due to its small quantum defect, long upper-state life time and wide gain width.

On the other hand, quasi phase matching (QPM) is a new technique instead of conventional birefringent phase matching for compensating phase velocity dispersion in frequency conversion. Inasmuch as the pool of mature nonlinear optical materials is limited and development of new materials takes time and cost, QPM is a useful method for extending the range of available nonlinear optical materials. The ability to pattern a QPM structure allows the nonlinear materials to be engineered for desired interactions, meaning molecular-science-specified lasers are obtainable through these artificial materials.

In this projects we research and develop new diode-pumped-solid-sate lasers and new frequency conversion devices. Especially, we will focus on the combination of Yb-doped lasers and QPM devices. These kinds of advanced tunable solid-state light sources which based on microchip lasers will be powerful tools in the research of molecular science.

Diode-pumped solid-state lasers can provide excellent spatial mode quality and narrow linewidths. The high spectral power brightness of these lasers has allowed high efficiency frequency extension by nonlinear frequency conversion. Moreover, the availability of new and improved nonlinear optical crystals makes these techniques more practical. Additionally, quasi phase matching (QPM) is a new technique instead of conventional birefringent phase matching for compensating phase velocity dispersion in frequency conversion. These kinds of advanced tunable solid-state light, so to speak "Chroma-Chip Lasers," will assist the research of molecular science. In this projects we are developing Chroma Chip Lasers based on diode-pumped-microchip-solid-sate lasers and advanced nonlinear frequency conversion technique.

Generation of Reactive Species via Electron Transfer on Metal Complexes, as Basis of Chemical Energy Conversion Systems

NAGATA, Toshi; HINO, Takami[1]; ITO, Hajime; ITO, Kaname; KIKUZAWA, Yoshihiro
(*[1]Kyoto Univ.*)

This project aims at developing redox catalysis reactions suitable for chemical energy conversion. Our current interest focuses on modeling photosynthesis, that is, driving endothermic chemical transformation by using light energy via photoinduced electron transfer. Progress has been made in the following topics during the last year:

A. Examination of various terdentate ligands as candidates for new electrocatalysis. 2,2':6',2"-Terpyridine (terpy) has been the ligand of choice for application of metal complexes on electrocatalysis. We found, however, that terpy tended to stabilize the complexes with first-row transition metals at their lower oxidation states (Fe(II), Mn(II), *etc.*), which prevented these complexes to serve as electro-catalysis at low overpotentials. We therefore examined other terdentate ligands that were to replace terpy. 2,2':6',2"-Terpyridine-1,1"-dioxide was a promising ligand which showed lower M(III)/M(II) potentials than the terpy analogs. Also being investigated are pyrrole-containing ligands, 2,6-bis(2-pyrrolyl)pyridine and 6-(2-pyrrolyl)-2,2'-bipyridine.

B. Multistep redox-active polymers were combined with photoactive pigment (porphyrin). This is another necessary step towards realizing photo-synthesis in artificial molecular systems. Multiple electron transfers from the polymer to quinones were

successfully observed. Development of other types of redox pools using dendrimer-related substances are currently under way.

Synthesis and Electron-Transport Properties of Perfluorinated Oligonaphthalenes

SAKAMOTO, Youichi; KOMATSU, Shingo; SUZUKI, Toshiyasu

We have synthesized perfluoro-2,6-ternaphthalene (**PF-3N**) and -quaternaphthalene (**PF-4N**). These oligomers are colorless crystalline solids, which showed sharp melting endotherms at 263 and 371 °C, respectively. **PF-3N** is slightly soluble in some solvents, but **PF-4N** is insoluble in common organic solvents. The cyclic voltammogram of **PF-3N** in THF exhibited a reversible reduction at –1.88 V. OLEDs were fabricated using these oligomers as the electron-transport layer. The luminance-voltage curves of **PF-3N** and **-4N** are almost identical to that of Alq_3. The maximum luminance of **PF-4N** reached 15940 cd/m^2 at 12.6 V. The low electron mobility of Alq_3 could be responsible for the saturation of luminance and current density.

Slurry Mixer for Bonded Lubricating Films

WATANABE, Michio; YOSHIDA, Hisashi; KONDOH, Takuhiko; MIYASHITA, Harumi; TAKAMATU, Gunzo

This year we have newly built a Slurry Mixer for Bonded Lubricating Films (Figure 1) to product bonded lubricating films.

Now we are evaluating the performance both in antigalling and in coefficient of friction for some samples by Ball on Disk Tribometer.

Figure 1. Slurry Mixer for Bonded Lubricating Films.

Investigation of Dynamics on Photo-Excited Solids and Surfaces by Using the Combination of Synchrotron Radiation and Laser

KAMADA, Masao; TAKAHASHI, Kazutoshi

Dynamics on solids and surfaces, which are excited by photons, has attracted much interest from both of basic and application sides, since it may provide new scientific fields and photo-controllable devices. We have been investigating the photo-induced phase transition using photoelectron spectroscopy based on the combination of synchrotron radiation and laser. Core-level and valence-band photoelectron spectra of organometalic complex showed clearly the characteristics of the photo-induced phase transition.

We have been also investigating the photo-induced phenomena on semiconductor surfaces using the combination of synchrotron radiation and laser. Photo-induced core-level shifts observed on GaAs (100) can be interpreted in terms of surface photo-voltage effects. This work is now extended to the super-lattice systems and another semiconductors such as GaN. We have constructed the experimental system for investigating the time-response on the semiconductor surfaces using photoelectron spectroscopy.

The dynamics on the photo-excited semiconductors is also observed in the optical response. We have conducted the two-photon excitation experiments using synchrotron radiation and laser. Excited carriers changed the surface band structures, resulting in the reflectivity spectra. The experiments are in progress on GaAs and ZnSe.

Development of Combined-function Focusing Magnet

KATOH, Masahiro; HAYASHI, Kenji; HORI, Yoichiro[1]; HOSAKA, Masahito; KINOSHITA, Toshio; KODA, Shigeru; TAKASHIMA, Yoshifumi; YAMAZAKI, Jun-ichiro
(*[1]IMS and KEK-PF*)

In the upgrade plan proposed for UVSOR, the original magnetic lattice will be modified to reduce the emittance and to increase the number of straight sections for insertion devices. We have completed the lattice design. We are designing and developing the lattice components, such as quadrupole/sextupole magnets and the vacuum chambers. Because of the space limitation, sextupoles will be integrated in quadrupoles. We have constructed a prototype of the combined-function magnets. Field measurements are in progress. It has been shown that the magnet is capable of producing required field strengths.
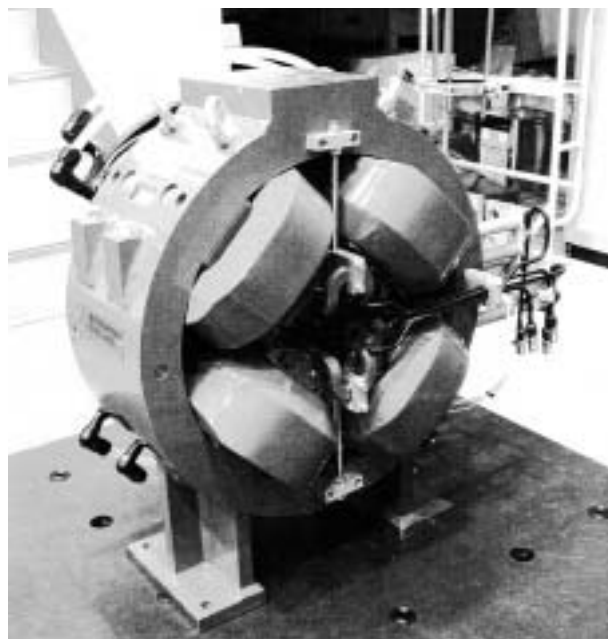
Figure 1. Prototype of the combined-function magnets.

Roles of Val-68 on the Oxidation Activity and Enantioselectivity by Sperm Whale Myoglobin

YANG, Hui-Jun; MATSUI, Toshitaka[1]; OZAKI, Shin-ichi[2]; UENO, Takafumi; WATANABE, Yoshihito
(*[1]Tohoku Univ.; [2]Yamagata Univ.*)

In the course of structural studies on H64D myoglobin (Mb) mutant, which is the first Mb mutant to afford compound I in its reaction with H_2O_2, we have solved the crystal structure of H64D/V68A Mb. The carboxylic acid in Asp-64 is found to interact with Arg-45 through a hydrogen bonding. According to the hydrogen bonding, a distal site immediate above the heme becomes vacant. In addition, the amino acid residue at the position of 68 appears to construct a big obstacle for incoming organic substrate such as sulfides and olefins. Thus, we have prepared H64D Mbs bearing a series of substituent for Val-68 whether or not the enzymatic activities could be regulated by the Va-l68 variants, so called H64D/V68X Mbs. A series of Mb mutants have been prepared by replacing Val-68 with Gly, Ala, Ser, Leu, Ile, and Phe in H64D Mb. All the mutant proteins, except for H64D/V68G Mb, are stable enough to be purified. The oxidation of thioanisole by compound I of H64D/V68X Mb (Mb-I) was directly monitored by stopped-flow spectrometer, and the sulfoxidation rate constants are found to increase in the order of Phe < Val < Leu < Ala < Ile. Unfortunately, H64D/V68S Mb-I is rapidly decay to Mb-II; therefore, the rate of Mb-I reduction with thioanisole was not determined accurately. The results suggest that the volume of hydrophobic residue at the 68 position influences the sulfoxidation activity. A similar trend is observed for the catalytic sulfoxidation of thioanisole by H64D/V68X Mbs with H_2O_2. The dominant product in the catalytic sulfoxidation is the (R)-isomer for the H64D/V68A and H64D/V68S mutants, with more than 84% enantiomeric excess (% ee). However, increasing the polarity of the distal pocket by substituting Ala-68 with Ser in H64D Mb decelerates the rate of sulfoxidation by 2-fold. On the other hand, the H64D/V68I mutant affords dominantly the (S)-enantiomer with the highest rate (*i.e.* 413 turnover/min). The substitution of Val-68 with Leu has little effect on enantioselectivity in the catalytic sulfoxidation but increases the reactivity with H_2O_2. Both the values of % ee and rate in the catalytic sulfoxidation decrease for H64D/V68F Mb in comparison with the values for H64D/V68A Mb, implying that a large benzyl side chain of phenylalanine at the 68 position inhibits the access of substrate to the heme pocket. In order to understand details of the transition state of the oxo-transfer step, we have examined enantioselective binding of (R)- and (S)-1-phenylethylamine to H64D/V68X Mb mutants, since the structure of 1-phenylethylamine–Mb adduct is expected to be very similar to the transition state of the thioanisole sulfoxidation (transition state analogue). Therefore, enantioselectivity sulfoxidation and enantioselective amine binding are compared. Finally, we have concluded that the enantioselectivity in the sulfoxidation is determining the step prior to the oxo-transfer step, possibly the substrate access step.

Molecular Mechanism of Oxygen Activation by Metalloenzymes

FUJII, Hiroshi

Metalloenzymes are a class of biologically important macromolecules which have various functions such as oxygen transport, electron transfer, oxidation, and oxygenation. These diverse functions of metalloenzymes have been thought to depend on the coordination structure of the active site in the protein matrices; the ligand donors, the geometry, and the coordination mode of reactant and substrate. Furthermore, it has been thought that protein structures in immediate vicinity of active metal ion are related to enzymatic function, regio-selectivity, and stereo-selectivity. In this project, we are studying the molecular mechanism of activation of molecular oxygen mediated by metalloenzymes.

(1) To understand the structure-function relationship of 3,4-PCD, there have been attempted over several decades to prepare inorganic model complexes that mimic the ferric iron site of 3,4-PCD, however, no ferric iron complex with the same coordination structure that in the enzyme has been characterized definitively. We have succeeded in an attainment to the ferric iron active site of 3,4-PCD by using sterically hindered salen ligand. Characterization of the model complex revealed the roles of the iron bound water ligand in the enzyme on the unique trigonal bipyramidal structure and the catechol degradation reaction.

(2) Cytochrome c oxidase (CcO) is the terminal oxidase that reduces molecular oxygen to water, coupling with proton pumping across the mitochondrial inner membrane. To reveal the reaction mechanism of CcO, we have synthesized model complexes of the heme-a_3 site of cytochrome c oxidase. We have

succeeded in the preparation of a high valent oxo iron porphyrin complexes as models for the intermediates P and F, which are detected as reaction intermediates in the catalytic cycle of CcO, by the oxidation of the ferric model complexes with m-chloroperbenzoic acid or ozone.

(3) Heme oxygenase catalyzes the regiospecific oxidative degradation of iron protoporphyrin IX (heme) to biliverdin, CO and Fe, utilizing molecular oxygen and electrons donated from the NADPH-cytochrome P450 reductase. To investigate the functionality of highly conserved polar amino acids in the distal helix of HO-1, we have prepared alanine mutants: T135A, R136A, D140A, and S142A, and found drastic changes in the heme degradation reactions of D140A. All of the experimental data clearly indicated that the carboxylate at position 140 has essential role on the activation of iron bound dioxygen and hydroperoxide.

OKAZAKI CONFERENCE

Okazaki COE Conference

Electronic Properties of Molecular Assemblies
—From Molecular Solid to Single Molecule—
(March 15–17, 2001)

Organizing members:
KOBAYASHI, Hayao (Chairperson); YAKUSHI,
Kyuya; NAKAMURA, Toshikazu; TADA,
Hirokazu; INOUE, Katsuya; YONEMITSU, Kenji;
SUZUKI, Toshiyasu

The International COE (Center of Excellence) Symposium of Institute for Molecular Science (IMS) of the last fiscal year was held on March 15–17, 2001 at Okazaki Conference Center. This symposium was organized by seven members of IMS whose research fields are concerned with the science of molecular assemblies.

The aim of this symposium was to overview the frontier of functional molecular science mainly from the view point of electronic properties of molecules and molecular assemblies. Up to now, there has been almost no chance that the leading scientists in the field of solid state science and those of molecular devices and electronics gather together to attend the same symposium. However, the communication between these two fields will be very important to get future prospect of molecular science. Under this idea, this symposium was organized. And the following topics are discussed: (1) magnetic organic metals and superconductors (2) single-component molecular metal (3) development of new functional molecules (4) organic and inorganic molecular magnets (5) organic/metal interfaces (6) Organic semiconductor transistor (7) molecular electronic devices. Besides, the lectures on the history of the discovery of conducting polyacetylene and its conduction mechanism were given by Profs. H. Shirakawa and Y. Ishiguro.

Since rapidly increasing interests are going to be attracted to the science and technology of nano-scale devices and electronic molecular functions, this COE conference was very timely and successful. About 150 attendants including 10 foreign leading scientists attended the conference. The 31 invited talks and 70 poster papers were presented. As mentioned above, this conference was an interdisciplinary one. Attendants could have a chance to see the recent progress in the field of functional molecular science.

JOINT STUDIES PROGRAMS

As one of the important functions of an inter-university research institution, IMS undertakes joint studies programs for which funds are available to cover research expenses as well as travel and living expenses of individuals. The proposals from domestic scientists are reviewed and controlled by an inter-university committee.

The programs are carried out under one of categories:

(1) Joint Studies on Special Projects (a special project of significant relevance to the advancement of molecular science can be carried out by a team of several groups of scientists).

(2) Research Symposia (a symposium on timely topics organized by collaboration between outside and IMS scientists).

(3) Cooperative Research (a research program carried out by outside scientists with collaboration from an IMS scientist).

(4) Use of Facility (a research program carried out by outside scientists at the research facilities of IMS except the UVSOR facility).

(5) Invited Research Project

(6) Joint Studies Programs Using beam lines of UVSOR Facility.
    A. Special Projects.   B. Use-of UVSOR Projects.

(7) Use of Facility Program of the Computer Center (a research program carried out by outside and inside IMS scientists at the research facilities of the Computer Center).

From October 2000, Cooperative Research Projects and Invited Research Projects for UVSOR Facility, which had belonged in the category (6), are included in the categories (3) and (4), respectively. In the fiscal year 2000, the numbers of joint studies programs accepted for the categories (1)–(5) and (7) were 3, 11, 110, 48, 5, and 156, respectively, and those accepted for subcategory (6)B was 161.

(1) Special Projects

A. Thermal and Optical Switching of Spin-Crossover Compounds

HAYAMI, Shinya[1]; MAEDA, Yonezo[1]; HOSOKOSHI, Yuko; INOUE, Katsuya; GU, Zhongze[2]; SATO, Osamu[2]
(*[1]Kyushu Univ.; [2]KAST*)

There has been a great interest in developing novel molecular compounds whose physical properties can be controlled by illumination. Along this line, photochemically tunable iron(II) spin-crossover complexes and a molecular photo-magnet have recently been reported. However, until now, the number of the optically switchable molecular solids reported has been quite small. This is because the strategy to achieve photo-induced switching in a solid state system is yet to be clarified. One of the requisites of optically switchable compounds is that they have nearly degenerate electronic states. Furthermore, it is known that the structural change accompanied with the switching phenomena should not be too large, because steric effects often prevent the photochemical transformation. For example, the azobenzene derivatives, which are representative photochromic molecules, do not undergo *trans*-to-*cis* photo-isomerization in the solid state due to the steric hindrance. This means that compounds with nearly degenerate electronic states and with only small structural changes occurring between the metastable state and the stable state are appropriate for optical switching. However, even if these requirements are satisfied, most never show photo-induced switching with long-lived metastable states. This is because,

although it is possible to produce a metastable state in such compounds by illumination, the metastable state rapidly relaxes back to the stable state as a result of tunneling effects due to the small structural change. Hence, in order to develop a variety of optically switchable molecular solids, strategies to prevent such a rapid relaxation from a metastable state to a ground state should be developed. We propose the introduction of strong intermolecular interactions in molecular compounds. It is thought that the cooperativity resulting from the intermolecular interaction operates to increase the activation energy for the relaxation processes, enabling the observation of a long-lived metastable state after illumination. That is, when the metastable molecular orientation reverts to the stable one, a large stress field might be built up in such compounds because of the presence of a strong binding energy between molecules.

A-1 A Novel LIESST Iron(II) Complex Exhibiting a High Relaxation Temperature

[*Inorg. Chem.* **40**, 3240 (2001)]

In the meantime a number of iron(II) compounds with long-live light-induced metastable HS states at low temperatures have been found. However, the LIESST effect has been observed only at sufficient low temperatures below 80 K so far. We directed toward to produce the compounds, which can be switched by illumination and the metastable HS state can be trapped at higher temperature. Temperature dependent spin-crossover phenomenon, $S = 0$ (LS) $\leftrightarrow$ $S = 2$ (HS) of the molecular complex, $[Fe(L)(CN)_2] \cdot H_2O$ (**1**) (L is Schiff-base macrocyclic ligand derived from the condensation of 2,6-diacetylpyridine with 3,6-dioxaoctane-1,8-diamine) has been extensively studied 15 years ago by König *et al.* They have been reported that the powder

samples of complex **1** exhibited unusual magnetic behaviors, but the physical properties of single crystals and photo-induced spin transition have not been reported yet. Here, we synthesized the single crystal form of the complex **1** and also investigated its crystal structure. Moreover, we have discovered that the complex **1** exhibits LIESST effects. The relaxation temperature from the metastable HS to the original LS state is above 130 K, which is the highest temperature investigated so far.
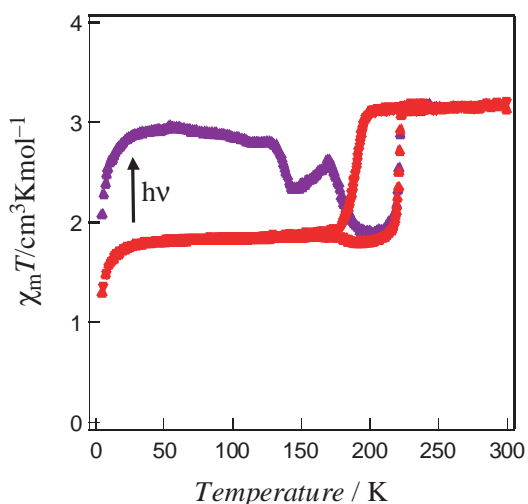

Figure 1. $\chi_m T$ *vs. T* plots for [Fe(L)(CN)$_2$]·H$_2$O before and after illumination at 550 nm.

A-2 Pressure-Stabilized Low-Spin State for Binuclear Iron(III) Spin-Crossover Compounds

[*Bull. Chem. Soc. Jpn.* in press]

Binuclear iron(III) spin-crossover complexes with salten ligand [Fe$_2$(salten)$_2$(L)](BPh$_4$)$_2$ were synthesized and characterized by single-crystal X-ray diffraction, Mössbauer spectra, magnetic susceptibilities and electronic spectra, where H$_2$salten is a pentadentate ligand derived from salicylaldehyde and 3,3'-diaminodipropylamine and L is a didentate axial ligand (az = azobis(4-pyridine) and cc = 4,4'-vinylenebis(pyridine)). The structures of [Fe$_2$(salten)$_2$(az)](BPh$_4$)$_2$ (**1**) and [Fe$_2$(salten)$_2$(cc)](BPh$_4$)$_2$ (**2**) were determined at both 100 K and 298 K. The complexes **1** and **2** exhibited the spin-crossover behavior depending on temperature within the temperature range of 200 to 350 K, and rapid spin equilibrium behavior was observed by means of Mössbauer spectroscopy at 293 K. The complexes **1** and **2** also exhibited a pressure-induced spin transition between the rapid spin equilibrium state and low-spin state at 300 K. Such a pressure-induced spin transition has not been reported earlier.
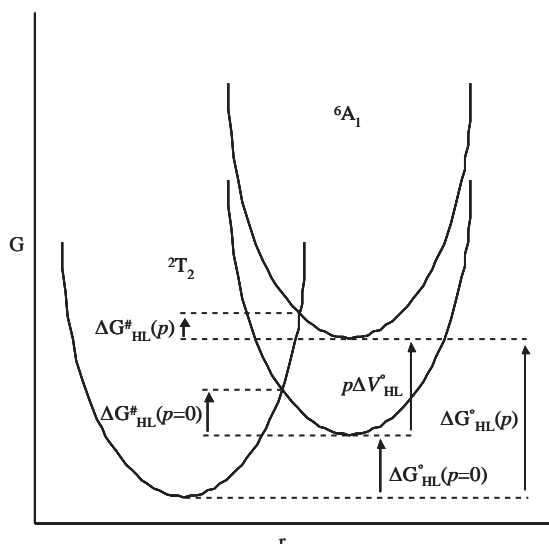
Figure 1. Schematic representation of the influence of pressure on the low-spin state ($^2T_2$) and high-spin state ($^6A_1$). Pressure increases the zero point energy difference, $\Delta G°_{HL}(p)$ by the work term $p\Delta V°_{HL}$ and decreases the activation energy $\Delta G^\#_{HL}(p)$, thus favouring the low-spin state and increaseing the rate constant k_{HL}.

A-3 Iron(III) Spin-Crossover Compounds with a Wide Apparent Thermal Hysteresis at around Room Temperature

[*J. Am. Chem. Soc.* in press]

The magnetic properties of the spin-crossover compounds, [Fe(qsal)$_2$]NCSe·MeOH (**1**) and [Fe(qsal)$_2$]NCSe·CH$_2$Cl$_2$ (**2**), have been measured. We have discovered that both compounds **1** and **2** have exhibited a wide thermal hysteresis loop of 140 K ($T_{1/2}\uparrow$ = 352 K and $T_{1/2}\downarrow$ = 212 K) and 180 K ($T_{1/2}\uparrow$ = 392 K and $T_{1/2}\downarrow$ = 212 K) respectively in the first cycle. Thermogravimetric analysis shows that solvent molecules escape from compounds **1** and **2** at around 340 K and 395 K, respectively. This means that the hysteresis loops observed for the first cycle are only apparent ones. Following the first loop, they show a two-step spin crossover in warming mode. The so-called "step 1" and "step 2" are centred around $T_{1/2(S1)}\uparrow$ = 215 K and $T_{1/2(S2)}\uparrow$ = 282 K, respectively. On the other hand, it shows a one-step spin crossover at $T_{1/2}\downarrow$ = 212 K in cooling mode. The hysteresis widths can be estimated to be 3 K (step 1) and 70 K (step 2), assuming that the widths in "step 1" and "step 2" are defined as the difference of $T_{1/2(S1)}\uparrow$ and $T_{1/2}\downarrow$, and $T_{1/2(S2)}\uparrow$ and $T_{1/2}\downarrow$, respectively. The hysteresis width of 70 K in "step 2" is one of the widest values reported so far for spin-crossover complexes. It is thought that the cooperativity operating in the complexes mainly arises from the intermolecular π interactions between quinoline and phenyl rings. Using the model reported by Kahn and Real *et al.* we are able to simulate the hysteresis loop with a two-step spin-crossover in warming mode and a one-step transition in cooling mode.
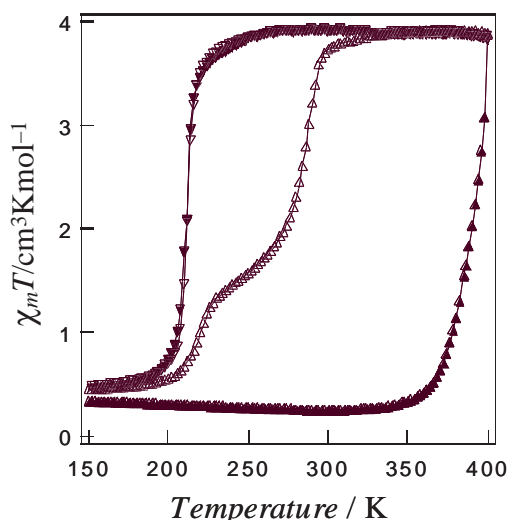
Figure 1. $\chi_m T$ versus T plots for **2**. The sample was warmed from 5 K to 400 K(▲) and then cooled from 400 K to 5 K (▼) in the first cycle, and the the sample was warmed from 5 K to 400 K (△) and then cooled from 400 K to 5 K (▽) in the second cycle at a rate of 2 K min⁻¹.

B. Photoinduced Energy Transfer in Meso-Acridine-Porphyrins

TANAKA, Yasutaka[1]; MATSUEDA, Satoshi[1]; YAMASHITA, Yoshinori[1]; SUZUKI, Hiroshi[1]; ISHIDA, Akito[2]
(*[1]Shizuoka Univ.; [2]Kyoto Pref. Univ.*)

Outline of the project:

Combination of several types of chromophores possessing distinct physical properties such as absorption coefficients and wavelengths leads to a valid light harvesting system with a broader absorption band and is thus attracting considerable attentions. In nature the light-harvesting complexes in photosynthetic systems consist of a few kinds of pigment molecules involving porphyrins and carotenoids and enable them to absorb and collect the solar energy comprised of many wavelengths where the intermolecular energy transfer between the pigments plays a central role in delocalizing and stabilizing the energy collected. In addition the spatial arrangement of the pigments affects the transfer efficiency in a striking manner. The importance and complexity of energy as well as electron transfer in nature have led many researchers to look into simplified model systems composed of donor and acceptor molecules for studying the fundamental process of energy and electron transfer and for constructing artificial photosynthetic systems capable of capturing and storing solar energy. We propose and design novel chemical structures of porphyrin molecules directly bound to an acridine ring(s) as a multi-chromophoric molecule. Acridine and porphyrin are both pigment possessing independent absorption coefficients and wavelengths. One may expect that a combination of these pigment lead to chromophores involving the physical properties drived from original molecules as well as an acquired property from the combination. Here the efficiency of the light harvesting and energy transfer in the acridine-porphyrins is

explained in terms of the spatial arrangement of the chromophores in grand and excited states.

Summery:

Multichromophoric molecules constituted of acridine and porphyrin moieties that are directly bound through covalent bonds were newly synthesized. Meso-monoacridinylporphyrin (**3**) and 5,15-bisacridinyl-porphyrin (**1**) exhibited that the fluorescence of the acridine chromopore was completely quenched by covalently bound porphyrin indicating the effective energy transfer from acridine to porphyrin. In contrast 5,10-bisacrydinylporphyrin (**2**) emits the fluorescence of both acridine and porphyrin when irradiated with light of acridine absorption showing partial energy transfer. The definitive discrepancy in the energy transfer behavior in acridine-porphyrins is expounded by mean of the dipole-dipole mechanism.

B-1 Syntheses of Acridine-Porphyrins

Acid catalyzed condensation of dipyrromethane (**5**) with 9-formylacridine (**6**), followed by oxidation using DDQ gave **1** as the prospective 2 (**5**) + 2 (**6**) condensation product along with porphyrins of **2**, **3**, and **4** (Figure 1). The unforeseen formation of these three porphyrins resulted from the scrambling (migration and loss) of meso-substituents. The scrambling occurred when the meso-substituents were bulky enough to unstabilize a porphyrinogen as a porphyrin precursor which is thus ultimately oxidized to give corresponding porphyrin. The porphyrin syntheses from 9-anthraldehyde and 1-naphthaldehyde with pyrrole were reported: the former fails (0%) and the latter succeeded (52%) although the two aldehydes possessed similar structures. Molecular model studies of the porphyrinogen molecules indicated that the anthracene 1-H is thrust into a severe eclipsing interaction with the *meso* hydrogen while the 8-H is unobstructed in the lower groove when 9-anthraldehyde or 9-formylacridiene were adopted as aldehyde (Figure 2(a)). Naphthaldehyde can avoid the meso hydrogen eclipsing interaction by rotation of the 8-H into the lower groove (Figure 2(b)). These are causes of the formation of the meso-substituents scrambling products as well as of the low yields. The structures of the porphyrins synthesized here were characterized by mean of ^{1}H, ^{13}C, and 2D (^{1}H-^{1}H COSY and NOESY, ^{1}H-^{13}C COSY) NMR spectra and mass spectroscopy.
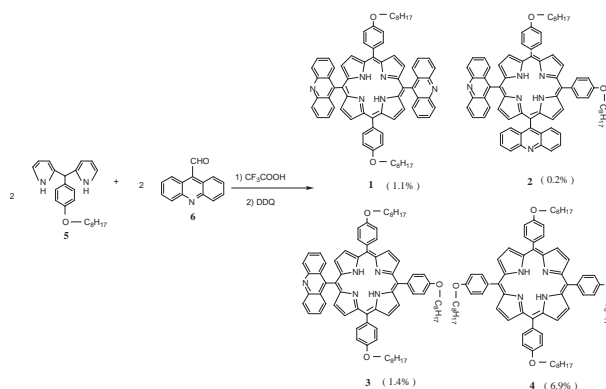
Figure 1. Synthesis of Acridiene-Porphyrins.

(a)

(b)

(X = C, N)
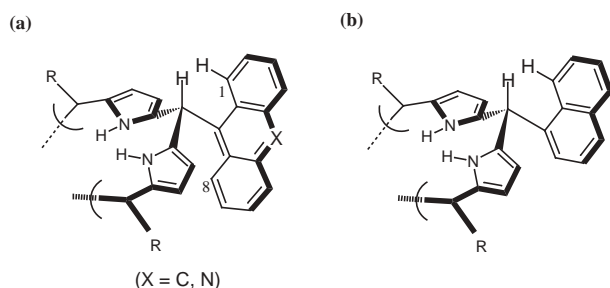
Figure 2. Steric structures of porphyrinoges possessing the moso-substituent of (a) 9-anthranyl or acrydin-9-yl and (b) 1-naphthyl.

B-2 Photoinduced Intramolecular Energy Transfer from Acridine to Porhyrin

Acridine-porphyrins (**1**, **2**, and **3**) closely resembled each other in their absorption spectra (Figure 1) except that the acridine absorption intensity (254 nm) in **1** and **2** is approximately double of that in **3** due to the number of acridine rings attached to porphyrin (B-1 Figure 1). The slight or no wavelength shifts in the Soret (426 nm) and acridine absorption (254 nm) bands in acridine-porphyrins from the absorptions of parent porphyrin (**4**, λ_{max} = 424 nm) and acridine (254 nm) suggested slight or no electronic interactions between the intramolecular chromophores. In particular PM3 semi-empirical calculation indicated that the acridine and porphyrin rings are almost orthogonal to one another in their energy minimized structures where the overlap of molecular orbitals of the chromophores thus seem to be scarce in the ground state (Figure 2).

When meso-tetraphenylporphyrin (TPP) was mixed with acridine in the ratio of 1:1 or 1:2 in CHCl$_3$ the fluorescence of acridine (broad luminescence at about 400 nm) was barely quenched by coexisting porphyrin indicating difficulty in transferring energy. In contrast **1** fluoresces light at 653 nm, the porphyrin fluorescence, without emitting the acridine fluorescence upon irradiation with light at 254 nm (Figure 3). **3** also fluoresces light at 653 nm with scanty fluorescence of acridine itself (Figure 4). These are clearly showing that the energy transfer between covalently bound chromophores efficiently takes place. The fluorescence life time measurements also proven the energy transfer. Two kinds of decay curves possessing respective rate constants were found in **3** on illumination at 250 nm and observation of the emission at larger than 300 nm (Figure 5(a)), the fluorescence life time of 10.7 nS being attributed to porphyrin and that of 1.8 ns being to acridine. In particular when irradiated at Soret band at 420 nm and observed the emission at larger than 600 nm the only life time afforded was to be 9.3 nS (Figure 5(b)), which is almost identical with that of the porphyrin fluorescence observed above. In marked contrast to **1** **2** emits light of both acridine and porphyrin fluorescence along with the decrease of the porphyrin fluorescence intensity as compared with those in **1** and **3** (Figure 6). This exhibits that the only partial energy transfer from acridine to porphyrin is occurring in **2** although **1** and **2** contain the same numbers of acridine and porphyrin rings in their structures.

The energy migrates from the excited to ground state

molecules when their orientation, distance, energy levels, and the other conditions is profitable to transfer. The inter- or intramolecular energy transfer is based on interacting transition dipole moments in energy donor and acceptor moieties in the dipole-dipole mechanism. Since the acridine fluorescence band gives a much greater overlap with the Soret band the intramolecular energy tranfer in **1**, **2**, and **3** should be driven by this mechanism. Thus the orientation of the acridine and porphyrin rings might be almost coplanar to one another in the excited state so as to induce the energy transfer. The molecular model studies including the PM3 calculation and CPK model exhibited that the two rings are capable of rotating along the C-C bond axis between the porphyrin meso and acridine 9 positions until the protons in the b in pyrrole and acridine 1- or 8-positions come into contact, where the two rings are nearly coplanar. The two chromophores in **1** and **3** seem to able to adopt this orientation (Figure 7(a)) while those in **2** seem to unable to do it due to a severe eclipsing interaction of an acridine 2- or 7-H with the adjacent acridene 2- or 7-H by rotation of the respective acridine rings (Figure 7(b)). Eventually the photo-excited acridine in **2** was deactivated by emitting the acridine fluorescence before the energy is migrating to porphyrin.

This is a quite unique example of an intramolecular energy transfer system since the definitive discrepancy in the energy transfer efficiency is derived only from the position of the acridine substituent in acridine-porphyrins, thus 5,15-bisacridinyl (**1**) or 5,10-bis-acridinyl (**2**). We are about to measure the fluorescence life time for **1** and **2** in order that we gaine a further insight into nature of novel synthesized porphyrins.
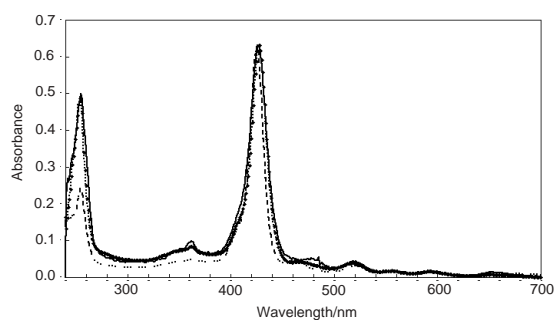
Figure 1. Absorption spectra of **1** (solid line), **2** (dotted line), and **3** (dashed line) in CHCl$_3$.
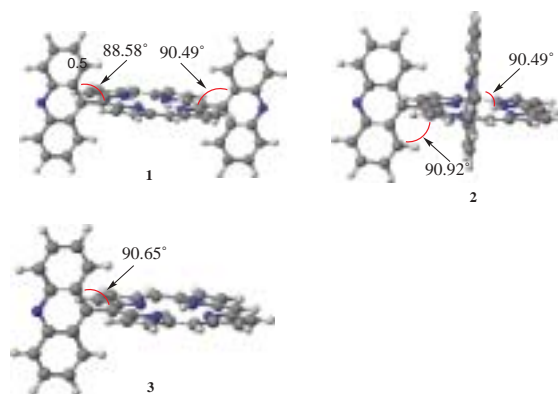
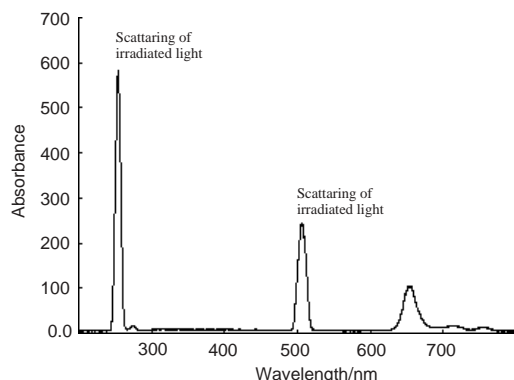**Figure 2.** Energy minimized structures of **1**, **2**, and **3** calculated by PM3.

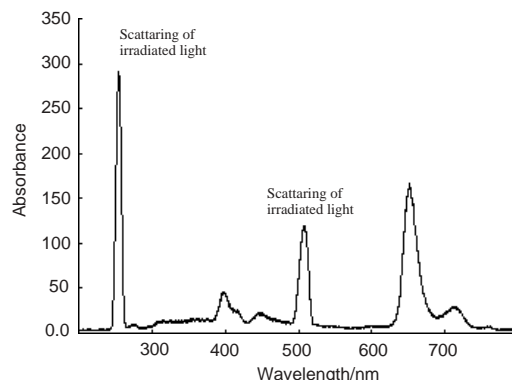**Figure 3.** Fluorescence spectrum of **1** in CH$_2$Cl$_2$ (excited at 254 nm).

Figure 4. Fluorescence spectrum of **3** in CH$_2$Cl$_2$ (excited at 254 nm).

Figure 5. Time-resolved fluorescence intensity of **3** in CH$_2$Cl$_2$, (a) EX 250 nm, EM > 300 nm, (b) EX 420 nm, EM > 600 nm.
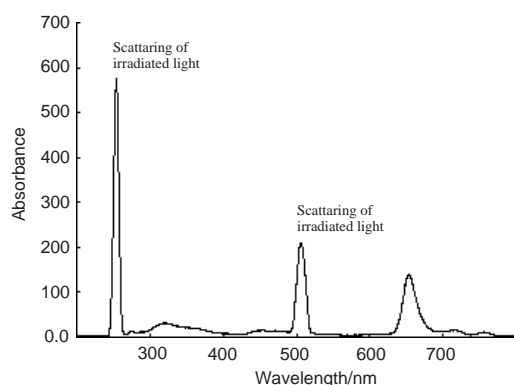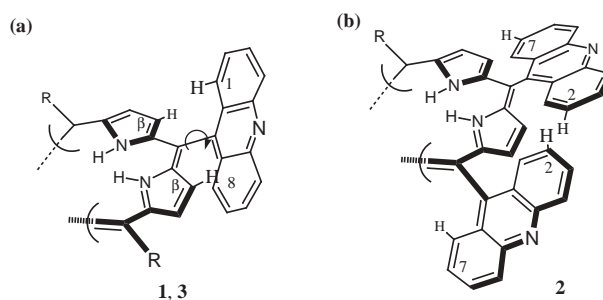

Figure 6. Fluorescence spectrum of **2** in CH$_2$Cl$_2$ (excited at 254 nm).

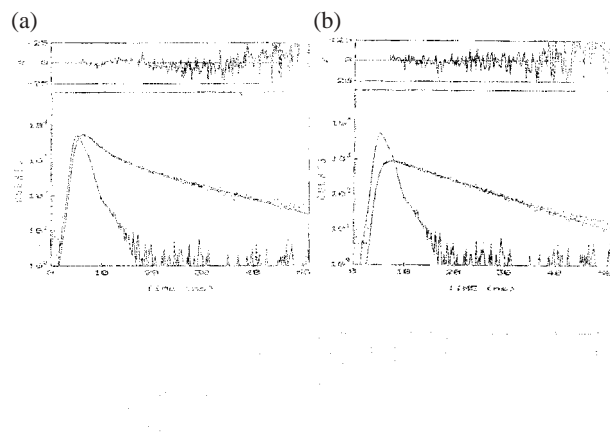**Figure 7.** Steric structures of acridine-porphyrins of (a) **1** and **3** (b) **2**.

(2) Research Symposia
(from September 2000 to August 2001)

1. Chemistry in Intense Laser Fields
    (September 4-5, 2000)
    Chair: **YAMAUCHI, Kaoru**

2. Present Status of VUV Light Sources and Its Application
    (September 17-19, 2000)
    Chair: **KUROSAWA, Kou**

3. Present Status and Future Trends of Fullerene Chemistry and Physics
    (November 23-25, 2000)
    Chair: **KOBAYASHI, Kaoru**

4. Future Prospect of Nano-Science by Electron Microscope
    (November 21-22, 2000)
    Chair: **TANAKA, Nobuo**

5. Molecular Science on Protein Dynamics: Toward Understanding of Fluctuation
    (December 25-27, 2000)
    Chair: **MIZUTANI, Yasuhisa**

6. Recent progress in functional organic molecules -- design, synthesis and physical properties
    (January 18-20 2001)
    Chair: **HOSOKOSHI, Yuko**

7. New Needs in the UV and VUV Region for

Synchrotron Radiation Application
(December 11-12)
Chair: **FUKUI, Toshikazu**

8. Application of VUV and SX Pulses and Future Prospect
(January 26-27, 2001)
Chair: **KAMATA, Masao**

9. Symposium on Physical Chemistry for Young Researcher of Molecular Science
(June 12, 2001)
Chair: **SHIBUYA, Kazuhiko**

10. Solution Chemistry in the 21st Century: A Perspective from the Molecular Science
(May 31- June 2, 2001)
Chair: **SATO, Hirofumi**

11. What kind of universality is present in functional mechanisms of proteins?
(July 17-18, 2001)
Chair: **MORIMOTO, Hideki**

(3) Cooperative Research

This is one of the most important categories that IMS undertakes for conducting its own research of the common interest to both outside and IMS scientists by using the facilities at IMS. During the first half of the fiscal year of 2000 ending on September 30, 61 outside scientists jointed Cooperative Research programs and during the second half, 49 outside scientists did. The names and affiliations of those collaborations are found in Research Activities.

(4) Use of Facility

The numbers of projects accepted for the Use-of-Facility program during the first half and the second half of the fiscal year of 2000 amounted to 3 and 2 for the Laser Research Center for Molecular Science, 21 and 20 for the Research Center for Molecular Materials, and 1 and 1 for Equipment Development Center, respectively.

(5) Invited Research

Under this joint-study program, several scientists were invited from other institutions of help for construction and improvement of instruments in IMS. The total number of the projects in this category was 5 (2 for the first half and 3 for the second half) in the fiscal year of 2000.

(6) UVSOR

In the UVSOR Facility with the 750 MeV electron storage ring, there are twenty beam lines available for synchrotron radiation research (see UVSOR ACTIVITY REPORT 2000). The Experimental facility of each beam line is also described in this report. Under the following programs, many users outside and inside IMS have carried out a number of synchrotron radiation studies: A. Special Projects. B. Use-of UVSOR Projects.

A. Special Projects

B. Use-of UVSOR Projects

Under this joint-study program, many synchrotron radiation experiments have been carried out with the beam lines of in-house staff in cooperation with scientists who were invited from other institutions. The total number of the projects in this category was 161 (86 for the first half and 75 for the second half) in the fiscal year of 2000.

(7) Use of Facility Program of the Computer Center

The number of projects accepted for the Use-of-Facility program of the Computer Center during the fiscal year of 2000 amounted to 156 (635 user) and computer time spent for these projects 143343 hours (converted to the IBM SP2 time), and amounted to 82% of the total annual CPU time used.

FOREIGN SCHOLARS

Visitors from abroad are always welcome at IMS and they have always played an important role in the research activities of the Institute. The foreign scientists who visited IMS during the past year (September 1999–August 2000) are listed below.

[1] indicates attendance at an Okazaki Conference; [2] a MONBUSHO (the Ministry of Education, Science, Sports and Culture, Japan) or JSPS (the Japan Society for the Promotion of Science) Invited Fellow; [3] an IMS councillor; [4] an IMS visiting professor or associate professor from abroad (period of stay from 6 to 12 months); [5] a JSPS Post-Doctoral or Ronpaku Fellow; [6] an IMS visiting scientist and [7] a visitor to IMS.

Scientists who would like to visit IMS under programs [2] and [4] are invited to make contact with IMS staff in their relevant field.

Prof. Wensheng Bian[5]	Shandong University	(China)	Feb. '00–
Prof. Myoungsik Cha[2]	Pusan National University	(Korea)	–Sep. '00
Prof. Benjamin Whitaker[2]	University of Leeds	(U.K.)	–Sep. '00
Prof. Jiri Hudecek[6]	Charles University	(Czech)	–Sep. '00
Prof. Alan Verma[7]	North Eastern Hill University	(India)	–Sep. '00
Prof. David Birch[5]	Univ. of Strathclyde	(U.K.)	Sep. '00
Prof. Evgueni Nikitin[7]	Technion, Haifa, Israel	(Israel)	Sep. '00
Dr. Curt Sander[7]	Danish Micro Engineering	(Denmark)	Sep. '00
Dr. Hocke Heiko[5]	Basel Univ.	(Switzerland)	Sep. '00–Aug. '02
Dr. Ranga Rao[7]	Indian Inst. of Technology	(India)	Oct. '00
Prof. Robert Byer[1]	Stanford Univ.	(U.S.A.)	Oct. '00
Prof. Sanford Asher[7]	Univ. of Pittsburgh	(U.S.A.)	Oct. '00
Prof. Jonathan Weissman[7]	Univ. of California	(U.S.A.)	Oct. '00
Prof. Devarajan Thirumalai[7]	Univ. of Maryland	(U.S.A.)	Oct. '00
Dr. Gennadiy Kozhukh[7]	Osaka Univ.	(Japan)	Oct. '00
Dr. Alam Mohammad[7]	Tokyo Inst. of Technology	(Japan)	Oct. '00
Dr. Tong Wang[7]	Tokyo Inst. of Technology	(Japan)	Oct. '00
Dr. Ruckman Hertadi[7]	Tokyo Inst. of Technology	(Japan)	Oct. '00
Prof. Voicu Lupei[2][4]	Inst. of Atomic Physics	(Rumania)	Oct. '00–Mar. '01
Dr. Harald Graaf[5]	Univ. of Bremen	(Germany)	Oct. '00–Sep. '01
Prof. Chun-Woo Lee[6]	Ajou Univ.	(Korea)	Nov. '00
Prof. Michael Grunze[6]	Univ. Heidelberg	(Germany)	Nov. '00
Prof. Sydney Leach[7]	CNRS	(France)	Nov. '00
Prof. James Brooks[6]	Univ. of Florida	(U.S.A.)	Nov. '00
Prof. Richard N. Zare[3]	Stanford Univ.	(U.S.A.)	Nov. '00
Prof. Lin Jianhua[7]	Peking Univ.	(China)	Nov. '00
Prof. Alexander Dalgano[7]	Harvard Univ.	(U.S.A.)	Nov. '00
Prof. Stanislav Nespurek[6]	Inst. of Macromolecular	(Czech)	Nov.–Dec. '00
Dr. Debabrata Mandal[5]	S.A.Jaipuria College	(India)	Nov. '00–Nov. '02
Prof. Peteanu Linda Anne[7]	Carnegie Mellon Univ.	(U.S.A.)	Dec. '00
Dr. Kim Cheal[2]	Seoul National Univ.	(Korea)	Dec. '00–Feb. '01
Dr. Mu Shik Jhon[2]	Korean Academy of Science and Technology	(Korea)	Jan. '01
Prof. Kwang Soo Kim[2]	Pohang Univ. of Science and Technology	(Korea)	Jan. '01
Prof. Seung Min Park[2]	Kyunghee Univ.	(Korea)	Jan. '01
Prof. Taiha Joo[2]	Pohang Univ. of Science and Technology	(Korea)	Jan. '01
Prof. Yong-Rock Kim[2]	Yonsei Univ.	(Korea)	Jan. '01
Prof. Hong Lae Kim[2]	Kangwon National Univ.	(Korea)	Jan. '01
Prof. Sang Kuk Lee[2]	Pusan National Univ.	(Korea)	Jan. '01
Prof. Sang Kyu Kim[2]	Inha Univ.	(Korea)	Jan. '01
Prof. Seung Koo Shin[2]	Pohang Univ. of Science and Technology	(Korea)	Jan. '01
Prof. Dongho Kim[2]	Yonsei Univ.	(Korea)	Jan. '01
Prof. Seokmin Shin[2]	Seoul National Univ.	(Korea)	Jan. '01
Prof. Sungyul Lee[2]	Kyunghee Univ.	(Korea)	Jan. '01
Prof. Yoon Sup Lee[2]	Korea Advanced Inst. of Sci. and Technology	(Korea)	Jan. '01
Dr. Naresh Patwari Ganpathi[7]	Tohoku Univ.	(Japan)	Jan. '01
Prof. James Brooks[7]	Univ. of Florida	(U.S.A.)	Jan. '01
Prof. Bernd A. Berg[7]	Florida State Univ.	(U.S.A.)	Jan. '01
Prof. Chul-Ho Jun[7]	Yonsei Univ.	(Korea)	Feb. '01
Dr. Dominique Mandon[7]	University Louis Pasteur	(France)	Feb. '01
Dr. Werner Fus[7]	Max-Planck Inst.	(Germany)	Feb. '01
Prof. Dong Hui Zhang[2]	National Univ. of Singapore	(Singapore)	Feb.–Mar. '01
Dr. Nicolaie Pavel[2][4]	Institute of Atomic Physics	(Rumania)	–Mar. '01

Dr. Olga Drozdova[*2*4]	Russian Academy of Sciences	(Russia)	–Mar. '01
Dr. Olga Gritsenko[*6]	Russian Academy of Sciences	(Russia)	–Mar. '01
Prof. Michael D. Fryzuk[*7]	Univ. of British Columbia	(Canada)	Mar. '01
Prof. Mark Johnson[*7]	Yale Univ.	(U.S.A.)	Mar. '01
Prof. Susan Sinnott[*2]	Univ. of Florida	(U.S.A.)	Mar. '01
Prof. R. Metzger[*7]	Univ. of Alabama	(U.S.A.)	Mar. '01
Prof. F. Wudl[*7]	Univ. of California	(U.S.A.)	Mar. '01
Prof. R. Superfine[*7]	Univ. of North Carolina	(U.S.A.)	Mar. '01
Prof. M. Kurmoo[*7]	Univ. of Strusburg	(France)	Mar. '01
Prof. Peter Day[*7]	Royal Institution of Great Britain	(U.K.)	Mar. '01
Prof. Dante Gatteschi[*7]	Univ. of Florence	(Italy)	Mar. '01
Prof. D. Allara[*7]	Pennsylvania State Univ.	(U.S.A.)	Mar. '01
Prof. H. Katz[*7]	Bell-Laboratories-Lucent Technologies	(U.S.A.)	Mar. '01
Prof. E. Coronado[*7]	Univ. of Valencia	(Spain)	Mar. '01
Prof. Patrick Cassoux[*7]	LCC-CNRS	(France)	Mar. '01
Dr. Benjamin Whitaker[*6]	Univ. of Leeds	(U.K.)	Mar.–Apr. '01
Prof. Yu-Jun Mo[*2*4]		(China)	–Apr. '01
Prof. Zhengqiang Li[*2*4]		(China)	–Apr. '01
Prof. Miller Roger[*7]	Univ. of North Carolina	(U.S.A.)	Apr. '01
Dr. Oleg I. Tolstikhin[*7]	Kurchatov Inst.	(Russia)	Apr. '01
Dr. Evgeni A. Solov'ev[*7]	Macedonian Academy of Sciences and Arts	(Macedonia)	Apr. '01
Dr. Claus Schulz[*7]	Max-Born Inst.	(Germany)	Apr. '01
Prof. Vladimir Osherov[*2]	Russian Academy of Sciences	(Russia)	Apr.–May '01
Prof. Rex Thomas Skodje[*2*4]	Univ. of Colorado	(U.S.A.)	Apr.–Dec. '01
Dr. Traian Dascalu[*7]	Inst. of Atomic Physics	(Rumania)	Apr. '01 –Mar. '02
Dr. Suyong Re[*5]	Rikkyo Univ.	(Japan)	Apr. '01 –Mar. '03
Dr. Yoong-Kee Choe[*6]	Univ. of Tokyo	(Japan)	Apr. '01 –Mar. '04
Prof. C. Dedonder-Kardeux[*7]	CNRS	(France)	May '01
Prof. Christoph Jouvet[*7]	CNRS	(France)	May '01
Prof. Henrik Kjaegaard[*7]	Univ. of Otago	(N. Z.)	May '01
Prof. Vincent Mckoy[*7]	Univ. of California	(U.S.A.)	May '01
Prof. Wolfgang Zinth[*7]	Ludwig-Maximilians-Univ.	(Germany)	May '01
Dr. Lawrence Ziegler[*7]	Boston Univ.	(U.S.A.)	May '01
Mr. Min-Chul Yoon[*7]	Yonsei Univ.	(Korea)	May '01
Mr. Jixin Yang[*7]	Univ. of Nottingham	(U.K.)	May '01
Prof. John Wright[*7]	Univ. of Wisconsin	(U.S.A.)	May '01
Prof. Wolfgang Werncke[*7]	Max Born Inst.	(Germany)	May '01
Prof. Gilbert Walker[*7]	Univ. of Pittsburgh	(U.S.A.)	May '01
Prof. Marten Vos[*7]	Ecole-Polytechnique-ENSTA	(France)	May '01
Prof. Costas Varotsis[*7]	Univ. of Crete	(Greece)	May '01
Prof. Siva Umapathy[*7]	Indian Inst. of Science	(India)	May '01
Prof. Michael Towrie[*7]	Rutherford Appleton Laboratory	(U.K.)	May '01
Prof. Andrei Tokmakoff[*7]	MIT	(U.S.A.)	May '01
Prof. James Terner[*7]	Virginia Commonwealth Univ.	(U.S.A.)	May '01
Prof. Friedrich Siebert[*7]	Albert-Ludwigs Univ.	(Germany)	May '01
Prof. Clarude Rulliere[*7]	Bordeaux I Univ.	(France)	May '01
Prof. Eberhard Riedle[*7]	Ludwig-Maximilians Univ.	(Germany)	May '01
Prof. David Phillips[*7]	Univ. of Hong Kong	(China)	May '01
Prof. Anthony Parker[*7]	Rutherford AppletonLaboratory	(U.K.)	May '01
Prof. Duohai Pan[*7]	Univ. of California	(U.S.A.)	May '01
Prof. Erik Nibbering[*7]	Max Born Inst.	(Germany)	May '01
Prof. Shaul Mukamel[*7]	Univ. of Rochester	(U.S.A.)	May '01
Mr. Alexander Mikhonin[*7]	Univ. of Pittsburgh	(U.S.A.)	May '01
Prof. Stephen Meech[*7]	Univ. of East Anglia	(U.K.)	May '01
Prof. John McGarvey[*7]	Queen's Univ. of Belfast	(U.K.)	May '01
Prof. Pavel Matousek[*7]	CLRC Rutherford Appleton Laboratory	(U.K.)	May '01
Prof. Tianquan Lian[*7]	Emory Univ.	(U.S.A.)	May '01
Prof. Steven Lewis[*7]	Univ. of Georgia	(U.S.A.)	May '01
Prof. Alfred Laubereau[*7]	Technische Univ. Muenchen	(Germany)	May '01
Prof. Robert Laenen[*7]	Technische Univ. Muenchen	(Germany)	May '01
Prof. Dongho Kim[*7]	Yonsei Univ.	(Korea)	May '01
Ms. Judy Kim[*7]	UC Berkeley	(U.S.A.)	May '01
Mr. Munira Khalil[*7]	Massachusetts Inst. of Technology	(U.S.A.)	May '01
Dr. Omar Sultan Jina[*7]	Univ. Park Nottingham	(U.K.)	May '01

Mr. Dae Hong Jeong[*7]	Yonsei Univ.	(Korea)	May '01
Prof. Thomas la Cour Jansen[*7]	Rijkssuniversiteit Groningen	(Holland)	May '01
Prof. Robin Hochstrasser[*7]	Univ. of Pennsylvania	(U.S.A.)	May '01
Prof. Edwin Heilweil[*7]	National Inst. of Standards and Technology	(U.S.A.)	May '01
Prof. Peter Hamm[*7]	Max Born Inst.	(Germany)	May '01
Prof. Terry Gustafson[*7]	Ohio State Univ.	(U.S.A.)	May '01
Prof. David Grills[*7]	Univ. Park Nottingham	(U.K.)	May '01
Prof. Keith Gordon[*7]	Univ. of Otago	(N.Z.)	May '01
Prof. Klause Gerwert[*7]	Ruhr-Universitat Boghum	(Germany)	May '01
Prof. Michael George[*7]	Univ. of Nottingham	(U.K.)	May '01
Prof. Henk Fidder[*7]	Uppsala Univ.	(Sweden)	May '01
Mr. Christopher Fecko[*7]	Massachusetts Inst. of Technology	(U.S.A.)	May '01
Ms. Joanne Dyer[*7]	Univ. of Nottingham	(U.K.)	May '01
Prof. Dana Dlott[*7]	Univ. of Illinois	(U.S.A.)	May '01
Prof. Jeffrey Cina[*7]	Univ. of Oregon	(U.S.A.)	May '01
Prof. Paul Champion[*7]	Northeastern Univ.	(U.S.A.)	May '01
Dr. Mike Carrabba[*7]	Chromex	(U.S.A.)	May '01
Prof. Mischa Bonn[*7]	Leiden Inst. of Chemistry	(Holland)	May '01
Prof. George Atkinson[*7]	Univ. of Arizona	(U.S.A.)	May '01
Prof. Sanford Asher[*7]	Univ. of Pittsburgh	(U.S.A.)	May '01
Prof. Andreas Albrecht[*7]	Cornell Univ.	(U.S.A.)	May '01
Dr. Peter Hamm[*7]	Max Born Inst.	(Germany)	May '01
Mr. Thomas La Cour Jansen[*7]	Groningen Univ.	(Germany)	May '01
Prof. Scott Anderson[*7]	Univ. of Utah	(U.S.A.)	May '01
Prof. Cornelis A. De Lange[*2]	Univ. of Amsterdam	(Holland)	May–Aug. '01
Dr. Sheng-Der Chao[*5]	Univ. of Colorado	(U.S.A.)	May–Dec. '01
Prof. Changshun Wang[*2*4]	Henan Univ.	(China)	May '01–Mar. '02
Dr. Viktor Gritsenko[*2*4]	Russian Academy of Sciences	(Russia)	–Jun. '01
Prof. Kwang Hyun Ahn[*6]	Kyung Hee Univ.	(Korea)	Jun. '01
Prof. Marcos Dantus[*7]	Michigan State Univ.	(U.S.A.)	Jun. '01
Prof. Myoung-Sik Cha[*7]	Pusan National Univ.	(Korea)	Jun.–Jul. '01
Prof. Anunay Samanta[*6]	Univ. of Hyderaband	(India)	Jul. '01
Prof. Mihir Chowdhury[*7]	Indian Association for the Cultivation of Sci.	(India)	Jul. '01
Prof. Kankan Bhattacharyya[*6]	Indian Association for the Cultivation of Sci.	(India)	Jul. '01
Prof. Michael Ashfold[*7]	Univ. of Bristol	(U.K.)	Jul. '01
Prof. Won Kweon Jang[*2]	Hanseo Univ.	(Korea)	Jun.–Aug. '01
Prof. Eok Kyun Lee[*2]	Korea Advanced Inst. of Sci. and Technology	(Korea)	Jun.–Aug. '01
Dr. Gennady Mil'nikov[*5]	Inst. of Structural Macrokinetics	(Russia)	Jun. '01–Mar. '02
Prof. Side Du[*2*4]	Fudan Univ.	(China)	Jun. '01–Apr. '02
Prof. Bin Zhang[*2*4]	Inst. of Chemistry Chinese Academy of Sci.	(China)	Jun. '01–May '02
Mr. Bodo Mayer[*5]	Darmstadt Univ. of Technology	(Germany)	Jul.–Aug. '01
Prof. Chun-Woo Lee[*6]	Ajou Univ.	(Korea)	Jul.–Aug. '01
Mr. Yong Hoon Kim[*6]	Yonsei Univ.	(Korea)	Aug. '01
Prof. John Dyke[*6]	Univ. of Southampton	(U.K.)	Aug. '01
Prof. Stanislav Nespurek[*6]	Inst. of Macromolecular	(Czech)	Aug. '01
Prof. James Lisy[*7]	Univ. of Illinois	(U.S.A.)	Aug. '01
Prof. Marek Janusz Wojcik[*7]	Jagiellonian Univ.	(Poland)	Aug. '01
Dr. Gennady Mil'nikov[*2]	Inst. of Structural Macrokinetics	(Russia)	Aug. '00–Mar. '01
Prof. Roman Sweitlik[*2*4]	Inst. of Molecular Phys. Polish Academy of Sci.	(Poland)	Aug. '01–Feb. '02

AWARDS

Professor Kaya's Scientific Achievements

Professor Koji Kaya, Director General of Institute for Molecular Science, received the Chemical Society of Japan Award in 2000 for his contribution to "Creation and Development of Cluster Chemistry—Composite Effects in Binary Components." Clusters, intermediate states of matter between the bulk and gas phases, have gained much attention recently as one of the key materials in nano-science. Professor Kaya has opened up new research field of cluster chemistry by focusing his attention on the composite effects observed in binary clusters. His scientific achievements relevant to the award are summarized as follows.

1) Investigation of electronic and geometrical structures of clusters of metal and semiconductor. He has developed a new diagnostics for the structures of the clusters based on extremely sensitive photoelectron spectroscopy and chemical doping method. One of the most important findings is that origin of photoluminescence from the semiconductor clusters is not due to the quantum size effects but to the surface oxide layers.

2) Production of novel organometallic clusters. Numbers of inorganic/organic hybrid clusters, having "sandwich" structures, have been prepared by laser vaporization of bulk metal in the presence of organic molecule. He has also developed a new method to deposit these novel clusters onto substrate without dissociation (soft landing method), which will be a powerful and promising technique to produce variety of cluster–assembled materials.

Professor Fumio Hirata

Professor Fumio Hirata of Department of Theoretical Studies won the Scientific Award of the Chemical Society of Japan in 2000 for his contributions to "Development of New Molecular Liquid Theory in Chemistry and Its Application." Professor Hirata's scientific achievements relevant to the award are summarized as follows:

1. Development of extended RISM theory.
   Although the original version of the reference interaction site model (RISM) theory enabled one to incorporate the effects of molecular geometry into the liquid theory, it was incomplete in the sense that it cannot deal with the electrostatic interactions. Professor Hirata extended the theory so that these interactions can be included. This is important because electrostatic interactions are essential in describing chemistry occuring in solution. His theory enabled researchers for the first time to study organic solvent, alcohol, and water in a quantitative manner.

2. Development of RISM-SCF theory.
   In quantum chemistry field the effects of solvent were usually included by continuum dielectric models. Professor Hirata developed the so-called RISM-SCF theory in which the effects of solvent on the electronic structure are incorporated by the RISM theory. The theory determines the electronic structures of solute and microscopic structures of solvent in a self-consistent manner.

3. Study of microscopic structures of liquid and its dynamics.
   Dynamics of liquid had been studied traditionally by spherical molecular models or those with embedded multipoles. Professor Hirata introduced the interaction-site description to liquid dynamics, which enables one to study dynamics of much more realistic system of chemical interests such as water and alcohol.

4. Study of electrode surface-solvent interactions and statistical mechanics of electrode reactions.
   Modern experimental techniques including STM, AFM, and SEIRAS have been revealing the electrode-solution interface in atomic detail, so that the current theories of electrode represented by the Gouy-Chapman double-layer theory is becoming senseless. By combining extended RISM, polymer RISM, and the density functional theory, Professor Hirata has been constructing a theory which is capable of exploring the electrode-solution interface in the same resolution as in the experimental methods. The theory allowed him to successfully study water structures near the electrode surfaces, electronic structures, and nonlinearity of charge transfer reactions.

5. Study of stability of biopolymers in solution and protein folding problem.
   Effects of solvent play an essential role in the stability of biopolymers in solution. Professor Hirata has been studying the elements of the stability from the physical-chemical viewpoint. In particular, he proposed to combine molecular simulations with extended RISM theory of solvation and also with extended scaled particle theory of solvation. He has given quantitative accounts of solvation effects on the stability of biomolecules as functions of tempearture, pressure, and ion concentration, etc. These studies give much information in the protein folding problem.

Professor Akasaka's Scientific Achievements

Professor Takeshi Akasaka, Department of Molecular Structure, received the Scientific Award of the Chemical Society of Japan in 2000 for his contribution to "Organic Chemistry of Fullerenes," and the Award of the Niigata Nippou in 2000 for his contribution to "Exohedral and Endohedral Chemistry of Fullerenes." Since the success of laboratory synthesis of C_{60} and other fullerenes, their chemical derivatives have been reported within a decade. Especially metallofullerenes (fullerenes with metal(s) inside the hollow spherical carbon cage) have interested people because of their possibilities of the free tune of "outside chemistry," and have been prepared and characterized. The electronic structure might reflect the chemical reactivity of metallofullerenes. Professor Akasaka has found a new photochemical exohedral derivatization of typical empty fullerenes such as C_{60} and C_{70} with disilirane. Moreover, he has found the chemical derivatization of endohedral metallofullerenes, La@C_{82} and Gd@C_{82} with disilirane. Recently he found that the anion of La@C_{82} had a unique stability toward air and water, and determined the molecular structure of the La@C_{82} anion by means of ^{13}C-NMR spectroscopy.

Professor Aida's Scientific Achievements

Professor Takuzo Aida (Department of Chemistry and Biotechnology, Graduate School of Engineering, The University of Tokyo), a visiting professor of Coordination Chemistry Laboratories (1999–2000), received "Nagoya Medal Seminar: Silver Medal Award 2000" and "Tokyo Techno Forum: Gold Medal Award 2001," for his outstanding contribution to "Design and Functions of Macromolecular and Supramolecular Materials." His scientific achievements relevant to these awards are summarized as follows.
1. Development of light-harvesting dendritic macromolecules and their nanoscopic photochemical and physical properties.
2. Development of a novel bioinspired fabrication of advanced polymeric materials by using mesoporous silicate materials.
3. Development of chirality-memory supramolecular systems for sensing asymmetric molecules.

Associate Professor Takasu's Scientific Achievements

Associate Professor Masako Takasu of Department of Applied Molecular Science received Molecular Simulation Award from the Molecular Simulation Society of Japan for her contribution to "Simulation of Quantum Systems in Random Media."
Her scientific achievements relevant to the award are summarized as follows.
1. Quantum calculations of electron in random media.
2. Simulation of superfluid transition of helium in random media.
This award is given annually to prospective scientists under 41 years old who made outstanding contribution in the area of molecular simulation.

Associate Professor Tahara's Scientific Achievements

Associate professor Tahei Tahara of Department of Vacuum UV Photoscience received the TRVS Outstanding Young Researcher Award (2001) for his contributions to "A new observation and a new method in time-resolved Raman spectroscopy." This award was given to the outstanding researchers who presented excellent scientific results in the 10th TRVS (Time-Resolved Vibrational Spectroscopy) international conference held at IMS in May, 21–25, 2001. In his invited talk, professor Tahara presented two new achievements in time-resolved Raman spectroscopy. First, he reported a picosecond Raman study of the local solvating structure around an electron injected in water (solvated electron). The solvated electron is the most fundamental ionic species in solution, and hence, the ultrafast dynamics has been extensively studied so far through time-resolved measurements of its electronic p ← s transition appearing in the near-infrared region. However, the local solvating structure cannot be unveiled by such an electronic spectroscopy. It is highly desirable to directly observe vibrational spectra of the water molecules that solvates the electron. He found that a transient Raman band appears in the OH bending region, when Raman spectra of water were measured under a probing condition resonant with the p ← s transition of the solvated electron. He successfully attributed the observed Raman signal to the solvating water molecules that strongly interact with the electron, and clarified the local structure of the water molecules in the solvation shell. The second topic was about the development of a new spectroscopic method for the study of low-frequency vibrations. In time-resolved Raman measurements using multichannel detectors, it is practically quite difficult to measure spectra in the low frequency region because of the disturbance of a strong Rayleigh scattering. In his efforts to overcome this difficulty, he has developed a novel method to study the low-frequency vibrations of short-lived transient species by

utilizing a time-domain Raman spectroscopy (impulsive stimulated Raman scattering, ISRS) as the probe process in time-resolved Raman measurements. Making the most use of this method, he recently succeeded in measuring ISRS signals of an excited-state polyatomic molecule in solution.

Associate Professor Mitsuke's Scientific Achievements

Associate professor Koichiro Mitsuke of Department of Vacuum UV Photoscience received the BCSJ Award of the Chemical Society of Japan in 2001 for his contribution entitled "UV and visible emission spectra from photodissociation of OCS using synchrotron radiation at 15–30 eV" published in the Bulletin of the Chemical Society of Japan. This work was fully accomplished at the UVSOR facility of IMS.

Professor Mitsuke has developed a new method of fluorescence spectroscopy by combining monochromatized undulator radiation with high sensitive imaging spectrograph. This method allows one to investigate various decay dynamics of transient superexcited states embedded in multiple dissociation continua. Professor Mitsuke has newly identified many electronic transitions and emission band systems arising from photodissociation of OCS. He has succeeded in presenting two powerful and complementary methods for gas-phase photoionization and photodissociation studies in the extreme UV region, *i.e.* two-dimensional photoelectron and fluorescence spectroscopies, both of which have been developed in the UVSOR facility.

Associate Professor Taira's Achievements

Associate professor Takunori Taira of Laser Research Center for Molecular Science received the promotion award of metal-structure photographs from the Japan Institute of Metal in 2001. This award was give to photographs of academic and technological excellence and the title of his award is "YAG ceramics for high-power laser oscillation." The award is shared with his collaborator, Dr. Ikesue of Japan Fine Ceramics Center, and their several-years achievements are widely accepted.

A cost effective and moldable ceramic material is inspiring into solid-state lasers emitting 1 µm wavelength although single crystal Nd:YAG is conventionally utilized in laser systems. Nd:YAG crystal is usually grown from liquid phase by the Cz method and growth speed is limited up to several mm/h to maintain crystal quality, which is an obstacle to low-cost and large-scale growth. It is

Highly Nd-Doped YAG Ceramic Microchip Laser

difficult to increase concentration of active Nd ions more than 1.4 at.% in the method because the crystal passes the liquid phase during growth. Low concentration is a drawback of single crystal Nd:YAG for achieving a microchip laser due to insufficient pump absorption. This is a main reason to use $Nd:YVO_4$ with high absorption coefficient in microchip lasers although it has low thermal conductivity.

Professor Taira and Dr. Ikesue have been pursuing a growth technique of Nd:YAG and discovered a sintering method for obtaining transparent ceramics with high Nd density, which lead to the first ceramic-based microchip laser. The figure shows a highly Nd-doped YAG ceramic microchip laser emitting 532 nm green light through wavelength conversion. This is a clear evidence of low scattering loss in laser materials allowing wavelength conversion even in a cavity. The ceramic technique will open the way to selective doping of active and saturable ions for integration of multifunctions.
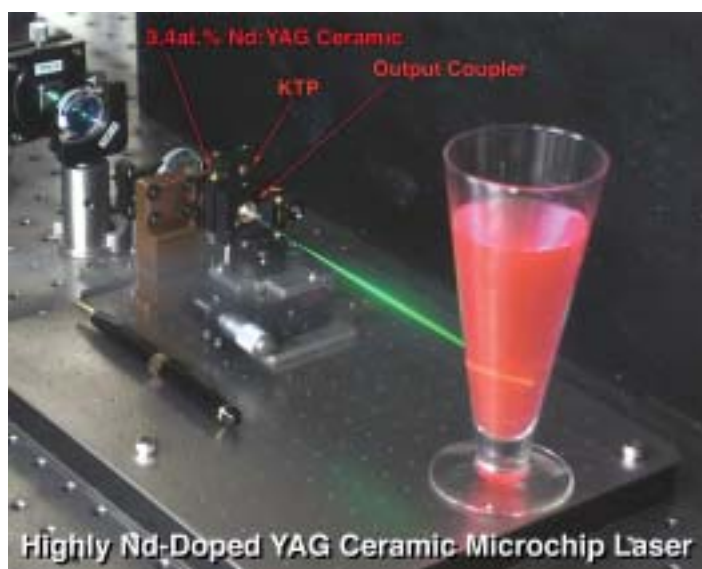
Associate Professor Iwata's Scientific Achievements

Associate professor Koichi Iwata, Department of Applied Molecular Science, received the Morino Science Award in 2000 for his contributions to "Development of time-resolved infrared and Raman spectroscopic methods and modeling of ultrafast reaction dynamics in solution." Time-resolved vibrational spectroscopy is very crucial for the study of the structure and dynamics of short-lived transient species. Professor Iwata has been making pioneering

contributions to the development of time-resolved vibrational spectrometers, such as a microsecond infrared spectrometer using a dispersive monochromator as well as a picosecond Raman spectrometer combined with a high-repetition-rate laser system. These spectrometers have enabled us to sensitively detect vibrational bands of the transient species, which is essential for the full elucidation of the chemical reaction dynamics. It can be said that these methods are now the most standard and popular system for the physicochemical study of the dynamical properties of molecules. Professor Iwata's achievements that have been made using these spectrometers are summarized as follows. (1) microsecond infrared study of the generation and annihilation dynamics of charged solitons in polyacetylene films, (2) picosecond Raman study of the vibrational cooling dynamics of S_1 *trans*-stilbene, which was then extended to (3) the elucidation of the solute-solvent energy transfer dynamics, (4) characterization of bimolecular reactions between aromatic compounds and solvent carbon tetrachloride by time-resolved infrared and visible absorption studies, and (5) modeling of the translational motion of solution-phase molecules in terms of the statistical diffusion in the picosecond time region.

Research Associate Mizutani's Scientific Achievement

Dr. Yasuhisa Mizutani, a research associate in Laboratory for Molecular Dynamics, Department of Molecular Structure, received the 17th Morino Science Award for his contribution to "Time-resolved Resonance Raman Studies of Photochemical Reactions in Solutions and Vibrational Energy Relaxation." Throughout his career he has been interested in structure and dynamics of complex systems such as liquids and proteins. When he joined IMS as a research associate, he decided to do some new experiments to answer a question, 'How do surrounding solvent molecules respond to a step-function like structural change of a solute molecule?' Practically, he planned to investigate the energy and structure relaxation of solute molecules using time-resolved vibrational spectroscopy, and started from the construction of a light source for measuring picosecond pump/probe time-resolved resonance Raman spectra with kiloheltz repetition in which the pump and probe wavelengths could be tuned independently. After a few years he succeeded in observing anti-Stokes time-resolved resonance Raman spectra of photodissociated carbonmonoxy myoglobin and unraveled the cooling dynamics of heme heated by photodissociation. The results were published in Science. Furthermore, he demonstrated that the expansion of porphyrin due to the low- to high-spin transition of iron occurs within 1 ps, but its out-of-plane movement and subsequent change of protein structures take place around ~10 ps and ~100 ps, respectively. On the other hand, he also investigated vibrational energy relaxation of metalloporphyrins in solutions and observed the vibrational energy redistribution process in a picosecond time regime. He pointed out the mode dependence of the vibrational relaxation for metalloporphyrins and heme proteins. Thus, he opened a new route to study molecular dynamics in solutions.

Dr. Hiroshi Noguchi's Scientific Achievements

Dr. Hiroshi Noguchi, a JSPS postdoctoral fellow in Takasu Group at the Department of Applied Molecular Science, received the Award for Encouragement of Research in Material Science in December 2000 for his contribution on "Electophoretic Behavior of Polyelectrolytes in Gel and Polymer Solutions."

This award is given to young scientists (under 36 years old) who made contribution in the area of material sciences and gave excellent presentation at the Annual Symposium of MRS-Japan.

LIST OF PUBLICATIONS

Department of Theoretical Studies

Y. SUGITA, A. KITAO and Y. OKAMOTO, "Multidimensional Replica-Exchange Method for Free-Energy Calculations," *J. Chem. Phys.* **113**, 6042 (2000).

Y. SUGITA and Y. OKAMOTO, "Replica-Exchange Multicanonical Algorithm and Multicanonical Replica-Exchange Method for Simulating Systems with Rough Energy Landscape," *Chem. Phys. Lett.* **329**, 261 (2000).

A. MITSUTAKE, M. KINOSHITA, Y. OKAMOTO and F. HIRATA, "Multicanonical Algorithm Combined with the RISM Theory for Simulating Peptides in Aqueous Solution," *Chem. Phys. Lett.* **329**, 295 (2000).

A. MITSUTAKE and Y. OKAMOTO, "Replica-Exchange Simulated Tempering Method for Simulations of Frustrated Systems," *Chem. Phys. Lett.* **332**, 131 (2000).

Y. ISHIKAWA, Y. SUGITA, T. NISHIKAWA and Y. OKAMOTO, "Ab Initio Replica-Exchange Monte Carlo Method for Cluster Studies," *Chem. Phys. Lett.* **333**, 199 (2001).

T. OKABE, M. KAWATA, Y. OKAMOTO and M. MIKAMI, "Replica-Exchange Monte Carlo Method for the Isobaric-Isothermal Ensemble," *Chem. Phys. Lett.* **335**, 435 (2001).

M. KINOSHITA, Y. OKAMOTO and F. HIRATA, "Solvent Effects on Conformational Stability of Peptides: RISM Analyses," *J. Mol. Liq.* **90**, 195 (2001).

T. YODA, M. SAITO, M. ARAI, K. HORII, K. TSUMOTO, M. MATSUSHIMA, I. KUMAGAI and K. KUWAJIMA, "Folding-Unfolding of Goat α-Lactalbumin Studied by Stopped-Flow Circular Dichroism and Molecular Dynamics Simulations," *Proteins: Struct., Funct., Genet.* **42**, 49 (2001).

K. NOBUSADA, H. NAKAMURA, Y. LIN and B. RAMACHANDRAN, "Quantum Reaction Dynamics of $O(^3P)$ + HCl on a New ab initio Potential Energy Surface," *J. Chem. Phys.* **113**, 1018 (2000).

K. NAGAYA, Y. TERANISHI and H. NAKAMURA, "Laser Control of Molecular Photodissociation with Use of the Complete Reflection Phenomenon," *J. Chem. Phys.* **113**, 6197 (2000).

Y. LIN, B. RAMACHANDRAN, K. NOBUSADA and H. NAKAMURA, "Quantum-Classical Correspondence in the $O(^3P)$ + HCl and $Cl(^2P)$+OH Reactions for Total Angular Momentum $J = 0$," *J. Chem. Phys.* **114**, 1549 (2001).

G. MIL'NIKOV, H. NAKAMURA and J. HORÁČEK, " Stable and Efficient Evaluation of Green's Function in Scattering." *Comput. Phys. Commun.* **135**, 278 (2001).

O. I. TOLSTIKHIN, V. N. OSTROVSKY and H. NAKAMURA, "Cumulative Reaction Probability and Reaction Eigenprobabilities from Time-Independent Quantum Scattering Theory," *Phys. Rev. A* **63**, 0402707 (2001).

V. I. OSHEROV and H. NAKAMURA, "Nonadiabatic Dynamics: Transitions between Asymptotically Degenerate States," *Phys. Rev. A* **63**, 052710 (2001).

C. ZHU, K. NOBUSADA and H. NAKAMURA, "New Implementation of the Trajectory Surface Hopping Method with Use of the Zhu-Nakamura Theory," *J. Chem. Phys.* **115**, 3031 (2001).

Y. TANIMURA and T. STEFFEN, "The Fifth and Seventh Order 2D Raman Spectroscopy for Harmonic System with Nonlinear System-Bath Interactions: Gaussian-Markovian Case," *J. Phys. Soc. Jpn.* **69**, 4095 (2000).

K. OKUMURA, D. M. JONAS and Y. TANIMURA, "Two-Dimensional Spectroscopy and the Harmonically Coupled Anharmonic Oscillators," *Chem. Phys.* **266**, 237 (2001).

T. KATO and Y. TANIMURA, "Multi-Dimensional Vibrational Spectroscopy Measured from Different Phase-Matching Conditions," *Chem. Phys. Lett.* **341**, 329 (2001).

Y. SUZUKI and Y. TANIMURA, "Quantum Theory of Two-Dimensional Rotator in a Dissipative Environment: Application to Infrared Spectroscopy," *J. Phys. Soc. Jpn.* **70**, 1167(2001).

Y. SUZUKI and Y. TANIMURA, "Nonequilibrium Initial Conditions of a Brownian Oscillator System Observed by Two-Dimensional Spectroscopy," *J. Chem. Phys.* **115**, 2267 (2001).

K. GOHDA, D. OHTA, A. KOZAKI, K. FUJIMORI, I. MORI and T. KIKUCHI, "Identification of Novel Potent Inhivitors for ATP-Phosphoribosyl Transferase Using Three-Dimensional Strcural Database Search Technique," *QSAR* **20**, 143 (2001).

H. YAJIMA, M. MORITA, M. HASHIMOTO, H. SASHIWA, T. KIKUCHI and T. ISHII, "Complex Formation of Chitosan with Iodine and Its Structure and Spectroscopic Properties—Molecular Assembly and Thermal Hysteresis Behavior," *Int. J. Thermodyn.* **22**, 1265 (2001).

S. OKADA, A. OSHIYAMA and S. SAITO, "Nearly Free Electron States in Carboon Nanotube Bundles," *Phys. Rev. B* **62**, 7634 (2000).

S. OKADA, S. SAITO and A. OSHIYAMA, "Energetics and Electronic Structures of Encapsulated C60 in a Carbon Nanotube," *Phys. Rev. Lett.* **86**, 3835 (2001).

S. OKADA, A. OSHIYAMA and S. SAITO, "Pressure and Orientation Effects on the Electronic Structure of Carbon Nanotube Bundles," *J. Phys. Soc. Jpn.* **70**, 2345 (2001).

K. KUWAMOTO and M. KINOSHITA, "Interaction between Solute Molecules in Medium Density Solvents," *Mol. Phys.* **98**, 725 (2000).

M. KINOSHITA, "Effects of a Trace Amount of Hydrophobic Molecules on Phase Transition for Water Confined between Hydrophobic Surfaces: Theoretical Results for Simple Models," *Chem. Phys. Lett.* **326**, 551 (2000).

M. YAMAMOTO, M. KINOSHITA and T. KAKIUCHI, "Structure of the Pt(111)/Liquid Interface: A First-Principles/RHNC Calculation," *Electrochim. Acta* **46**, 165 (2000).

M. KINOSHITA, "Long-Range Interaction between Hydrophilic Surfaces Immersed in a Hydrophobic Fluid Containing a Hydrophilic Component at Low Concentration," *Chem. Phys. Lett.* **333**, 217 (2001).

M. KINOSHITA and Y. SUGAI, "Methodology for Predicting Approximate Shape and Size Distribution of Micelles," *Stud. Surf. Sci. Catal.* **132**, 109 (2001).

M. KINOSHITA, Y. OKAMOTO and F. HIRATA, "Solvent Effects on Conformational Stability of Peptides: RISM Analyses," *J. Mol. Liq.* **90**, 195 (2001).

T. NAKABAYASHI, H. SATO, F. HIRATA and N. NISHI, "Theoretical Study on the Structures and Energies of Acetic Acid Dimers in Aqueous Solution," *J. Phys. Chem. A* **105**, 245 (2001).

A. SETHIA, S. MIURA and F. HIRATA, "Density Matrix and Eigenstates for an Excess Electron in Water," *J. Mol. Liq.* **90**, 225 (2001).

A. SETHIA, S. SANYAL and F. HIRATA, "Quantum Dynamics: Path Integral Approach to Time Correlation Functions in Finite Temperature," *J. Chem. Phys.* **114**, 5097 (2001).

A. KOVALENKO, F. HIRATA and M. KINOSHITA, "Hydration Structure and Stability of Met-enkephalin Studied by a Three-Dimensional Reference Interaction Site Model with a Repulsive Bridge Correction and a Thermodynamic Perturbation Method," *J. Chem. Phys.* **113**, 9830 (2000).

Y. HARANO, T. IMAI, A. KOVALENKO, M. KINOSHITA and F. HIRATA, "Theoretical Study for Partial Molar Volume of Amino Acids and Poly-Peptides by the Three-Dimensional Reference Interaction Site Model," *J. Chem. Phys.* **114**, 9506 (2001).

K. NISHIYAMA, F. HIRATA and T. OKADA, "Importance of Acoustic Solvent Mode and Solute-Solvent Radial Distribution Functions in Solvation Dynamics: Studied by RISM Theory," *J. Chin. Chem. Soc.* **47**, 837 (2000).

K. NISHIYAMA, F. HIRATA and T. OKADA, "Relaxation of Average Energy and Rearrangement of Solvent Shells in Various Polar Solvents in Connection with Solvation Dynamics: Studied by RISM Theory," *Chem. Phys. Lett.* **330**, 125 (2000).

K. NISHIYAMA, F. HIRATA and T. OKADA, "Nonlinear Response of Solvent Molecules Induced by Instantaneous Change of Solute Electronic Structure: Studied by RISM Theory," *J. Mol. Struct.* **565-566**, 31 (2001).

K. NISHIYAMA, F. HIRATA and T. OKADA, "Average Energy Relaxation and Rearrangement of Solute-Solvent Radial Distribution Function in Solvation Dynamics: A Connection between Spectroscopic Results and RISM Theory," *J. Mol. Liq.* **90**, 251 (2001).

A. KOVALENKO and F. HIRATA, "Self-Consistent, Kohn-Sham DFT and Three-Dimensional RISM Description of a Metal-Molecular Liquid Interface," *J. Mol. Liq.* **90**, 215 (2001).

A. KOVALENKO and T. N. TRUONG, "Thermochemistry of Solvation: A Self-Consistent Three-Dimensional Reference Interaction Site Model Approach," *J. Chem. Phys.* **113**, 7458 (2000).

J. KISHINE and K. YONEMITSU, "Interplay of Randomness, Electron Correlation, and Dimensionality Effects in Quasi-One-Dimensional Conductors," *Phys. Rev. B* **62**, 13323 (2000).

J. KISHINE, N. FURUKAWA and K. YONEMITSU, "Two-Loop Renormalization of the Quasiparticle Weight in Two-Dimensional Electron Systems," *Int. J. Mod. Phys. B* **15**, 1381 (2001).

K. YONEMITSU and J. KISHINE, "Charge Gap and Dimensional Crossovers in Quasi-One-Dimensional Organic Conductors," *J. Phys. Chem. Solids* **62**, 99 (2001).

J. KISHINE, "One- and Two-Band Hubbard Models in $d = 1 + \varepsilon$ Dimensions: Dimensionality Effects on the Charge and Spin Gap Phases," *J. Phys. Chem. Solids* **62**, 369 (2001).

M. MORI and K. YONEMITSU, "Anisotropic Collective Excitations around Various Charge Ordering States," *J. Phys. Chem. Solids* **62**, 409 (2001).

M. KUWABARA and K. YONEMITSU, "Charge Ordering and Lattice Modulation in MMX Chains," *J. Phys. Chem. Solids* **62**, 435 (2001).

Y. SHIMOI, M. KUWABARA and S. ABE, "Highly Doped Nondegenerate Conjugated Polymers: A Theory Using the DMRG Method," *Synth. Met.* **119**, 213 (2001).

K. YONEMITSU, "Intra- and Inter-Chain Dynamic Response Functions in Quasi-One-Dimensional Conductors," *Synth. Met.* **120**, 845 (2001).

M. MORI and K. YONEMITSU, "Stability and Cation Dependence of Magnetic Orders in $(Et_nMe_{4-n}Z)[Pd-(dmit)_2]_2$," *Synth. Met.* **120**, 945 (2001).

M. KUWABARA and K. YONEMITSU, "Charge Excitations in an Alternate Charge Polarization Phase of a One-Dimensional Two-Band Extended Peierls-Hubbard Model for MMX Chains," *Synth. Met.* **120**, 947 (2001).

J. KISHINE, P. A. LEE and X. G. WEN, "Staggered Local Density of States around the Vortex in Underdoped Cuprates," *Phys. Rev. Lett.* **86**, 5365 (2001).

Department of Molecular Structure

Y. MORIWAKI and N. MORITA, "Laser Spectroscopic Measurements of Fine Structure Changing Cross Sections of Ca^+ and Sr^+ Ions in Collisions with He Atoms," *J. Phys. B* **33**, 5099 (2000).

Y. MORIWAKI and N. MORITA, "Spectroscopic Studies on Yb^+ Ions in Liquid Helium," *Eur. Phys. J. D* **13**, 11 (2001).

B. KETZER, T. VON EGIDY, F. J. HARTMANN, C. MAIERL, R. POHL, J. EADES, E. WIDMANN, T. YAMAZAKI, M. KUMAKURA, N. MORITA, R. S. HAYANO, M. HORI, T. ISHIKAWA, H. A. TORII, I. SUGAI and D. HORVATH, "Collisional Quenching of Metastable States of Antiprotonic Helium by Hydrogen and Deuterium Molecules," *Eur. Phys. J. D* **13**, 305 (2001).

T. AKASAKA, T. WAKAHARA, S. NAGASE, K. KOBAYASHI, M. WAELCHLI, K. YAMAMOTO, M. KONDO, S. SHIRAKURA, Y. MAEDA, T. KATO, M. KAKO, Y. NAKADAIRA, X. GAO, E. Van CAEMELBECKE and K. M. KADISH, "Structural Determination of the $La@C_{82}$ Isomer," *J. Phys. Chem. B* **105**, 2971 (2001).

Y. KUBOZONO, T. TAKABAYASHI, S. KASHINO, M. KONDO, T. WAKAHARA, T. AKASAKA, K. KOBAYASHI, S. NAGASE, S. EMURA and K. YAMAMOTO, "Structure of $La_2@C_{80}$ Studied by La K-Edge XAFS," *Chem. Phys. Lett.* **335**, 163 (2001).

Y. SASAKI, M. FUJITSUKA, O. ITO, Y. MAEDA, T. WAKAHARA, T. AKASAKA, K. KOBAYASHI, S. NAGASE, M. KAKO and Y. NAKADAIRA, "Photoinduced Electron-Transfer Reactions between C_{60} and Cyclic Disiliranes," *Heterocycles* **54**, 777 (2001).

T. AKASAKA, Y. MAEDA, T. WAKAHARA, T. MIZUSHIMA, W. ANDO, M. WAELCHLI, T. SUZUKI, K. KOBAYASHI, S. NAGASE, M. KAKO, Y. NAKADAIRA, M. FUJITSUKA, O. ITO, Y. SASAKI, K. YAMAMOTO and T. ERATA, "First Photochemical Bis-Germylation of C_{60} with Digermirane," *Org. Lett.* **2**, 2671 (2000).

Y. MAEDA, R. SATO, T. WAKAHARA, M. OKAMURA, T. AKASAKA, M. FUJITSUKA, O. ITO, K. KOBAYASHI, S. NAGASE, M. KAKO, Y. NAKADAIRA and E. HORN, "C_{60}-Sensitized Bis-Silylation of Nitrile and Carbonyl Compounds with Disilirane," *J. Organomet. Chem.* **611**, 414 (2000).

T. WAKAHARA, T. KONDO, M. OKAMURA, T. AKASAKA, Y. HAMADA, T. SUZUKI, M. KAKO and Y. NAKADAIRA, "Photochemical Bis-Silylation of C_{60}: Synthesis of a C_{60} Main Chain Polysilane," *J. Organomet. Chem.* **611**, 78 (2000).

Y. SASAKI, T. KONISHI, M. FUJITSUKA, O. ITO, Y. MAEDA, T. WAKAHARA, T. AKASAKA, M. KAKO and Y. NAKADAIRA, "Photoinduced Electron-Transfer Reaction between C_{60} and Cyclic Silicon Compounds," *J. Organomet. Chem.* **599**, 216 (2000).

K. OZAWA, T. MEIKARI, K. MOTOHASHI, M. YOSHIDA and H. AKUTSU, "Evidence for the Presence of F-Type ATPsynthase Involved in Sulfate-Respiration in *Desulfovibrio vulgaris*," *J. Bacteriol.* **182**, 2200 (2000).

T. FUJIWARA, P. KHANDELWAL and H. AKUTSU, "Compound Radio-Frequency Driven Recoupling Pulse Sequences for Efficient Magnetization Transfer by Homonuclear Dipolar Interaction under Magic Angle Spinning Conditions," *J. Magn. Reson.* **145**, 73 (2000).

K. OZAWA, A. TSAPIN, K. H. NEALSON, M. A. CUSANOVICH and H. AKUTSU, "Expression of a Tetraheme Protein, *Desulfovibrio vulgaris* Miyazaki F Cytochrome c_3, in *Shewanella oneidensys* MR-1," *Appl. Environ. Microbiol.* **66**, 4168 (2000).

K. OZAWA, F. YASUKAWA, Y. FUJIWARA and H. AKUTSU, "A Simple, Rapid, HIghly Efficient Gene Expression System for Multiheme Cytochrome *c*," *Biosci., Biotechnol., Biochem.* **65**, 185 (2001).

L. YU, T. ISHIDA, K. OZAWA, H. AKUTSU and K. HORIIKE, "Purification and Characterization of Homo- and Hetero-Dimeric Acetate Kinases from the Sulfate-Reducing Bacterium *Desulfovibrio vulgaris*," *J. Biochem.* **129**, 411 (2001).

C. NAKAMURA, K. NODA, N. A. ZORIN, H. AKUTSU and J. MIYAKE, "Cytochrome c_3-Langmuir Blodgett Film for Hydrogen Evolving Device," *Synth. Met.* **117**, 285 (2001).

A. I. TSAPIN, I. VANDENBERGHE, K. H. NEALSON, J. H. SCOTT, T. E. MEYER, M. A. CUSANOVICH, E. HARADA, T. KAIZU, H. AKUTSU, D. LEYS and J. J. VAN BEEUMEN, "Identification of a Small Tetraheme Cytochrome *c* and a Flavocytochrome *c* as Two of the Principal Soluble Cytochromes *c* in *Shewanella Oneidensis* Strain MR1," *Appl. Environ. Microbiol.* **67**, 3236 (2001).

T. AKASAKA, T. WAKAHARA, S. NAGASE, K. KOBAYASHI, M. WAELCHLI, K. YAMAMOTO, M. KONDO, S. SHIRAKURA, S. OKUBO, Y. MAEDA, T. KATO, M. KAKO, Y. NAKDAIRA, R. NAGAHATA, X. GAO, E. VAN CAEMELBECKE and K. M. KADISH, "$La@C_{82}$ Anion. An Unusually Stable Metallofullerene," *J. Am. Chem. Soc.* **122**, 9316 (2000).

M. KUMAGAI, H. KANAMORI, M. MATSUSHITA and T. KATO, "Quasimicrowave Spectroscopy of Nonpolar Diatomic Molecules by Using Optical Phase-Locked Lasers," *J. Chem. Phys.* **113**, 7031 (2000).

N. HAYASHI and T. KATO, "Investigations of Orientational Order for an Antiferroelectric Liquid Crystal by Polarized Raman Scattering Measurements," *Phys. Rev. E* **63**, 021706 (2001).

T. AKASAKA, T. WAKAHARA, S. NAGASE, K. KOBAYASHI, M. WAELCHLI, K. YAMAMOTO, M.

KONDO, S. SHIRAKURA, Y. MAEDA, T. KATO, M. KAKO, Y. NAKDAIRA, X. GAO, E. VAN CAEMELBECKE and K. M. KADISH, "Structure Determination of the La@C_{82} Isomer," *J. Phys. Chem. B* **105**, 2971 (2001).

C. YAMAMOTO, T. HAYASHI, Y. OKAMOTO, S. OKUBO and T. KATO, "Direct Resolution of C_{76} Enantiomers by HPLC Using an Amylose-Based Chiral Stationary Phase," *Chem. Commun.* 925 (2001).

N. HAYASHI, T. KATO, T. AOKI, T. ANDO, A. FUKUDA and S.-S. SEOMUN, "Probable Langevin-Like Director Reorientation in an Interface-Induced Disordered SmC*-Like State of Liquid Crystals Characterized by Frustration between Ferro- and Antiferro-Electricity," *Phys. Rev. Lett.* **87**, 015701 (2001).

Department of Electronic Structure

Y. KODAMA, T. NAKABAYASHI, K. SEGAWA, E. HATTORI, M. SAKURAGI, N. NISHI and H. SAKURAGI, "Time-Resolved Absorption Studies on the Photochromic Process of 2H-Benzopyrans in the Picosecond to Submillisecond Time-Domain," *J. Phys. Chem. A* **104**, 11478 (2000).

T. NAKABAYASHI, H. SATO, F. HIRATA and N. NISHI, "Theoretical Study on the Structures and Energies of Acetic Acid Dimers in Aqueous Solution," *J. Phys. Chem. A* **105**, 245 (2001).

K. KOSUGI, Y. INOKUCHI and N. NISHI, "Charge Transfer Interaction in the Acetic Acid-Benzene Cation Complex," *J. Chem. Phys.* **114**, 4805 (2001).

Y. INOKUCHI and N. NISHI, "Photodissociation Spectroscopy of Benzene Cluster Ions in Ultraviolet and Infrared Regions: Static and Dynamic Behavior of Positive Charge in Cluster Ions," *J. Chem. Phys.* **114**, 7059 (2001).

T. NAKABAYASHI, S. KAMO, H. SAKURAGI and N. NISHI, "Time-Resolved Raman Studies of Photoionization of Aromatic Compounds in Polar Solvents: Picosecond Relaxation Dynamics of Aromatic Cation Radicals," *J. Phys. Chem. A* **105**, 8605 (2001).

M. SAEKI, T. TSUKUDA and T. NAGATA, "Ab initio Study of $(CO_2)_n^-$: Structures and Stabilities of Isomers," *Chem. Phys. Lett.* **340**, 376 (2001).

K. SUZUKI, Y. EMURA, S. ISHIUCHI and M. FUJII, "Internal Methyl Group Rotation in o-Cresol Studied by Pulsed Field Ionization - ZEKE Photoelectron Spectroscopy," *J. Electron Spectrosc.* **108**, 13 (2000).

K. SUZUKI, S. ISHIUCHI and M. FUJII, "Pulsed Field Ionization - ZEKE Spectroscopy of Cresoles and Their Aqueous Complex: Internal Rotation of Methyl Group and Intermolecular Vibrations," *Faraday Discuss.* **115**, 229 (2000).

K. TAKAZAWA and M. FUJII, "Butterfly Vibration of the Tetrafluorobenzene Cation Studied by Pulsed Field Ionization-ZEKE Photoelectron Spectroscopy," *J. Electron Spectrosc.* **112**, 241 (2000).

M. MITSUI, Y. OHSHIMA, S. ISHIUCHI, M. SAKAI and M. FUJII, "Structure and Dynamics of 9(10H)-Acridone and Its Hydrated Clusters. II. Structural Characterization of Hydrogen-Bonding Networks," *J. Phys. Chem. A* **104**, 8649 (2000).

K. SAKOTA, N. YAMAMOTO, K. OHASHI, H. SEKIYA, M. SAEKI, S. ISHIUCHI, M. SAKAI and M. FUJII, "Electronic and Infrared Spectra of Jet-Cooled 4-Aminiobenzonitrile-H_2O. Change of NH_2 from Proton Acceptor to Proton Donor by CN Substitution," *Chem. Phys. Lett.* **341**, 70 (2001).

M. TSUBOUCHI, B. J. WHITAKER, L. WANG, H. KOHGUCHI and T. SUZUKI, "Photoelectron Imaging on Time-Dependent Molecular Alignment Created by a Femtosecond Laser Pulse," *Phys. Rev. Lett.* **86**, 4500 (2001).

H. KOHGUCHI, T. SUZUKI and M. H. ALEXANDER, "Fully State-Resolved Differential Cross Sections for the Inelastic Scattering of the Open-Shell NO Molecule by Ar," *Science* **294**, 832 (2001).

J. K. SONG, M. TSUBOUCHI and T. SUZUKI, "Femtosecond Photoelectron Imaging on Pyrazine: Spectroscopy of 3s and 3p Rydberg States," *J. Chem. Phys.* **115**, 8810 (2001).

B. BOTAR, T. YAMASE and E. ISHIKAWA, "A Highly Nuclear Vanadium-containing Tungstobismutate: Synthesis and Crystal Structure of $K_{11}H[(BiW_9O_{33})_3Bi_6(OH)_3(H_2O)_3V_4O_{10}]\cdot28H_2O$," *Inorg. Chem. Commun.* **3**, 578 (2000).

T. YAMASE and E. ISHIKAWA, "Photochemical Self-Assembly Reaction of β-$[Mo_8O_{26}]^{4-}$ to Mixed-Valence Cluster $[Mo_{37}O_{112}]^{26-}$ in Aqueous Media," *Langmuir* **16**, 9023 (2000).

T. YAMASE, H. MAKINO, H. NARUKE and A. M. S. JOSÉ WÉRY, "A Spherical Potassium-Capped Vanadium Methylphosphonate as Another ε-Keggin Fragment, $[H_6KV_{12}O_{27}(VO_4)(PO_3CH_3)_3]^{5-}$," *Chem. Lett.* 1350 (2000).

T. YAMASE, B. BOTAR, E. ISHIKAWA and K. FUKAYA, "Chemical Structure and Intramolecular Spin-Exchange Interaction of $[(VO)_3(SbW_9O_{33})_2]^{12-}$," *Chem. Lett.* 56 (2001).

H. NARUKE and T. YAMASE, "Synthesis and Structure of $Ln(W_5O_{18})$-Capped Mixed-Ligand Polyoxotungsto-lanthanoate $[Ln(W_5O_{18})\{Ln(H_2O)_2(SbW_9O_{33})(W_5O_{18})\}]^{15-}$ (Ln = Sm and Er)," *Bull. Chem. Soc. Jpn.* **74**, 1289 (2001).

L. YANG, C. HU, H. NARUKE and T. YAMASE, "Three-Dimensional Inorganic/Organic Hybrid Material, $[Ni_2-(4,4'-bipy)_3(H_2O)_2V_4O_{12}]\cdot2.5H_2O$," *Acta Crystallogr., Sect. C: Cryst. Struct. Commun.* **57**, 799 (2001).

M. MITSUI and Y. OHSHIMA, "Structure and Dynamics of 9(10H)-Acridone and Its Hydrated Clusters. I. Electronic Spectroscopy," *J. Phys. Chem. A* **104**, 8638 (2000).

M. MITSUI, Y. OHSHIMA, S. ISHIUCHI, M. SAKAI and M. FUJII, "Structure and Dynamics of 9(10H)-Acridone and Its Hydrated Clusters. II. Structural Characterization of Hydrogen-Bonding Networks," *J. Phys. Chem. A* **104**, 8649 (2000).

M. MITSUI, Y. OHSHIMA and O. KAJIMOTO, "Structure and Dynamics of 9(10H)-Acridone and Its Hydrated Clusters. III. Microscopic Solvation Effects on Nonradiative Dynamics," *J. Phys. Chem. A* **104**, 8660 (2000).

T. IIMORI and Y. OHSHIMA, "Size Reassignments of the S_1–S_0 Vibronic Spectra of Benzene Clusters," *J. Chem. Phys.* **114**, 2867 (2001).

K. EGASHIRA, Y. OHSHIMA and O. KAJIMOTO, "Structural Characterization of 9-Cyanoanthracene–(Ar)$_n$ (n = 0–3) by Rotational Coherence Spectroscopy," *J. Phys. Chem. A* **105**, 1131 (2001).

K. EGASHIRA, Y. OHSHIMA and O. KAJIMOTO, "Structural Characterization of 9-Cyanoanthracene–Water by Rotational Coherence Spectroscopy," *Chem. Phys. Lett.* **334**, 285 (2001).

K. EGASHIRA, Y. OHSHIMA and O. KAJIMOTO, "Structural Characterization of 1:1 van der Waals Complexes of 9-Cyanoanthracene with Aprotic Solvents by Rotational Coherence Spectroscopy," *J. Phys. Chem. A* **105**, 4781 (2001).

Department of Molecular Assemblies

L. V. ZORINA, S. S. KHASANOV, R. P. SHIBAEVA, M. GENER, R. ROUSSEAU, E. CANADELL, L. A. KUSHCH, E. B. YAGUBSKII, O. O. DROZDOVA and K. YAKUSHI, "A New Stable Organic Metal Based on the BEDO-TTF Donor and the Doubly Charged Nitroprusside Anion, (BEDO-TTF)$_4$[Fe(CN)$_5$NO]," *J. Mater. Chem.* **10**, 2017 (2000).

K. TAKEDA, I. SHROTANI, C. SEKINE and K. YAKUSHI, "Metal to Insulator Transition of One-Dimensional Bis(1,2-benzoquinonedioximato) Platinum(II), Pt(bqd)$_2$, at Low Temperatures and High Pressures," *J. Phys.: Condens. Matter* **12**, L483 (2000).

M. URUICHI, Y. YAMASHITA and K. YAKUSHI, "Optical Properties and Metal-Insulator Transitions in (BEDT-ATD)$_2$X(solvent) (X = PF$_6$, AsF$_6$, BF$_4$; solvent = THF, DHF, DO) [BEDT-ATD= 4,11-bis(4',5'-ethylene-dithio-1',3'-dithiole-2'-ylidene)-4,11- dihydroanthra[2,3-c][1,2,5] thiadiazole]," *J. Mater. Chem.* **10**, 2716 (2000).

J. OUYANG, K. YAKUSHI, Y. MISAKI and K. TANAKA, "Raman Spectroscopic Evidence for the Charge Disproportionation in a Quasi-Two-Dimensional Organic Conductor θ-(BDT-TTP)$_2$Cu(NCS)$_2$," *Phys. Rev. B* **63**, 54301 (2001).

M. SIMONYAN, Y. YONEHARA, Y. DING and K. YAKUSHI, "Hyperfine Structure and Exchange Coupling between Local and Itinerant Magnetic Moments in Quasi-One-Dimensional Organic Metal Co$_{0.01}$Ni$_{0.99}$Pc(AsF$_6$)$_{0.5}$," *Phys. Rev. B* **63**, 113103 (2001).

Y. HARUYAMA, T. KINOSHITA, K. TAKIMIYA, T. OTSUBO, C. NAKANO and K. YAKUSHI, "Electronic Structures of Organic Salt DMTSA-BF$_4$ Using Photoelectron Spectromicroscopy," *J. Electron Spectrosc.* **114-116**, 1013 (2001).

M. J. KONSTANTINOVIC, J. DONG, M. E. ZIAEI, B. P. CLAYMAN, J. C. IRWIN, K. YAKUSHI, M. ISOBE and Y. UEDA, "Charge Ordering and Optical Transitions of Li$_2$VO$_5$ and NaV$_2$O$_5$," *Phys. Rev B* **63**, 121102 (2001).

L. MARTIN, S. S. TURNER, P. DAY, P. GUIONNEAU, J. A. K. HOWARD, D. E. HIBBS, M. E. LIGHT, M. B. HURSTHOUSE, M. URUICHI and K. YAKUSHI, "Crystal Chemistry and Physical Properties of Superconducting and Semiconducting Charge Transfer Salts of the Type (BEDT-TTF)$_4$[A^{I}M^{III}(C$_2$O$_4$)$_3$]·PhCN (A^I = H$_3$O, NH$_4$, K; M^{III} = Cr, Fe, Co, Al; BEDT-TTF =Bis(ethylenedithio) tetrathiafulvalene)," *Inorg. Chem.* **40**, 1363 (2001).

S. HASEGAWA, T. HORIGOME, K. YAKUSHI, H. INOKUCHI, K. OKUDAIRA-KAMIYA, N. UENO, K. SEKI, R. J. WILLICUT, R. L. McCARLEY, E. MORIKAWA and V. SAILE, "Angle-Resolved Photoemission Measurements of ω-(*n*-pyrrolyl)alkanethiol Self-Assembled Monolayers Using in-situ Sample Preparation Apparatus," *J. Electron Spectrosc.* **113**, 101 (2001).

Y. DING, M. SIMONYAN, Y. YONEHARA, M. URUICHI and K. YAKUSHI, "Preparation and Characterization of Organic Alloy Co$_x$Ni$_{1-x}$Pc(AsF$_6$)$_{0.5}$ ($0 \leq x \leq 1$)," *J. Mater. Chem.* **11**, 1469 (2001).

J. ULANSKI, K. YAKUSHI, H. YAMOCHI and G. SAITO, "Observation of Plasmons in 2-D Organic Metal BO$_{2.4}$I$_3$ by Reflection Spectroscopy," *Synth. Met.* **120**, 721 (2001).

K. YAMAMOTO and K. YAKUSHI, "Electronic Ground State of θ-(BEDT-TTF)$_2$RbZn(SCN)$_4$ Studied by Raman Spectroscopy," *Synth. Met.* **120**, 791 (2001).

J. OUYANG, K. YAKUSHI, Y. MISAKI and K. TANAKA, "Phase Transition of θ-(BDT-TTP)$_2$Cu(NCS)$_2$," *Synth. Met.* **120**, 843 (2001).

O. DROZDOVA, H. YAMOCHI, K. YAKUSHI, M. URUICHI, S. HORIUCHI and G. SAITO, "Raman Spectroscopy as a Method of Determination of the Charge on BO in Its Complexes," *Synth. Met.* **120**, 721 (2001).

T. YAMAMOTO, H. HANASAKI, J. YAMAURA, S. AONUMA, H. TAJIMA, K. YAKUSHI, M. URUICHI and R. KATO, "Phase Diagrams of (DMe-DCNQI)$_2$Li$_{1-x}$Cu$_x$ System," *Synth. Met.* **120**, 873 (2001).

T. KAMBE, N. FUJIMURA, Y. NOGAMI, K. OSHIMA, K. YAKUSHI, J. DONG, K. TAKIMIYA and T. OTSUBO, "Low Temperature X-Ray and ESR Study of Quasi-1D DMT*C*A-BF$_4$ (*C* = S, Se) with Half-Filled

Band," *Synth. Met.* **120**, 931 (2001).

O. DROZDOVA, G. SAITO, H. YAMOCHI, K. OOKUBO, K. YAKUSHI, M. URUICHI and L. OUAHAB, "Composition and Structure of the Anion Layer in the Organic Superconductor κ'-(ET)$_2$Cu$_2$(CN)$_3$: Optical Study," *Inorg. Chem.* **40**, 3265 (2001).

N. MATSUNAGA, K. NOMURA, T. NAKAMURA, T. TAKAHASHI, G. SAITO, S. TAKASAKI, J. YAMADA, S. NAKATSUJI and H. ANZAI, "Static Magnetic Susceptibility in (TMTTF)$_2$Br and (TMTSF)$_2$-AsF$_6$," *Physica B* **284-288**, 1583 (2000).

Y. MISAKI, T. KAIBUKI, M. TANIGUCHI, K. TANAKA, T. KAWAMOTO, T. MORI and T. NAKAMURA, "A Novel Organic Conductor with Three-Dimensional Molecular Array: (TM-TPDS)$_2$AsF$_6$," *Chem. Lett.* 1274 (2000).

T. NAKAMURA, "Possible Successive SDW Transition in (EDT-TTF)$_2$AuBr$_2$," *J. Phys. Soc. Jpn.* **69**, 4026 (2000).

T. NAKAMURA, "Low-Temperature Electronic States in (EDT-TTF)$_2$AuBr$_2$," *J. Phys. Chem. Solids* **62**, 381 (2001).

R. CHIBA, H. YAMOAMOTO, K. HIRAKI, T. TAKAHASHI and T. NAKAMURA, "Charge Disproportionation in (BEDT-TTF)$_2$RbZn(SCN)$_4$," *J. Phys. Chem. Solids* **62**, 389 (2001).

Y. TAKANO, K. HIRAKI, H.M. YAMAMOTO, T. NAKAMURA and T. TAKAHASHI, "Charge Disproportionation in the Organic Conductor, α-(BEDT-TTF)$_2$I$_3$," *J. Phys. Chem. Solids* **62**, 393 (2001).

K. NOMURA, N. MATSUNAGA, A. ISHIKAWA, H. KOTANI, K. YAMASHITA, T. SASAKI, T. HANAJIRI, J. YAMADA, S. NAKATSUJI, H. ANZAI, T. NAKAMURA, T. TAKAHASHI and G. SAITO, "Spin Density Wave in Quasi-One-Dimensional Organic Conductors," *Phys. Status Solidi B* **223**, 449 (2001).

A. ISHIKAWA, N. MATSUNAGA, K. NOMURA, T. NAKAMURA, T. TAKAHASHI and G. SAITO, "Pressure and Magnetic Field Dependence of SDW Transition in (TMTTF)$_2$Br," *Phys. Status Solidi B* **223**, 539 (2001).

T. NAKAMURA, "Observation of SDW Sub-Phase in Q1D 1/4-Filled System, (EDT-TTF)$_2$AuBr$_2$," *Synth. Met.* **120**, 831 (2001).

H. TSUKADA, T. NAKAMURA, Y. MISAKI and K. TANAKA, "Magnetic Investigation of Organic Conductors Based on TTP Derivatives," *Synth. Met.* **120**, 869 (2001).

H. OHTA, T. SAKURAI, S. OKUBO, R. KATO and T. NAKAMURA, "High Field ESR Measurements of Me$_4$As[Pd(dmit)$_2$]$_2$," *Synth. Met.* **120**, 891 (2001).

A. ISHIKAWA, N. MATSUNAGA, K. NOMURA, T. NAKAMURA, T. TAKAHASHI and G. SAITO, "Pressure Dependence of the SDW Transition in (TMTTF)$_2$Br," *Synth. Met.* **120**, 905 (2001).

R. CHIBA, H. YAMAMOTO, K. HIRAKI, T. TAKAHASHI and T. NAKAMURA, "Charge Ordering in θ-(BEDT-TTF)$_2$RbZn(SCN)$_4$," *Synth. Met.* **120**, 919 (2001).

Y. TAKANO, K. HIRAKI, T. TAKAHASHI, H. YAMAMOTO and T. NAKAMURA, "Charge Ordering in α-(BEDT-TTF)$_2$I$_3$," *Synth. Met.* **120**, 1081 (2001).

B. NARYMBETOV, A. OMERTZU, M. TOKUMOTO, H. KOBYASHI and D. MIHAILOVIC, "Origin of Ferromagnetic Exchange Interactions in a Fullerene—Organic Compound," *Nature* **407**, 883 (2000).

H. MORI, N. SAKURAI, S. TANAKA, H. MORIYAMA, T. MORI, H. KOBAYASHI and A. KOBAYASHI, "Control of Electronic State by Dihedral Angle in θ-Type Bis(ethylenedithio)-Tetraselenafulvalene Salts," *Chem. Mater.* **12**, 2984 (2000).

D. ZHANG, K. ANDRES, Ch. PROST, W. BIEBERACHER, N. D. KUSH and H. KOBAYASHI, "Indication for an Antiferromagnetically Ordered state in the Organic Conductor, κ-(BETS)$_2$FeCl$_4$," *Solid State Commun.* **115**, 433 (2000).

H. TANAKA, H. KOBAYASHI, A. KOBAYASHI and P. CASSOUX, "Superconductivity, Antiferromagnetism and Phase Diagram of a Series of Organic Conductor, λ-(BETS)$_2$Fe$_x$Ga$_{1-x}$Br$_y$Cl$_{4-y}$," *Adv. Mater.* **12**, 1685 (2000).

L. BALICAS, J. S. BROOKS, K. STORR, D. GRAF, S. UJI, H. SHINAGAWA, E. OJIMA, H. FUJIWARA, H. KOBAYASHI, A. KOBAYASHI and M. TOKUMOTO, "Shubnikov-de Haas Effect and Yamaji Oscillations in the Antiferromagnetically Ordered Organic Superconductor κ-(BETS)$_2$FeBr$_4$: A Fermiology Study," *J. Solid State Commun.* **116**, 557 (2000).

H. TANAKA, Y. OKANO, H. KOBAYASHI, W. SUZUKI and A. KOBAYASHI, "A Three-Dimensional Synthetic Metallic Crystal Composed of Single Component Molecules," *Science* **291**, 285 (2001).

H. FUJIWARA, E. FUJIWARA, Y. NAKAZAWA, B. Zh. NARYMBETOV, K. KATO, H. KOBAYASHI, A. KOBAYASHI, M. TOKUMOTO and P. CASSOUX, "A Novel Antiferromagnetic Organic Superconductor κ-(BETS)$_2$FeBr$_4$ [where BETS = bis(ethylenedithio)tetraselenafulvalene], *J. Am. Chem. Soc.* **123**, 306 (2001).

B. Zh. NARYMBETOV, E. CANADELL, T. TOGONIDEZE, S. S. KHASANOV, L. V. ZORINA, R. P. SHIBAEVA and H. KOBAYASHI, "First-Order Phase Transition in the Organic Metal κ-(BETS)$_2$C(CN)$_3$," *J. Mater. Chem.* **11**, 332 (2001).

S. UJI, H. SHINAGAWA, T. TERASHIMA, C. TERAKURA, T. YAKABE, Y. TERAI, M. TOKUMOTO, A. KOBAYASHI, H. TAKAKA and H. KOBAYASHI, "Magnetic Field Induced Superconductivity in Two-dimensional Conductor," *Nature* **410**, 908 (2001).

T. OTSUKA, A. KOBAYASHI, Y. MIYAMOTO, J. KIUCHI, S. NAKAMURA, N. WADA, E. FUJIWARA,

H. FUJIWARA and H. KOBAYASHI, "Organic Antiferromagnetic Metals Exhibiting Superconducting Transitions κ-(BETS)$_2$FeX$_4$ (X = Cl, Br): Drastic Effect of Halogen Substitution on the Successive Phase Transitions," *J. Solid State Chem.* **159**, 407 (2001).

T. ADACHI, T. TANAKA, H. KOBAYASHI and T. MIYAZAKI, "Electrical Resistivity Measurements on Fragile Organic Single Crystals in the Diamond Anvil Cell," *Rev. Sci. Instrum.* **72**, 2358 (2001).

A. KOBAYASHI, H. TANAKA and H. KOBAYASHI, "Molecular Design and Development of Single-Component Molecular Metals," (Feature Article) *J. Mater. Chem.* **11**, 2078 (2001).

S. UJI, H. SHINAGAWA, T. TERAI, T. YAKABE, C. TERAKURA, T. TERASHIMA, L. BALICAS, J. S. BROOKS, E. OJIMA, H. FUJIWARA, H. KOBAYASHI, A. KOBAYASHI and M. TOUMOTO, "Fermi Surface Studies in the Magnetic-Field-induced Superconductor λ-(BETS)$_2$FeCl$_4$," *Phys. Rev. B* **64**, 024531-1 (2001).

L. BALICAS, J. S. BROOKS, K. STOORR, S. UJI, M. TOKUMOTO, H. TANAKA, H. KOBAYASHI, A. KOBAYASHI, V. BARZYKIN and L. P. GORKOV, "Superconductivity in an Organic Insulator at Very High Magnetic Field," *Phys. Rev. Lett.* **87**, 067002-1 (2001).

S. UJI, H. SHINAGAWA, Y. TERAI, T. YAKABE, C. TERAKURA, T. TERASHIMA, L. BALICAS, J. S. BROOKS, E. OJIMA, H. FUJIWARA, H. KOBAYASHI, A. KOBAYASHI and M. TOKUMOTO, "Two-Dimensional Fermi Surface for the Organic Conductor κ-(BETS)$_2$FeBr$_4$," *Physica B* **298**, 557 (2001).

H. KOBAYASHI, H. TANAKA, E. OJIMA, H. FUJIWARA, T. OTSUKA, A. KOBAYASHI, M. TOKUMOTO and P. CASSOUX, "Coexistence of Magnetic Order and Superconductivity in Organic Conductors," *Polyhedron* **20**, 1587 (2001).

H. KOBAYASHI, H. TANAKA, E. OJIMA, H. FUJIWARA, Y. NAKAZAWA, T. OTSUKA, A. KOBAYASHI, M. TOKUMOTO and P. CASSOUX, "Antiferromagnetism and Superconductivity of BETS Conductors with Fe^{3+} Ions," *Synth. Met.* **120**, 663 (2001).

A. KOBAYASHI, H. TANAKA, T. ADACHI and H. KOBAYASHI, "Molecular Design of a 'Neutral Metal' Composed of Single Component Molecules," *Synth. Met.* **120**, 1087 (2001).

H. TANAKA, H. KOBAYASHI and A. KOBAYASHI, "Novel Conductor Based on Metal Complexes with Extended TTF Ligands," *Synth. Met.* **129**, 1037 (2001).

H. FUJIWARA, E. OJIMA and H. KOBAYASHI, "Synthesis and Properties of a New Organic Donor Containing a TEMPO Radical," *Synth. Met.* **120**, 971 (2001).

E. OJIMA, H. FUJIWARA, H. KOBAYASHI and M. TOKUMOTO, "Synthesis and Properties of a New TSeF Derivative Containing a Pyrazino-Ring," *Synth. Met.* **120**, 887 (2001).

T. KAWASAKI, M. A. TANATAR, T. ISHIGURO, H. TANAKA, A. KOBAYASHI and H. KOBAYASHI, "In-Plane Anisotropy of the Upper Critical Field of λ-(BETS)$_2$GaCl$_4$," *Synth. Met.* **120**, 771 (2001).

H. TADA, T. TOJO, M. KAKO, Y. NAKADAIRA and K. MATSUSHIGE, "Energy Transfer in Highly Oriented Permethyldodecasilane and -octadecasilane Films," *J. Organomet. Chem.* **611**, 85 (2000).

Y. NISHIO, M. TAMURA, K. KAJITA, S. AONUMA, H. SAWA, R. KATO and H. KOBAYASHI, "Thermodynamical Study of (DMe-DCNQI)$_2$Cu System—Mechanism of Reentrant-Metal-Insulator Transition—," *J. Phys. Soc. Jpn.* **69**, 1414 (2000).

H. M. YAMAMOTO and R. KATO, "Design, Preparation, and Characterization of Novel ET Salts with Supramolecular Assembly—Sheet and Chain Structures Based on Difluorotetraiodobenzene—," *Chem. Lett.* 970 (2000).

R. KATO, E. WATANABE, M. FUJIWARA, Y. KASHIMURA, Y. OKANO and J. YAMAURA, "Conducting Properties of Assembled Metal Complexes," *Mol. Cryst. Liq. Cryst.* **343**, 1 (2000).

T. NAKAMURA, H. TSUKUDA, T. TAKAHASHI, S. AONUMA and R. KATO, "Low Temperature Electronic States of β'-Type Pd(dmit)$_2$ Compounds," *Mol. Cryst. Liq. Cryst.* **343**, 187 (2000).

N. BISKUP, J. S. BROOKS, R. KATO and K. OSHIMA, "Angular Magnetoresistance in the (DMET-TSeF)$_2$X Family: (X = AuCl$_2$, AuI$_2$) : Field-Induced Spin-Density Waves and Commensurability Effects," *Phys. Rev. B* **62**, 21 (2000).

R. KATO, M. FUJIWARA, Y. KASHIMURA and J. YAMAURA, "Development of Molecular Conductors Derived from Metal Dithiolene Complexes," *Synth. Met.* **120**, 675 (2001).

T. YAMAMOTO, N. HANASAKI, J. YAMAURA, S. AONUMA, H. TAJIMA, K. YAKUSHI, M. URUICHI and R. KATO, "Phase Diagram of (DMe-DCNQI)$_2$Li$_{1-x}$Cu$_x$ System," *Synth. Met.* **120**, 873 (2001).

T. IMAKUBO, T. IIJIMA, K. KOBAYASHI and R. KATO, "A New Synthetic Route to TTF-Vinylogues," *Synth. Met.* **120**, 899 (2001).

T. KAWAMOTO, M. ASHIZAWA, T. MORI, J. YAMAURA, R. KATO, Y. MISAKI and K. TANAKA, "Ground States of One-Dimensional Organic Conductors Based on ChTM-TTP," *Synth. Met.* **120**, 793 (2001).

T. IMAKUBO, A. MIYAKE, H. SAWA and R. KATO, "Synthesis and Physical Properties of (DIETS)$_2$[Au-(CN)$_4$]: A New θ-Salt with a Unique Donor⋯Anion Network," *Synth. Met.* **120**, 927 (2001).

J. YAMAURA, M. FUJIWARA, R. KATO, T. CHONAN and K. TAKAHASHI, "Cation Effect on Structural and Physical Properties of Purely One-Dimensional Electronic System [D](CPDT-TCNQ)$_2$ [D = Cation]," *Synth. Met.* **120**, 913 (2001).

H. M. YAMAMOTO, R. MAEDA, J. YAMAURA and R. KATO, "Multicomponent Molecular Conductors with

Supramolecular Assembly—Supramolecules with Various Dimensionality—," *Synth. Met.* **120**, 781 (2001).

H. OHTA, T. SAKURAI, S. OKUBO, R. KATO and T. NAKAMURA, "High Field ESR Measurements of Me$_4$-As[Pd(dmit)$_2$]$_2$," *Synth. Met.* **120**, 891 (2001).

H. M. YAMAMOTO, R. MAEDA, J. YAMAURA and R. KATO, "Structural and Physical Properties of Conducting Cation Radical Salts Containing Supramolecular Assemblies Based on *p*-Bis(iodoethynyl)benzene Derivatives," *J. Mater. Chem.* **11**, 1034 (2001).

M. ISHIDA, O. TAKEUCHI, T. MORI and H. SHIGEKAWA, "Comparison of the Symmetry Breaking in the Surface Molecular Structures of One- and Two-Dimensional Bis(ethylenedithio)tetrathia-fulvalene Compounds," *Jpn. J. Appl. Phys.* **39**, 3823 (2000).

M. ARAGAKI, H. HOSHINO, T. MORI, Y. MISAKI, K. TANAKA, H. MORI and S. TANAKA, "TCNQ Complex with θ-Type Donor Arrangement: (TMET-TS-TTP)$_2$(TCNQ)," *Adv. Mater.* **12**, 983 (2000).

T. MORI, "Estimaion of Off-Site Coulomb Integrals and Phase Diagrams of Charge Ordered States in the θ-Phase Organic Conductor," *Bull. Chem. Soc. Jpn.* **73**, 2243 (2000).

M. KATSUHARA, M. ARAGAKI, T. MORI, Y. MISAKI and K. TANAKA, "1:1 Composition Organic Metal Including a Magnetic Counteranion, (TTM-TTP)FeBr$_{1.8}$Cl$_{2.2}$," *Chem. Mater.* **12**, 3186 (2000).

T. KAWAMOTO, T. MORI, T. YAMAMOTO, H. TAJIMA, Y. MISAKI and K. TANAKA, "Marginal Paramagnetic State of a One-Dimensional Half-Filled Alternating Chain in (TTM-TTP)AuI$_2$," *J. Phys. Soc. Jpn.* **69**, 4066 (2000).

S. KIMURA, H. KURAI, T. MORI, H. MORI and S. TANAKA, "Tetrathiapentalene Derivatives with Long Alkyl Chains," *Bull. Chem. Soc. Jpn.* **74**, 59 (2001).

T. ISE, T. MORI and K. TAKAHASHI, "Preparation, Crystal Structures and Electrical Properties of PF$_6$ and AsF$_6$ Salts of a Novel Furopyrazine-Extended Donor (BDTFP) with a Two-Leg Ladder Type Orbital Overlapping Mode," *J. Mater Chem.* **11**, 264 (2001).

T. MORI, M. KATSUHARA, H. HOSHINO, M. ARAGAKI, T. KAWAMOTO, Y. MISAKI, K. TANAKA, H. MORI and S. TANAKA, "Metallic 1:1-Composition Organic Conductors and the Estimated U and V," *Synth. Met.* **120**, 821 (2001).

T. KAWAMOTO, M. ASHIZAWA, T. MORI, J. YAMAURA, R. KATO, Y. MISAKI and K. TANAKA, "Ground States of One-Dimensional Organic Conductors Based on ChTM-TTP," *Synth. Met.* **120**, 793 (2001).

M. KATSUHARA, M. ARAGAKI, T. MORI, Y. MISAKI and K. TANAKA, "Metallic Organic Conductor with 1:1 Composition Including Magnetic Anion," *Synth. Met.* **120**, 823 (2001).

S. KIMURA, H. KURAI, T. MORI, H. MORI and S. TANAKA, "Tetrathiapentalene Derivatives Having Long Alkyl Chains," *Synth. Met.* **120**, 829 (2001).

M. ARAGAKI, Y. TOMINAGA and T. MORI, "Preparation and Properties of Oxacyclopentylenedithio and Cyclopentylenedithio Substituted TTP Donors," *Synth. Met.* **120**, 827 (2001).

K. TAKAHASHI, K. TANAKA, M. TANIGUCHI, Y. MISAKI, K. TANAKA and T. MORI, "Preparation and Electrical Properties of the Novel TTP Donors Including the BETS Unit," *Synth. Met.* **120**, 955 (2001).

M. ARAGAKI, S. KIMURA, M. KATSUHARA, H. KURAI and T. MORI, "Selenium Analogs of Tetrathia-pentalene Derivatives with Long Alkyl Chains," *Bull. Chem. Soc. Jpn.* **74**, 833 (2001).

M. ARAGAKI, H. HOSHINO and T. MORI, "Universal Phase Diagram of θ-Type TMET-TTP Salts," *J. Phys. Soc. Jpn.* **70**, 1642 (2001).

H. FURUTA, T. ISHIZUKA, A. OSUKA and T. OGAWA, "'N-Fused Porphyrin': A New Tetrapyrrolic Porphyrinoid with a Fused Tri-Pentacyclic Ring," *J. Am. Chem. Soc.* **122**, 5748 (2000).

Y. WADA, M. TSUKADA, M. FUJIHIRA, K. MATSUSHIGE, T. OGAWA, M. HAGA and S. TANAKA, "Prospects and Problems of Single Molecule Information Devices," *Jpn. J. Appl. Phys.* **39**, 3835 (2000).

T. OGAWA, H. FURUTA, A. MORINO, M. TAKAHASHI and H. UNO, "Synthesis and Characterization of N-Confused Porphyrinatoantimony(V): Toward Low Energy Gap Molecular Wire," *J. Organomet. Chem.* 551 (2000).

H. FURUTA, N. KUBO, H. MAEDA, T. ISHIZUKA, A. OSUKA, H. NANAMI and T. OGAWA, "N-Confused Double-Decker Porphyrins," *Inorg. Chem.* **39**, 5424 (2000).

T. OGAWA, K. KOBAYASHI, G. MASUDA, T. TAKASE, Y. SHIMIZU and S. MAEDA, "Chemical Approach toward Molecular Electronic Device." *Trans. Mater. Res. Soc. Jpn.* **26**, 733 (2001).

S. HASEGAWA, T. HORIGOME, K. YAKUSHI, H. INOKUCHI, K. KAMIYA-OKUDAIRA, N. UENO, K. SEKI, R. J. WILLICUT, R. L. McCARLEY, E. MORIKAWA and V. SAILE, "Angle-Resolved Photoemission Measurements of ω-(n-pyrrolyl)alkanethiol Self-Assembled Monolayers Using *in-situ* Sample Preparation Apparatus," *J. Electron. Spectrosc. Relat. Phenom.* **113**, 101 (2001).

Department of Applied Molecular Science

T. GOTO, M. I. BARTASHEVICH, Y. HOSOKOSHI, K. KATOH and K. INOUE, "Observation of a Magnetization Plateau of 1/4 in a Novel Double Spin Chain of Ferromagnetic Dimers Formed by Organic Tetraradicals," *Physica B* **294**, 43 (2001).

S. AONUMA, H. CASELLAS, C. FAULMANN, B. G. de BONNEVAL, I. MALFANT, P. CASSOUX, P. G

LACROIX, Y. HOSOKOSHI and K. INOUE, "Structure and Properties of Novel M(dmit)$_2$ Salts with the Me$_3$N-TEMPO Radical (Me$_3$N-TEMPO = *N,N,N*-trimethyl(1-oxyl-2,2,6,6-tetramethylpiperidin-4-yl)ammonium)," *J. Mater. Chem.* **11**, 337 (2001).

Y. HOSOKOSHI, K. KATOH, A. S. MARKOSYAN and K. INOUE, "Magnetic Properties of Organic Spin Ladder Systems," *Synth. Met.* **121**, 1838 (2001).

S. AONUMA, H. CASELLAS, C. FAULMANN, B. G. de BONNEVAL, I. MALFANT, P. G LACROIX, P. CASSOUX, Y. HOSOKOSHI and K. INOUE, "Structure and Properties of M(dmit)$_2$ Salts of Cations with a Magnetic Nitroxide Radical," *Synth. Met.* **120**, 993 (2001).

K. MUKAI, S. JINNO, Y. SHIMOBE, N. AZUMA, Y. HOSOKOSHI, K. INOUE, M. TANIGUCHI, Y. MISAKI and K. TANAKA, "Syntheses and Properties of Genuine Organic Magnetic Conductors: (1:1) and (1:2) Salts of Ethyl-Pyridinium-Substituted Verdazyl Radicals with TCNQ," *Polyhedron* **20**, 1537 (2001).

Y. HOSOKOSHI, K. KATOH, Y. NAKAZAWA, H. NAKANO and K. INOUE, "Approach to a Single-Component Ferrimagnetism by Organic Radical Crystals," *J. Am. Chem. Soc.* **123**, 7921 (2001).

M. TANAKA, Y. HOSOKOSHI, A. S. MARKOSYAN, H. IWAMURA and K. INOUE, "Magnetic Properties of Layered Complexes [M(hfac)$_2$]$_3$·(R)$_2$, M = Mn(II) and Cu(II), with Trisnitroxide Radicals Having Various Metal-Radical Exchange Interactions," *J. Phys.: Condens. Matter* **13**, 7429 (2001).

H. KUMAGAI, M. AKITA TANAKA, K. INOUE and M. KURMOO, "Hydrothermal Synthesis and Characterization of New Porous 3-D-networks Containing the Versatile *cis*, *cis*-1,3,5-cyclohexanetricarboxilate," *J. Mater. Chem.* **11**, 2146 (2001).

P. S. GHALSASI, K. INOUE, S. D. SAMANT and J. V. YAKHMI, "A Complex of a Chiral Substituent-Based Nitroxide Triradical Having Two Chiral Centers with Mn(hfac)$_2$," *Polyhedron* **20**, 1495 (2001).

H. KUMAGAI, Y. HOSOKOSHI, A. S. MARKOSYAN and K. INOUE, "Synthesis, Structure and Magnetic Properties of Bis(hexafluoroacetylacetonato) Mn(II) Complex with a Novel Ttriplet Organic Radical, 4-*N-tert*-butylaminoxyl-4'-nitronylnitroxylbiphenyl," *Polyhedron* **20**, 1329 (2001).

H. SAKIYAMA, R. ITO, H. KUMAGAI, K. INOUE, M. SAKAMOTO, Y. NISHIDA and M. YAMASAKI, "Dinuclear Cobalt(II) Complexes of an Acyclic Phenol-Based Dinucleating Ligand with Four Methoxyethyl Chelating Arms—First Magnetic Analyses in an Axially Distorted Octahedral Field," *Eur. J. Inorg. Chem.* 2027 (2001).

A. S. OVCHINNIKOV, I. G. BOSTREM, V. E. SYNITSYN, N. V. BARANOV and K. INOUE, "The Ground State Properties of One-dimensional Heterospin Chain (5/2, 1/2, 1/2) with Alternating Exchange," *J. Phys.: Condens. Matter* **13**, 5221 (2001).

V. G. PLESCHOV, N. V. BARANOV, A. N. TITOV, K. INOUE, M. I. BARTASHEVICH and T. GOTO, "Magnetic Properties of Cr-Intercalated TiSe$_2$," *J. Alloys Compd.* **320**, 13 (2001).

K. ADACHI, S. KAWATA, M. K. KABIR, H. KUMAGAI, K. INOUE and S. KITAGAWA, "Design and Construction of Coordination Polymers Based on the Topological Property of the Multidentate Ligand," *Chem. Lett.* 50 (2001).

K. INOUE, H. KUMAGAI and A. S. MARKOSYAN, "Synthesis of Asymmetric One-Dimensional Molecular-Based Magnets," *Synth. Met.* **121**, 1772 (2001).

H. SAKIYAMA, A. SUGAWARA, M. SAKAMOTO, K. UNOURA, K. INOUE and M. YAMASAKI, "Manganese(II) Complexes of an Acyclic Phenol-based Dinucleating Ligand with Four Methoxyethyl Chelating Arms: Synthesis, Structure, Magnetism and Electrochemistry," *Inorg. Chim. Acta* **310**, 163 (2000).

H. KITAMURA, K. ANDO, T. OZAWA, K. JITSUKAWA, H. MASUDA and H. EINAGA, "Electron Transfer Reaction Induced by Self-assembly of Biguanidato and Violurato Complexes through Triple Hydrogen-Bond," *Kobunshi Ronbunshu* **57**, 188 (2000).

N. OHATA, H. MASUDA and O. YAMAUCHI, "Unique Self-Organized Structures of Metal(II)-Arginine Complexes through Directed Hydrogen Bonds," *Kobunshi Ronbunshu* **57**, 167 (2000).

N. OHATA, H. MASUDA and O. YAMAUCHI, "Dianion-Controlled Supramolecular Assembly of Copper(II)-Arginine Complex Ion," *Inorg. Chim. Acta* **300-302**, 749 (2000).

H. KITAMURA, T. OZAWA, K. JITSUKAWA, H. MASUDA and H. EINAGA, "Unique Self-Organization System Formed between Biguanidato and Biuretato Complexes with Triple Hydrogen-Bonds," *Mol. Cryst. Liq. Cryst.* **342**, 69 (2000).

H. KITAMURA, T. OZAWA, K. JITSUKAWA, H. MASUDA, Y. AOYAMA and H. EINAGA, "Syntheses, Structures, and Properties of Tetrakis(μ-acetato)-dirhodium(II) Complexes with Axial Pyridine Nitrogen-Donor Ligands with and/or without Assistance of Hydrogen Bonds," *Inorg. Chem.* **39**, 3294 (2000).

R. YAMAHARA, S. OGO, Y. WATANABE, T. FUNABIKI, K. JITSUKAWA, H. MASUDA and H. EINAGA, "(Catecholato)iron(III) Complexes with Tetradentate Tripodal Ligands Containing Substituted Phenol and Pyridine Units as Structural and Functional Model Complexes for the Catechol-bound Intermediate of Intradiol-Cleaving Catechol Dioxygenases," *Inorg. Chim. Acta* **300-302**, 587 (2000).

H. KUMITA, N. ASAI, T. SAKURAI, K. JITSUKAWA, T. OZAWA, H. MASUDA and H. EINAGA, "Stereoselective Electron-Transfer Reactions of the Optically Active Ruthenium(III) Complexes with Hydrophobic Side-Chains with Azurin(I) from Alacaligenes Xylosoxidans GIFU 1051," *Inorg. Chem. Commun.* **3**, 185 (2000).

H. ARII, S. NAGATOMO, T. KITAGAWA, T. MIWA, K. JITSUKAWA, H. EINAGA and H. MASUDA, "A Novel Diiron Complex as a Functional Model for Hemerythrin," *J. Inorg. Biochem.* **82**, 153 (2000).

K. JITSUKAWA, T. IRISA, H. EINAGA and H. MASUDA, "A Substrate-Specific α-Hydroxylation of Dipeptides Mediated upon a Co(III)-Terpyridine Complex: A Functional Model for Peptidylglycine α-Hydroxylating Monooxygenase," *Chem. Lett.* 30 (2001).

H. KUMITA, T. MORIOKA, T. OZAWA, K. JITSUKAWA, H. EINAGA and H. MASUDA, "Site-Selective Recognition of Amino Acids by The Co(III) Complexes Containing (N)(O)$_3$-Type Tripodal Tetradentate Ligand," *Bull. Chem. Soc. Jpn.* **74**, 1035 (2001).

K. MATSUMOTO, T. OZAWA, K. JITSUKAWA, H. EINAGA and H. MASUDA, "Crystal Structure and Redox Behavior of a Novel Siderophore Model System: A Trihydroxamato-Iron(III) Complex with Intra- and Interstrand Hydrogen Bonding Networks," *Inorg. Chem.* **40**, 190 (2001).

H. KUMITA, K. JITSUKAWA, H. EINAGA and H. MASUDA, "Characterization of an NH-π Interaction in Co(III) Ternary Complexes with Aromatic Amino Acids," *Inorg. Chem.* **40**, 3936 (2001).

K. JITSUKAWA, Y. OKA, H. EINAGA and H. MASUDA, "Reverse Reactivity in Hydroxylation of Adamantane and Epoxidation of Cyclohexene Catalyzed by the Mononuclear Ruthenium-oxo Complexes with 6-Substituted Tripodal Polypyridine Ligands," *Tetrahedron Lett.* **42**, 3467 (2001).

K. MATSUMOTO, T. OZAWA, K. JITSUKAWA, H. EINAGA and H. MASUDA, "A Structural Model of the Ferrichrome Type Siderophore: Chiral Preference Induced by Intramolecular Hydrogen Bonding Networks in Ferric Trihydroxamate," *Chem. Commun.* 978 (2001).

K. MATSUMOTO, N. SUZUKI, T. OZAWA, K. JITSUKAWA and H. MASUDA, "Crystal Structure and Solution Behavior of the Iron(III) Complex of the Artificial Trihydroxamate Siderophore with Tris(3-aminopropyl)-amine Backbone," *Eur. J. Inorg. Chem.* **10**, 2481 (2001).

K. IMURA, T. KAWASHIMA, H. OHOYAMA, T. KASAI, A. NAKASHIMA and K. KAYA, "Non-Destructive Selection of Geometrical Isomers of Al(C$_6$H$_6$) Cluster by a 2-Meter Electrostatic Hexapole Field," *Phys. Chem. Chem. Phys.* **3**, 3593 (2001).

H. OHOYAMA, M. YAMATO, S. OKADA, T. KASAI, B. G. BRUNETTI and F. VECCHIOCATTIVI, "Direct Measurement of Oscillating Behavior in Ar(^{3}P) + CH$_3$Cl → Ar + CH$_3$Cl$^+$ + e$^-$ Ionization Cross Section by Velocity and Orientational Angle Selected Collisions," *Phys. Chem. Chem. Phys.* **3**, 3598 (2001).

K. IMUARA, T. KAWASHIMA, H. OHOYAMA and T. KASAI, "Direct Determination of the Permanent Dipole Moments and Structures of Al–CH$_3$CN and Al–NH$_3$ by Using 2-Meter Electrostatic Hexapole Field," *J. Am. Chem. Soc.* **123**, 6367 (2001).

M. YAMATO, H. OHOYAMA and T. KASAI, "2D-Measurement of Penning Ionization Cross Section upon Molecular Orientation and Collision Energy in Ar(^{3}P$_{2,0}$) + CHCl$_3$ Crossed Beam Reaction," *J. Phys. Chem.* **105**, 2967 (2001).

B. G. BRUNETTI, P. CANDORI, S. FALCINELLI, T. KASAI, H. OHOYAMA and F. VECCHIOCATTIVI, "Velocity Dependence of the Ionization Cross Section of Methyl Chloride Molecules Ionized by Metastable Argon Atoms," *Chem. Phys. Phys. Chem.* **3**, 807 (2001).

M. NOSAKA and M. TAKASU, "Structure Analysis of Chemical Gel Using Monte Carlo Simulation," *Trans. Mater. Res. Soc. Jpn.* **26**, 557 (2001).

H. NOGUCHI and M. TAKASU, "Linear-Shaped Motion of DNA in Entangled Polymer Solutions under a Steady Field," *J. Phys. Soc. Jpn.* **69**, 3792 (2000).

H. NOGUCHI and M. TAKASU, "Dynamics of DNA in Entangled Polymer Solutions: An Anisotropic Friction Model," *J. Chem. Phys.* **114**, 7260 (2001).

H. NOGUCHI, "Electrophoretic Behavior of Polyelectrolytes in Gel and Polymer Solutions," *Trans. Mater. Res. Soc. Jpn.* **26**, 687 (2001).

Department of Vacuum UV Photoscience

A. N. DE BRITO, S. SUNDIN, R. R. MARINHO, I. HJELTE, G. FRAGUAS, T. GEJO, N. KOSUGI, S. SORENSEN and O. BJÖRNEHOLM, "Memories of Excited Femtoseconds: Effects of Core-Hole Localization after Auger Decay in the Fragmentation of Ozone," *Chem. Phys. Lett.* **328**, 177 (2000).

N. KOSUGI and T. ISHIDA, "Molecular Field and Spin-Orbit Splittings in the 2p Ionization of Second-Row Elements: A Breit-Pauli Approximation Applied to OCS, SO$_2$, and PF$_3$," *Chem. Phys. Lett.* **329**, 138 (2000).

Y. TAKATA, E. SHIGEMASA and N. KOSUGI, "Mg and Al K-Edge XAFS Measurements with a KTP Crystal Monochromator," *J. Synchrotron Radiat.* **8**, 351 (2001).

Y. TAKATA, T. IWAZUMI and N. KOSUGI, "Resonant X-Ray Emission Spectra of K$_2$Ni(CN)$_4$·H$_2$O at the Ni K-Edge," *J. Synchrotron Radiat.* **8**, 404 (2001).

Y. TAKATA, T. HATSUI, N. KOSUGI, A. AGUI, M. MAGNUSON, C. SÅTHE, J.-E. RUBENSSON and J. NORDGREN, "Valence Excitations Observed in Resonant Soft X-Ray Emission Spectra of K$_2$Ni(CN)$_4$·H$_2$O at the Ni 2p Edge," *J. Electron Spectrosc.* **114-116**, 909 (2001).

C. MIRON, M. SIMON, P. MORIN, S. NANBU, N. KOSUGI, S. L. SORENSEN, A. N. DE BRITO, M. N. PIANCASTELLI, O. BJÖRNEHOLM, R. FEIFEL, M. BÄSSLER and S. SVENSSON, "Nuclear Motion Driven by the Renner-Teller Effect as Observed in the Resonant Auger Decay to the $X^2\prod$ Electronic Ground State of N$_2$O$^+$," *J. Chem. Phys.* **115**, 864 (2001).

A. SHIMOJIMA and T. TAHARA, "Picosecond Time-Resolved Resonance Raman Study of Photoisomerization of Retinal," *J. Phys. Chem. B* **104**, 9288 (2000).

S. Yu. ARZHANTSEV, S. TAKEUCHI and T. TAHARA, "Ultrafast Excited-State Proton Transfer Dynamics of 1,8-Dihydroxyanthraquinone (Chrysazin) studied by Femtosecond Time-Resolved Fluorescence Spectroscopy," *Chem. Phys. Lett.* **330**, 83 (2000).

T. FUJINO, S. ARZHANTSEV and T. TAHARA, "Femtosecond Time-Resolved Fluorescence Study of Photoisomerization of trans-Azobenzene," *J. Phys. Chem. A* **105**, 8123 (2001).

K. IWATA, S. TAKEUCHI and T. TAHARA, "Photochemical Bimolecular Reaction between Biphenyl and Carbon Tetrachloride: Observed Ultrafast Kinetics and Diffusion-Controlled Reaction Model," *Chem. Phys. Lett.* **347**, 331 (2001).

M. MIZUNO and T. TAHARA, "Novel Resonance Raman Enhancement of Local Structure around Solvated Electron in Water," *J. Phys. Chem. A* **105**, 8823 (2001).

S. TAKEUCHI and T. TAHARA, "Excitation-Wavelength Dependence of the Femtosecond Florescence Dynamics of 7-Azaindole Dimer: Further Evidence for the Concerted Double Proton Transfer in Solution," *Chem. Phys. Lett.* **347**, 108 (2001).

H. NODA, T. URISU, Y. KOBAYASHI and T. OGINO, "Initial Stage of Hydrogen Etching of Si Surfaces Investigated by Infrared Reflection Absorption Spectroscopy," *Jpn. J. Appl. Phys.* **39**, 6985 (2000).

M. TAKIZAWA, S. BANDOW, M. YUDASAKA, Y. ANDO, H. SIMOYAMA and S. IIJIMA, "Change of Tube Diameter Distribution of Single-Wall Carbon Nanotubes Induced by Changing the Bimetallic Ratio of Ni and Y Catalysts," *Chem. Phys. Lett.* **326**, 351 (2000).

Y. NONOGAKI, Y. GAO, H. MEKARU, T. MIYAMAE and T. URISU, "STM Observation of Surface Nanostructures on Si(111) Formed after Synchrotron Radiation Stimulated Cleaning," *Trans. Mater. Res. Soc. Jpn.* **26**, 751 (2001).

Y. NONOGAKI, Y. GAO, H. MEKARU, T. MIYAMAE and T. URISU, "Nanostructure Formation on Si(111) Surface Assisted by Synchrotron Radiation Illumination —Characterization by Scanning Tunneling Microscopy—," *J. Electron Spectrosc. Relat. Phenom.* **119**, 241 (2001).

T. URISU, Y. NONOGAKI, T. KATO and Y. ZHANG, "Device and Material Processes Using Synchrotron Radiation —from Micron to Nanometers—," *J. Jpn. Soc. Synchrotron Radiat. Res.* **14**, 112 (2001).

S. BANDOW, M. TAKIZAWA, K. HIRAHARA, M.YUDASAKA and S. IIJIMA, "Raman Scattering Study of Double-Wall Carbon Nanotubes Derived from the Chains of Fullerenes in Single-Wall Carbon Nanotubes," *Chem. Phys. Lett.* **337**, 48 (2001).

S. MORÉ, A. P. SEITSONNEN, W. BERNDT and A. M. BRADSHAW, "Ordered Phases of Na Adsorbed on Pt(111): Experiment and Theory," *Phys. Rev. B* **63**, 75406 (2001).

K. MITSUKE, H. HATTORI and Y. HIKOSAKA, "Superexcitation and Subsequent Decay of Triatomic Molecules Studied by Two-Dimensional Photoelectron Spectroscopy," *J. Electron Spectrosc. Relat. Phenom.* **112**, 137 (2000).

M. ONO, H. YOSHIDA, H. HATTORI and K. MITSUKE, "Performance of the 18 m-Spherical Grating Monochromator Newly Developed in the UVSOR Facility," *Nucl. Instrum. Methods Phys. Res., Sect. A* **467–468**, 577 (2001).

K. MITSUKE and M. MIZUTANI, "Laser Induced Fluorescence Spectroscopy of CN($X^2\Sigma^+$) Radicals Produced by Vacuum UV Photoexcitation of CH_3CN with Synchrotron Radiation," *J. Electron Spectrosc. Relat. Phenom.* **119**, 155 (2001).

K. MITSUKE and M. MIZUTANI, "UV and Visible Emission Spectra from Photodissociation of Carbonyl Sulfide Using Synchrotron Radiation at 15–30 eV," *Bull. Chem. Soc. Jpn.* **74**, 1193 (2001).

K. KUROSAWA, N.TAKEZOE, H.YANAGIDA, J. MIYANO, Y. MOTOYAMA, K. TOSHIKAWA, Y. KAWASAKI and A. YOKOTANI, "Silica Film Preparation by Chemical Vapor Depositionj Using Vacuum Ultraviolet Excimer Lamps," *Appl. Surf. Sci.* **168**, 37 (2000).

K. TOSHIKAWA, J. MIYANO, Y. MOTOYAMA, Y. YAGI, H. YANAGIDA, K. KUROSAWA, A. YOKOTANI and W. SASAKI, "Characterization of SiO_2 Dielectric Films in Photo-Chemical Vapor Deposition Using Vacuum Ultraviolet Excimer Lamp," *199th Meeting of Electrochemical Society* **2001-1**, 241 (2001).

Y. MOTOYAMA, J. MIYANO, K. TOSHIKAWA, Y. YAGI, K. KUROSAWA, A. YOKOTANI and W. SASAKI, "Electrical Properties of SiO_2 Films Prepared by VUV Chemical Vapor Deposition," *199th Meeting of Electrochemical Society* **2001-1**, 257 (2001).

J. MIYANO, Y. MOTOYAMA, K. TOSHIKAWA, Y. YAGI, H. YANAGIDA, K. KUROSAWA, AQ. YOKOTANI and W. SASAKI, "SiO_2 Film Deposition on Different Substrate Materials by Photo-CVD Using Vacuum Ultraviolet Radiation," *199th Meeting of Electrochemical Society* **2001-1**, 258 (2001).

A. KAMEYAMA, A. YOKOTANI and K. KUROSAWA, "Identification of Defects Associated with Second-Order Optical Nonlinearity in Thermally Poled High-Purity Silica Glasses," *J. Appl. Phys.* **89**, 4707 (2001).

K. KUROSAWA, Y. MAEZONO, J. MIYANO, T. MOTOYAMA and A. YOKOTANI, "GeO_2 and SiO_2 Thin Film Preparation with CVD Using Ultraviolet Excimer Lamps," *J. Phys.* **11**, 739 (2001).

Y. MAEZONO, H. YANAGIDA, K. NISHI, J. MIYANO, A. YOKOTANI, K. KUROSAWA, N.

HISHINUMA and H. MATSUNO, "Room Temperature Deposition of GeO_2 Thin Film Using Dielectric Barrier Discharge Driven Excimer Lamps," *J. Phys.* **11**, 811(2001).

Y. MOTOYAMA, J. MIYANO, K. TOSHIKAWA, Y. YAGI, H. YANAGIDA, K. KUROSAWA and A. YOKOTANI, "Study of SiO_2 Films Deposited by Adding N_2O or O_2 to TEOS in Photo-Chemical Vapor Deposition at Room Temperature," *J. Phys.* **11**, 1131(2001).

T. UCHIHASHI, T. ISHIDA, M. KOMIYAMA, M. ASHINO, Y. SUGAWARA, W. MIZUTANI, K. YOKOYAMA, S. MORITA, H. TOKUMOTO and M. ISHIKAWA, "High-Resolution Imaging of Organic Monolayers Using Noncontact AFM," *Appl. Surf. Sci.* **157**, 244 (2000).

M. KOMIYAMA and N. GU, "Study of Catalyst Preparation Processes by Atomic Force Microscopy (AFM): Adsorption of a Pt Complex on a Zeolite Surface," *Stud. Surf. Sci. Catal.* **130**, 3173 (2000).

A. MOTOGAITO, M. YAMAGUCHI, K. HIRAMATSU, M. KOTOH, Y. OHUCHI, K. TADATOMO, Y. HAMAMURA and K. FUKUI, "Characterization of GaN-Based Schottky Barrier Ultraviolet (UV) Detectors in the UV and Vacuum Ultraviolet (VUV) Region Using Synchrotron Radiation," *Jpn. J. Appl. Phys., Part 2* **40**, L368 (2001).

K. KINOSHITA, K. FUKUI, S. ASAKA, H. YOSHIDA, M. WATANABE, T. HORIGOME, MA PEIJUN, K. OHTSUKA, M. IWANAGA and E. OHSIMA, "Development of A Surface Profiler for Optical Elements," *Nucl. Instrum. Methods Phys. Res., Sect. A* **467–468**, 329 (2001).

K. FUKUI, H. MIURA, H. NAKAGAWA, I. SHIMOYAMA, K. NAKAGAWA, H. OKAMURA, T. NANBA, M. HASUMOTO and T. KINOSHITA, "Performance of IR-VUV Normal Incidence Monochromator Beamline at UVSOR," *Nucl. Instrum. Methods Phys. Res., Sect. A* **467–468**, 601 (2001).

S. TANAKA, K. MASE, M. NAGASONO, S. NAGAOKA, M. KAMADA, E. IKENAGA, T. SEKITANI and K. TANAKA, "Electron-Ion Coincidence Spectroscopy as a New Tool for Surface Analysis –an Application to the Ice Surface," *Jpn. J. Appl. Phys.* **39**, 4489 (2000).

S. NAGAOKA, T. IBUKI, N. SAITO, Y. SHIMIZU, Y. SENBA, K. KAMIMORI, Y. TAMENORI, H. OHASHI and I. H. SUZUKI, "Resonant Auger Spectrum Following Kr:$2p \rightarrow 5s$ Photoexcitation," *J. Phys. B: At. Mol. Opt. Phys.* **33**, L605 (2000).

N. SAITO, K. UEDA, M. SIMON, K. OKADA, Y. SHIMIZU, H. CHIBA, Y. SENBA, H. OKUMURA, H. OHASHI, Y. TAMENORI, S. NAGAOKA, A. HIRAYA, H. YOSHIDA, E. ISHIGURO, T. IBUKI, I. H. SUZUKI and I. KOYANO, "Molecular Deformation in the O $1s^{-1}2\pi_u$ Excited States of CO_2 Probed by the Triple-Differential Measurement of Fragment Ions," *Phys. Rev. A* **62**, 042503 (2000).

S. NAGAOKA, S. TANAKA and K. MASE, "Site-Specific Fragmentation following C:1s Core-Level Photo-ionization of 1,1,1-Trifluoroethane Condensed on a Au Surface and of a 2,2,2-Trifluoroethanol Monolayer Chemi-sorbed on a Si(100) Surface," *J. Phys. Chem. B* **105**, 1554 (2001).

Y. NISHIOKU, K. OHARA, K. MUKAI and S. NAGAOKA, "Time-Resolved EPR Investigation of the Photo-Induced Intramolecular Antioxidant Reaction of Vitamin K-Vitamin E Linked Molecule," *J. Phys. Chem. A* **105**, 5032 (2001).

H. OHASHI, E. ISHIGURO, Y. TAMENORI, H. OKUMURA, A. HIRAYA, H. YOSHIDA, Y. SENBA, K. OKADA, N. SAITO, I. H. SUZUKI, K. UEDA, T. IBUKI, S. NAGAOKA, I. KOYANO and T. ISHIKAWA, "Monochromator for a Soft X-Ray Photochemistry Beamline BL27SU of SPring8," *Nucl. Instrum. Methods Phys. Res., Sect. A* **467–468**, 533 (2001).

K. UEDA, H. YOSHIDA, Y. SENBA, K. OKADA, Y. SHIMIZU, H. CHIBA, H. OHASHI, Y. TAMENORI, H. OKUMURA, N. SAITO, S. NAGAOKA, A. HIRAYA, E. ISHIGURO, T. IBUKI, I. H. SUZUKI and I. KOYANO, "Angle-Resolved Electron and Ion Spectroscopy Apparatus on the Soft X-Ray Photochemistry Beamline BL27SU at SPring-8," *Nucl. Instrum. Methods Phys. Res., Sect. A* **467–468**, 1502 (2001).

E. MORIKAWA, V. SAILE, K. K. OKUDAIRA, Y. AZUMA, K. MEGURO, Y. HARADA, K. SEKI, S. HASEGAWA and N. UENO, "Pendant Group Orientation of Poly(2-vinylnapthalene) Thin Film Surface Studied by Near-edge X-ray Absorption Fine Structure Spectroscopy (NEXAFS) and Angle-resolve Ultraviolet Photoelectron Spectroscopy (ARUPS)," *J. Chem. Phys.* **112**, 10476 (2000).

H. YASUFUKU, K. MEGURO, K. K. OKUDAIRA, N. UENO and Y. HARADA, "Reaction at the Outermost Surface Selectivity Induced by Metastable-Atom Beams," *Jpn. J. Appl. Phys., Part 1* **39**, 4126 (2000).

S. KERA, H. SETOYAMA, K. KIMURA, A. IWASAKI, K. K. OKUDAIRA, Y. HARADA and N. UENO, "Direct Observation of S-Au Bonding State of Self-Assembled Monolayers by Outermost-surface Spectroscopy Using Metastable Atom Beam," *Surf. Sci.* **482–485**, 1192 (2001).

H. YASUFUKU, M. OKUMURA, T. IBE, K. K. OKUDAIRA, Y. HARADA and N. UENO, "Surface Images of SiO_2/Si(100) Pattern Using Electron Emission Microscopy with Metastable Atoms, Photons and Low-Energy Electrons," *Jpn. J. Appl. Phys., Part 1* **40**, 2447 (2001).

H. YASUFUKU, T. IBE, M. OKUMURA, S. KERA, K. K. OKUDAIRA, Y. HARADA and N. UENO, "Diffusion of Chloroaluminum Phthalocyanine on MoS_2 Surface Detected by Photoemission Electron Microscopy and Metastable Electron Emission Microscopy," *J. Appl. Phys.* **90**, 213 (2001).

S. KERA, K. K. OKUDAIRA, Y. HARADA and N. UENO, "Molecular Orientation and Aggregation of Titanyl

Phthalocyanine Molecules on Graphite Substrates: Effects of Surface Topography of the Substrate," *Jpn. J. Appl. Phys., Part 1* **40**, 783 (2001).
S. KERA, H. SETOYAMA, M. ONOUE, K. K. OKUDAIRA, Y. HARADA and N. UENO, "Origin of Indium-[perylene-3,4,9,10-tetracarboxilic dianhydride] Interface States Studied by Outermost Surface Spectroscopy Using Metastable Atoms," *Phys. Rev. B* **63**, 115204 (2001).
A. ABODUREYIM, K. K. OKUDAIRA, Y. HARADA, S. MASUDA, S. AOKI, K. SEKI, E. ITO and N. UENO, "Characterization of 4-Mercaptohydrocynnamic Acid Self-Assembled Film on Au(111) by means of X-Ray Photoelectron Spectroscopy," *J. Electron Spectrosc. Relat. Phenom.* **114–116**, 371 (2001).
H. YASUFUKU, M. OKUMURA, S. KERA, K. K. OKUDAIRA, Y. HARADA and N. UENO, "PEEM and MEEM of Chloroaluminum Phthalocyanine Ultrathin Film on MoS$_2$," *J. Electron Spectrosc. Relat. Phenom.* **114–116**, 1025 (2001).
S. HINO, K. UMISHITA, K. IWASAKI, M. AOKI, K. KOBAYASHI, S. NAGASE, T. JOHN, S. DENNIS, T. NAKANE and H. SHINOHARA, "Ultraviolet Photoelectron Spectra of Metallofullerenes, Two Ca@C$_{82}$ Isomers," *Chem. Phys. Lett.* **337**, 65 (2001).

S. FUJIKI, Y. KUBOZONO, S. EMURA, Y. TAKABAYASHI, S. KASHINO, A. FUJIWARA, K. ISHII, H. SUEMATSU, Y. MURAKAMI, Y. IWASA, T. MITANI and H. OGATA, "Structure and Raman Scattering of Cs$_3$C$_{60}$ under High Pressure," *Phys. Rev. B* **62**, 5366 (2000).
Y. KUBOZONO, Y. TAKABAYASHI, T. KAMBE, S. FUJIKI, S. KASHINO and S. EMURA, "Structure and Physical Properties of Na$_4$C$_{60}$ under Ambient and High Pressures," *Phys. Rev. B* **63**, 45418 (2001).
S. IIDA, Y. KUBOZONO, Y. SLOVOKHOTOV, Y. TAKABAYASHI, T. KANBARA, T. FUKUNAGA, S. FUJIKI, S. KASHINO and S. EMURA, "Structure and Electronic Properties of Dy@C$_{82}$ Studied by UV-VIS Absorption, X-Ray Powder Diffraction and XAFS," *Chem. Phys. Lett.* **338**, 21 (2001).
Y. KUBOZONO, Y. TAKABAYASHI, S. KASHINO, M. KONDO, T. WAKAHARA, T. AKASAKA, K. KOBAYASHI, S. NAGASE and S. EMURA, "Structure of La$_2$@C$_{80}$ Studied by La K-Edge XAFS," *Chem. Phys. Lett.* **335**, 163 (2001).
T. KANBARA, Y. KUBOZONO, Y. TAKABAYASHI, S. FUJIKI, S. IIDA, Y. HARUYAMA, S. KASHINO and S. EMURA, "Dy@C$_{60}$: Evidence for Endohedral Structure and Electron Transfer," *Phys. Rev. B* **64**, 113403 (2001).

Coordination Chemistry Laboratories

Y. UOZUMI, T. ARII and T. WATANABE, "Double Carbonylation of Aryl Iodides with Primary Amines under Atmospheric Pressure Conditions Using Pd/PPh$_3$/DABCO/THF System," *J. Org. Chem.* **66**, 5272 (2001).
S.-I. NAGAI, T. MIYACHI, T. NAKANE, T. UEDA and Y. UOZUMI, "Synthesis and Potential Central Nervous System Stimulant Activity of 5,8-Methanoquinazolines and Bornano-[1,2,4]triazines Fused with Imidazole and Pyrimidine," *J. Heterocycl. Chem.* **38**, 379 (2001).
T. HAYASHI, J. W. HAN, A. TAKEDA, J. TANG, K. NOHMI, K. MUKAIDE, H. TSUJI and Y. UOZUMI, "Modification of Chiral Monodentate Phosphine Ligands (MOP) for Palladium-Catalyzed Asymmetric Hydrosilylation of Cyclic 1,3-Dienes," *Adv. Synth. Catal.* **343**, 279 (2001).
T. HAYASHI, S. HIRATE, K. KITAYAMA, H. TSUJI, A. TORII and Y. UOZUMI, "Asymmetric Hydrosilylation of Styrenes Catalyzed by Palladium-MOP Complexes: Ligand Modification and Mechanistic Studies," *J. Org. Chem.* **66**, 1441 (2001).
Y. UOZUMI and K. SHIBATOMI, "Catalytic Asymmetric Allylic Alkylation in Water with a Recyclable Amphiphilic Resin-Supported *P,N*-Chelating Palladium Complex," *J. Am. Chem. Soc.* **123**, 2919 (2001).
Y. UOZUMI, K. YASOSHIMA, T. MIYACHI and S.-I. NAGAI, "Enantioselective Desymmetrization of *Meso*-Cyclic Anhydrides Catalyzed by Hexahydro-1*H*-pyrrolo[1,2-c]imidazolones," *Tetrahedron Lett.* **42**, 411 (2001).
Y. UOZUMI, K. MIZUTANI and S.-I. NAGAI, "A Parallel Preparation of a Bicyclic *N*-Chiral Amine Library and Its use for Chiral Catalyst Screening," *Tetrahedron Lett.* **42**, 407 (2001).
T. HAYASHI, S. HIRATE, K. KITAYAMA, H. TSUJI, A. TORII and Y. UOZUMI, "Modification of Chiral Monodentate Phosphine (MOP) Ligands for Palladium-Catalyzed Asymmetric Hydrosilylation of Styrenes," *Chem. Lett.* 1272 (2000).
K. SHIBATOMI, T. NAKAHASHI and Y. UOZUMI, "Michael Reactions in Water Using Amphiphilic Resin-Supported Quaternary Ammonium Hydroxides," *Synlett* **11**, 1643 (2000).
M. KAWATSURA, Y. UOZUMI, M. OGASAWARA and T. HAYASHI, "Palladium-Catalyzed Asymmetric Reduction of Racemic Allylic Esters with Formic Acid: Effects of Phosphine Ligands on Isomerization of π-Allylpalladium Intermediates and Enantioselectivity," *Tetrahedron* **56**, 2247 (2000).

I. TANIGUCHI, S. YOSHIMOTO, M. YOSHIDA, S. KOBAYASHI, T. MIYAWAKI, Y. AONO, Y. SUNATSUKI and H. TAIRA, "Simple Methods for Preparation of a Well-Defined 4-Pyridinethiol Modified Surface on Au(111) Electrodes for Cytochrome c Electrochemistry," *Electrochim. Acta* **45**, 2843 (2000).
T. SAWAGUCHI, S. YOSHIMOTO, F. MIZUTANI and I. TANIGUCHI, "Voltammetric and In Situ STM Studies on Self-Assembled Monolayers of 4- and 2-Mercaptopyridines and Thiophenol on Au(111) Electrodes," *Electrochim. Acta* **45**, 2861 (2000).

C.-Z. LI, K. NISHIYAMA and I. TANIGUCHI, "Electrochemical and Spectroelectrochemical Studies on Cobalt Myoglobin," *Electrochim. Acta* **45**, 2883 (2000).

Y. MIE, K. SONODA, M. KISHITA, E. KRESTYN, S. NEYA, N. FUNASAKI and I. TANIGUCHI, "Effect of Rapid Heme Rotation on Electrochemistry of Myoglobin," *Electrochim. Acta* **45(18)**, 2903 (2000).

A. OHIRA, T. ISHIZAKI, M. SAKATA, I. TANIGUCHI, C. HIRAYAMA and M. KUNITAKE, "Formation of the 'Nanotube' Structure of β-Cyclodextrin on Au(111) Surfaces Induced by Potential Controlled Adsorption," *Colloids Surf., A* **169**, 27 (2000).

K. NISHIYAMA, A. UEDA, S. TANOUE, T. KOGA and I. TANIGUCHI, "Direct Observation of Perchlorate Induced by Redox Reaction of Ferrocene Terminated Self-Assembled Monolayer Studied by in situ FT-Surfaces Enhanced Raman Spectroscopy," *Chem. Lett.* 930 (2000).

S. UEMURA, M. SAKATA, I. TANIGUCHI, M. KUMITAKE and C. HIRAYAMA, "Novel Wet Process Technique Based on Electrochemical Replacement for the Preparation of Fullerene Epitaxial Adlayers," *Langmuir* **17**, 5 (2001).

M. TOMINAGA and I. TANIGUCHI, "Electrochemically Regulated Iron Uptake and Release for Ferritin Immobilized on Self-Assembled Monolayer-Modified Gold Electrodes," *Chem. Lett.* 705 (2001).

T. WADA, K. TSUGE and K. TANAKA, "Syntheses and Redox Properties of Bis(hydroxoruthenium) Complexes with Quinone and Bipyridine Ligands. Water-Oxidation Catalysis," *Inorg. Chem.* **40**, 329 (2001).

T. TOMON, D. OOYAMA, T. WADA, S. KAZUSHI and K. TANAKA, "A Ru–Carbene Complex with a Metallacycle Involving a 1,8-Naphthylidine Framework," *Chem. Commun.* 1100 (2001).

E. FUJITA, M. CHOU and K. TANAKA, "Characterlzation of Ru(bpy)$_2$(CO)(COO) Prepared by CO$_2$ Addition to Ru(bpy)$_2$(CO) in Acetonitrile," *Appl. Organomet. Chem.* **14**, 844 (2000).

D. OOYAMA, T. TOMON, K. TSUGE and K. TANAKA, "Structural and Spectroscopic Characterization of Ruthenium(II) Complexes with Methyl, Formyl, and Acetyl Groups as Model Species in Multi-Step CO$_2$ Reduction," *J. Organomet. Chem.* **619**, 299 (2001).

T. NAGATA and K. TANAKA, "Pentadentate Terpyridine-Catechol Linked Ligands and Their Cobalt(III) Complexes," *Inorg. Chem.* **39**, 3515 (2000).

H. SUGIMOTO, K. TSUGE and K. TANAKA, "Ruthenium Terpyridine Complexes with mono- and bi-Dentate Dithiolene Ligands," *J. Chem. Soc., Dalton Trans.* 57 (2001).

H. SUGIMOTO and K. TANAKA, "Syntheses of New Ruthenium Carbonyl Terpyridine o-Phenylene Complexes: Strong Interaction Between Carbonyl and o-Phenylene Ligands," *J. Organomet. Chem.* **622**, 280 (2001).

H. KAWAGUCHI and K. TATSUMI, "Synthesis of a Pentamethylcyclopentadienyl Complex of Tungsten with Three Different Chalcogenido (O^{2-}, S^{2-}, Se^{2-}) Ligands," *Angew. Chem., Int. Ed. Engl.* **113**, 1306 (2001).

K. WAKITA, N. TOKITOH and R. OKAZAKI, "Separation of Orientational Disorder in the X-Ray Analysis of the Kinetically Stabilized 2-Silanaphthalene," *Bull. Chem. Soc. Jpn.* **73**, 2157 (2000).

T. SAIKI, K. GOTO, N. TOKITOH, M. GOTO and R. OKAZAKI, "Syntheses and Structures of Novel *m*-Xylylene-Bridged Calix[6]arenes: Stabilization of a Sulfenic Acid in the Cavity of Calix[6]arene," *J. Organomet. Chem.* **611**, 146 (2000).

T. SASAMORI, Y. ARAI, N. TAKEDA, R. OKAZAKI and N. TOKITOH, "The First Chemical Trapping of Stibinidene, a Monovalent Antimony Compound," *Chem. Lett.* 42 (2001).

Y. KAWAI, Y. INABA and N. TOKITOH, "Asymmetric Reduction of Nitroalkenes with Baker's Yeast," *Tetrahedron: Asymmetry* **12**, 309 (2001).

Y. KAWAI, Y. INABA, M. HAYASHI and N. TOKITOH, "Asymmetric Synthesis of a Nitroalkane by the Use of Novel Nitroalkene Reductases from Baker's Yeast," *Tetrahedron Lett.* **42**, 3367 (2001).

N. TOKITOH, Y. ARAI, T. SASAMORI, N. TAKEDA and R. OKAZAKI, "Formation of Antimony-Sulfur Double-Bond Compounds and Their Trapping with Nitrile Oxides," *Heteroatom Chem.* **12**, 244 (2001).

N. TOKITOH, "Synthesis, Structures, and Reactivities of Novel Silacyclic Systems: The First Stable Silabenzene and Silacyclopropabenzene," *Phosphorus, Sulfur Silicon Relat. Elem.* **168**, 31 (2001).

T. SASAMORI, N. TAKEDA and N. TOKITOH, "Novel Disproportionation Reaction of Stable Stibabismuthene via 1,2,3,4-Distibadibismetane Derivative," *Phosphorus, Sulfur Silicon Relat. Elem.* **169**, 89 (2001).

I. HAMACHI, R. EBOSHI, J. WATANABE and S. SHINKAI, "Guest-Induced Umpolung on a Protein Surface: A Strategy for Regulation of Enzymatic Activity," *J. Am. Chem. Soc.* **122**, 4530 (2000).

I. HAMACHI, N. KASAGI, S. KIYONAKA, T. NAGASE, Y. MITO-OKA and S. SHINKAI, "Pd(en) as a Sequence-Selective Molecular Pinch for α-Helical Peptides," *Chem. Lett.* 16 (2001).

Y. MITO-OKA, S. TSUKIJI, T. HIRAOKA, N. KASAGI, S. SHINKAI and I. HAMACHI, "Zn(II) Dipicolylamine-Based Artificial Receptor as a New Entry for Surface Recognition of α-Helical Peptides in Aqueous Solution," *Tetrahedron Lett.* **42**, 7059 (2001).

N. OHSHIRO, A. SHIMIZU, R. OKUMURA, F. TAKEI, K. ONITSUKA and S. TAKAHASHI, "Living Polymerization of Aryl Isocyanides by Multifunctional Initiators Containing Pd–Pt μ-Ethynediyl Units," *Chem. Lett.* 786 (2000).

K. ONITSUKA, N. OHSHIRO, M. FUJIMOTO, F. TAKEI and S. TAKAHASHI, "Synthesis of Hyper-branched Platinum-Poly(yne) Polymers by Self Polycondensation," *Mol. Cryst. Liq. Cryst.* **342**, 159 (2000).
K. ONITSUKA, A. IUCHI, M. FUJIMOTO and S. TAKAHASHI, "Synthesis of Organometallic Dendrimers by Ligand Exchange Reactions: Reversible Bonding of Dendrons to a Core in Transition Metal Acetylide Dendrimers," *Chem. Commun.* 741 (2001).

Laser Research Center for Molecular Science

K. SAITOW, K. NISHIKAWA, H. OHTAKE, N. SARUKURA, H. MIYAGI, Y. SHIMOKAWA, H. MATSUO and K. TOMINAGA, "Supercritical-Fluid Cell with Device of Variable Optical Path Length Giving Fringe-Free Terahertz Spectra," *Rev. Sci. Instrum.* **71**, 4061 (2000).
K. SHIMAMURA, T. FUJITA, H. SATO, A. BENSALAH, N. SARUKURA and T. FUKUDA, "Growth and Characterization of $KMgF_3$ Single Crystals by the Czochralski Technique under CF_4 Atmosphere," *Jpn. J. Appl. Phys., Part 1* **39**, 6807 (2000).
Z. LIU, T. KOZEKI, Y. SUZUKI, N. SARUKURA, K. SHIMAMURA, T. FUKUDA, M. HIRANO and H. HOSONO, "Chirped-Pulse Amplification of Ultraviolet Femtosecond Pulses by Use of $Ce^{3+}:LiCaAlF_6$ as a Broadband, Solid-State Gain Medium," *Opt. Lett.* **26**, 301 (2001).
S. ONO, T. TSUKAMOTO, E. KAWAHATA, T. YANO, H. OHTAKE and N. SARUKURA, "Terahertz Radiation from a Shallow Incidence-Angle InAs Emitter in a Magnetic Field Irradiated with Femtosecond Laser Pulses," *Appl. Opt.* **40**, 1369 (2001).
K. SHIMAMURA, S. L. BALDOCHI, I. M. RANIERI, H. SATO, T. FUJITA, V. L. MAZZOCCHI, C. B. R. PARENTE, C. O. PAIVA-SANTOS, C. V. SANTILLI, N. SARUKURA and T. FUKUDA, "Crystal Growth of Ce-Doped and Undoped $LiCaAlF_6$ by the Czochralski Technique under CF_4 Atmosphere," *J. Cryst. Growth* **223**, 382 (2001).
Z. LIU, T. KOZEKI, Y. SUZUKI, N. SARUKURA, K. SHIMAMURA, T. FUKUDA, M. HIRANO and H. HOSONO, "Ultraviolet Femtosecond Pulse Amplification with High Gain Using Solid-State, Broad-Band Gain Medium $Ce^{3+}:LiCaAlF_6$," *Jpn. J. Appl. Phys., Part 1* **40**, 2308 (2001).
K. SAITOW, H. OHTAKE, N. SARUKURA and K. NISHIKAWA, "Terahertz Absorption Spectra of Supercritical CHF_3 to Investigate Local Structure Through Rotational and Hindered Rotational Motions," *Chem. Phys. Lett.* **341**, 86 (2001).
T. KOZEKI, Y. SUZUKI, M. SAKAI, H. OHTAKE, N. SARUKURA, Z. LIU, K. SHIMAMURA, K. NAKANO and FUKUDA, "Observation of New Excitation Channel of Ceriumion through Highly Vacuumultra-violet Transparent LiCAF Host Crystal," *J. Cryst. Growth* **229**, 501 (2001).

I. SHOJI, Y. SATO, S. KURIMURA, T. TAIRA, A. IKESUE and K. YOSHIDA, "Optical Properties and Laser Characteristics of Highly Nd^{3+}-Doped $Y_3Al_5O_{12}$ Ceramics," *Appl. Phys. Lett.* **77**, 939 (2000).
A. IKESUE, T. TAIRA, Y. SATO and K. YOSHIDA, "High-Performance Microchip Lasers Using Polycrystalline Nd:YAG Ceramics," *J. Ceram. Soc. Jpn.* **108**, 428 (2000).
N. PAVEL, J. SAIKAWA and T. TAIRA, "Radial-Pumped Microchip High-Power Composite Yb:YAG Laser: Design and Power Characteristics," *Jpn. J. Appl. Phys.* **40**, 146 (2001).
N. PAVEL, J. SAIKAWA, S. KURIMURA and T. TAIRA, "High Average Power Diode End-Pumped Composite Nd:YAG Laser Passively Q-switched by Cr^{4+}:YAG Saturable Absorber," *Jpn. J. Appl. Phys.* **40**, 1253 (2001).
N. SENGUTTUVAN, K. OOTSUKA, N. KIDOKORO, M. ISHII, M. KOBAYASHI, T. TAIRA, Y. SATO, S. KURIMURA and M. IMAEDA, "Crystal Growth and Characterization of New Laser Crystal $Bi_4Si_3O_{12}$:Nd," *Memoirs Shonan Inst. Tech.* **35**, 29 (2001).
N. SENGUTTUVAN, N. KIDOKORO, K. OOTSUKA, M. ISHII, M. KOBAYASHI, T. TAIRA, Y. SATO and S. KURIMURA, "Crystal Growth and Optical Properties of $Bi_4Si_3O_{12}$:Nd," *J. Cryst. Growth* **229**, 188 (2001).
V. LUPEI, A. LUPEI, N. PAVEL, T. TAIRA, I. SHOJI and A. IKESUE, "Laser Emission under Resonant Pump in the Emitting Level of Concentrated Nd:YAG Ceramics," *Appl. Phys. Lett.* **79**, 590 (2001).
V. LUPEI, T. TAIRA, A. LUPEI, N. PAVEL, I. SHOJI and A. IKESUE, "Spectroscopy and Laser Emission under Hot Band Resonant Pump in Highly Doped Nd:YAG Ceramics," *Opt. Commun.* **195**, 225 (2001).
N. PAVEL, J. SAIKAWA and T. TAIRA, "Diode End-Pumped Passively Q-Switched Nd:YAG Laser Intra-Cavity Frequency Doubled by LBO Crystal," *Opt. Commun.* **195**, 233 (2001).

Research Center for Molecular Materials

Y. TAKAHASHI, M. TOMURA, K. YOSHIDA, S. MURATA and H. TOMIOKA, "Triplet Di(9-anthryl)carbene Undergoes Trimerization," *Angew. Chem., Int. Ed. Engl.* **39**, 3478 (2000).
K. SUZUKI, M. TOMURA, S. TANAKA and Y. YAMASHITA, "Synthesis and Characterization of Novel Strong Electron Acceptors: Bithiazole Analogues of Tetracyanodiphenoquinodimethane (TCNDQ)," *Tetrahedron Lett.* **41**, 8359 (2000).
Y. WADA, M. TSUKADA, M. FUJIHIRA, K MATSUSIGE, T. OGAWA, M. HAGA and S. TANAKA, "Prospects of Single Molecule Devices for Future High Performance Infromation Technologies," *Jpn. J. Appl. Phys.*

39, 3835 (2000).

M. TOMURA and Y. YAMASHITA, "Tetrathiafulvalene with a Fused Pyrazine Ring," *Acta Crystallogr., Sect. E: Struct. Rep.* **57**, o307 (2001).

M. AKHTARZZAMAN, M. TOMURA and Y. YAMASHITA, "One-Dimensional Hydrogen-Bonded Molecular Tapes in 1,4-Bis[(4-pyridinium)ethynyl]-benzene Chloranilate," *Acta Crystallogr., Sect. E: Struct. Rep.* **57**, o353 (2001).

M. TOMURA and Y. YAMASHITA, "A Molecule with a C_1-Homobasketane Framework," *Acta Crystallogr., Sect. C: Cryst. Struct. Commun.* **57**, 619 (2001).

M. B. ZAMAN, M. TOMURA and Y. YAMASHITA, "Linear Hydrogen-Bonded Molecular Tapes in the Co-Crystals of Squaric Acid with 4,4'-Dipyridylacetylene or 1,2-Bis(4-pyridyl)ethylene," *Acta Crystallogr., Sect. C: Cryst. Struct. Commun.* **57**, 621 (2001).

M. TOMURA and Y. YAMASHITA, "One-Dimensional Zigzag Chain Structures with Intermolecular C–H⋯π and C–H⋯O Interactions Consisted of Phthalic Acid and Pyridine Derivatives," *Chem. Lett.* 532 (2001).

M. AKHTARZZAMAN, M. TOMURA and Y. YAMASHITA, "4,7-Bis[(4-pyridyl)ethynyl]-2,1,3-benzo-thiadiazole and Its Dipyridinium Diperchlorate," *Acta Crystallogr., Sect. C: Cryst. Struct. Commun.* **57**, 751 (2001).

M. B. ZAMAN, M. TOMURA and Y. YAMASHITA, "Synthesis and Crystal Structures of Decamethyl-ferrocenium Salts of Anilate Anion Derived from Bromanilic Acid, Chloranilic Acid and Cyananilic Acid," *Inorg. Chim. Acta* **318**, 127 (2001).

Y. YAMASHITA, M. TOMURA and K. IMAEDA, "Hydroxyphenyl Substituted Tetrathiafulvalene Vinylogues Affording Stable Cation Radical Salts with Unusual Crystal Structures," *Tetrahedron Lett.* **42**, 4191 (2001).

S. TANAKA and Y YAMASHITA, "Novel Synthetic Approaches to Multifunctional π-Conjugated Oligomers for Molecular Scale Electronics," *Trans. Mater. Res. Soc. Jpn.* **26**, 739 (2001).

S. TANAKA and Y YAMASHITA, "Novel Synthetic Approach to 5–10 nm Long Functionalized Oligo-thiophenes," *Synth. Met.* **119**, 67 (2001).

S. B. HEIDENHAIN, Y. SAKAMOTO, T. SUZUKI, A. MIURA, H. FUJIKAWA, T. MORI, S. TOKITO and Y. TAGA, "Perfluorinated Oligo(*p*-Phenylene)s: Efficient n-Type Semiconductors for Organic Light-Emitting Diodes," *J. Am. Chem. Soc.* **122**, 10240 (2000).

Y. SAKAMOTO, S. KOMATSU and T. SUZUKI, "Tetradecafluorosexithiophene: The First Perfluorinated Oligothiophene," *J. Am. Chem. Soc.* **123**, 4643 (2001).

M. IKAI, S. TOKITO, Y. SAKAMOTO, T. SUZUKI and Y. TAGA, "Highly Efficient Phosphorescence from Organic Light-Emitting Devices with an Exciton-Block Layer," *Appl. Phys. Lett.* **79**, 156 (2001).

H. FUJIMORI, D. KUWAHARA, T. NAKAI and S. MIYAJIMA, "Transient 13C-1H Nuclear Overhauser Effect in Liquid Crystal," *J. Phys. Soc. Jpn.* **70**, 1117 (2001).

D. KUWAHARA, T. NAKAI, J. ASHIDA and S. MIYAJIMA, "Real Figure of Two-Dimensional Spin-Echo NMR Spectra for a Homonuclear Two-Spin System in Rotating Solids," *Mol. Phys.* **99**, 939 (2001).

D. KUWAHARA, T. NAKAI, J. ASHIDA and S. MIYAJIMA, "Novel Structure Discovered on Two-Dimensional Spin-Echo NMR Spectra for a Homonuclear Two-Spib System in Rotating Solids," *Proceedings of 14th Conference of the International Society of Magnetic Resonacene* 130 (2001).

UVSOR (Ultraviolet Synchrotron Orbital Radiation) Facility

S. TANAKA, K. MASE, M. NAGASONO, S. NAGAOKA, M. KAMADA, E. IKENAGA, T. SEKITANI and K. TANAKA, "Spectroscopy as a New Tool for Surface Analysis—Application to the Ice Surface," *Jpn. J. Appl. Phys.* **39**, 4489 (2000).

S. TANAKA, K. MASE, M. NAGASONO, S. NAGAOKA and M. KAMADA, "Electron-Ion Coincidence Study for the TiO_2(110) Surface," *Surf. Sci.* **451**, 182 (2000).

S. WAKO, M. SANO, Y. OHNO. T. MATSUSHIMA, S. TANAKA and M. KAMADA, "Orientation of Oxygen An-Molecules on Stepped Platinum (112)," *Surf. Sci.* **461**, L537 (2000).

S. ASAKA, M. ITOH and M. KAMADA, "Ultraviolet Light Amplification within a Nanometer-Sized Layer," *Phys. Rev. B* **63**, 81104 (2001).

R. GUILLEMIN, E. SHIGEMASA, K. LE GUEN, D. CEOLIN, C. MIRON, N. LECLERCQ, K. UEDA, P. MORIN and M. SIMON, "New Setup for Angular Distribution Measurements of Auger Electrons from Fixed in Space Molecules," *Rev. Sci. Instrum.* **71**, 4387 (2000).

T. KIYOKURA, F. MAEDA, Y. WATANABE, Y. IKEKAKI, K. NAGAI, Y. HORIKAWA, M. OSHIMA, E. SHIGEMASA and A. YAGISHITA, "Throughput Measurement of a Multilayer-Coated Schwarzschild Objective Using Synchrotron Radiation," *Opt. Rev.* **7**, 576 (2000).

K. ITO, J. ADACHI, R. HALL, S. MOTOKI, E. SHIGEMASA, K. SOEJIMA and A. YAGISHITA, "Photoelectron Angular Distributions from Dissociative Photoionization Channels of Fixed-in-Space Molecular Hydrogen," *J. Phys. B: At., Mol. Opt. Phys.* **33**, 527 (2000).

Y. TAKATA, E. SHIGEMASA and N. KOSUGI, "Mg and Al K-Edge XAFS Measurements with a KTP Crystal Monochromator," *J. Synchrotron Radiat.* **8**, 351 (2001).

M. KATOH, K. HAYASHI, T. HONDA, Y. HORI, M. HOSAKA, T. KINOSHITA, S. KODA, Y. TAKASHIMA and J. YAMAZAKI, "New Lattice for UVSOR," *Nucl. Instrum. Methods Phys. Res., Sect. A* **467–8**, 68 (2001).

H. OKAMURA, M. MATSUNAMI, T. INAOKA, T. NANBA, S. KIMURA, F. IGA, S. HIURA, J. KLIJN and T. TAKABATAKE, "Optical Conductivity of $Yb_{1-x}Lu_xB_{12}$: Energy Gap and Mid-Infrared Peak in Diluted Kondo Semiconductors," *Phys. Rev. B* **62**, R13265 (2000).
S. KIMURA, F. ARAI and M. IKEZAWA, "Optical Study on Electronic Structure of Rare-Earth Sesquioxides," *J. Phys. Soc. Jpn.* **69**, 3451 (2000).

Computer Center

J. I. CHOE, S. K. CHANG, S. W. HAM, S. NANBU and M. AOYAGI, "Ab Initio Study of *p-tert*-Butylcalix[4]-crown-6-ether Complexed with Alkyl Ammonium Cations," *Bull. Korean Chem. Soc.* **22**, 356(2001).

Center for Integrative Bioscience

M. P. ROACH, W. J. PUSPITA and Y. WATANABE, "Proximal Ligand Control of Heme Iron Coordination Structure and Reactivity with Hydrogen Peroxide: Investigations of the Myoglobin Cavity Mutant H93G with Unnatural Oxygen Donor Proximal Ligands," *J. Inorg. Biochem.* **81**, 173 (2000).
S. OZAKI, I. HARA, T. MATSUI and Y. WATANABE, "Molecular Engineering of Myoglobin: The Improvement of Oxidation Activity by Replacing Phe-43 with Tryptophan," *Biochemistry* **40**, 1044 (2001).
N. MAKIHARA, S. OGO and Y. WATANABE, "pH-Selective Hydrogenation of Water-Soluble Carbon Compounds and Alkenes with $[Cp*Ir^{III}(H_2O)_3]^{2+}$ ($Cp* = \eta^5C_5H_5$) as a catalyst Precusor in Very Acidic Media," *Organometallics* **20**, 497 (2001).
H. OHTSU, S. ITOH, S. NAGATOMO, T. KITAGAWA, S. OGO, Y. WATANABE and S. FUKUZUMI, "Characterization of Imidazolate-Bridged Dinuclear and Mononuclear Hydroperoxo Complexes," *Inorg. Chem.* **40**, 3200 (2001).
N. HARUTA, M. AKI, S. OZAKI, Y. WATANABE and T. KITAGAWA, "Protein Conformation Change of Myoglobin upon Ligand Binding Probed by Ultraviolet Resonance Raman Spectroscopy," *Biochemistry* **40**, 6956 (2001).
S. HEROLD, T. MATSUI and Y. WATANABE, "Peroxynitrite Isomerization Catalyzed by His64 Myoglobin Mutants," *J. Am. Chem. Soc.* **123**, 4085 (2001).

K. Y. HARA, H. NOJI, D. BALD, R. YASUDA, K. KINOSITA, Jr. and M. YOSHIDA, "The Role of the DELSEED Motif of the β Subunit in Rotation of F_1-ATPase," *J. Biol. Chem.* **275**, 14260 (2000).
Y. HARADA, O. OHARA, A. TAKATSUKI, H. ITOH, N. SHIMAMOTO and K. KINOSITA, Jr., "Direct Observation of DNA Rotation during Transcription by *Escherichia coli* RNA Polymerase," *Nature* **409**, 113 (2001).
R. YASUDA, H. NOJI, M. YOSHIDA, K. KINOSITA, Jr. and H. ITOH, "Resolution of Distinct Rotaitonal Substeps by Submillisecond Kinetic Analysis of F_1-ATPase," *Nature* **410**, 898 (2001).
H. NOJI, D. BALD, R. YASUDA, H. ITOH, M. YOSHIDA and K. KINOSITA, Jr., "Purine But Not Pyrimidine Nucleotides Support Rotation of F_1-ATPase," *J. Biol. Chem.* **276**, 25480 (2001).

H. FUJII, X. ZHANG, T. TOMITA, M. IKEDA-SAITO and T. YOSHIDA, "A Role for Highly Conserved Carboxylate, Aspartate-140, in Oxygen Activation and Heme Degradation by Heme Oxygenase-1," *J. Am. Chem. Soc.* **123**, 6475 (2001).

M. AKI, T. OGURA, K. SHINZAWA-ITOH, S. YOSHIKAWA and T. KITAGAWA, "A New Measurement System for UV Resonance Raman Spectra of Large Proteins and Its Application to Cytochrome *c* Oxidase," *J. Phys. Chem.* **104**, 10765 (2000).
M. NAGAI, M. AKI, R. LI, Y. JIN, H. SAKAI, S. NAGATOMO and T. KITAGAWA, "Heme Structure of Hemoglobin M Iwate [α87(F8)His → Tyr]: A UV and Visible Resonance Raman Study," *Biochemistry* **39**, 13093 (2000).
K. YAMAMOTO, Y. MIZUTANI and T. KITAGAWA, "Construction of Novel Nanosecond Temperature Jump Apparatuses Applicable to Raman Measurements and Direct Observation of Transient Temperature," *Appl. Spectrosc.* **54**, 1591 (2000).
H. OHTSU, S. ITOH, S. NAGATOMO, T. KITAGAWA, S. OGO, Y. WATANABE and S. FUKUZUMI, "Characterization of Imidazolate-Bridged Cu(II)–Zn(II) Heterodinuclear and Cu(II)–Cu(II) Homodinuclear Hydroperoxo Complexes as Reaction Intermediate Models of Cu, Zn-SOD," *J. Roy. Soc. Chem. Commun.* 1051 (2000).
S. ITOH, M. TAKI, H. KUMEI, S. TAKAYAMA, S. NAGATOMO, T. KITAGAWA, N. SAKURADA, R. ARAKAWA and S. FUKUZUMI, "Model Complexes for the Active Form of Galactose Oxidase. Physicochemical Properties of Cu(II)- and Zn(II)-Phenoxyl Radical Complexes," *Inorg. Chem.* **39**, 3708 (2000).
T. UCHIDA, H. ISHIKAWA, K. ISHIMORI, I. MORISHIMA, H. NAKAJIMA, S. AONO, Y. MIZUTANI

and T. KITAGAWA, "Identification of Histidine 77 as the Axial Heme Ligand of Carbonmonoxy CooA by Picosecond Time-Resolved Resonance Raman Spectroscopy," *Biochemistry* **39**, 12747 (2000).

M. TAKI, H. KUMEI, S. NAGATOMO, T. KITAGAWA, S. ITOH and S. FUKUZUMI, "Active Site Models for Galactose Oxidase Containing Two Different Phenol Groups," *Inorg. Chim. Acta* **300-302**, 622 (2000).

T. OHTA, T. TACHIYAMA, K. YOSHIZAWA, T. YAMABE, T. UCHIDA and T. KITAGAWA, "Synthesis, Structure, and H_2O_2-Dependent Catalytic Functions of Disulfide-Bridged Dicopper(I) and Related Thioether-Copper(I) and Thioether-Copper(II) Complexes," *Inorg. Chem.* **39**, 4358 (2000).

H. ARII, S. NAGATOMO, T. KITAGAWA, T. MIWA, K. JITSUKAWA, H. EINAGA and H. MASUDA, "A Novel Diiron Complex as a Functional Model for Hemerythrin," *J. Inorg. Biochem.* **82**, 153 (2000).

N. SUZUKI, T. HIGUCHI, Y. URANO, K. KIKUCHI, T. UCHIDA, M. MUKAI, T. KITAGAWA and T. NAGANO, "First Synthetic NO-Heme-Thiolate Complex Relevant to Nitric Oxide Synthase and Cytochrome P450nor," *J. Am. Chem. Soc.* **122**, 12059 (2000).

T. UCHIDA, M. TSUBAKI, T. KUROKAWA, H. HORI, J. SAKAMOTO, T. KITAGAWA and N. SONE, "Active Site Structure of SoxB-Type Cytochrome *bo*₃ Oxidase from Thermophilic *Bacillus*," *J. Inorg. Biochem.* **82**, 65 (2000).

Y. KIM, K. SHINZAWA-ITOH, S. YOSHIKAWA and T. KITAGAWA, "Presence of the Heme-Oxo Intermediate in Oxygenation of Carbon Monoxide by Cytochrome c Oxidase Revealed by Resonance Raman Spectroscopy," *J. Am. Chem. Soc.* **123**, 757 (2001).

N. HARUTA, M. AKI, S. OZAKI, Y. WATANABE and T. KITAGAWA, "Protein Conformation Change of Myoglobin upon Ligand Binding Probed by Ultraviolet Resonance Raman Spectroscopy," *Biochemistry* **40**, 6956 (2001).

T. EGAWA, D. A. PROSHLYAKOV, H. MIKI, R. MAKINO, T. OGURA, T. KITAGAWA and Y. ISHIMURA, "Effects of a Thiolate Axial Ligand on the $\pi \pi^*$ Electronic States of Oxoferryl Porphyrins: A Study of the Optical and Resonance Raman Spectra of Compounds I and II of Chloroperoxidase," *J. Biol. Inorg. Chem.* **6**, 46 (2001).

T. TOMITA, N. HARUTA, M. AKI, T. KITAGAWA and M. IKEDA-SAITO, "UV Resonance Raman Detection of a Ligand Vibration on Ferric Nitrosyl Heme Proteins," *J. Am. Chem. Soc.* **123**, 2666 (2001).

Y. MIZUTANI and T. KITAGAWA, "A Role of Solvent in Vibrational Energy Relaxation of Metalloporphyrins," *J. Mol. Liq.* **90**, 232 (2001).

S. G. KRUGLIK, P. MOJZES, Y. MIZUTANI, T. KITAGAWA and P-Y. TURPIN, "Time-Resolved Resonance Raman Study of the Exciplex Formed between Excited Cu-Porphyrin and DNA," *J. Phys. Chem.* **105**, 5018 (2001).

REVIEW ARTICLES AND TEXTBOOKS

Department of Theoretical Studies

S. ABE and Y. OKAMOTO, Eds., *Lecture Notes in Physics: Nonextensive Statistical Mechanics and Its Applications*, Springer-Verlag, pp. 1–277 (2001).

Y. OKAMOTO, "Monte Carlo Simulated Annealing in Protein Folding," in *Encyclopedia of Optimization Vol. III*, C. A. Floudas and P. M. Pardalos, Eds., Kluwer Academic, pp. 425–439 (2001).

U. H. E. HANSMANN and Y. OKAMOTO, "Protein Folding: Generalized-Ensemble Algorithms in Protein Folding," in *Encyclopedia of Optimization Vol. IV*, C. A. Floudas and P. M. Pardalos Eds., Kluwer Academic, pp. 392–401 (2001).

A. MITSUTAKE, Y. SUGITA and Y. OKAMOTO, "Generalized-Ensemble Algorithms for Molecular Simulations of Biopolymers," *Biopolymers (Pept. Sci.)* **60**, 96–123 (2001).

Y. OKAMOTO, "Simulations for Tertiary Structure Prediction," in *New Developments in Genome Informatics: From the Viewpoint of Biophysics*, (in Japanese) *Biophysics* **40**, 308–309 (2000).

Y. SUGITA and A. KITAO, "Theoretical Studies on Formation of Tertiary Structure of Protein," (in Japanese) *Biophysics* **40**, 368–373 (2000).

M. KINOSHITA, Y. OKAMOTO and F. HIRATA, "Solvent Effects on Formation of Tertiary Structure of Protein," (in Japanese) *Biophysics* **40**, 374–378 (2000).

Y. OKAMOTO, "Post-Genome Analyses by Computer Simulations," in *Genome, Life, and Computer*, (in Japanese) *Computer Today* **101**, 26–30 (2001).

Y. OKAMOTO, "How Far Can Computational Chemistry Approach the Full Understanding of Biological Phenomena," in *Challenges in Theoretical Chemistry and Computational Chemistry*, (in Japanese) *Chemistry in the 21st Century* **9**, Chemical Society of Japan, pp. 65–70 (2001).

M. KINOSHITA, Y. OKAMOTO and F. HIRATA, "Theoretical Analysis of Peptide Conformations in Water and in Alcohol," (in Japanese) *Protein, Nucleic Acid and Enzyme* **46**, May, pp. 713–718 (2001).

Y. SUGITA, A. MITSUTAKE and Y. OKAMOTO, "Protein Folding Simulations by Generalized-Ensemble Algorithms," (in Japanese) *Butsuri* **56**, 591–599 (2001).

Y. OKAMOTO, "Biomolecular Simulations in the Post Genome Era," in *New Frontiers of Genome Science*, (in Japanese) *Mathematical Sciences* **458**, 36–43 (2001).

K. MITSUKE and H. NAKAMURA, "Photo-Dynamics and Reaction Dynamics of Molecules (Satellite of XXI-ICPEAC)," *Comm. Atom. & Molec. Phys. Comm. Modern Phys.* **2**, Part D, 75 (2000).

C. ZHU, Y. TERANISHI and H. NAKAMURA, "Nonadiabatic Transitions due to Curve Crossings: Complete Solutions of the Landau-Zener-Stueckelberg Curve Crossing Problems and Their Applications," *Adv. Chem. Phys.* **117**, 127 (2001).

Y. TERANISHI, K. NAGAYA and H. NAKAMURA, "New Way of Controlling Molecular Processes by Lasers," in *Quantum Control of Molecular Reaction Dynamics*, R. J. Gordon and Y. Fujimura, Eds., World Scientific, **14**, 215 (2001).

S. SAITO and K. UMEMOTO, "Electronic Structure of Body-Centered Lattice Fullerides," in *Electronic Propeerties of Novel Materials—Molecular Nanostuructures*, H. Kuzmany *et al.*, Eds., American Institute of Physics Conference Proceedings, **544**, 14 (2000).

S. SAITO, "Electronic Properties of Nanotube Based Materials," in *Tours Symposium on Nuclear Physics IV*, A. Arnould *et al.*, Eds., American Institute of Physics Conference Proceedings, **561**, 214 (2000).

M. KINOSHITA, Y. OKAMOTO and F. HIRATA, "Solvent Effects on Formation of Tertiary Structure of Protein," *Seibutsu Butsuri* (in Japanese) **40**, 374 (2000).

M. KINOSHITA, Y. OKAMOTO and F. HIRATA, "Theoretical Analysis of Peptide Conformations in Water and in Alcohol," *Tanpakusitsu Kakusan Kouso* (in Japanese) **46**, 713 (2001).

F. HIRATA, H. SATO, S. TEN-NO and S. KATO, "The RISM-SCF/MCSCF Approach for the Chemical Processes in Solutions," in *Computational Biochemistry and Biophysics*, O. M. Becker, A. D. MacKerell, Jr., B. Roux and M. Watanabe, Eds., Marcel Dekker Inc.; New York, pp. 417–439 (2001).

H. SATO, "Theory for Solvent Effects: A combination of Electronic Structure Theory and Liquid Theory—Quantum Mechanics, Statistical Mechanics and Acid-Base—," *Kagaku to Kogyo (Chemistry and Chemical Industry)* (in Japanese) **54–2**, pp. 119–123 (2001).

M. KUWABARA and K. YONEMITSU, "Charge Ordering and Optical Conductivity of MMX Chains," in *Physics in Local Lattice Distortions*, H. Oyanagi and A. Bianconi, Eds., American Institute of Physics; Melville, N.Y., 465 (2001).

Department of Molecular Structure

Y. MAEDA, T. WAKAHARA, T. AKASAKA, M. FUJITSUKA, O. ITO, K. KOBAYASHI and S. NAGASE, "Metal-free Bis-silylation and Bis-germiration: C_{60}-Sensitized Reaction of Unsaturated Compounds with disilirane and digermirane," *Recent Research Developments in Organic Chemistry* **5**, 151–163 (2001).
T. KATO, T. AKASAKA, K. TASHIRO and T. AIDA, "An Inclusion Complex of a cyclic Dimer of Metallo-porphyrin with La@C_{82}," in *Recent Advances in the Chemistry and Physics of Fullerenes*, P. V. Kamat, D. M. Guldi and K. M. Kadish, Eds., The Electrochemical Society; Pennington, NJ (2001).
T. AKASAKA, T. WAKAHARA, M. KONDO, S. SHIRAKURA, Y. MAEDA, S. NAGASE, K. KOBAYASHI, M. WAELCHLI, K. YAMAMOTO, T. KATO, M. KAKO, Y. NAKADAIRA, X. GAO, E. V. CAEMELBECKE and K. M. KADISH, "Chemistry of Endohedral Metallofullerenes: Structural Determination of the La@C_{82} Isomer," in *Recent Advances in the Chemistry and Physics of Fullerenes*, P. V. Kamat, D. M. Guldi and K. M. Kadish, Eds., The Electrochemical Society; Pennington, NJ (2001).
T. WAKAHARA, T. AKASAKA, K. KOBAYASHI and S. NAGASE, "Recent Advances in Chemistry of Endohedral Metallofullerenes," *Kagaku* **56**, 60–61 (2001).
T. AKASAKA, T. WAKAHARA, S. NAGASE and K. KOBAYASHI, "Silylfullerenes," *J. Syn. Org. Chem. Japan* **58**, 1066–1076 (2000).
M. FUJITSUKA, O. ITO, K. YAMAMOTO and T. AKASAKA, "Photophysical and Photochemical Properties of Higher Fullerenes," *Recent Research Developments in Physical Chemistry* **4**, 135–148 (2000).

S. OKUBO, T. KATO, M. INAKUMA and H. SHINOHARA, "Spin Dynamics of ESR-active Lanthanum Endohedral Fullerenes," in *Proceedings of the Symposium on Chemistry and Physics of Fullerenes and Carbon Nanomaterials* **10**, P. V. Kamat, D. M. Guldi and K. M. Kadish, Eds., The Electrochemical Society, Inc.; Pennington, pp. 291–297 (2000).

Department of Electronic Structure

Y. UOZUMI and T. TSUKUDA, "Preparations and New Functions of Metal Nanoparticles," *Kagaku* (in Japanese) **56**, 68 (2001).

T. SUZUKI and B. J. WHITAKER, "Non-adiabatic dynamics effects in Chemistry revealed by time-resolved charged particle imaging," *Int. Rev. Phys. Chem.* **20**, 313 (2001).
T. SUZUKI, "Non-adiabatic bending dissociation of OCS," in *ACS symposium series, American Chemical Society*, K. Dyall and M. Hoffmann, Eds. (2001).

T. YAMASE, "Molecular Aspect of Energy Transfer from Tb^{3+} to Eu^{3+} in Polyoxometalate Lattices: An Approach for Molecular Design of Rare-Earth Metal-oxide Phosphors," in *Polyoxometallates: From Topology to Industrial Applications*, M. T. Pope and A. Müller, Eds., Kluwer Academic Publishers, pp. 187–203 (2001).

Department of Molecular Assemblies

K. YAKUSHI, "Reflection spectroscopic study of organic conductors," *Bull. Chem. Soc. Jpn.* **73**, 2643 (2000).
K. YAKUSHI, M. SIMONYAN and Y. DING, "Spectroscopic Studies of Solid Phthalocyanines and Their Charge-Transfer Salts," *J. Porphyrins Phthalocyanines* **5**, 13 (2001).

H. KOBAYASHI, A. KOBAYASHI and P. CASSOUX, "BETS as a Source of Molecular Magnetic Super-conductors (BETS = bis(ethylenedithio)tetraselenafulvalene)," *Chem. Soc. Rev.* **29**, 325 (2000).

R. KATO, "Conductive Copper Salts of 2,5-Disubstituted *N,N'*-Dicyanobenzoquinonediimines (DCNQIs): Structural and Physical Properties," *Bull. Chem. Soc. Jpn.* **73**, 515 (2000).

T. OGAWA, "Structural Chemistry of Organobismuth Compounds," in *Organobismuth Chemistry*, H. Suzuki, Ed., Elsevier Science S.A.; Lausanne (2001).

Department of Applied Molecular Science

M. K. KABIR, N. MIYAZAKI, S. KAWATA, K. ADACHI, H. KUMAGAI, K. INOUE, S. KITAGAWA, K. IIJIMA and M. KATADA, "Novel Layered Structures Constructed from Iron-chloranilate Compounds," *Coord. Chem. Rev.* **198**, 157 (2000).

H. MASUDA, H. KITAMURA, K. JITSUKAWA and H. EINAGA, "Unique Inorganic-Organic Hybrid Systems Self-Organized by Triply-Hydrogen Bonding Interaction and Their Functions," in *Precision Polymers and Nano-Organized Systems*, Kodansha Scientific, pp. 239–242 (2000).

Department of Vacuum UV Photoscience

N. KOSUGI, "Highly bright synchrotron radiation gives a new horison to resonant photoelectron spectroscopy," (in Japanese) *KAGAKU (CHEMISTRY)* **56**, 60–61 (2001).

M. KOMIYAMA and T. SHIMAGUCHI, "Recent Applications of Atomic Force Microscopy to the Study of Pyridine-Base Molecules Adsorbed on the (010) Surfaces of Heulandite and Stilbite Crystals," in *Natural Zeolites for the Third Millennium*, C. Colella and F. A. Mumpton, Eds., De Frede Editore; Naples, pp. 315–320 (2000).
M. KOMIYAMA, "AFM Observations of Adsorbed Molecular Structure on Zeolite (010) Surface," (in Japanese) *Hyomen Kagaku (J. Surf. Sci. Soc. Jpn.)* **21**, 576–583 (2000).
M. NAGAI, A. ONAKA, M. KOMIYAMA, K. DOMEN and T. FUJITA, "Catalyst Study for the 21st Century," (in Japanese) *Shokubai (Catalyst and Catalysis)* **42**, 546–551 (2000).
M. KOMIYAMA, "Shokubai-no-Jiten (Encyclopaedia of Catalysis)," (in Japanese) M. Misonou, Y. Ono and Y. Morooka Eds., Asakura; Tokyo (2000).

I. H. SUZUKI, N. SAITO, S. NAGAOKA, T. IBUKI, Y. SHIMIZU, Y. TAMENORI, H. OHASHI, Y. SENBA and H. OHASHI, "Observation of Resonant Auger Electron Emission Following Photoexcitation of the Kr 2p Electron to the 5s Orbital," *Atomic Collision Res. Jpn.* **26**, 69 (2000).

Coordination Chemistry Laboratories

I. TANIGUCHI, "Bioelectrochemistry" in *Denki-kagaku Binran* (in Japanese), Electrochem. Soc. Jpn., Ed., Maruzen; Tokyo (2000).
I. TANIGUCHI, "Chemically Modified Electrode" and "Photovolatge" in *Shokubai-Jiten*, (in Japanese), Y. Ono, M, Misonoo and Y. Morooka, Eds., Asakura-shoten; Tokyo (2000).
I. TANIGUCHI, "Bioelectroanalytical Chemistry Using Functionalized Electrodes: Fundamentals and Applications," in *Proc. Workshop cum Seminar on Electroanaltytical Chemistry and Allid Topics (ELAC-2000)*, S. K. Aggarwar, H. S. Sharma, N. Gopinath and D. S. C. Purushotham, Eds., BARC; Munbai (2000).

R. OKAZAKI and N. TOKITOH, "Heavy Ketones, the Heavier Element Congeners of a Ketone," *Acc. Chem. Res.* **33**, 625 (2000).
N. TOKITOH and R. OKAZAKI, "Recent Topics in the Chemistry of Heavier Congeners of Carbenes," *Coord. Chem. Rev.* **210**, 251 (2000).
N. TOKITOH, "New Aspects in the Chemistry of Low-Coordinated Inter-Element Compounds of Heavier Group 15 Elements," *J. Organomet. Chem.* **611**, 217 (2000).
N. TOKITOH and R. OKAZAKI, "Recent Advances in the Chemistry of Group 14-Group 16 Double Bond Compounds," *Adv. Organomet. Chem.* **47**, 121 (2001).

I. HAMACHI, J. WATANABE, R. EBOSHI, T. HIRAOKA and S. SHINKAI, "Incorporation of Artificial Receptors into a Protein/Peptide Surface: A Strategy for On/Off Type of Switching of Semisynthetic Enzymes," *Biopolymers* **55**, 459 (2001).

K. ONITSUKA and S. TAKAHASHI, "Synthesis and catalysis of organotransition metal dendrimers," *Yuki Gosei Kagaku Kyokaishi (J. Synth. Org. Chem. Jpn.)* (in Japanese) **58**, 988 (2000).

Laser Research Center for Molecular Science

K. TOMINAGA, H. OHTAKE, N. SARUKURA, K. SAITOW, H. SASAKAWA, A. TAMURA, I. V. RUBTSOV and K. YOSHIHARA, "Spectroscopic Application of the THz Radiation Generated by Ultrashort Pulses—Static Far Infrared Absorption Measurement in Condensed Phases—," in *Advances in Multiphoton Process and Spectroscopy* **14**, S. H. Lin, A. A. Villaeys and Y. Fujimura, Eds., World Scientific; Singapore (2001).

I. SHOJI and T. TAIRA, "Trend of Microchip laser development," *Optical Alliance* **12**, 19–24 (2001).

Center for Integrative Bioscience

Y. WATANABE, "Asymmetric Oxidation of Sulfides and olefins by Myoglobin Mutants," *Review on Heteroatom Chemistry* **22**, 135 (2001).
L. QUE, Jr. and Y. WATANABE, "Oxygenase Pathways: Oxo, Peroxo, and Superoxo," *Science* **292**, 651 (2001).

K. KINOSITA, Jr., R. YASUDA and H. NOJI, "F_1-ATPase: a Highly Efficient Rotary ATP Machine," *Essays Biochem.* **35**, 3 (2000).
K. KINOSITA, Jr., R. YASUDA, H. NOJI and K. ADACHI, "A Rotary Molecular Motor That Can Work at Near 100% Efficiency," *Phil. Trans. Roy. Soc. Lond. B.* **355**, 473 (2000).

R. YASUDA, H. NOJI, K. ADACHI, T. NISHIZAKA, Y. KATO-YAMADA, M. YOSHIDA and K. KINOSITA, Jr., "Rotation of ATP Synthase," in *Na/K-ATPase and Related ATPases*, K. Taniguchi and S. Kaya, Eds., Elsevier; Amsterdam (2000).

S. ISHIWATA, J. TADASHIGE, I. MASUI, T. NISHIZAKA and K. KINOSITA, Jr., "Microscopic Analysis of Polymerization and Fragmentation of Individual Actin Filaments," in *Results and Problems in Cell Differentiation, Vol. 32: Molecular Interactions of Actin*, C. dos Remedios, Ed., Springer-Verlag; Berlin (2001).

T. KITAGAWA, "Structures of reaction intermediates of cytochrome c oxidase probed by time-resolved vibrational spectroscopy," *J. Inorg. Biochem.* **82**, 9 (2000).

T. KITAGAWA, "Progress report on molecular biometallics (1996-2000), a project of the priority areas for research under the auspices of the Japanese government," *J. Biol. Inorg. Chem.* **5**, 410 (2000).

AUTHOR INDEX

to "Research Activities" and "Special Research Projects"